FULL-FIELD STRAIN MEASUREMENTS OF METAL PLATE CONNECTIONS USING DIGITAL IMAGE CORRELATION TECHNIQUE

By

DEEMA RASHAD ALSHEIAB

Bachelor of Science in Civil Engineering
Jordan University of Science and Technology
Irbid, Jordan
2002

Master of Science in Civil Engineering
Oklahoma State University
Stillwater, Oklahoma
2006

Submitted to the Faculty of the
Graduate College of the
Oklahoma State University
in partial fulfillment of
the requirements for
the Degree of
DOCTOR OF PHILOSOPHY
December, 2013

FULL-FIELD STRAIN MEASUREMENTS OF

METAL PLATE CONNECTIONS USING DIGITAL

IMAGE CORRELATION TECHNIQUE

Dissertation Approved:

Dissertation Adviser: Dr. Robert Emerson

Dissertation Adviser

Committee Member : Dr. Garold Oberlender

Committee Member : Dr. Tyler Ley

Outside Committee Member : Dr. Damon Chandler

ACKNOWLEDGEMENTS

I wish to express my appreciation and gratitude to the people who were most supportive of me as I engaged this study.

First, I wish to thank my advisor Dr. Robert Emerson, I wish to express my highest degree of thanks for his support and opinions to make this wok happen.

To my committee members, Dr.Garold Oberlender, Dr. Tyler Ley and Dr. Damon Chandler, I appreciate their time and comments.

I offer my gratitude to David Porter (lab manager) who helped me in making all the wood joints, to Alex Morrison who helped me in conducting all the experimental tests, to brother Sayeed Mohammad, to my husband, Aymen Kassaimih, and my little kids Ali (7 years) and Sandy (5 years) who suffered from being me at school to finish my research work.

Finally, I owe my deepest thanks to my Mother (Tuffaha Nusir) and my father (Rashad Alsheiab) who always pray for me and wish me the best.

Name: Name: DEEMA RASHAD ALSHEIAB

Date of Degree: DECEMBER, 2013

Title of Study: FULL-FIELD STRAIN MEASUREMENTS OF METAL PLATE CONNECTIONS USING DIGITAL IMAGE CORRELATION TECHNIQUE

Major Field: CIVIL ENGINEERING

Abstract:

Metal plate connections (MPC) are a very important element in the truss design industry; however, they are considered the least understood part and their design is not well understood. The complications in MPC joint modeling, analysis, and design are related to the combined nature of the metal plate and wood as well as the geometry of the system. Widespread use of metal plate connections to connect wood-truss-joints (in industrial buildings, residential and housing, and commercial buildings) opened the doors to create opportunities for more research in studying the behavior of MPC's. Thus, the need for an accurate understanding of the performance and properties of the metal plate connectors and the wood members has risen to get an efficient and accurate analysis and design of MPC which could mean major savings in time and money. None of the previous research in metal plate connections contained measurements of the entire surface displacements or strain (local) of the metal plate connections. The measurement of strain (displacements) plays an important role in experimental stress analysis and in the evaluation of material properties. Several experimental methods and devices are used to measure displacements: Moiré techniques, laser speckle, Strain gauges etc. However, digital image correlation (DIC) has been successfully applied to measure the full-field strain and displacements.

Digital image correlation (DIC) technique is a well-established approach that is used to find the full-field strain (local) measurements for MP connected joint surface. The MPC were studied in four-tensile joint configuration and heel joint. 2D-DIC code is used to find the full-field strain measurements. The results from the DIC are used to find the yielding stress for the first test AA under tensile force. The heel joint full-field strain measurements show the changes in the strain under loading and the influence of the rotation of the top chord wood member.

TABLE OF CONTENTS

LIST OF TABLES

LIST OF FIGURES

Notations

MPC: Metal Plate Connections or Connectors

MP: Metal Plate

LVDT: Linear Variable Differential Transducers

DIC: Digital Image Correlation

HJ: Heel Joint

Ft: Fracture tensile stress

Fy: Yielding stress

AA: the load is parallel to the plate's major axis and to the wood grain

AE: the load is parallel to the plate's major axis and perpendicular to the wood grain

EA: the load is perpendicular to the plate's major axis and parallel to the wood grain

EE: the load is perpendicular to the plate's major axis and to the wood grain

CHAPTER I

INTRODUCTION

1.1 An Overview on Metal Plate Connections MPC and Research Motivation

The invention of metal plate connectors was a revolution in the wood truss industry. Metal plate connections (MPC) were invented in Florida in 1952. Since then, hundreds of millions of MPC have been manufactured and widely used in wood construction. Currently, most residential homes and apartments in the U.S.A are constructed by using MPC joints (Carlson 1991). Figure 1.1 shows an example of MPC.

Figure 1-1: Metal plate connected wood joint (ref. On Line Building Safety Journal)

There are many types of connectors that have been developed to connect wood members together such as nails, bolts, split rings etc. However, MPC are the most economical and efficient connectors compared to the other types of connectors. Their uncomplicated installation and low labor requirements have made the MPC the most widely used connector in the manufacturing of light frames and trusses.

Metal Plate Connectors are punched from light-gauge steel coil. A high-speed stamping machine punches out the teeth to required dimensions for a variety of different forms. The plates are pressed into the wood by hydraulic or roller equipment. The strength capacity of the metal plate is based on the tensile and the shear capacity of metal plate in addition to the teeth-gripping. MPC are designed to connect wood members together and to transfer the load between wood members at the joints. The function of the teeth is to join the MPC to the wood and to transfer the shear forces which should not exceed the allowable load per tooth or per unit area (Truss Plate Institute TPI, 2007). In 2003, the yearly sales of the trusses and MPC industry were over two billion dollars (Slabinski, 2005). These statistical sales numbers show the significant expansion and rising demand for MPC.

Thus, the need for an accurate understanding of the performance and properties of MPC and the wood members has risen. An efficient and accurate analysis and design of MPC is therefore required which would lead to savings in individual connection design. The accumulation of these savings over millions of plates leads to a large overall savings in money and resources. MPC are an important element in the truss design industry; however, they are considered the least understood part and their design is not well understood. The complications in MPC joint modeling, analysis and design are related to the combined nature of the metal plate and wood and the geometry of the system (Cabrero and Gebremedhin, 2009). Widespread use of MPC to connect wood-truss-joints (in industrial buildings, residential and housing, and commercial buildings) opened the doors to create opportunities for more research in studying the behavior of MPC.

Indeed, several factors may affect the performance and the behavior of metal plate connectors such as the plate dimensions, plate directions or orientations, steel plate properties, teeth design or layout, teeth length and more.

None of the previous research in MPC contained measurements of the entire surface displacements or strain (local) of the metal plate connections. Most previous studies on MP connected joints were focused on only the displacements in the area between the two wood members that are connected by the MPC. A linear variable differential transducer (LVDT) was generally used to find this displacement. The continuously growing development in the digital image technology and machines has also made several digital cameras available at reasonable cost, opening the door to utilize this developing technology. Digital image correlation (DIC) techniques are effective and applicable in the processing of images, providing for full-field strain (local) measurements regardless of the nature of the loading conditions or any other environmental effects. These techniques save both time and money to find full-field strain (local) distribution. In this research, the DIC technique was used to find the full field strain measurements on the surface of MPC. This strain is used to study the materials properties and the failure mode which can be used in modeling approaches.

1.1.1 Heel Joints

A heel joint is one of the joints in a truss, a structural frame comprising a triangular unit. These triangular units have straight members connected at joints or nodes. The truss members will transfer the load to the reaction points.

The arrangement of truss members provides high strength-to-weight ratios and permits long spans without intermediate support. Wood trusses are widely used in residential, commercial, agricultural, and institutional buildings, etc. due to the availability of required strength in the wood trusses. Wood trusses provide economical framing solutions (cost and time effectiveness), flexibility and versatility of wood trusses, and environmental benefits. Light weight wood trusses are designed in almost any size or shape with some limitations such as the manufacturing capabilities and shipping and handling.

Light frame trusses connected by MPC were originally developed in U.S.A in the 1950's. Since then the system has grown and now is highly developed. In 1960, the Truss Plate Institute (TPI) was established in the U.S. to maintain and develop an industry-wide wood truss design standards. Since then, several other associations were also established.

The metal plate in the truss is used to connect two or more members of lumber. The metal pate will transfer the loads between the adjoining members through the plate's teeth. The strength of the steel plate depends on several factors including (a) shear capacity of the plate, (b) tensile capacity of the plate, and (c) grip of the teeth. The size of the plate is not fixed, the width can be at least 1 inch and up to 12 inches, and the length of plate can be 2 feet or more. The length of teeth is also not fixed and can be 0.25 inch or more.

1.2 Digital Image Correlation DIC

Digital image correlation (DIC) technique is a well-established approach that can be used to find full-field strain measurements. In this research, the behavior of MPC was investigated by testing many samples and configurations. The full-field strain measurements for the MPC were obtained from digital image correlation technique at different loading increments. The MPC were coated with a white pattern then with a random black pattern known as speckles. A digital camera was used to capture the deformation of each specimen under loading at different stages until failure. The digital images represent the intensity of the light and can be represented as a matrix. This intensity matrix was used for correlation between the deformed and non-deformed images. Thus, DIC technique relies on comparison between two speckled images to retrieve the required data. DIC is an optical methodology based on image processing and numerical calculations (Bing Pan, 2009).

The measurement of strain plays an important role in experimental stress analysis and in the evaluation of material's properties. There are several experimental methods and devices for measuring in-plane and out-of-plane displacements. Moiré techniques, laser speckle, photo-elasticity, etc. Each of these methods has its own limitations and characteristics. The equipment and preparation for these methods are expensive. They require special treatments to the surface and changes in the mechanical properties in addition to special attachment considerations. Strain gauges, clip on electrical transducers, and linear variable differential transducers (LVDT's) are devices that can measure the distance between two points over a limited gauge length. Strain is important for material's properties. To have full-field strain measurements is more practical than having a displacement over a limited length.

The needs for a non-contacting method to find the full-field strain measurement opened the door to focus on DIC, which has been successfully applied to measure the displacements and strain (local strain). DIC technique (also called digital speckle photography) was developed as an application of computer vision and has proven its effectiveness in several scientific and life fields. This technique has been used in dynamics, rigid body mechanics, fluid mechanics, biomechanics, and others.

This technique is used to compare two similarly speckled images, one of them representing the object before deformation and the other the object after deformation, which have been captured by a charge-coupled device (CCD) camera, which operates by the movement of electrical charge, usually from within the device to an area where the charge can be manipulated then converted into a digital value. This is achieved by "shifting" the signals between stages within the device one at a time. CCDs move charge between capacitive bins in the device, with the shift allowing for the transfer of charge between bins. Once digitized, an image can be characterized by the patterns of various levels of light intensity. Differences between two digitized images can be obtained by correlating and comparing them using an algorithm. Therefore, whole field displacement measurements for plane structures can be obtained using the optical technique of DIC (Chu, Ranson et al., 1985; Bruck, 1989; Choi, 1997; Wattrisse, Chrysochoos et al., 2001) . The resolution of the strain measurements using DIC technique is determined by (1) the magnification of the acquisition system such as optical lenses, scanning microscope, etc. and (2) the features of the image sensing elements such as the pixel pitch of the CCD (Wang and Cuitiño, 2002). DIC is a straightforward technique that can provide the measurements in2D and 3D. But the

2D concepts are easier to understand and to use. The implementation of 2D DIC technique can be done in three steps:

1) Preparing the specimen (experimental testing)

2) Capturing images for the specimen before and after loading

3) Processing the images using computer algorithm to obtain the strain measurements.

Digital Image Correlation has been used in various applications in many fields. It has been used to determine the displacement of and to describe the deformation mechanism for many materials (metal, wood, polymer etc.) as they are subjected to different kinds of loading such as mechanical, thermal, or others. Full-field strain (local strain) measurements and displacements (local displacement),obtained using DIC technique, can be used to identify the elastic properties of materials (Hild and Roux, 2006; Avril, Bonnet et al., 2008). Also, several mechanical parameters (Poisson's ratio, Young's modulus, stress intensity factor, residual stress, and thermal expansion coefficient) can be determined (Lyons 1996, Zhang D 1999, Cho 2005, Sabaté 2006, Zhang 2006). It can be expected that the coming years will see further extended DIC applications in several additional research fields.

In this research, DIC technique was used to find the full-field strain measurements (local strain) for the surface of the MPC. There are two main tests; the first test is a tension test of the four cases-standard metal plate connections tension test as shown in figure 1.2. The second test is the heel joint test by making a simple truss.

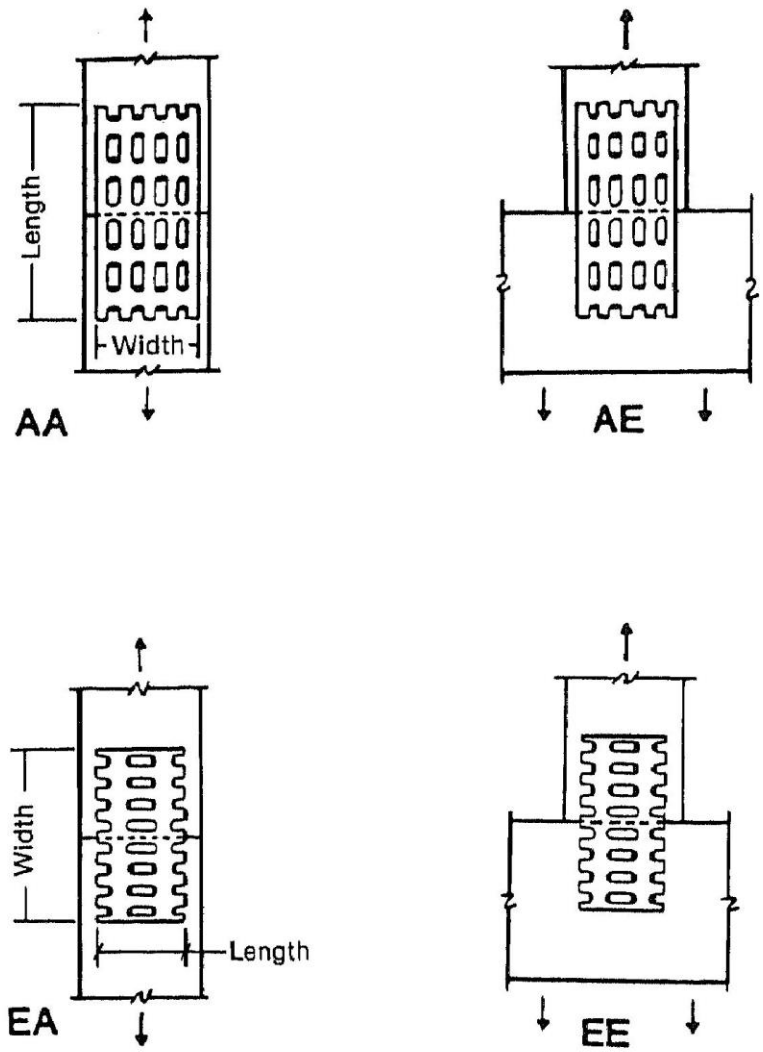

Figure 1-2: The four Canadian Standard Plate tests

The first letter in the coding refers to the orientation of the plate primary axis to the load (A = parallel, E = perpendicular).

The second letter refers to the orientation of the wood grain to the load (A = parallel, E = perpendicular).

(Canadian Standard Association 1980)

A Nikon camera (CCD camera) was used to capture the digital images under a certain increment of load until failure from a fixed place. The acquired images were then implemented in a digital image correlation Vic-2D code to find the full-field displacement measurements for the surface of the MPC under different levels of loadings. Vic-2D is a widely used digital image correlation code created by Dr. Michael Sutton (University of South Carolina) and others. Dr. Sutton is considered one of the early founders of digital image correlation technique.

1.3 Main Objectives of this Study

This study is divided into two parts. First, the experimental laboratory tests were conducted and second, the digital image correlation techniques were used for the images that had been captured during the experimental laboratory tests. The experimental laboratory tests are divided into two main parts:

- Four basic tension tests
- Heel joint test

The metal plate connectors (MPC) were used to connect the wood members together. The CCD camera was used to capture the image at every 200 pounds of loading. The deformed images were then run through the digital image correlation (DIC) code to find the full-field strain (local strain) measurements of the MPC. The local strain behavior that is obtained from digital image correlation was used to describe the behavior of the plate under loading until failure.

Thus, the main objectives of this research are:

- Developing and applying DIC to obtain full-field strain measurements
- Studying the behavior of MP connected joints focusing on localized strain behavior
- Developing a deeper understanding for the failure mode based on strain analysis
- Describing the general behavior of MP connected joints under different loadings and situations to improve the future structural modeling

1.4 Dissertation Outline

This dissertation consists of five chapters. This first section provides a brief overview of the layout of this study to assist the reader in accessing the portions of his/her interest. Chapter 2- describes the previous research work and studies focusing on the beginning of the metal plate connections and its history from the first invention to date. Chapter 2 also describes the history of the digital image correlation techniques and its applications.

Chapter 3- describes the methodology in this research. It explains the experimental tests that were conducted in the lab and describes the conditions of each test. Then, it explains the digital image correlation technique as a method to find the full-field strain measurement and present the conditions related to this technique and the work procedures.

Chapter 4- discusses the results from the experimental laboratory tests and the full-field strain measurements that were obtained from the digital image correlation code. Each test is repeated three times, and the fourth chapter describes each individual test and discusses the full-field strain measurements results. Also a graphical analysis for the strain behavior of the MPC at different loading stages is provided. Then at the end of each test a summary and discussion is provided. Finally,

Chapter 5- lists the conclusion of this research. It summarizes the results of all the tests, their significance and limitations of the research and suggestions of future work.

CHAPTER II

LITERATURE REVIEW

2.1 The Previous MPC Joints-Strain Studies

Since the invention of MPC, several researchers have studied the behavior of MP connected joints either experimentally or theoretically under tension forces or compressive forces. Numerous studies have been conducted to improve the MPC industry by focusing on improving the stiffness and strength of the joints. Previous studies have focused on analyzing and modeling the metal plate connected joints using several assumptions in their models and then the general strain based on their model was obtained. They measured the general strain in the area that connects two pieces of lumber together by MPC using LVDT (linear variable differential transformer) testing machine experimentally. Abrero, J. M. and K. G. Gebremedhin (2009) show the strain in the wood around the teeth using their finite element model. None of the previous researchers have studied the strain behavior of the MPC itself. The displacement and strain of MPC can be tracked under different loadings and conditions using the DIC technique.

2.2 Previous Analysis and Modeling of MPC

A large number of research studies have analyzed and modeled metal plate connections (MPC). Accurate modeling of metal plate connectors and wood is very complex (Triche and Suddarth, 1988) because of the nature of the wood as a material and the difficult nature of the connector-wood combination. In fact, the behavior of MP connected joints is complicated and affected by several factors and variables. One of the most important issues in modeling the metal plate connected joint is the connection type between the wood and the metal plate connector, which is conventionally counted as either rigid (assumed infinite stiffness) or pinned (no moments are transferred), but the actuality of many connections is not purely rigid or not purely pinned. In other words, it is semi-rigid connection joint. Thus, there are some relative movements axially, transversely, and rotationally between the connected wood members. Another issue in modeling is the nature of the wood. Most of the past research to date considers the wood as isotropic or orthotropic material, which is between anisotropic and isotropic, for simplicity. In reality, wood is anisotropic material and its mechanical properties vary in each direction. Because of the nature of wood as anisotropic, it is too complex to model as such.

Since the invention of MPC, many researchers have studied the behavior of MPC joints either experimentally or theoretically under tension forces or compressive forces, but the research's interest focused on the tension forces to determine the strength capacity of MPC. Several models were developed by using different programs and procedures. The interest in the teeth of MPC is a part of the general model except for a few studies which focused more on the teeth analysis and design. Some models have considered the teeth as a beam on wood foundations; other models have considered the teeth as a set or a group of springs.

Demarkles (1955), Misra (1964), Isyumov (1967), Cramer (1968), Lantos (1969), and Rassam and Goodman (1970) were the earliest researchers who attempted to analyze metal plate connectors by focusing on the interaction between the MPC and the wood member. Beineke and Suddarth (1979) started with the results of the last five researchers' studies and compared their theories by calculating the forces' distribution on the connector and the joint at different places. They presented their study to show more details in the interaction between the MPC and the wood members and to produce a new analytical method that described the behavior of metal plate connectors. Their goal was to reduce the large number of necessary lab tests to examine the MPC joints. However, they observed that results of load-slip behavior of MPC joints from lab tests did not match the ones from the previous earliest analytical models (Riley May 1998) besides, their model was identical to what Foschi (1977) had already done with the exception of a single methodology.

The connections' behavior could be simulated by means of equivalent springs or fictitious members. However, using this simulation was difficult because it required taking into account all possible properties for the equivalent springs or other fictitious member affecting the behavior of the connection. Foschi (1977) is considered to be the first to present a theoretical expression to characterize the nonlinear load-slip characteristics of the connectors. He developed a model using a computer program called SAT (Structural Analysis of Trusses). In his empirical model, the wood and the plate (flat) was considered as rigid while each tooth that connect the wood and the metal plate was represented by non-linear spring. The non-linear springs properties were found based on the size of the tooth-wood contact area and the grain orientation of wood with respect to the teeth. Then, he developed a function to work on a per-tooth basis and to consider the nonlinear relationship of the connection (spring) load-slip curve. The truss plate stiffness was calculated based on the number of teeth per plate. The nonlinear relationship of connections is modeled with the following equation 2.1.

$$F(\delta) = (m_0 + m_1\delta)\left[1 - EXP\left\{-\frac{K\delta}{m_0}\right\}\right] \tag{2.1}$$

Where F = Load or the Force required to create the deformation (slip) (N)

δ = Slip (mm), K = slope of the (P-δ) curve (N/mm)

m_1 = slope of the (P-δ) curve at failure (N/mm)

m_0 = y-intercept of the tangent to the (P-δ) curve at failure (N)

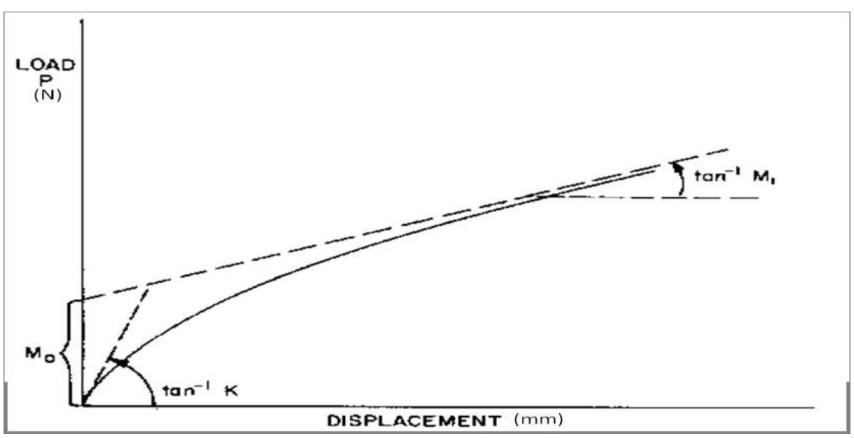

Figure 2-1: Tooth Load-Slip Relationship (used by Foschi 1977)

The experimental load-slip curve result was very close to the theoretical one (developed from the model). The assumption of Foschi's method was that the steel connector plate did not deform and remained rigid. Thus, the wood deformation, which occurred around the teeth of MPC, caused the joint displacement or the relative displacement between the wood and the plate. Furthermore, the assumption that the load was uniformly distributed over each tooth did not match with the non-uniform real load distribution in MPC (Crovella and Gebremedhin, 1990). In the end, Foschi's model could not determine the forces on individual teeth. However, most theoretical works that were created later to model the MP connected joints and explain their characteristics were based on Foschi's model (Cabrero and Gebremedhin, 2009).

Suddarth and Wolfe (1984) modeled MPC joints by a program called Purdue Plane Structures Analyzer II (PPSA II). This program treated the MPC joints members' behavior as linear and elastic. The connections between the members were considered as either pinned or rigid but with a third possibility by inserting fictitious members among actual members to estimate the partial fixity of the connections. The fictitious members helped to treat the connection as a semi-rigid connection through the modeling. The properties of fictitious members were determined separately from experimental results. However, the real interaction between the teeth and the wood members was not clear in this model.

Triche and Suddarth (1988) were aware that the essential problem in the analysis and design of MP connected joints was its complication. How tooth connections react to force depends not only on the tooth geometry but on wood grain orientation as well. These two factors should be involved in any MPC solution. Since Foschi considered this problem in his work, they expanded a new methodology using his mathematical method. Their method was considered as one of the first finite element approaches for analysis and design of MP connected joints. In their method, they used the results of load-slip relationship from Foschi's methodology to examine the distribution of forces on each tooth of the array of the MPC and to estimate the relative displacement between the wood and the teeth. In their study, the steel plate was assumed to remain rigid under all conditions and the displacement of the MPC and the wood member was assumed to result from the deformation of the wood encircling the teeth. In addition, the wood functioned as a nonlinear-elastic foundation. The finite element model predictions were close to the experimental results. However, their study did not present the stress or the force distribution at different positions or different points of the MPC.

All previous models considered the wood and the plate as rigid material and the deformation was found for the spring and the contact area. The assumption of considering the wood and the plate as a rigid (and remaining rigid) and the assumption of considering the deformation as just a spring deformation at the spring area had made inaccurate results in the stresses distribution and the deformation situations in the connection.

Sasaki and Takemura (1990) presented a nonlinear analysis of trusses connected with semi rigid joint connections by using a matrix analysis. A model for MPC joints was created based on replacing the MP connected joints with three linear-elastic springs. The three elastic springs represent the axial, shear, and rotational stiffness. Based on the load-slip characteristics, they found that the increase in the stiffness characteristics of the joint was more efficient to increase the strength of the whole truss than increasing in the modulus of elasticity. These researchers' mathematical procedures and expressions were similar to Foschi's work. They did not show the real interaction between the wood and the metal plate connection and the teeth function.

Cramer, Shrestha et al. (1990) created a new nonlinear-two dimensional-plane stress finite element model for MP connected joints. They used finite element analysis software called TPAR (Truss Plate Analysis Routine). The tooth-wood interaction was considered as a spring with the plate (flat) modeled as non-linear isotropic continuum and the wood as orthotropic-linear elastic material. Taking advantage of developments in technology and computer programs, they analyzed and described MP connected joints in more detail than previous models. They used a more powerful finite element program which described and treated the stiffness contributions of the tooth-wood interface, the wood, and the flat steel plate separately. This model computed the bending of a splice joint by using the stiffness of a tooth-wood spring found from tension tests. The real test behavior of stiffness values and the theoretical stiffness values, predicted from the model, were very close. However, the current model characterized unrealistic approximations of the behavior for large plate connectors and realistic approximations of the behavior for relatively small plates. Therefore, the size of plate affects the lateral tooth resistance of MPC. Their study was limited to MPC joints loaded in tension and bending. furthermore, it did not discuss any other kind of joints. After three years, Cramer, Shrestha et al. (1993) developed "a more efficient scheme for computing the stiffness of a metal-plate-connected joint ". They created a new analysis method that can be used to analyze MB connected joints. Stiffness and forces of MPC joints was computed by this method taking into account the nonlinear, semi-rigid joint and the joint eccentricity. Each MPC joint was modeled as one element and the tooth was represented by springs. A single element included three springs, two springs represented translational movement and one spring represented the rotational movement, connected to the metal plate through rigid link assumption and located at the center of gravity of the metal plate-wood contact area. The stiffness was computed from the geometric characteristics of each plate-wood contact surface and the single tooth load-deflection relationship of the metal plate from the testing.

Gebremedhin and Crovella (1991) tested four different metal plate connector types to describe the load distribution alongside the tooth array. They used the elastic foundation model as the study theoretical technique which considered the tooth as a cantilever beam inside an elastic supporting foundation (Schriver and Wood, 1990) as shown in Figure (2.2).

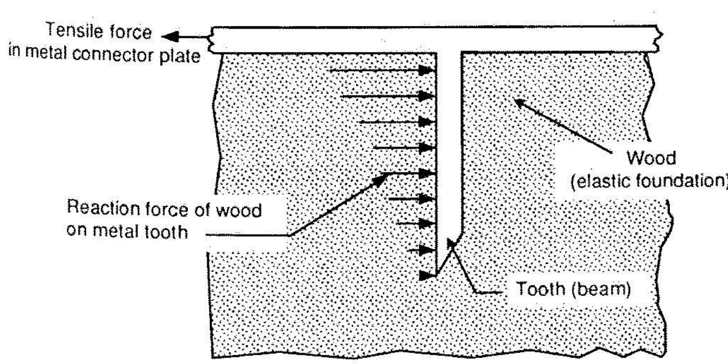

Figure 2-2: Profile of embedded tooth in elastic foundation (Schriver and Wood) when a tensile force is applied on the plate

They found that the load distribution along the tooth was non uniform and the nearest row of the teeth to the centerline of MPC was found the most effective row to transfer the maximum load more than the farther rows of teeth. The length of the tooth was one of the characteristics that could affect the stiffness of the MPC. The parameter $\beta 1$ was critical to find the optimal tooth length and so the stiffness.

$\beta 1 = (b_o\ k/4\ EI)^{l/4}$

b_o = beam width,

k = foundation modulus of the wood surrounding the beam

E = modulus of elasticity of the beam

I = moment of inertia of the beam

l = tooth length

According to $\beta 1$, beams could be classified into three types:

1. Short beams, $\beta 1<1$
2. Medium length beams, $1< \beta 1<3$
3. Long beams, $\beta 1>3$

The authors found that the variability value of the wood foundation modulus (modulus of elasticity of the wood) and the moment of inertia of the beam (tooth) were critical parameters that affect the deformation of the teeth and so the stiffness of MPC.

In another study, Crovella and Gebremedhin (1990) created two models of a uniaxial loaded tension splice joint by using two different theoretical techniques. The first was a two-dimensional-linear finite element model, and the second was an elastic foundation model. Besides the theoretical model, experimental investigations were also conducted to find the stiffness of MPC by applying a tension force until failure, and then the stiffness could be calculated from the load-deflection relationship. As a result, the joint stiffness results from the experimental results were very close to the joint stiffness results from the elastic foundation model with the assumption that the tooth was a cantilever beam with one free end and the other end was rigid. This method was more reasonable than a beam with one end-pinned-assumption. While, the joint stiffness results from the finite element model over predicted due to the properties of triangular elements used to generate the mesh, they used three linear node-triangular elements to represent the joint. However, they did not predict the teeth bending. In general, the tooth withdrawal was general failure mode occurred to three different metal plates out of four. The load distribution along the metal plate connector surface was non-uniform. This study was limited to MP connected joints subjected to axial tension only. The study did not discuss any other joint model or loading conditions.

Groom and Polensek (1992) developed a theoretical model that correctly predicted the mechanisms of load transfer, ultimate load, load-displacement curve, and failure modes under different conditions for MPC truss joints. The model considered the tooth as a beam on an inelastic foundation with inelastic behavior between the tooth and the wood. This model considered the wood-grain orientation so K (stiffness= slope of the Load-displacement curve) can be calculated under different loading situations. The theoretical and the experimental results of the load-displacement curve were in good agreement. However, the tooth-wood interaction was not that clear, and the model did not discuss the effects of some other conditions on the results such as the moisture content, specific gravity, and the eccentric loading.

Vatovec (1995) developed a finite element model using ANSYS software to model the MPC on a per- tooth basis. The single tooth was represented by three nonlinear spring elements and the plate steel was assumed to be a flat plate without slots between the teeth. The three dimensional- nonlinear models was developed for axial load and then the load-displacement relationship was created afterward. The model did not exactly show wood-tooth interaction, as it was modeled for the whole MP connected joint in general.

Vatovec, Miller et al. (1996) created a three dimensional finite element model that described MPC joints' performance and behavior in service. This model provided information about joint displacement and the forces in joint members after loading. The model considered the teeth-grain-direction of force-orientation and the properties of the materials. The wood was modeled as a linear-elastic-isotropic beam and the steel plate was rigid. Each single tooth was represented by one set of three uniaxial spring elements. "Each spring element accounts for tooth-wood behavior (stiffness) in one major plate direction: parallel to slots, perpendicular to slots in the plane of the plate, and perpendicular to the plane of the plate". For each spring element, tension splice joints tests were conducted to get the nonlinear load-slip curve. The results of load-displacement curve from the finite element model compared closely to results from experimental tests (tensile and bending tests). The spring elements (teeth) played the major role in governing joint behavior. In this model, too many numbers of degrees of freedom were allowed, making the modeling procedures long and time consuming. The model did not show if the holes of the plate were considered to have an effect on the performance of the joint in addition to the effects of modulus of elasticity of the wood and the steel. Also, the teeth were not modeled in three dimensions.

Riley and Gebremedhin (1999) developed a semi analytical model for metal-plate-connected wood truss joints based on elastic foundation theory. A cantilever beam was represented by punched-tooth embedded on an elastic foundation. The main goal of the model was to predict the axial and the rotational stiffness value of the MP connected tension-splice joints and heel joints. The theory of this model was that the deformation of wood produced a reaction force in the wood (foundation) then this deformation affected the tooth (beam) at the point of deformation. Figure (2.3) shows the layout of this model.

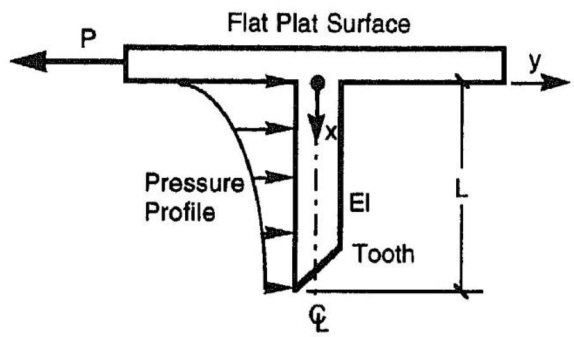

Figure 2-3: Layout of the tooth as a cantilever beam on an elastic foundation

(Schriver and Wood)

The following equation was used to represent the deflection of the beam (tooth) but the friction between the tooth and wood interface was neglected:

$$EI\frac{d^4y}{dx^4} = -Ky \tag{2.3}$$

Where

X = distance along the neutral axis of the tooth

E = modulus of elasticity of the tooth

I = cross-sectional moment of inertia of the tooth

Y = deflection of the tooth

K = foundation modulus (wood modulus)

The model was used to investigate other properties that may affect the results such as tooth geometry (length, width), tooth layout (coordinates), plate geometry (length, width, thickness), wood moisture content, and specific gravity and loadings conditions (concentric or eccentric). This model did not exactly describe the interaction of the tooth-wood connection, as elastic behavior was the basic assumption of this model.

Amanuel, Gebremedhin et al.(2000) developed a two-dimensional finite element model that can predict the axial stiffness of MP-connected tension-splice joints. The model focused on the teeth-wood interface by using contact elements. A commercial computer software, a linear-elastic, finite elements ANSYS was used to generate the contact elements and to model the teeth, metal plate face, and the wood. This paper discussed the contact elements, a component which had rarely been discussed before. “The contact elements transfer the normal forces between two surfaces remain in contact and/or tangential forces along two surfaces where one surface slips relative to the other” .Therefore, the slip between the tooth and the wood interface was modeled by nonlinear contact elements. Accounting for transferred forces in modeling procedures by the contact elements provided an efficient and useful model. The error percentage between the absolute predicted value and the experimental value was within 5%. In this model, the frictional forces between the teeth and the wood were ignored and the wood was assumed isotropic. On the other hand, this study considered the wood modulus of elasticity and the MPC thickness in stiffness calculations.

Ellegaard (2006) improved Foschi's (1977) model by providing more details and description about the idea and the theory of using the finite-element model program to design and analyze the metal plate connections MPC.

Cabrero and Gebremedhin (2009) created a two-dimensional finite-element model using a commercial software *ABAQUS* to predict the axial stiffness of MPC. The model was applied on tension-splice joints and heel-joints and considered the isotropic and linear behavior of the wood and the metal plate. In this study, the slip of the teeth and shear at the wood-tooth interface were modeled by contact surfaces. The interface friction between the wood and the tooth was considered. The predicted stiffness values were within 5% of the experimental stiffness values.

Suddarth and Percival (1972) also tested a heel joint within a big truss to estimate the axial stiffness and bending properties of heel joints. Gupta and Gebremedhin (1990) created a new testing apparatus to find the stiffness and failure modes for heel joints under different conditions. Redlinger (1998) examined many tensions splice joints and heel joints against the wind and impact loads as a part of truss. Several researchers involved the load-slip behavior of the joints to find a perfect technique that can predict global features of trusses. They examined the whole truss joints together to obtain the global truss-joints characteristics.

2.3 Factors Affects Modeling and Analyzing of MPC

The factors that can affect modeling and analyzing of MPC including the teeth also had been discussed by many researchers. Gupta, Vatovec et al. (1996), Quaile and Keenan (1979) , Suddarth, Percival et al. (1979), and Truss Plate Institute TPI (2007) discussed the variables that could influence the stiffness and the strength of MP connected joints and should be considered in modeling and analyzing. Some of the important factors are listed below:

- Location and Orientation of plate and lumber grain and the load angle
- Specific gravity of wood
- Lumber/wood species
- Size of plate (length, width and thickness)
- Size, shape and number of teeth
- Moisture content of wood
- Installation method that is used to press the MPC in to the wood
- Properties of metal (size, thickness, stiffness, geometry etc.)
- Tooth length and tooth layout on the overall joint performance
- Time between fabrication and testing

Gupta and Wagner (2002) studied the influence of metal plate's teeth on the bending strength of wood. They applied bending tests on wood beams with and without MPC then the results were compared. The results did not show a significant difference in the bending strength between wood beams with MPC and wood beams without MPC. So tooth damage does not appear to affect the bending strength of wood members.

The metal plate's teeth characteristics such as stiffness and strength can be improved. Groom (1991) proved that the tensile behavior of MPC can be modified by addition of an adhesive layer to the tip of each tooth of MPC immediately prior to joint assembly. During the pressing process, the adhesive layer extended along most of the tooth length. Tensile testing showed that the initial stiffness values of adhesive teeth increased by around 90% compared with the non-adhesive teeth. Further, a load-slip diagram (Fig. 2.4) shows that non-adhesive teeth begin to yield at around 25% of ultimate load compared to %50 for adhesive teeth. Thus, the adhesive layer around the teeth increased the strength of the connection between the MPC and the wood member. The adhesive layer reorganizes the stresses along the length of the teeth to support the applied lateral force which increases the resistance of the teeth to withdrawal forces.

Tooth damage occurred because of the occurrence of knots, cracks, or splits in the wood, or when pressing or rolling the metal plate connector on the wood during fabrication (Gebremedhin and Crovella 1991) .

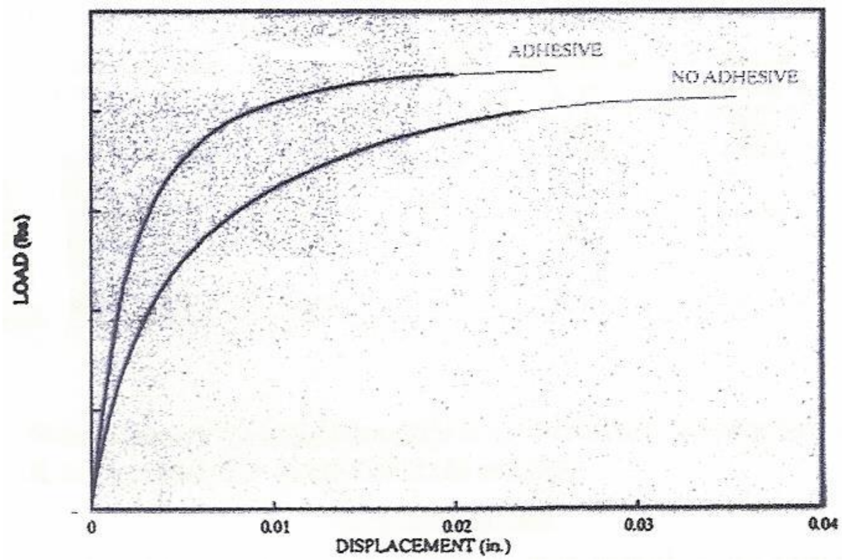

Figure 2-4: Average load-displacement traces for 30 metal plate connections with and without adhesive (Groom 1991)

Several standards used in the U.S.A include procedures to test metal plates and metal plate connected wood truss joints. The basic load-displacement characteristics of metal plate-wood connection can be determined from the four tests of the Canadian Standards Association (CSA) (Canadian Standard Association, 1980). CSA provided a method to test and to evaluate metal plate connections. It also provided the main procedures to determine the lateral resistance and the stiffness of many types of metal plate connected joints and to determine the shear and tensile strengths for the net section of the plate. The design procedures provided by the Truss Plate Institute (ANSI/TPI, 1995) for MPC wood truss joints is considered the most widely used and recognized in United States building codes.

2.4 Literature Review of Digital Image Correlation (DIC) Technique

The digital image correlation technique was developed in the 1980’s, and many algorithms were created and proposed for two dimensional and three dimensional measuring systems. Several researchers used the DIC technique in different fields and created different algorithms to reduce the errors and obtain more accurate results, to reduce the computation complexity, and to expand the application range. The major disadvantage of the digital image speckle technique was the long processing time required for analysis. Over the last years, different methods and approaches were presented to reduce the processing time for analysis using the digital image technique (Huntley 1996, Amodio, Broggiato et al., 2003).

Use of digital image correlation (DIC) as a surface strain and displacement measurement technique was introduced for the first time by Peters and Ranson (1982) at the University of Southern Carolina. The authors subjected a specimen to ultrasonic waves before loading (non-deformed image) and after loading (deformed image). Then the authors created an approach to compare between the recorded digital images (reflected from wave pattern) using a small subset before and after loading. Then, in 1983 other researchers (Sutton, 1983) built upon this previous approach to develop numerical algorithms that can be used to analyze the results obtained from optically recorded images. Today this method is known as 2D Digital Image Correlation.

In 1986, (Sutton, 1986) Sutton and other researchers developed the most commonly used algorithm in DIC today. They focused on using subset comparison to get the 2D full-field displacement measurements. Later the technique was used to study the two dimensional solid mechanics displacements. The procedures were validated, developed, modified and many other algorithms were refined and used. Within ten years, the concepts of DIC were modified and the optical approach was adopted. The DIC technique has been successfully applied in the field of experimental mechanics. Thus, the first DIC technique creators or founders (Sutton, 1983; Chu, Ranson et al., 1985; Bruck 1989) used a computer algorithm for analyzing images to find the displacements and strains using speckle technique. In their study, they measured a simple deformation of a solid body. The Newton-Raphson approach was used by some researchers in 1989 (Bruck, 1989) and was widely adopted by many others since its ability to decrease the computational work (Wang and Cuitiño 2002) is higher than other methods. Alternate algorithms have been proposed in different research papers (Sjödahl, 1994; Vendroux and Knauss, 1998; Lu and Cary, 2000; Cheng, Sutton et al., 2002) either to increase the accuracy of results or to presents a new technique. The greatest disadvantage of the digital image speckle technique was the long processing time required for analysis. Over the last years, different methods and approaches were presented to reduce the processing time for analysis using the digital image technique (Huntley, 1996; Amodio, Broggiato et al., 2003).

In the literature, the DIC technique has been used with different names such as texture correlation, digital speckle correlation method (DSCM), electronic speckle photography (ESP) and computer-aided speckle interferometry (CASI) (Chen, 1993; Sjodahl, 1993; Sjodahl, 1994; Sjodahl, 1994; Bay, 1995; Sjodahl, 1997; Zhang D, 1999; Gaudette, 2001, Zhou, 2001).

In 2000, (Rastogi, 2000; Sutton, 2000; Sutton, McNeill et al., 2000) presented the DIC technique in great detail with emphasis on theory and applications. Su and Anand (2003) developed a new digital image correlation algorithm for non-contact and two-dimensional whole field strain measurements. This algorithm reduced the calculation time by using the neighborhood available data technique to determine the full-field strain measurements.

Hung and Voloshin (2003) also presented a new detection algorithm using digital image correlation to find the surface deformation. The new algorithm was based on pixel level and used fine search pixel by pixel.

Amodio, Broggiato et al. (2003) used numerical processing of digital images to find small strain measurements. This new technique was considered as extension to the digital image technique in which the authors improved the DIC white light speckle method. It requires a very simple object preparation and numerical elaboration to do the strain calculations.

Schreier (2000) focused on improving the accuracy of the matching process by using image reconstruction displacement. He used higher order spline interpolation function to reconstruct the pattern of the image intensity. Schreier (2002) confirmed that the quadratic shape functions had some advantages if they were used in the DIC algorithm without seriously affecting processing time. Several research papers presented amendments to the features of DIC technique and process. He (2006) and Zhang (2006) introduced a different search procedure to use as new algorithm in DIC technique.

2.5 Applications of DIC as Deformation Measurements Technique

Digital image correlation technique has been adopted in many scientific fields. The wide range of applications of DIC technique indicates its usefulness and flexibility. In addition to being used in fracture mechanics, DIC is also used to understand the deformation behavior of different materials such as plastics, ceramics, wood, and metals as well as damage to composite materials and concrete etc. He, Sutton et al. (1984) have used the DIC technique to measure the fluid velocity-field. Mizuno, Kawasaki et al., (1995) have used the DIC technique to develop an in-situ system for monitoring sintering shrinkage of powder compacts. Two dimensional deformation measurements could be obtained by the system, although it would not address the non-uniform and anisotropic shrinkage of the powder filling. Caárdenas-García, Yao et al. (1998) have used the DIC technique to track movement changes of points on the surface of a soil specimen to determine the surface displacement and then to characterize the surface layer cracking in the soil. Tong (1997) has created a new technique to find the whole field in-plane strain in aluminum sheet metals based on the DIC technique. The new technique can monitor the plastic deformation and the microscopic surface grain deformation for the aluminum sheets.

Digital image correlation has been used to find the velocities of discrete points in rigid body (field-velocity) and in seeded flows (Peters, 1983; He, 1984). Digital image correlation is also used in biomechanics (Wu W., 1987; Durig, Peters et al., 1988) in which the strain fields have been successfully measured.

Wood is a non-homogeneous and anisotropic material which also displays anatomical variability. Given these properties, it is quite difficult to find quality strain and displacement measurements for wood. However, researchers have used DIC to study the deformation of single wood cells (Mott, 1996). Several researchers have used DIC to describe and characterize the mechanical properties of wood (Choi, 1991; Choi, 1996; Zink, 1996; Stelmokas, 1997). DIC technique was also used by researchers to investigate the drying process in wood (Kifetew, 1996; Kifetew, 1997).

Digital image correlation technique has also been applied in civil engineering. Carroll (2011) focused on finding the full-field quantitative measurements of a fatigue crack growth in titanium using DIC technique. Digital Image Correlation Vic-2D was used to process the images and to obtain the results. The research showed the full-field strain measurements for the specimen surface at multiple scales associated with material damage during fatigue crack growth. Strain evolution with increased loading was investigated. Another application for DIC is in concrete to find macro deformation under compression forces (Choi, 1997). DIC technique is employed as a fracture mechanics tool to find the surface displacements measurements in two concrete projects. It has been applied on deformed samples to find the surface displacements and the results were higher in resolution than other experimental technique (Corr, 2007). Helm (2008) has created a method using DIC technique to determine surface displacement and provides the required analysis in spite of the existence of growing cracks on the surface. This technique permits surface displacement to be accurately measured on a concrete slab with growing cracks.

Digital image correlation technique is mainly used in experimental mechanics with emphasis on fracture mechanics. There are many applications of 2D strain field measurements based on DIC technique. Lyons, Liu et al. (1996), Liu, Lyons et al. (1998), and Mahmoud and Lease (2003) determined strain field measurements near crack-tips. This shows the capability of DIC technique to accurately measure strain fields at high temperature. An in-plane deformation and strain measurement was accurately found near stationary and growing tips (Sutton, Turner et al., 1992; Han, Sutton et al., 1994; Han, Sutton et al., 1995). Also, in a growing crack, the crack tip opening displacement is measured by using DIC technique (Dawicke and Sutton, 1994; Amstutz, Sutton et al., 1995; Dawicke, Sutton et al., 1995; McNeill, Sutton et al., 1997; Sutton, 2000). Zhang D (1999) proposed an optimized digital speckle correlation algorithm which he named "big-window correlation" in which he measured the compression strain for polyurethane foam plastics materials. Other researchers used the same technique (Zhang D, 1999) for aluminum alloy foams (Bart-Smith, Bastawros et al., 1998; Bastawros, Bart-Smith et al., 2000). Wang and Cuitiño (2002) illustrated how the DIC technique can be used to measure heterogeneous deformation in low density polymeric foams under compressive forces using the Newton-Raphson approach.

Montemayor (2003) used the Vic-3D code (digital image correlation technique) to measure the strain during a displacement controlled cyclic tri-axial test of a clay specimen. He compared the deformation results from the DIC technique to the results from LVDT. The research showed the ability of the digital image correlation technique to process and analyze images and to provide data sufficient to model accurately the behavior of a clay specimen. The results from using Vic-3D digital image correlation software successfully replicated the LVDT results.

2.6 Sources of Errors and Strain Measurements Using DIC Technique

S.F. Hwang (2008) obtained strain and displacement information by using a hybrid genetic algorithm that was implemented in the DIC technique. The author replaced the Newton-Raphson method with a hybrid genetic algorithm. The DIC/hybrid genetic algorithm was used to obtain the strain–gradient in a high strain region around a hole in a plate under a uniaxial tensile testing (Hwang, 2012).

The measurement accuracy using DIC is influenced by several factors such as lens distortion (lens aberration), subset shape function, subset size, image quality, noise, correlation algorithm chosen etc. Sun (1997) used a CCD camera mounted on an optical microscope system. The images were used to measure the displacement by using the DIC technique. The results were in-plane surface displacement at high magnification (around 1000-2000 pixels/mm). Powder materials were used to create the speckled pattern. The sources of errors were also determined and discussed. Schreier (2000) investigated systematic errors in digital image correlation caused by intensity interpolation. Schreier (2002) also investigated systematic errors in DIC caused by shape. Pan Bing (2006) investigated three types of sub-pixel displacement algorithms. The results from each algorithm were used to compare the performance of each registered algorithm. Yoneyama (2006) investigated the effects of lens distortion on surface displacement results measured by DIC. The authors proposed a lens distortion correction that can eliminate the influence of lens distortion on DIC accuracy in displacement results. The lens distortion coefficient was determined by using the least square method then the corrected displacement distribution was reached. The experimental displacement results proved that the proposed lens distortion correction method can reduce the influence of lens distortion error on the accuracy of measured displacements. Zhang (2006) introduced a simple calibration method to reduce the effects of lenses distortion in DIC displacements measurements.

Bornert (2009) proposed a general method to evaluate DIC displacement errors. The authors tested DIC parameter combinations using six versions of DIC-software to obtain the parameters results to use as a reference. Wang (2009) presented a procedure to quantitatively evaluate the errors in the pattern matching in DIC. Brillaud (2002) developed a software to measure displacement by correlating two images. Some limitations that affected the strain results were discussed such as the subset size. Yoneyama (2006) proposed a lens distortion correction method to eliminate the lens distortion error on measured displacement.

Sources of errors that may affect strain measurements results using DIC were studied by several researchers. Haddadi (2008) presented different (experimental and numerical) tests to define the errors related to different sources. The errors were classified into two categories. The first category included the quality of the measurement devices and environmental conditions such as lens distortion, lighting, CCD sensor, the preparation of the devices in the workspace, and out of plane displacement presence. The second category was related to the correlation principle such as the quality of speckle pattern, the size of subset, and the correlation algorithm and functions used. The research offered recommendations that could help to reduce the errors. Lecompte (2006) investigated speckle pattern quality by describing the speckle size distribution of the speckle patterns. The authors compared three different speckle patterns that were numerically deformed using finite element simulation. The results showed that the size of the speckle patterns and the subset affected the measured displacements. The subset size was related to the speckle size. When the speckle size was small then the mean speckle size should also be small and so on. The ideal speckle size and subset size for many experimental tests can be obtained using a simulation system such as finite element simulation. However, in real life this was difficult because the speckle pattern was obtained using paint-spray method. An evenly distributed speckle pattern should be achieved to obtain accurate displacement results.

Sun (1997) discussed three sources of errors: contrast adequacy pattern on the surface of interest, out of plane displacement, and the errors from the lens aberration. Schreier (2000) investigated systematic errors caused by gray-value interpolation (intensity interpolation). Many interpolation functions were investigated and the results of each one compared. Smith (1998) defined two types of errors: digitization errors and optical errors. Digitization errors were related to the resolution and interpolation of the digital imaging devices and software used while optical errors were related to imaging and focusing technique such as lens distortion, specimen illumination, specimen displacement, etc. Wang (2009) proposed a quantitative procedure for error assessment in speckle pattern matching. Errors were analyzed quantitatively in a matrix as a function of sub-pixel motion, interpolation technique, intensity pattern noise, speckle contrast, subset size, and level of uniaxial normal strain.

2.7 Advantages and Disadvantages of Digital Image Correlation (DIC) Technique:

As with any other technique, DIC has advantages and disadvantages.

Advantages:

- Non-contacting technique
- Insensitive to material properties , environmental effects and temperature changes
- Can be employed in both 2D and 3D
- Specimen size is not a problem or an issue
- Provide a full-field strain measurement of the deformed surface, which is important when the deformation is non-homogeneous
- Inexpensive technique and easily accessible with commercially available equipment
- Easy to use hardware and software skills for the digital images processing
- It is practical technique for strain measurements at microscale or nanoscale
- Suitable for static and dynamic situation
- Simple experimental setup and specimen preparation
- Require a white light source of natural light which makes the processing applicable to use in the laboratory or the field.
- In case of large strain, there is no issue with using DIC technique unless the specimen moves out from the field of the camera view.

Disadvantages:

- Only applied on flat services
- Sensitive to light fluctuations
- Computation time is high and mathematics involved is a challenging
- Speckle pattern for the specimen
- Depending highly on the quality of the imaging system

Due to several advantages and wide spread applications, DIC technique has become a well-established method and a significant technique for measuring the full-field surface strain in solid mechanics (Jin and Bruck, 2005). It is viewed as one of the fastest developing areas in experimental methods Laurence Mott, 1994). In the area of metal plate connections, none of the previous researchers have tried to find the strain measurements on the surface of MPCs. All previous studies have focused on finding the displacement at the gap between the two pieces of lumber connected by the MPC using the LVDT device. Digital image correlation may provide a strain map for the surface of MPCs under different loading conditions starting from zero loading until failure. Changes in strain under loading can be used to develop a deeper understanding of the behavior of these connections. Additionally, strain mapping may be used to more accurately describe failure mechanisms for implementing model design.

CHAPTER III

MATERIALS AND METHODS

3.1 General

This chapter describes the materials used and the fabrication of the tension test joints (specimens) connected by metal plate connectors. Four joints are fabricated based on the direction of the tension load and the wood grain. This chapter explains the fabrication of the simple trusses to obtain a heel joint. Four simple trusses are fabricated under the same conditions. The procedures for each test are also provided. LVDTs (Linear Voltage Displacement Transducers) also have been used in the experimental test to verify the digital image correlation results. The moisture contents of the wood have been investigated for six samples of wood members to obtain the weight loss with time before testing them.

Digital Image Correlation technique is a methodology that is used to find full-field strain measurements for the surface of the metal plate connections under loading. This chapter explains the theory and basics of digital image correlation DIC as a methodology to find the full-field strain measurements for surfaces.

3.2 Materials and Fabrication of the Joints

The wood specimens were fabricated from Douglas fir. The 2 x 6 in cross sectional wood was cut into 17-inch pieces. The wood members that were cut were allowed to sit in the lab for a time sufficient to allow the moisture content to stabilize at room temperature. The moisture contents for the wood specimens were calculated based on weight loss every 24 hours. The weight loss with time is presented in Appendix B. The wood members were set in the lab for almost two months before testing until the moisture contents had reached the room moisture content.

Standard metal plate connections were used in the tests. The thickness of the plate was 0.0345 in (20gauge). Table 3.1 shows the properties of the metal plate connections and the teeth.

Table 3-1: The physical properties of MPC

Property of Plate	**Value**
Thickness	0.0345 in
Tooth Length	0.375 in
Slot Length	0.5 in
Slot Width	0.22 in
Plate Width	4 in
Plate length	5 in
Teeth shape or Pattern	waived pattern teeth

After the moisture contents had become fixed, the joints are fabricated. Four basic tension joints were made. Each test was repeated three times. The four tensile joints were fabricated the follows:

- AA-Joint : the tensile force is parallel to the plate's major axis and the wood grain

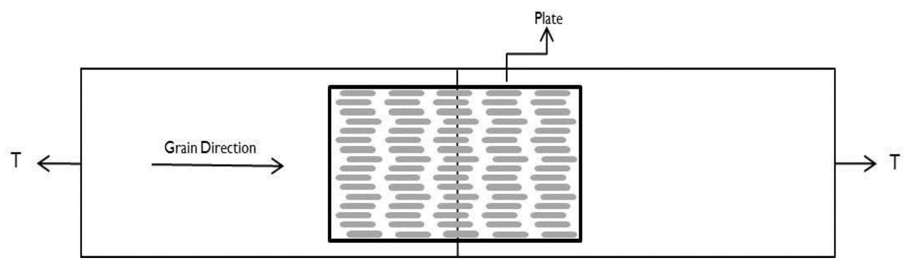

Figure 3-1: AA-tension joint

- AE-Joint: the tensile force is parallel to the plate's major axis, perpendicular to the wood grains.

Figure 3-2: AE-tension

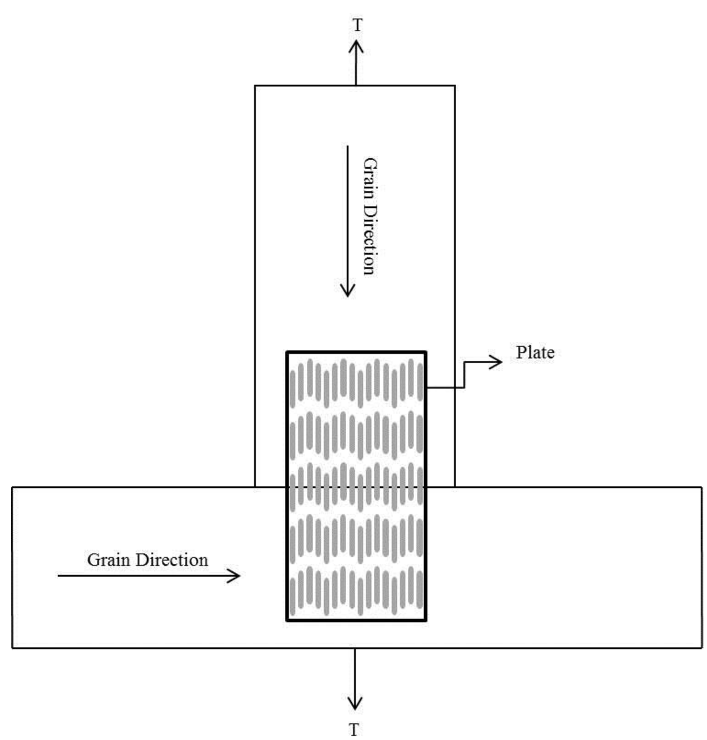

- EA-Joint: the tensile force

is perpendicular to the plate's major axis and parallel to the wood grain.

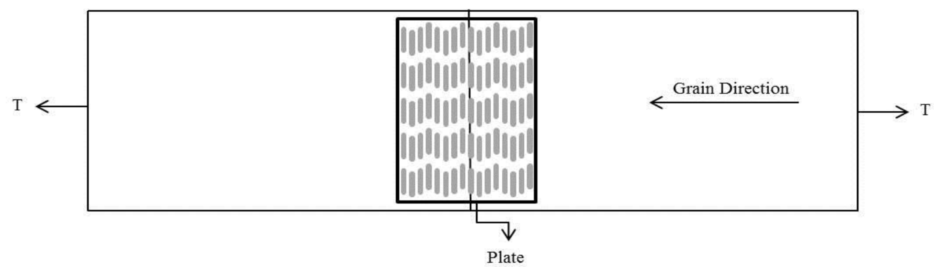

Figure 3-3: EA-tension joint

- EE-Joint: the tensile force is perpendicular to the plate's major axis and the wood grain.

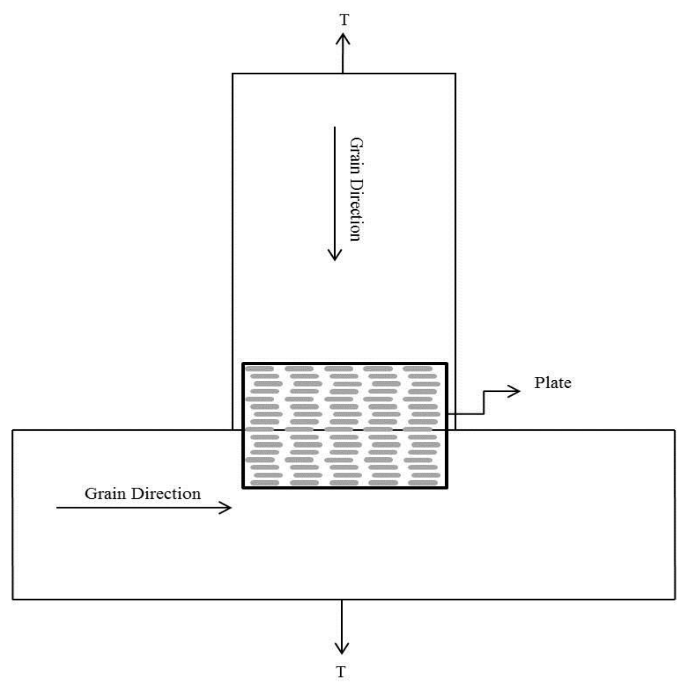

Figure 3-4: AA-tension

Note: the letter A means parallel, the letter E means perpendicular, the first letter indicates the plate's major axis and the second letter incidents the wood grain direction.

The teeth of the metal plate connection were pressed inside the wood members to build the joints using a pressing machine in the civil engineering lab. After fabrication of 12-joints, they were placed in the lab for seven days. This time allows for the relaxation of the teeth inside the wood. After 7 days each test configuration was tested in the lab using the Universal Testing Machine. All joints specimens were loaded until failure.

Figure 3-5: The Universal Testing Machine in civil engineering lab

Linear Voltage Displacement Transducer (LVDT) was used for the first four basic tension tests. The LVDT was placed on the right and the left of the joint to obtain the displacements between the two wood members. The displacements were taken as voltages then they converted to displacements in inches. The displacements were found for increments of load on either side or one side for some tests. Then the displacements from the LVDT machine were compared to the displacements found from the digital image correlation code. Thus, the LVDT displacements results were used to confirm the results of the DIC software.

The other main test is the heel joint. Four heel joints are fabricated at a slope of 4:12. The heel joints are fabricated by building 4-simple trusses. All the wood members are connected by the same metal plate that was used in the first four tensile tests. The 4:12 slope is frequently used in housing construction.

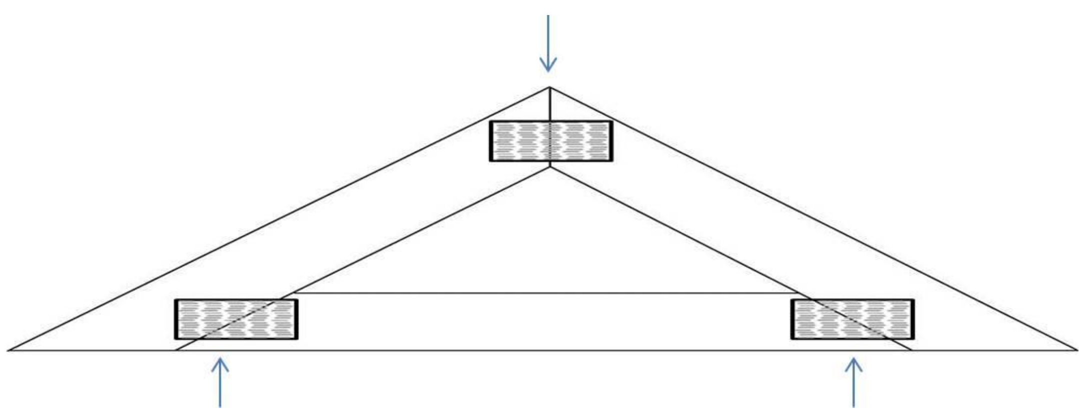

Figure 3-6: Simple truss -Heel joint

In the design of the plate, three strength sources of plate are based on TPI:

- Lateral resistance (tooth withdrawal): the plate area should be designed to provide the required number of teeth that will develop one of the required design strength in the plate.
- Tension strength of plate net section (width)
- Shear strength of plate net section (width)

3.3 Strain

The general definition of strain is the change in the length of a specimen divided by the original length.

$$\varepsilon = \frac{\Delta l}{l_0} = \frac{l - l_0}{l_0}$$

Where:

ε = Strain

l_0 = The original length of the specimen

l = The new length of the specimen

Δl = The displacement or the change in the length of the specimen

The strain is related to the measurement of length. The length can be measured either using the traditional measuring devices which measure the distance between two points or using the field method in which the coordinates of the point on the surface of the specimen are determined. The traditional contact measuring devices such as gauges or extensometers were used to find deformation. The contact methods are accurate but very limited. The field methods are non-contact methods. These include the grid method, moiré method, speckle laser, and digital image correlation technique. Non-contact methods have advantages over contact methods by measuring the strain field without coming into contact with it. Also these methods are useful for studying heterogonous materials and composite materials. These non-contact methods have been successfully used to study crack growth (Avril, 2004) and other damage in materials (Claire, 2002).

The strain that is found using traditional measuring approaches between two points across the entire specimen is called a global strain. The measured global strain represents the average behavior of the whole specimen. Local strain represents a strain for a small part of the specimen. The summation of the local average strains represents the strain field.

Many kinds of devices are used to measure displacement including mechanical or electrical devices on the one hand or imaging devices on the other. Imaging device are applicable and suitable for full-filed strain and displacement measurements.

Strain is considered to be one of the most important mechanical properties of any material. It defines the mechanical behavior of that material. This requires an applicable and appropriate strain measuring technique. Each material is different in its behavior under loading conditions. However, having an appropriate strain measuring technique is required when the material has complex heterogeneous deformation. Many methods have been used to measure strain and displacement, but DIC technique can be considered an appropriate technique to measure the strain in many cases. Digital image correlation technique has been used to study the mechanical behavior of materials under different loading conditions.

Digital image correlation tracks the black speckle pattern between two images, one image before loading and the other after loading, to determine the in plane (surface) displacement field under various loading conditions. Using DIC technique, the strain is obtained by differentiating the in-plane displacement of the plate surface. This is determined by comparing two digital images that are captured before and after deformation.

3.4 Axial Displacement Measurements Using LVDT

Axial displacement measurements in this research were performed using the LVDT (linear variable differential transformer). The LVDT measurements values were compared to the Digital image correlation values and results. The LVDT measured the displacement between the two wood members through the test (gap-displacement).

3.5 Digital Image Correlation Technique (DIC)

Digital Image Correlation is an optical, numerical, non-destructive, and non-contact measuring technique in which the surface deformation of the interested object can be correlated using digital images (Poissant and Barthelat, 2010).

Digital Image Correlation is mainly used for two-dimensional applications in which one camera is used to obtain the in-plane displacement measurements. However, it can be used for three-dimensional displacement measurements by using two cameras at the same time.

Digital image correlation technique depends on tracking the movements of pixels. A pixel is the smallest controllable single element of an image and is represented using dots or squares. All pixels together represent the full image, so to get more accurate representation for the original image; a high resolution camera should be used to provide more image-pixels. The pixels represent the intensity of light. Each pixel has a value corresponding to its brightness. In this research the grayscale image is used which means just a black and white colors. The light intensity can range from 0 for pure black to 255 for pure white with a total of 256 levels of colors (8-bit grayscale image system). A digital image can be represented as a matrix with positive integer elements (element = pixel=number) which represents the surface brightness. Each value of this matrix is in a range from 0 to 255 (gray-scale image).

3.5.1 How Does DIC Tracking Pixels Work?

The digital image is divided into tiny dots called pixels. Each pixel has a value number between 0 to 255 depending on the light intensity or the brightness. Assume there is a pixel with a value of 0 in the reference image. To track this pixel, one will look for a pixel with a value of 0 in the deformed image. However, a pixel with a value of 0 may be repeated many times in the deformed image. Thus, to make it easy, practical and beneficial, a unique way is required to identify these pixels. To solve this problem, a region of points called subsets is used.

A subset is a group of pixels in the reference image and is called a point. A point is a subset which contains more than one pixel. The intensity of the point or the subset is the average value of the pixels which are involved in the subset. Now, for the purpose of tracking subsets between the reference and the deformed image, the average intensity value of the subset has a good chance to be unique. The subset size is considered one of the factors that affect the accuracy of the DIC technique results, so much study has gone into determining the best size (Pan, 2008). Figure 3.7 shows the relationship between subset, pixel and speckle.

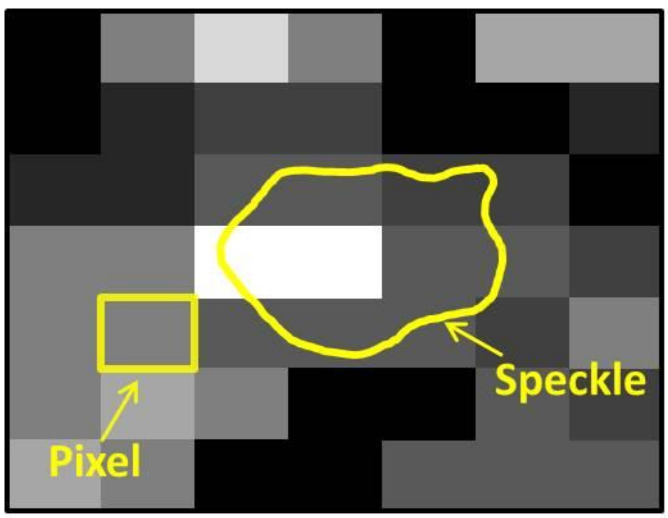

Figure 3-7: A 7 X 7 subset array. The relationship between pixel, subset, and speckle

Digital image correlation (DIC) programs determine the displacement of each subset by correlating the deformed image to the reference image. The program can recognize and track a specific pixel by looking at other pixels around it.

The images can be classified as:

- Colored images: red, green, blue (R,G,B) color pixel vector, there are parameterizations each with its own advantages and disadvantages
- Grayscale images: is preferred over the colored image in order to avoid the various nuances involved with different parameterizations. Limited dynamic range of pixel values (0-255), (8 bits/pixel) = 2^8 = 256 gray levels = more emphasis or more effective with details (high quality). For example (5 bits/pixel) = 32 = 2^5 gray level and (1 bit/pixel) = 2 = 2^1 gray level which represent the color depth and intensity. Figure 3.8 explains the intensity of light in matrix form.

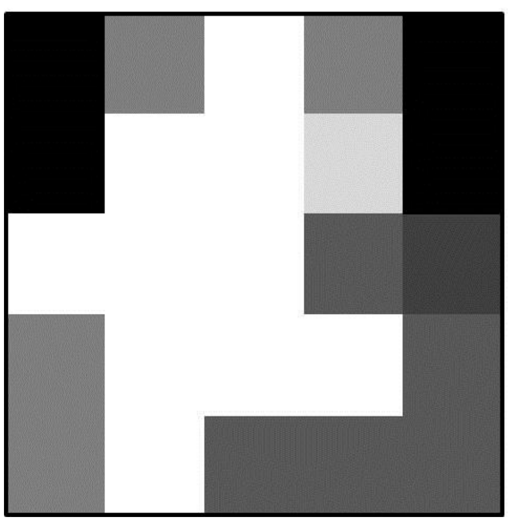

0	100	255	100	0
0	255	255	200	0
255	255	255	85	80
100	255	255	255	90
100	255	90	90	90

Figure 3-8: Image in matrix format showing the intensity of light

The accuracy of DIC technique results depends on many factors such as the algorithm used, subset size, subset shape, sub-pixel intensity interpolation pattern, and the image quality and noise such as lens distortion. Figure 3.9 shows how to track a subset.

Reference

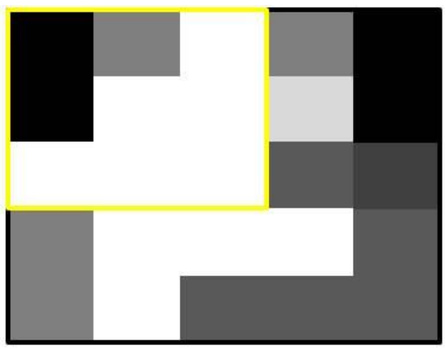

0	100	255	100	0
0	255	255	200	0
255	255	255	85	80
100	255	255	255	90
100	255	90	90	90

Deformed

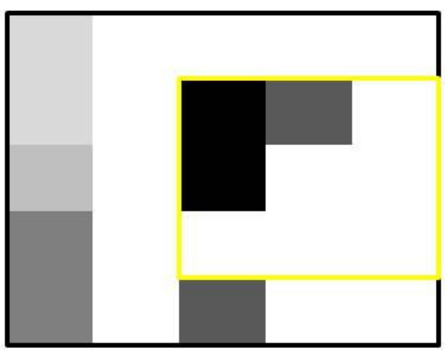

220	255	255	255	255
220	255	0	100	255
190	255	0	255	255
120	255	255	255	255
120	255	100	255	255

Figure 3-9: Image in matrix format before and after deformation

3.5.2 Digital Image Correlation Algorithms

Since the invention of DIC method, many approaches have been created to find the measurements of displacement and strain fields. Some approaches are considered standard-two dimensional 2D-DIC approaches. The standards methods are well documented in much of the literature (Bruck, 1989; Vendroux and Knauss, 1998; Schreier 2000; Schreier, 2002). The standard methods include the basics such as random speckled specimen, digital images for the speckled specimens, a reference image in non-deformed state, and a deformed image in deformed state. In the DIC standard method, the subset is defined using the displacement u , v . For small deformation and first order approximation the displacement gradients are u_x, u_y, v_x, v_y. Or u_{xx}, u_{yy}, v_{xx}, v_{yy}, u_{xy},v_{xy} for second order and large deformation approximation. Each pixel has a number (discrete value) then the interpolation is used to find values between pixel positions. The well-known used interpolation systems are the Bicubic Spline Interpolation and the Quintic Interpolation. The interpolation system tries to smooth the discrete values and allow measuring the displacement with subpixel accuracy. The Bicubic B-splines approach is used to find the continuous description of the intensity distribution for the interpolated deformed image.

3.5.3 Mapping Displacements:

In 2D-displacement fields a point (subset) P(x,y) in the reference image (non-deformed image) is tracked and mapped into point P^* $(\tilde{x}, \tilde{y})$ in the deformed image.

The subset location can be expressed by:

$$\tilde{x} = x + u(x, y)$$

$$\tag{3.1}$$

$$\tilde{y} = y + v(x, y)$$

where:

u and v are the displacement components in x and y directions respectively.

(x, y) is the point's original location.

The displacement components can be expressed using a second order Taylor series expansion about the point P(x_0,y_0) then the last equation (3.1) can be expressed as:

$$\tilde{x} = x_0 + u_0 + \frac{\partial u}{\partial x}\Delta x + \frac{\partial u}{\partial y}\Delta y + \frac{1}{2}\frac{\partial^2 u}{\partial x^2}\Delta x^2 + \frac{1}{2}\frac{\partial^2 u}{\partial y^2}\Delta y^2 + \frac{\partial^2 u}{\partial x \partial y}\Delta x \Delta y$$

$$\tag{3.2}$$

$$\tilde{y} = y_0 + v_0 + \frac{\partial v}{\partial x}\Delta x + \frac{\partial v}{\partial y}\Delta y + \frac{1}{2}\frac{\partial^2 v}{\partial x^2}\Delta x^2 + \frac{1}{2}\frac{\partial^2 v}{\partial y^2}\Delta y^2 + \frac{\partial^2 v}{\partial x \partial y}\Delta x \Delta y$$

where , $\Delta x = x - x_0$ and $\Delta y = y - y_0$ (Dally 2005).

In case of large strains, first order expansion is suitable for most cases:

$$\tilde{x} = x_0 + u_0 + \frac{\partial u}{\partial x}\Delta x + \frac{\partial u}{\partial y}\Delta y$$

$$\tag{3.3}$$

$$\tilde{y} = y_0 + v_0 + \frac{\partial v}{\partial x}\Delta x + \frac{\partial v}{\partial y}\Delta y$$

where:

$\frac{\partial u}{\partial x}, \frac{\partial u}{\partial y}, \frac{\partial v}{\partial x}\ and\ \frac{\partial v}{\partial y}$ Are the first order displacement gradients (slopes) or linear subset

Deformations and they are related to strains as the following:

$$\varepsilon_x = {\partial u}/{\partial x}$$

$$\varepsilon_y = {\partial v}/{\partial y}$$

$$\gamma_{xy} = {\partial v}/{\partial x} + {\partial u}/{\partial y}$$

$\varpi_{xy} = \frac{1}{2}\left(\frac{\partial v}{\partial x} - \frac{\partial u}{\partial y}\right)$ Rotation

and,

$\frac{\partial^2 u}{\partial x^2}, \frac{\partial^2 u}{\partial y^2}, \frac{\partial^2 u}{\partial x \partial y}, \frac{\partial^2 v}{\partial x^2}, \frac{\partial^2 v}{\partial y^2}, \frac{\partial^2 v}{\partial x \partial y}$ are the second order displacement gradients.

If the subset in the reference image is matched to the subset in the deformed one, then the parameters in the last equations can be adjusted to obtain the best match between the subset in the deformed image to the original subset. Thus, the strain field can be calculated from differentiating the displacement field.

A digital image contains thousands of pixels with different intensity values. The data is smoothed in the two matched images to reduce the mathematical difficulties. This process is called the interpolation. Generally, bilinear and cubic are the two interpolation schemes used for this purpose. The Newton-Raphson method is used to determine the displacement vector. Figure 3.10 explains the basic principle of subset in DIC.

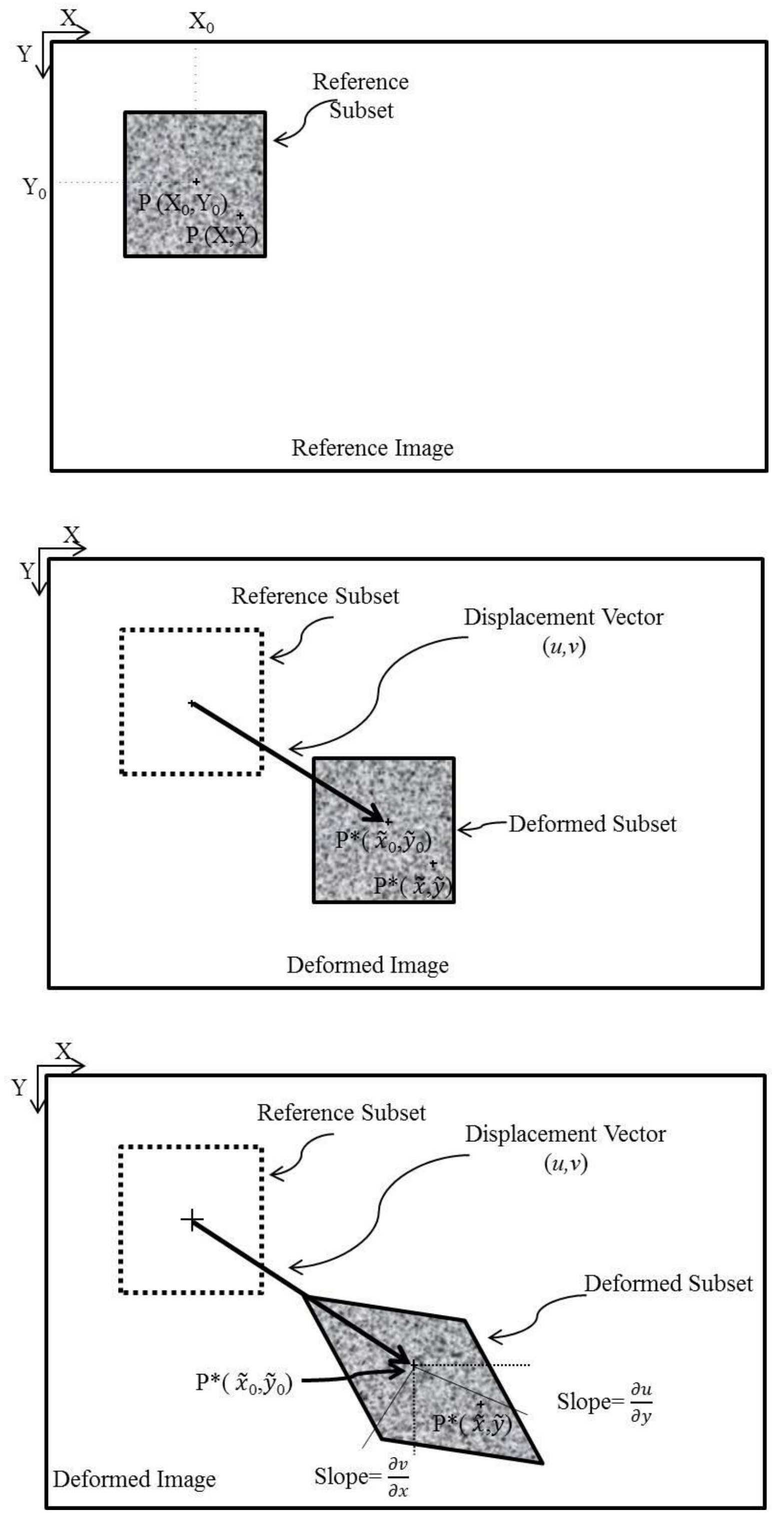

Figure 3-10: Mapping the displacement and shape functions. Basic principle of subset in the reference and deformed image

3.5.4 Correlation Coefficient and DIC-Algorithms

Correlation in DIC is the intensity pattern matching method. The correlation coefficient is the factor that can identify the quality of the match between the subset in the deformed to the subset in the non-deformed image. Different correlation coefficients are defined and used depending to the program used. The well known and most used is the least square correlation coefficient, C, which is defined mathematically as:

$$C = \frac{\sum_{S_p \in S}\{g(S_p) - h(S_p, P)\}^2}{\sum_{S_p \in S}\{g^2 S_p\}} \tag{3.4}$$

where:

g ≡ the intensity in the original non-deformed subset.

h ≡ the intensity in the deformed subset.

S ≡ all the points that surround a single point S_p in the subset.

The correlation coefficient C in equation (3.4) means the measurement of error at a point of interest. This is done by subtracting the values of intensity in the original and deformed subset and then dividing by the original intensity value. This C value is calculated at each point in the subset. If the correlation coefficient C is zero that means a perfect match between the deformed and non-deformed original subset is met. This operation is repeated for each subset. Because DIC technique programs can consume a great deal of time correlating each subset to the best match, minimization techniques have been used to decrease the time consumed. The Newton Raphson method is one of the techniques that have been used by many researchers to obtain fast correlation. But this method requires very accurate initial subset guesses.

Mathematically, the correlation coefficient (C) was found for the best match between the non-deformed and the deformed subset using the least square method. Also Newton-Raphson approach is usually used to minimize the C value which means best match. These standard methods are accurate and already have been used in different applications; however, they fail to find the displacement near cracks or any discontinuous displacement. Other approaches were created to decrease the limitations of the standard DIC approach. Jin and Bruck (2005) created a pointwise DIC method that includes a genetic algorithm. Each pixel will be assessed individually so a large number of unknowns will be optimized in the related correlation function. This approach can measure the discontinuous deformation, but it is computationally expensive. Another approach based on the finite element method in which the image is meshed and the nodal displacement is considered as the required displacement can be used to find the discontinuous displacement (Réthoré, 2007; Réthoré, 2008).

The DIC technique requires an algorithm to track the surface point movements and changes and to measure the surface deformation of a specimen. The digital camera will capture the non-deformed image then deformed images through the test until failure. The algorithm of DIC will match the intensity matrices between the non-deformed and the deformed images. The match will start by selecting a subset window, a small finite region on the surface of the non-deformed image, and then the DIC algorithm recognizes the corresponding region on the digital deformed image. The DIC algorithm then repeats the same process for the whole neighboring region until covering the whole area of the image. The process may take three to four hours to be done. Then a result of the full-field strain measurements should be successfully provided. More mathematical explanations and details can be found in many research papers (Sutton, 1983; Bruck, 1989; Sutton, 2000; Sutton, 2009). More than one correlation criterion can be used in advance to assess the correlation (similarity) degree between the reference subset and the deformed subset. Cross correlation (CC) and sum-squared difference (SSD) are two criteria, and each one has also other approaches (Bing Pan, 2009). The DIC technique, a reference square subset with different intensity variations is selected from the original non-deformed image. The DIC code then searches for a matching subset in the deformed image. To have accurate matching between the deformed and the non-deformed image, the selected subset should be unique and have adequate intensity variations.

The matching process between the original non-deformed subset and deformed subset is an essential step in DIC technique. Four types of correlation criteria have been used in DIC methods for assessing the similarity degree between images (Pan, 2011). These include the sum of absolute difference SAD (Giachetti, 2000), cross correlation CC and sum of squared difference SSD criteria (Giachetti, 2000; Tong, 2005), and parametric sum of squared difference PSSD (Pan, 2009; Sutton, 2009).

Another MATLAB DIC program has been developed by Poissant and Barthelat (2010). This code is capable of giving a full-field strain measurement for the deformed MPC and also has another advantage over other codes that it can correlate the images near displacement discontinuities, where standard DIC methods tend to perform poorly. The subsets in the reference and the deformed images can be correlated correctly when the deformation is continuous. However, the Poissant and Barthelat DIC algorithm named “subset splitting” can capture discontinuous deformation as it can track and measure the jumps in displacements. The algorithm has been tested and validated on digital images with a crack opening. The advantage of this subset splitting algorithm over other algorithms is being considered as a direct extension for the standard DIC. In this research a DIC code that can cut out the slots is needed. The metal plate connection has slots all over the surface so not any DIC program can work on it to obtain the full-field strain measurements. Vic-2D digital image correlation code is flexible code that can cut off some areas of the surface of interest and process the images, as these areas are not there. Many universities are using this code. Recently, Carroll (2011) (Civil Engineering) has used this code in his research and has proved its accuracy.

3.5.5 Camera Calibration

The calibration of the camera is important to provide the data for analysis and conversion the pixel to units. The factors that affect the calibration are as follow:

- The magnification factor: is the dimension of specimen to a corresponding dimension on the image plane of the camera. This can be determined by applying a scale on the surface of the plate (specimen).
- Lens distortion: The lens center of the camera has to coincide with the center of the specimen to avoid the effect of lens distortion. Lens with long focal length (200 to 300 mm is usually used) is required with CCD camera to help reduce the effect of lens distortion.

3.5.6 Image Processing Fundamentals

Spatial resolution: a measure of the smallest discernible resolution in an image, stated with dots (pixels) per unit distance, dots per inch (dpi).

Intensity resolution: the smallest discernible change in intensity level, stated with 8 bits, 12bits, etc.

In DIC, intensity resolution is used.

Common image file format:

- PNG (Portable Network Graphics)
- JPEG (Joint Photographic Expert Group)
- GIF (Graphic Interchange Format)
- PGM (Portable Gray Map)
- FITS (Flexible Image Transport System)
- TIFF (Tagged Image File Format)
- BMP (Bitmap Image Format) is used in this research

3.5.7 Speckles

The speckle pattern plays a main role in the DIC system. Speckle patterns in DIC can be lines, dots, grids, and arrays but the random pattern is the most commonly used. If the type of target is the same, then it would be impossible to distinguish between them. Thus, a unique shape is required for each point. This can be accomplished by using speckles. To obtain more accurate results, Speckle should cover at least 3x3 pixel areas.

The repeating texture may lead to some problems, so the texture should be non-periodic. A good speckle pattern is one with high information content. This allows accurate pattern matching on the surface (Figure 3.11). This leads to the use of a group of pixels which is referred to as a subset or a window sometimes.

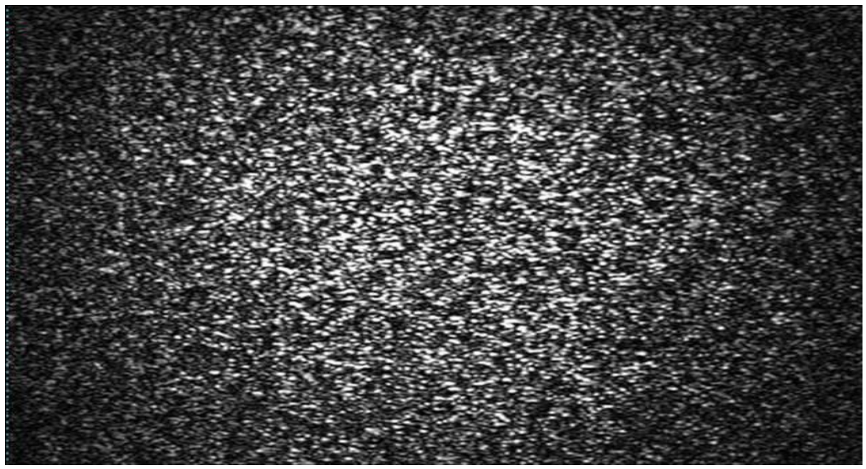

Figure 3-11: A typical speckle

There are two ways to create the speckle pattern:

1) Coherent laser illumination (the surface of interest is under illumination of a coherent light such as laser)

2) Creating random speckle pattern on the surface (digital speckle correlation).

The variation of the intensity is represented by the speckle size and the contrast of pattern. These two factors are important to the algorithm to be effective. The average size of the speckle depends on the size of the pixel of CCD sensor. Using coarse fine search, the speckle size should cover two to three pixels of the CCD sensor (Bruck, 1989). If the speckles are small, then the intensity of speckle will be unclear if it is compared to bigger speckle size. The general rule is that the speckle should cover most of the area of the subset size.

To get accurate results from DIC processing many features of speckle pattern should be considered:

- the quality of the speckle pattern is very important
- Black and white colors are usually used for speckle pattern because they give the best difference for pattern matching. So, using other colors is not prohibited but the white and black is the best.
- The paint that will be used on the surface should strongly stick to the surface. And during the test, it should stretch without cracking or peeling.
- The average size (pixels) of the speckle pattern is also an important feature. The subset (small finite region) size should cover at least three to five speckles.

The speckle patterns techniques:

- Very high resolution: use fluorescent nanoparticles. The fluorescent particles create finer surface pattern than the paint.
- Small speckles: spray white paint and then sprinkle carbon particles.
- Moderated speckles: spray white paint and then spray black paint with light pass.
- Large speckles: spray white paint then brush black paint

Speckle size in the research papers: Speckle method is considered one of the optical methods that can effectively be used for measurement in-plane displacements of the investigated surface (Yuanhao, 2004).The average size (speckle diameter) of randomly distributed speckles is an important factor in the correlation-algorithm. Bruck (1989) found that the speckle size should be two to three pixels. Hung and Voloshin (2003) investigated strains against speckle sizes and found that, in tension tests, the average speckle size was between 2 to 10 pixels. And in compression test it is between 4 to 7 pixels. If the speckle size is less than 2 pixels then the light intensity and the actual speckle location will be uncertain which will affect the accuracy of the results. On the other hand, if the speckle size is larger than 10 pixels, the speckle will be too large, making the measuring of small strain impossible (Hung and Voloshin, 2003).

3.5.8 Shape Function

The shape function is a mathematical approach used in DIC algorithm to transform the pixel coordinates in the reference subset into coordinates in the deformed image. The average displacement of a typically square subset by matching between two images is not always straightforward. However, the displacement it is generally complex, as the specimen might experience compression, elongation, shear, or rotation. Then the similarity between the subsets in the reference image and the deformed image decreases. Therefore, the subset shape function is required to decrease the de-correlation between the subsets in the reference and the deformed images (Sutton, 2009). In most of the matching DIC algorithms, the subset shape function is incorporated.

3.5.9 Subset

The main principle of 2D-DIC is tracking the pixels between two images before and after deformation. To find the displacement of any point, a reference square subset on the reference image with a specific pixel dimension will be chosen where the interested point will be at the center of this subset window. Then the subset on the reference image (non-deformed subset) will be used to track its corresponding new location in the deformed one (deformed subset). The tracking procedure used will be square subset (more than one pixel) not individual pixels because the subset includes more variation in gray levels which will help to recognize and identify itself from other subsets in the deformed image (Bing Pan, 2009). To obtain accurate results from the DIC, the 2D-DIC algorithm requires an accurate initial guess. The large subset size usually gives larger errors in the results.

The size of subset is one of the critical characters that can influence the displacement results using DIC. Many researchers have studied the subset size effects since creating the DIC technique (Knauss, 2003; Lecompte, 2006). To obtain a reliable correlation analysis, the selected subset size should be large enough to have a sufficient unique intensity pattern that makes it looks different from all other subsets on the surface. On the other hand, a small subset has been accurately used to find displacements using first order and second order subset shape function while the larger subset size may end up with larger errors than the smaller subset size. Thus, a small subset will give reliable displacement measurements. The fact is the speckle pattern is sprayed on the surface randomly so different grayscale distribution features, different speckle size, and intensity pattern will appear. Getting a proper subset size can be confusing. The specimen surface conditions and the image noise define the speckle pattern image quality. The subset size is very important and effective. It will interact with the subset image quality and displacements functions.

For assessing the quality of speckle patterns, Lecompte (2006) developed three different speckle patterns. The displacements were measured using the DIC technique for the three different speckle patterns specimen. The results show the effect of speckle size on the accuracy of the in-plane displacements. Yaofeng (2007) investigated the effect of subset size on the accuracy of DIC displacement measurements. The image pattern quality and the used subset displacement functions have been associated with the subset size investigation. At the end, the paper recommended using a sufficiently large subset size. Pan (2008) investigated the subset size selection in the reference image and create a theoretical model to check the DIC displacement accuracy. The model has been used to find the proper subset size in the reference image. The Sum of Squared Differences (SSD) method for correlation has been used. The experimental tests show three different speckle patterns, and the authors have proposed a simple algorithm that can be used to select the best subset size.

The displacements results from using the DIC technique are affected by many factors and limits such as the measurement system, lighting conditions, and speckle pattern. Hung (2003) investigated the appropriate DIC-speckle size (average speckle diameter) to find the strain. The results indicated that the most suitable speckle size should be between two and ten pixels to obtain accurate displacement results in uniaxial tension test. And four to seven pixels in compression test. The problem with larger speckle size is the capability to measure small displacement accurately will be reduced.

Orteu (2006) proposed a procedure to simulate a speckle pattern (a speckle-texture image generator framework) which can be achieved using the regular speckle methods (spray painting) using Parlin's noise function. The speckle generation framework is suitable for performance valuation of DIC technique as a measurement system. This can help to limit the introduction of any bias due to interpolation.

3.5.10 The Procedures for Using DIC Technique:

There are some special procedures should be followed to obtain correct results using the DIC:

- Generating a random speckle pattern :
  1- The specimen surface should be clean and dry.
  2- Coat the surface of specimen with a thin white paint by spraying the whole area of MPC.
  3- Over the white coating, spray randomly a black paint pattern. This procedure is considered as a regular speckle application as shown in figure 3.12.

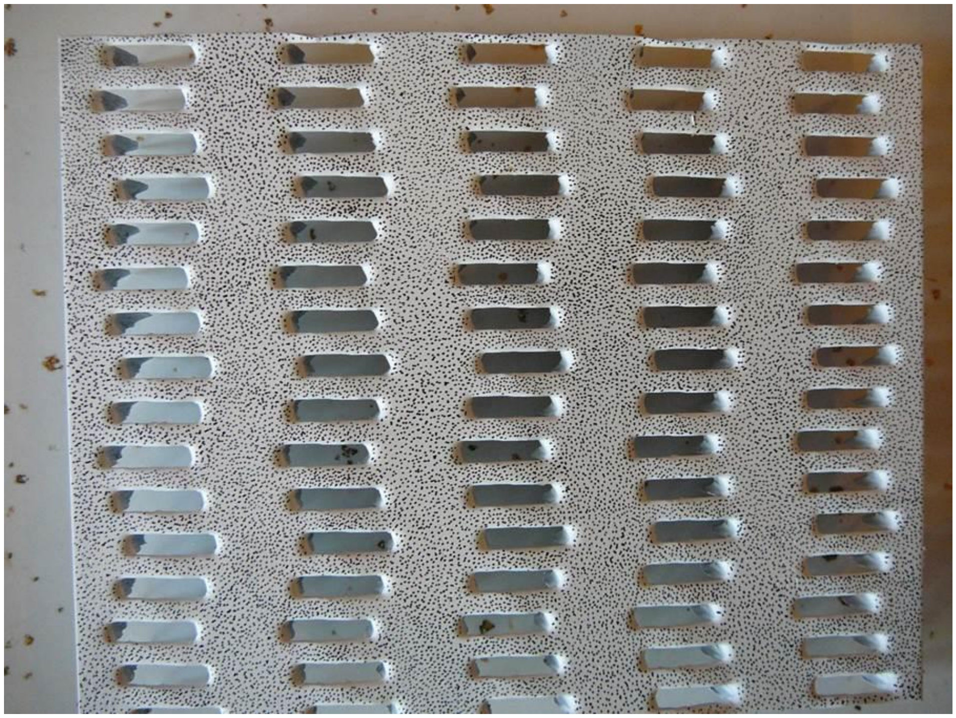

Figure 3-12: A typical speckled plate

4- Leave the specimen to dry before being used.

5- Average speckle size of 5 pixels and imaged with a magnification of 10 pixels /mm (TIWARI 2008)

6- Increase the contrast of speckle pattern during the experiment in order to avoid errors and achieve high accuracy results.

- Camera: digital camera has sensors that convert the light into electrons then an intensity value will be assigned to each pixel. All pixels beside each other (looks like mosaic) represent the image. High speed cameras have several developed combination of special features such as lenses and prisms all of which can be used to increase the light intensity and provide high contrast images. There are two basic categories of cameras: vidicon tube cameras and solid state CCD (charged-coupled device) cameras. The vidicon cameras are expensive and require frequent adjustment and maintenance besides having advantages over the CCD cameras but the CCD cameras are have lower cost and are easily available commercially which make it the most often used type in DIC technique (Laurence Mott, 1994). For 2D DIC configuration, a single digital camera should be used. The camera will be located on a fixed place. The lens of the camera (CCD array) will be orthogonal to the speckled specimen. The digital camera will capture the image. The image will be recorded by the CCD array as intensity of light falling on a net of pixels. High digital quality camera has rectangular array. The array contains thousands of pixels/line and thousands of lines/image (Dally, 2005) and will save it as a discrete intensity matrix then using the computer to transfer the digital image data into the algorithm to finish the correlation process. In this research a CCD Nikon Camera has been used.

Figure 3-13: The Nikon camera used in the tests

- Take the first grayscale image to be the reference image from a fixed camera.
- Take other images for the surface of MPC as it deforms with a specific increment of load. The format of the images is uncompressed image format “tiff “format not JPG.
- Using the program of DIC to choose the area of interest and run the code using the DIC- mat-lab code.
- To obtain the full-field displacement measurements of the surface, the subsets from the original non-deformed and deformed image will be compared and correlated to determine the full displacement fields. Digital image correlation depends on the correlation values between the pixels in the reference image and the deformed one. Figure 3.14 shows a typical arrangement equipment system for 2D DIC technique.

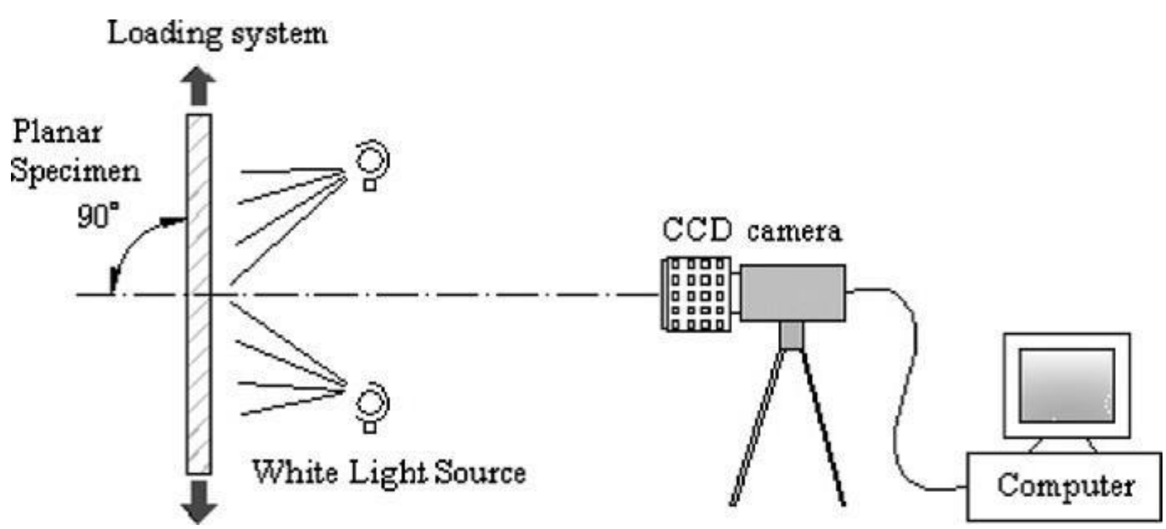

Figure 3-14: a typical arrangement equipment system for 2D DIC technique

3.6 DIC Code Used in this Study

In this research, the taken images were in NEF (raw) format. NEF images were changed to BMP images. Then the images were implemented in Vic-2D DIC code. The initial guess was chosen based on the least place that had changed or deformed during the test.

The Vic-2D code is a well-established digital image correlation code created by Dr. Sutton and others. It is considered one of the best codes. Its accuracy with respect to strain gauges is 99%. The code Vic-2D can measure in-plane displacements and strains from 50 micro-strains and above. The Vic-2D code presents three types of strain to calculate the local strain values in the full field strain measurements. However, the default and the preferred strain in 2D is the Lagrange strain. The presented strains are the Von Mises, Tresca strain and Lagrange strain.

Von Mises strain theory: When a load is applied on a ductile material or solid material, the load will be saved or stored as a potential energy. Under the stress strain curve this energy is $U = 0.5\ \sigma\ \varepsilon$ (strain energy density). The strain energy density consists of two components: change in the volume and change in the shape. According to Von Mises strain theory, the ductile solid material will yield when the distortion energy density reaches a critical value (of the material). The critical value can be found from the uniaxial test at yielding. Thus, the distortion energy density is associated by yielding stress of the material. The material yields when the Von Mises stress exceeds the yield stress (from uniaxial test) or in other words, the yielding of the material occurs when the distortion strain energy per unit volume reaches or exceeds the distortion strain energy per unit volume for yield in simple uniaxial test. Von Mises stress is used to determine if the material will yield when it is subjected to complex loading conditions in 3D.

Tresca strain theory: the idea is that the ductile material yields due to slipping of the contact planes of particles or crystals that make up the material. Thus, slipping is due to shear stress. This failure idea by shear stress was proposed by Henri Tresca (1868) and it is known as maximum shear stress theory or Tresca yield theory where $\varepsilon_y = \sigma_y/2$. Associated with the stresses the strain also can be found known as Tresca strain.

Lagrange strain: the motion is described by the material coordinate and the time for tracking the material point. It is preferred for solid mechanics. Lagrange strain is the default one in Vic-2D. It is a finite strain measure which includes higher order displacement terms.

The strain that can be obtained from this code and used in this project is the Lagrange strain. The following equations show the difference between the Lagrange strain and other kinds of strain.

$$\varepsilon = \frac{1}{k}\,(\lambda^k - 1), \quad where\ \lambda = \frac{l}{l_o}\ , \quad 0 < \lambda < \infty$$

- Engineering strain (k=1): $\varepsilon^{eng} = \lambda - 1 = \frac{l-l_o}{l_o}$
- True strain (k=-1): $\varepsilon^{true} = 1 - \frac{1}{\lambda} = \frac{l-l_o}{l_o}$
- Logarithmic strain ($K \longrightarrow 0$): $\varepsilon^{log} = ln\lambda = \ln(\frac{l}{l_o})$
- Lagrange strain (k=2): $\varepsilon^{lag} = \frac{1}{2}(\lambda^2 - 1)$

At such small strain values of (0.01) or less, the difference between these strains is as much as 1.5%. The processing time is almost 1-minute / image. At the end, the full-field strain measurements can be obtained in both major axes x and y.

CHAPTER IV

RESULTS AND DISCUSSION

This chapter presents the results obtained from the laboratory tests and the digital image correlation software. Two types of experimental results are included in this chapter:

1) Tension splice joint tests
2) Heel joint tests

The tension splice joint tests are four basic tests based on the direction of the tensile load with respect to the plate's major axis and on the direction of tensile load with respect to the wood grain direction. The four basic tension joint tests are: AA, AE, EA and EE. Each tension joint test was repeated three times. The heel joint tests were also conducted and a comparison of these tests is also presented in this chapter. Digital image correlation code (Vic-2D) was used to obtain the full-field strain measurements for each captured image for both tests.

4.1 Tension Joint Tests

4.1.1 AA – Tension Test

The first test conducted in the laboratory was the AA-tension test. It was performed by using two members of wood connected by the metal plate connector (MPC). The tension load was parallel to the metal plate slots (plate's major axis) and to the wood grain as shown in Figure 4-1. Three specimens were made for this test style. After seven days the three specimens were tested in the department laboratory using the universal testing machine. The camera was set on a fixed stand and perpendicular to the MPC. White lights were also used and images were taken at every 200 pounds (load increment) of loadings.

The LVDT machine was used to verify the results from the digital image correlation software. The first test was performed without using the LVDT. In the second test the LVDT was used on the right side of the specimen whereas in the third test, the LVDT was used for both sides of the specimen of wood members. Thus, the second and third tests are described in detail.

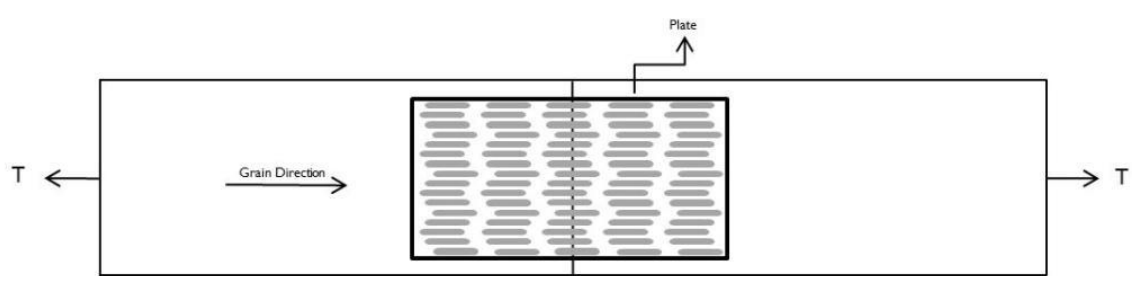

Figure 4-1:AA- sample test shape

4.1.1.1 Plate's Axes Direction Based on DIC Software

The direction of the x and y axis was obtained from the digital image correlation software as shown in the next two Figures 4-2. and 4-3.

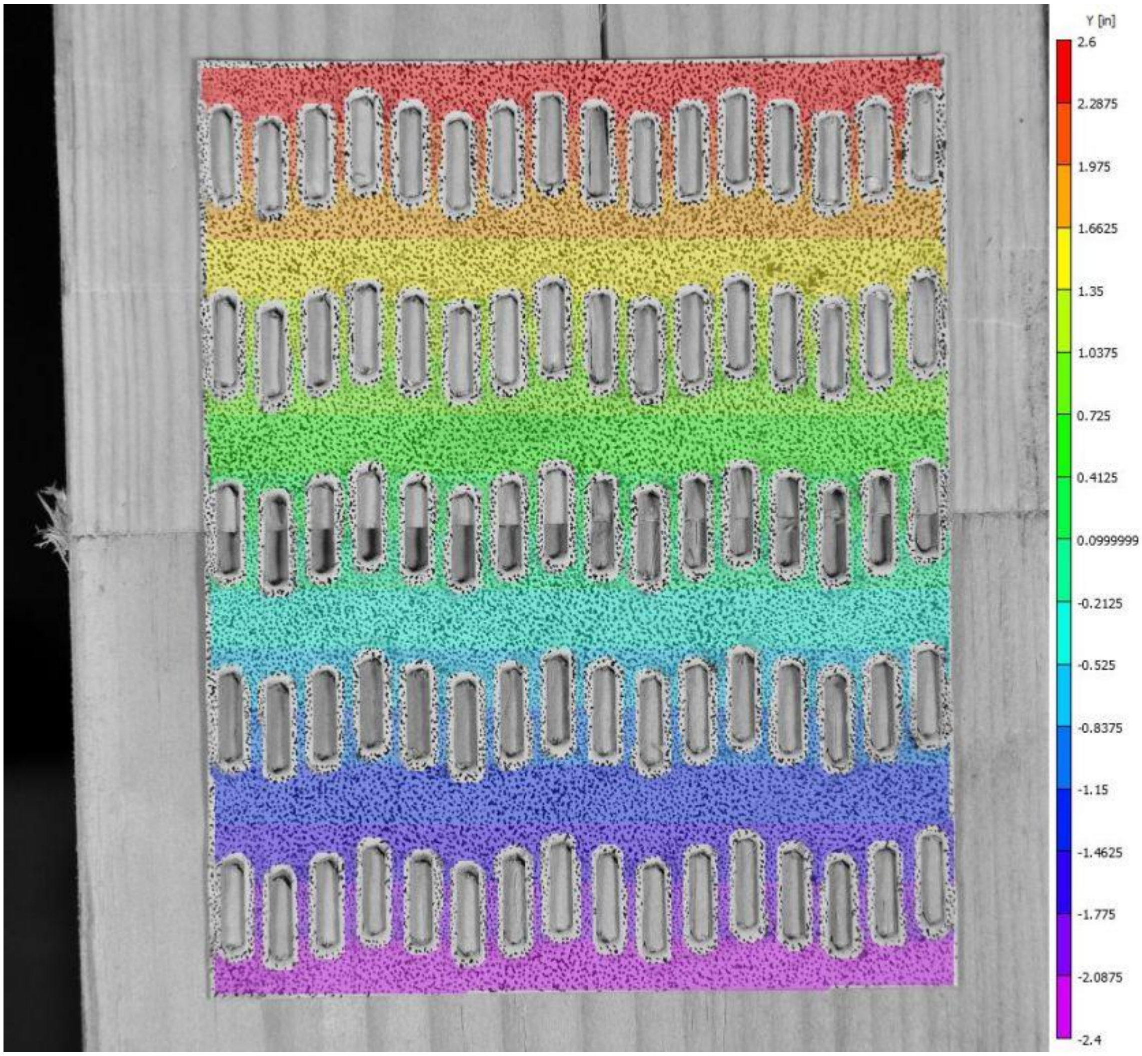

Figure 4-2:y-axis coordination system obtained from DIC software

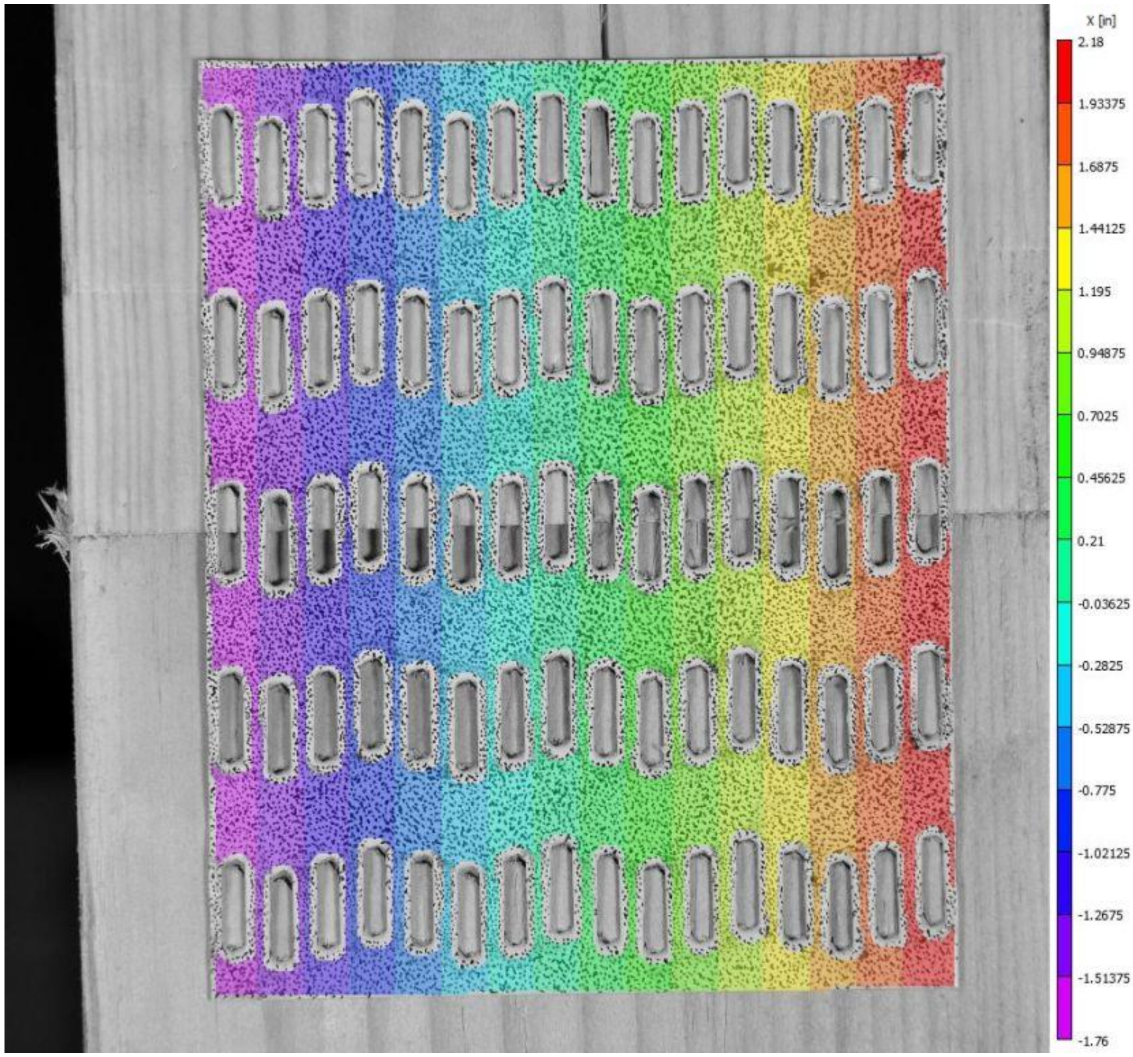

Figure 4-3:x-axis coordination system obtained from DIC software

4.1.1.2 The First Tension Test (AA-1st)

In this test, the two members of wood were connected by the MPC. The specimen was set on the universal testing machine. The first reference image was taken before applying any load. Figure 4-4 shows the first image which is considered as the reference image in digital image correlation technique.

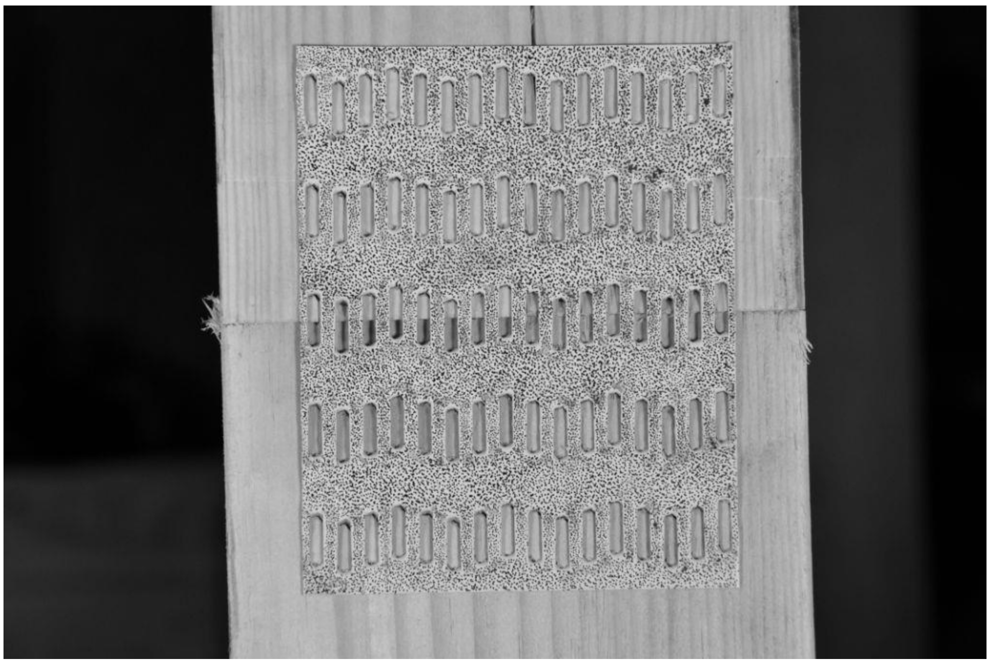

Figure 4-4: First image /reference image

After the first reference image was taken at load zero, the load was increased on the specimen until failure. The camera was placed at a fixed location and the MPC was kept perpendicular to the camera's lenses. Images were taken for the MPC specimen at each load increment of 200 pounds until failure. The failure in the member occurred in the metal plate connector. Figure 4-5 shows the last image at the failure.

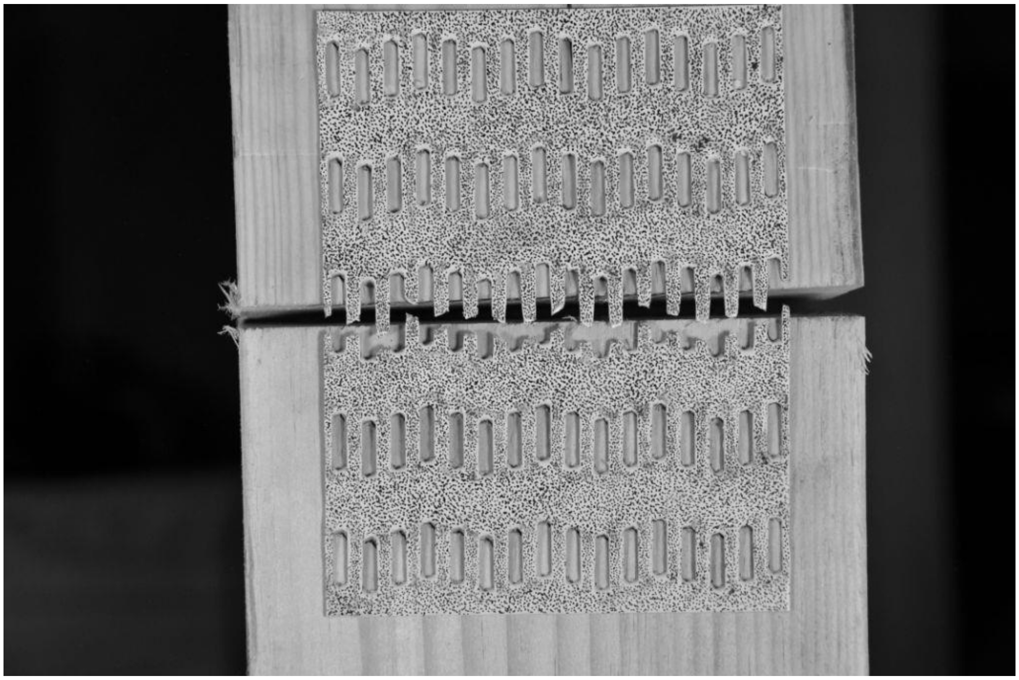

Figure 4-5: The last image at the failure

A total of 43 deformed images were obtained and the plate failed when the load was about 8,550 pounds. The plate was ruptured along the horizontal middle gap line of the plate. Digital image correlation software Vic-2D was used to process the 42 deformed images to obtain the local full-field strain measurements. The last image at failure was not processed because of the splitting of the plate into two parts so the DIC code was not able to process the splitting parts after the plate tear.

4.1.1.2.1 Analysis of the Full-Field Strain Results Obtained From DIC-Software

All the test images, which were obtained from the laboratory test, were implemented in the digital image correlation software Vic-2D. Each image was analyzed in relation to a reference image. Therefore, each deformed image was compared to the non-deformed reference image. The full-field strain measurements were obtained from the digital image correlation software for each deformed image. Figure (4-6)-(4-8) shows the strain field for three images.

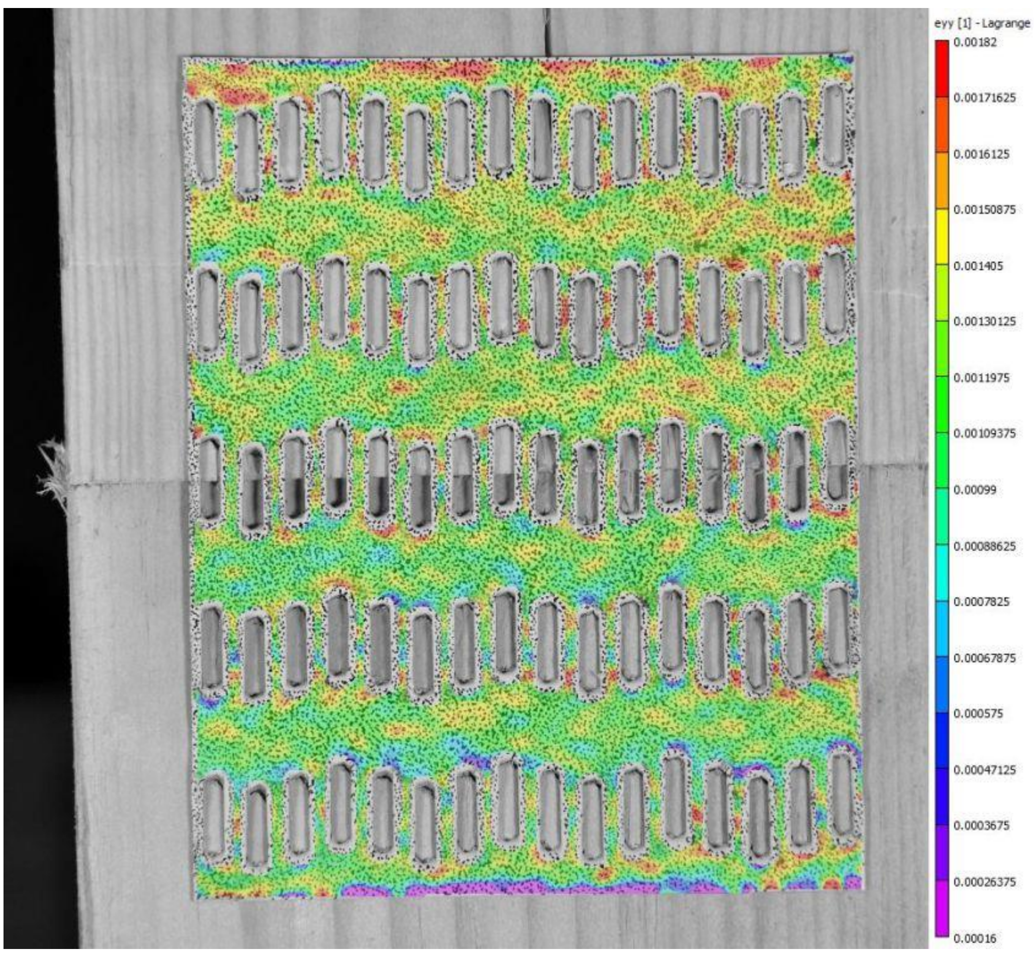

Figure 4-6: Full-field strain measurements (ε_{yy}) for the MPC at 200 pounds

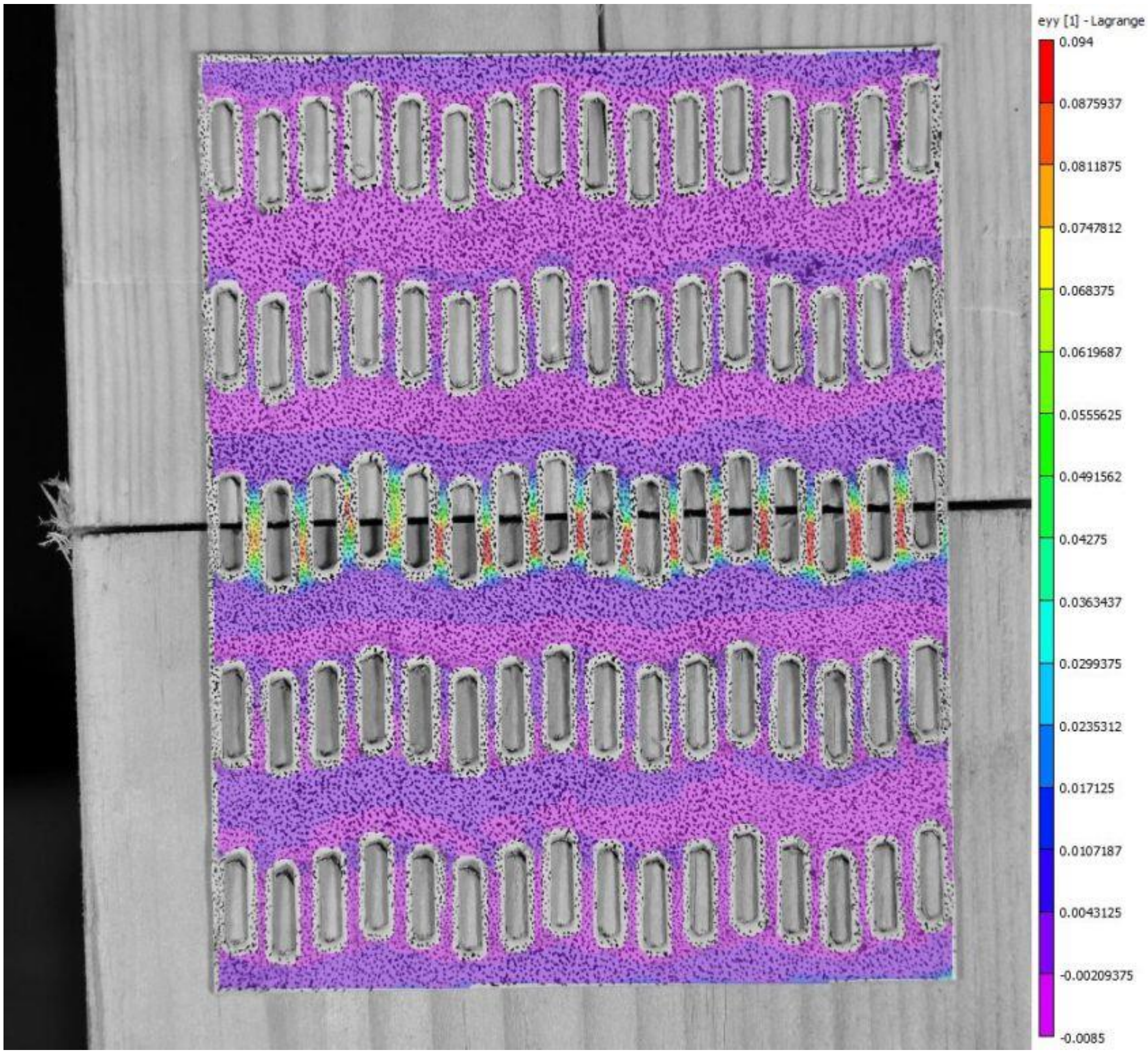

Figure 4-7: Full-field strain measurements (ε_{yy}) for the last image before the failure at 8,550 pounds

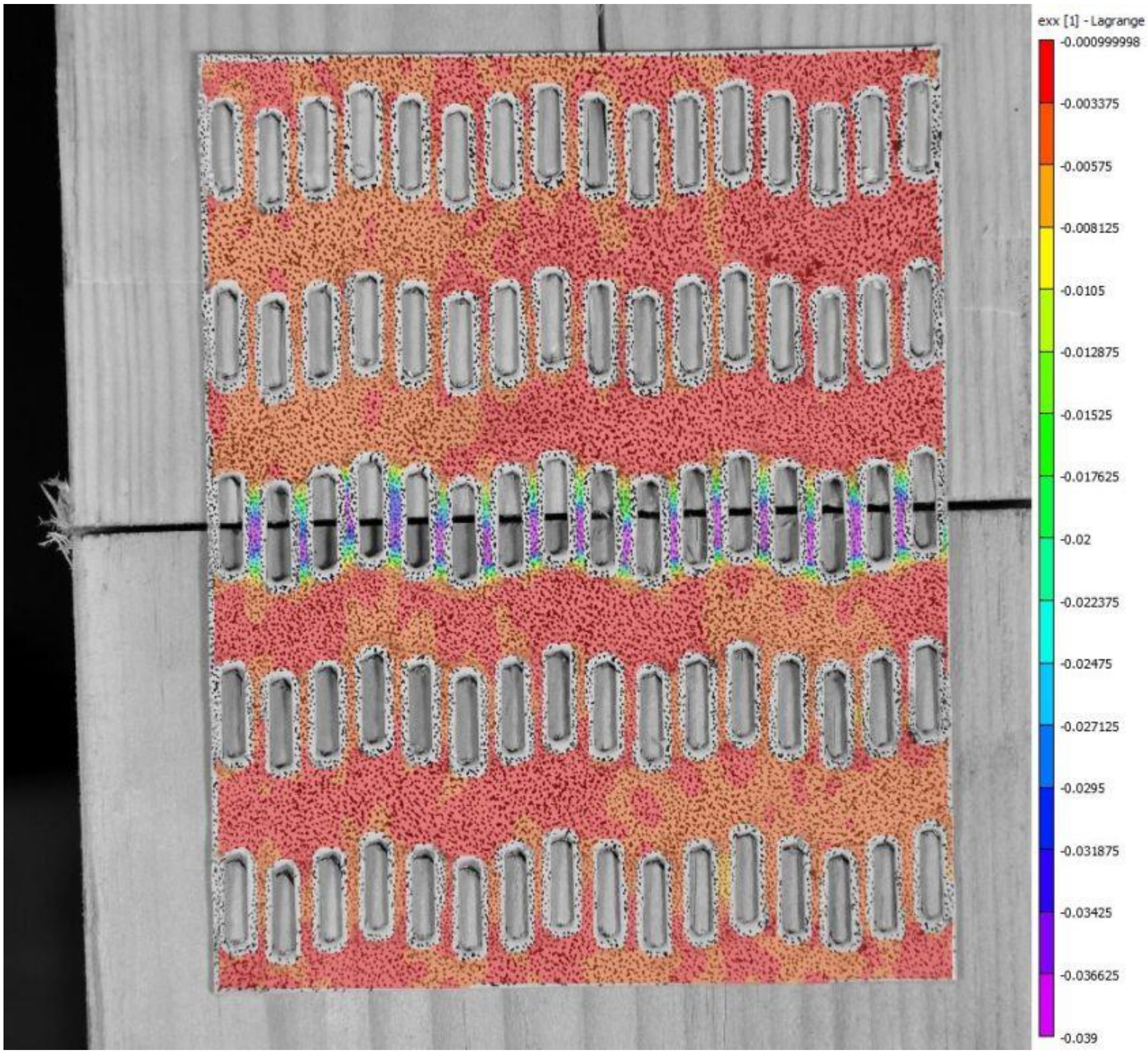

Figure 4-8: Full-field strain in x-direction (ε_{xx}) at load 8,550 pounds (the last image before failure)

4.1.1.3 The Second Tension Test (AA-2nd)

In this test, the two members of wood were connected by the MPC. The specimen was set on the universal testing machine. The first reference image was taken before applying any load. Figure 4-9 shows the first image which is considered as the reference image in digital image correlation technique.

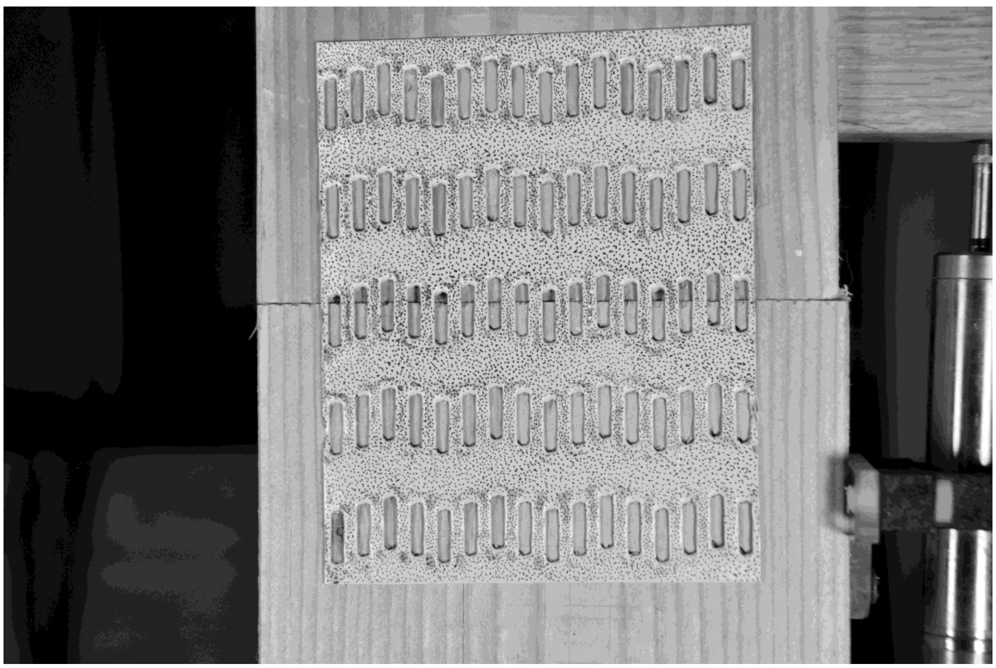

Figure 4-9: First image /reference image

After the first reference image was taken at load zero, the load was increased on the specimen gradually until failure occurred. The camera was placed on a fixed place and the MPC was perpendicular to the camera's lenses. Images were taken for the MPC specimen at each load increment of 200 pounds until failure. The failure in the member occurred in the metal plate connection. Figure 4-10 shows the last image after the failure.

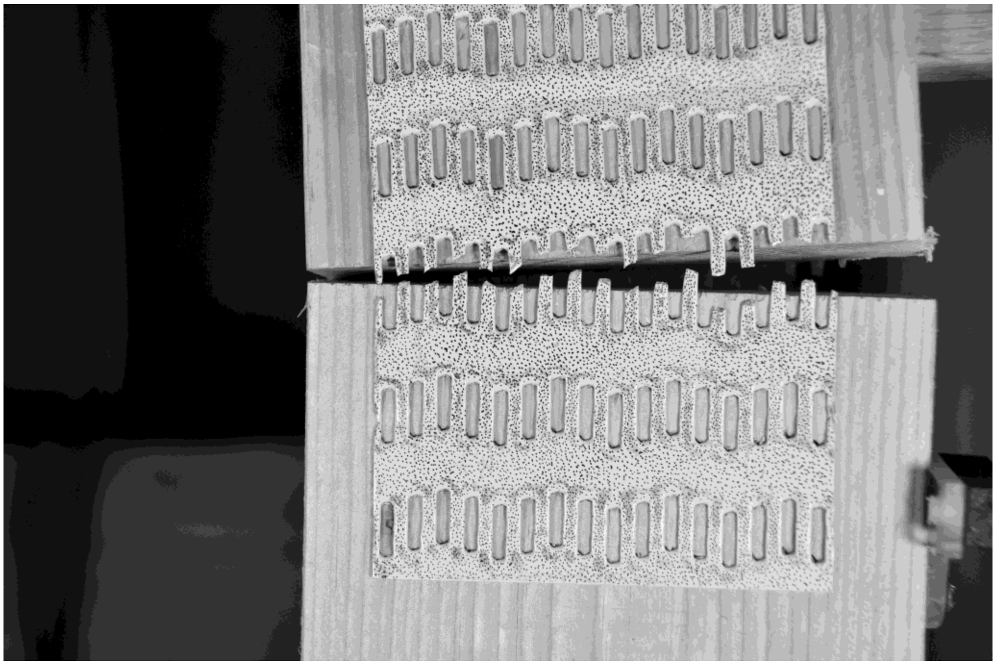

Figure 4-10: The last image after the failure

Forty three (43) images were taken in addition to the reference image and the last failure image. The metal plate failed at load equal to 8,650 pounds. The plate was ruptured from the right side and then it failed. Images were implemented in DIC-software to find the full-field strain measurements.

4.1.1.3.1 Analysis of the Full-Field Strain Results Obtained From DIC-Software

All the test images, which were obtained from the laboratory test, were implemented in the digital image correlation software Vic-2D. The software analyzed each image related to the reference one. Thus each deformed image was compared to the non-deformed reference image. The full-field strain measurements were obtained from the digital image correlation software for each deformed image. Figure 4-11 shows the strain in y direction (ε_{yy}) for the image at 200 pounds.

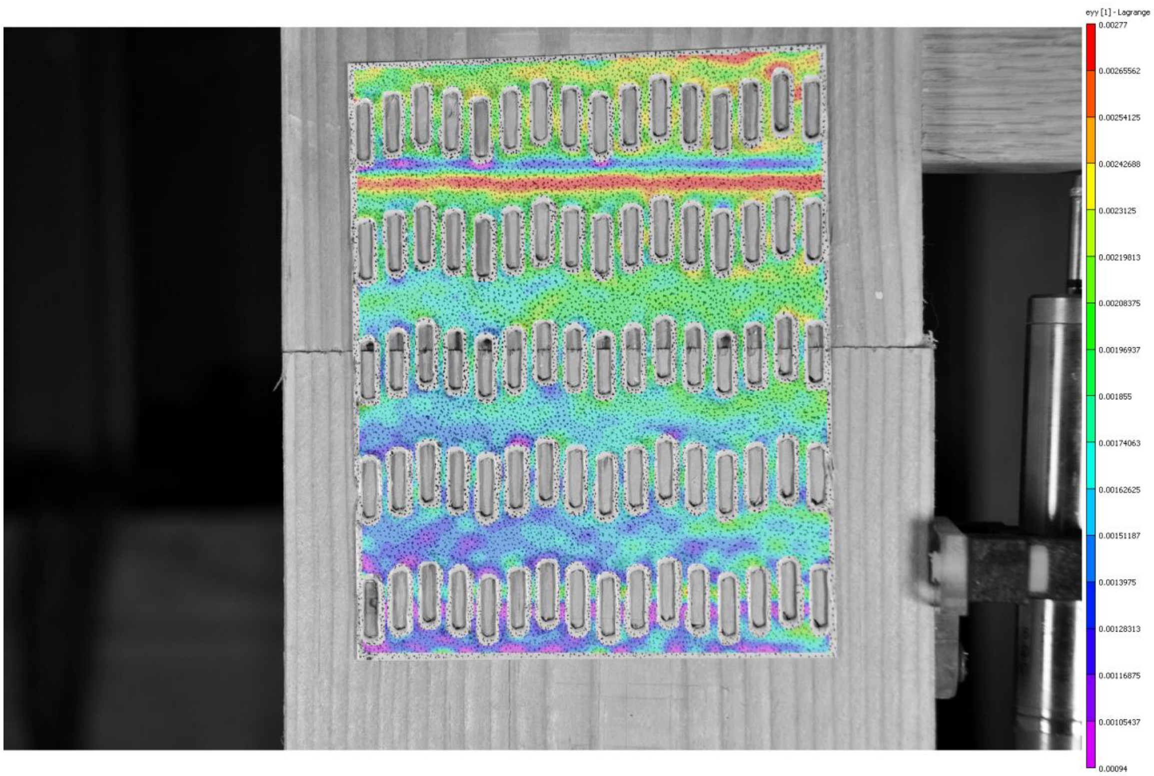

Figure 4-11: Full-field strain measurements (ε_{yy}) for the MPC at 200 pounds

The last figure shows the metal plate at 200 pounds which is very low loading. The digital image correlation software presents the results of strain as a strain color contour plots. The strain field's results show different levels of colors and show that each level of color represents a number. The full-field strain measurements at 200 pounds show changes for the strain values over the plate. These changes are due to the presence of the teeth distributed everywhere on the plate and driven into wood, which has different properties in all directions. The increment of loading is 200 pounds. After increasing the load, the strain field will show more changes and the external force will hold more influence on the plate. The strain (ε_{yy}) is a tensile strain starting from the beginning of this test at load 200 pounds until failure. The full-field strain images show that the strain (ε_{yy}) increases with loading. The area of the plate above the middle horizontal gap line holds higher strain (ε_{yy}) than the underneath area with very low difference. The significant change in the strain (ε_{yy}) is at 6,400 pounds. The middle horizontal gap line shows high tensile strain over some areas of the plate. The upper area of the plate is holding high tensile strain from the beginning but the middle area of the plate is just showing the high strain at load 6,400 pounds as shown in Figure 4-12. The strain (ε_{yy}) on the middle horizontal gap line shows high tensile strain over some areas. The strain (ε_{yy}) above the middle horizontal line is slightly bigger than the strain underneath the horizontal middle gap line. After 6,400 pounds the significant increase in strain along the middle horizontal gap line of the plate continues increasing up and it becomes clear on the full-field strain (ε_{yy}) images. The full-field strain (ε_{yy}) images from 6,400 pounds until failure at 8,650 pounds shows that the strain (ε_{yy}) on the upper and lower areas of the plate becomes very close and looks like a mirror to each other. These similarities increase with loading. As more load is applied, the more similarities grow between the two halves of the plate.

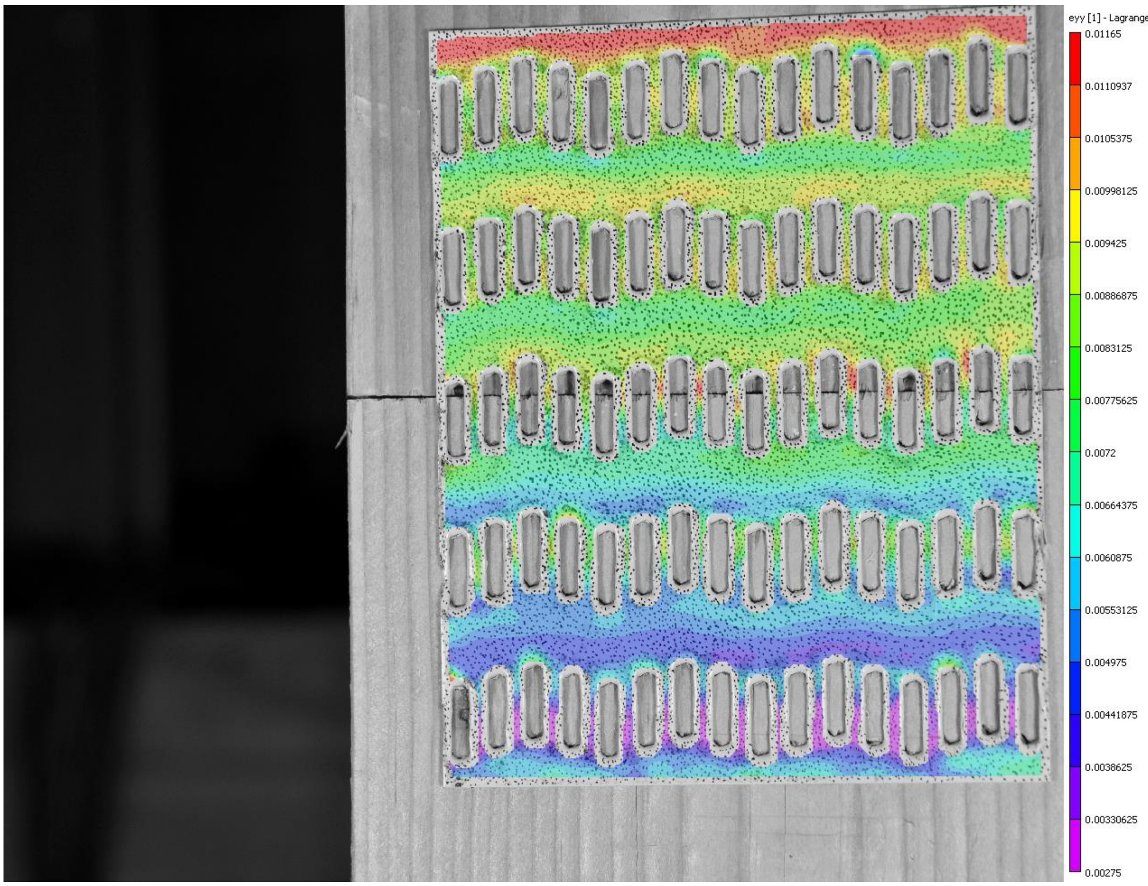

Figure 4-12: Full-field strain measurements (ε_{yy}) for the image at 6,400 pounds

The last image before failure at 8,600 pounds is shown in Figure 4-13. The full-field strain (ε_{yy}) before the failure occurs at 8,650 pounds shows that the strain (ε_{yy}) is very high along the middle horizontal gap line of the plate and the right strain is higher than the left strain. In general the strain (ε_{yy}) above and below the middle horizontal gap line is very close with only a slight difference between them. The strain over the entire plate in this test is a tensile strain. The failure occurred at 8,650 pounds with the rupture of the plate from the right side to the left side showing a complete split between the two halves of the plates.

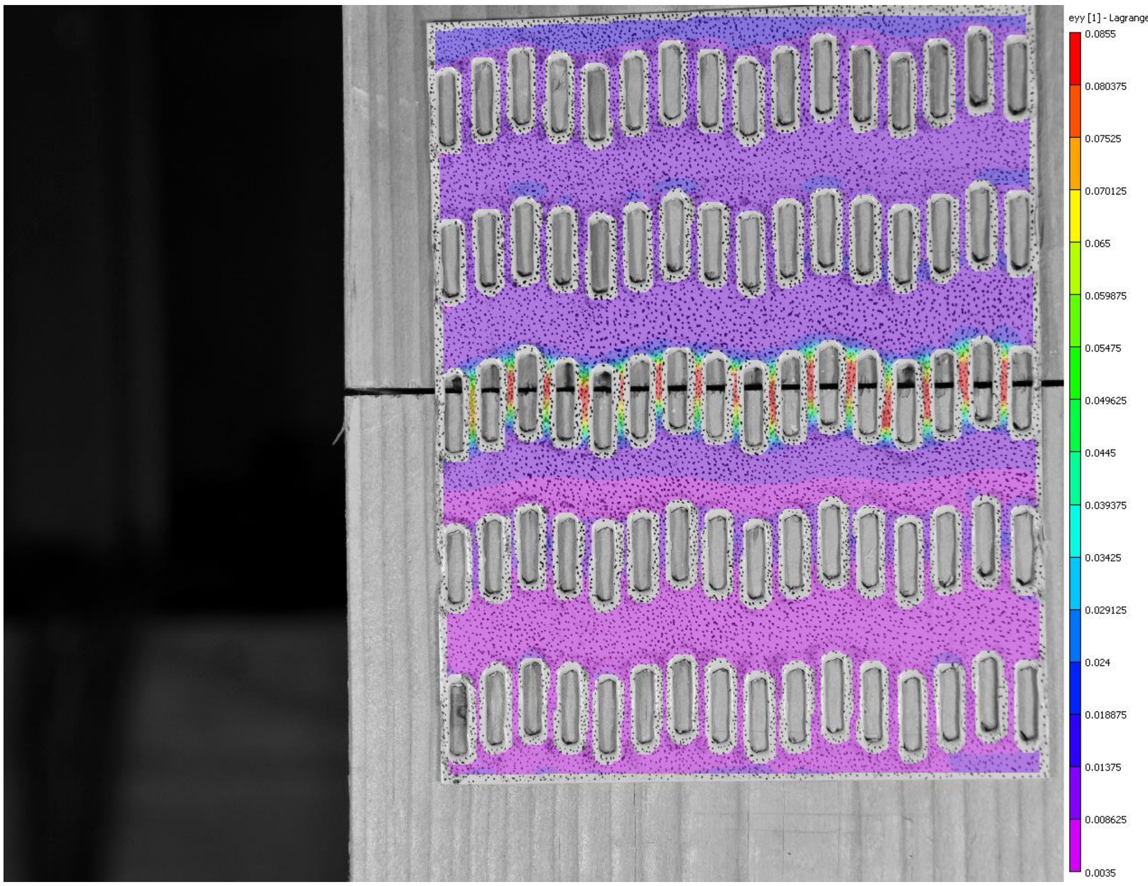

Figure 4-13: Full-field strain measurements (ε_{yy}) for the last image before the failure at 8,600 pounds

The failure image is showed earlier in this section. The complete rupture of the plate indicates that the plate in the middle horizontal line has yielded then ruptured. At 6,400 pounds the strain in the middle reaches 0.01 while on the other plate’s area it is 0.002 or less. So the plate's area along the middle horizontal starts to yield after applying 6,400 pounds then the rupture at 8,650 pounds. The presence of the slots makes this area weaker than any other place on the plate. The significant changes in the strain (ε_{yy}) occur along the middle horizontal gap line due primarily to the presence of the gap between the two wood members and the fact that the area of the plate is halved by virtue of the slots. The gap between the two connected wood members increases with increased load through the test.

The full-field strain (ε_{xx}) images in x-direction can also be obtained from digital image correlation software. The strain (ε_{xx}) also changes with loading, and (ε_{xx}) is a positive strain from the beginning of the test. Then it continues tensile strain over the whole plate. The middle horizontal line of the plate shows decreasing values of strain with loading until this strain turns to negative strain which is a compressive strain. Figure 4-14 shows the strain field behavior at 8,000 pounds.

The strain above and below the horizontal middle line is almost the same but has a slight difference. Figure 4-15 shows the strain in x-direction for the last image before failure. The figure shows high compressive strain in the middle of the plate. However, a tensile strain on the top and the bottom of the plate is almost equal to it.

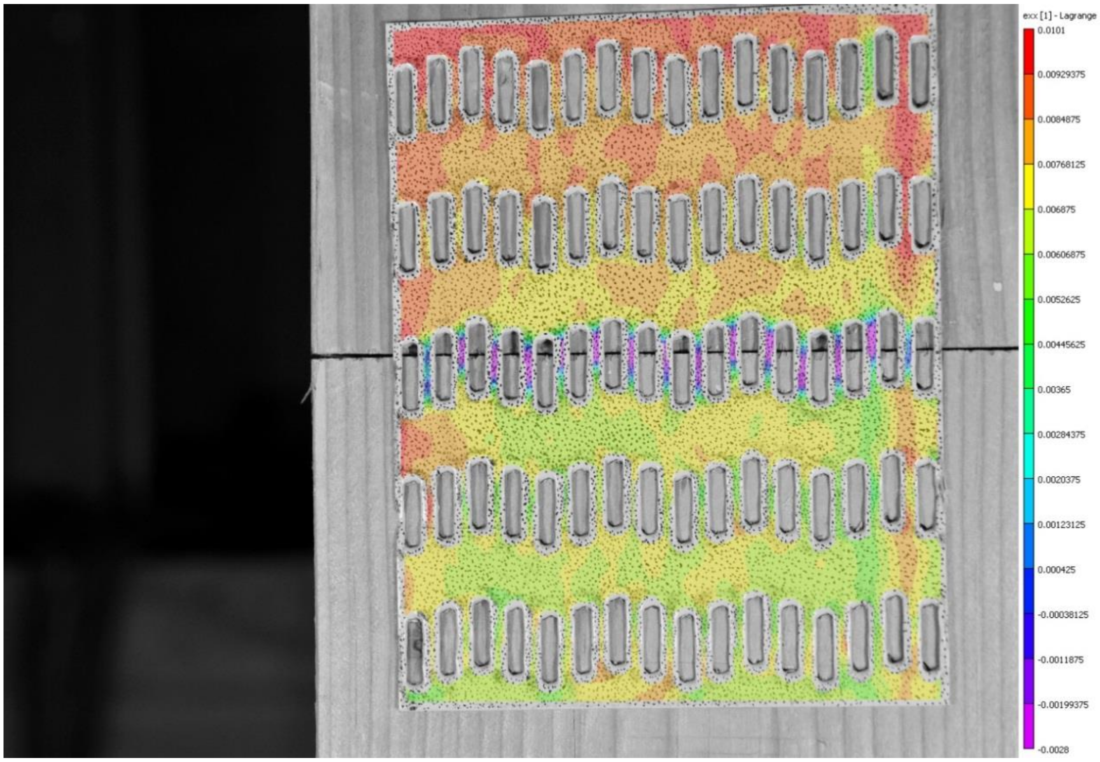

Figure 4-14: Full-field strain in x-direction (ε_{xx}) at 8,000 pounds

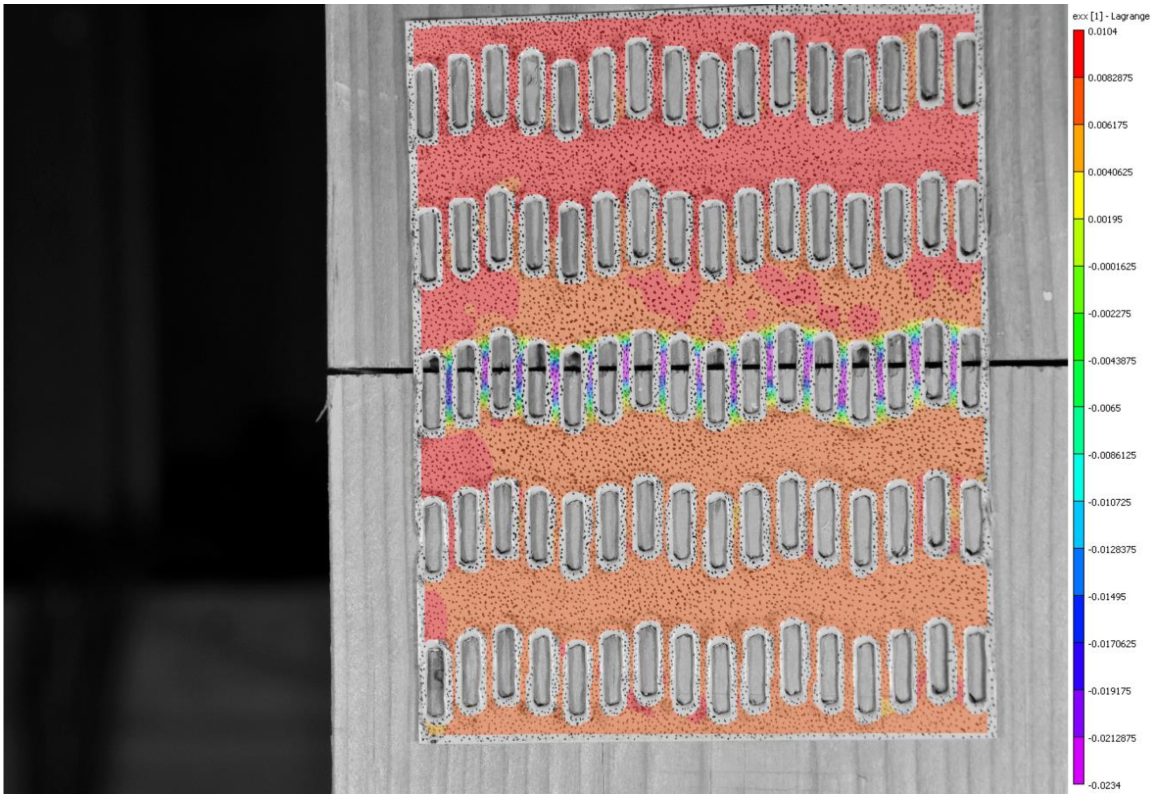

Figure 4-15: Full-field strain in x direction (ε_{xx}) under load 8,600 pounds (the last image before failure)

Thus, the last image for full-field strain shows that the middle of the plate has the highest tensile strain (ε_{yy}) and the highest compressive strain (ε_{xx}) which is a logical result. When a deformable body is subjected to an axial tensile force it will elongate and also contract laterally.

4.1.1.3.2 Numerical Analysis for the Results

To analyze the DIC results numerically, a vertical cross section line from the top of the plate to the bottom is taken for some images starting with the first image at 200 pounds and ending with the last image before failure. The cross section is taken in three different locations as shown if Figure 4-16.

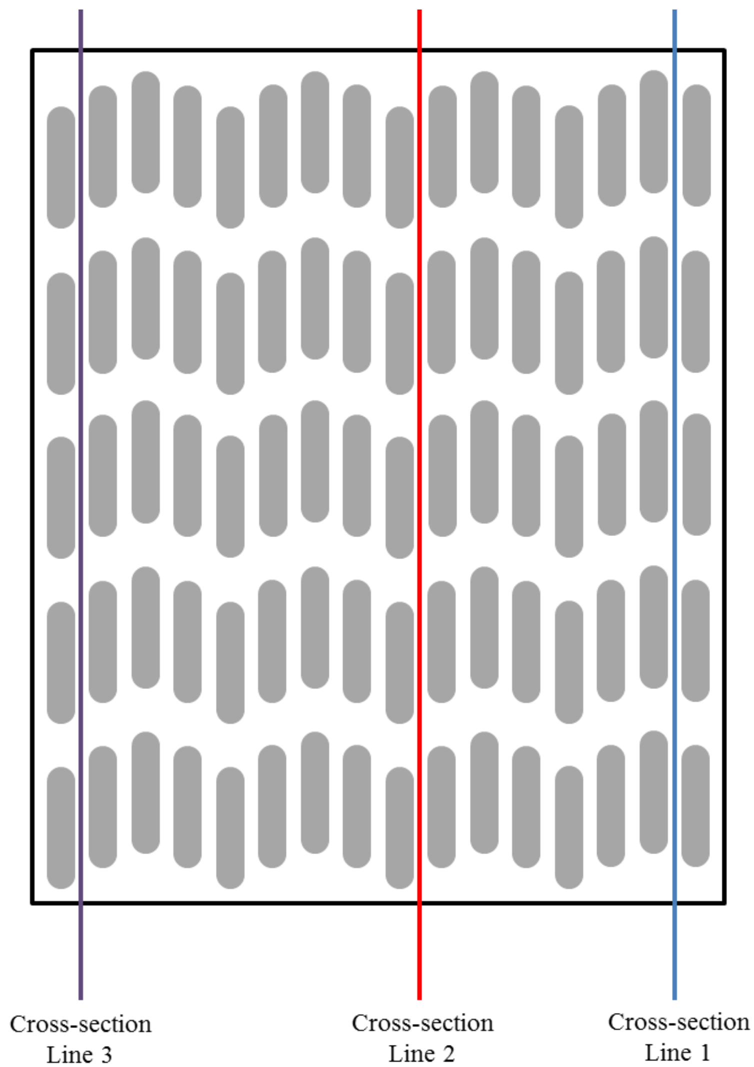

Figure 4-16: Metal plate with the cross-section lines along the vertical direction

The cross section lines locations are based on the following:

- The first cross section line (1-1) is from the right side of MPC @ x = 2.095 in.
- The second cross section line (2-2) is near the middle of the MPC @ x = 0.5452 in.
- The third cross section line (3-3) is from the left side of MPC @ x = -1.40746 in.

Three cross-section lines are taken over the strain field (ε_{yy}). The next three Figures 4-17 to 4-19 show the distribution of strain (ε_{yy}) at three different locations for 14 images. Each image represents the value of the loading that is applied on the specimen of the two wood members connected by the metal plate connections. The curves show that the first considered load is 200 pounds then the increment of loading is almost 1,000 pounds until the image of load 7,000 pounds then the increment of loading decreases to 400 pounds and then 200 pounds for the last four images. These changes in the increment of loading and so in the curves because of the significant changes in the strain after applying 6,000 pounds. And the last images before failure are the most important images that show the significant change in the plate under loading before failure occurs. The failure of the plate has occurred along the middle of the plate and the middle of the plate is clearly shown in the next three figures that they hold the maximum tensile strain. The strain along the middle horizontal line of the plate is significantly higher than any other strain on the plate.

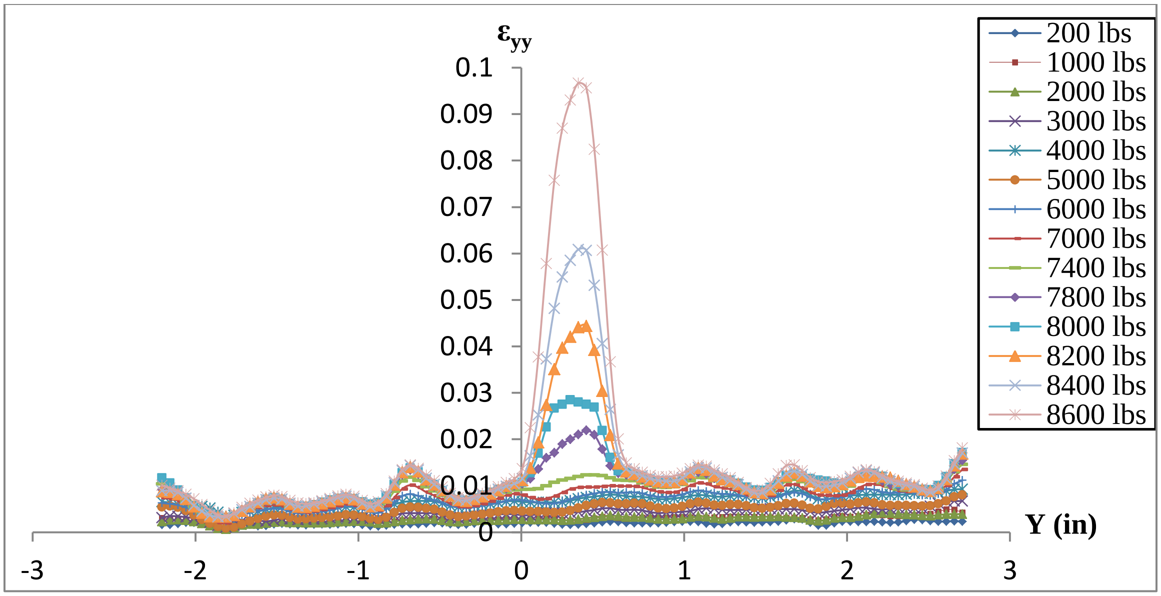

Figure 4-17: The strain distribution (ε_{yy}) along a cross section line (1-1) located on the right side of the plate

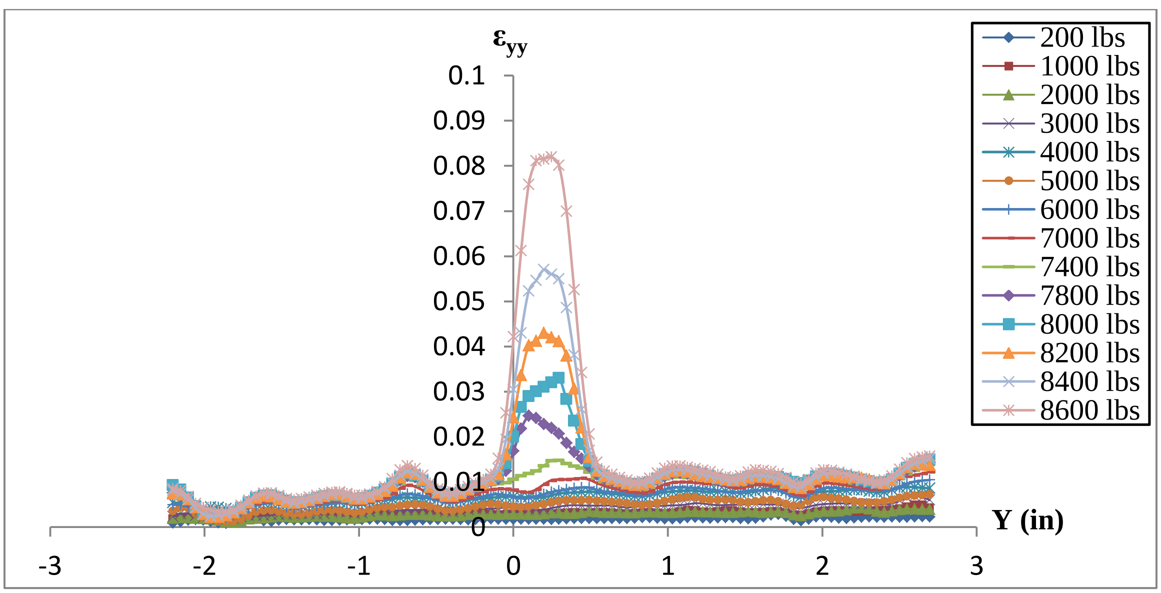

Figure 4-18: The strain (ε_{yy}) distribution along a cross section line (2-2) located near the middle of the plate

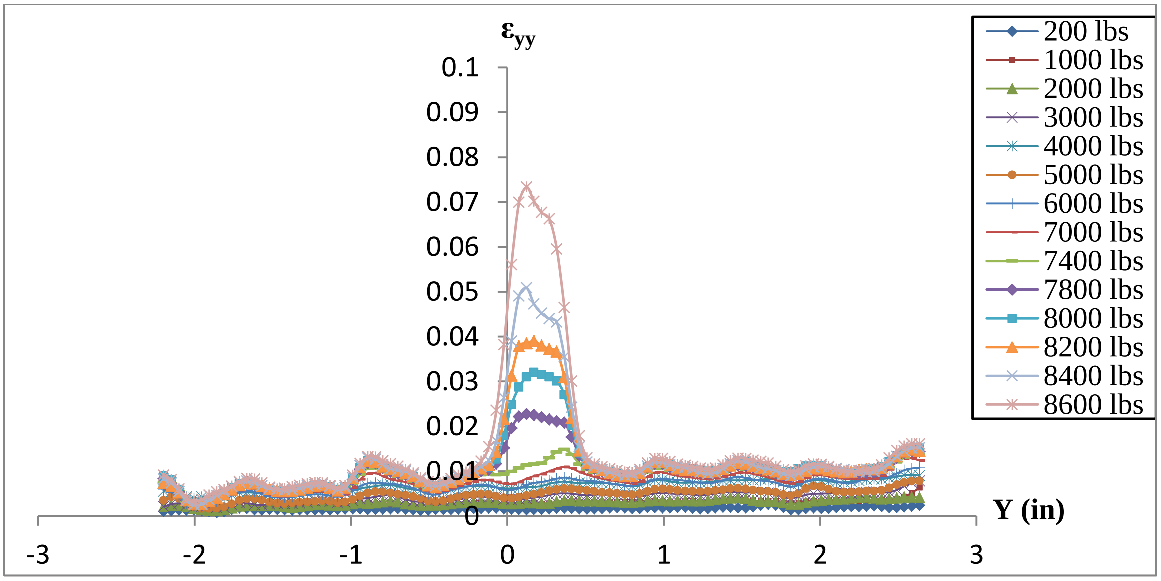

Figure 4-19: The strain (ε_{yy}) distribution along a cross section line (3-3) located on the left side of the plate

The strain distribution over the surface of the MPC (based on the full-field strain measurements and the cross sections lines) starts with very low strain values and almost equal strain values over the whole surface of the metal plate. The strain on the upper part of the plate nearly mirrors the strain on the lower part of plate. The plate fails at load around of 8,650 pounds. The total images for this test are 43 images. In the previous cross section strain curves, it shows that the plate starts to yield and the strain (ε_{yy}) becomes a significant and clear at almost image 35 which is at load equal to 7,000 pounds. Then the strain (ε_{yy}) in the middle of the plate becomes higher and continues to increase until failure.

The strain (ε_{yy}) curves show some repeating-rotating jumps up and down from the top to the bottom of the plate. Thus the strain is not a flat strain. These jumps are due to the change in the cross sectional area of the plate because of the presence of the slots. Moreover, the slots also are not perfectly distributed horizontally, and they are also distributed in a wavy shape. Also the wood is non-homogeneous material so the properties of wood are different from position to another. The angles of the teeth that are embedded in the wood are not the same for the entire plate. These teeth can affect the strain values.

The strain (ε_{yy}) shows high values along the first cross-section (1-1). The lowest strain values along the three cross-section lines are the left cross section line (3-3). The last image before failure which is at the maximum load (8,600 pounds) has the maximum strain (ε_{yy}) of values in all of the cross-section lines. In the middle of each cross-section line, which represents the horizontal middle of the plate, the increase in the strain is obvious. The plate yields then fractures along the horizontal middle gap line of the plate while the other regions of the plate still far from yielding. The difference between the strain values in the middle and the strain on any other area of the plate is high. In cross section line (1-1) the percentage of the increase in the strain between the strain on the middle and the strain from the upper area of the plate is 572.3%.

Failure occurs at 8,650 pounds where the two halves of the plate are completely split. The split from the right side is bigger than the left side. This is obvious in the strain curves. The strain (ε_{yy}) on the right side of the plate at cross section line (1-1) is the highest. The strain (ε_{yy}) along cross section line (2-2) in the middle is higher than the strain (ε_{yy}) on the left side of the plate at cross section line (3-3). So the strain (ε_{yy}) is explaining the failure behavior for the plate. The failure occurs along the middle horizontal gap line where the two wood members are connected which makes that gap line the weakest region.

On the other hand, the metal plate also shows strain in x-direction (ε_{xx}). The strain (ε_{xx}) along y-direction for the cross-section lines (1-1), (2-2) and (3-3) is also found in the next Figures 4-20 to 4-22.

The strain (ε_{xx}) is a tensile strain over the entire plate with some exceptions starting from the first image at 200 pounds. The tensile (ε_{xx}) increases with loading as shown in the strain (ε_{xx}) curves. At high load approximately 7,000 pounds the middle horizontal line of the plate shows decreasing tensile strain. The decreasing in the tensile strain continues with loading until the strain (ε_{xx}) turns to negative strain along the horizontal gap line of the plate as shown in the strain curves (ε_{xx}). The strain (ε_{xx}) turns to compressive strain along the middle line of the plate at around load 7,800 pounds. Figure 4-20 shows the strain (ε_{xx}) along the first cross section line (1-1) located on the right side of the plate. The strain (ε_{xx}) is tensile strain from load 200 pounds until 8,000 pounds. At 8,000 pounds the strain (ε_{xx}) on the middle of the plate turns to compressive strain. And the strain on the rest area of the plate is tensile strain. Although the strain (ε_{xx}) is tensile strain, its values slightly decrease after 8,000 pounds. The compressive strain in the middle continues to increase until failure. The strain (ε_{xx}) for the last image before failure at 8,600 pounds has the highest compressive strain. The strain (ε_{yy}) curves show that the strain (ε_{yy}) has the highest tensile strain at load 8,600 where the strain (ε_{xx}) has the highest compressive strain along the cross section line (1-1). This confirms when a deformable body is subjected to an axial tensile force, it will elongate and also contracts laterally.

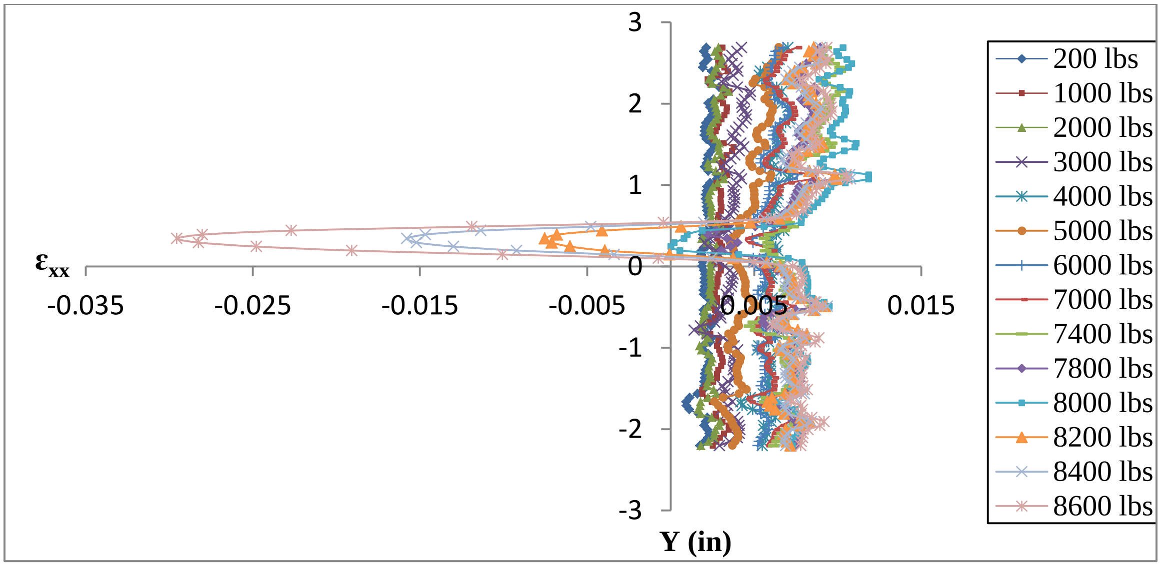

Figure 4-20: The strain distribution (εxx) along a cross section line (1-1) located on the right side of the plate

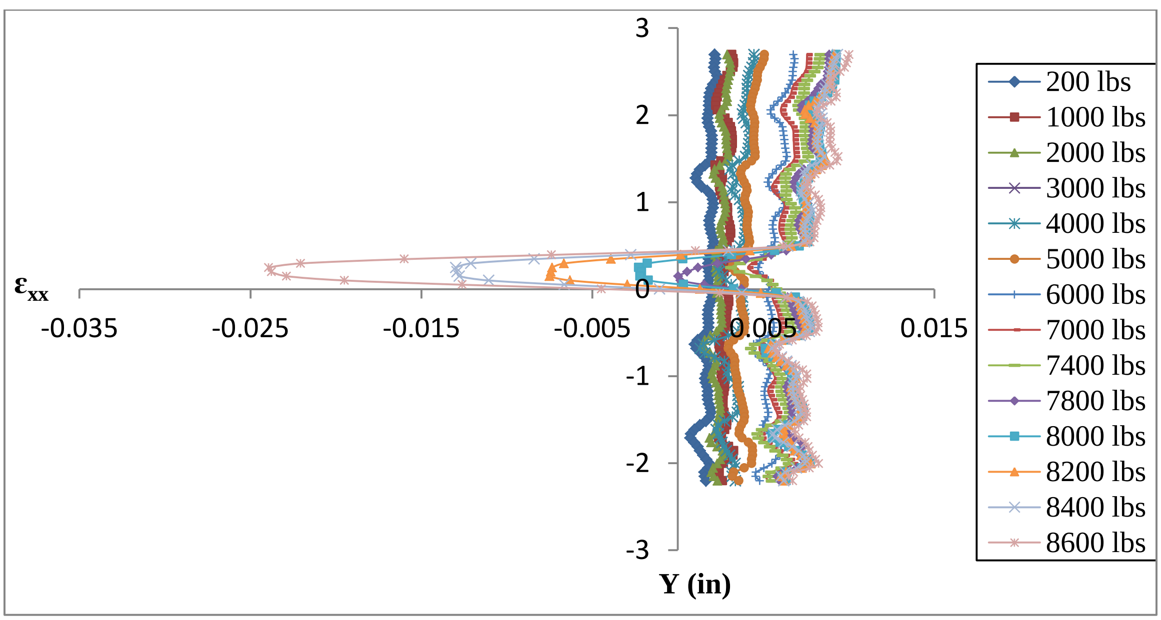

Figure 4-21: The strain (εxx) distribution along a cross section line (2-2) located near the vertical middle of the plate

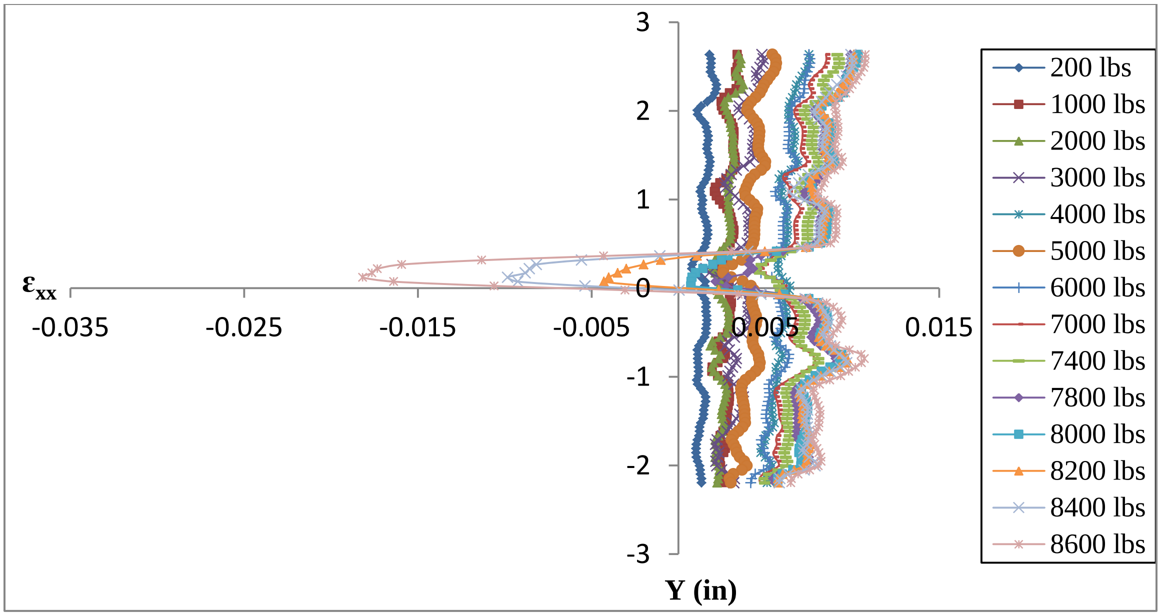

Figure 4-22: The strain (εxx) distribution along a cross section line (3-3) located on the left side of the plate

The other two section lines (2-2) and (3-3) behave in the same way as cross section line (1-1). But the increase in the compressive strain (ε_{xx}) in the middle of cross section line (2-2) is bigger than (3-3), and the compressive strain (ε_{xx}) at cross section line (1-1) is the biggest. The maximum compressive strain (ε_{xx}) value from the curves at 8,600 pounds is -0.029 at cross section line (1-1). And the mean tensile strain (ε_{xx}) for the last image at 8,600 pounds is 0.008. So the strain (ε_{xx}) is obvious and clear. To design the metal plate connection this strain (ε_{xx}) should be considered over the entire plate. The average (ε_{xx}) for the first section (1-1) is over 0.01 in and it is lower than that in the other sections.

The strain curves are not flat curves or linear curves. The strain curves are jumping up and down along the vertical direction lines. These repeating sudden changes are due to the presence of the slots on all the plate’ s surface. These sudden jumping strain changes also can be seen in the strain curves (ε_{yy}).

In general, the shape for the strain (ε_{xx}) is opposite to the shape of the strain (ε_{yy}) along the middle horizontal gap line of the plate. This illustrates the digital image correlation results. Where the strain (ε_{xx}) is high as a compressive strain, the strain (ε_{yy}) is high as a tensile strain in the same area. The other areas of plate in general are influenced by tensile strain (ε_{yy}) and tensile strain (ε_{xx}). Although the middle horizontal line gap of the plate is holding high compressive strain (ε_{xx}) and high tensile strain (ε_{yy}). This result shows that the strain with loading is still under the influence of the shear force from the teeth. The teeth are distributed over the entire plate in a wavy shape. The cross sectional area also, where the teeth are, is very tinny and less than the cross sectional area on other regions. These two factors beside the fact that the wood has different properties in all directions makes the tensile strain still the dominant strain on the plate. The middle horizontal region where the failure occurs has half cross sectional plate’s area and it is along the gap between the two connected wood members. This region is the only region showing the influence of the tensile load. The other area on the plate’s surface is still under the influence of the teeth gripping and strength.

4.1.1.3.3 A Comparison between the Strain in y and x direction [(ε_{xx}) vs. (ε_{yy})]

In this section, the strain values {**(ε_{xx})** vs. **(ε_{yy})}** for the last image before failure at load 8,600 pounds is compared. The next Figures 4-23 and 4-24 show the three cross-section lines for the last image before failure at load 8,600 pounds for strain (ε_{yy}) and (ε_{xx}).

The strain curves for the lines show that the middle of the plate has yielded. The upper and lower plates have not yielded and are not close when compared to the big jump in the strain values in the middle of the plate. So, the local strain values are very high in the middle part of the plate. The cross sectional area there is half of the plate cross sectional area because of the slots. Thus, these changes in the cross sectional area makes the failure easier in the middle than any other place.

The figures show that there is a strain along x-axis (ε_{xx}) which should not be ignored. The general shape of strain in y-direction (ε_{yy}) is very close to the shape of the strain in x-direction (ε_{xx}) but on the negative side. Both (ε_{yy}) and (ε_{xx}) have almost the same strain on the upper and lower part of the plate around the line of connection between the two wood members, however they have high strain in the middle of the plate although in different directions. The maximum strain is in the right side of the plate as shown in cross-section line (1-1). This explains the direction of the rupture in the plate. The failure starts from the right side then the middle then the left side which has the smallest local strain values. On the other hand, the strain in x-direction (ε_{xx}) in the middle of the plate is in compression and has the highest compressive strain in x-direction where the steel has yielded and then ruptured.

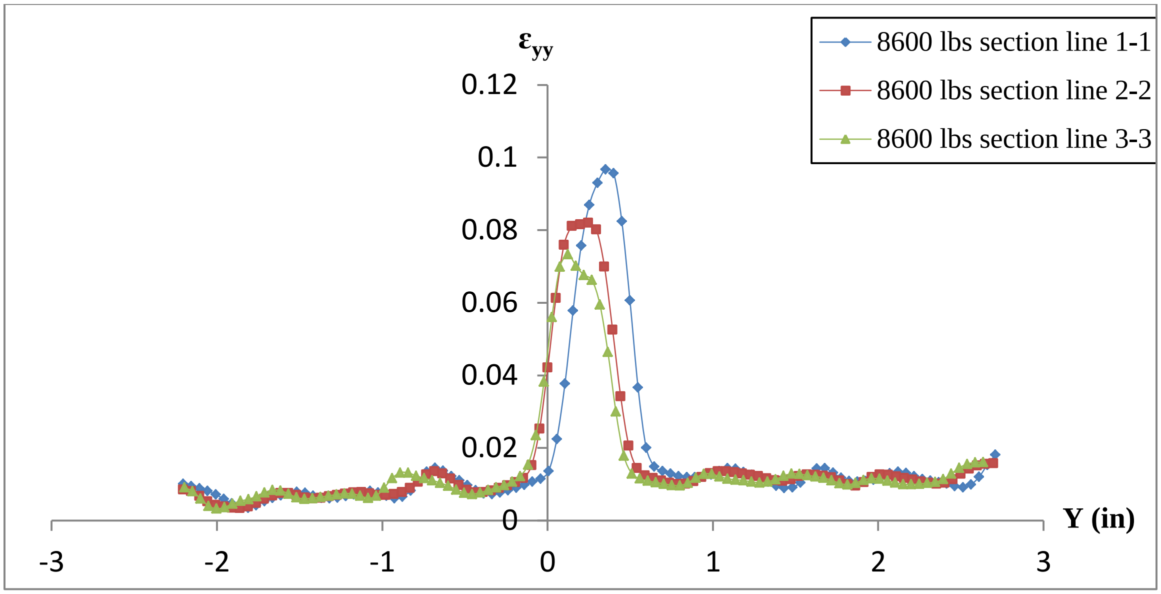

Figure 4-23: The strain (ε_{yy}) distribution along the three cross-section lines (1-1), (2-2), (3-3) for the last image before failure at load 8,600 pounds

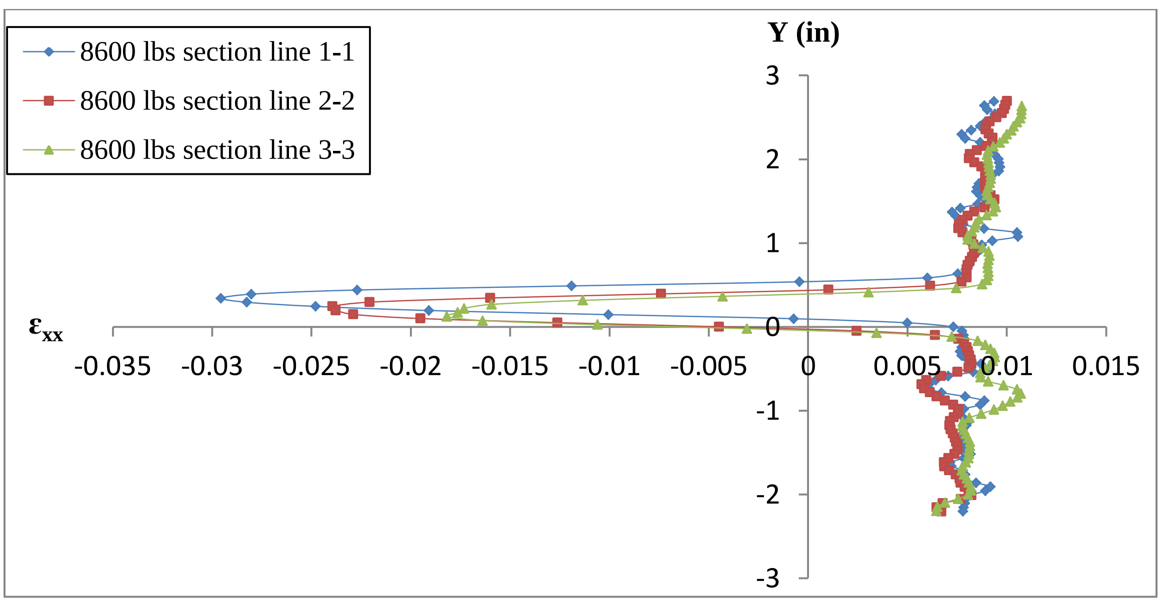

Figure 4-24: The strain (ε_{xx}) distribution along the three cross-section lines (1-1), (2-2), (3-3) for the last image before failure at load 8,600 pounds

4.1.1.4 The Third Tension Test (AA-3rd)

In this test, the two members of wood were connected by the MPC. The specimen was set on the universal testing machine. The first reference image was taken before applying any load. Figure 4-25 shows the first image which is considered as the reference image in digital image correlation technique.

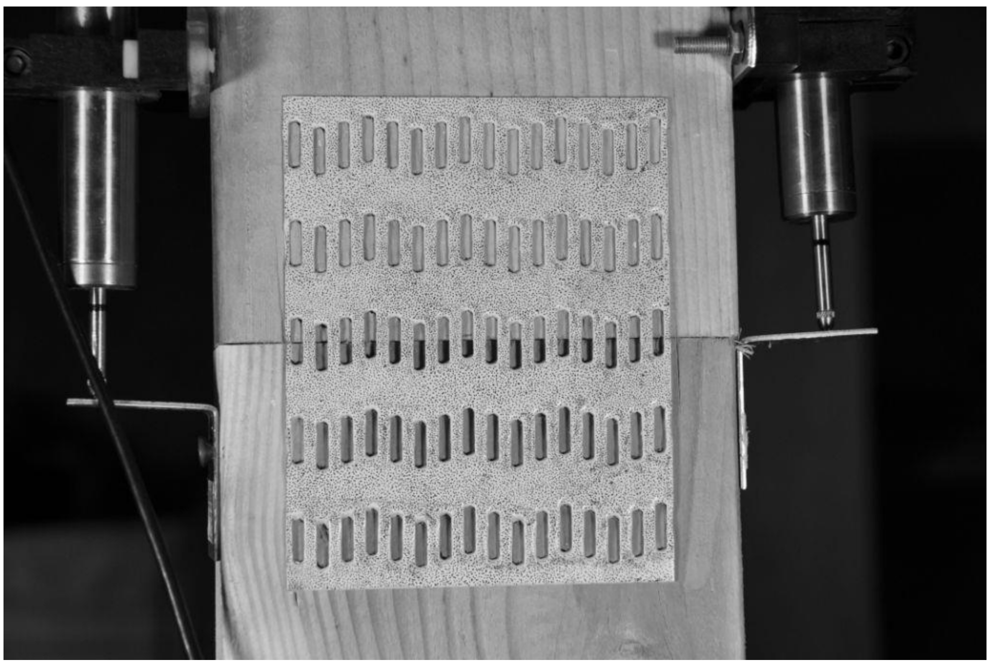

Figure 4-25: First image /reference image

After the first reference image was taken at load zero, the load was increased on the specimen until failure. The camera was placed on a fixed place, and the MPC was perpendicular to the camera's lenses. Images were taken for the MPC specimen at each load increment of 200 pounds until failure. The failure in the member occurred in the metal plate connection. Figure 4-26 shows the last image after the failure.

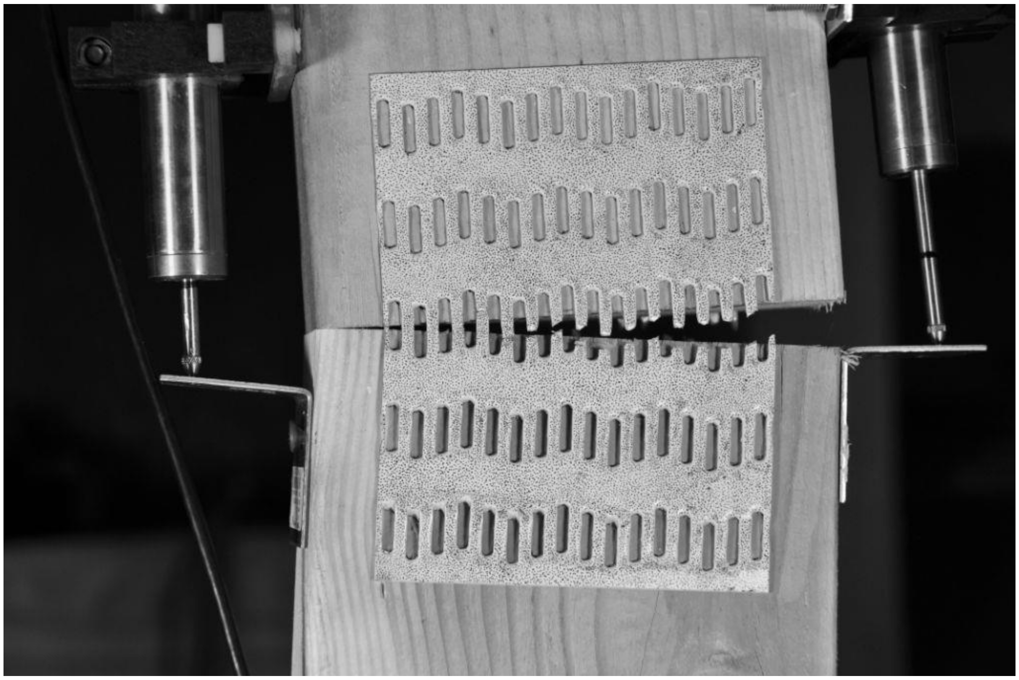

Figure 4-26: The last image after the failure

The total deformed images were 43 images and the plate failed at about 8,640 pounds load. The plate was horizontally ruptured in the middle with an increasing slope from left to right. Digital image correlation software Vic-2D was used to process the 43 deformed images to obtain the local full-field strain measurements. Each single image was compared to the reference image to find the full-field strain measurements.

4.1.1.4.1 Analysis of the Full-Field Strain Results Obtained From DIC-Software

All the test images, which were obtained from the laboratory test, were implemented in the digital image correlation software Vic-2D. The software analyzed each image and related it to the reference one. The full-field strain measurements were obtained from the DIC software for each deformed image. Figure 4-27 shows the strain in y-direction (ε_{yy}) for the image at 200 pounds.

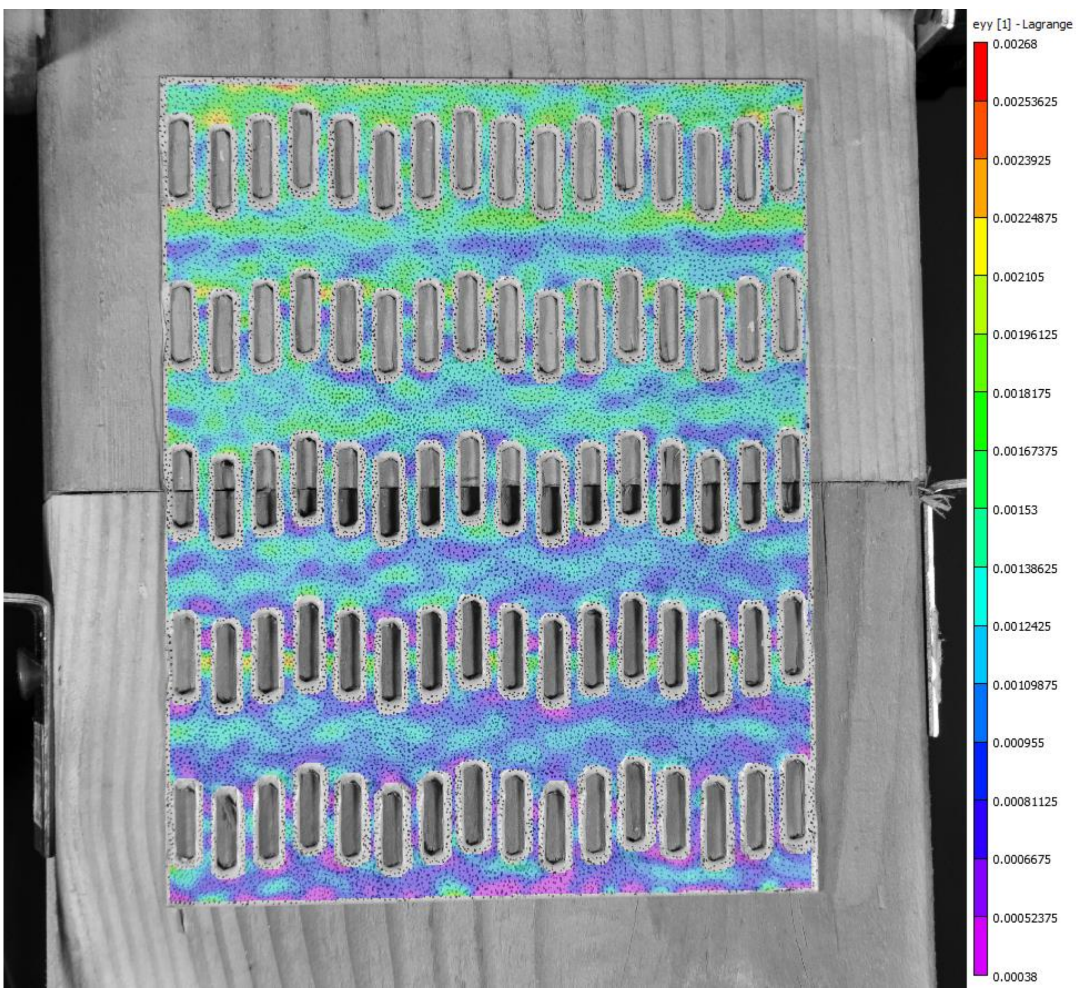

Figure 4-27: Full-field strain measurements (ε_{yy}) for the MPC after applying 200 pounds

The digital image correlation software presents the results of strain as a color contour plots strain field. The strain field's results show different levels of color and show that each level of color represents a number. The previous figure shows the metal plate at 200 pounds which is the first load on the plate. The strain (ε_{yy}) is low. The strain contour plot fluctuates over the surface of the plate but in general the top part of plate almost looks like the bottom part of the plate.

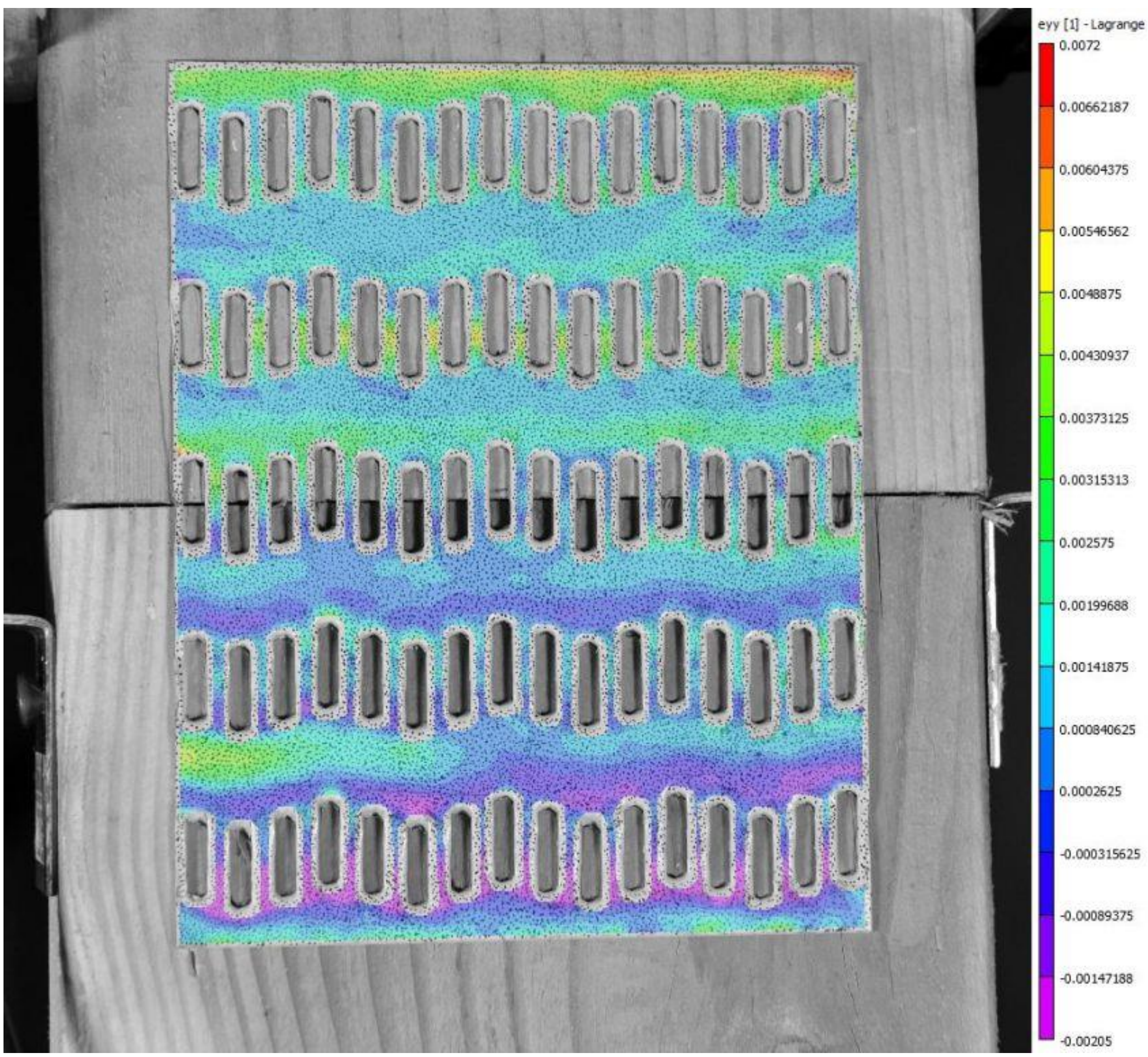

Figure 4-28: Full-field strain measurements (ε_{yy}) for the image at 6,000 pounds

By increasing the load with 200 pounds increment, the strain (ε_{yy}) field changes in value and direction. The strain (ε_{yy}) is tensile strain over the plate's area with some limited exception areas. After applying 4,000 pounds the strain goes up as a tensile strain (ε_{yy}) and it increases with load. A full-field strain measurement for the image at 6,000 pounds is shown in Figure 4-28. The strain image at 6,000 pounds shows higher tensile strain on the area of the plate above the horizontal gap line than on the area below it. Some areas of the plate beneath the horizontal gap hold a low strain (ε_{yy}) values. The strain (ε_{yy}) is still fluctuating strain in its values and distribution over the whole area of the plate. The image shows sudden changes from one region to another. Increasing the load causes the strain in the plate to keep increasing in the same way. The plate-strain behavior at 7,400 pounds shows different contour strain color than the previous strain images in the horizontal middle of the plate along the horizontal gap. The strain on the middle of the plate starts to be higher than any other strain on the plate as shown in Figure 4-29. The strain field (ε_{yy}) shows a significant increase in its values that are located along the horizontal middle gap of the plate.

After applying 7,400 pounds the plate starts to yield in the middle from the right side. The full-field strain measurements images (ε_{yy}) from 7,400 pounds until the last image before the failure at 8,600 pounds shows high increase in the strain (ε_{yy}) along the horizontal gap line in the middle of the plate. The increase in the strain along this middle line is not equal and it starts from the right side of the plate middle gap line. The strain field image before the failure shows that the strain (ε_{yy}) above the middle horizontal gap line is almost equal to the strain beneath the middle line.

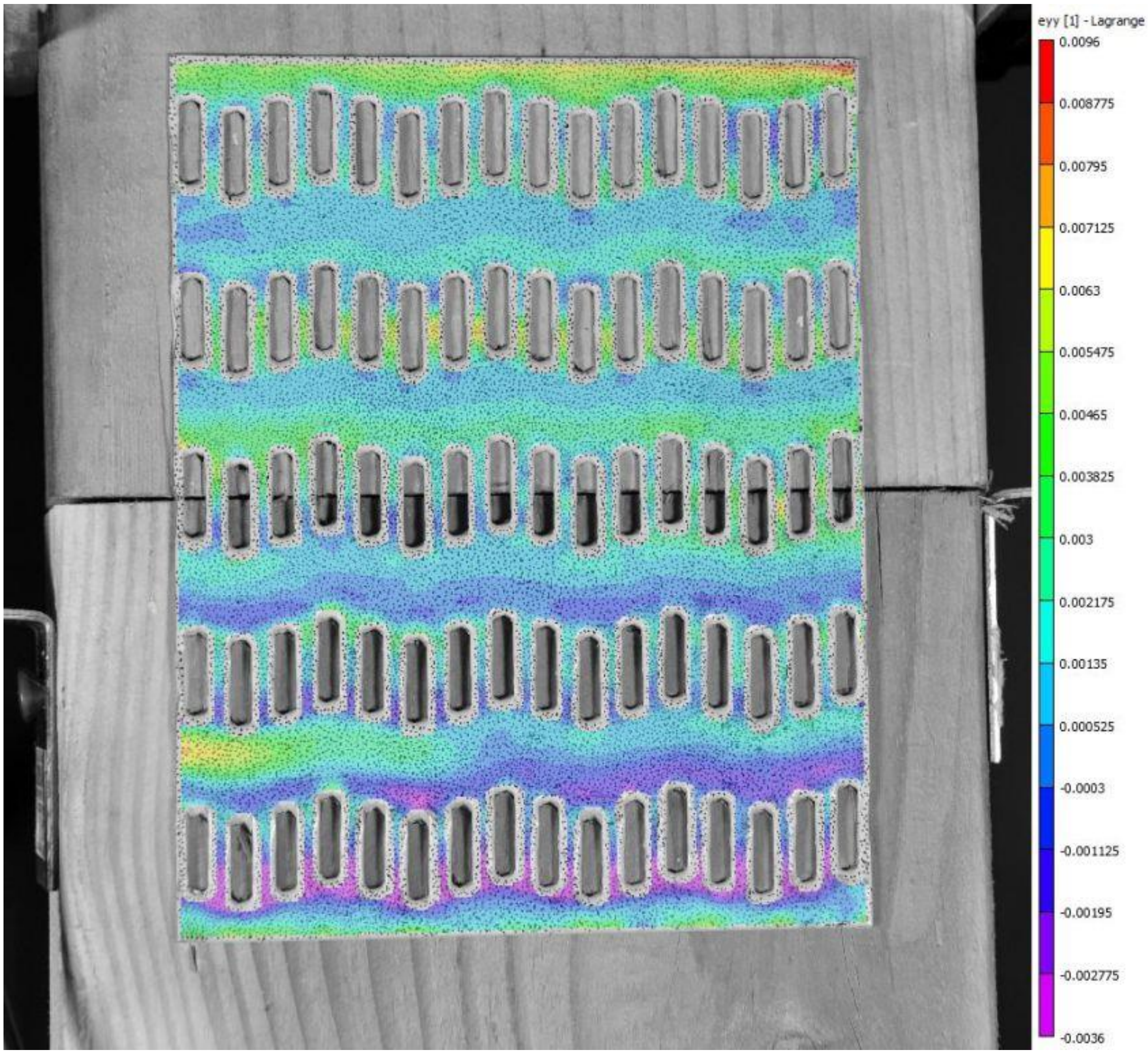

Figure 4-29: Full-field strain measurements (ε_{yy}) for the MPC at 7, 400 pounds

The full-field strain measurements (ε_{yy}) for the last DIC-processed image before failure at 8,600 pounds are shown in Figure 4-30. Digital image correlation software has analyzed all images except the image at failure because of the complete splitting of the plate from the horizontal-middle. The image at failure was presented earlier in this section. The full-field strain (ε_{yy}) is tensile strain all the entire plate with some limited exceptions in the bottom part of the plate which show some pulling out for the plate.

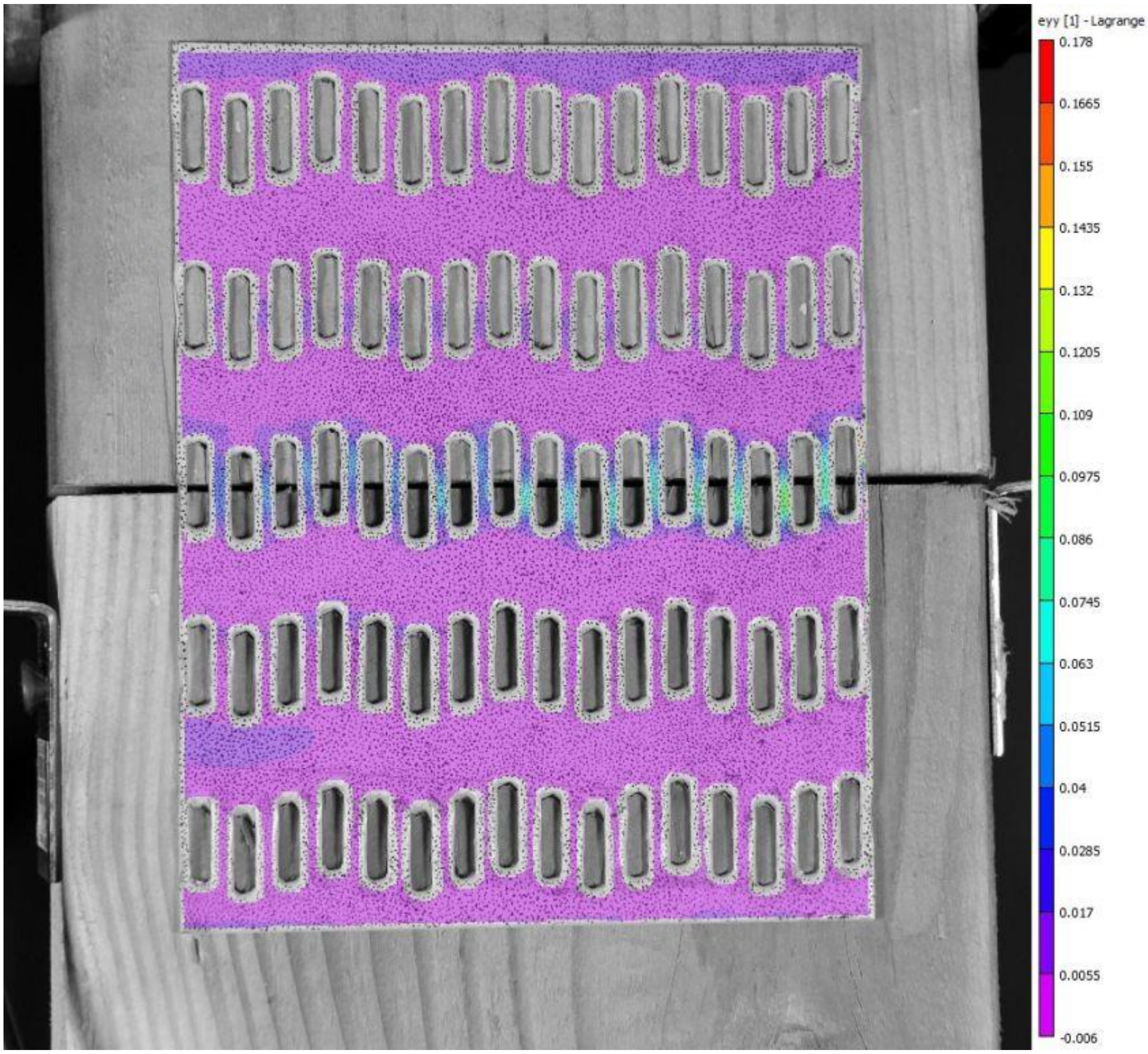

Figure 4-30: Full-field strain measurements (ε_{yy}) for the last image before the failure at 8,600 pounds

The strain (ε_{yy}) above the horizontal middle gap line almost mirrors the strain (ε_{yy}) beneath this line. The strain along the horizontal middle gap line holds very high tensile strain. It is low on the left side of the gap line and increases from left to right. The right side of the middle horizontal line on the plate has the maximum tensile strain, which reaches up to 0.09 while other tensile strain is almost close to zero.

The area of the plate which is located in the middle along the horizontal gap line where the two wood members are connected has half of the area because of the presence of the slots. This makes the area there weaker than any other place on the plate. Also the wood members tend to fail in the gap between the two wood members where the MPC connect them. The gap increases with increasing load through the test.

The full-field strain (ε_{xx}) images in x-direction are also found using the digital image correlation software. The full-field strain (ε_{xx}) images show very low strain (ε_{xx}) values from the beginning of the test. The strain (ε_{xx}) fluctuates and changes over the plate area with loading. Negative and positive values over the entire plate's surface are shown. The top and bottom strain tends to have very close values. By increasing the load, some parts over the surface of the plate possess negative strain and other parts display positive strain. But in general, the strain over the surface of the plate is moving up toward negative values which are compressive strain whereas some places over the plate possess tensile strain. The horizontal middle gap line over the plate shows significant changes in the strain (ε_{xx}) at high loading. Figure 4-31 shows the full-field strain measurements for the image at 8,000 pounds. The strain (ε_{xx}) over the plate's area is almost equally distributed while the strain (ε_{xx}) along the horizontal middle diagonal gap line shows different strain color than other strain areas and also high compressive strain.

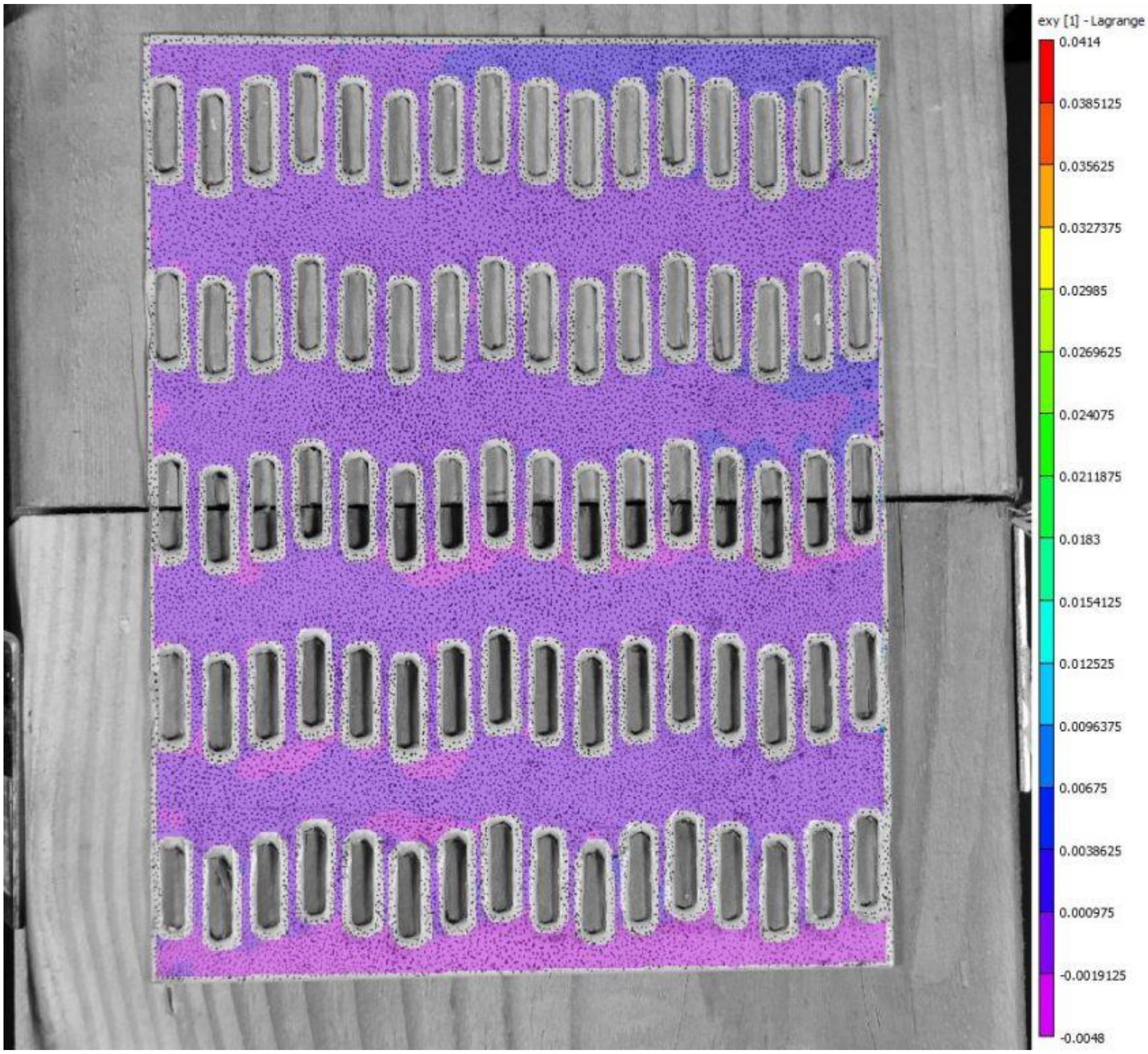

Figure 4-31: Full-field strain in x- direction (ε_{xx}) at 8,000 pounds

The strain (ε_{xx}) increases significantly by loading especially in the middle of the plate. Figure 4-32 shows the strain in x-direction for the image before failure at 8,600 pounds. The figure shows high compressive strain along the middle horizontal gap line. But the strain has fewer values in the top and the bottom of the middle horizontal gap line. The strain above the horizontal middle gap line is almost mirror to the strain (ε_{xx}) underneath this line.

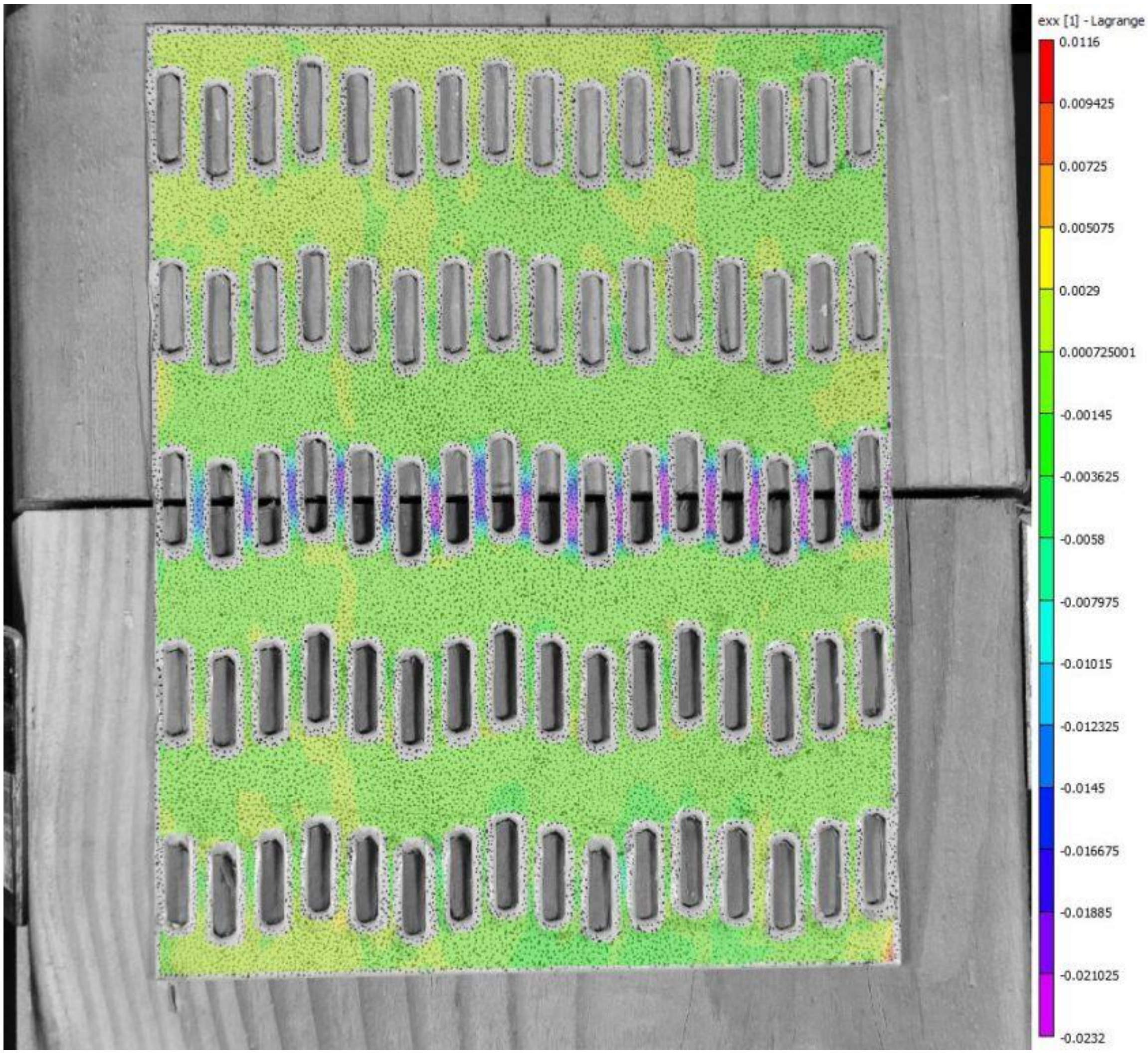

Figure 4-32: Full-field strain in x- direction (ε_{xx}) at load 8,600 pounds (the last image before failure)

The last image for full-field strain shows that the horizontal middle gap line of the plate has the highest tensile strain (ε_{yy}) and the highest compressive strain (ε_{xx}), which is a logical result. When a deformable body is subjected to an axial tensile force it will elongate and also contract laterally.

4.1.1.4.2 Numerical Analysis for the Results

To analyze the DIC results numerically, a vertical cross section line from the top of the plate to the bottom is taken for some images starting with the first image at 200 pounds and ending with the last image before failure. The cross section lines are taken in three different locations. Figure 4-33 shows the cross section lines on the metal plate surface.

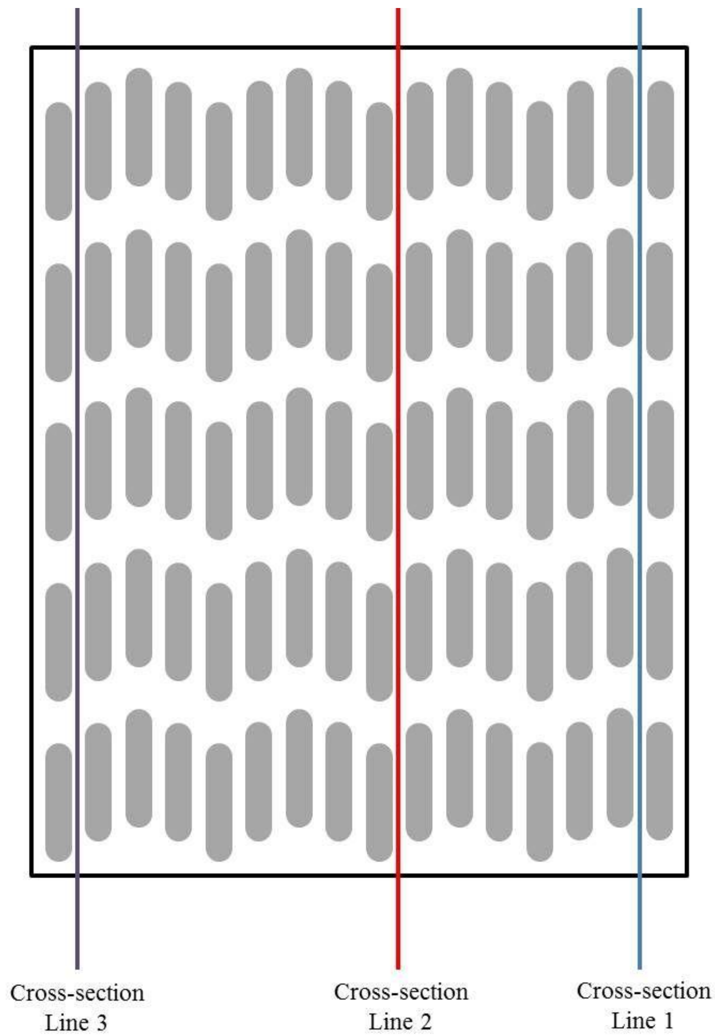

Figure 4-33: Metal plate with the three cross-section lines along the vertical direction

The three cross section lines are located on the plate surface as the following:

- The first cross section line (1-1) is from the right side of MPC @ x = 1.55 in.
- The second cross section line (2-2) is near the middle of the MPC @ x = 0.07 in. cross-section 2-2.
- The third cross section line (3-3) is from the left side of MPC @ x = -1.92 in.

Based on the three cross-section lines that are taken over the strain field (ε_{yy}), the next three Figures 4-34 to 4-36 show the distribution of strain (ε_{yy}) at three different locations for 14 images. Each image represents the value of the loading that is applied on the specimen of the two wood members connected by the metal plate connections.

The curves show that the first considered load is 200 pounds then the increment of loading is almost 1,000 pounds until the image at load 7,000 pounds, and then the increment of loading decreases to 400 pounds and then 200 pounds for the last five images. These changes in the increment of loading in the curves because the significant changes in the strain occur after applying 7,000 pounds. The last images before failure are the most important images that show the significant change in the plate under loading before failure occurs.

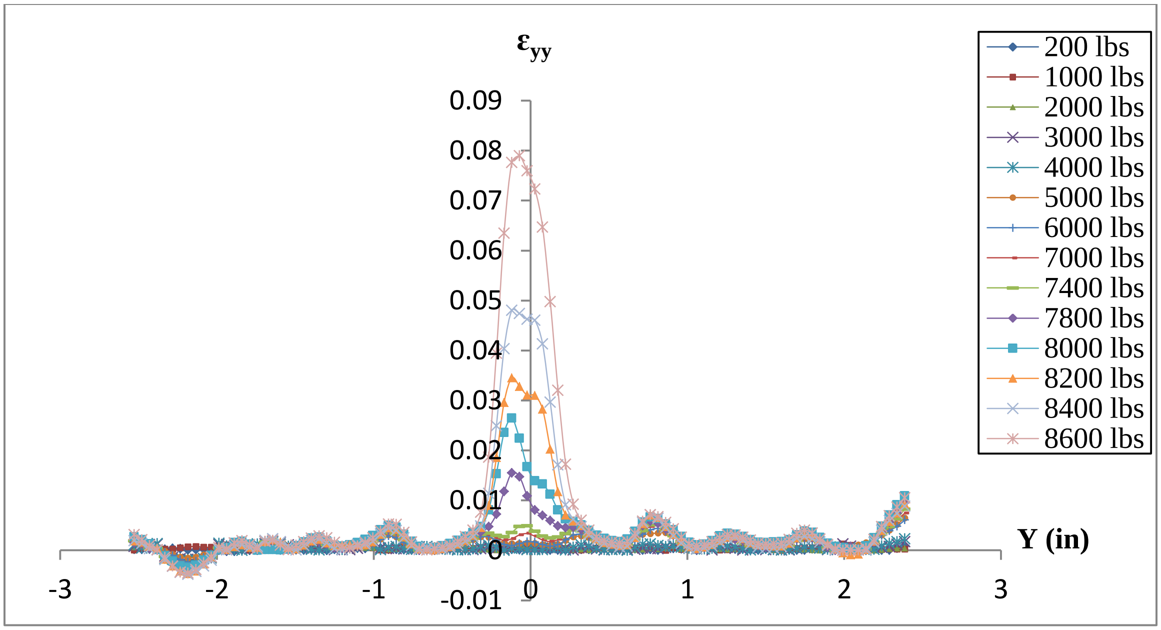

Figure 4-34: The strain distribution (ε_{yy}) along a cross section line (1-1) located on the right side of the plate

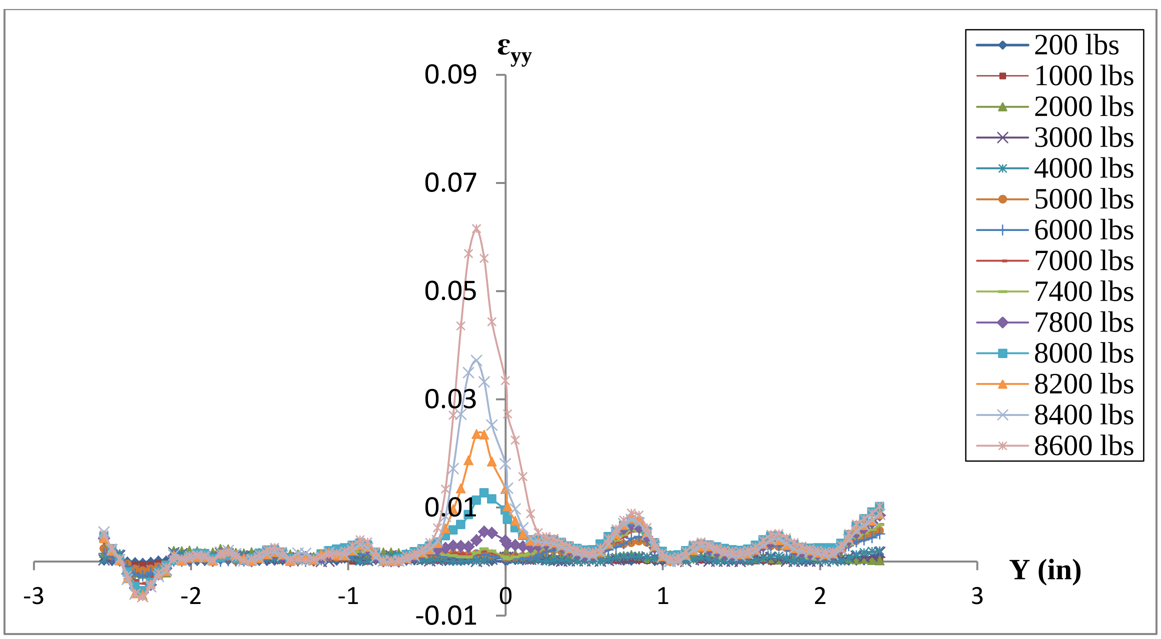

Figure 4-35: The strain (ε_{yy}) distribution along a cross section line (2-2) located near the middle of the plate

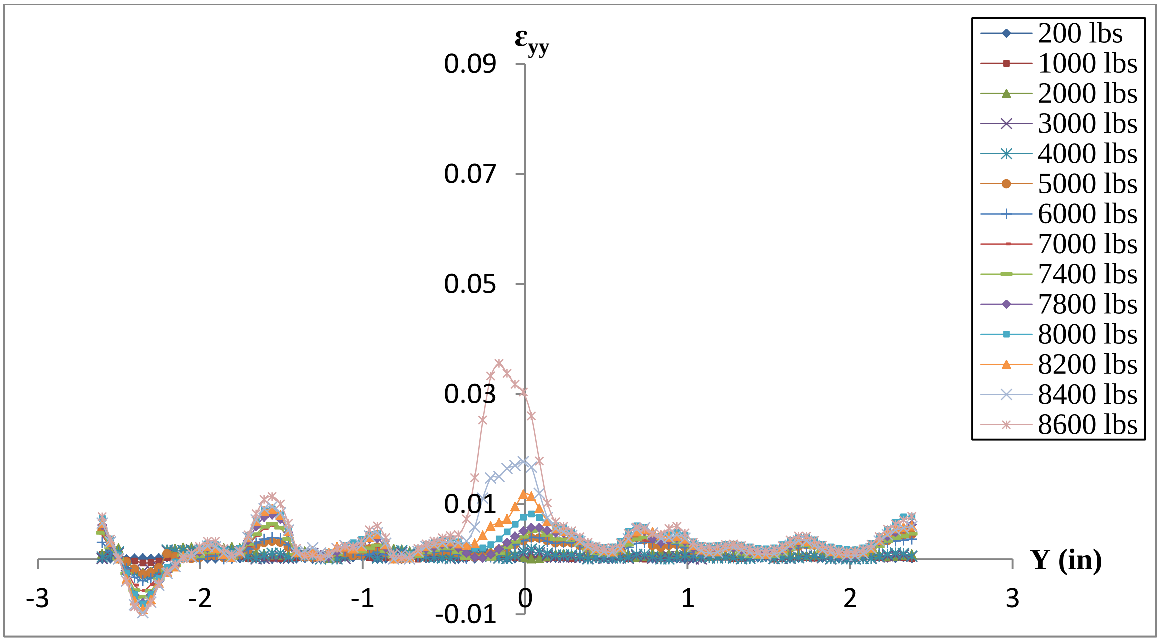

Figure 4-36: The strain (ε_{yy}) distribution along a cross section line (3-3) located on the left side of the plate

The strain distribution over the surface of the MPC (based on the full-field strain measurements and the cross sections lines) displays very low values and almost equal strain values are observed all over the surface of the metal plate. The strain on the upper part of the plate is almost mirror to the strain on the lower part of plate surface. The plate fails at a load of around of 8,640 pounds. The total images for this test are 43 images. The previous cross section curves show that the plate starts to yield and the strain becomes significant at image 40, which is at a load equal to 7,400 pounds. Then the strain on the horizontal middle gap line of the plate's surface increases significantly with loading until the failure.

The curves show some rotating and repeating spike from the top to the bottom of the plate and the strain is not a flat strain. These spikes are due to many factors such as the change in the cross sectional area through the entire plate because of the presence of the slots. The slots also are not distributed horizontally but they are distributed in a wavy shape. Since the wood is a non-homogeneous material, the properties of wood are different from one position to another. The angles of the teeth that are embedded in the wood are not the same for the entire plate teeth. These teeth can affect the strain values. Due to the above reason it can be seen that the strain is varying continuously.

The strain (ε_{yy}) shows high values along the first cross-section (1-1). The lowest strain values along the three cross-section lines are the left line section (3-3). The image before failure which is under the maximum load has the maximum strain (ε_{yy}) values in all of the cross-section lines. In the middle of each cross-section line, which represents the horizontal middle of the plate, the increase in strain is noticeable. The plate yields then tears in the middle. While the other parts of the plate is not near to yield point.

The direction of failure is evident. From the images, it can be seen that very high strain values occur on the right side of the plate and very low strain on the left side which explains the direction of failure.

On the other hand, the metal plate also shows strain in x-direction (ε_{xx}). The strain (ε_{xx}) along y-direction for the cross-section lines (1-1), (2-2) and (3-3) is also found in the next Figures 4-37, 4-38 and 4-39.

The figures show that the strain (ε_{xx}) possesses the highest compressive strain values on the area of the highest tensile strain (ε_{yy}) values on the horizontal middle gap line of the plate. The previous three figures for the strain (ε_{yy}) show that the tensile strain is high in the middle of the plate, compared to the strain (ε_{xx}) in x-direction it is the highest compressive strain in the same place.

The strain (ε_{xx}) in the middle of the plate is negative strain which denotes compressive strain. This occurs in the first cross-section line (1-1) at load 7,400 pounds where the strain (ε_{xx}) possesses negative values along the horizontal middle line of the plate. However, the strain (ε_{xx}) is positive and negative over the entire plate. The tensile strain areas are distributed on the areas that are close to the high negative strain in the middle. High compressive strain (ε_{xx}) along the horizontal middle of the plate surface especially in the last five images is clearly shown in the next three figures.

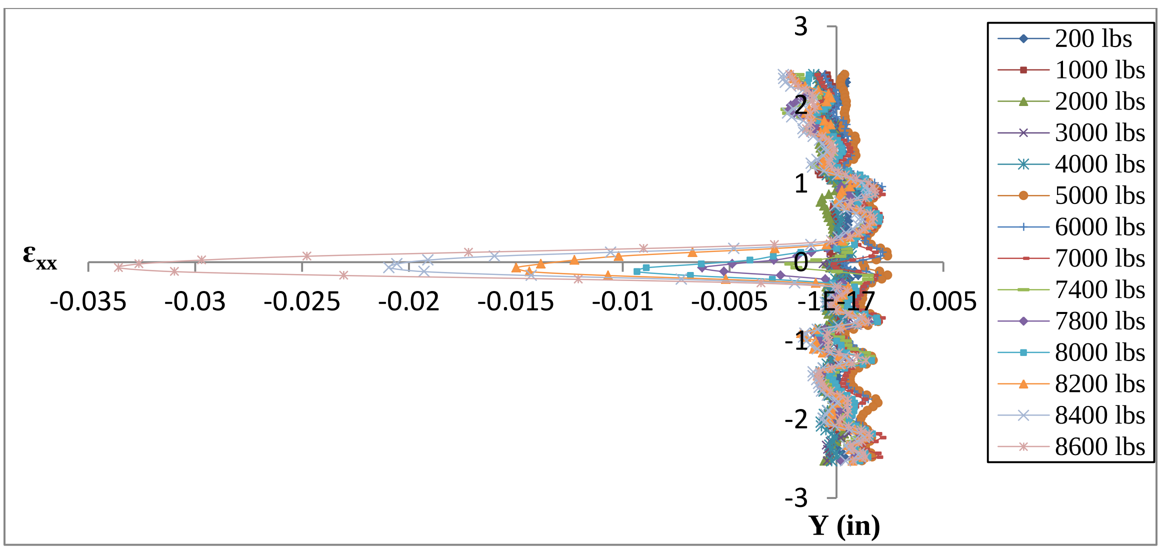

Figure 4-37: The strain distribution (ε_{xx}) along a cross section line (1-1) located on the right side of the plate

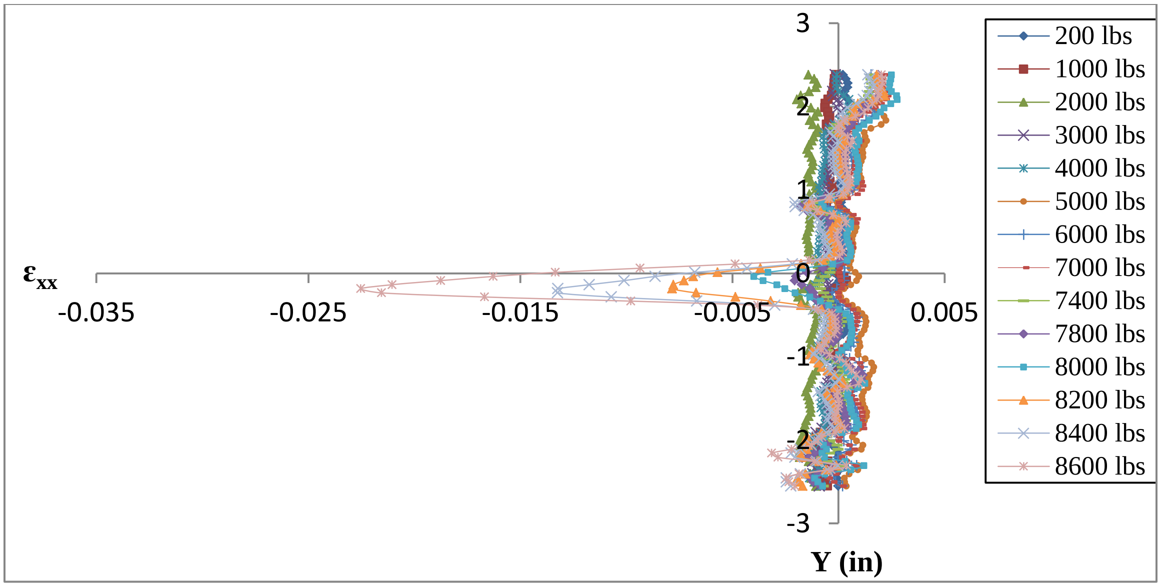

Figure 4-38: The strain (ε_{xx}) distribution along a cross section line (2-2) located almost on the vertical middle of the plate

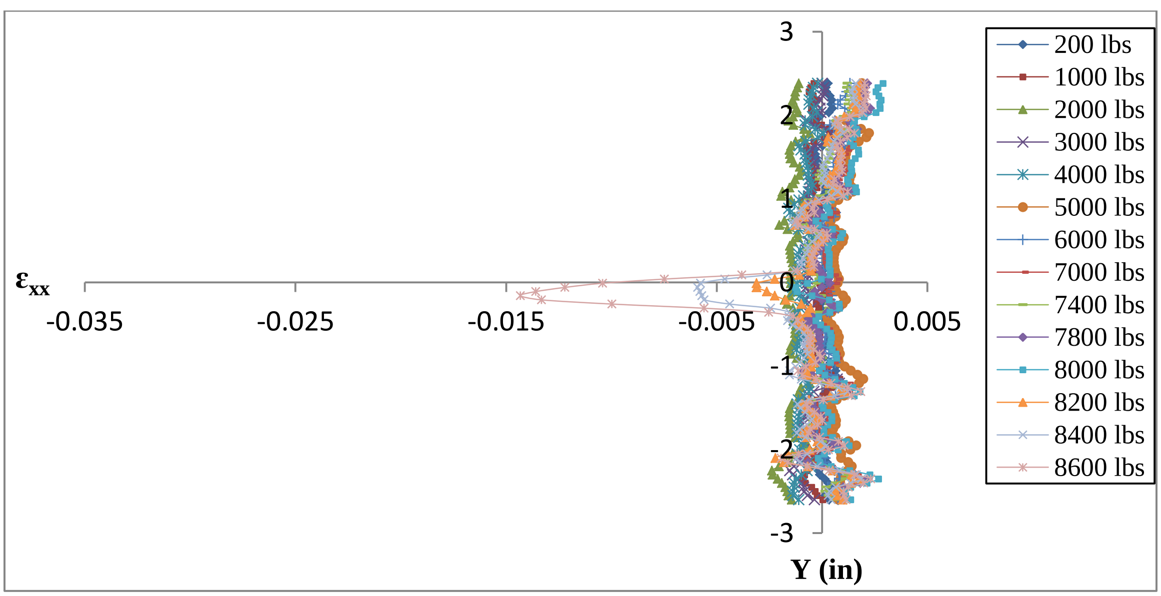

Figure 4-39: The strain (ε_{xx}) distribution along a cross section line (3-3) located on the left side of the plate

The last section line (3-3) possesses the lowest compressive-strain (ε_{xx}) values in the horizontal middle of the plate where the two wood members are connected. The cross-section line (1-1) possesses the highest compressive-strain (ε_{xx}) values along the same area. The changes in strain in the images between compressive and tensile strain are due to some pulling out of the plate and the teeth out of wood. Therefore, it is obvious that before failure the middle of the plate shows the most uniform compressive strain over the surface of the plate. In general, the strain (ε_{xx}) displays a significant change in the middle of the plate after applying 7,400 pounds.

In general, the shape for the strain (ε_{xx}) is opposite to the shape of the strain (ε_{yy}) along the horizontal middle of the plate. This agrees well with the digital image correlation results. The strain (ε_{xx}) is high as a compressive strain then the strain (ε_{yy}) is high as a tensile strain along the horizontal middle gap. The rest areas of the plate are controlled by the teeth. The teeth's gripping is still strong and this is shown on the plate full-field strain and the strain curves. The strain curves shows spikes in the strain curve and these repeat along the cross section line. These changes are due to the presence of the slots which makes the cross sectional area also different. The teeth shear strength are losing their shear affect along the horizontal middle gap line and it is obvious from the strain (ε_{xx}) and (ε_{yy}) curves and how the strain (ε_{xx}) is a compressive strain at that area and (ε_{yy}) is tensile strain. The strain (ε_{xx}) is quite clear. Therefore, to design the metal plate connection this strain (ε_{xx}) should be considered over the entire plate. The maximum compressive strain (ε_{xx}) is -0.033 on the right side surface of the plate.

4.1.1.4.3 A Comparison between the Strain in y and x Direction [(ε_{xx}) vs. (ε_{yy})]

In this section, the strain values {**(ε_{xx})** vs. **(ε_{yy})}** for the last image before failure at load 8600 pounds will be compared. The next Figures 4-40 and 4-41 show the three cross-section lines for the last image before failure at load 8,600 pounds for strain (ε_{yy}) and (ε_{xx}) respectively.

The curves for the lines show that the middle of plate has yielded. The upper and lower plate still has not yielded yet especially when compare it to the large increase in the strain values on the horizontal middle of the plate. Therefore, the local strain values are very high on the middle part of the plate. The cross sectional area in the middle is half of the plate's cross sectional area because of the slots. This change in the cross sectional area makes the failure easier in the middle than at any other place.

The figures show that there is a strain along x-axis (ε_{xx}) that should not be ignored. The general shape of strain in y-direction (ε_{yy}) is close to the shape of the strain in x-direction (ε_{xx}) but in the negative side. Both (ε_{yy}) and (ε_{xx}) have almost the same strain on the area of the plate above the horizontal middle gap line and beneath this horizontal line, however, they also have high strain in the middle of the plate in different directions. The maximum strain is in the right side of the plate as shown in cross-section (1-1). This explains the direction of the rupture in the plate. The failure starts from the right side then the middle then the left side which has the smallest local strain values. On the other hand, the strain (ε_{xx}) in the middle of the plate is compressive strain and possesses the highest compressive strain in x-direction where the steel has yielded and then ruptured. The strain (ε_{yy}) increases in the vertical direction with an

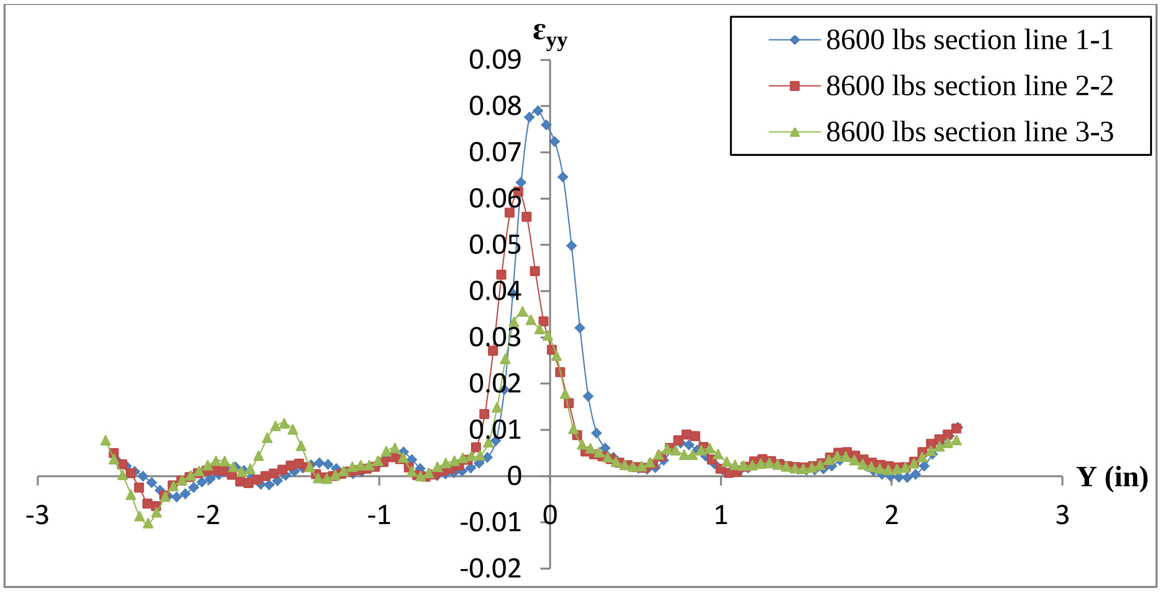

Figure 4-40: The strain (ε_{yy}) distribution along the three cross-section lines (1-1), (2-2), (3-3) for the last image before failure at load 8600 pounds

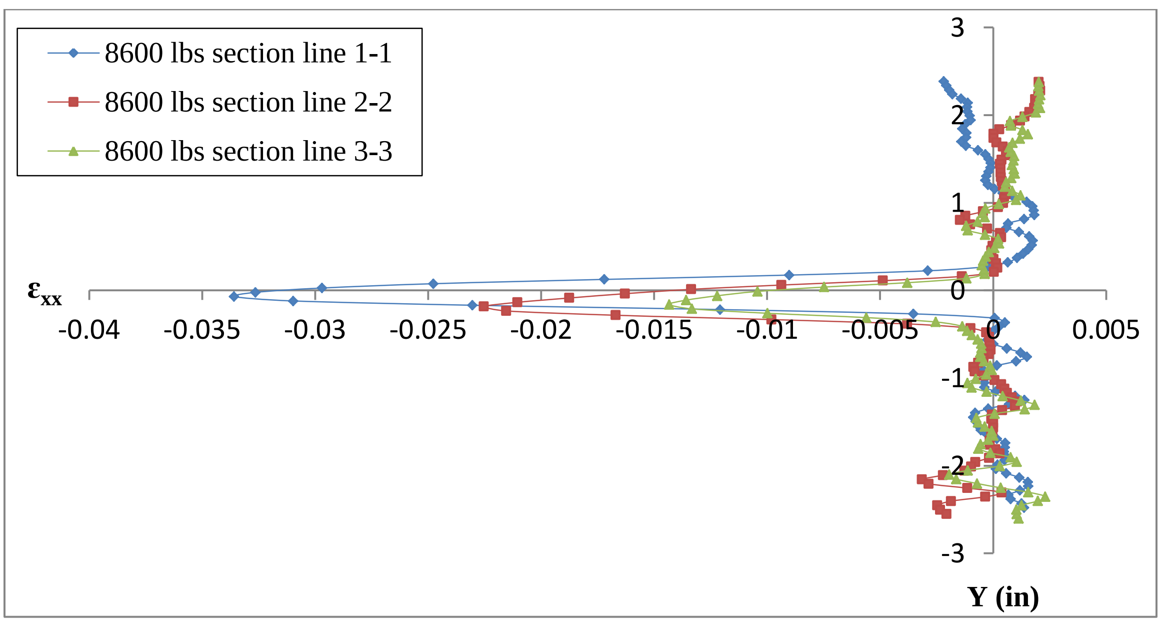

Figure 4-41: The strain (ε_{xx}) distribution along the three cross-section lines (1-1), (2-2), (3-3) for the last image before failure at load 8600 pounds

Increase slope from left to the right side. This exactly explains the rupture in the plate. The crack starts from the right side. The upper part of the plate moves with an increase slope from the left to the right. These results appear to be consistent and prove the validity of using the DIC technique to find the strain measurements behavior of materials.

In general, the metal plate in this test shows significant changes in the strain at approximately 7,400 pounds. The horizontal middle gap line along the middle of the plate shows high tensile strain (ε_{yy}) and high compressive strain (ε_{xx}). The rest region over the plate is in good shape and the teeth gripping are high when their strain values are compared to the middle strain values. The teeth are distributed in a wavy shape over the entire plate. The strain results show that the teeth are losing their control along the middle horizontal of the plate at the gap between the two wood members. The area of the plate along that line is half of the area in other regions because of the slots. The failure behavior is from the right to the left which proves the high tensile strain (ε_{yy}) and high compressive strain (ε_{xx}) from the right side that are obtained from DIC software. The other region over the plate is under control of the teeth as shown in the failure image.

4.1.1.5 Comparison between the Displacement from LVDT and DIC-Code

LVDT was used to verify the results from the digital image correlation software. The first test was done without using the LVDT. In the second test the LVDT was set on the right side of the specimen as shown in Figure 4-42. The curves show very close results. But in the third test, the LVDT was used for both sides of the specimen of wood members as shown in Figure 4-43 and 4-44. The DIC results measure the gap between the two wood members by counting for the pixels on that gap length.

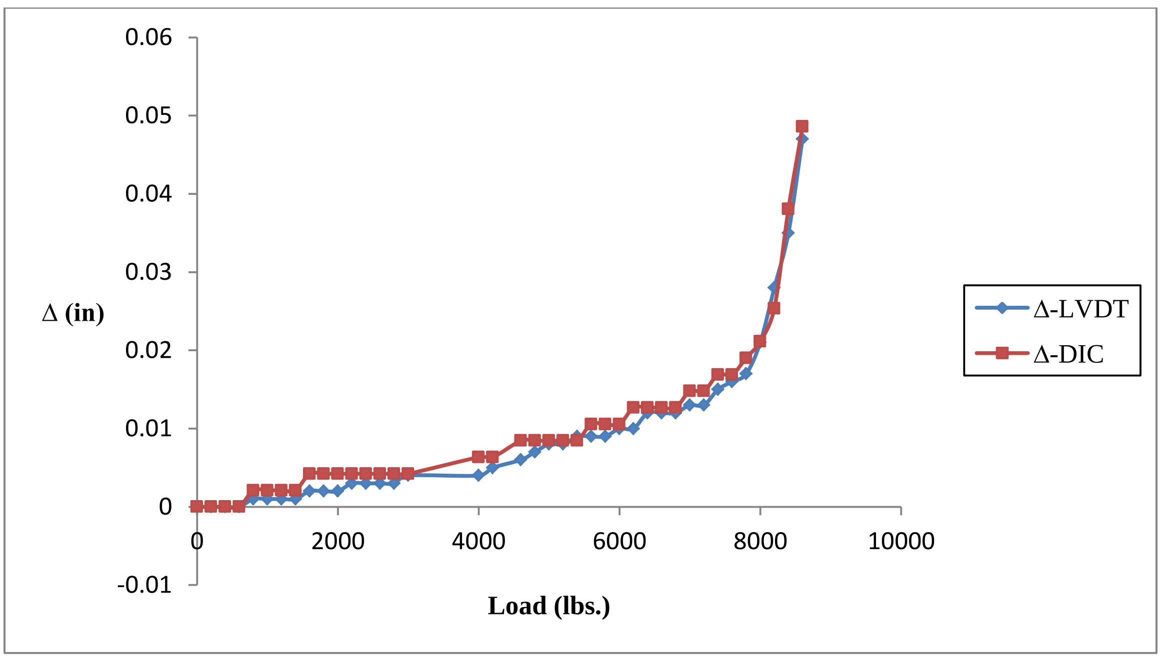

Figure 4-42: The displacement from LVDT vs. the displacement from DIC-code for the 2nd AA test –the right side gap

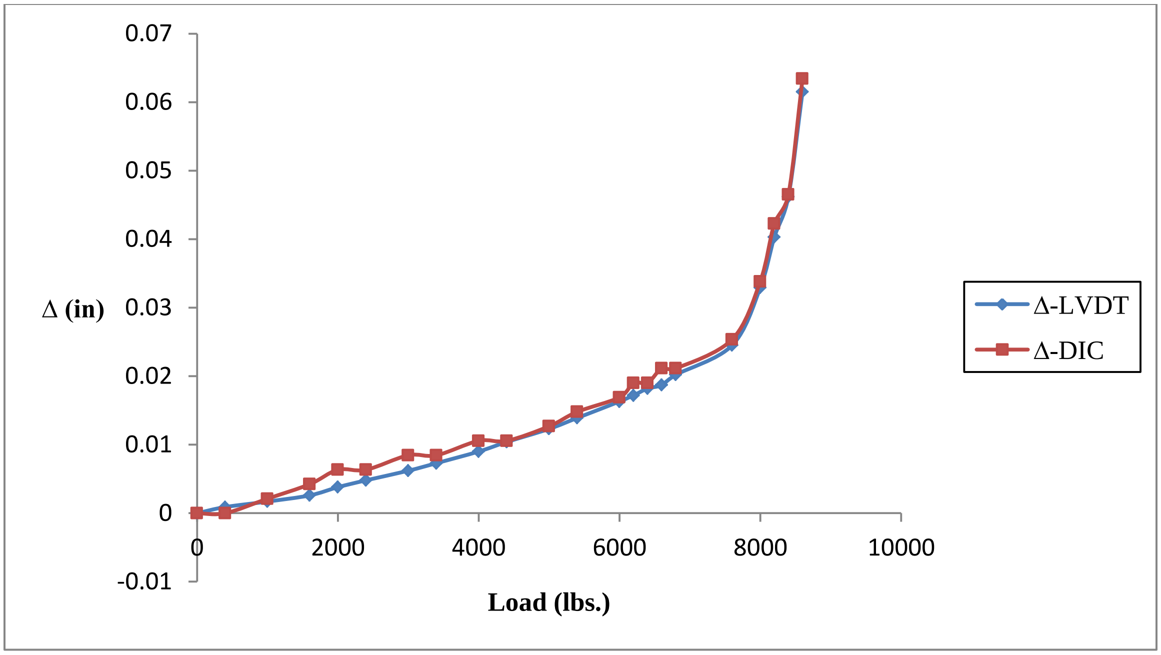

Figure 4-43: The displacement from LVDT vs. the displacement from DIC-code for the 3rd AA test –the right side gap

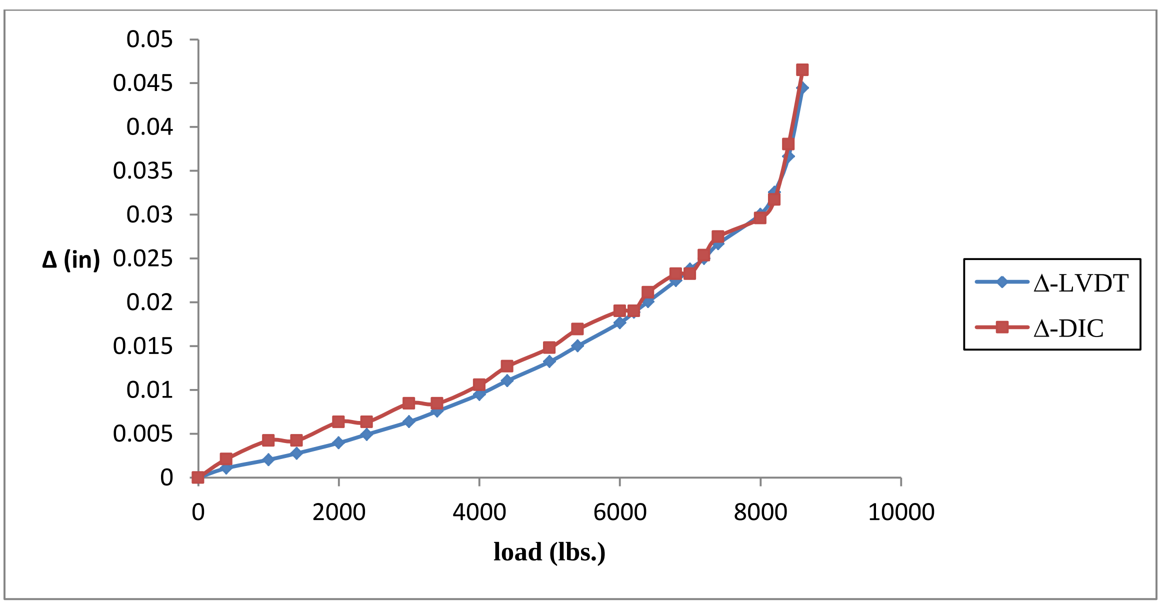

Figure 4-44: The displacement from LVDT vs. the displacement from DIC-code for the 3rd AA test –the left side gap

4.1.1.6 Manual Check to Confirm the DIC Strain in Test AA-1st

A Manuel check for the first tension joint test AA-1st has been done for the last image before the failure as shown in the next figure.

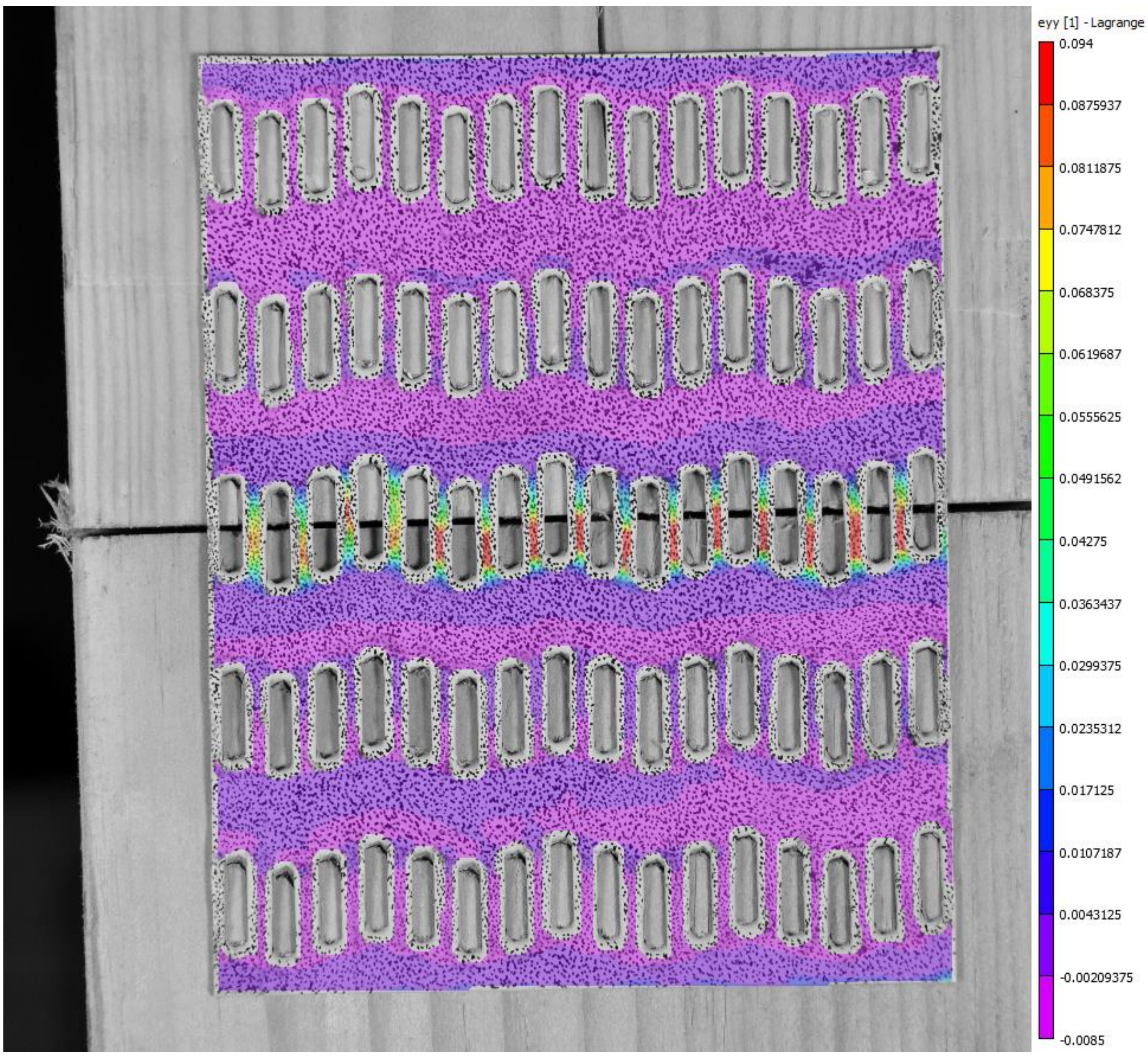

Figure 4-45: the last image before the failure for the first tension test AA-1st

In the embedded image, I've chosen a region on the deformed image where there is a very high strain as shown in figure 4-46. Choose two speckles (relatively far from each other) in the red and yellow region and write down their pixel coordinates (X,Y).

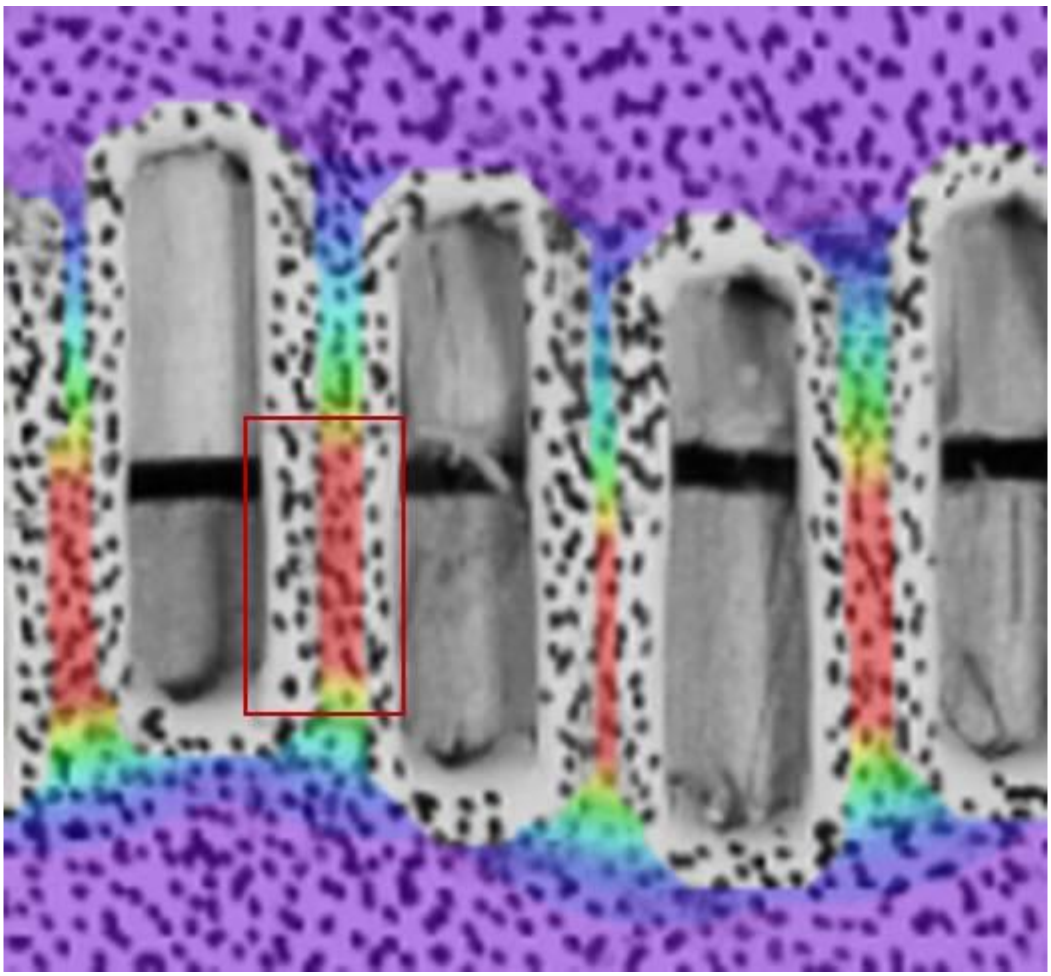

Figure 4-46: Choose a region on the deformed image of AA-1st

On the reference image, zoom in on the same location where there is a maximum stress in the deformed image and write down the pixel coordinates of the same speckles.

Then do the following calculations:

V_1 = Y coordinate of speckle 1 on deformed image { $Y_{1(D)}$} – Y coordinate of speckle 1 on reference image { $Y_{1(R)}$ } as the following

$$V_1 = Y_{1(D)} - Y_{1(R)}$$

V_2 = Y coordinate of speckle 2 on deformed image { $Y_{2(D)}$} – Y coordinate of speckle 2 on reference image { $Y_{1(R)}$} as the following.

$$V_2 = Y_{2(D)} - Y_{2(R)}$$

Then,

$$dv = V_2 - V_1$$

$$dy = Y_{2(R)} - Y_{1(R)}$$

$\boldsymbol{\varepsilon}_{yy}$ = (V_2 – V_1) / (distance between speckle 1 and 2 on ***reference image***).

$$\varepsilon_{yy} = \frac{dv}{dy}$$

The next table shows the points and the coordinates then the strain is calculated.

Table 4-1: the two chosen points coordinates and the strain calculations AA-1st

	Reference image (Pixel)	Deformed image (Pixel)
Y_1	549	542
Y_2	578	573

V_1 =	-7
V_2 =	-5
$dV=V_2-V_1$ =	2
$dy = Y_2(R.) - Y_1(R.)$ =	29
ε_{yy}=dv/dy =	**0.068965517**

The strain ε_{yy} is 0.06896 which is almost equal to the strain that found from DIC image by checking the earlier full-field strain images.

4.1.1.7 The AA-Tests Summary and Discussion

Three AA tests were conducted in the lab. The specimens were loaded until failure. A Nikon digital camera was used to capture images every 200 pounds of loading. All the captured images were implemented in digital image correlation software Vic-2D. All the three tests failed at the plate. The plate had split into two parts as a result of tensile force influence. Tables 4-2, 4-3 and 4-4 show a brief description for each test.

Table 4-2: Brief description for each test-AA

AA-Test #	**Failure load (lbs.)**	**Total Deformed Processed Images by DIC Code**	**Failure Behavior Description**
1	8,550	42	plate failure/ plate was ruptured along the horizontal middle gap line from right side
2	8,650	43	plate failure/ plate was ruptured along the horizontal middle gap line from right side
3	8,640	43	plate failure/ plate was ruptured along the horizontal middle gap line from right side

Table 4-3: Brief comments for each test-AA

AA Test #	**Comments on the Test and the Failure**
1	The available captured images are 43 images plus the reference one. The last image at failure was not processed by DIC-code due to complete split of the plate into two halves.
2	The available captured images are 44 images plus the reference one. The last image at failure was not processed by DIC-code due to complete split of the plate into two halves.
3	The available captured images are 44 images plus the reference one. The last image at failure was not processed by DIC-code due to split of the plate into two halves.

Table 4-4: Brief strain changes description for each test-AA

AA-Test #	**The Strain (ε_{yy}) Changes**
1	the change of the strain starts at load 6,000 pounds but it is very clear at 7,000 pounds in which the strain starts to show some changes along the middle horizontal line of the plate above the gap.
2	the change of the strain starts at load 6,000 pounds but it is very clear at 7,000 pounds in which the strain starts to show some changes along the middle horizontal line of the plate above the gap.
3	at load 7,400 pounds the strain starts to show some changes along the middle horizontal line of the plate above the gap.

The previous tables describe the behavior of each plate under tensile load until failure. The entire three specimens failed in the same way by splitting the plate along the horizontal middle gap line from the right side of the plate. The dominant strain (ε_{yy}) is tensile strain. At an average of 7,000 pounds, the strain along the horizontal middle line changes and a curvature is observed in the strain curves. Then the strain curvature increases with loading until the failure. The strain curvature of the three tests shows a sharp rise between the maximum strain (ε_{yy}) value at the middle of the plate and another strain above or below the horizontal middle gap line. In one of the tests the increase in the maximum value with respect to other strain (ε_{yy}) value at last image before the failure is 572.3%. The strain curves show several spikes in the strain curves along the vertical cross section lines. These spikes are due to the change in the cross sectional area of the plate because of the presence of the slots. Moreover, the slots also are not distributed horizontally but they are distributed in a wavy shape. Wood is anisotropic material and its mechanical properties vary in each direction. The angles of the teeth that are embedded in the wood are not the same for the entire plate. These teeth can affect the strain values.

The strain curves are not flat curves or linear curves. The strain curves contain spikes along the vertical direction lines due to the presence of the slots on all the plate' s surface. In general, the shape for the strain (ε_{xx}) is opposite to the shape of the strain (ε_{yy}) along the middle horizontal gap line of the plate. This proves the digital image correlation results. When the strain (ε_{xx}) is high as a compressive strain, the strain (ε_{yy}) is high as a tensile strain at the same area. The other areas of plate in general are influenced by tensile strain (ε_{yy}) and tensile strain (ε_{xx}). Although the middle horizontal line gap of the plate is holding high compressive strain (ε_{xx}) and high tensile strain (ε_{yy}). This result show that the strain with loading is still under the influence of the shear force from the teeth.

The strain curves show that the strain possesses the highest tensile (ε_{yy}) and the highest compressive strain (ε_{xx}) along the horizontal middle gap line of the plate at load 8,600 pounds or 8,400 pounds in the last three tests before the failure. This confirms when a deformable body is subjected to an axial tensile force it will elongate and also contract laterally.

The strain curves show that the strain is high in the middle and the right side of the plate's surface along the horizontal middle gap line. This exactly explains the rupture in the plate. The plate has failed due to split of the plate into two parts along the horizontal middle gap line. The gap between the two wood members is higher in the right and the middle side than the left side. These results are logical and prove the validity of using the DIC technique to find the strain measurements behavior of materials. The strain behavior explains the failure behavior of the plate.

The rest region of the plate above and underneath the horizontal middle gap line is in very good shape and the teeth gripping are high comparing their strain values to the middle strain values. The presence of the teeth wavy-distributed over the entire plate makes low strain values in both directions. The strain results show that the teeth are having very strong gripping with wood. The failure occurs along the horizontal middle where the area of the plate along that line is half of the area in other regions because of the slots. The two wood members are connected at a gap between them so the connection tends to fail along this gap. The failure behavior is from the right to the left which proves the high tensile strain (ε_{yy}) and high compressive strain (ε_{xx}) from the right side that are obtained from DIC software. The other region over the plate is still under control of the teeth as shown in the failure image.

The displacement of the gap between the two pieces of wood was found using the DIC Vic-2D software based on the number of pixels in the vertical direction in each image under loading. Then the calibration from the software is used to change the pixels to inches. The calibration factor is 0.002113. The results from the LVDT are used to compare the displacement of the gap from LVDT to the displacement that is found using the digital image correlation software Vic-2D. The results are not identical between the two methods but they are very close. Many factors can affect the difference between the DIC method and the LVDT. In DIC, the pixels are counted based on the image and the surface while the LVDT will measure the displacement from the middle of the wood side. Also, the resolution of images plays an important role in the accuracy of pixels numbers. The manner in which the LVDT is placed may also have affected the results.

4.1.2 AE–Test

In AE- tension test the tension load is parallel to the plate slots or the plates' major axis but perpendicular to the wood grain as shown in Figure 4-47. Three specimens of two members of wood are connected by a metal plate connector. After seven days, the specimens were tested under tension force in the in the civil engineering lab using the universal testing machine.

The LVDT machine is used to verify the results from the digital image correlation software. Two LVDT machines are used one on the right side of the joint and the other on the left side of the joint. The displacements between the two connected wood members at the gap can be measured by LVDT machine at different loading stages.

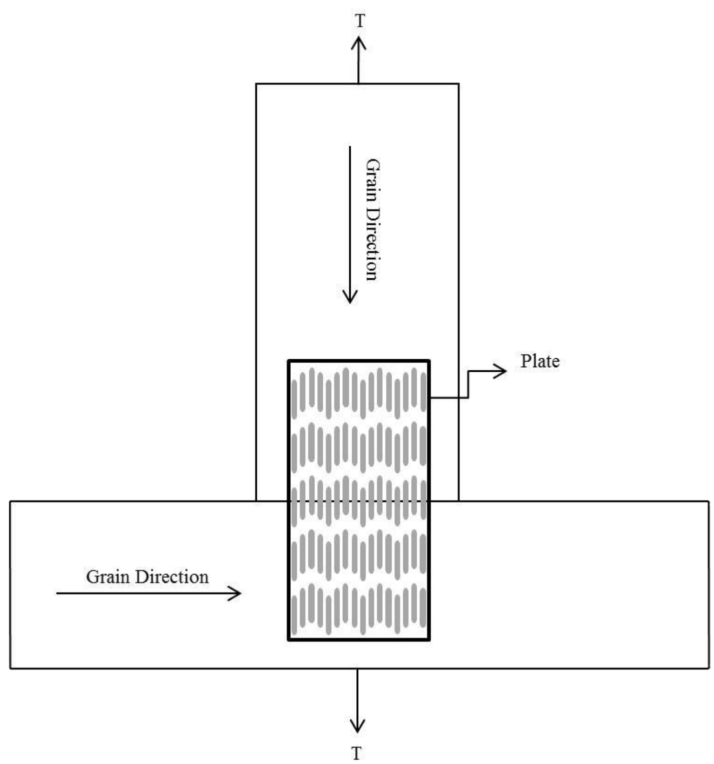

Figure 4-47: AE- sample test shape

4.1.2.1 Plate's axis direction

The direction of the x and y axis was obtained from the digital image correlation software as shown in the next two Figures 4-48, 4-49.

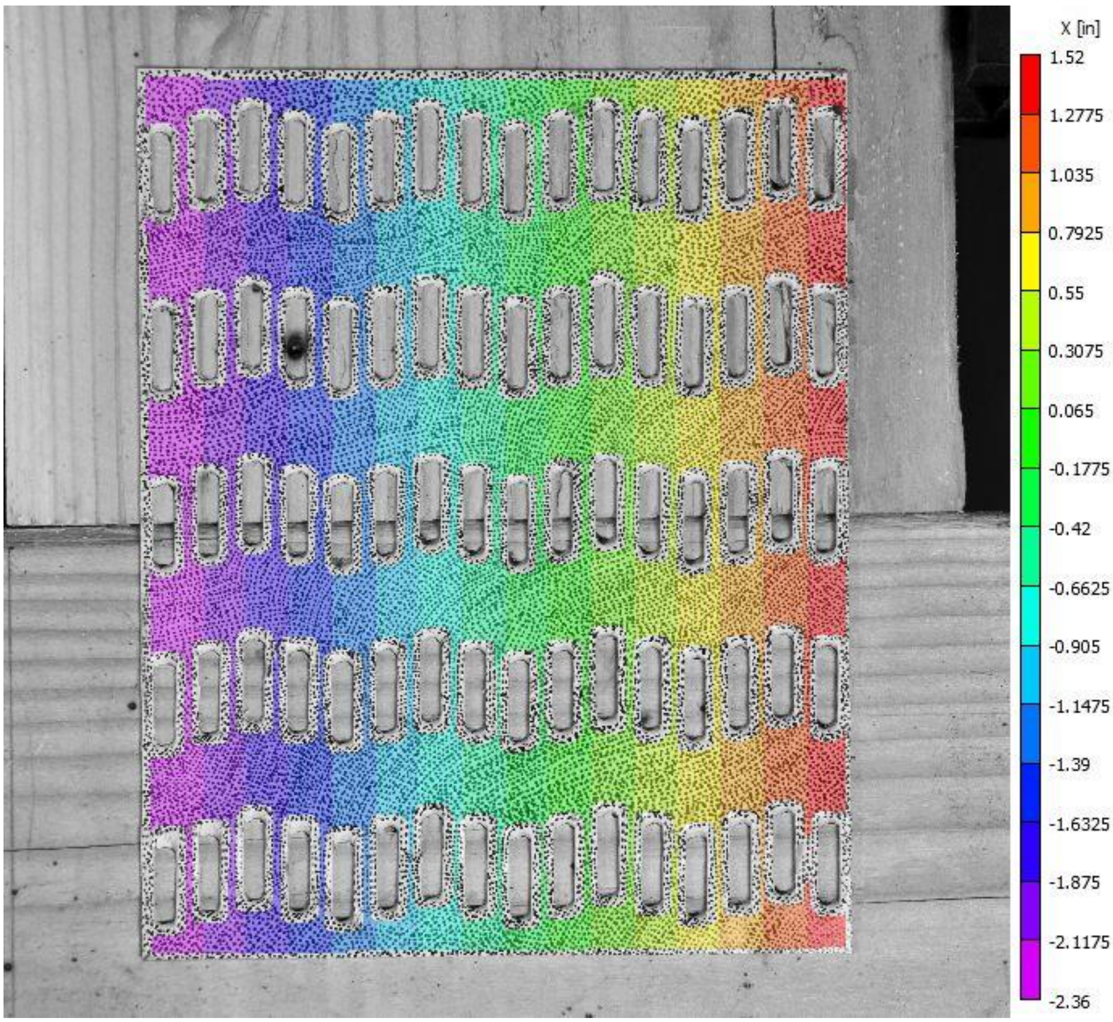

Figure 4-48: x-axis coordination system obtained from DIC software

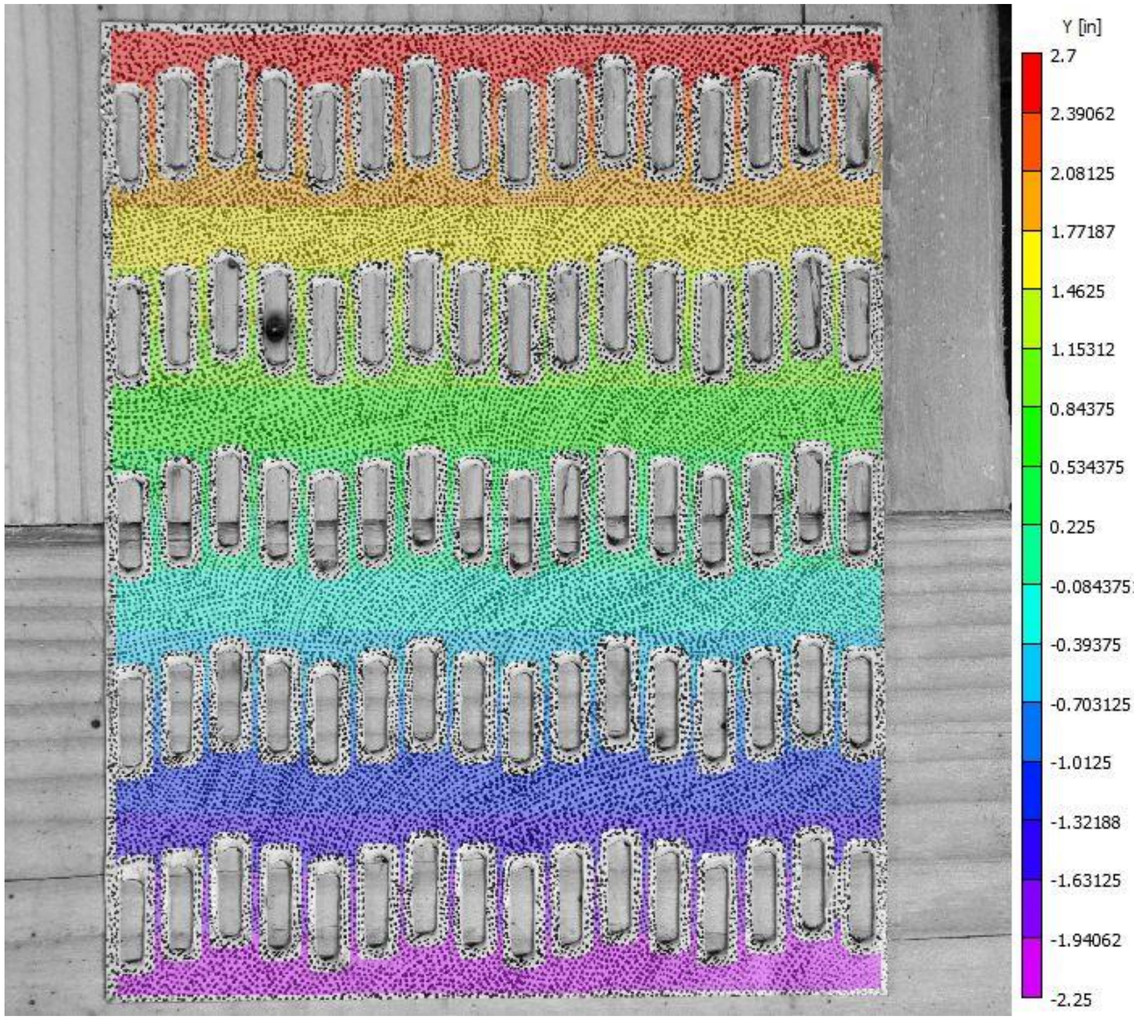

Figure 4-49: y-axis coordination system obtained from DIC software

4.1.2.2 The First Tension Test (AE-1^{st})

In this test, the two members of wood were connected by the MPC. The specimen was set on the universal testing machine. The first reference image was taken before applying any load. Figure 4-50 shows the first image which is considered as the reference image in digital image correlation technique.

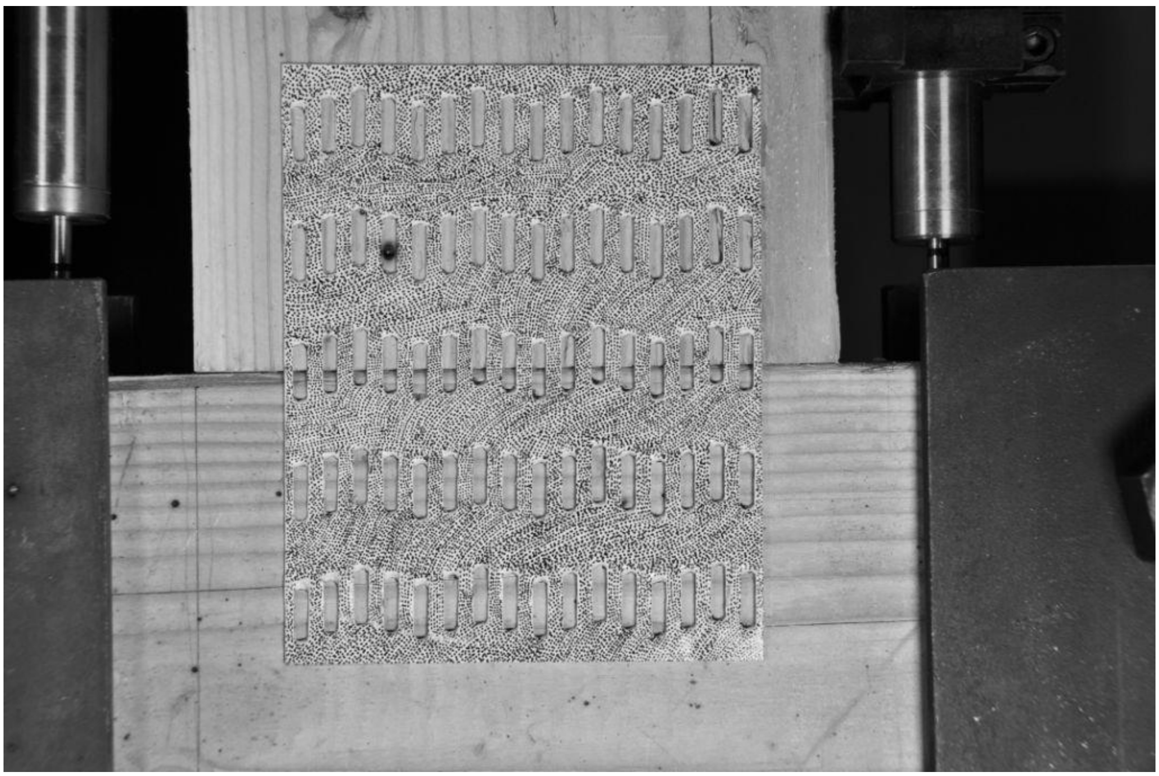

Figure 4-50: First image / reference image

After the first reference image was taken at load zero, the load was increased on the specimen until failure. The camera was placed on a fixed place and the MPC was perpendicular to the camera's lenses. Images were taken for the MPC specimen at each load increment of 200 pounds until failure. The failure in the member occurred in the wood. Figure 4-51 shows the last image at the failure.

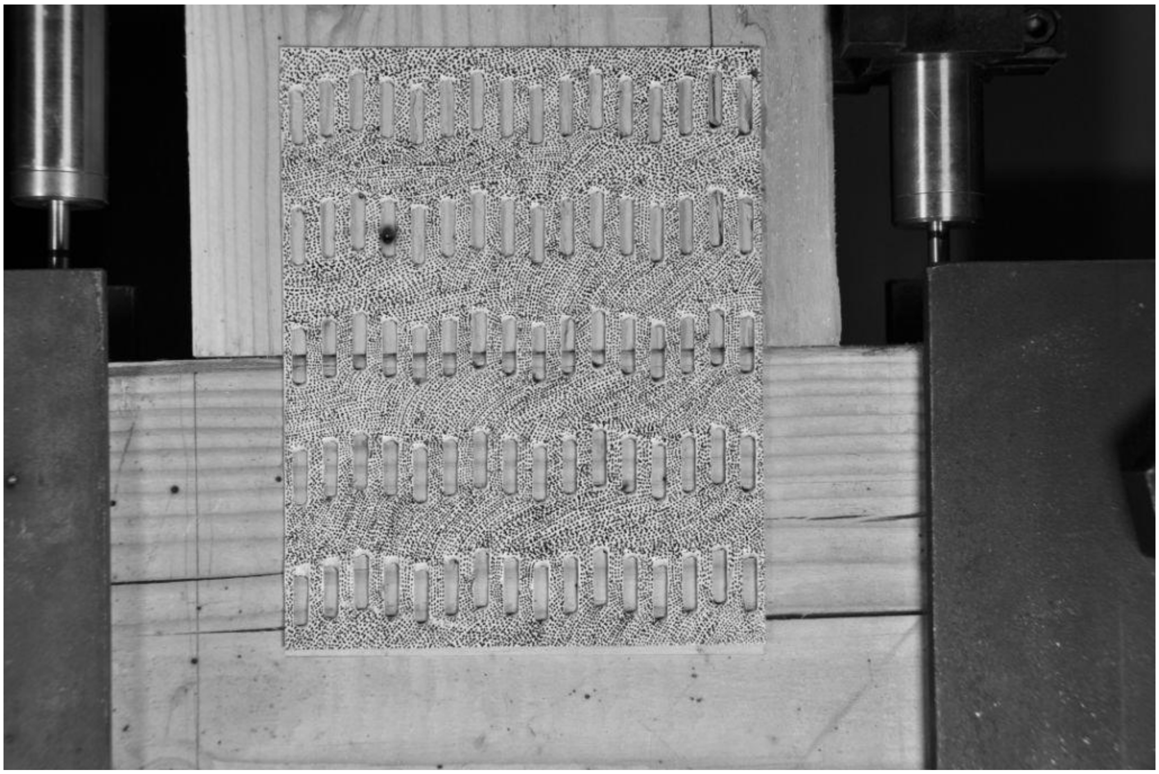

Figure 4-51: The last image at the failure

Ten (10) images were taken in addition to the reference image. The metal plate did not fail directly; however, some places had tooth withdrawal. The main reason for failure was wood cracks. The wood failed at load equal to 1940 pounds. The bottom wood member had cracked horizontally. The captured images were implemented in DIC-software to find the full-field strain measurements.

4.1.2.2.1 Analysis of the Full-Field Strain Results That Obtained From DIC Software

All the test images, which were obtained from the lab test, were implemented in the digital image correlation software Vic-2D. Each image was analyzed in relation to a reference image. Each deformed image was compared to a non-deformed reference image. The full-field strain measurements were obtained from the digital image correlation software. Figure 4-52 shows the strain (ε_{yy}) at 200 pounds.

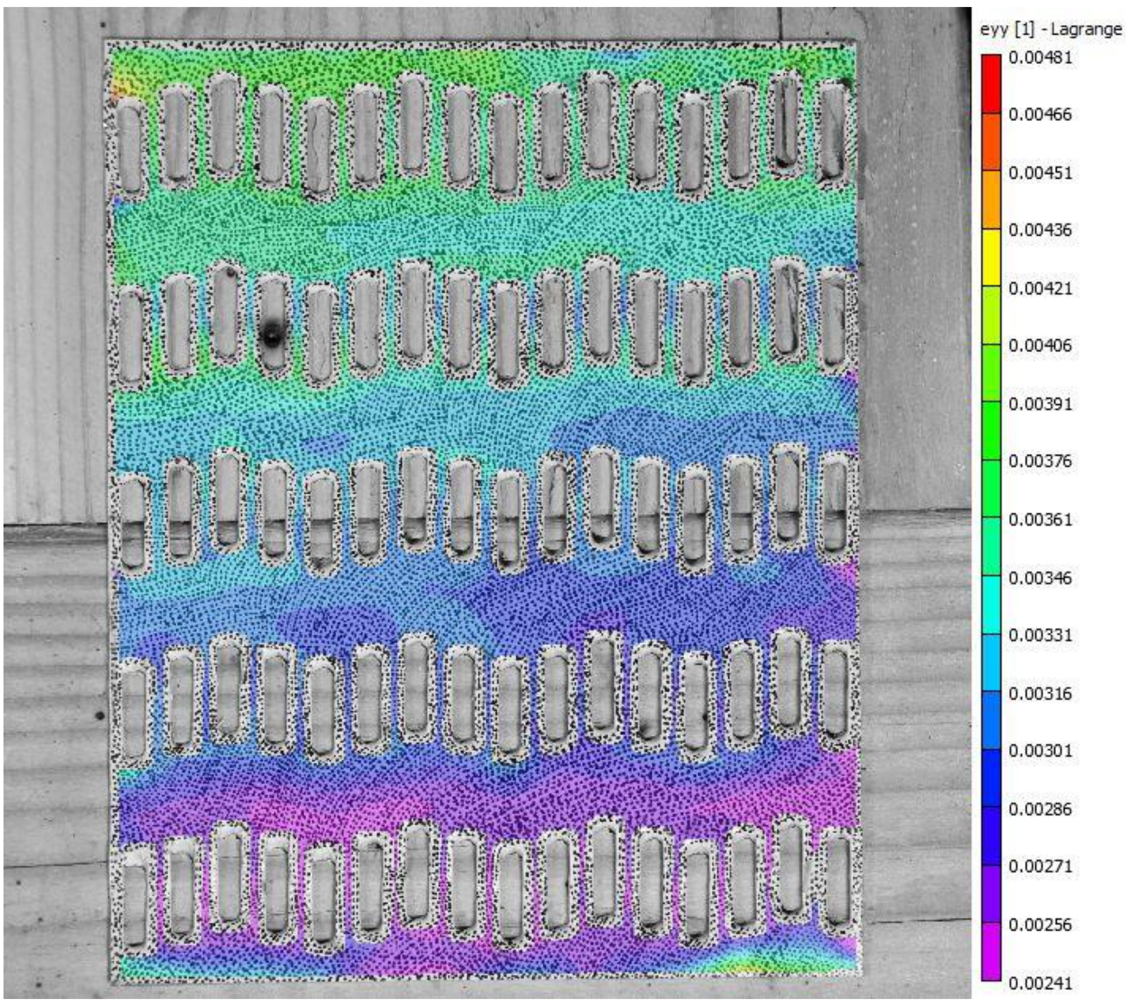

Figure 4-52: Full-field strain measurements (ε_{yy}) for the MPC at 200 pounds

The strain field's results show different levels of color and shows that each level of color represents a number. The failure in this test was in the bottom wood member so the changes in the strain over the surface of the plate are not that significant. But DIC software can be used to show the changes in strain under different low loading increments. The previous figure shows that the strain (ε_{yy}) is a tensile strain over the entire plate and that it is almost uniform over the entire plate's surface after applying 200 pounds. The strain values fluctuate over the entire plate's surface. The range of strain is in between 0.002 and 0.003. The strain above the horizontal middle gap line is slightly higher than the strain underneath this line with high strain near the edge of the plate.

Loading the strain (ε_{yy}) increases the values uniformly. From load 200 pounds until 600 pounds the full-field strain measurements show an increase in the strain values over the entire plate. Figure 4-53 shows the full-field strain measurements for the image at load 600 pounds. The average strain values are almost 0.004. The difference of strain (ε_{yy}) above and below the horizontal middle gap line is less than the difference of the strain at 200 pounds. After 600 pounds the strain (ε_{yy}) shows a decrease in the strain values until load 1,600 pounds. At 1,600 pounds the full-fields strain measurements shows an increase in the strain (ε_{yy}) until the strain at failure at 1,940 pounds. The strain at 1,940 pounds on some areas of the plate shows lower values than the strain at 600 pounds. The load 1,940 pounds does not represent the failure load for the plate. The plate is still in good conditions and the teeth maintain their grip as shown in the failure image. However, the strain results from digital image correlation can show the behavior of the plate's strain at very low loadings before any sign of failure.

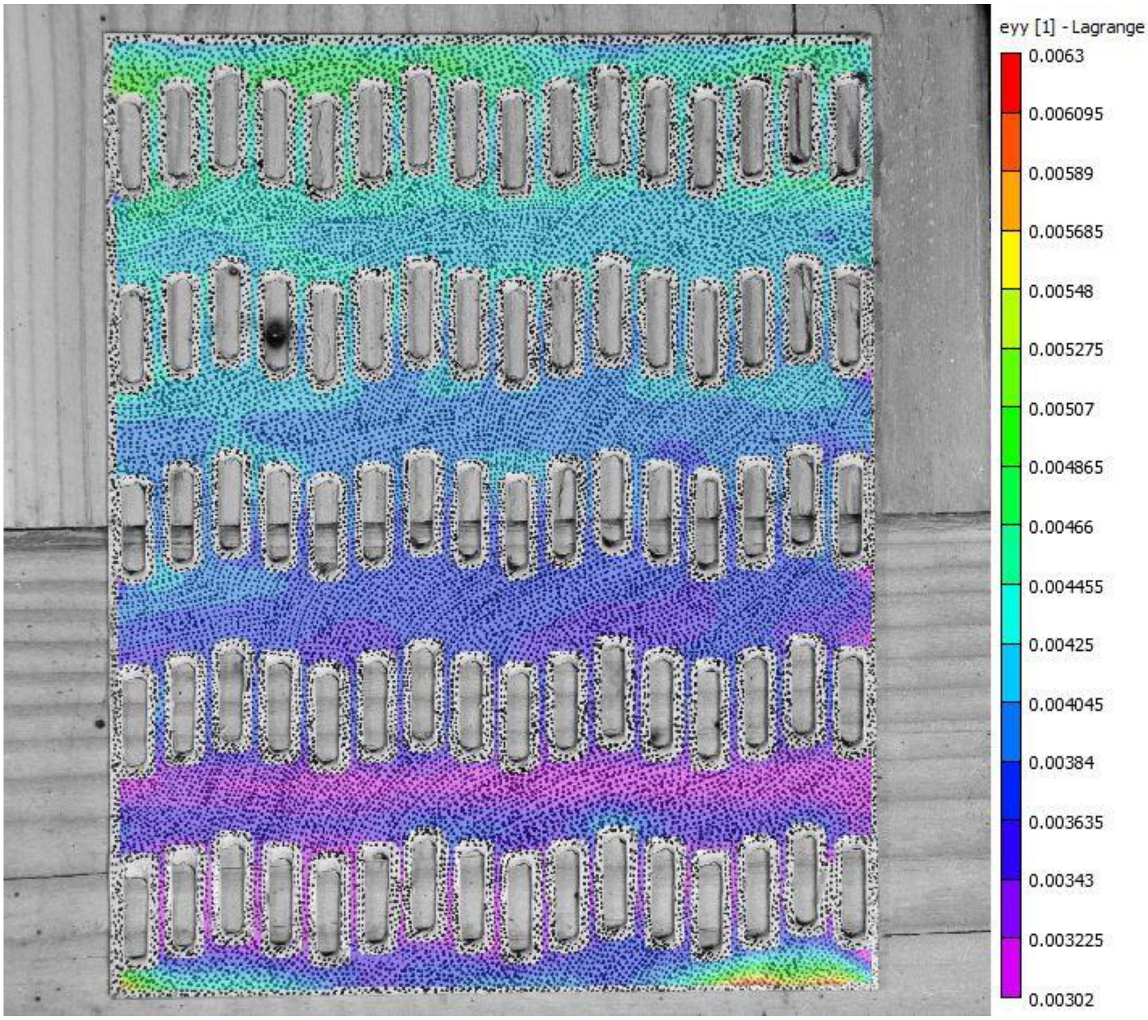

Figure 4-53: Full-field strain measurements (ε_{yy}) at 600 pounds

The bottom wood member, which holds the grain that is perpendicular to the tension force, failed first. The images show that there are two horizontal cracks in the bottom wood member. Both cracks are under the plate in the bottom. These cracks caused some tooth withdrawal through the test especially the bottom crack. The full-field strain figures show the change in the strain's color and values due to the presence of the crack. The lower crack is more effective and wider than the upper one and so failure has occurred in the bottom wood member due to this bottom horizontal crack. The full-field strain measurement for the image at the failure is shown in Figure 4-54.

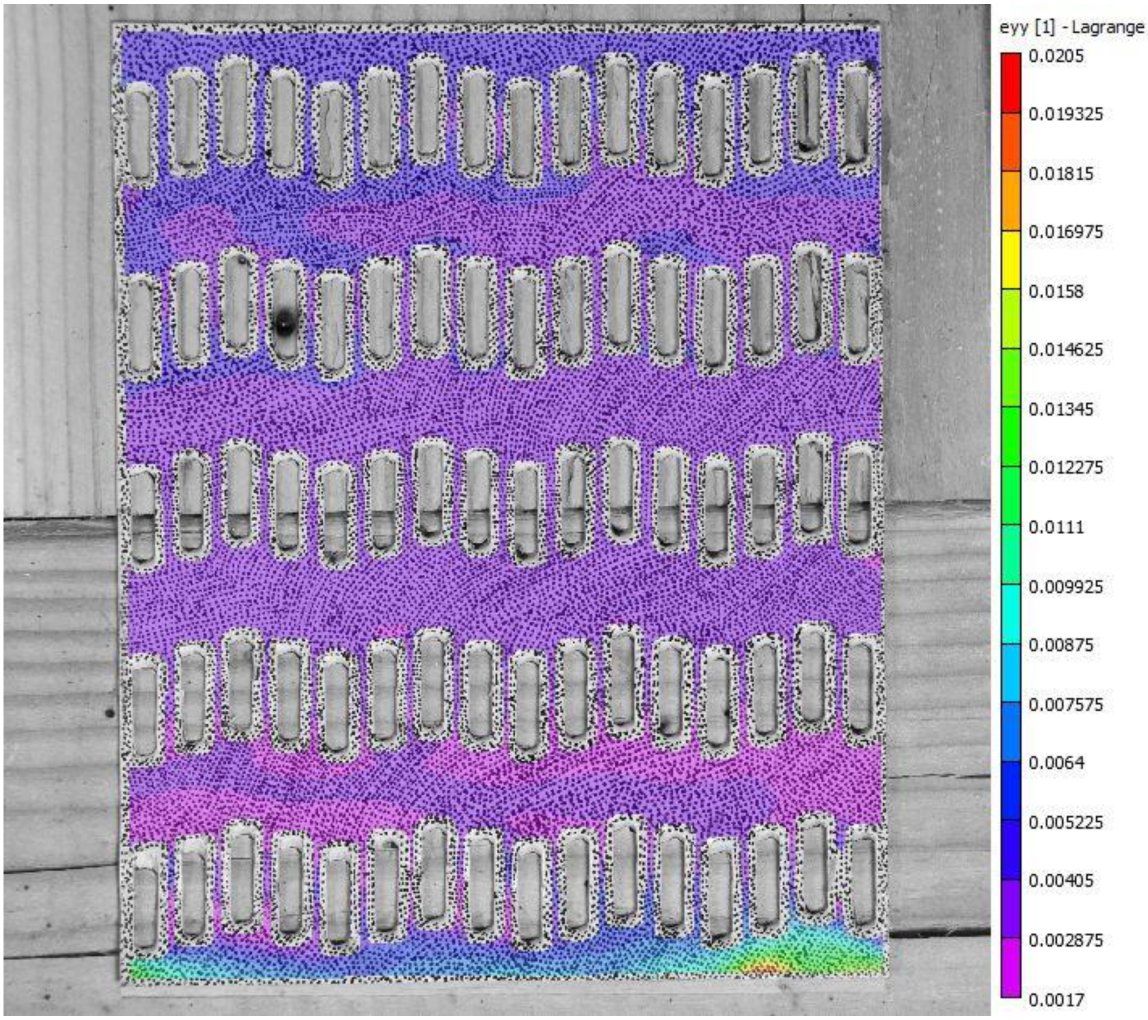

Figure 4-54: Full-field strain measurements (ε_{yy}) for the last image at the failure at 1,940 pounds

The full-field strain measurement (ε_{yy}) at 1,940 shows that the strain (ε_{yy}) is more organized over the plate's surface. High strain is shown near the bottom edge of the plate which is above the main horizontal crack in the wood. The average strain value is around 0.0035. No significant strain change is observed along the horizontal middle gap line due to the wood failure.

The full-field strain (ε_{xx}) image in x- direction can also be obtained from DIC code. The full-field strain measurements (ε_{xx}) is a tensile strain all over the 10 captured images. The strain (ε_{xx}) at 200 pounds is shown in Figure 4-55. The figure shows that the strain (ε_{xx}) is tensile strain with low and very close values over the entire plate.

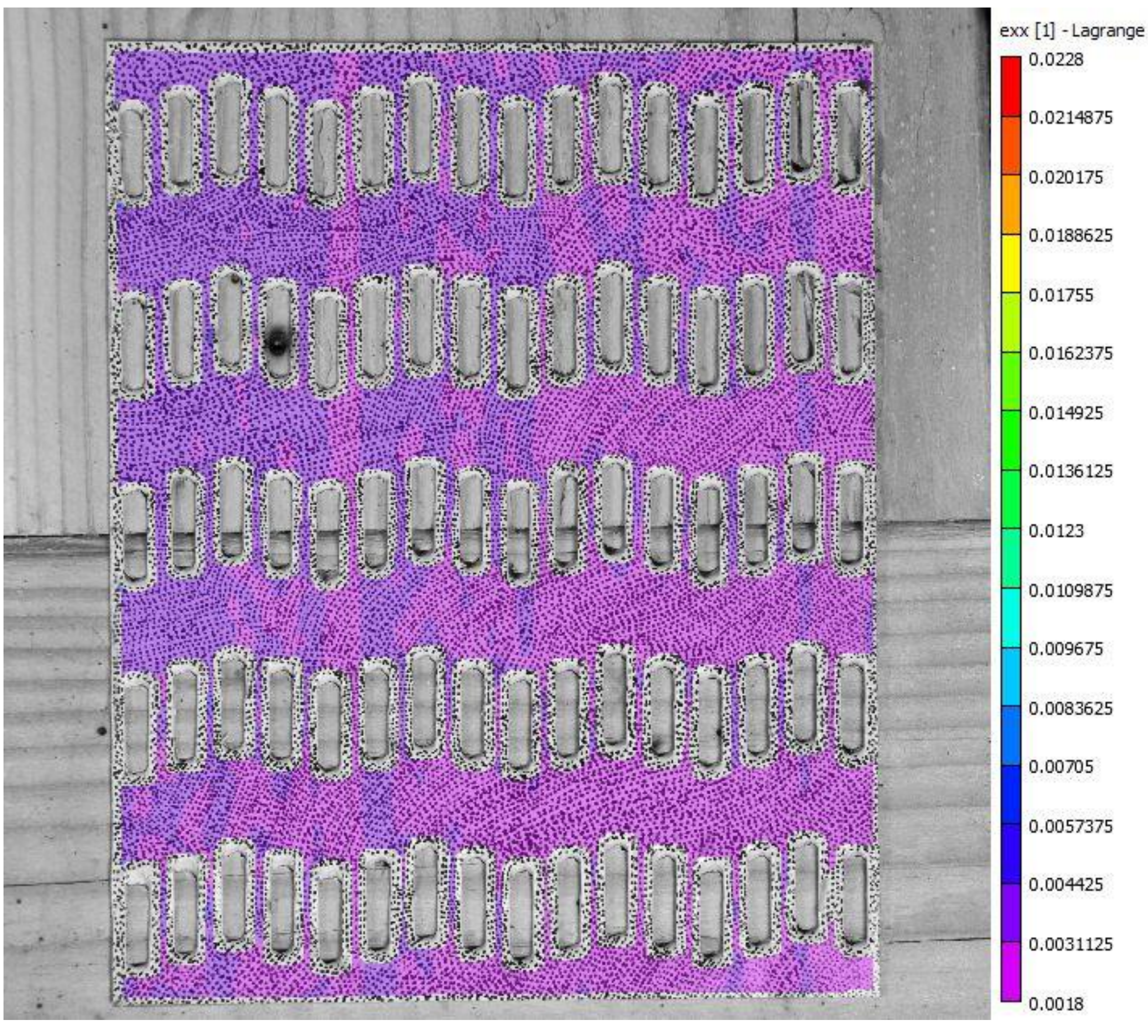

Figure 4-55: Full-field strain in x-direction (ε_{xx}) at load 200 pounds

The strain (ε_{xx}) increases with loading from 200 pounds until 600 pounds where the strain (ε_{xx}) at 600 pounds is the highest. Therefore, the strain (ε_{xx}) follows the strain (ε_{yy}) in this behavior. Figure 4-56 shows the strain (ε_{xx}) at 600 pounds.

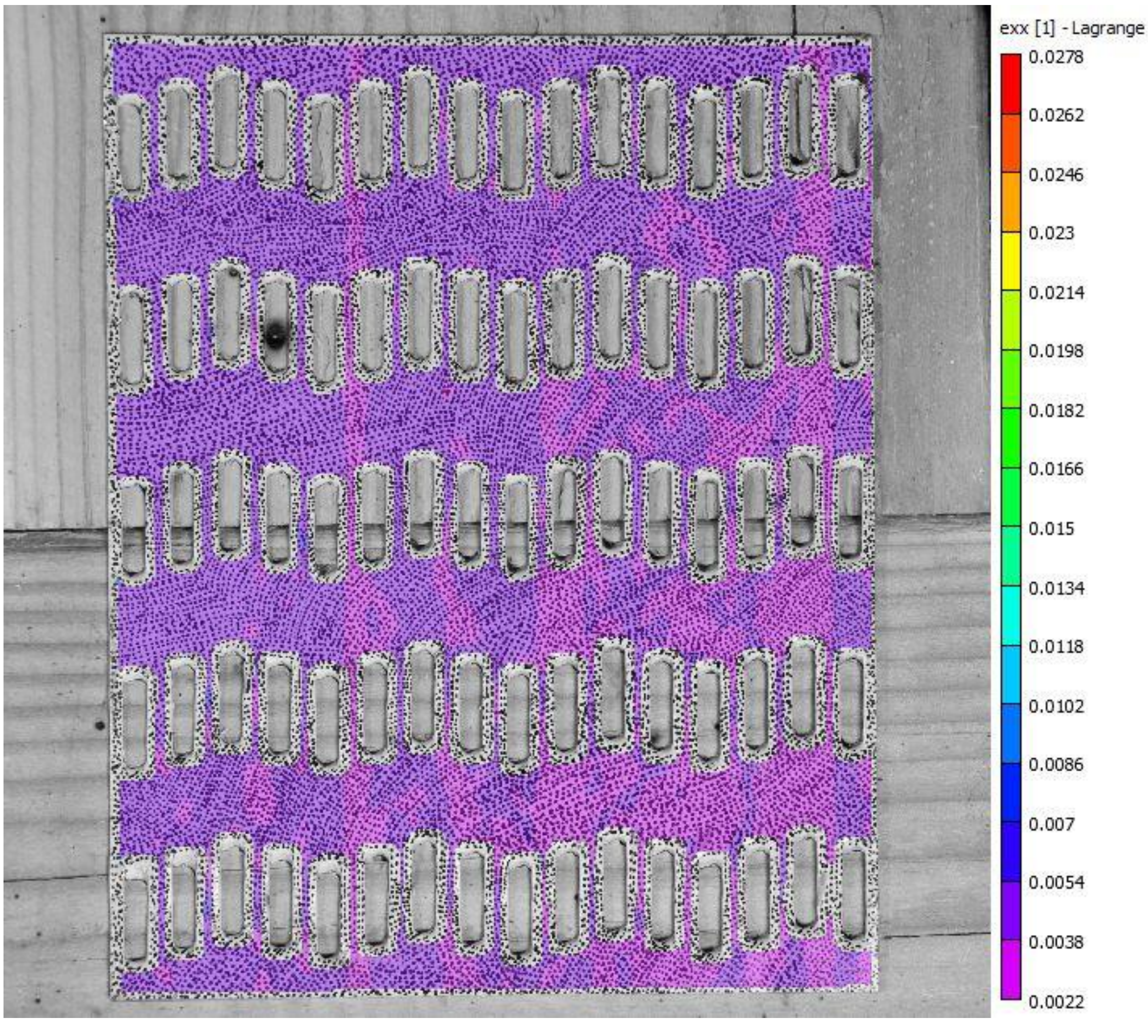

Figure 4-56: Full-field strain in x-direction (ε_{xx}) at load 600 pounds

After applying 600 pounds the strain (ε_{xx}) decreases again exactly as previously described for the strain behavior (ε_{yy}). At highest load of 1,940 pounds the strain (ε_{xx}) shows high strain values again but over some plate's regions they are less than the strain (ε_{xx}) at 600

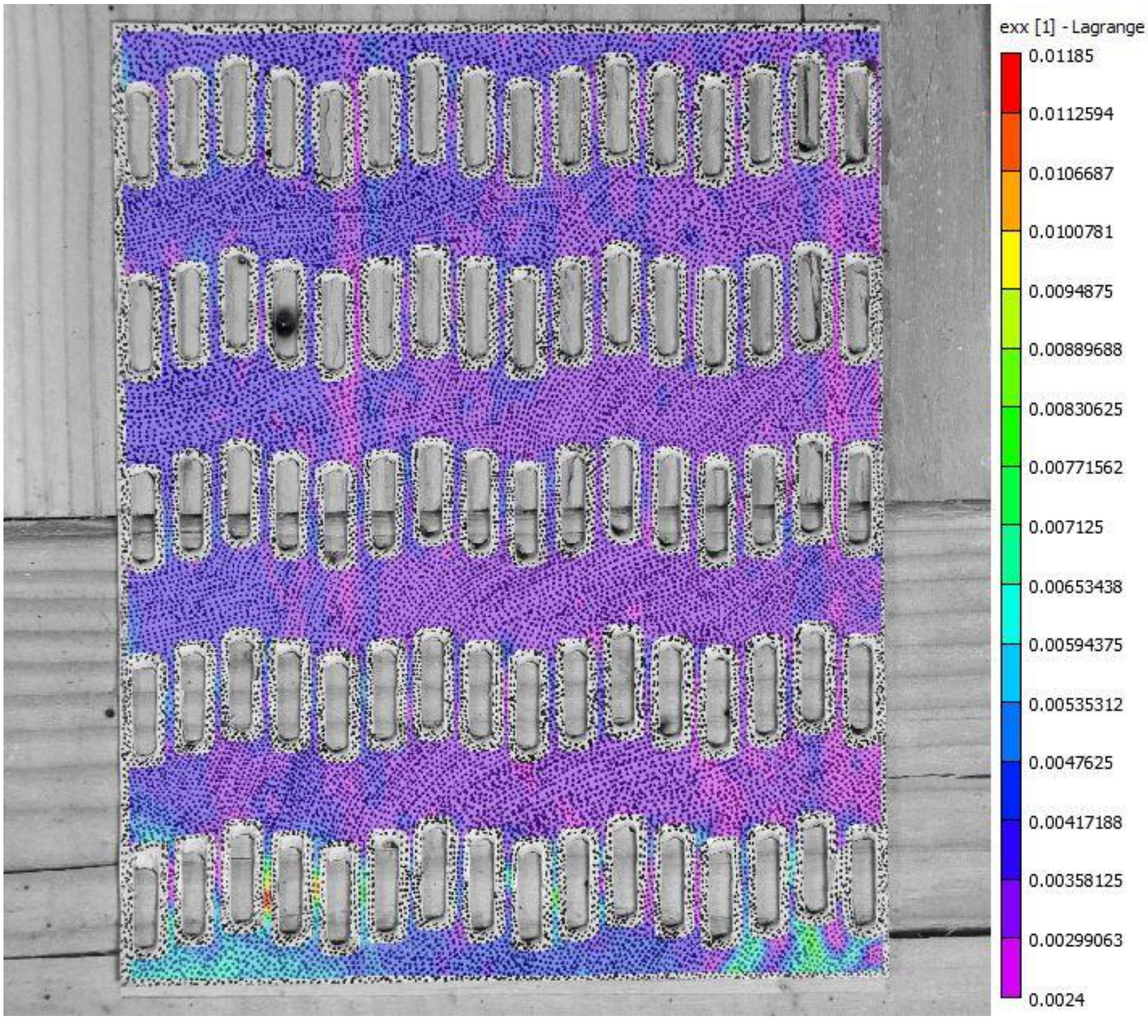

Figure 4-57: Full-field strain in x-direction (ε_{xx}) at load 1,940 pounds (the last image at failure)

pounds. The full-field strain measurements (ε_{xx}) for the last image at the maximum load are shown in figure 4-57. The strain (ε_{xx}) is tensile strain and shows very close but lower values than the tensile train (ε_{yy}). The bottom part of the plate shows some significant changes in the strain contour color and so the strain values due to the failure of wood at these places as shown earlier with strain (ε_{yy}) behavior.

4.1.2.2.2 Numerical Analysis for the Results

To analyze the DIC results numerically, a vertical cross section line from the top of the plate to the bottom is taken for some images starting with the first image at 200 pounds and ending with the last image at failure. The cross section is taken in three different locations as shown in Figure 4-58.

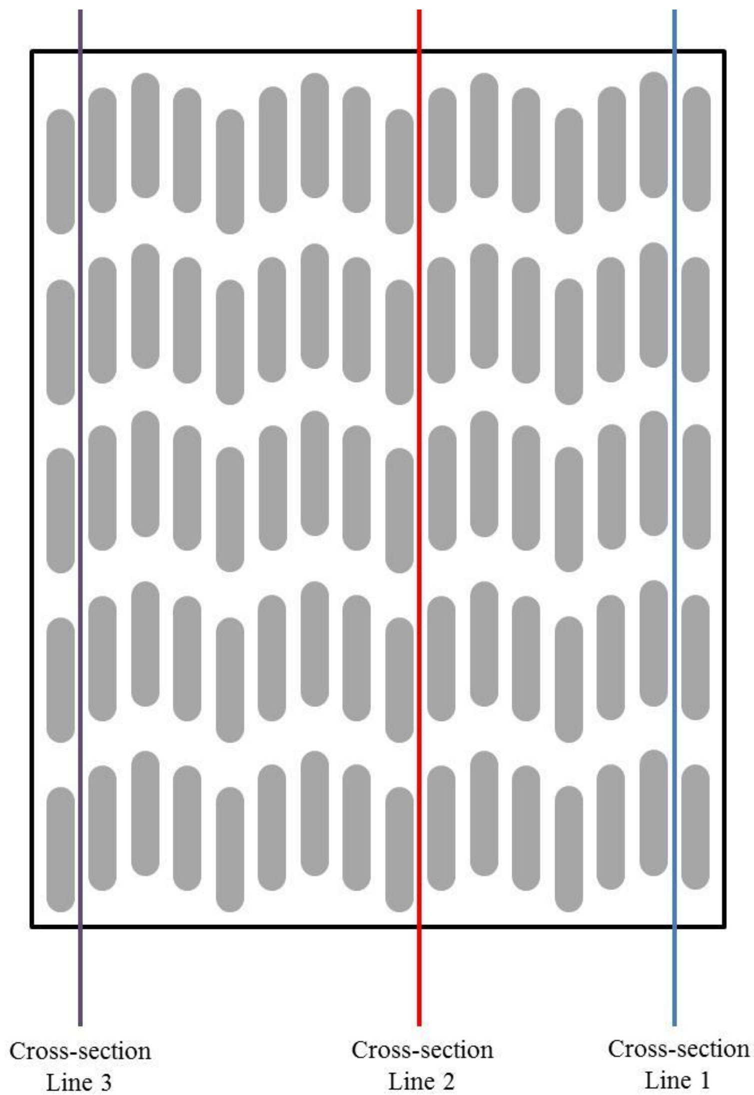

Figure 4-58: Metal plate with the cross-section lines along the vertical direction

The three locations of the cross section lines are as the following:

- The first cross section line (1-1) is from the right side of MPC @ x = 1.245 in.
- The second cross section line (2-2) is near the middle of the MPC @ x = -0.1952 in.
- The third cross section line (3-3) is from the left side of MPC @ x = -2.237 in.

Three cross-section lines are taken for the strain field (ε_{yy}). The next three Figures 4-59, 4-60 and 4-61 show the distribution of strain (ε_{yy}) at three different locations for 10 images. Each image represents the value of the loading that is applied on the specimen of the two wood members connected by the metal plate connector.

The curves show that the first considered load is 200 pounds then the increment of loading is 200 pounds until the failure. The failure is in the wood, not in the plate. The curves show that the tensile strain (ε_{yy}) increases with an increase the load from 200 pounds until 600 pounds. After applying 600 pounds the strain (ε_{yy}) shows a decrease in the strain (ε_{yy}) curves. Then at around 1,600 pounds, the strain curves increase again. Then at the failure at 1,940 pounds the strain curve is on some plate's regions less than the strain curves at 600 pounds. In general the strain (ε_{yy}) curve at each load shows very close values above and underneath the horizontal middle gap line with some exception. The strain (ε_{yy}) at the bottom edge of the plate which is located above the main horizontal crack in the wood shows higher tensile strain values with respect to the other strain values on the plate's surface. These higher values are due to pulling out the edge of the plate due to tooth withdrawal especially on the right side of the plate.

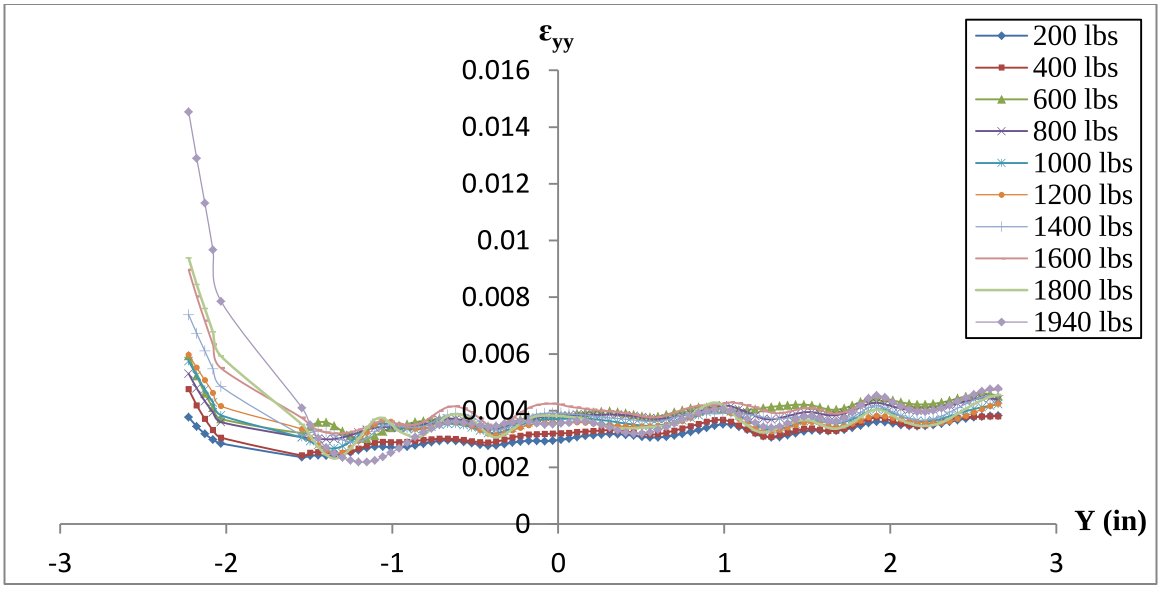

Figure 4-59: The strain distribution (ε_{yy}) along a cross section line (1-1) located on the right side of the plate

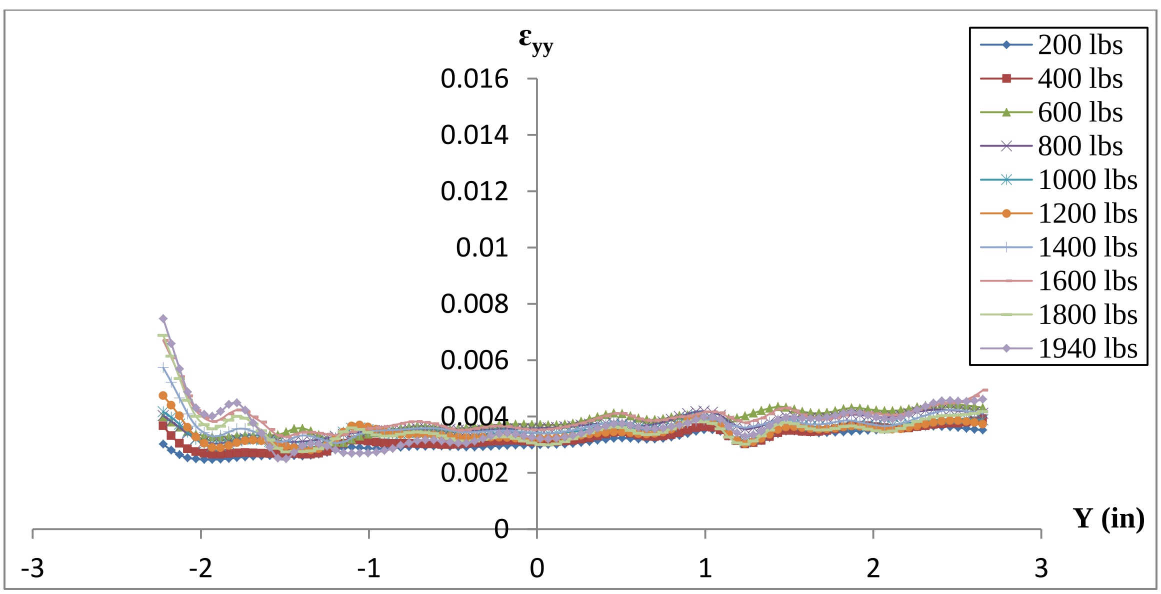

Figure 4-60: The strain (ε_{yy}) distribution along a cross section line (2-2) located near the middle of the plate

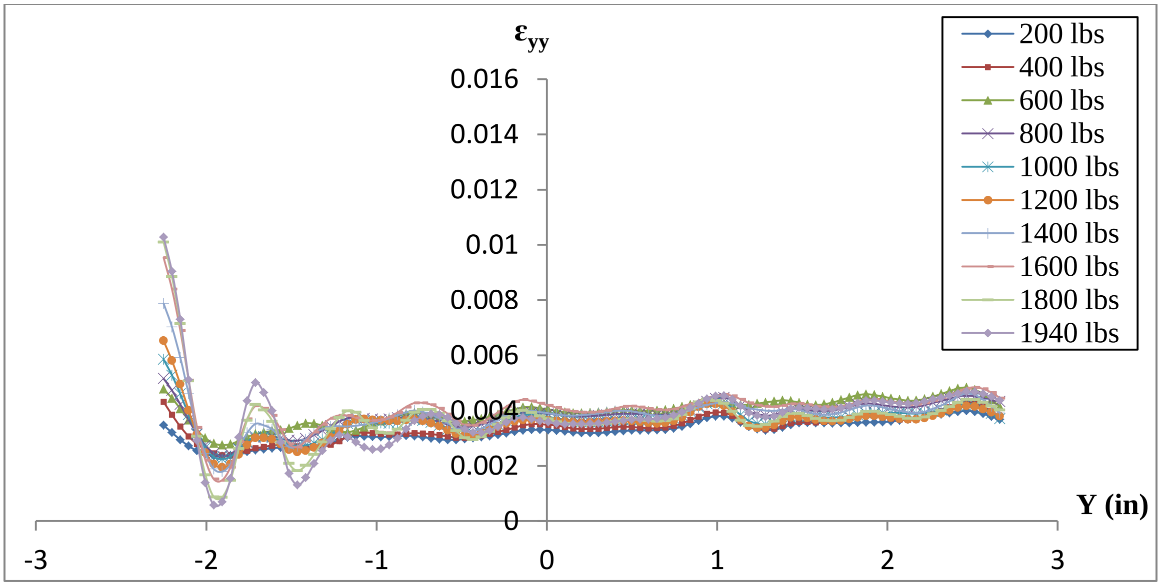

Figure 4-61: The strain (ε_{yy}) distribution along a cross section line (3-3) located on the left side of the plate

The right side of the plate is influenced by larger wood horizontal crack than the left side of the plate. The strain (ε_{yy}) at load 1,940 holds the highest strain values among all images at different loading due to tooth withdrawal. While on other full-field strain curves some regions of the plate surface show strain values at 600 pounds larger than the strain values at the same places at load 1,940 pounds. The strain curves at the bottom of the plate along the cross section line (1-1) shows that the last strain curve at 1,940 pounds is influenced by high strain (ε_{yy}) at the bottom of the plate. The strain (ε_{yy}) curve along the middle cross section line (2-2) shows sudden rise in the strain at the bottom higher than other strain curve's load. However, the bottom strain at the vertical middle of the plate is lower than the vertical strain at the right side of the plate. The strain (ε_{yy}) along the left vertical cross section (3-3) also influenced by an increase in the strain (ε_{yy}) at the bottom area of the plate and also shows steep rise of the strain. The maximum strain (ε_{yy}) value there is less than the strain (ε_{yy}) maximum value at cross section line (1-1).

However, it is higher than the middle cross section line (2-2).The strain at 600 pounds on some plate's regions is higher than the strain at 1,940 pounds. This result shows that when it comes to the plate's failure the strain is high at higher load. Also this result shows that the external load is not controlled by the plate, and the plate has higher strength against the external force. The teeth gripping are high. So the strain curve is still not fully organized with respect to external loading. Some spikes of the strain curves are shown along the vertical curves due to the waived-distributed slots that are distributed on the whole plate's surface.

The only area on the plate's surface showing influence by the higher load values is the bottom region at the edge of the plate which is affected by tooth withdrawal due to the horizontal crack in the wood. But the other regions of the plate's surface are in very good conditions, and there are no indications for sudden low or high strain changes. The horizontal middle areas of the plate along the gap line does not show any significant changes in the strain curves which indicate that the plate is under very low load to fail. The horizontal gap line is the place where the two wood members are connected and the area of the plate along this gap line is the half of the plate's area on other plate's surface. Therefore, the failure of the plate is expected to start there. In this test, the failure starts in the wood and slightly affected the bottom edge of the plate.

The gap between the two connected wood members increases with an increase in the load. The crack in the wood is developed from the right side of the plate makes the lower wood member to go up and at the last image it shows that the gap closes instead of opening. This explains why some tensile strain curves in the previous figures have lower strain values than other curves that have less applying loads. This can be seen especially for the last image at load 1,940 pounds. The strain curve for the last image is lower than that for other images with lower load. Therefore, the pressing of the wood due to crack also influences the fluctuating change in the strain curves at different loading.

On the other hand, the metal plate also shows the strain in x-direction (ε_{xx}). The strain (ε_{xx}) along y-direction for the cross-section lines (1-1), (2-2) and (3-3) is also found in the next Figures 4-62, 4-63 and 4-64.

The figures show that the strain (ε_{xx}) is a tensile strain. The tensile strain (ε_{xx}) shows very close values to the previously described tensile strain (ε_{yy}).

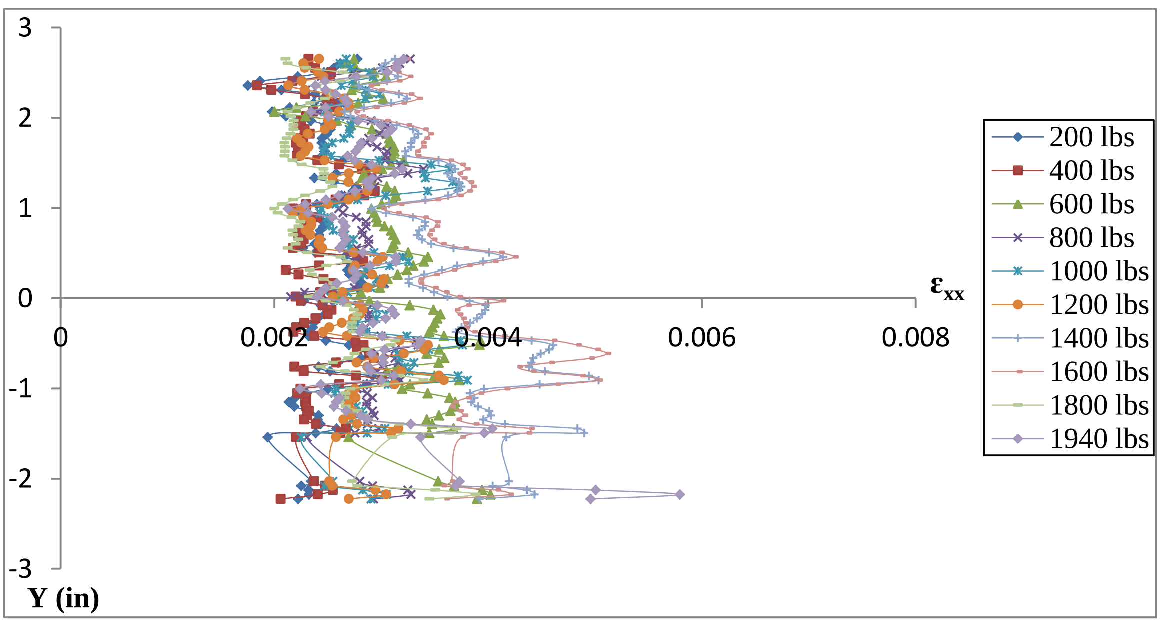

Figure 4-62: The strain distribution (ε_{xx}) along a cross section line (1-1) located on the right side of the plate

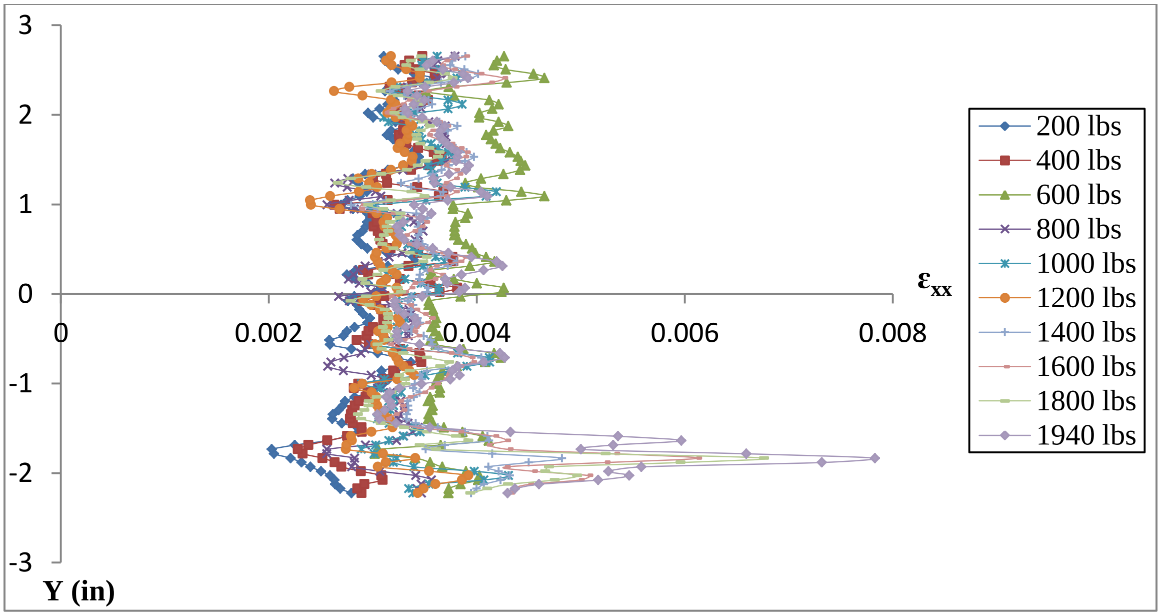

Figure 4-63: The strain (ε_{xx}) distribution along a cross section line (2-2) located near the vertical middle of the plate

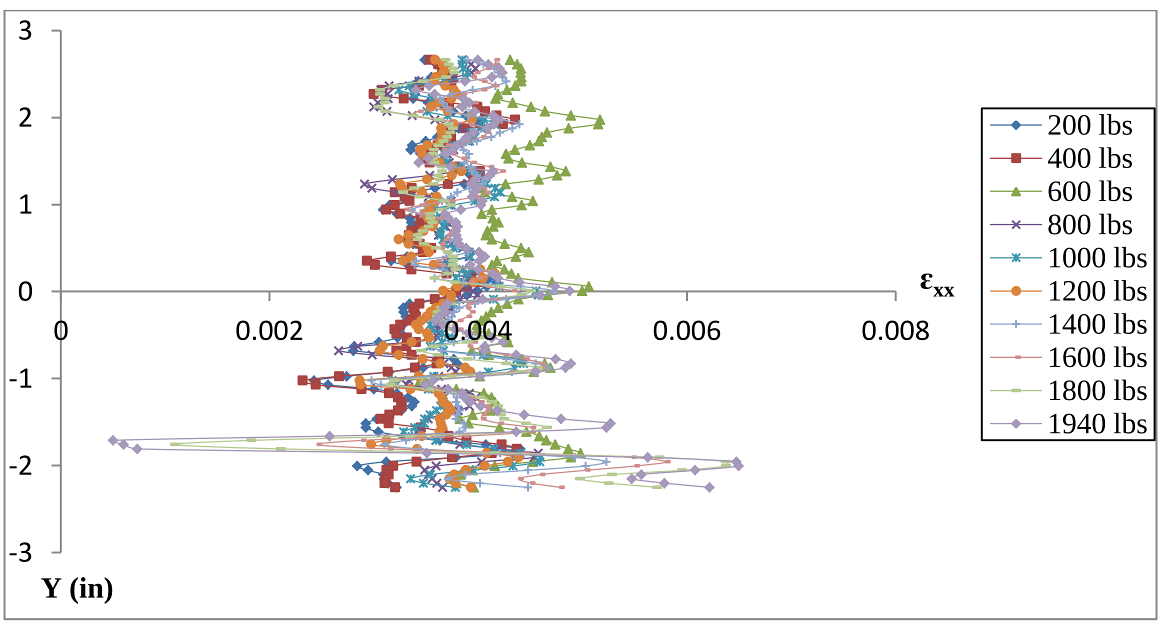

Figure 4-64: The strain (ε_{xx}) distribution along a cross section line (3-3) located on the left side of the plate

The strain curves (ε_{xx}) show low tensile strain at 200 pounds. Then the strain (ε_{xx}) increases until load 600 pounds. The strain (ε_{xx}) curves at 600 pounds are one of the highest strain curves the plate in this test has. Then strain (ε_{xx}) values decrease. The strain curve (ε_{xx}) at the last maximum load at 1,940 is less than the strain at 600 pounds on some regions over the plate. The strain curves (ε_{xx}) are fluctuating with load as the strain (ε_{yy}). Sudden jumps in the strain can be shown at the very low end of the plate near the edge where the horizontal wood crack developed. The dominant significant strain (ε_{xx}) at the edge regions is the strain at the maximum load 1,940 pounds. This indicates that the failure of the plate is influenced by high strain at high load. The strain (ε_{xx}) decreases at the crack region with significant values. On the other hand the strain (ε_{yy}) significantly increases on the same place.

In general the tensile strain (ε_{xx}) is as high as the tensile strain (ε_{yy}). No indication appeared for changes in the strain along the horizontal gap line which has the weakest line to show significant changes in the strain (ε_{xx}) values and behavior. The plate is in good condition and shape. The tooth grip is very strong. Thus the fluctuation in the strain values and behavior among the images under different load are obvious. The external load is very low to make significant changes in the plate and the plate's strain behavior. The strain from the top to the bottom of the plate holds very close to strain values. The failure in this test is in the wood by a main horizontal crack in the bottom member that has a grain perpendicular to the external tension force. The cracks in the bottom wood member play an important role to show fluctuations in the strain curves by making one split wood part to press to the top and the other part to the bottom. Thus the horizontal gap closes at load 1,940 pounds instead of increasing.

4.1.2.2.3 A Comparison between the Strain in y and x direction [(ε_{xx}) vs. (ε_{yy})]

In this section, the strain values {**(ε_{xx})** vs. **(ε_{yy})}** for the last image at the failure at load 1,940 pounds will be compared. The next Figures 4-65 and 4-66 show the three cross-section lines for the last image at the failure at load 1,940 pounds for strain (ε_{yy}) and (ε_{xx}).

The curves show the significant changes and spikes in the strain values that can be found in the strain curves (ε_{xx}). Figure 4-65 shows that the right cross section line (1-1) has the lowest strain (ε_{xx}) values then the middle. The last cross section line (3-3) in general has the highest **(ε_{xx})** values. The middle cross section line (2-2) has very high **(ε_{xx})** in the bottom plate and very low **(ε_{xx})** in the same level for the strain at cross section line (3-3). This change in strain is due to the crack in the wood that is under the plate and caused tooth withdrawal to some locations of the plate. The middle section has one crack at the rear end while the cross section (3-3) has two cracks one at the rear end and another one to the top of this rear end one. The middle cross section has the highest (ε_{xx}) value where the (ε_{yy}) is going down.

Figure 4-66 shows the strain curves (ε_{yy}). The curves look like very close with some exceptions at the bottom due to the tooth withdrawal at the places of the wood crack. The change in the cross-section (1-1) is obvious the bottom of the plate and shows one significant change while there are two big jumps in the strain curve for the cross section line (3-3) due to presence of two wood cracks at that area which reflects on the strain curve directions.

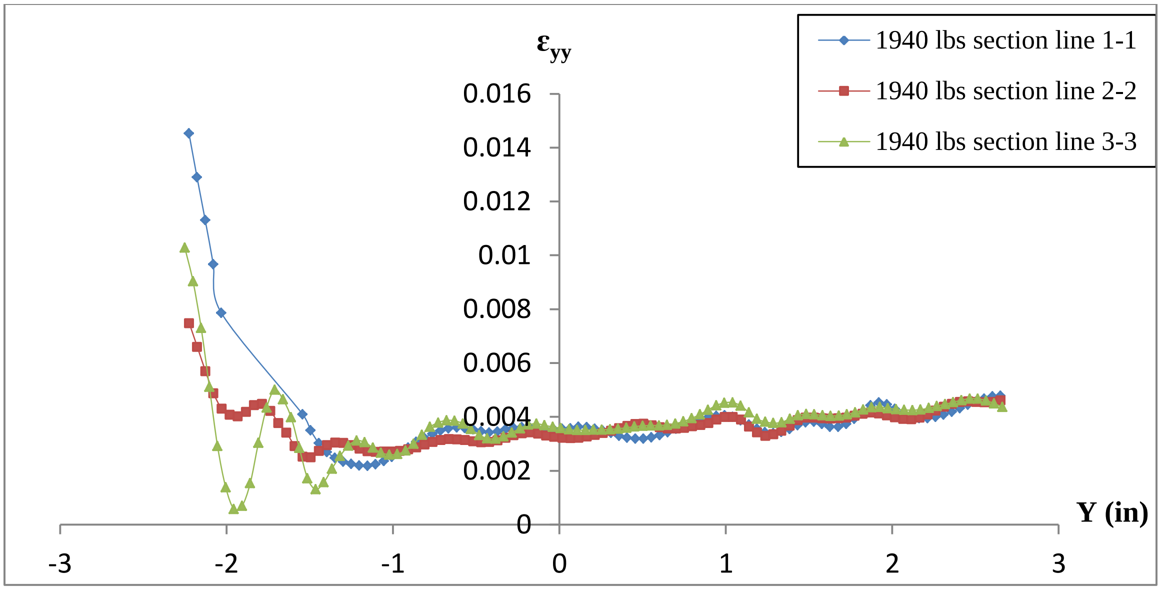

Figure 4-65: The strain (ε_{yy}) distribution along the three cross-section lines (1-1), (2-2), (3-3) for the last image at the failure at load 1,940 pounds

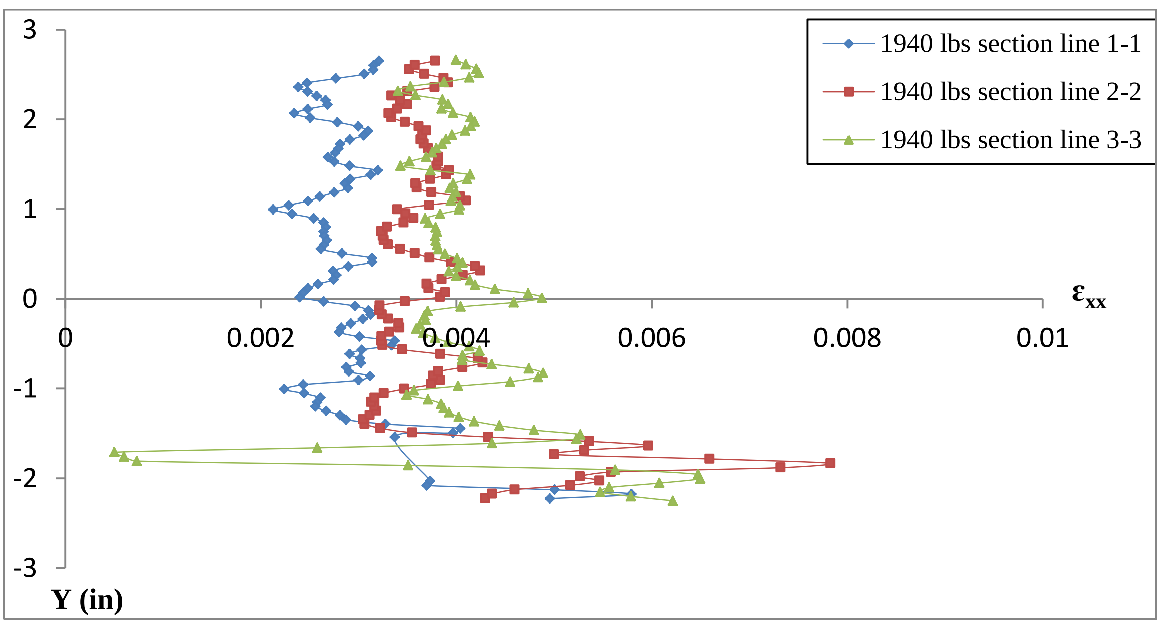

Figure 4-66: The strain (ε_{xx}) distribution along the three cross-section lines (1-1), (2-2), (3-3) for the last image at the failure at load 1,940 pounds

4.1.2.3 The Second Tension Test (AE-2nd)

In this test, the two members of wood were connected by the MPC. The specimen was set on the universal testing machine. The first reference image was taken before applying any load. Figure 4-67 shows the first image which is considered as the reference image in digital image correlation technique.

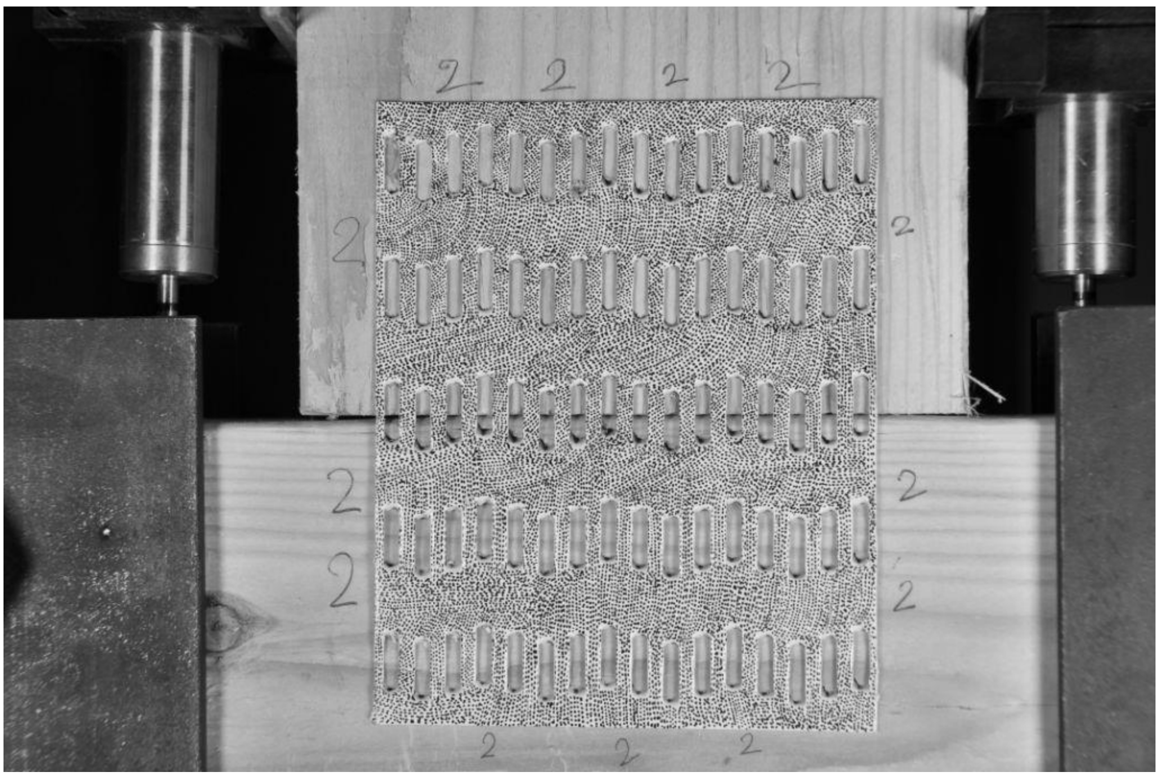

Figure 4-67: First image / reference image

After the first reference image was taken at load zero, the load was increased on the specimen until failure. The camera was placed on a fixed place and the MPC was perpendicular to the camera’s lenses. Images were taken for the MPC specimen at each load increment of 200 pounds until failure. The failure in the member occurred in the wood. Figure 4-68 shows the last image after the failure.

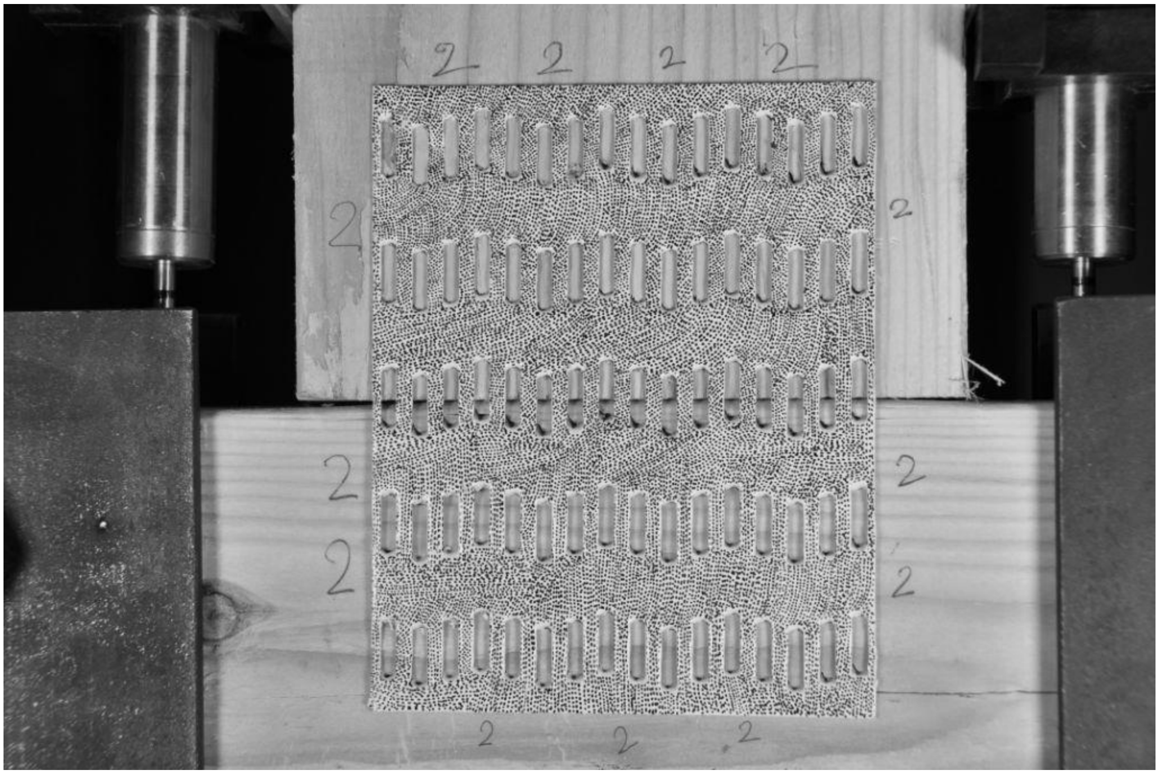

Figure 4-68: The last image after the failure

Seventeen (17) images were taken in addition to the reference image. The metal plate had not failed directly but some regions on the plate had tooth withdrawal. The main reason for failure was wood failure. The wood had failed at load equal to 3,400 pounds. The bottom wood member had cracked horizontally at failure. The captured images were implemented in DIC-software to find the full-field strain measurements.

4.1.2.3.1 Analysis of the Full-Field Strain Results Obtained From DIC Software

All the test images, which were obtained from the lab test, were implemented in the digital image correlation software Vic-2D. Each image was analyzed in relation to a reference image. Thus each deformed image was compared to the non-deformed reference image. The full-field strain measurements were obtained from the digital image correlation software. Figure 4-69 shows the strain (ε_{yy}) at 200 pounds.

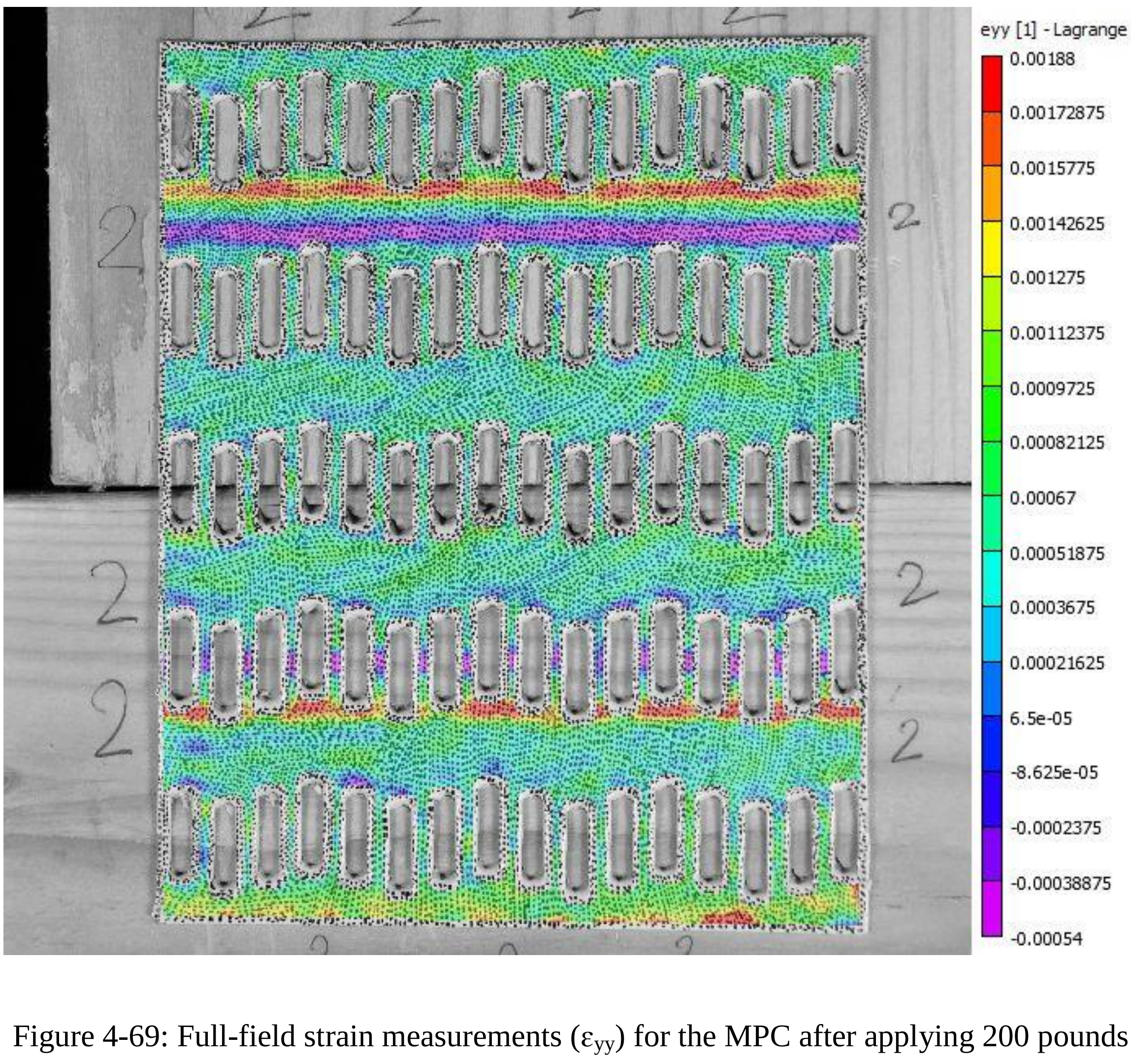

Figure 4-69: Full-field strain measurements (ε_{yy}) for the MPC after applying 200 pounds

The strain field's results show different levels of colors and shows that each level of color represents a number. The failure in this test is in the bottom wood member under the right support. Thus, the changes in the strain over the surface of the plate are not that significant. But DIC software can be used to show the changes in strain stages under different loading increments until wood failure. The image shows that the strain contour plot over the surface of the plate in general is a tensile strain (ε_{yy}) and it has very low values. The strain (ε_{yy}) average is almost 0.0006. The strain contour plot shows some regions on the plate have negative strain especially in the top part of the plate. There is a continuous strip of negative strain on the top region of the plate. This negative strain is a result of compression force on that region due to due to the influence of the angle of implemented teeth.

The strain (ε_{yy}) increases with loading until image at load 2,600 pounds. Figure 4-70 shows the full-field strain measurement (ε_{yy}) at 2,600 pounds. The strain (ε_{yy}) is high related to the previous strain field images. The strain field values over the plate contain fluctuation; however they have, in general, close values. The bottom of the plate shows high tensile strain due to pulling out for the edge of the plate. A wood crack also appears there. The strain field values fluctuate from the top to the bottom of the plate due to repeat changing of the plate's cross sectional areas because of the slots. The teeth also are distributed on the plate in wavy shape based on the slots locations. The angle of the teeth affects the strain behavior based on their direction of influence. At 2,600 pounds the plate in good shape and condition and no special changes in the strain behavior to indicate the plate's failure. The horizontal middle gap line has normal strain values as the other plate's area.

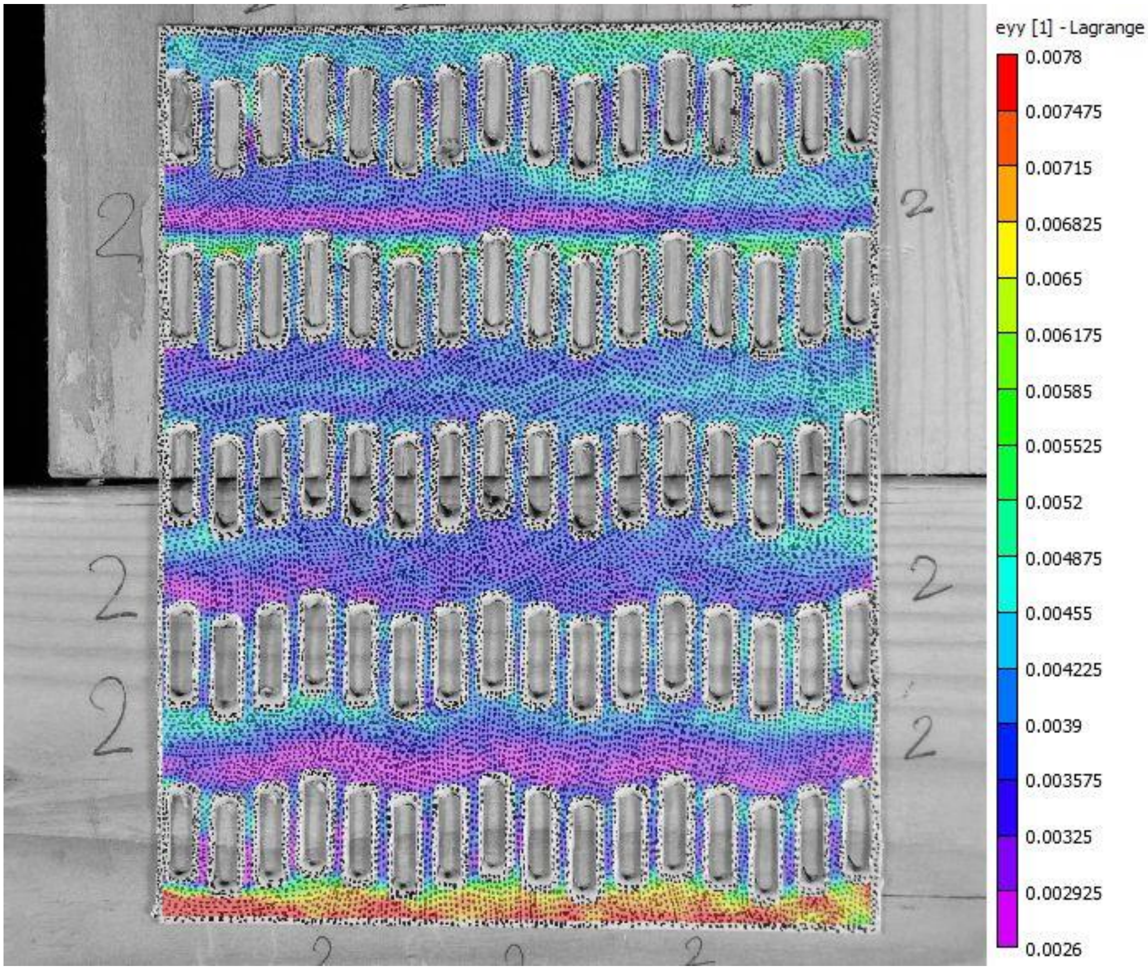

Figure 4-70: Full-field strain measurements (ε_{yy}) at 2,600 pounds

By increasing the load from 2,600 to the failure at 3,400 the strain fields shows very close strain (ε_{yy}) values until failure. Figure 4-71 shows the strain contour plot for the plate at failure. The bottom wood member shows a horizontal crack. The specimen has failed due to a crack in the wood especially under the support. So no significant changes in the plate or the strain (ε_{yy}) are shown. Very high strain (ε_{yy}) values at the edge of the plate due to the tooth withdrawal. The wood crack crosses the bottom region of the plate where the tensile strain (ε_{yy}) is high.

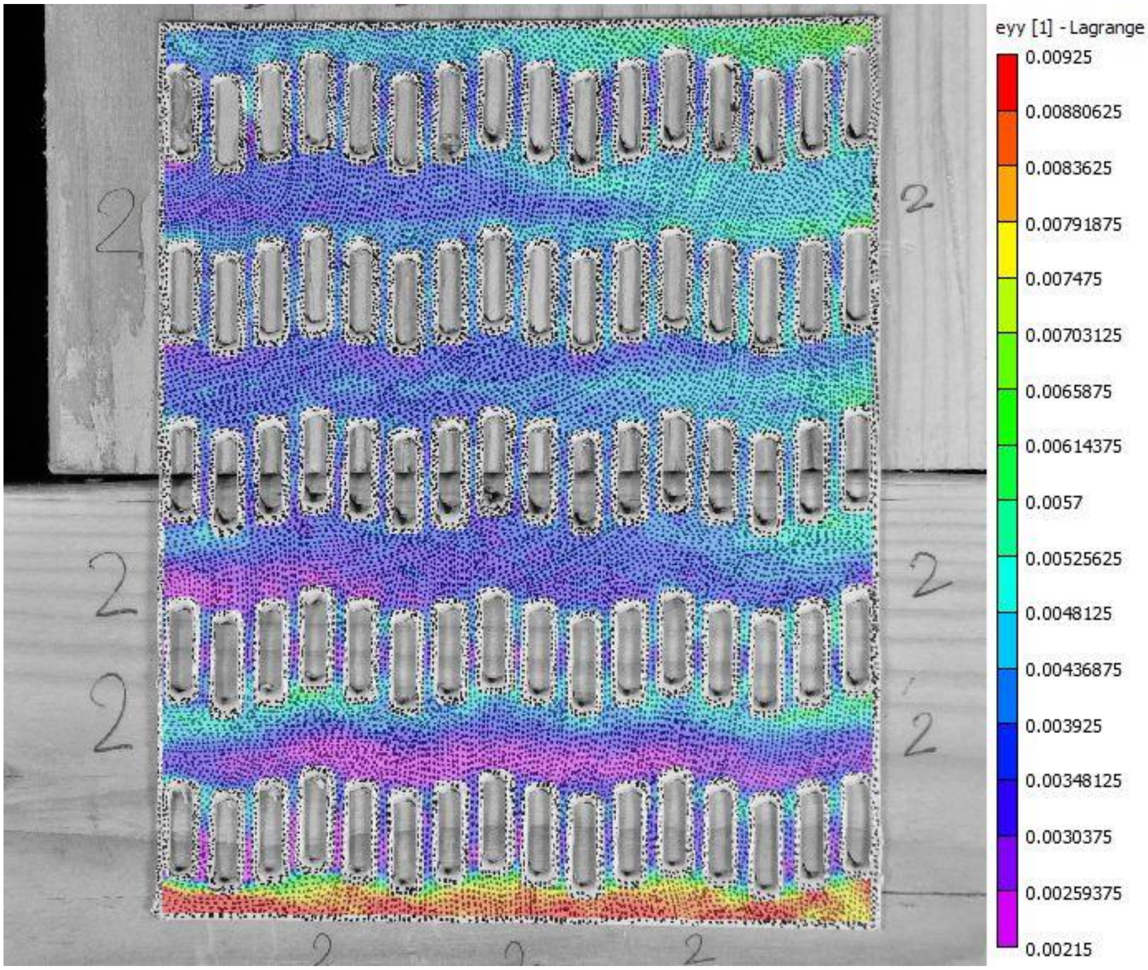

Figure 4-71: Full-field strain measurements (ε_{yy}) for the last image at the failure at 3,400 pounds

The bottom wood member, which holds the grain that is perpendicular to the tension force, failed first. The images show that there is a horizontal crack in the wood to the right side of the plate. This is observable after applying 600 pounds. This crack caused some tooth withdrawal through the test. The gap between the two connected wood members increases with load. There are no significant changes in the strain (ε_{yy}) are shown in this test to be an indication for plate's failure. The plate is in good shape and the teeth gripping are very strong and can resist the external forces.

The full-field strain (ε_{xx}) image in x-direction can also be obtained from DIC code. The full-field strain measurements (ε_{xx}) are a tensile strain all over the captured images. The strain (ε_{xx}) at 200 pounds is shown in Figure 4-72. The figure shows that the strain (ε_{xx}) is tensile strain with low and very close values over the entire plate with some limited exceptions over the plate's surface.

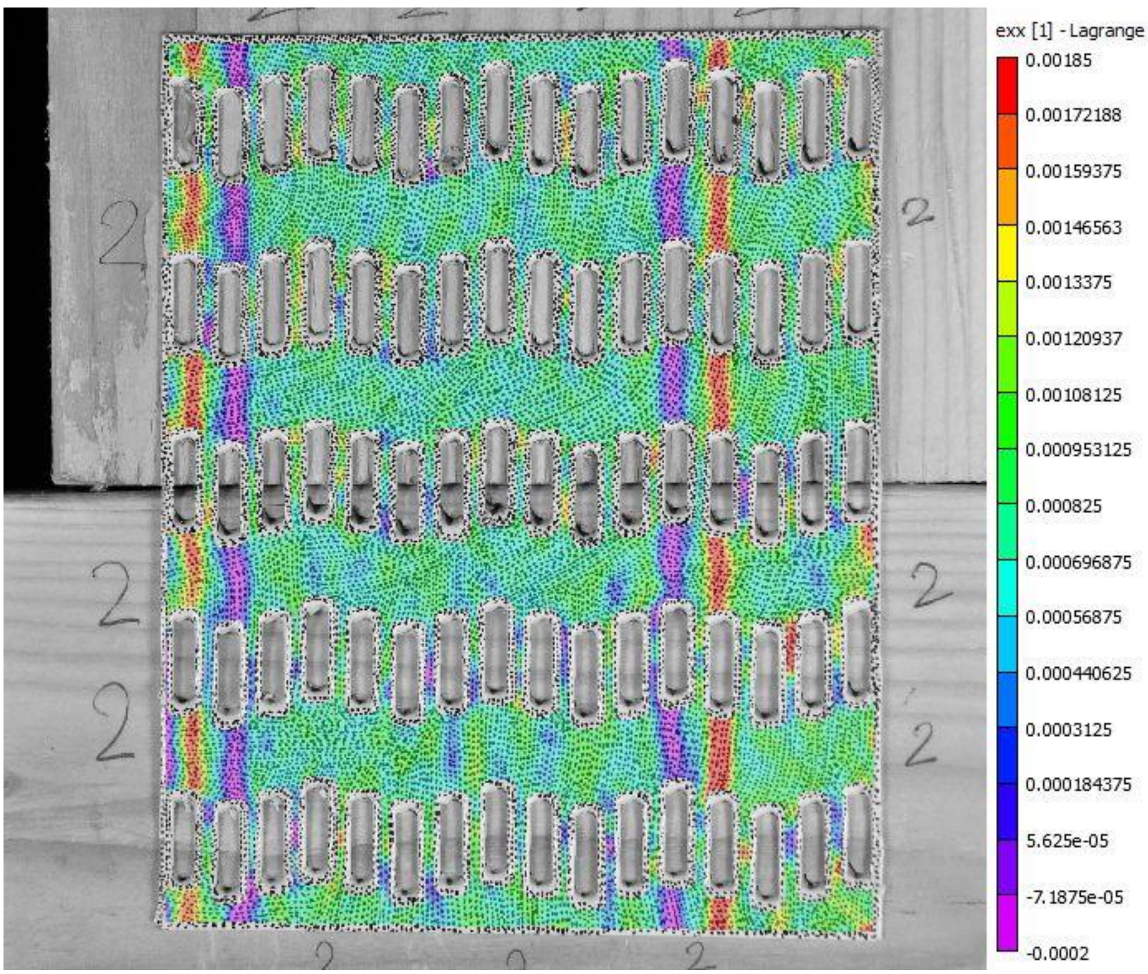

Figure 4-72: Full-field strain in x-direction (ε_{xx}) at load 200 pounds

The strain (ε_{xx}) increases with loading from 200 pounds to 2,600 pounds. The strain full-field measurements at 2,600 pounds are shown in Figure 4-73. The strain (ε_{xx}) at 2,600 pounds is one of the highest strains. Thus, the strain (ε_{xx}) follows the strain (ε_{yy}) in this behavior.

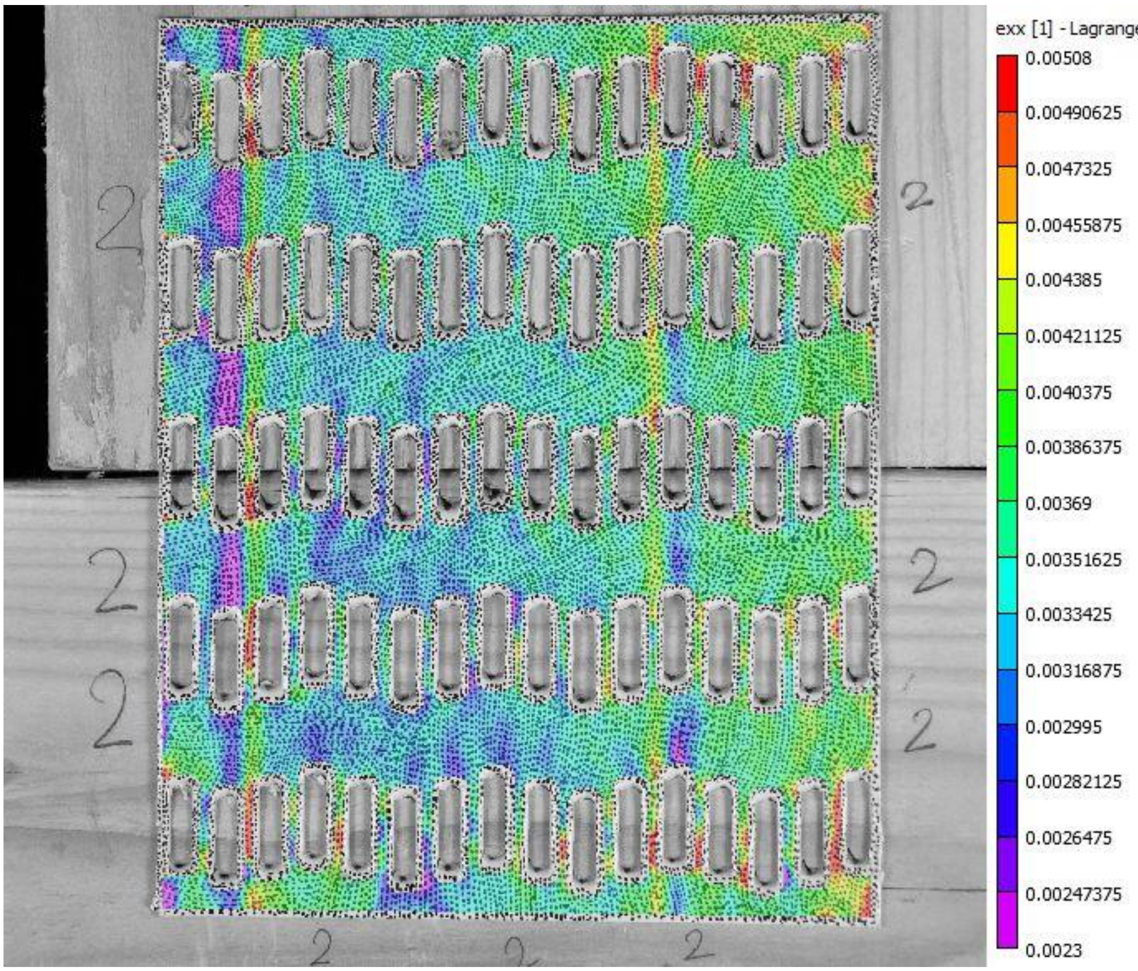

Figure 4-73: Full-field strain in x-direction (ε_{xx}) at load 2,600 pounds

The previous figure shows that the strain (ε_{xx}) possesses higher strain values at the right side more than the left side. The strain (ε_{xx}) continues to increase with loading until the failure at 3,400 pounds. Figure 4-74 shows the full-field strain measurements (ε_{xx}) at 3,400 pounds.

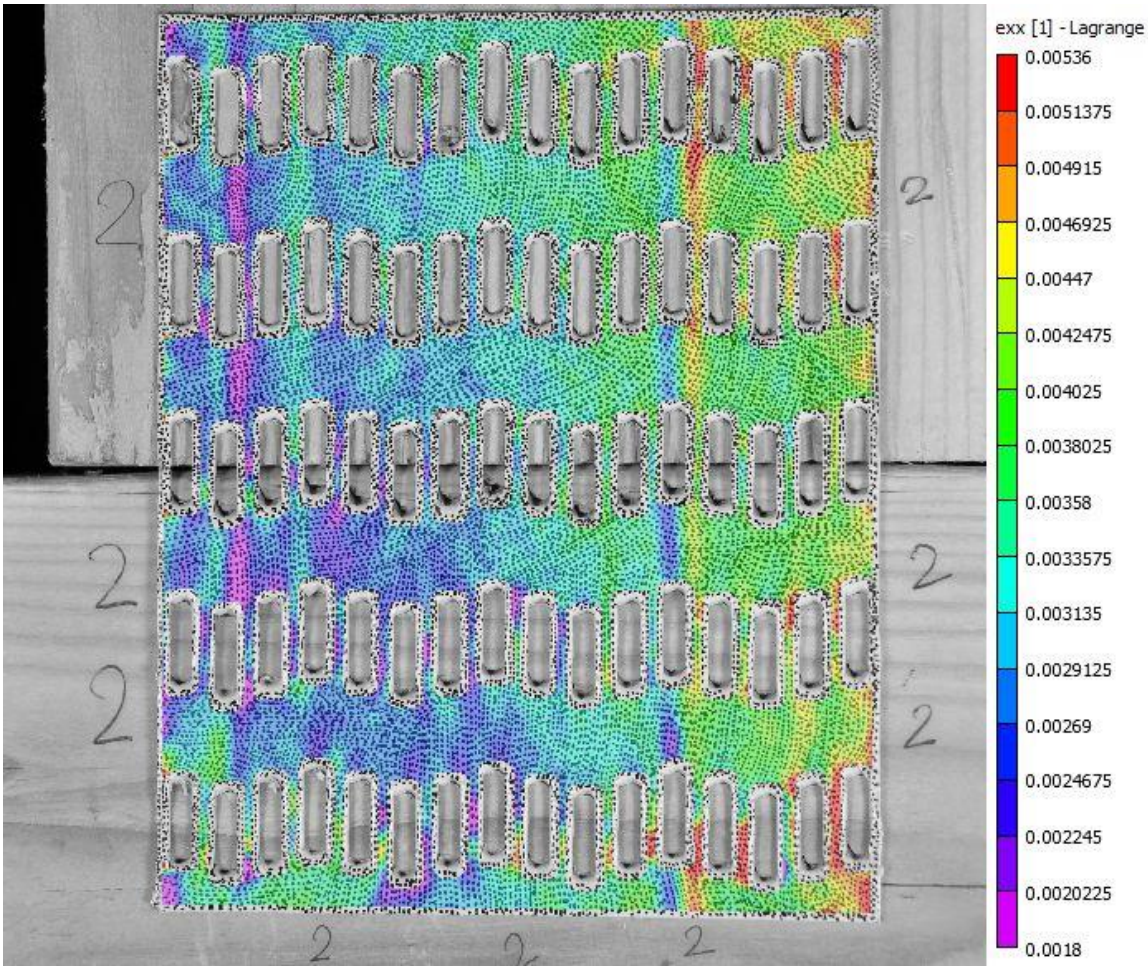

Figure 4-74: . Full-field strain in x-direction (ε_{xx}) at load 3,400 pounds (the last image at failure)

The strain (ε_{xx}) at the last image shows very close results to the image at 2,600 pounds. The strain is higher along the right side than the left side. However, the difference between the strains (ε_{xx}) is also very low. The top part of the plate above the horizontal middle gap line is almost equal to the strain (ε_{xx}) beneath the horizontal gap line.

4.1.2.3.2 Numerical Analysis for the Results

To analyze the DIC results numerically, a vertical cross section line from the top of the plate to the bottom is taken for some images starting with the first image at 200 pounds and ending with the last image before failure. The cross section is taken in three different locations as shown in Figure 4-75.

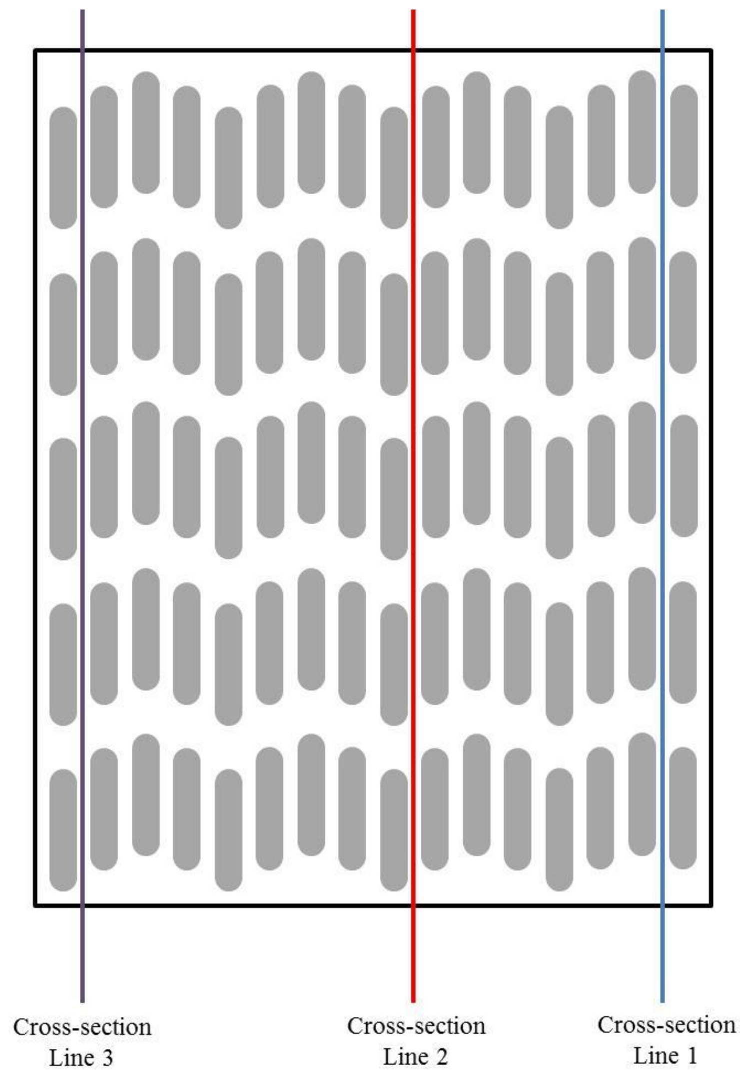

Figure 4-75: Metal plate with the cross-section lines along the vertical direction

The three locations of the cross section lines are as the following:

- The first cross section line (1-1) is from the right side of MPC @ x = 2.118 in.
- The second cross section line (2-2) is near the middle of the MPC @ x = 0.6157 in.
- The third cross section line (3-3) is from the left side of MPC @ x = -1.368 in.

Three cross-section lines are taken for the strain field (ε_{yy}). The next three Figures 4-76, 4-77 and 4-78 show the distribution of strain (ε_{yy}) at three different locations for 10 images. Each image represents the value of the loading that is applied on the specimen of the two wood members connected by the metal plate connector.

The curves show that the first considered load is 200 pounds then different increment of loading is used until the failure as shown in the next strain curves.

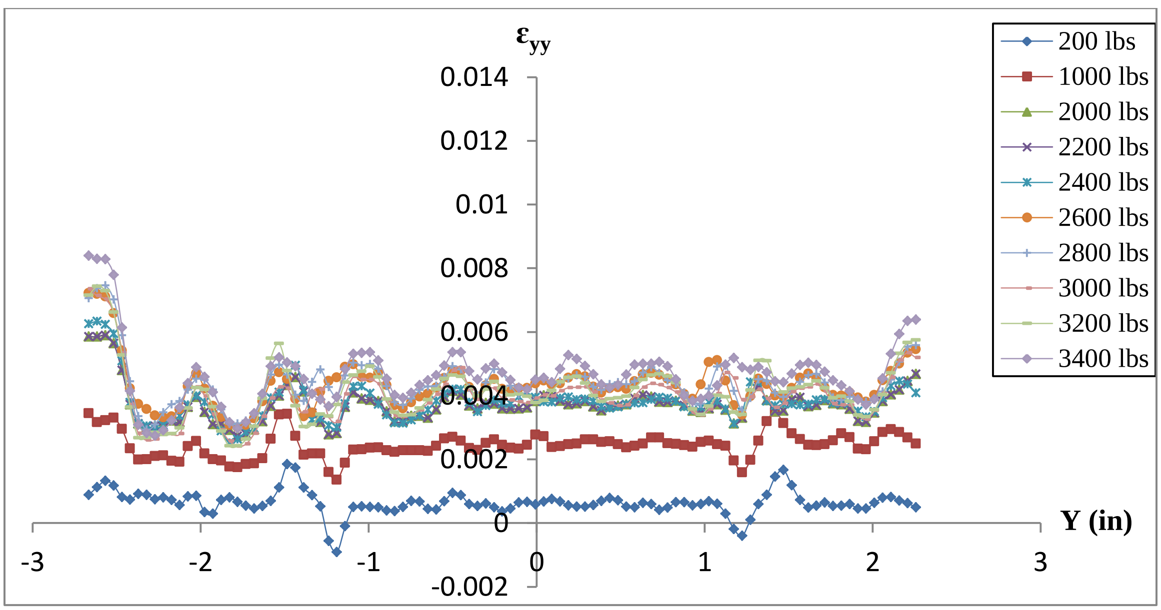

Figure 4-76: The strain distribution (ε_{yy}) along a cross section line (1-1) located on the right side of the plate

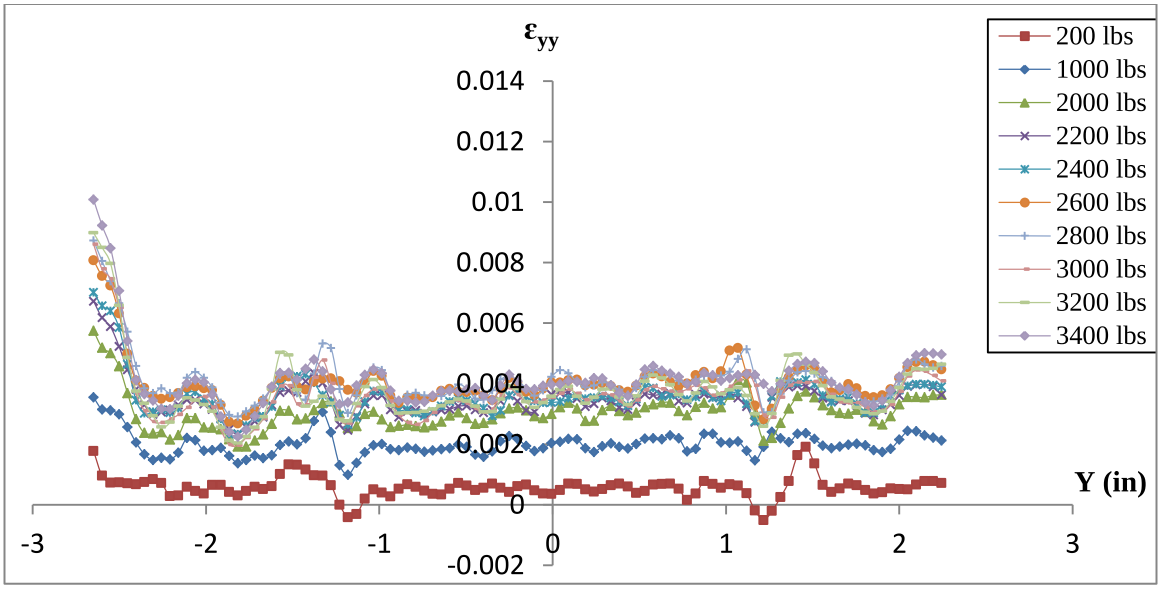

Figure 4-77: The strain (ε_{yy}) distribution along a cross section line (2-2) located near the middle of the plate

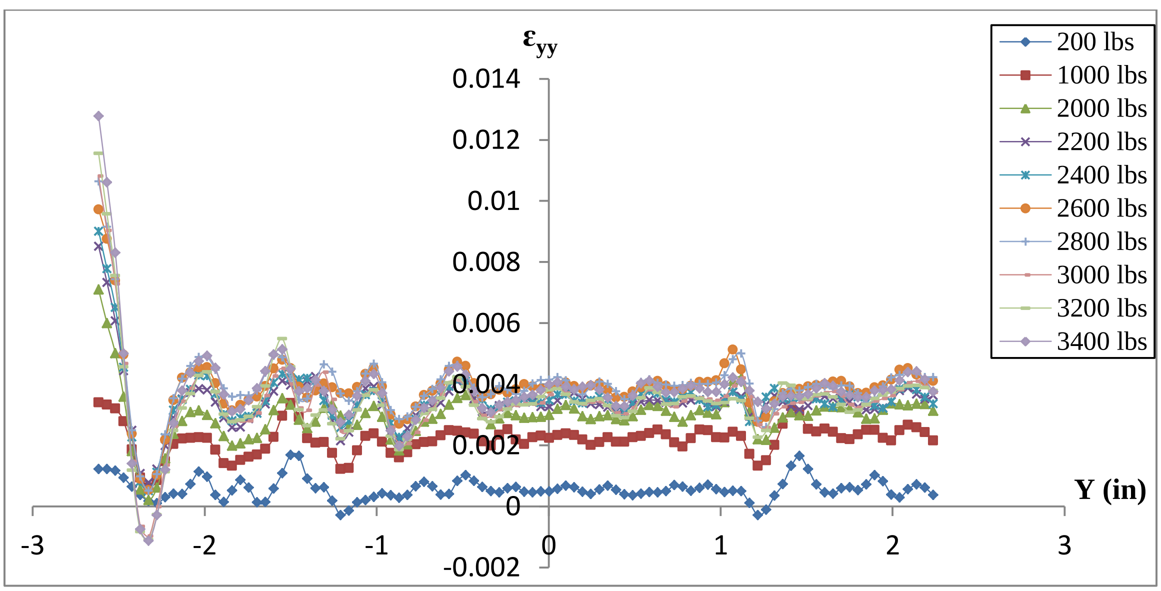

Figure 4-78: The strain (ε_{yy}) distribution along a cross section line (3-3) located on the left side of the plate

The strain (ε_{yy}) curves show that the strain at load 200 pounds has the lowest tensile strain curve. Then the strain (ε_{yy}) curves increase with loading. By increasing the load to 1,000 pounds the strain curve of 1,000 pounds is almost the same as the strain curve of 200 pounds but with higher strain values. This is similar to shifting the curve to the top. The 2,000 pounds strain curve is almost a shift of 1,000 pounds strain curve also. The strain at 2,600 pounds shows high strain curve values. The strain curves at the next loading look similar to each other until the failure curve.

The curve in the bottom shows very high tensile strain (ε_{yy}) in the bottom with respect to other strain values. This high strain is due to pulling out of the bottom edge of the plate and the teeth. The strain (ε_{yy}) curves are not flat lines from the top to the bottom of the plate along the cross section lines. Several spikes in the strain (ε_{yy}) curves are shown and repeated over the vertical cross section line. These sudden changes of the strain are due to the changes in the plate cross sectional area through the entire plate surface because of the slots. The slots are wavy distributed over the entire plate. Also the angle of the teeth that are embedded in the wood members also plays a big role in strain and the plate behavior.

Cross section line (1-1) shows the highest average strain (ε_{yy}) curve as shown in the figures. But the maximum strain (ε_{yy}) value the bottom edge of the plate is at cross section line (3-3). At cross section line (3-3) the strain (ε_{yy}) at the bottom of the plate decreases down to the negative strain values at limited regions of the plate.

In this test the specimen failed due to wood cracks along the bottom wood member. The crack occurred under the support. The high tensile strain (ε_{yy}) occurs at the bottom where the tooth withdrawal appears. This result shows that when it comes to the plate's failure the strain is high at higher load. The plate is in good shape. No cracks or damage were observed. The bottom tooth withdrawal is due to wood cracks not to losing tooth strength because of the load. The external load is not controlling the plate and the plate has very high strength against the external force. The tooth gripping is very high. So the strain curve is not fully organized with respect to external loading. Several spikes of the strain curves are shown along the vertical curves due to the waived-distributed slots that are distributed on the whole plate's surface.

The horizontal middle areas of the plate along the gap line does not show any significant changes in the strain curves which indicate that the plate is under very low load to fail. The plate tends to fail along that gap line because this is the place where the two wood members are connected and the area of the plate along this gap line is half of the plate's area on other plate's surface. Therefore, the failure of the plate is expected to start there. In this test, the failure stared in the wood and slightly affected the bottom edge of the plate.

The gap between the two connected wood members increases with an increase the load. The crack in the wood is developed from the right side of the plate and crosses below the bottom edge of the plate.

On the other hand, the metal plate also shows strain in x-direction (ε_{xx}). The strain (ε_{xx}) along y-direction direction for the cross-section lines (1-1), (2-2) and (3-3) is also found in the next Figures 4-79, 4-80 and 4-81.

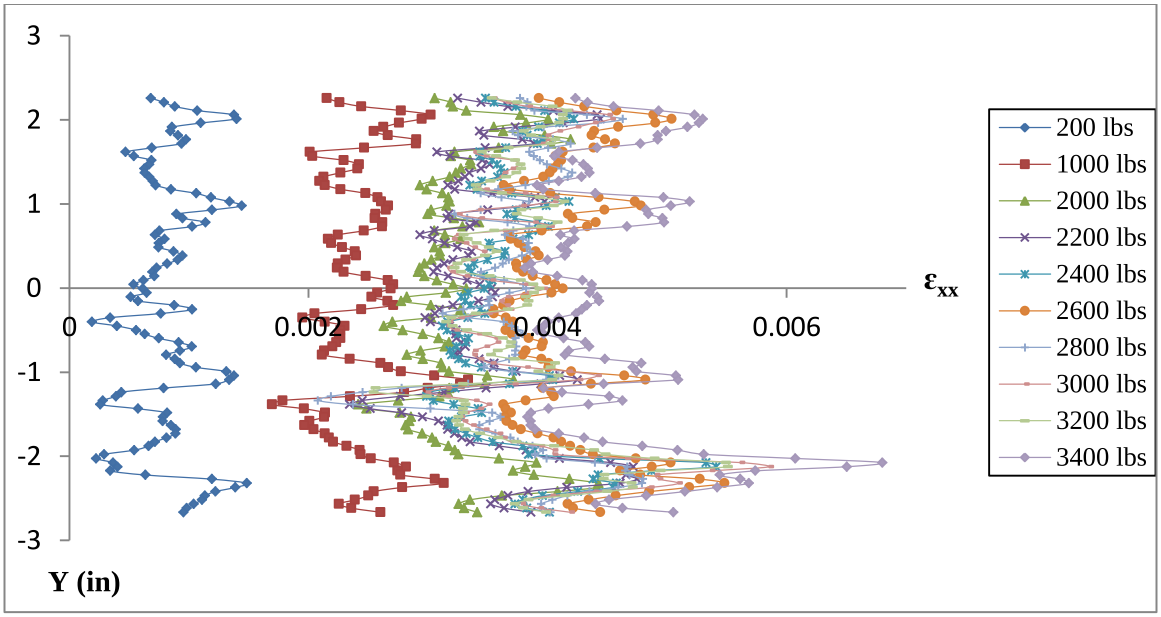

Figure 4-79: The strain distribution (ε_{xx}) along a cross section line (1-1) located on the right side of the plate

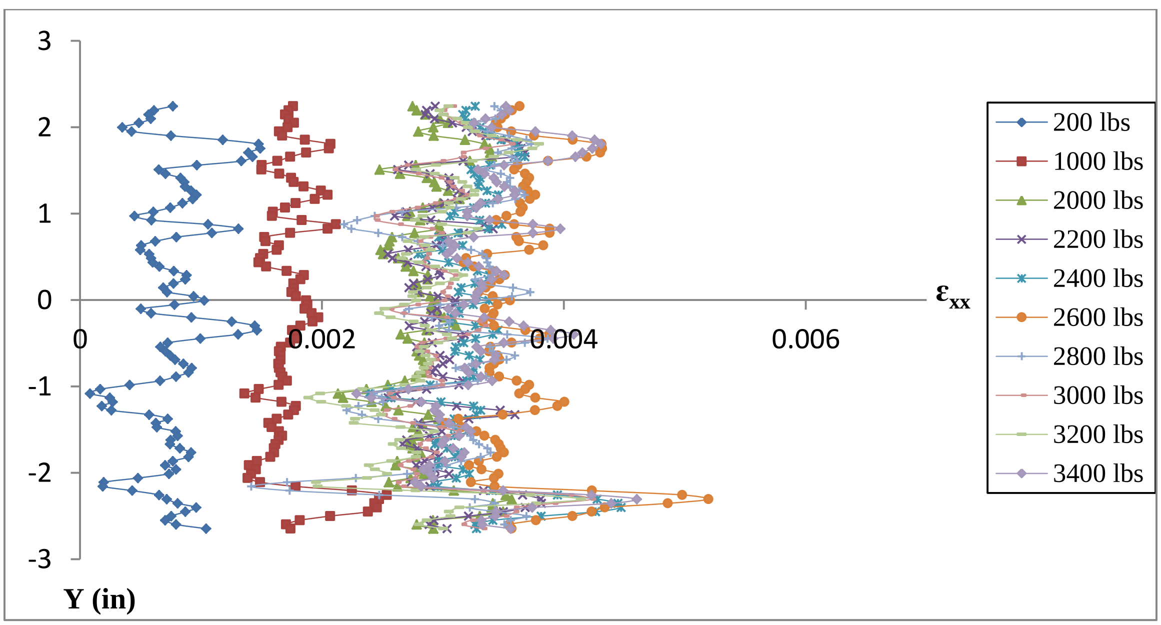

Figure 4-80: The strain (ε_{xx}) distribution along a cross section line (2-2) located near the vertical middle of the plate

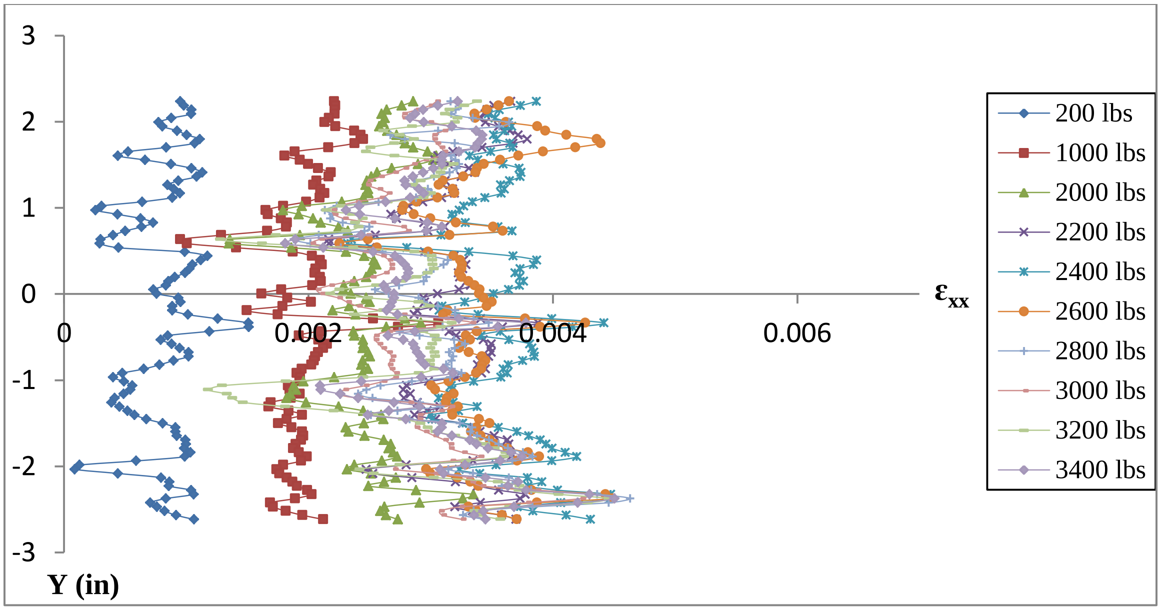

Figure 4-81: The strain (ε_{xx}) distribution along a cross section line (3-3) located on the left side of the plate

The figures show that the strain (ε_{xx}) is a tensile strain at all loading stages. The tensile strain (ε_{xx}) shows very close values to the previously described tensile strain (ε_{yy}). At 200 pounds the (ε_{xx}) curve has the lowest values in this test. Then the strain (ε_{xx}) increases with loading until 2,600 pounds. At 2,600 pounds the strain curve is one of the highest shown in the previous curves. At failure the strain curve (ε_{xx}) also shows high strain curve values.

In the bottom of the plate, where the wood crack has occurred, the strain (ε_{yy}) is high while the strain (ε_{xx}) is going down and it is very low. The strain curves along the cross section lines are not flat and fluctuate in the values. The reasons are described earlier in the strain curves (ε_{yy}) curves behavior. No significant changes in the strain (ε_{xx}) due to failure in the wood not in the plate.

4.1.2.3.3 A Comparison between the Strain in y and x Direction [(ε_{xx}) vs. (ε_{yy})]

In this section, the strain values {**(ε_{xx})** vs. **(ε_{yy})**} for the last image exactly at the failure at load 3,400 pounds will be compared. The next Figures 4-82 and 4-83 show the three cross-section lines for the last image exactly at the failure at 3,400 pounds for strain (ε_{yy}) and (ε_{xx}).

The curves in Figure 4-82 show that the first section line (1-1) has the highest strain (ε_{yy}) in the top part of the plate then cross-section line (2-2) then (3-3). There is very low strain (ε_{yy}) in the third cross-section line (3-3) and even goes to negative strain due to plate and tooth withdrawal at that left side edge of the plate.

The strain (ε_{xx}) in the Figure 4-83 show the three strain (ε_{xx}) curves. Cross section line (1-1) has the highest (ε_{xx}) values then the middle and the last is the left cross-section line (3-3). By checking the high (ε_{xx}) values in the same place you find low strain (ε_{yy}) in the strain curve.

Thus the strain curves (ε_{xx}) and (ε_{xx}) along the vertical cross section line are organized based on the high strain values. Where the strain (ε_{xx}) is high then the strain (ε_{yy}) is low. At high external load the strain in both directions show more organized strain distribution than the strain at lower load values. Both of the strains (ε_{xx}) and (ε_{yy}) are tensile strain with some exceptions. The strain (ε_{xx}) is not low and it is very close to (ε_{yy}). Thus, at low external loads the strain (ε_{xx}) should not be ignored.

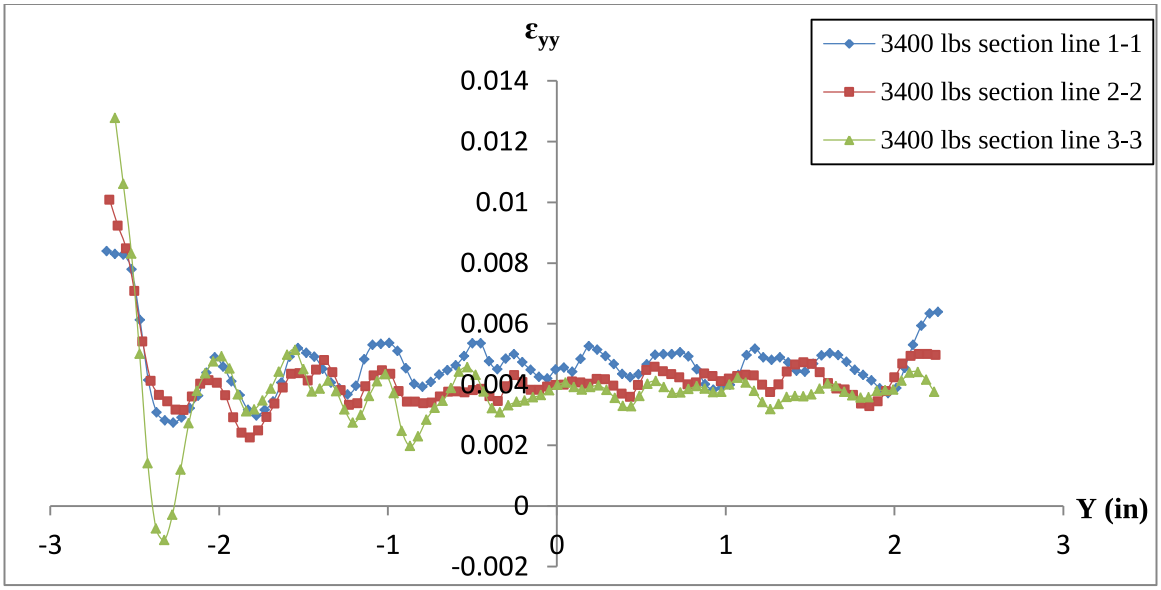

Figure 4-82: The strain (ε_{yy}) distribution along the three cross-section lines (1-1), (2-2), (3-3) for the last image at the failure at load 3,400 pounds

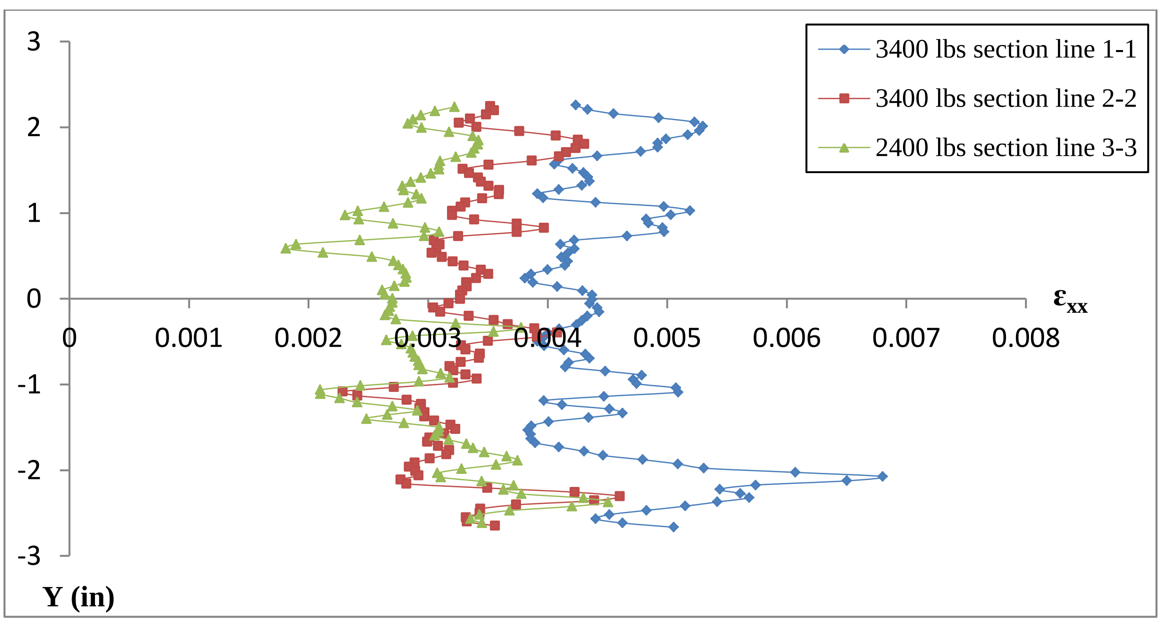

Figure 4-83: The strain (εxx) distribution along the three cross-section lines (1-1), (2-2), (3-3) for the last image before failure at load 3,400 pounds

4.1.2.4 The Third Tension Test (AE-3rd)

In this test, the two members of wood were connected by the MPC. The specimen was set on the universal testing machine. The first reference image was taken before applying any load. Figure 4-84 shows the first image which is considered as the reference image in digital image correlation technique.

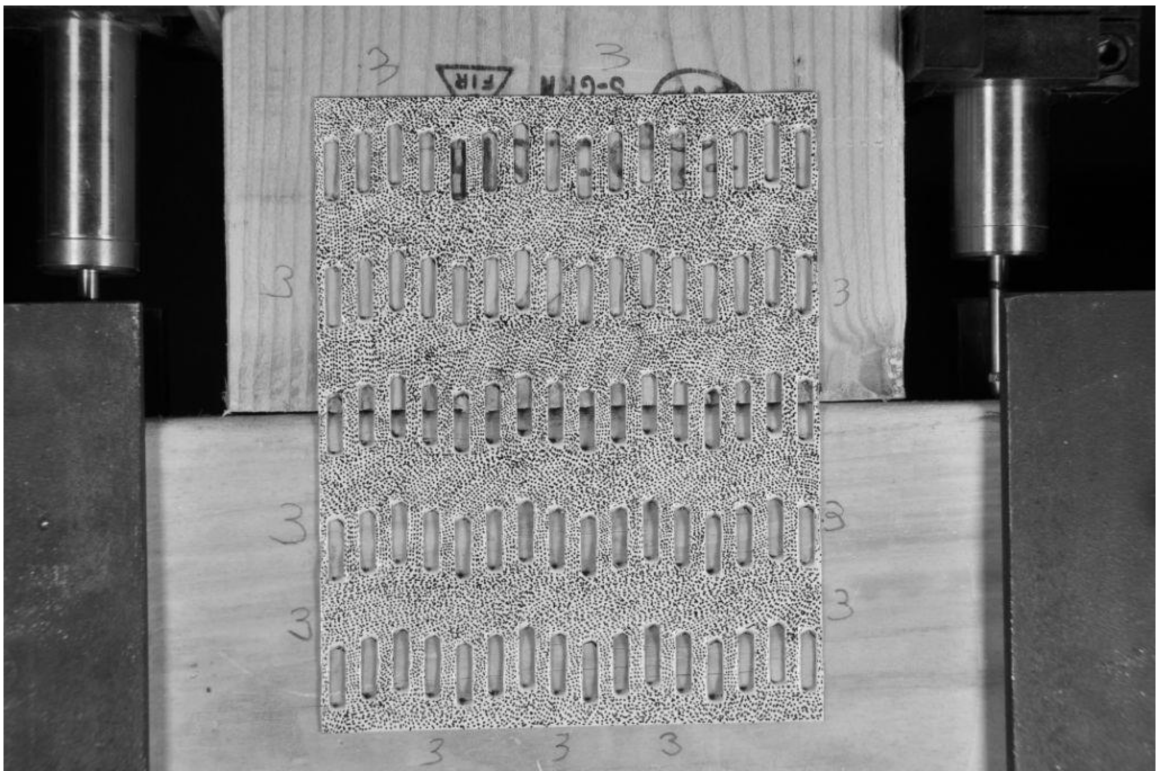

Figure 4-84: First image / reference image

After the first reference image was taken at load zero, the load was increased on the specimen until failure. The camera was placed on a fixed place and the MPC was perpendicular to the camera's lenses. Images were taken for the MPC specimen at each load increment of 200 pounds until failure. The failure in the member occurred in the wood. Figure 4-85 shows the last image after the failure.

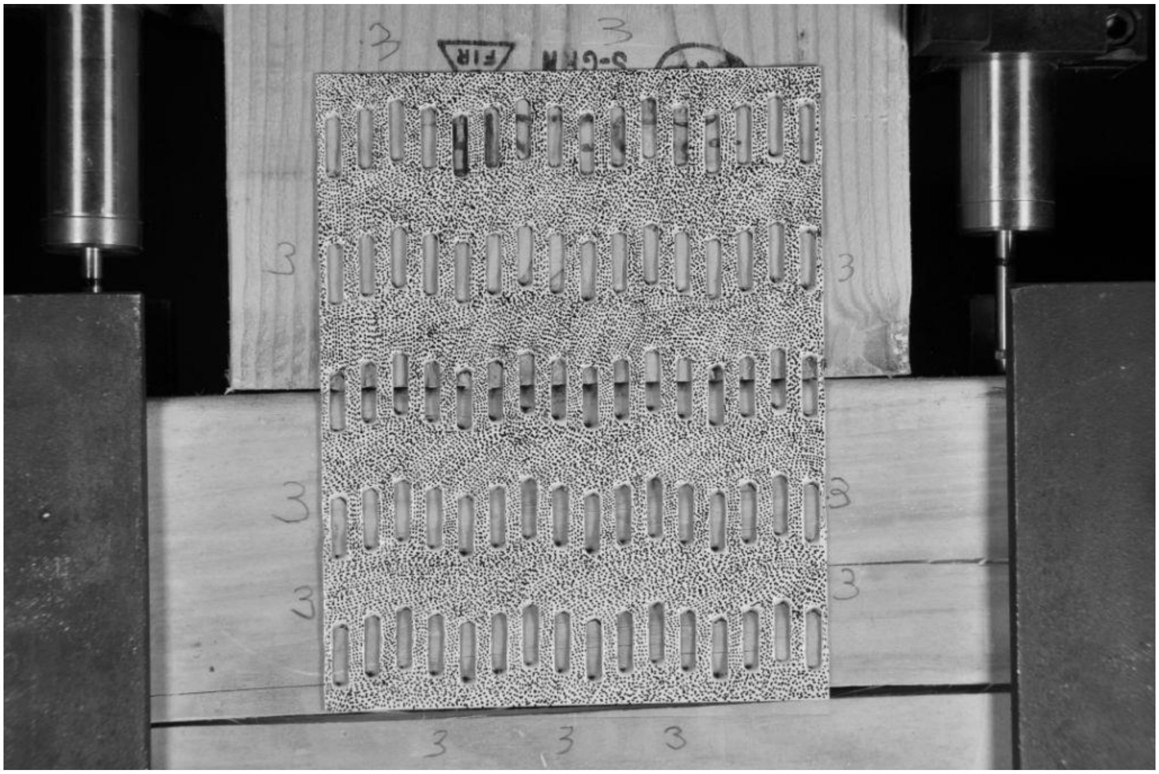

Figure 4-85: The last image after the failure

Fourteen (14) images were taken in addition to the reference image. The metal plate did not fail directly; however, some regions on the plate had tooth withdrawal. The main reason for failure was wood cracks. The wood failed at load equal to 2,800 pounds. The bottom wood member had a deep horizontal crack. The last image at the failure shows that the wood crack continues even after the machine stopped. The captured images were implemented in DIC-software to find the full-field strain measurements.

4.1.2.4.1 Analysis of the Full-Field Strain Results That Obtained From DIC Software

All the test images, which were obtained from the lab test, were implemented in the digital image correlation software Vic-2D. Each image was analyzed in relation to a reference image. The full-field strain measurements were obtained from the digital image correlation software. Figure 4-86 shows the strain in y-direction (ε_{yy}) for the image at 200 pounds.

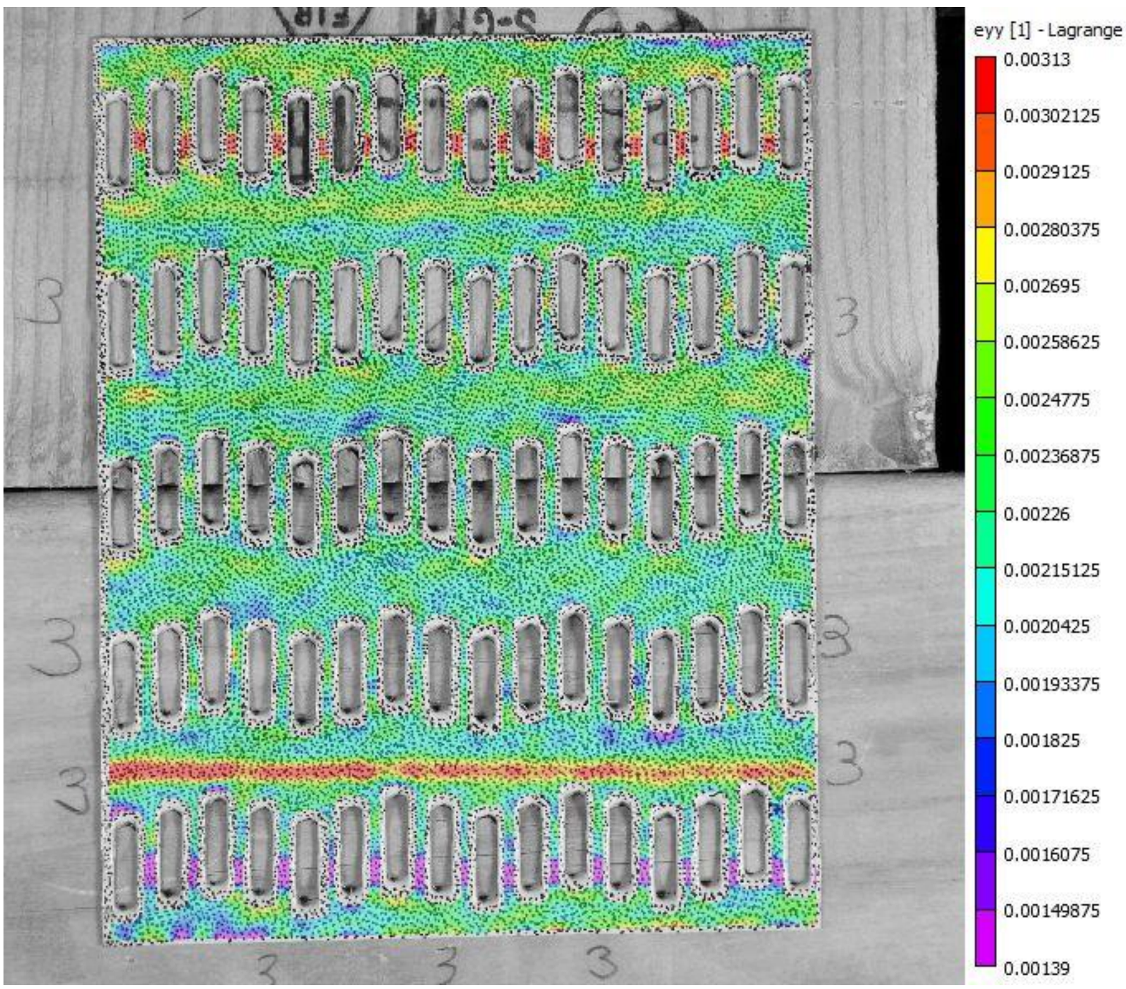

Figure 4-86: Full-field strain measurements (εyy) for the MPC at applying 200

The strain field's results show different levels of color and shows that each level of color represents a number. The failure in this test is in the bottom wood member so the changes in the strain over the surface of the plate are not that significant. However, DIC software can be used to show the changes in strain behavior under different loading increments. The image at 200 pounds shows that the strain (ε_{yy}) tensile strain over the entire plate. The strain field has values almost very close to each other with some high or low values with some exceptions. Although the strain (ε_{yy}) show fluctuation in the values over the plate's surface but in general they are very close. The full-field strain above the horizontal middle gap line is almost the same as the strain (ε_{yy}) underneath this line.

By loading, the strain (ε_{yy}) increases to higher tensile strain values. The full-field strain measurements for the image at 1,800 pounds and 2,000 pounds are very close. The strain field at this load is high and it is considered one of the highest strain field images in this test. Figure 4-87 shows the strain (ε_{yy}) field at 2,000 pounds. The figure shows that the strain (ε_{yy}) is higher at right side than the left side. The strain (ε_{yy}) above the horizontal middle gap line is almost very close to the strain field underneath this line. The highest strain (ε_{yy}) is shown at the bottom edge of the plate due to appearing of the wood cracks at those regions. The wood cracks also can be seen in between the bottom slots. The plate at 2,000 pounds is in very good conditions. No significant changes in the strain values or clear had tooth withdrawal. The cracks in the wood are starting from the bottom member in which the grain is perpendicular to tension load. The wood cracks also expand and develop through the wood under the support at this stage of loading. But the tooth gripping is still high over the entire plate at this stage.

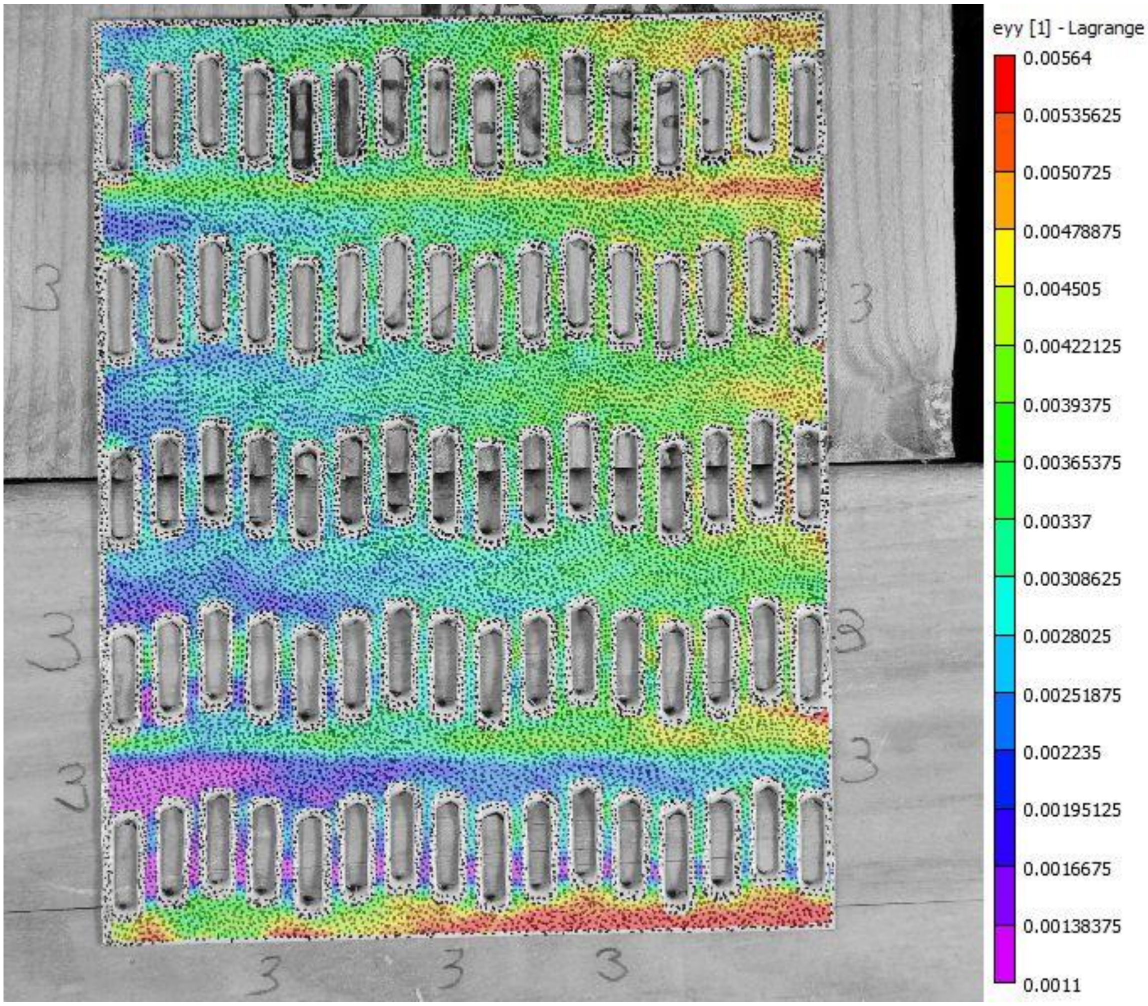

Figure 4-87: Full-field strain measurements (ε_{yy}) at 2,000 pounds

By an increase the load the strain (ε_{yy}) fields retreat back in its values until load 2,600. But at 2,800 pounds the strain field (ε_{yy}) proceeds again and it shows high full-field strain values as shown in Figure 4-88. The images show that the full-field strain measurements at 2,000 pounds are very close to the image at 2,800 pounds. The image does not show any significant high strain changes or special strain changes along the horizontal middle gap line where the two wood members are connected there. The bottom horizontal crack in the wood member shows more increasing in the crack's gap than

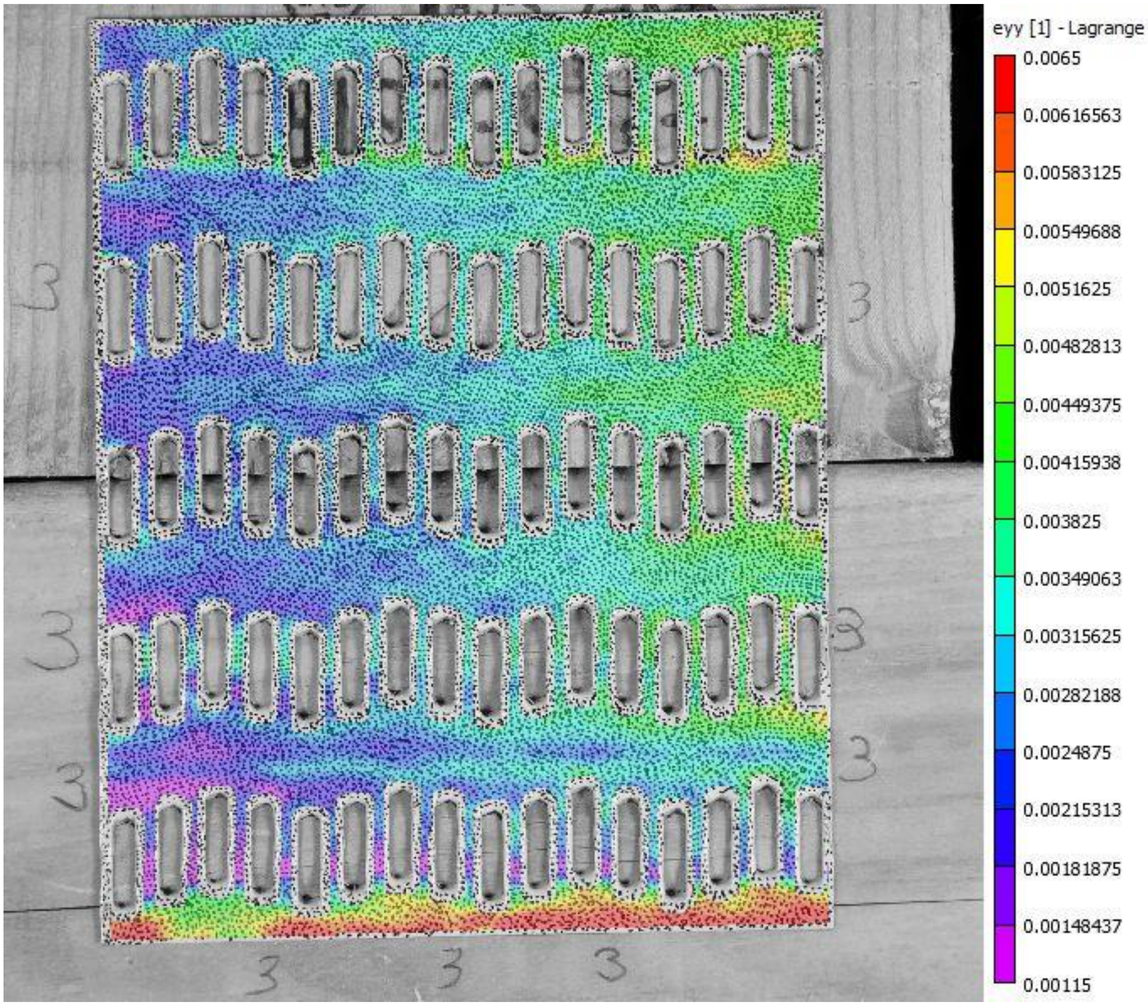

Figure 4-88: Full-field strain measurements (ε_{yy}) for the last image at the failure at 2,800 pounds

the previous images. At 2,800 pounds the machine stopped working due to the wood failure. Then the crack in the wood continues even after stopping the machine. The bottom horizontal crack at failure has expanded more. There is another crack under the support is seen after failure. The strain (ε_{yy}) is the highest at the bottom edge due to tooth withdrawal there. The strain (ε_{yy}) above the horizontal middle gap line is almost very close to the strain underneath the horizontal gap line.

On the other hand, the full-field strain (ε_{xx}) image in x-direction can also be obtained from digital image correlation software. The full-field strain measurements (ε_{xx}) is a tensile strain all over the 14 captured images. The strain (ε_{xx}) at 200 pounds is shown in figure 4-89. The figure shows that the strain (ε_{xx}) is tensile strain with low and very close values over the entire plate. But it fluctuates from one area to another. Some limited areas show high strain (ε_{xx}) while others show very low strain (ε_{xx}). The maximum strain (ε_{xx}) value is 0.003 while the minimum is 0.0012.

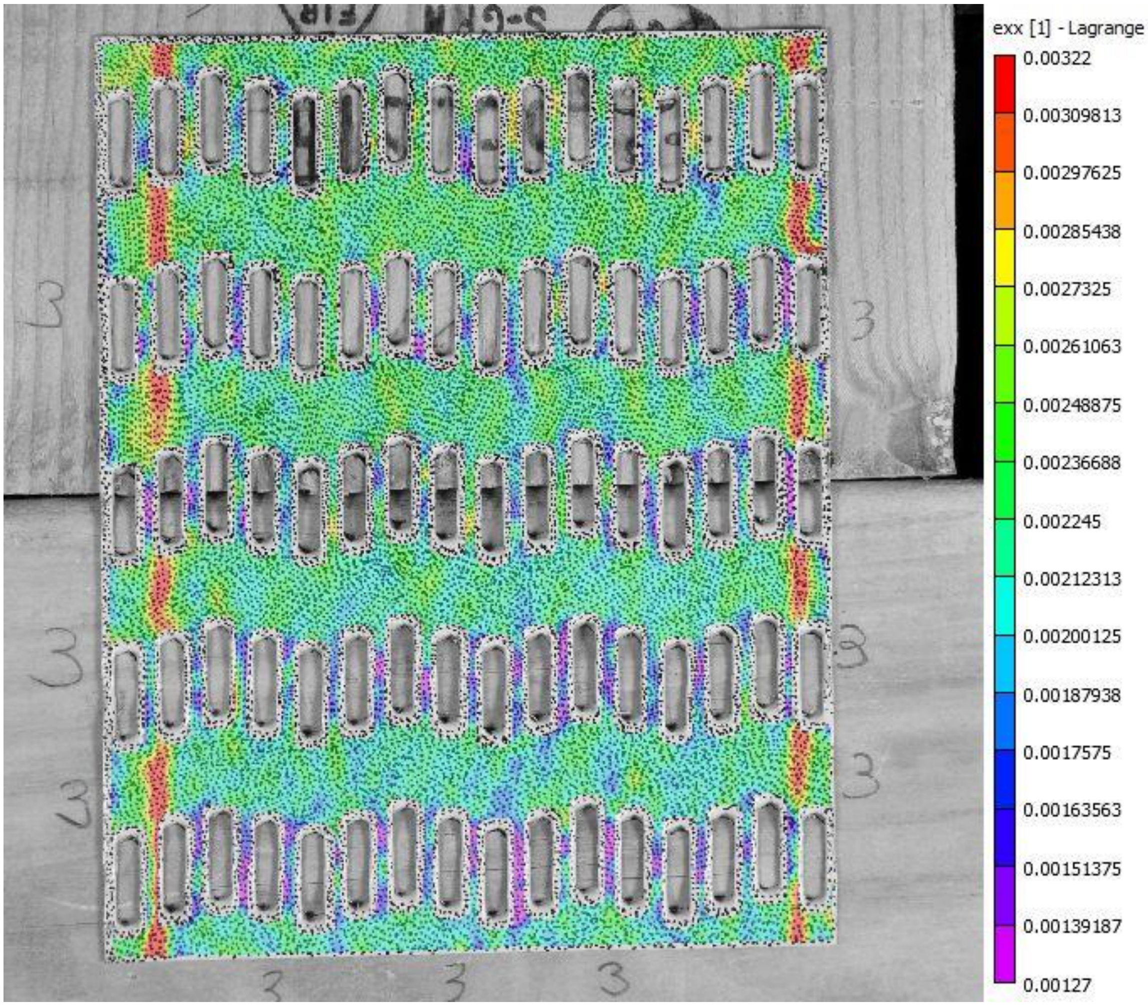

Figure 4-89: Full-field strain in x-direction (ε_{xx}) at load 200 pounds

The strain (ε_{xx}) increases with loading. The full-field strain measurement for the image at 2,000 pounds is shown in figure 4-90.

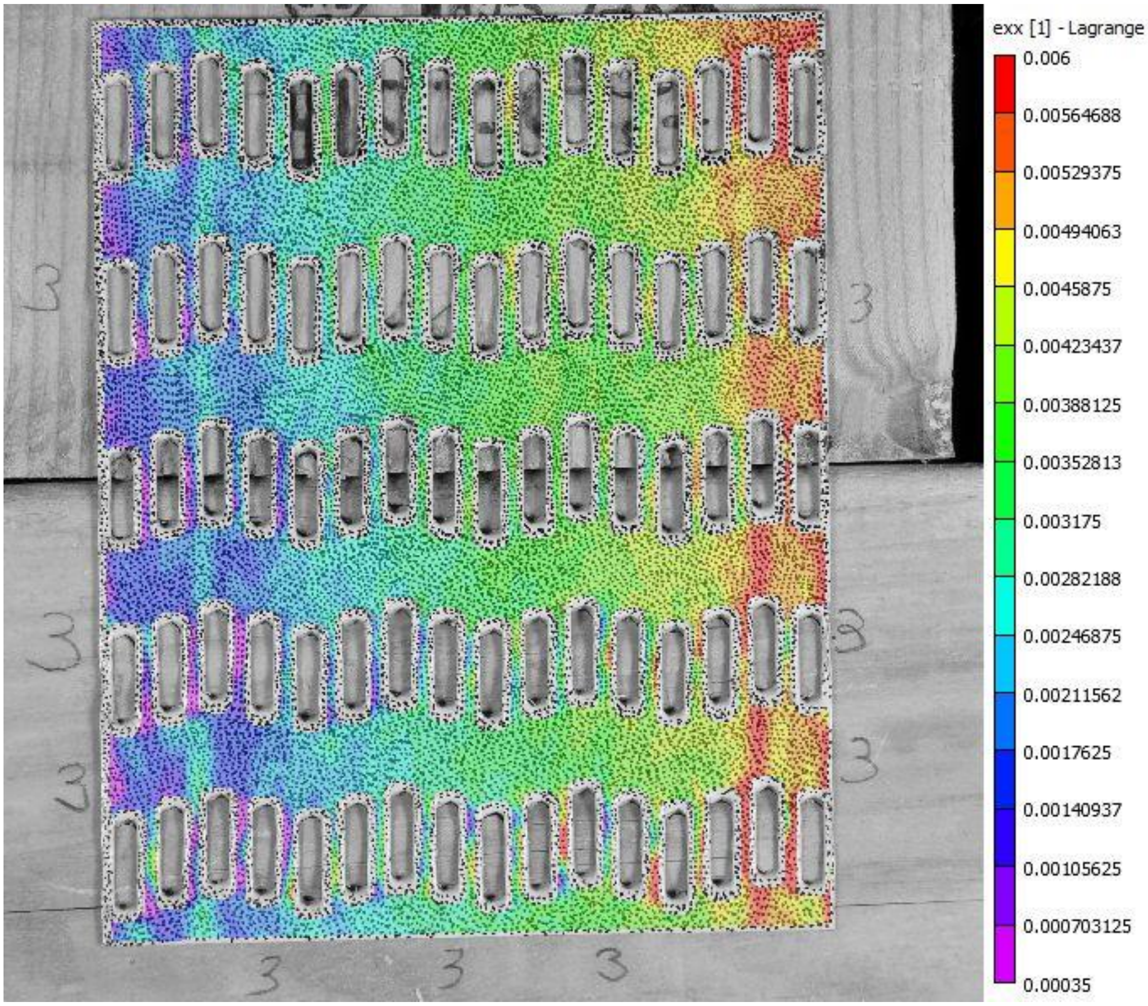

Figure 4-90: Full-field strain in x-direction (ε_{xx}) at load 2,000 pounds

The image at 2,000 pounds shows that the strain (ε_{xx}) on the right side is higher than the strain in the middle and the left side. In general the strain (ε_{xx}) is a tensile strain. The strain (ε_{xx}) above the horizontal middle gap line is almost identical to the strain below this line. The strain values can go high up to 0.006 on the right said of the plate and can go down to .0002 on the left side of the plate. The strain at 2,000 pounds shows more organized strain field behavior than the strain field at 200 pounds. By increasing the load the strain (ε_{xx}) is increasing and decreasing at some load. The full-field strain measurements (ε_{xx}) for the last image at the failure load 2,800 pounds is shown in figure 4-91. The strain (ε_{xx}) is high on the vertical right side then it is gradually vertically decreasing to the left side of the plate.

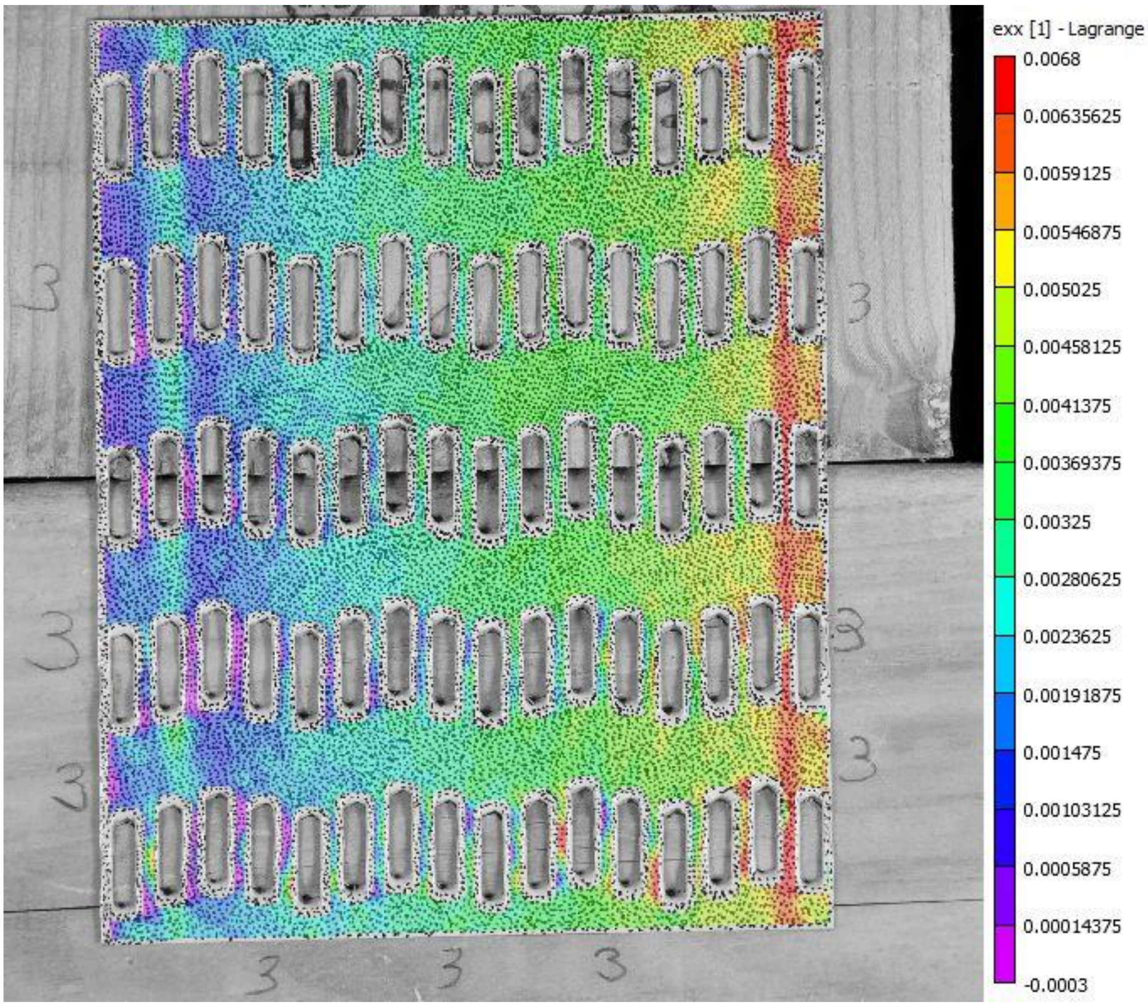

Figure 4-91: Full-field strain in x-direction (ε_{xx}) under load 2,800 pounds (the last image at failure)

4.1.2.4.2 Numerical Analysis for the Results

To analyze the DIC results numerically, a vertical cross section line from the top of the plate to the bottom is taken for some images starting with the first image at 200 pounds and ending with the last image at failure. The cross section is taken in three different locations as shown in Figure 4-92.

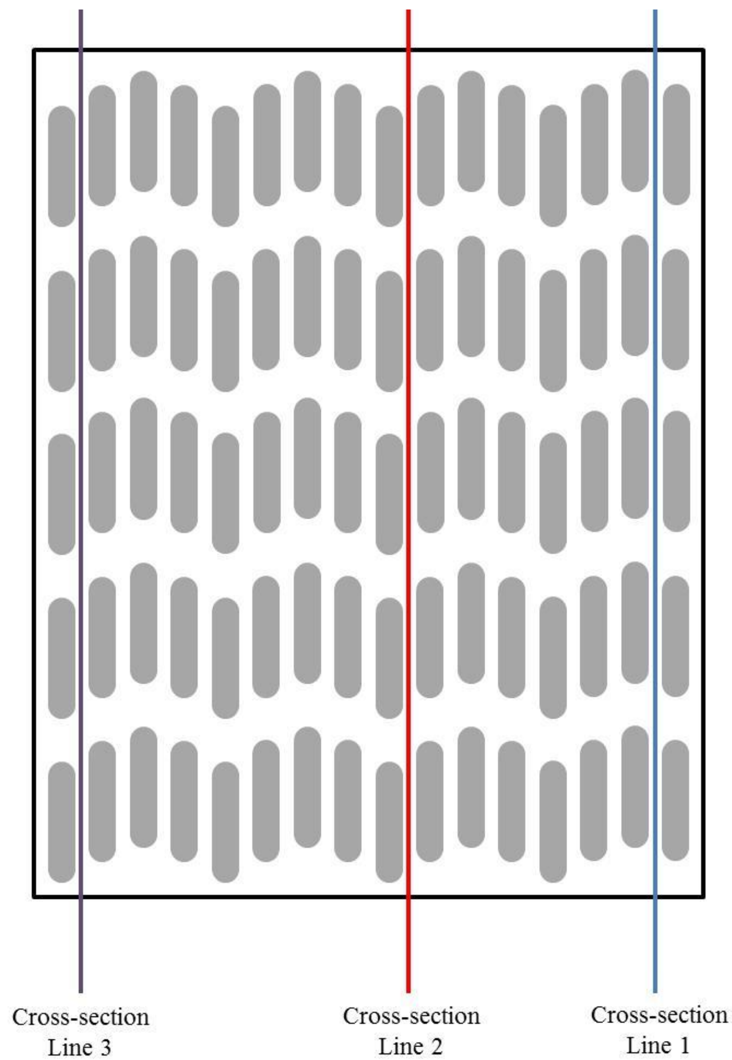

Figure 4-92: Metal plate with the cross-section lines along the vertical direction

The three locations of the cross section lines are as the following:

- The first cross section line (1-1) is from the right side of MPC @ x = 1.664 in.
- The second cross section line (2-2) is near the middle of the MPC @ x = 0.1521in.
- The third cross section line (3-3) is from the left side of MPC @ x = -1.86 in.

Three cross-section lines are taken for the strain field (ε_{yy}). The next three Figures 4-93, 4-94 and 4-95 show the distribution of strain (ε_{yy}) at three different locations for 8 images. Each image represents the value of the loading that is applied on the specimen of the two wood members connected by the metal plate connector.

The curves show that the first considered load is 200 pounds then the load increases gradually until failure. The failure is in the wood not in the plate. The curves show that the tensile strain (ε_{yy}) increases with an increase in the load. The strain along vertical cross section lines shows high strain along the vertical cross section line (1-1) then decreases gradually to (2-2) then (3-3). The strain (ε_{yy}) curve increases with loading until 2,000 pounds along the cross section line (1-1) and (2-2). The third cross section is shown less affected by loading than (1-1) and (2-2). Then the strain (ε_{yy}) shows retreating down. But the strain curve at 2,800 pounds shows high strain curve values along cross section line (1-1) and (2-2). At cross section line (3-3) it is high but less than the strain curve at 1,000 pounds. The strain fields images reveal that the left side of the plate shows a decrease in the strain (ε_{yy}) and also (ε_{xx}) with loading. This decreasing gradually decreases with loading.

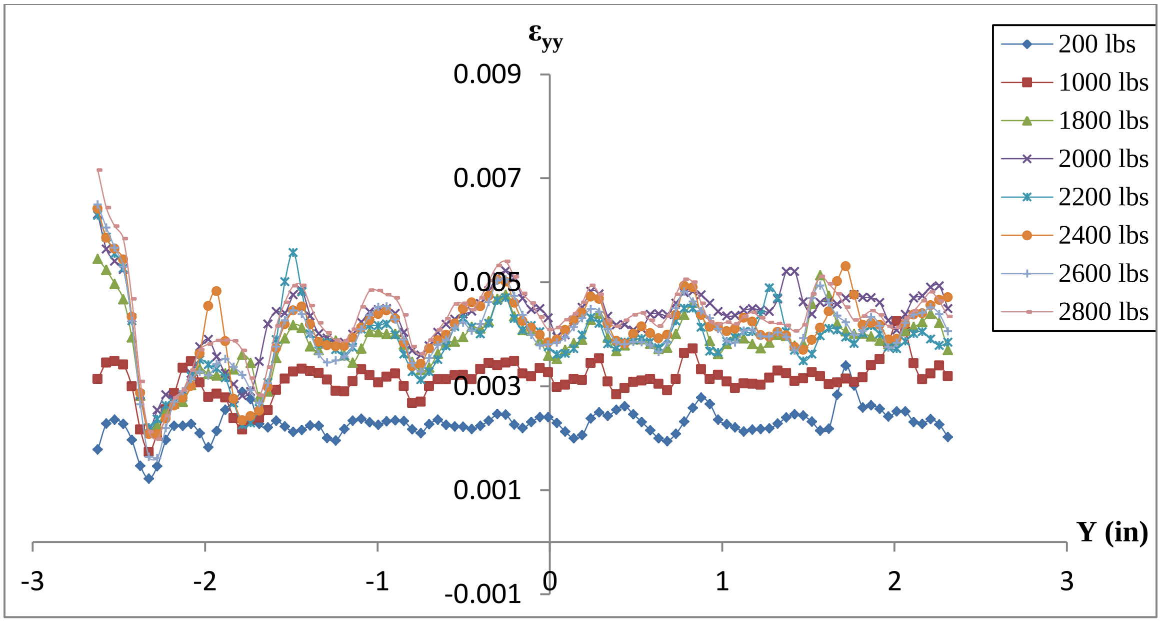

Figure 4-93: the strain distribution (ε_{yy}) along a cross section line (1-1) located on the right side of the plate

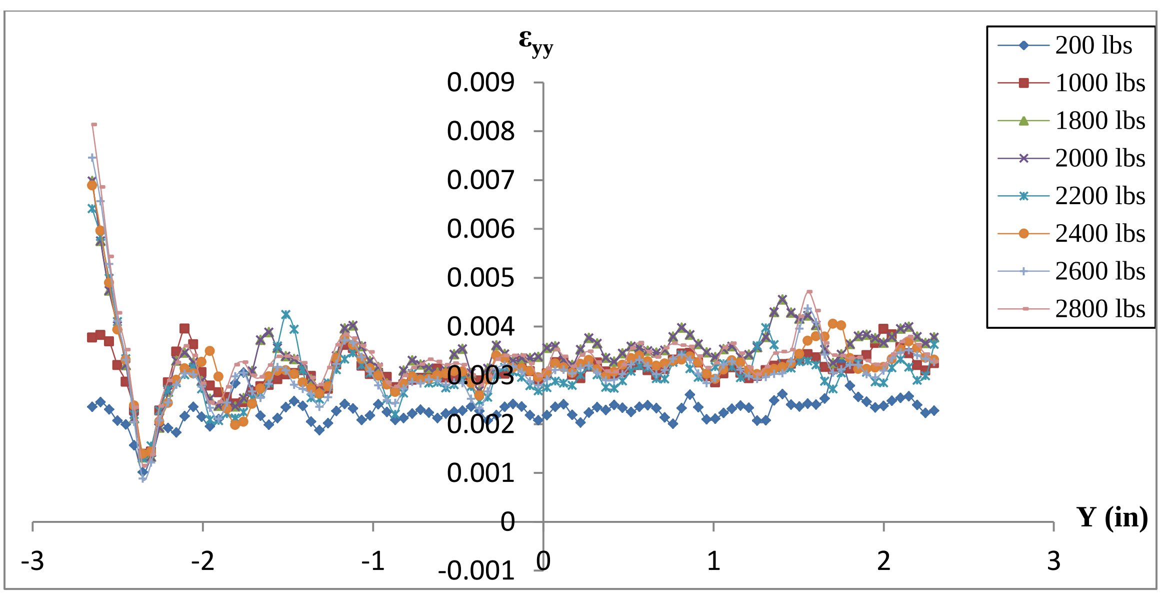

Figure 4-94: The strain (ε_{yy}) distribution along a cross section line (2-2) located near the middle of the plate

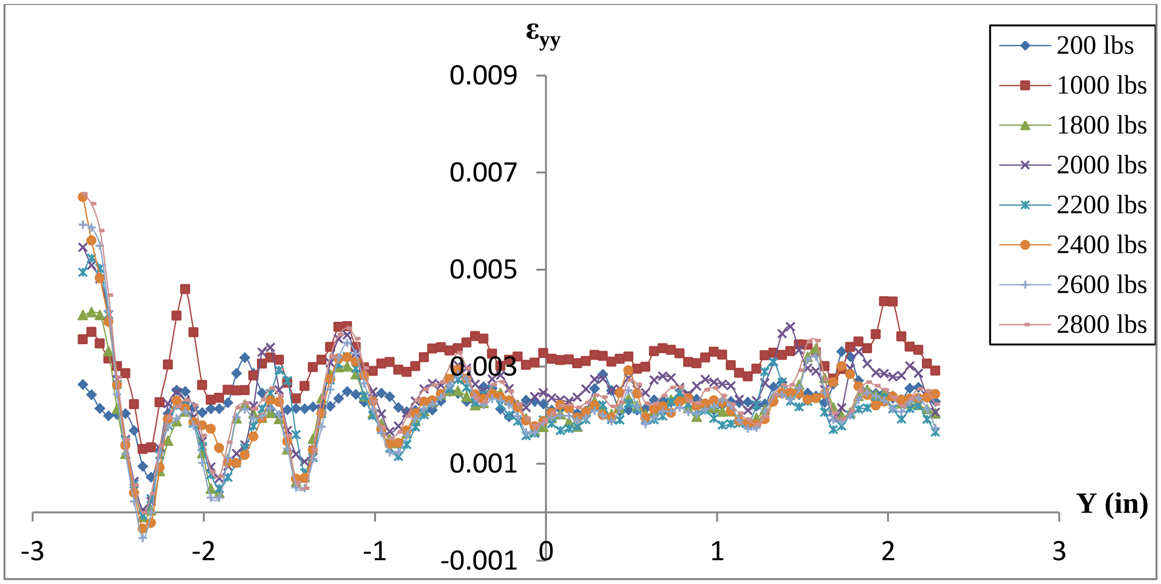

Figure 4-95: The strain (ε_{yy}) distribution along a cross section line (3-3) located on the left side of the plate

The higher strain changes is along the cross section line (1-1) then the middle cross section line (2-2) as shown in the strain (ε_{yy}) curves. The curves show that the strain (ε_{yy}) is highest at the end of the curves which is located at the bottom edge of the plate. The strain (ε_{yy}) decreases to compressive strain over a limited area between the slots located above the bottom edge of the plate. The bottom edge shows very high tensile strain and so a pulling out of the plate's edge. This pulling out of the plate's edge at the bottom presses on the little areas between the slots and causes a compressive strain.

The strain curve along the cross section line (2-2) is the most organized strain curves distribution all over the test. The strain curves fluctuate in their values up and down along the vertical cross section line. The least fluctuated strain curves is the strain curves at the cross section line (2-2). These changes in strain are due to many factors that affect the plate. The cross sectional areas over the plate's regions are not the same due to the presence of the slots over the entire plate. The angles of the teeth that are embedded in the wood also affect the direction of the shear forces that resists the external forces.

The specimen in this test failed due to wood cracks. The strain curves (ε_{yy}) do not show any significant changes in the strain that can lead to a plate failure. The cracks in the wood start horizontally in the bottom wood member. These cracks are along the bottom edge of the plate. Therefore, these cracks cause a high tensile strain in the bottom of the strain curves and also low tensile strain. Sometimes it is compressive strain as a result of pulling out of the bottom edge of the plate. This result shows that when it comes to a plate failure the strain reaction is obvious in the curves.

The plate is in good condition with no significant changes in its dimensions. No clear tooth withdrawal or any indication for significant continuous changes in the strain over the plate's surface is evident. So the tooth grip is very high and can resist higher external forces. The plate can stand more loads. The more load values may be a way over 3,000 pounds. This is the result here because the strain's distribution over the plate's surface fluctuates and changes with loading. This indicates that the teeth resist the external load and the direction of the angle of the teeth and the cross sectional area is still controlling the strain over the entire plate's surface. So the external force needs to be higher to resist and to take over the influence of the teeth over the plate. Also the external force can take advantage of the lower cross sectional areas on some regions over the plate's surface.

On the other hand, the metal plate also shows the strain curves in x-direction (ε_{xx}). The strain (ε_{xx}) along y-direction for the cross-section lines (1-1), (2-2) and (3-3) is also found in the next Figures 4-96, 4-97 and 4-98.

The figures show that the strain (ε_{xx}) is tensile strain with some limited exceptions along the cross section line (3-3). In general the cross section lines show high tensile strain curves values along the cross section line (1-1) and less than that at cross section (2-2) then the cross section line (3-3) shows the least tensile strain values and sometimes even go to compressive over some limited areas of the plate. The strain curves at the left side cross (3-3) decreases after applying 1,000 pound as shown in the next figure.

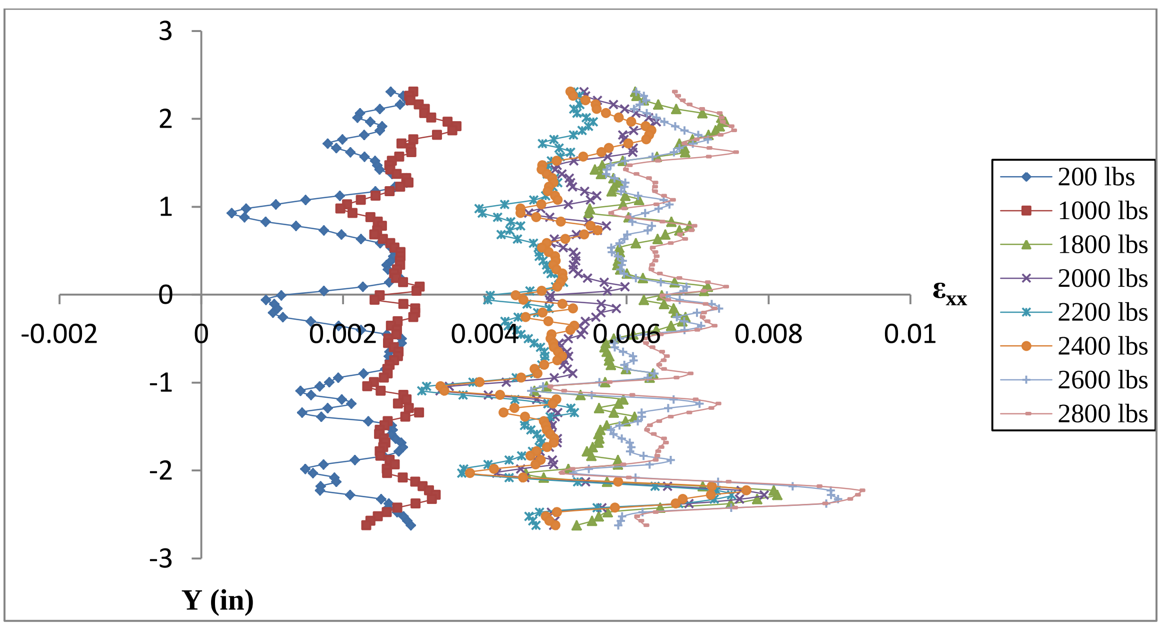

Figure 4-96: The strain distribution (ε_{xx}) along a cross section line (1-1) located on the right side of the plate

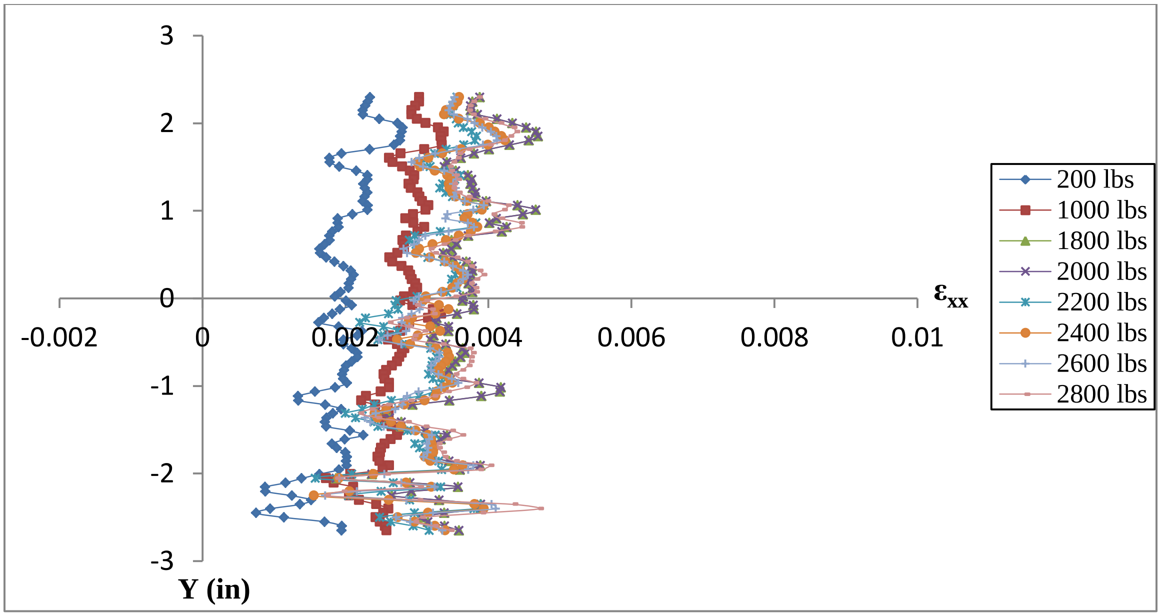

Figure 4-97: The strain (ε_{xx}) distribution along a cross section line (2-2) located near the vertical middle of the plate

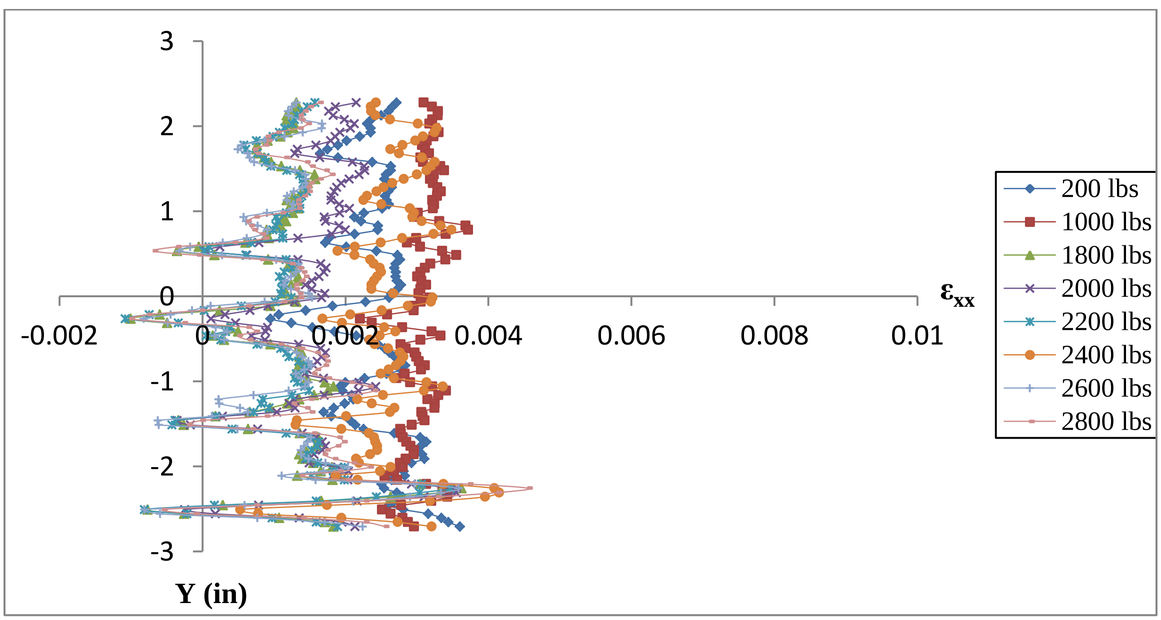

Figure 4-98: The strain (ε_{xx}) distribution along a cross section line (3-3) located on the left side of the plate

Tracking the strain curves in all the sections reveals that the strain (ε_{xx}) increases by loading from the top to the bottom of the plate. The strain (ε_{xx}) curves show decreasing and then they justify their behavior with loading and return back to increase. The plate tends to have high strain (ε_{xx}) on the right side of the plate and very low strain (ε_{xx}) or even compressive strain (ε_{xx}) on the left side. The strain curves (ε_{yy}) along the cross section line (3-3) also show lower tensile strain values than the other two cross sections. The strain (ε_{yy}) is negative strain values at a limited area of the plate while the plate behavior on the right side and the middle of the plate is different than the left side. The strain there is higher. Thus, the left side of the plate is more resistant to the load than the middle or the right side of the plate which hold higher strains.

The repeat spikes in strain curve along the cross section lines can also be shown through the strain curves (ε_{xx}). Cross section line (2-2) shows the most stable strain curve line. The external force is very low to make the strain curve behavior more organized. The effect of the teeth shear force that resists the external force is high. The teeth are distributed in a wavy shape through the entire plate. And the cross sectional areas are also different due to the presence of the slots everywhere the teeth are.

No significant changes in the strain behavior in this test are evident to show any indication for the plate's failure behavior. The distribution of the strains over the entire plate is not stable and they change gradually or non-gradually.

4.1.2.4.3 A Comparison between the Strain in y and x Direction [(ε_{xx}) vs. (ε_{yy})]

In this section, the strain values {**(ε_{xx})** vs. **(ε_{yy})}** for the last captured image at the failure at load 2,800 pounds will be compared. The next Figures 4-99 and 4-100 show the three cross-section lines for the last image before the failure at load 2,800 pounds for strain (ε_{yy}) and (ε_{xx}).

The cross section (1-1) which is located on the right side of the plate has the highest strain (ε_{yy}) followed by the middle then the third cross section line (3-3) which has the lowest (ε_{yy}). On the other hand, the same arrangement for the strain in x-direction (ε_{xx}) in Figure 4-99 at section (3-3) shows very low values and decreases to negative values which mean compressive strain. All the strains (ε_{yy}) values are tensile strain. The strain (ε_{xx}) are tensile strain along cross section line (1-1) and (2-2). The strain (ε_{xx}) along cross section line (3-3) shows some negative strain values which means compressive strain. Thus, the plate's strain (ε_{yy}) and (ε_{xx}) in general is a tensile strain. The strain values (ε_{xx}) are in general higher than (ε_{yy}) values in section (1-1). It can reach up to 0.009 and in average of 0.006-0.007 as shown in Figure 4-100. The strain (ε_{xx}) in the middle cross section line (2-2) tends to approach a higher value than the strain (ε_{yy}) values while the strain (ε_{xx}) in the third cross section line (3-3) is lower than the strain (ε_{yy}) and also it is a compressive strain. The bottom member of wood which has the grain perpendicular to the direction of load has a crack pass under the plates causing the plate to pull out and some areas to have tooth withdrawal. These changes in the wood and the plate affect the strain values in all directions.

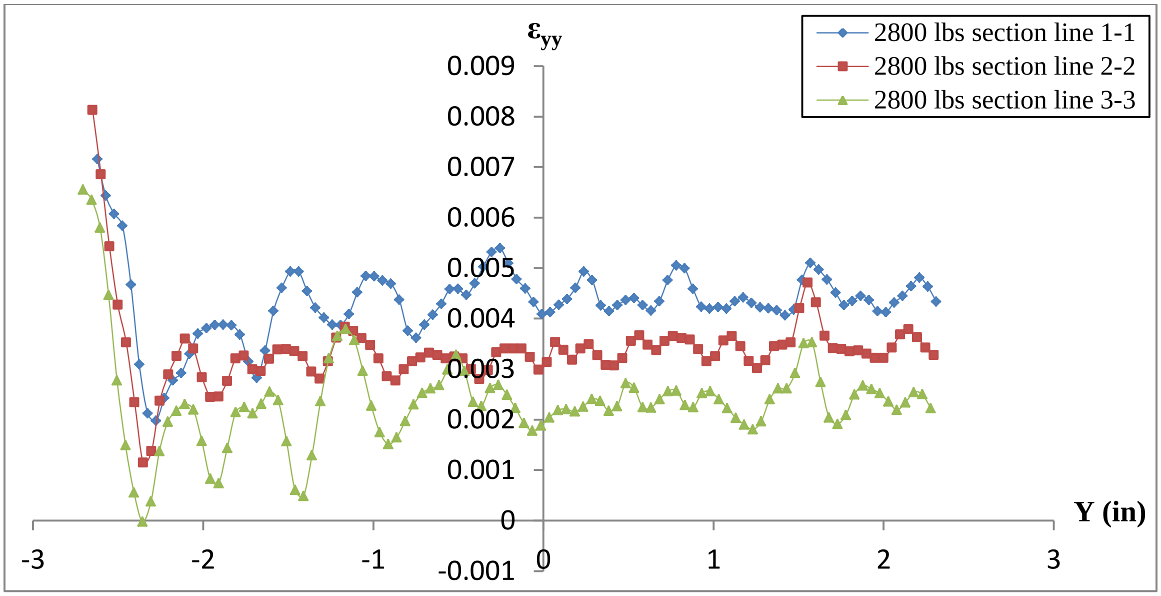

Figure 4-99: The strain (ε_{yy}) distribution along the three cross-section lines (1-1), (2-2), (3-3) for the last image before failure at load 2,800 pounds

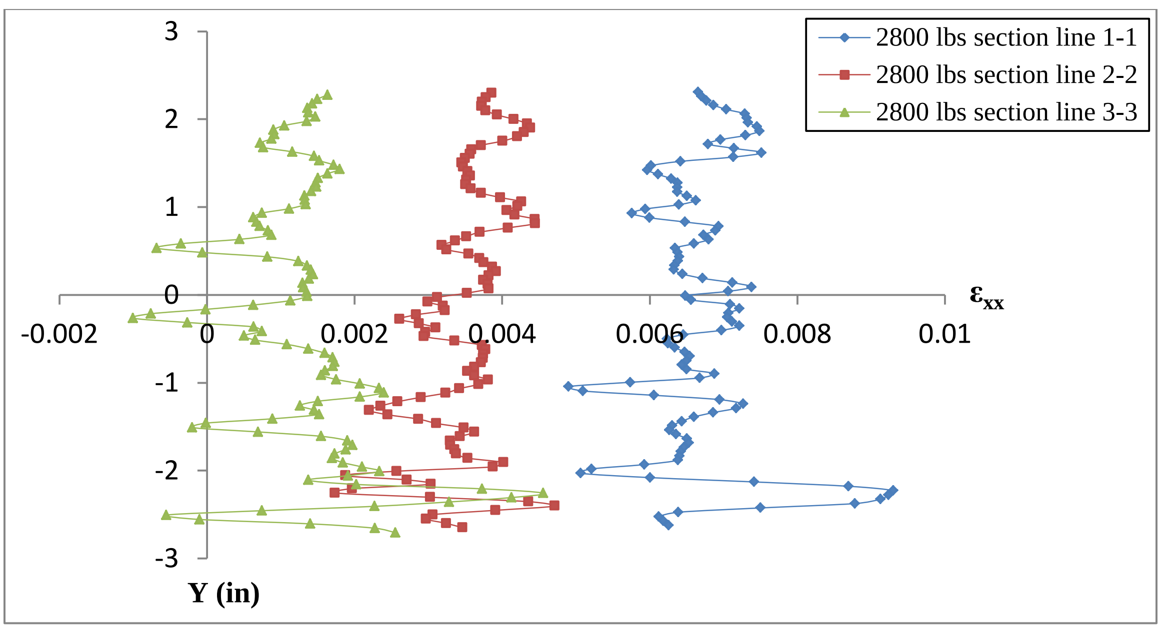

Figure 4-100: The strain (εxx) distribution along the three cross-section lines (1-1), (2-2), (3-3) for the last image before failure at load 2,800 pounds

4.1.2.5 Comparison between the Displacement from LVDT and DIC-Code

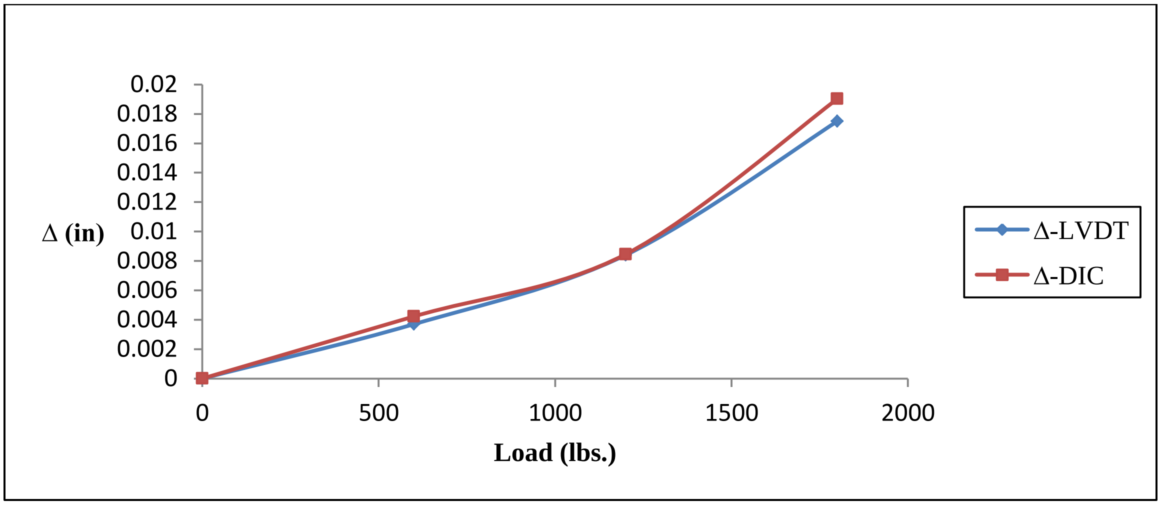

Figure 4-101: The displacement from LVDT vs. the displacement from DIC-code for the 1st AE test –the right side gap

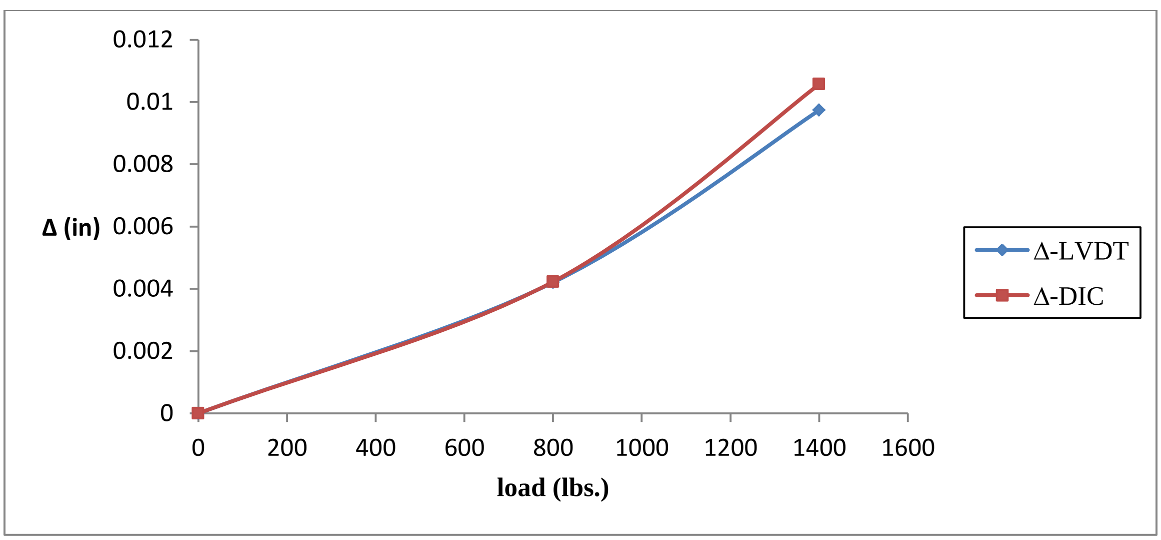

Figure 4-102: The displacement from LVDT vs. the displacement from DIC-code for the 1st AE test –the left side gap

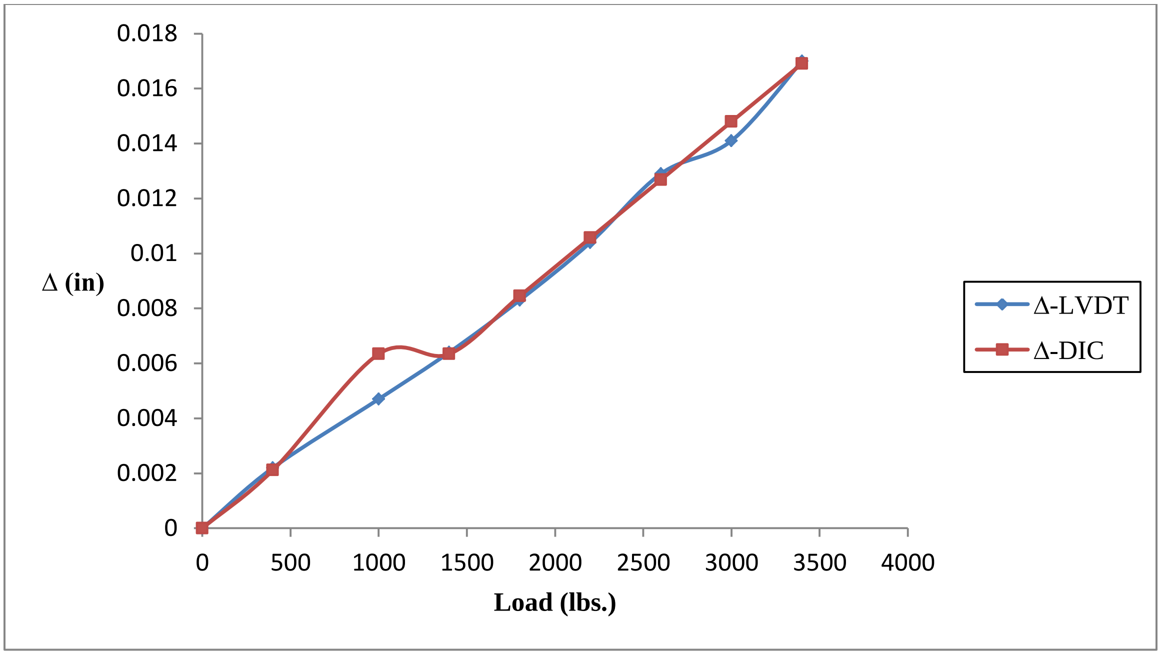

Figure 4-103: The displacement from LVDT vs. the displacement from DIC-code for the 2nd AE test –the right side gap

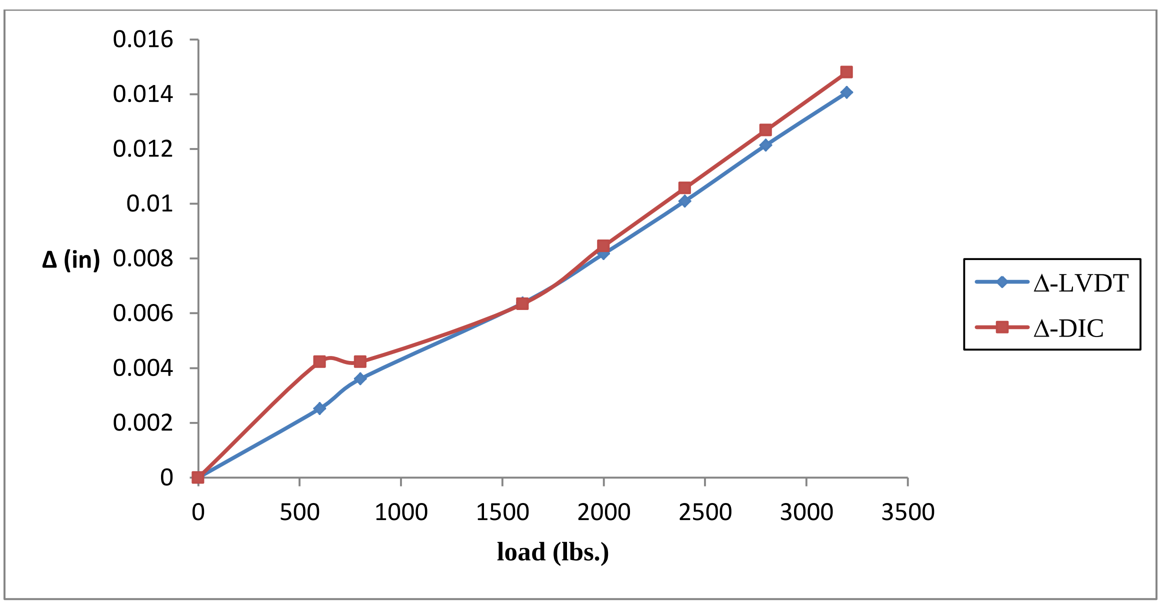

Figure 4-104: The displacement from LVDT vs. the displacement from DIC-code for the 2nd AE test –the left side gap

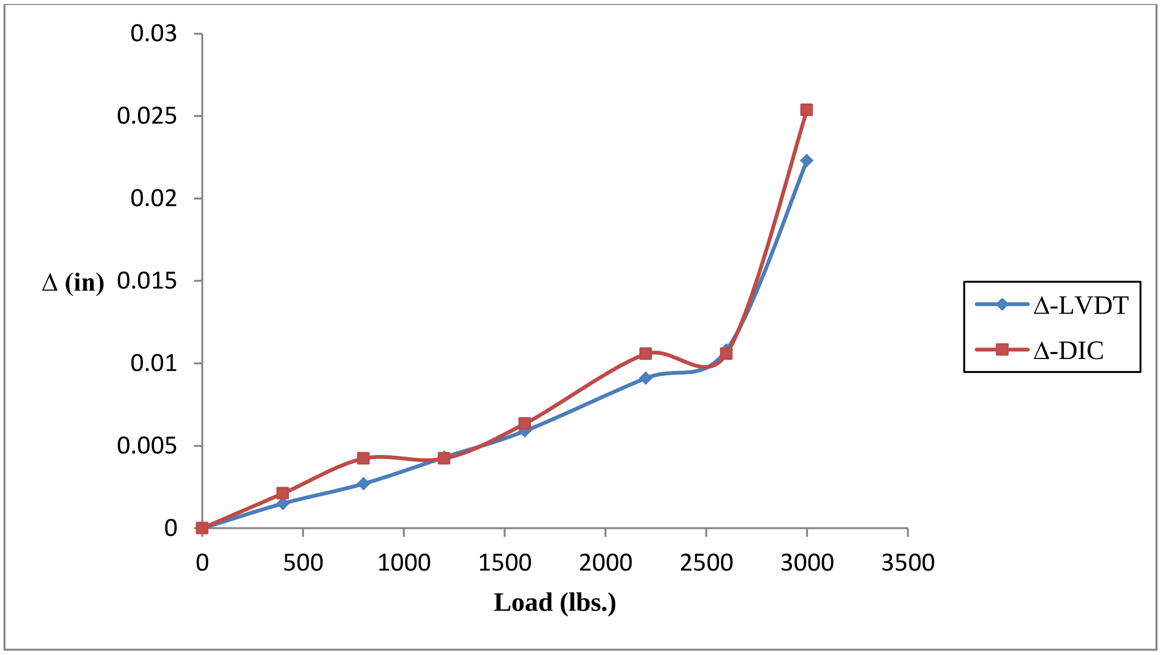

Figure 4-105: The displacement from LVDT vs. the displacement from DIC-code for the 3rd AE test –the right side gap

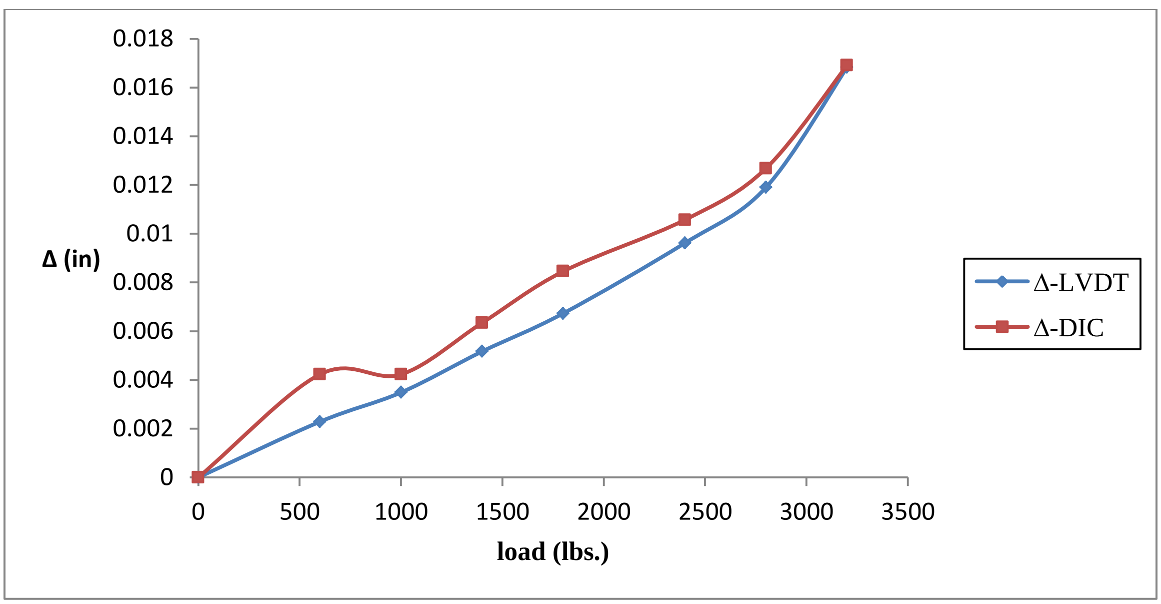

Figure 4-106: The displacement from LVDT vs. the displacement from DIC-code for the 3rd AE test –the left side gap

4.1.2.6 The AE-Tests Summary and Discussion

Three tests (AE) were conducted in the lab. The specimens were loaded until failure. A digital camera was used to capture images every 200 pounds. All the captured images were implemented in digital image correlation software Vic-2D. All the three tests failed at the bottom wood member. Horizontal wood cracks occurred in the bottom wood member and under the steel support. The plate is in good shape at the failure load. Tables 4-5, 4-6 4-7 show a brief description for each test.

Table 4-5: Brief description for each test-AE

AE-Test #	Failure load (lbs.)	Total Deformed Processed Images by DIC Code	Failure Behavior Description
1	1,940	10	wood failure/ The bottom wood member cracked horizontally
2	3,400	17	wood failure/ The bottom wood member cracked horizontally especially below the support
3	2,800	14	wood failure/ The bottom wood member cracked horizontally in more than one position

Table 4-6: Brief comments on each AE-test

AE Test #	Comments on the Test and the Failure
1	The available captured images are 10 images plus the reference one. The last image at failure has been processed by DIC-code due to wood failure. No significant changes on the plate itself. (ε_{yy}) and (ε_{xx}) are tensile strain most of the times.
2	The available captured images are 17 images plus the reference one. The last image at failure has been processed by DIC-code due to wood failure. No significant changes on the plate itself. (ε_{yy}) and (ε_{xx}) are tensile strain most of the times.
3	The available captured images are 15 images plus the reference one. The last image at failure has not been processed by DIC-code because the failure happened and continues so the last image represents the complete failure not the beginning of failure. (ε_{yy}) and (ε_{xx}) are tensile strain most of the times.

Table 4-7: Brief strain changes description for each AE-test

AE-Test #	The Strain (ε_{yy}) Changes
1	The tensile strain increases until load 600 pounds. Then the strain decreases. The strain at 1,940 pounds shows higher tensile strain near the wood crack.
2	The tensile strain increases until load 2,600 pounds then a slight decrease is shown in the strain values. The strain at failure is also as high as the strain at 2,600 and higher over some plate's areas. The strain is high at the crack region.
3	The tensile strain increases until load 2,000 pounds then a slight decrease is shown in the strain values. The strain at failure is also as high as the strain at 2,000 and higher over some plate's regions. The strain is high at the crack region.

All the three (AE) tests are described in the previous three tables. All the last three tests show that the failure is in the bottom wood where the wood's grain direction is perpendicular to the plate's major axis and to the external tension force. The maximum load that the last test could reach before wood failure occurs is 3,400 pounds. The bottom horizontal wood cracks cause tooth withdrawal and pulling out of the edge of the plate away from the wood. This causes a high strain on the full-field strain images.

The strain (ε_{yy}) at load 1,940 holds the highest strain values among all images at different loading due to tooth withdrawal there. On other full-field strain curves, some regions of the plate surface shows strain values at 600 pounds higher than the strain values at the same places at load 1,940 pounds. The strain at 600 pounds on some plate's regions is higher than the strain at 1,940 pounds. This result shows that when it comes to the plate's failure the strain is high at higher load. Also this result shows that the external load does not control the plate and the plate has very high strength against the external force. The tooth grip tends to remain secure. Thus, the strain curve is not fully organized with respect to external loading. Some spikes of the strain curves shown along the vertical curves are due to the waived-distributed slots that are distributed on the whole plate's surface. The full-field strain measurement for the last image at the failure load shows that the strain (ε_{xx}) is as high as the strain (ε_{yy}). Thus, at early stages of loading before 3,400 pounds the strain (ε_{xx}) cannot be ignored and should be considered along with the strain (ε_{yy}).

Both strains (ε_{xx}) and (ε_{yy}) are tensile strain in the test with some limited exceptions. This indicates that the stretch in the wood is also a factor that can affect the strain results and so the plate's behavior. The presence of teeth distributed in a wavy pattern on the plate also plays a major role in changing the strain (ε_{xx}) proposed behavior. The wood is anisotropic material, and the external load should be high enough to control the strain behavior and wood properties.

This test does not show any significant changes in the strain field or strain curves of the plate. The strain curves in this test, as described earlier in this section, increase with loading then they retreat down then they increase again at higher loading stages. This fluctuation in the strain curves and strain values at different loading stages is clearly in the strain curves behavior. This indicates that the external tension force that affects the specimen is very low to show a significant change in the strain behavior. The strain behavior is not organized very well over the plate's surface even at the last load at the failure. The plate is in a very good shape and condition. No clear tooth withdrawal or cracks occurred in the plate. In general, the plate is in good condition and no indications for sudden low or high strain changes were observed. The horizontal middle areas of the plate along the gap line doesn't show any significant changes in the strain curves which indicate that the plate is under very low load at failure. This horizontal gap line is the place where the two wood members are connected and the area of the plate along this gap line is half of the plate's area on other plate's surface. Thus, the failure of the plate is expected to start there. In this test the failure starts in the wood and only slightly affected the bottom edge of the plate.

The plate is in good condition with no significant changes in its dimensions. No clear tooth withdrawal or any indication for significant continuous changes in the strain over the plate's surface is evident. The tooth grip is secure and can resist higher external forces. The plate can withstand more loads. The added load values could be over 3,400 pounds. The strain's distribution over the plate's surface fluctuates and changes with loading. This indicates that the teeth resist the external load. The direction of the teeth angle and the cross sectional area controls the strain over the entire plate's surface. Thus, the external force needs to be higher to take over the influence of the teeth over the plate. Also the external force can take advantage of the lower cross sectional areas on some regions over the plate's surface.

The gap between the two connected wood members increases with an increase in the load. The crack in the wood developed from the right side of the plate makes the lower wood member to rise up so that the last image shows that the gap closes instead of opening. This explains why some tensile strain curves in the previous figures have lower strain values than other curves even when they are under less load. This effect of wood crack can be seen clearly in the last image at load 1,940 pounds in the first AE test. The strain curve for the last image is lower than that for other images with lower load. Thus, the pressing of the wood due to crack also influences the fluctuation in the strain curves at different loading.

The displacement of the gap between the two pieces of wood was found using the DIC Vic-2D software based on the number of pixels in the vertical direction in each image under loading. Then the calibration from the software is used to change the pixels to inches. The calibration factor is 0.002113. The results from the LVDT are used to compare the displacement of the gap from LVDT to the displacement that is found using the digital image correlation software Vic-2D.

4.1.3 EA–Tension Test

In the EA-tension test the tension load is perpendicular to the plate slots or the plates' major axis but parallel to the wood grain. Three specimens of two members of wood connected by a metal plate connector were prepared for testing. After preparing the specimens they sat for 7 days before the test. They were tested under tension force in the in the civil engineering lab using the universal testing machine. The load increment is 200 pounds and an image was taken at each load increment until failure using a CCD camera that set at a fixed stand. The captured images have been implemented into the digital image correlation software (Vic-2D) to obtain the full-field strain measurements.

LVDT machine is used to verify the results from the digital image correlation software. Two LVDT machines are used on the right side and the other on the left side of the joint. The displacements between the two connected wood members at the gap can be measured by LVDT machine at different loading stages.

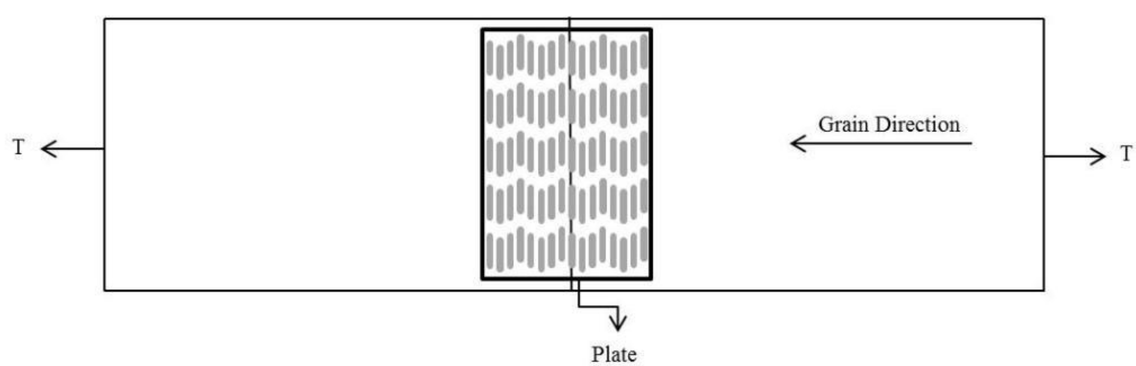

Figure 4-107: EA- sample test shape

4.1.3.1 Plate's Axis Direction Based on DIC Software

The direction of the x and y axis was obtained from the digital image correlation software as shown in the next two Figures 4-108 and 4-109.

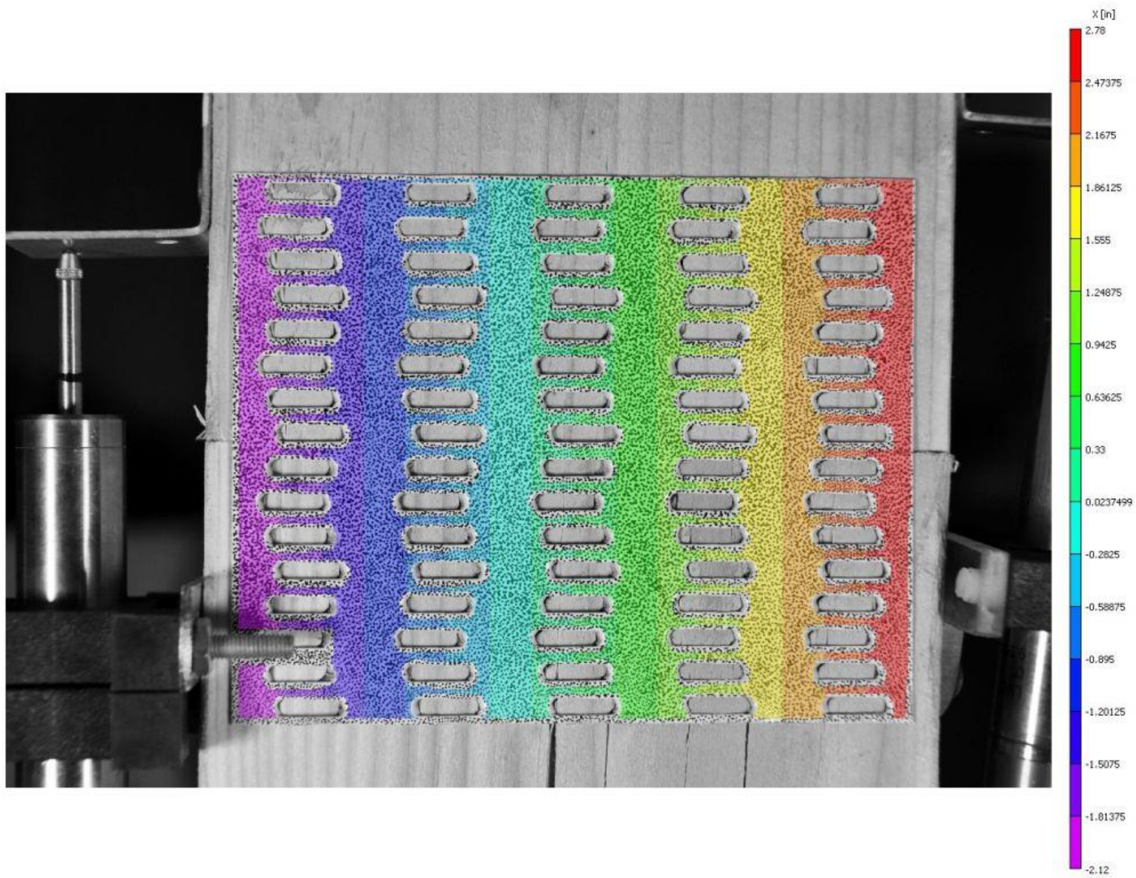

Figure 4-108: x-Axis coordination system obtained from DIC software

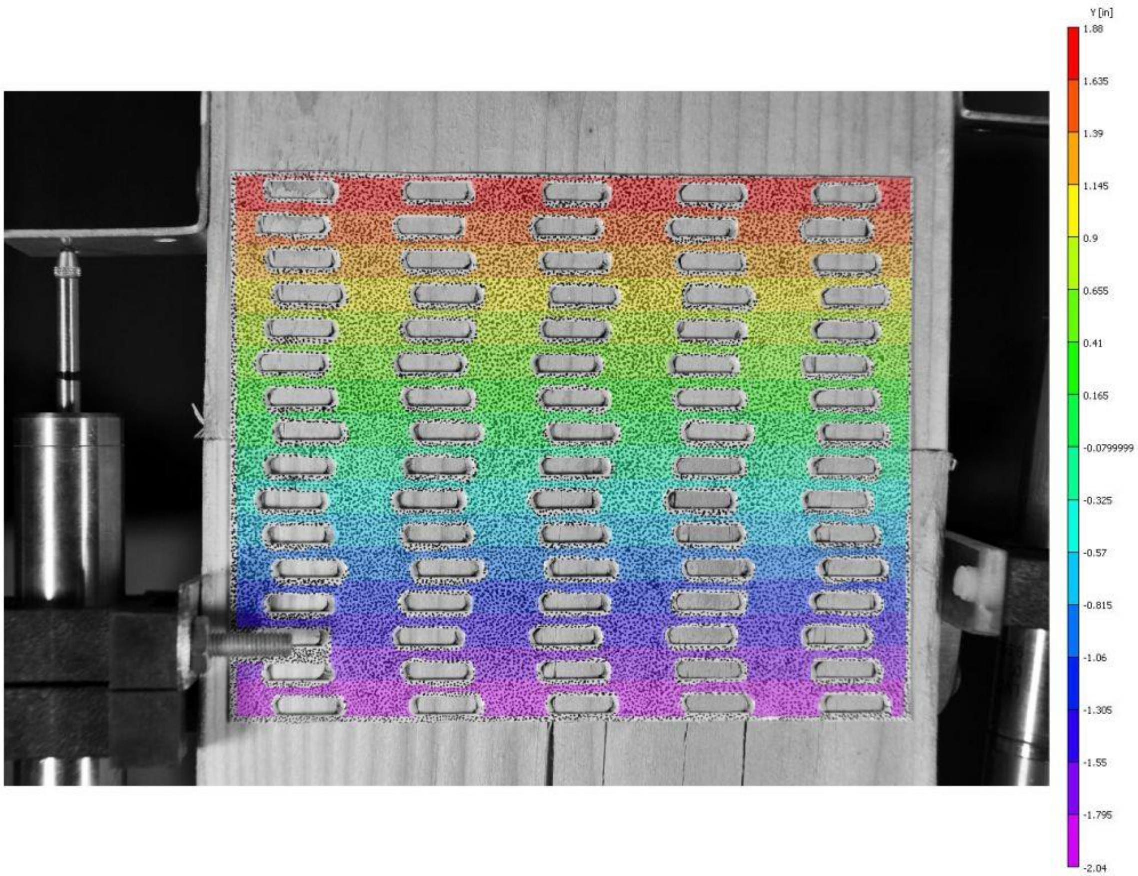

Figure 4-109: y-Axis coordination system obtained from DIC software

4.1.3.2 The First Tension Test (EA-1st)

In this test, the two members of wood were connected by the MPC. The specimen was set on the universal testing machine. The first reference image was taken before applying any load. Figure 4-110 shows the first image which was considered as the reference image in digital image correlation technique.

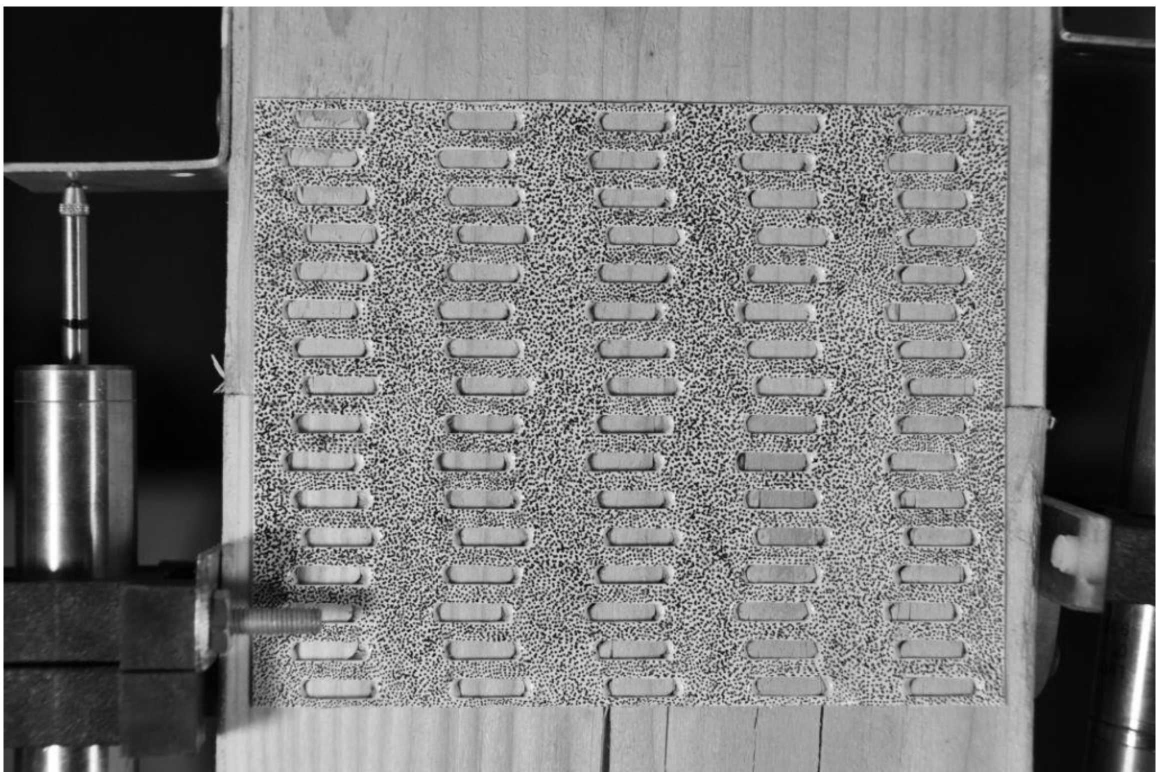

Figure 4-110: First image / reference image

After the first reference image was taken at load zero, the load was increased on the specimen until failure. The camera was placed on a fixed stand and the MPC was perpendicular to the camera's lenses. Images were taken for the MPC specimen at each

load increment of 200 pounds until failure. The failure in the member occurred in the metal plate due to tooth withdrawal. Figure 4-111 shows the last image at the failure.

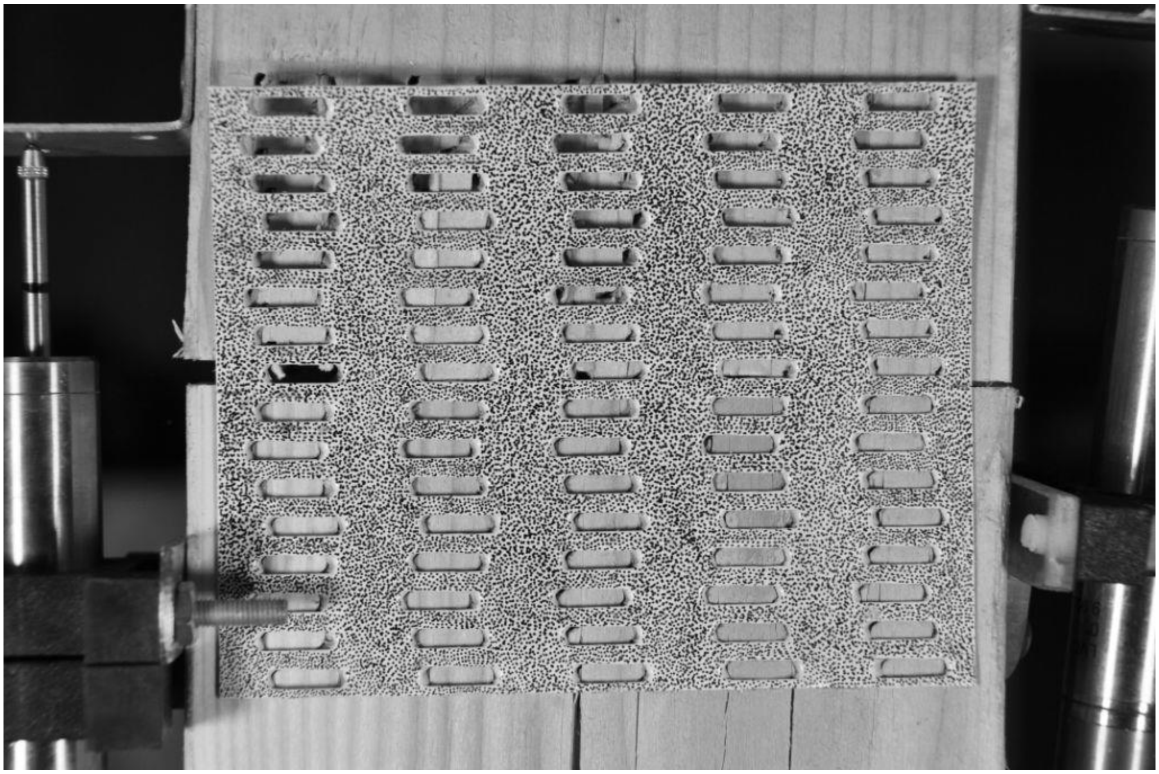

Figure 4-111: The last image after the failure

Thirty seven (37) images were taken in addition to the reference image. The metal plate failed due to tooth withdrawal. As shown in the previous figure the wood member in the top and the bottom was cracked. However, the main reason for failure was the tooth withdrawal. The plate failed at load equal to 7,300 pounds. The captured images were implemented in DIC-software to find the full-field strain measurements.

4.1.3.2.1 Analysis of the Full-Field Strain Results Obtained From DIC Software

All the test images, which were obtained from the lab tests, were implemented in the digital image correlation software Vic-2D. Each image was analyzed in relation to a reference image. Thus, each deformed image was compared to the non-deformed reference image. The full-field strain measurements were obtained from the digital image correlation software. Figure 4-112 shows the strain in y-direction (ε_{yy}) for the first image at 200 pounds.

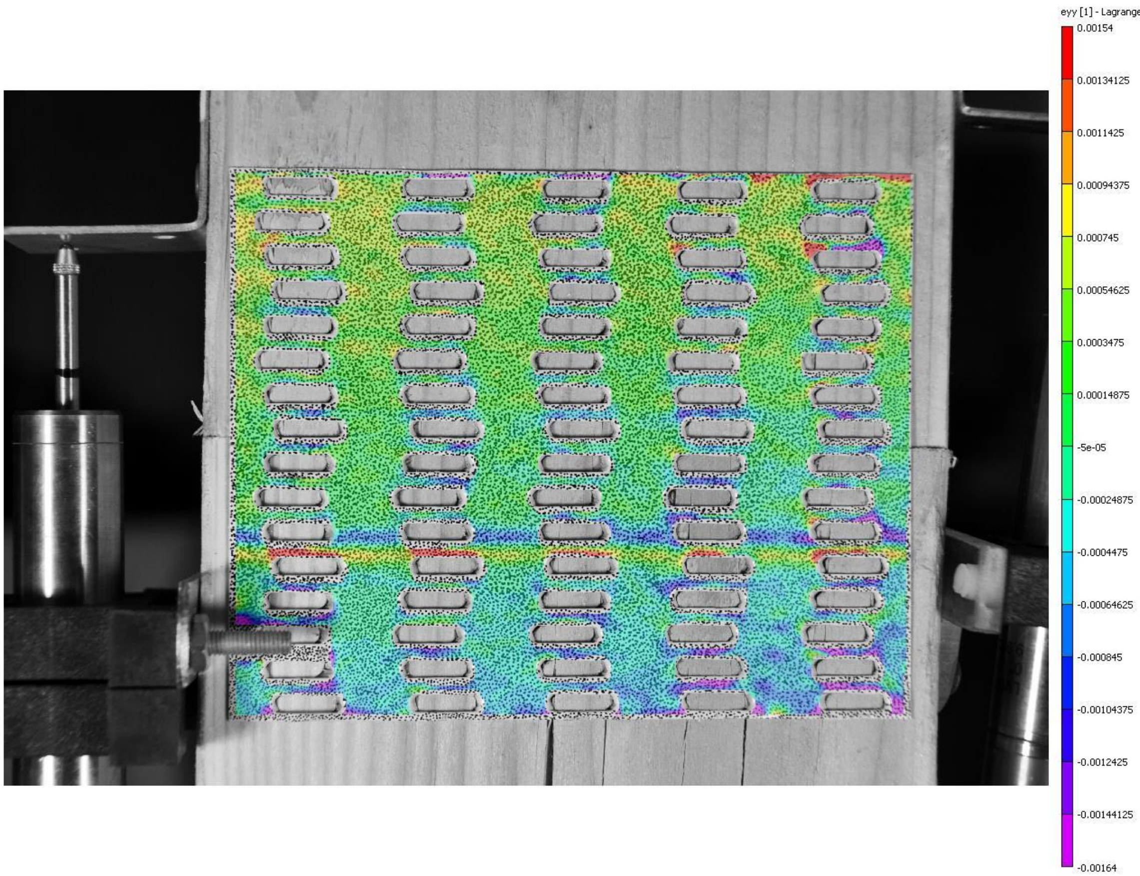

Figure 4-112: Full-field strain measurements (ε_{yy}) for the MPC at 200 pounds

The strain field's results at 200 pounds show different levels of colors all around the plate's surface but they are all very close to each other from the top to the bottom of the plate. The strain (ε_{yy}) is positive strain which means a tensile strain.

As the load increases, the strain (ε_{yy}) increases as a tensile strain until 1,000 pounds. Then the strain retreats down again until load 3,000 pounds which means it increases as a tensile strain. Above 3,000 pounds the strain increases as a tensile strain. At 6,000 pounds, the strain (ε_{yy}) shows a significant increase and also a turn to high tensile strain as shown in Figure 4-113.

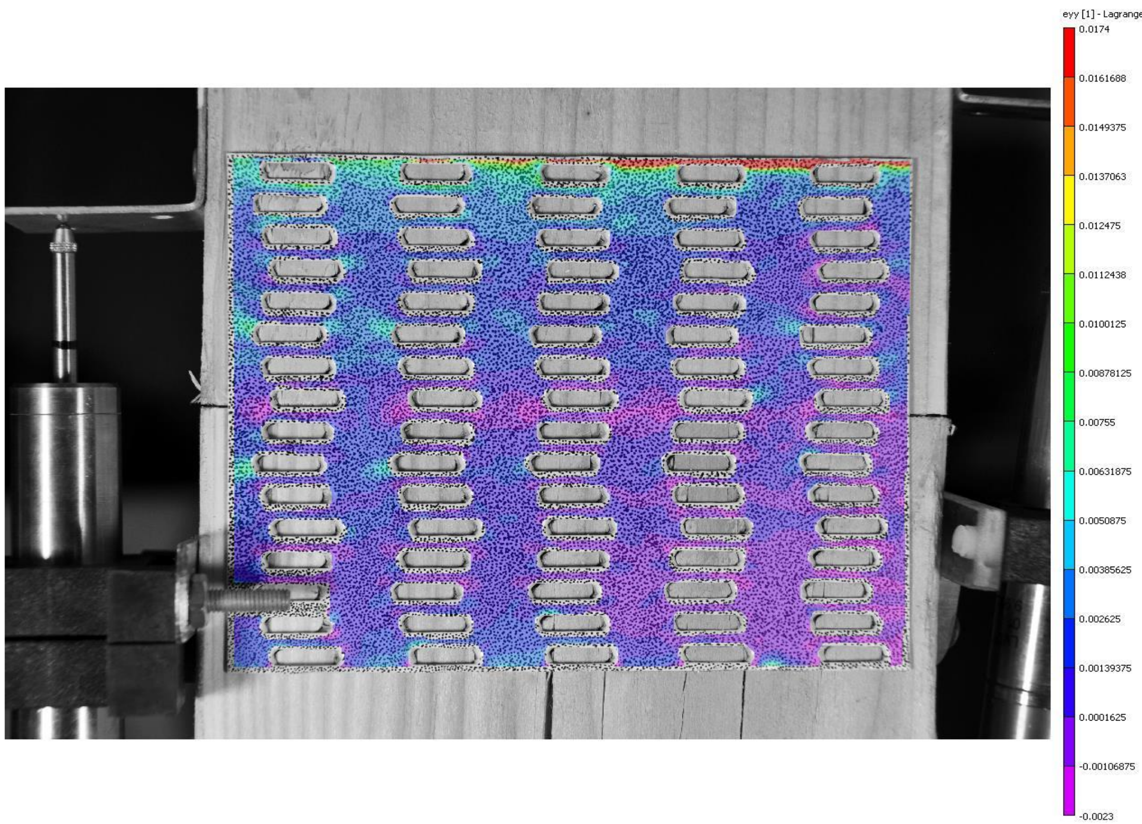

Figure 4-113: Full-field strain measurements (ε_{yy}) at 6,000 pounds

The full-field strain measurements at 6,000 pounds show that the strain is a tensile strain on the top half of the plate, which is above the horizontal middle gap line. The strain in the middle of the plate cross the horizontal middle gap line shows much lower strain values than the other strain around. After an increase in the load, the strain (ε_{yy}) has lower values along the horizontal line and this becomes quite noticeable especially in the middle area of the plate. The strain from 6,000 pounds until the failure at 7,300 pounds is a tensile strain (ε_{yy}) above and beneath the horizontal middle gap line, and it is compressive strain along the horizontal middle gap line.

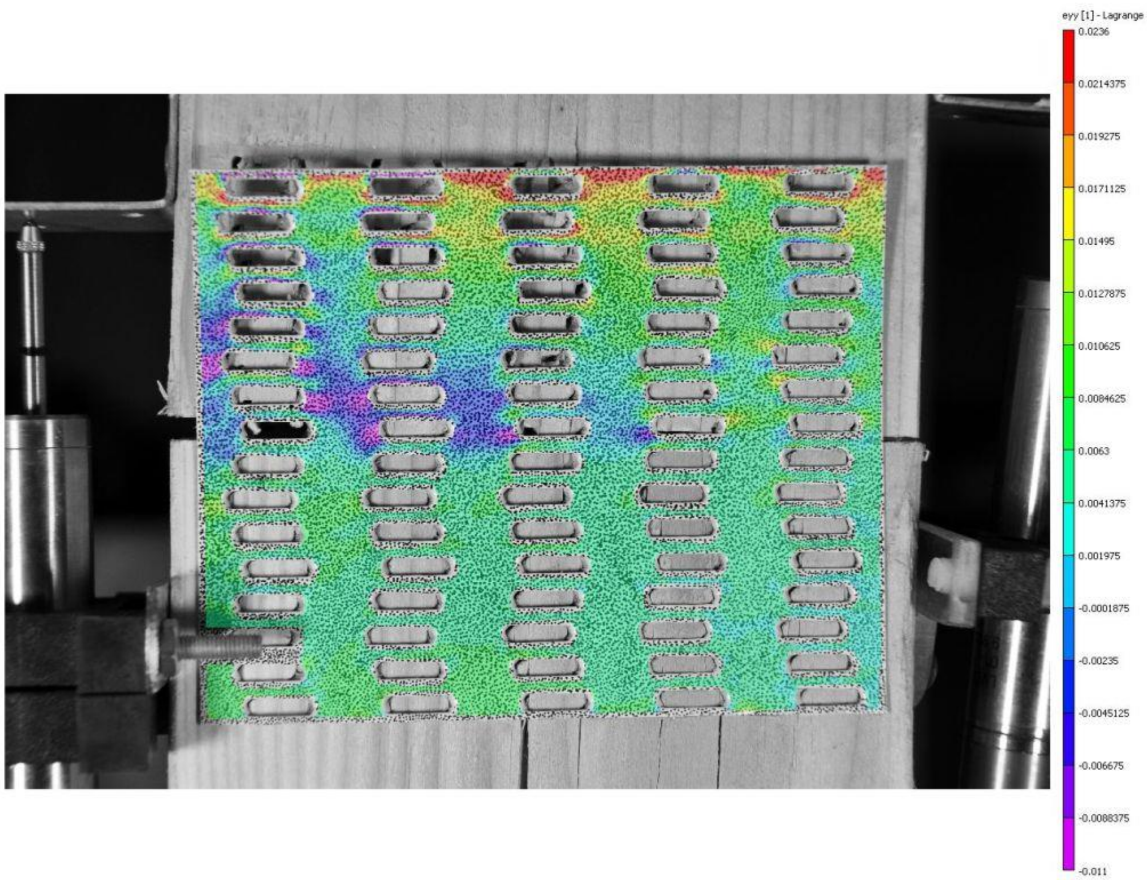

Figure 4-114: Full-field strain measurements (ε_{yy}) for the last image at failure at 7,300 pounds

In general, the strain on the top half of the plate is slightly higher than the bottom half of the plate. The top edge of the plate is influenced by high tensile strain due to pulling out for that edge almost at load 4,000 pounds. At this top edge the strain (ε_{yy}) shows a continuous increase in the tensile strain with loading until failure. The full-field strain measurements for the last image at failure are shown in Figure 4-114. The figure shows that the strain (ε_{yy}) is increased due to an increase in the load amount and it reaches up to 0.0234 as a maximum value. The middle of the plate on the left side clearly shows the negative strain due to the failure there.

In this test failure is due to tooth withdrawal in the top area of the plate especially on the left side. The plate's region on the left shows complete tooth withdrawal and the middle horizontal gap line that is near to that area goes to compressive strain instead of tensile strain. The strain (ε_{yy}) underneath the middle horizontal gap line is stable and holds a tensile strain. While the strain above the horizontal middle gap line is a tensile, it has a high tensile strain on the top edge of the plate due to pulling out of the plate's edge and the tooth withdrawal there. The plate shows a circular shape deformation due to tooth withdrawal. The tooth withdrawal in the left side is quite obvious more than the right side of the plate.

The bottom wood member, which holds the grain that is parallel to the tension force, has some vertical cracks before the test but the cracks were developed more by loading. The top wood member shows a wood crack under the middle slots row and this crack support the tooth withdrawal in that row and this is shown in Figure 4-114. The last image shows that the whole top left-quarter of the metal plate has been pulled out of the wood due to tooth withdrawal.

The gap in the left side of the specimen is a larger than the gap size on the right side. This result is logical due to tooth withdrawal of the top left-quarter of metal plate. Looking at all images from the first one to the image at 6,000 pounds reveals the gap increasing slightly. However, after applying 6,000 pounds, the gap increases rapidly, especially from the left side, and it has taken in the neighborhood of 900 pounds until failure.

The strain results in x-direction (ε_{xx}) can also be obtained from DIC-code. The strain at 200 pounds is shown in Figure 4-115. The strain (ε_{xx}) is almost equally distributed over the entire plate with some exceptions near the slots. The strain (ε_{xx}) is compressive strain and has very low values. Increasing the load causes the strain (ε_{xx}) to follow the strain (ε_{yy}) behavior. The strain (ε_{xx}) decreases until 1,000 pounds then increases to 3,000 pounds as a compressive strain. At 4,000 pounds the strain decreases as a compressive strain and continues until the strain turns to tensile strain. The strain shows a tensile strain at 6,000 pounds and some big region of plate is influenced by compressive strain. The full-field strain (ε_{xx}) measurements at 6,000 pounds are shown in Figure 4-116.

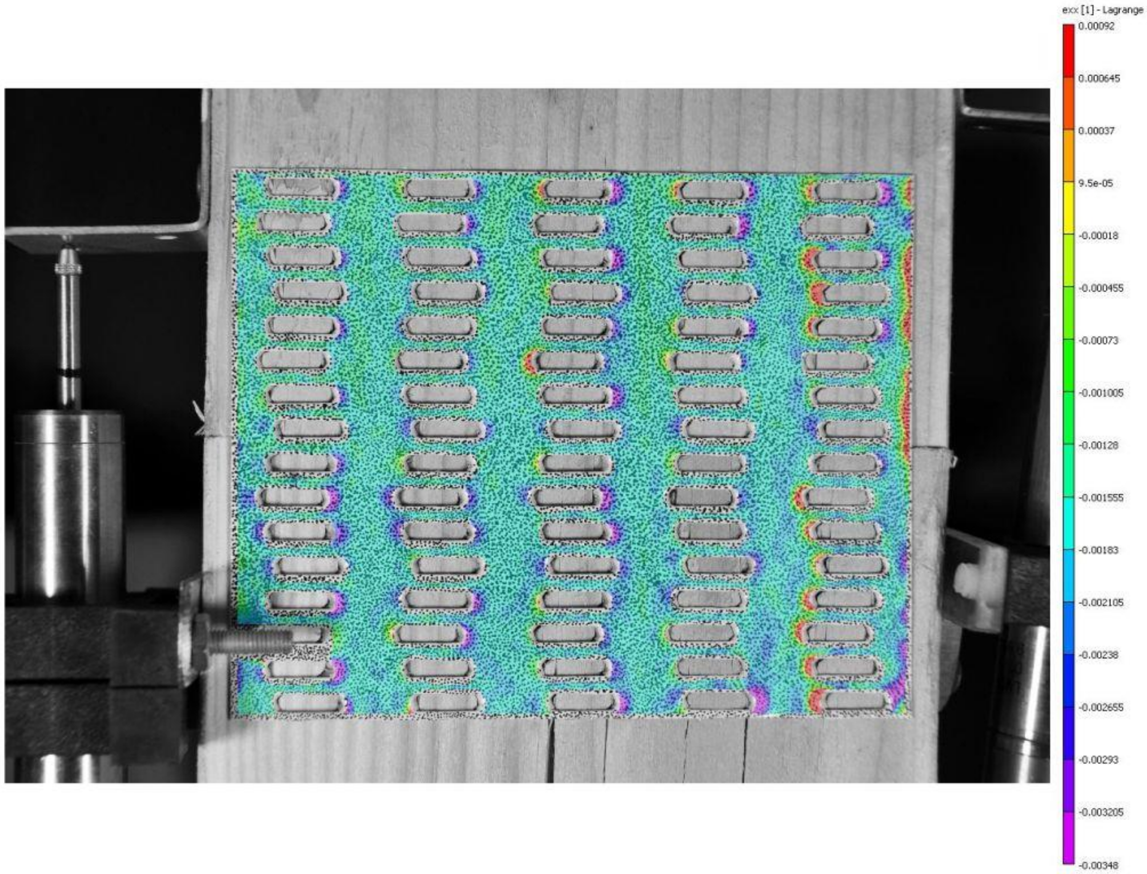

Figure 4-115: Full-field strain in x-direction (ε_{xx}) at load 200 pounds

The failure in this test is due to tooth withdrawal of the top half of the plate. The left quarter top of the plate shows complete tooth withdrawal. Thus the right side of the plate has less strain change than the other regions of the plate. It is considered the least affected part by the failure. However, due to tooth withdrawal the strain in the top half of the plate has changed and fluctuated in its values while the bottom half of the plate remains stable. The strain (ε_{xx}) behavior confirms the strain (ε_{yy}) behavior. Thus, at the end the last image for full-field strain (ε_{xx}) shows that the top left side of the plate has the highest strain (ε_{yy}) and the highest strain (ε_{xx}).

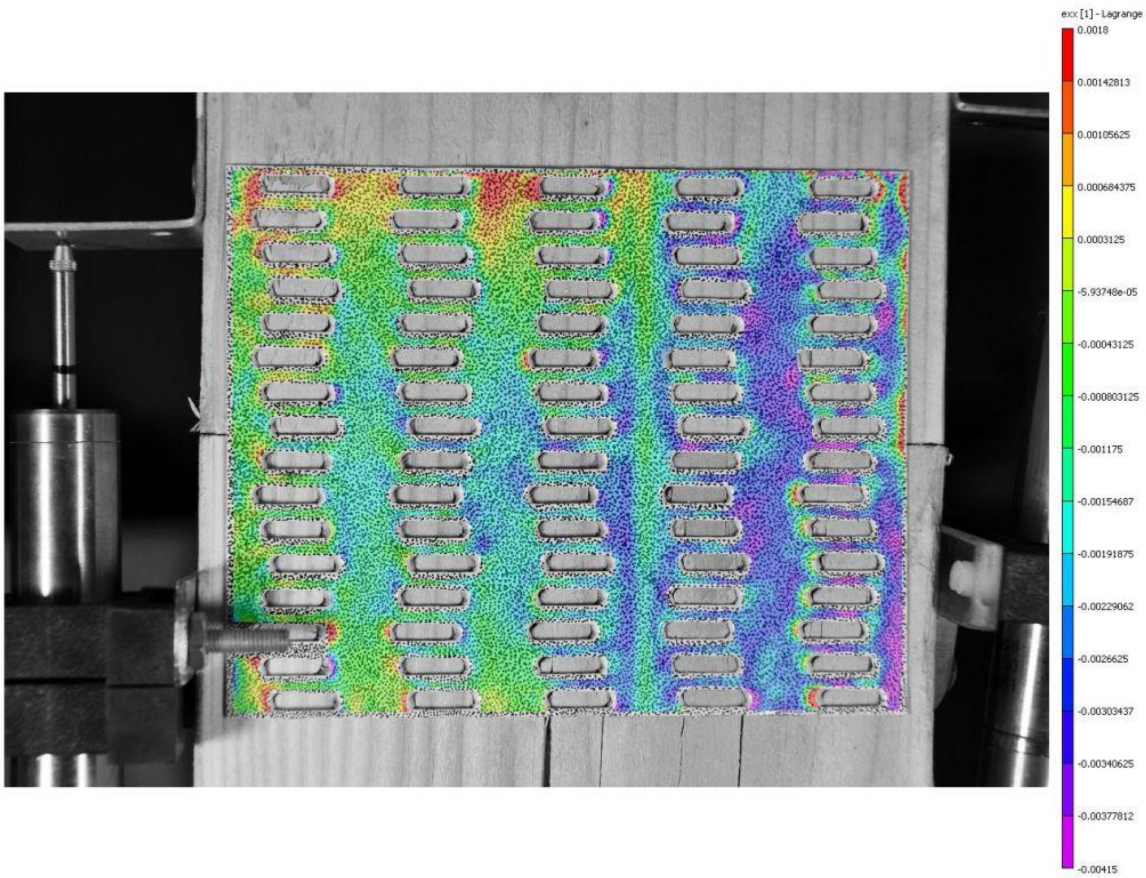

Figure 4-116: Full-field strain in x-direction (εxx) at load 6,000 pounds

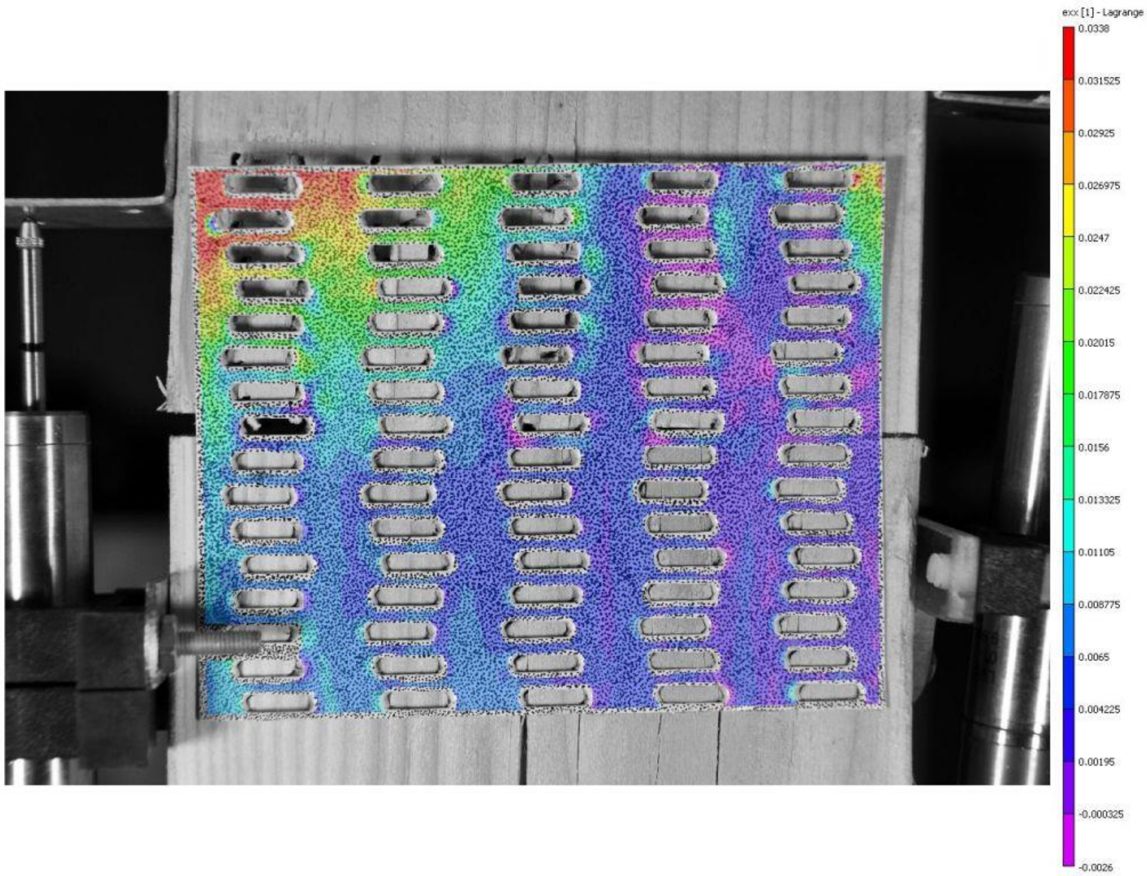

Figure 4-117: Full-field strain in x-direction (εxx) at load 7,300 pounds (the last image at failure)

4.1.3.2.2 Numerical Analysis for the Results

Two types of numerical analysis for the results are performed here based on the strain direction. The strain (ε_{yy}) is along the vertical direction and (ε_{xx}) is along the horizontal direction.

4.1.3.2.2.1 Strain in y-direction (ε_{yy}) along y-axis

To analyze the DIC results numerically, vertical cross section lines from the top of the plate to the bottom are taken for some images starting with the first image at 200 pounds and ending with the last image at failure. The cross section lines are taken in four different locations as shown in Figure 4-118.

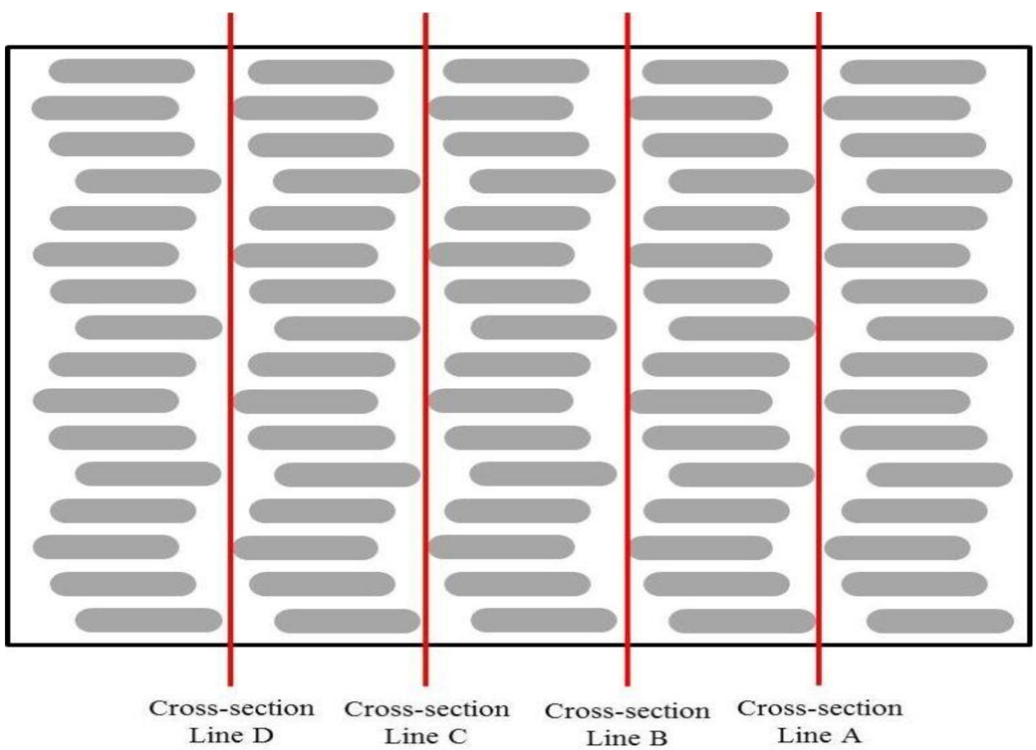

Figure 4-118: Metal plate with the cross-section lines along the vertical direction

The four locations of the cross section lines are as the following:

- The first cross section line (A-A) is from the right side of MPC @ x = 1.83 in.
- The second cross section line (B-B) is @ x = 0.904 in.
- The third cross section line (C-C) is @ x= -0.154 in.
- The fourth cross section line (D-D) is from the left side of MPC @ x= -1.59 in.

Four cross-section lines are taken for the strain field (ε_{yy}). The next four Figures 4-119 to 4-122 show the distribution of strain (ε_{yy}) at four different locations for 13 images. Each image represents the value of the loading that is applied on the specimen of the two wood members connected by the metal plate connector.

The curves show that the first considered load is 200 pounds then the increment of loading is 1,000 pounds until the load is 6,000 pounds. Another loading increment of 200 pounds is taken starting from 6,400 pounds until the failure is observed at 7,300 pounds. The failure occurred in the plate due to tooth withdrawal in addition to some cracks in the wood members.

The curves show that the strain (ε_{yy}) is negative strain and continues from load of 200 pounds until 5,000 pounds. At 6,000 pounds strain (ε_{yy}) shows some changes and starts to be positive as a tensile strain. The strain (ε_{yy}) continues to increase with loading until the failure at 7,300 pounds. In general, the cross section lines show higher positive strain in the top half of the plate than the bottom half of the plate. From the images and also the curves' results it is obvious that the top of the plate is the first part of the plate affected by the loading then it starts to pull out from the wood member at load around 4,000 pounds.

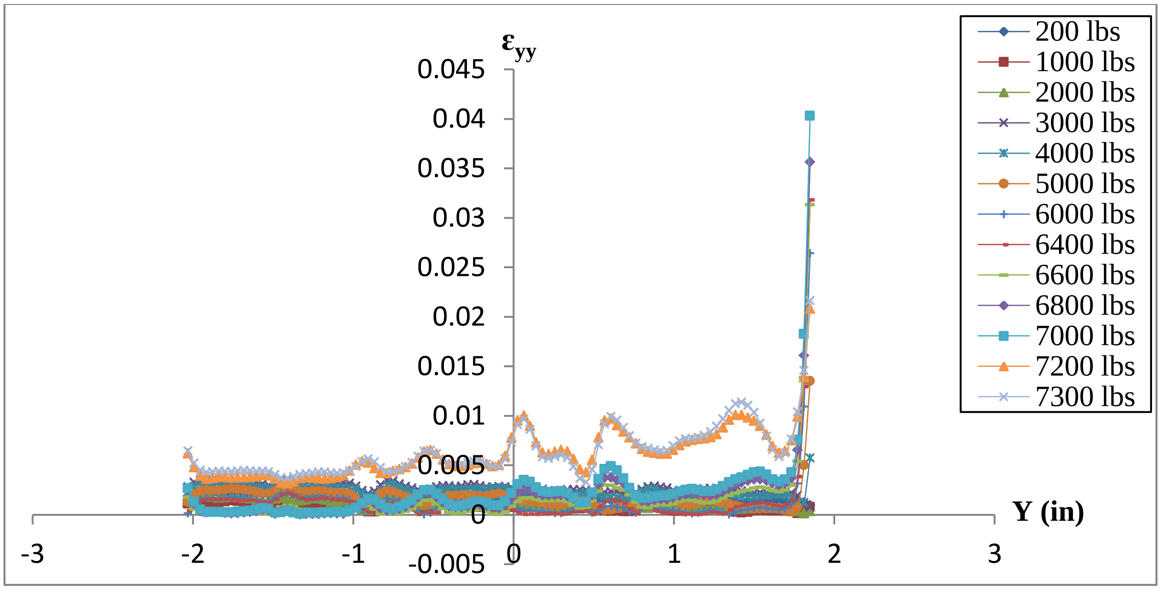

Figure 4-119: The strain distribution (ε_{yy}) along a cross section line (A-A) located on the right side of the plate

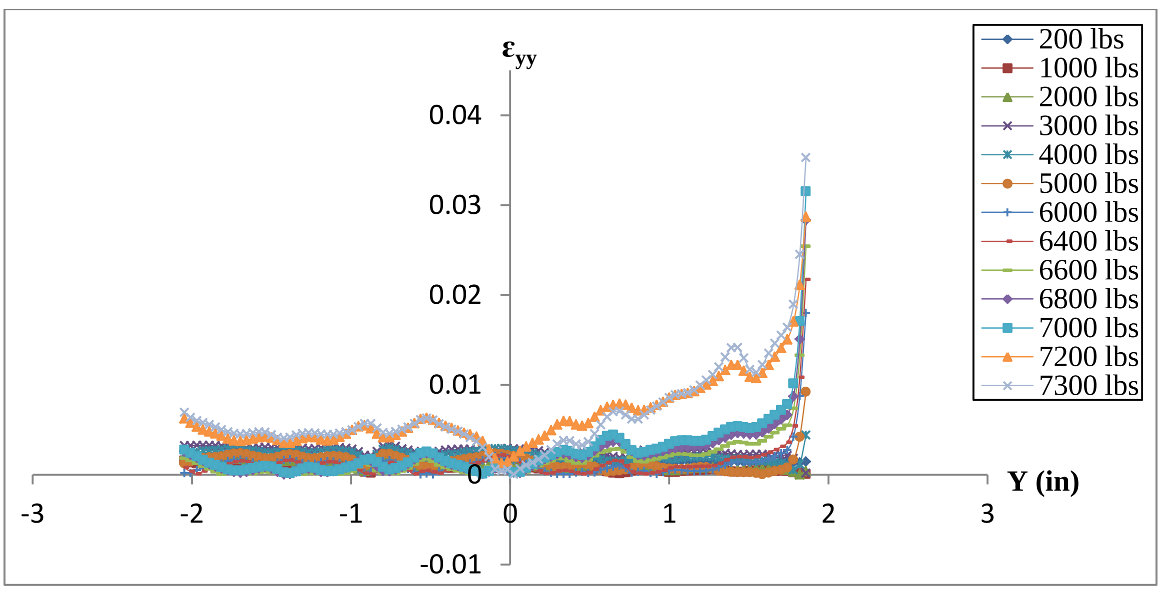

Figure 4-120: The strain distribution (ε_{yy}) along a cross section line (B-B)

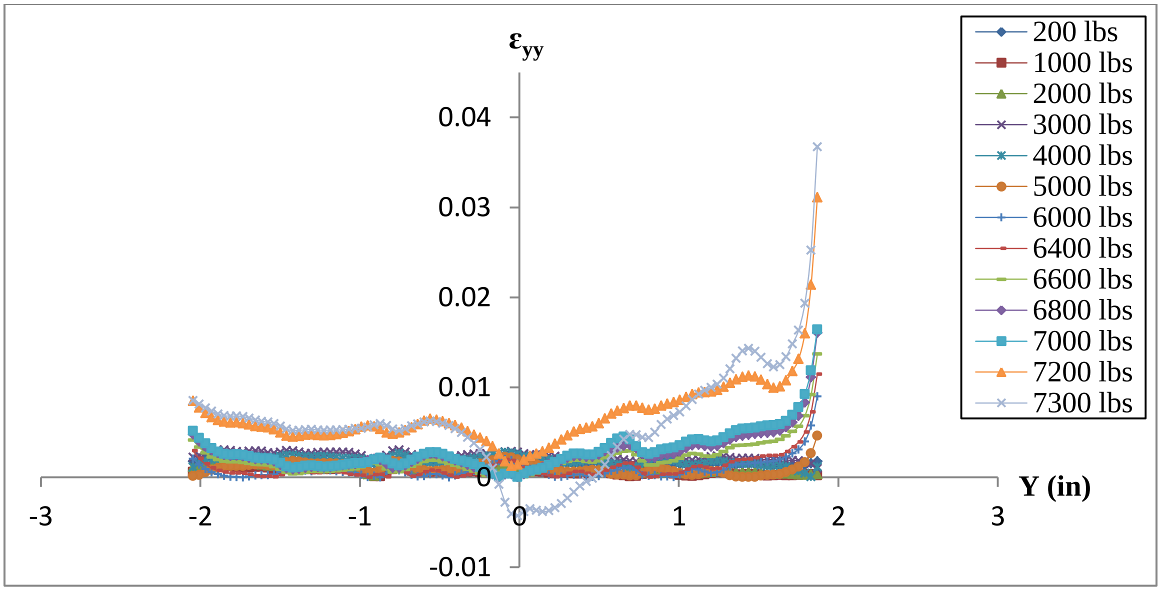

Figure 4-121: The strain distribution (ε_{yy}) along a cross section line (C-C)

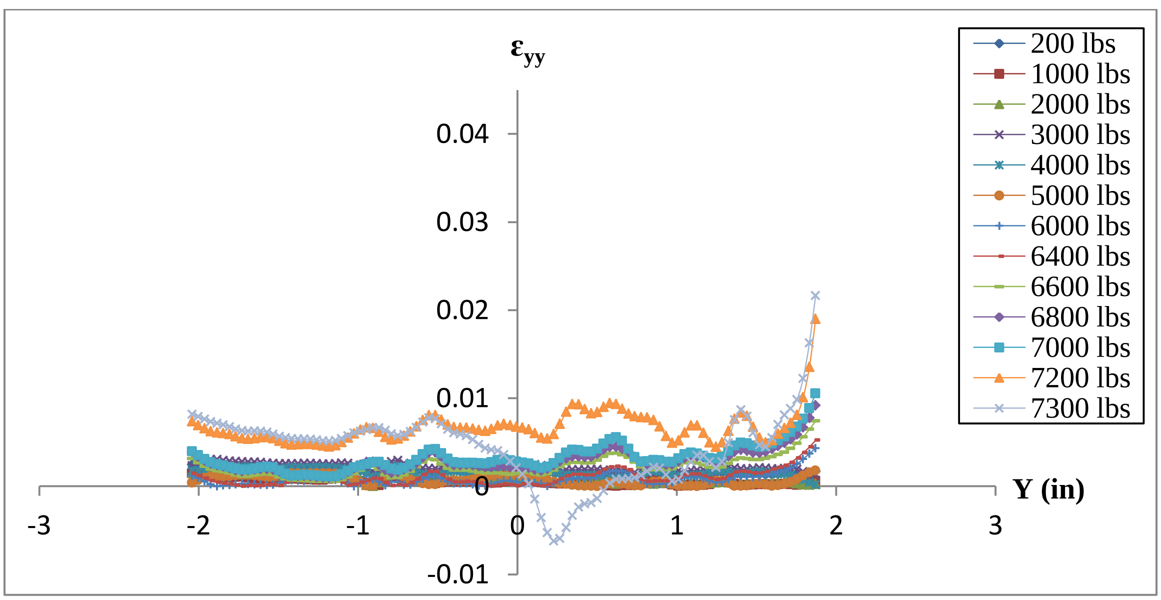

Figure 4-122: The strain distribution (ε_{yy}) along a cross section line (D-D) located on the left side of the plate

The strain (ε_{yy}) in the top of the plate is not mirror to the strain (ε_{yy}) in the bottom part of the plate. The images show that the top part has tooth withdrawal while the bottom part undergoes little change.

The left side of the specimen shows high gap between the two wood members more than the right side gap. By an increase in the load, the left side gap increases then tooth withdrawal occurs. The tooth withdrawal in the left side is quite clear and it is considered the main feature of the failure. However, the cross section line (D-D) and (C-C) shows low strain in the middle of the plate due to pulling out of the plate in the middle of the plate. The right side of the plate in the middle is affected by tooth withdrawal so the cross sections line (A-A) does not show any sudden changes in the strain curves. A comparison between the strain curves at the four cross section lines for the image at the failure is shown in Figure 4-123.

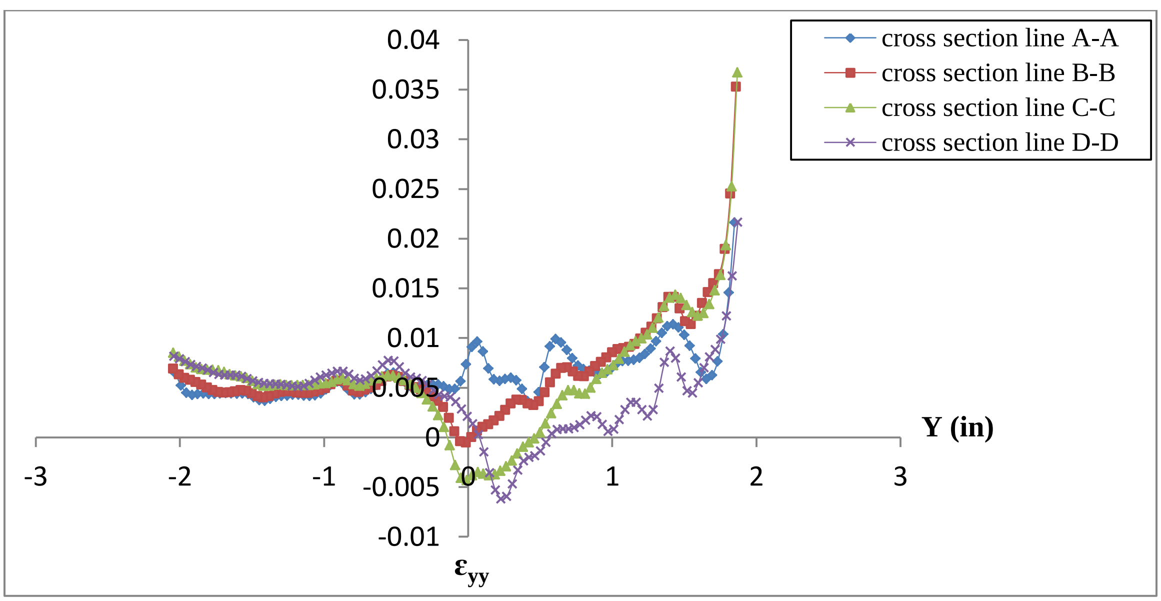

Figure 4-123: The strain (εyy) distribution along the four cross-section lines (A-A), (B-B) and (C-C), (D-D) for the last image at failure at load 7,300 pounds.

4.1.3.2.2.2 Strain in x-direction (ε_{xx}) along x-axis

To analyze the DIC results numerically, horizontal cross sectional lines from the right of the plate to the left are taken .The cross section lines are taken in three different locations as shown in Figure 4-124.

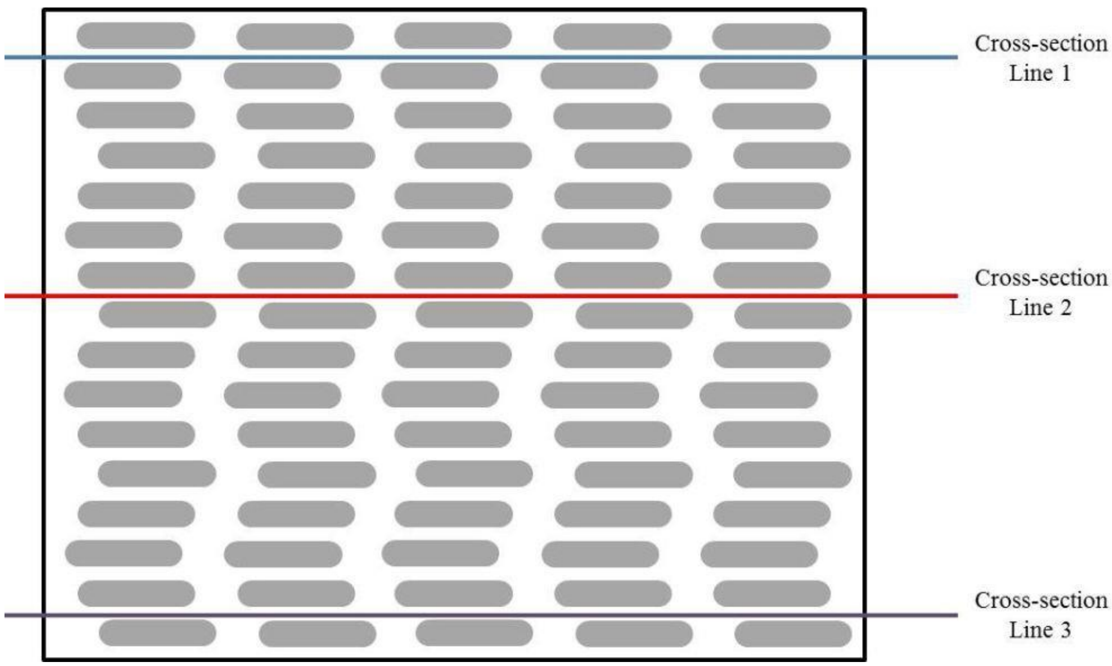

Figure 4-124: Metal plate with the cross-section lines along the horizontal direction

The three locations of the cross section lines are as the following:

- The first cross section line (1-1) is at the top of MPC @ y = 1.631 in.
- The second cross section line (2-2) is along the middle of the MPC @ y =- 0.112 in.
- The third cross section line (3-3) is from the bottom of the MPC @ y = -1.872 in.

The strain (ε_{xx}) along x-direction can be obtained from digital image correlation software. The next Figures 4-125, 4-126 and 4-127 show the strain (ε_{xx}) along x-axis.

The curves in the three different places (top, middle, bottom of the plate) show different results. At 200 pounds the strain (ε_{xx}) is compressive strain then it decreases until 1,000 pounds as a compressive strain. Then the strain increases again as a compressive strain until load 3,000 pounds. At 4,000 pounds the strain shows a decrease in the curves and goes toward the positive side.

The strain (ε_{xx}) at load 7,000 pounds, which is the stage before the clear tooth withdrawal occurs, shows negative strain in the middle and the bottom half of the plate. The top side contains fluctuation in the strain values and behavior. The strain (ε_{xx}) there is going up and down as a tensile strain with some exceptions. The bottom cross section line (3-3) displays the least effective line by the failure as shown in the figures. The top cross sectional line is the worst regarding the strain because of the tooth withdrawal at that part of the plate. The strain (ε_{xx}) fluctuates and changes from the right to the left side as shown in the curves. The tensile strain is high in the three cross sectional lines on the vertical-left side of the plate. The gap between the wood members is larger on the left side than on the right. The strain in the left side is higher than that on right side, which makes sense. The third cross section line in the bottom of the plate (3-3) increases with loading, and left side strain is higher than the right side strain. Cross sectional line (3-3) is the least cross sectional line affected by loading.

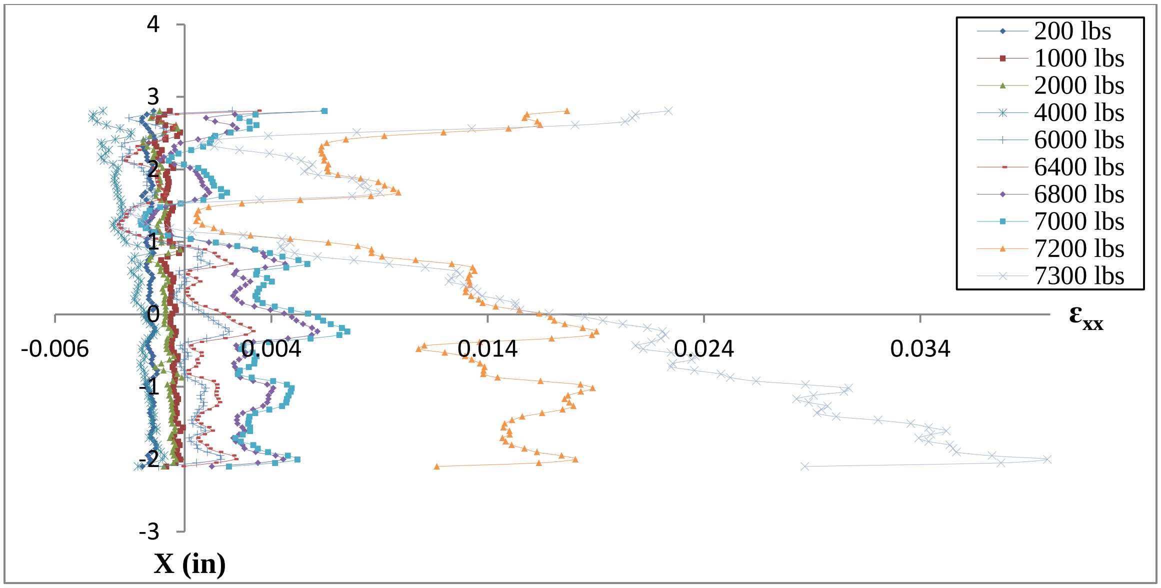

Figure 4-125: The strain distribution (ε_{xx}) along a cross section line (1-1) located on the top of the plate

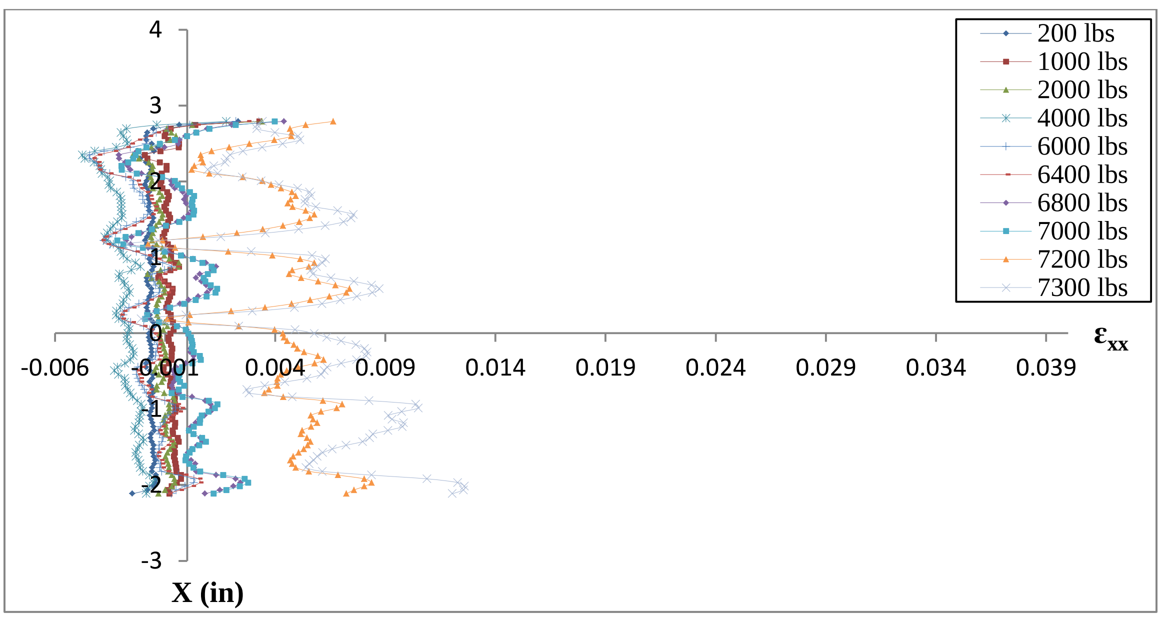

Figure 4-126: The strain distribution (ε_{xx}) along a cross section line (2-2) located on the middle of the plate

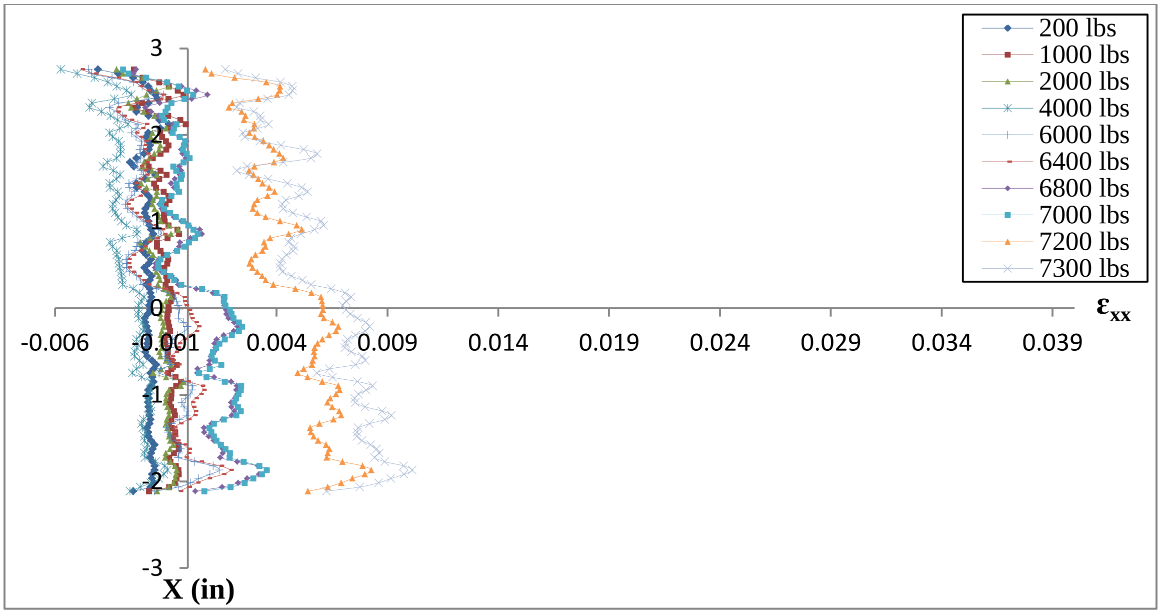

Figure 4-127: The strain distribution (ε_{xx}) along a cross section line (3-3) located on the bottom of the plate

Figure 4.137 shows the three lines strain (ε_{xx}) curves for the last image at 7,300 pounds.

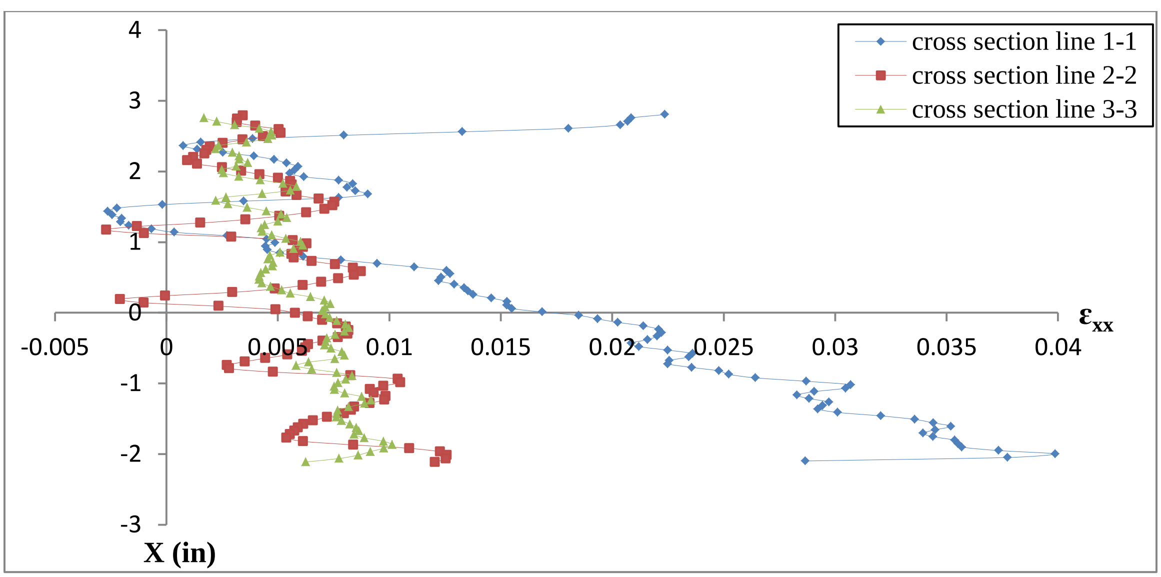

Figure 4-128: The strain (ε_{xx}) distribution along the three cross-section lines (1-1), (2-2), and (3-3) for the last image at the failure at load 7,300 pounds

4.1.3.3 The Second Tension Test (EA-2nd)

In this test, the two members of wood were connected by the MPC. The specimen was set on the universal testing machine. The first reference image was taken before applying any load. Figure 4-129 shows the first image which was considered as the reference image in digital image correlation technique.

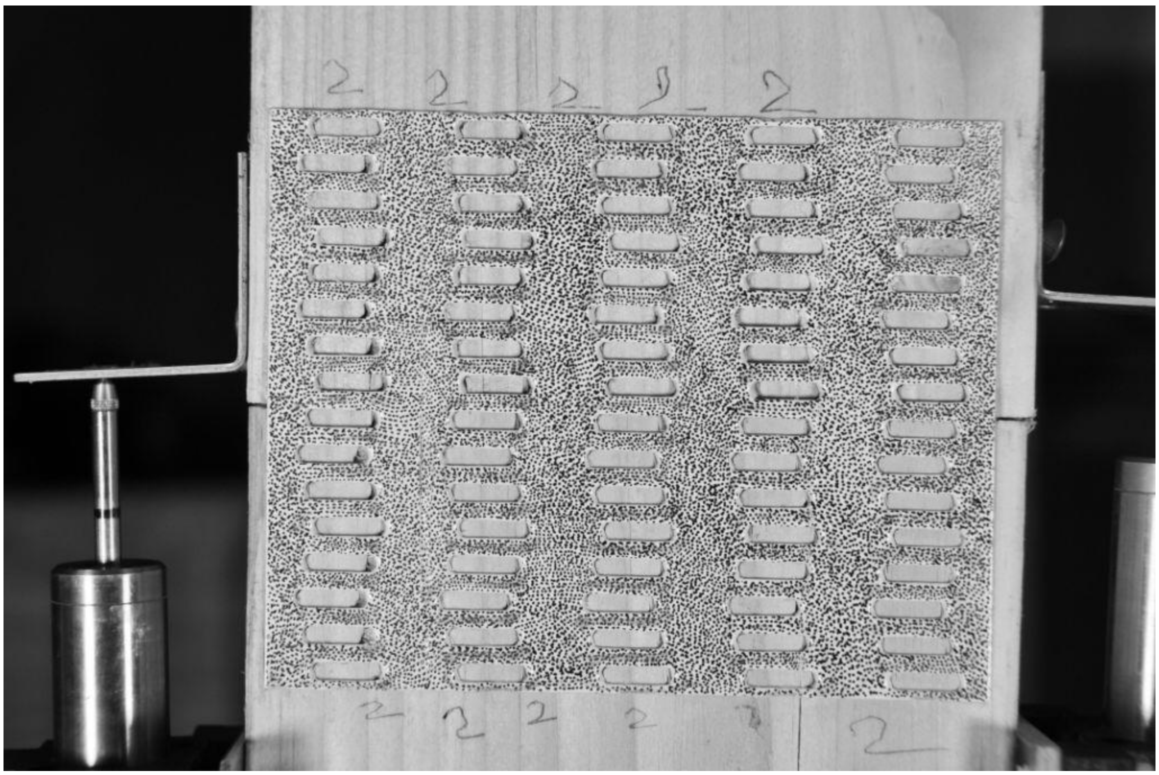

Figure 4-129: First image / reference image

After the first reference image was taken at load zero, the load was increased on the specimen until failure. The camera was placed on a fixed stand and the MPC was perpendicular to the camera's lenses. Images were taken for the MPC specimen at each

load increment of 200 pounds until failure. The failure in the member occurred in the metal plate due to tooth withdrawal. Figure 4-130 shows the last image after the failure.

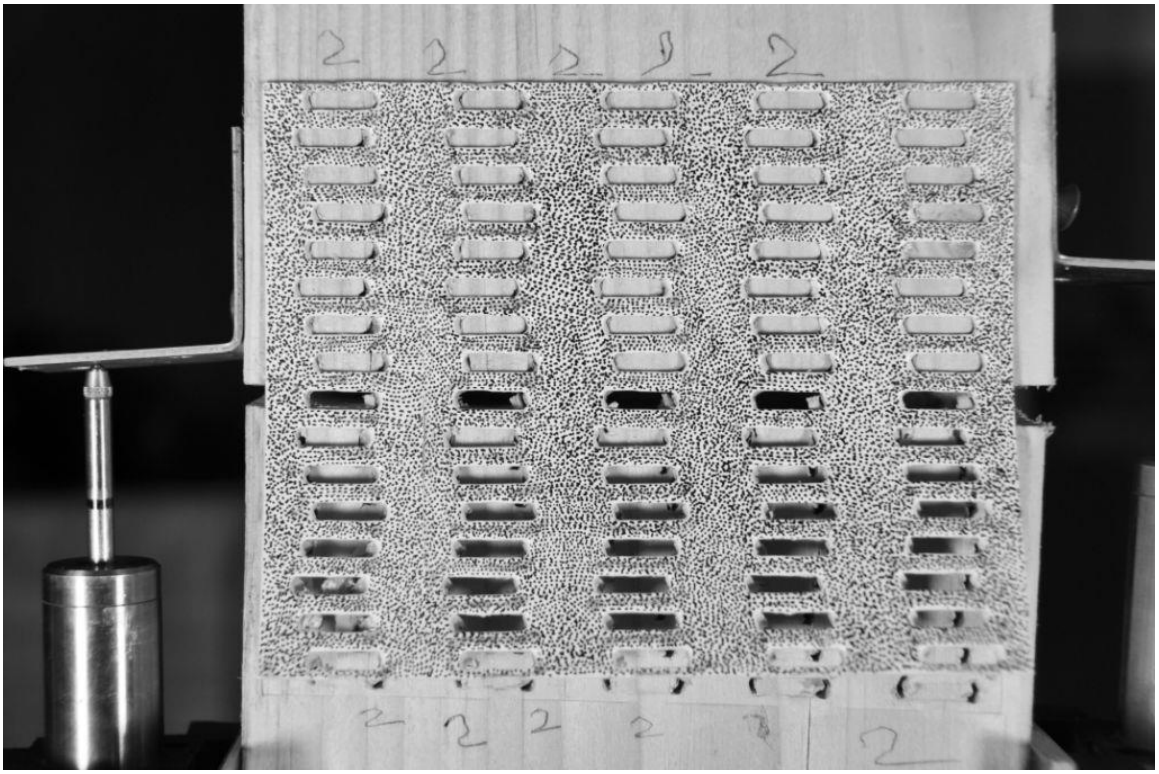

Figure 4-130: The last image at the failure

Forty seven (43) images were taken in addition to the reference image. The metal plate failed due to tooth withdrawal. As shown in Figure 4-129 and 4-130 the wood member in the bottom already had cracks before any loading and no major cracks developed in the wood members through the test until failure. Thus, the main reason for failure was the tooth withdrawal. The plate had failed at load equal to 8,300 pounds. The captured images were implemented in DIC-software to find the full-field strain measurements.

4.1.3.3.1 Analysis of the Full-Field Strain Results That Obtained From DIC Software

All the test images, which were obtained from the lab tests, were implemented in the digital image correlation software Vic-2D. Each image was analyzed in relation to a reference image. So each deformed image was compared to the non-deformed reference image. The full-field strain measurements were obtained from the digital image correlation software. Figure 4-131 shows the strain in y-direction (ε_{yy}) for the image at 8,000 pounds.

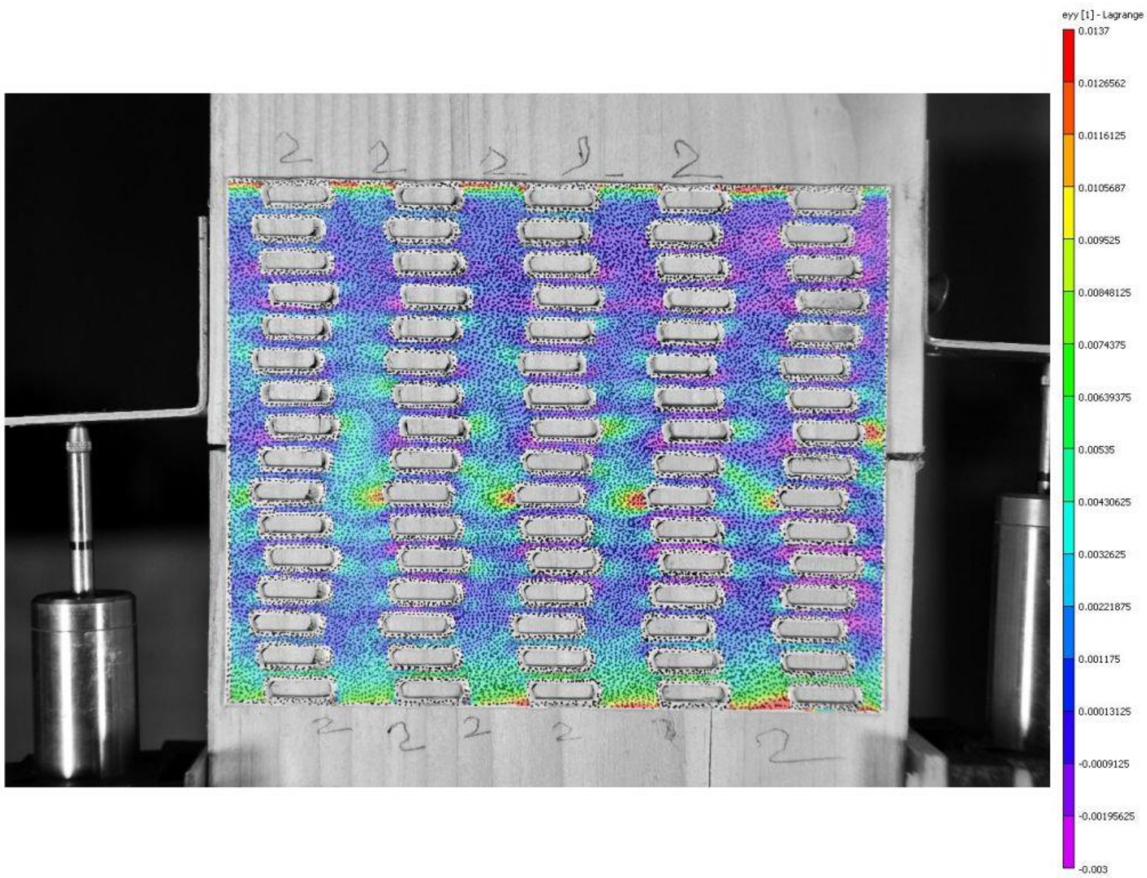

Figure 4-131: Full-field strain measurements (ε_{yy}) at 8,000 pounds

The strain from load 6,000 pounds to failure shows an increase in the tensile strain (ε_{yy}). The full-field strain measurements show that the strain along the horizontal middle gap line rises up with increased loading as a tensile strain. The strain above and below the horizontal middle gap line are not mirror to each other with loading. Before applying 6,000 pounds, the strain above and underneath the horizontal middle gap line shows very close behavior. However, after applying 6,000 pounds the strain (ε_{yy}) behavior shows more unstable distribution. The strain varies as a tensile strain and a significant change along the horizontal middle gap line. The last image at failure is shown in Figure 4-132.

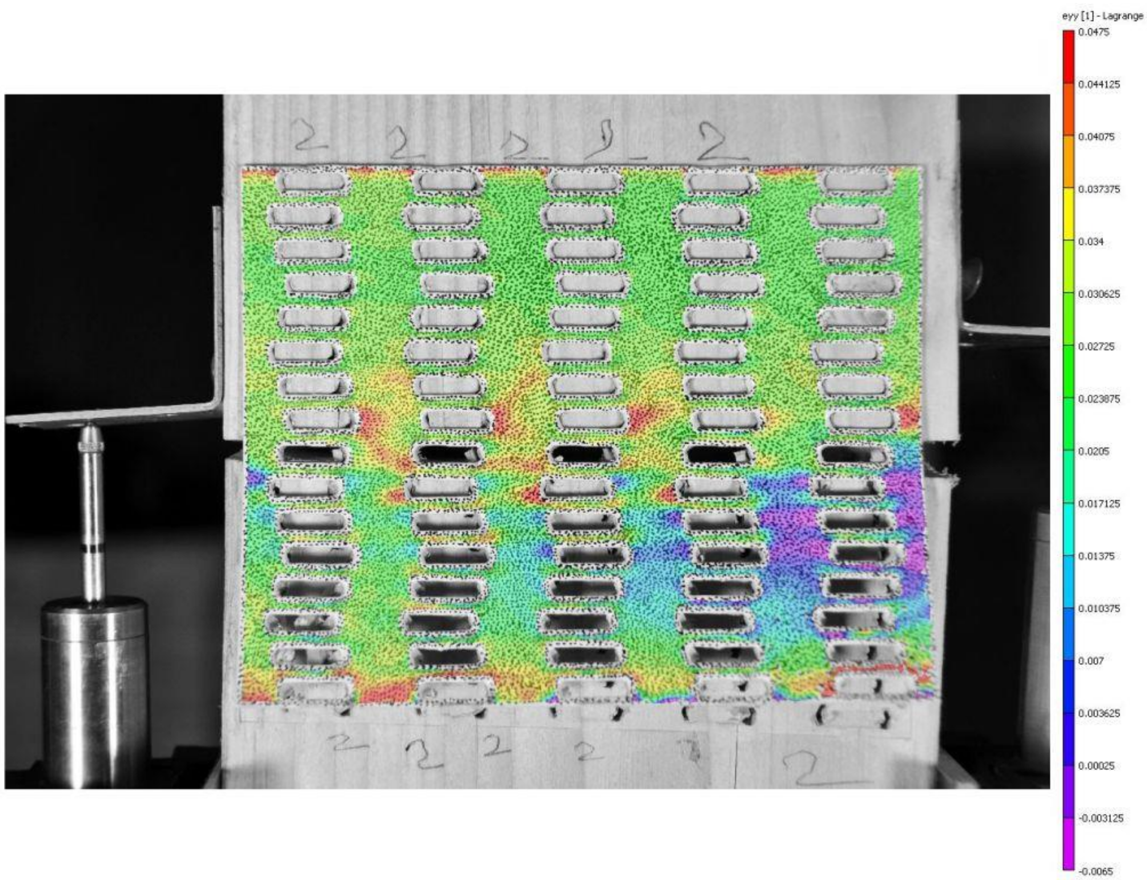

Figure 4-132: Full-field strain measurements (εyy) for the last image at the failure at 8,300 pounds

The failure in this test is due to tooth withdrawal to the bottom half of the plate. The indications for tooth withdrawal started at load 8,000 pounds. The tensile strain (ε_{yy}) increased with different shape behaviors over the plate's surface. The strain distribution was not organized. This behavior was due to the effect of external factor of tooth withdrawal which changes the strain's behavior. The gap between the two wood members is higher on the right side than on the left.

The strain results in x-direction (ε_{xx}) can also be obtained from digital image correlation software. The strain (ε_{xx}) is compressive strain at 200 pounds and the strain (ε_{xx}) is equally distributed from the top to the bottom of the plate. As the load increases, the strain (ε_{xx}) follows the strain (ε_{yy}) behavior. From load 200 until 7,000 pounds, the strain is compressive. Once the indication for tooth withdrawal occurs, the compressive strain (ε_{xx}) decreases as a compressive strain and also turns with loading to tensile strain. At 8,000 pounds, the strain (ε_{xx}) shows a tensile strain as shown in Figure 4-133.

The left side of the plate is influenced by tensile strain while the right side of the plate is influenced by low compressive strain. The strain (ε_{xx}) above and underneath the horizontal middle gap line is almost mirror to each other.

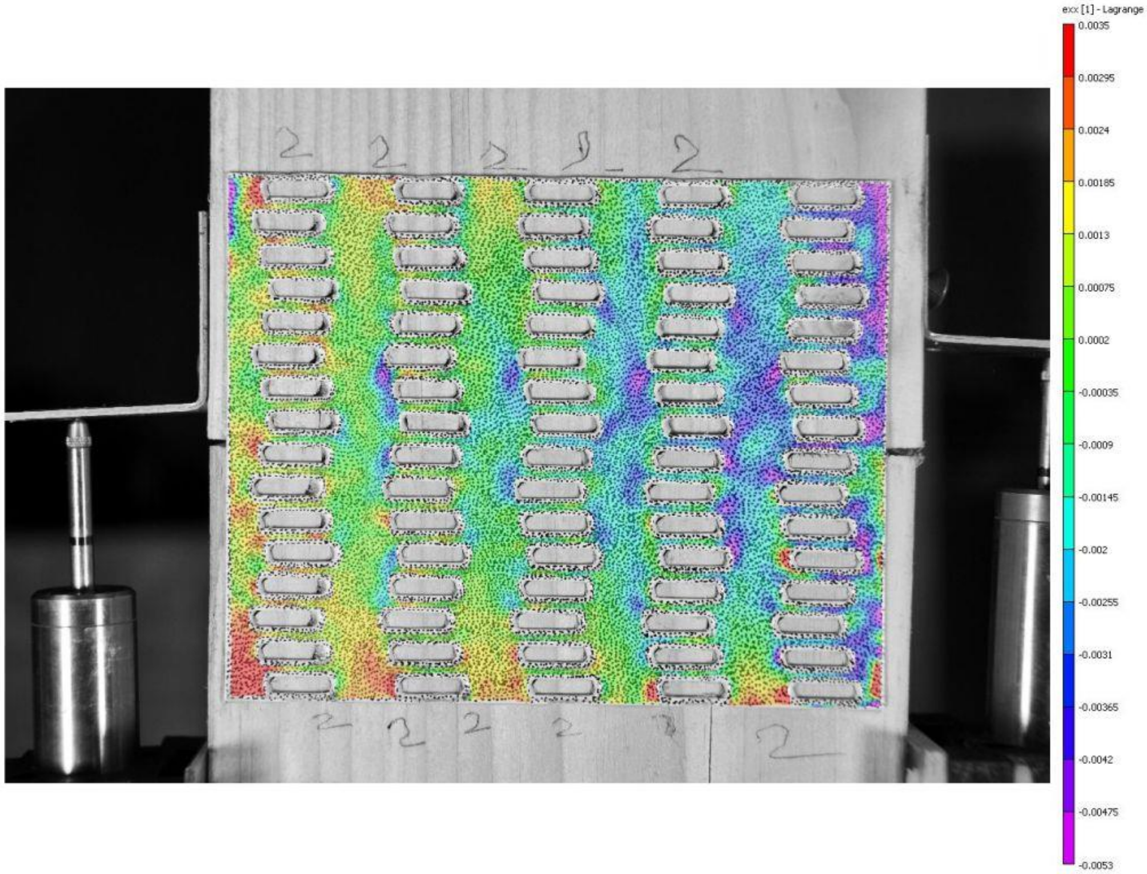

Figure 4-133: Full-field strain in x-direction (ε_{xx}) at load 8,000 pounds

Increasing the load more than 8,000 pounds increases the strain (ε_{xx}) as a tensile strain over the entire plate. The strain on the right side of the plate is influenced by tensile strain at load almost equal to 8,300 pounds. The spikes in the strain values as a result of tooth withdrawal failure along the middle horizontal gap line is shown in the full-field strain measurement images starting at load 6,000 pounds. At 8,300 pounds the strain (ε_{xx}) holds the highest tensile strain on the plate. Figure 4-134 shows the full-field (ε_{xx}) at load 8,300 pounds. It shows very stable tensile strain on the top half of the plate and also a fluctuation in strain on the bottom half of the plate due to tooth withdrawal. The gap also shows larger deformation on the right side than on the left side.

Figure 4-134: Full-field strain in x-direction (ε_{xx}) at load 8,300 pounds

4.1.3.4 The Third Tension Test (EA-3rd)

In this test, the two members of wood were connected by the MPC. The specimen was set on the universal testing machine. The first reference image was taken before applying any load. Figure 4-135 shows the first image which was considered as the reference image in digital image correlation technique.

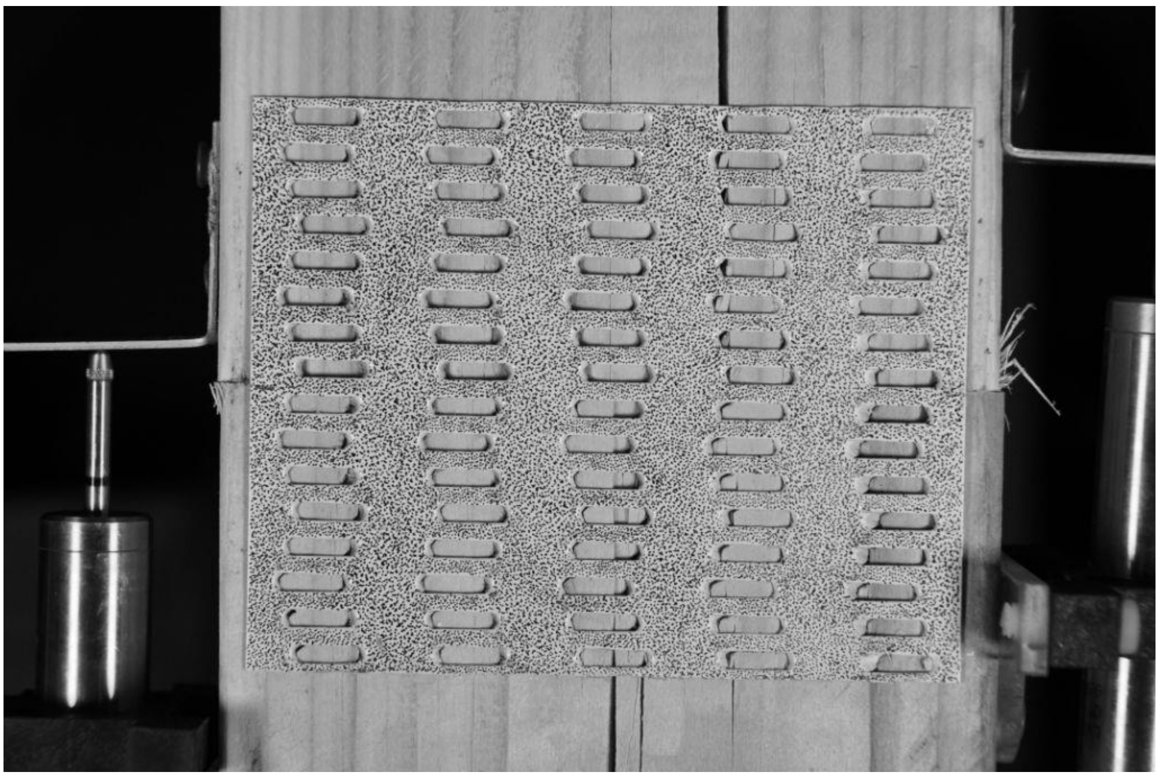

Figure 4-135: First image / reference image

After the first reference image was taken at load zero, the load was increased on the specimen until failure. The camera was placed on a fixed stand and the MPC was perpendicular to the camera's lenses. Images were taken for the MPC specimen at each

load increment of 200 pounds until failure. The failure in the member occurred in the wood. The specimen also rotated horizontally to the left side.

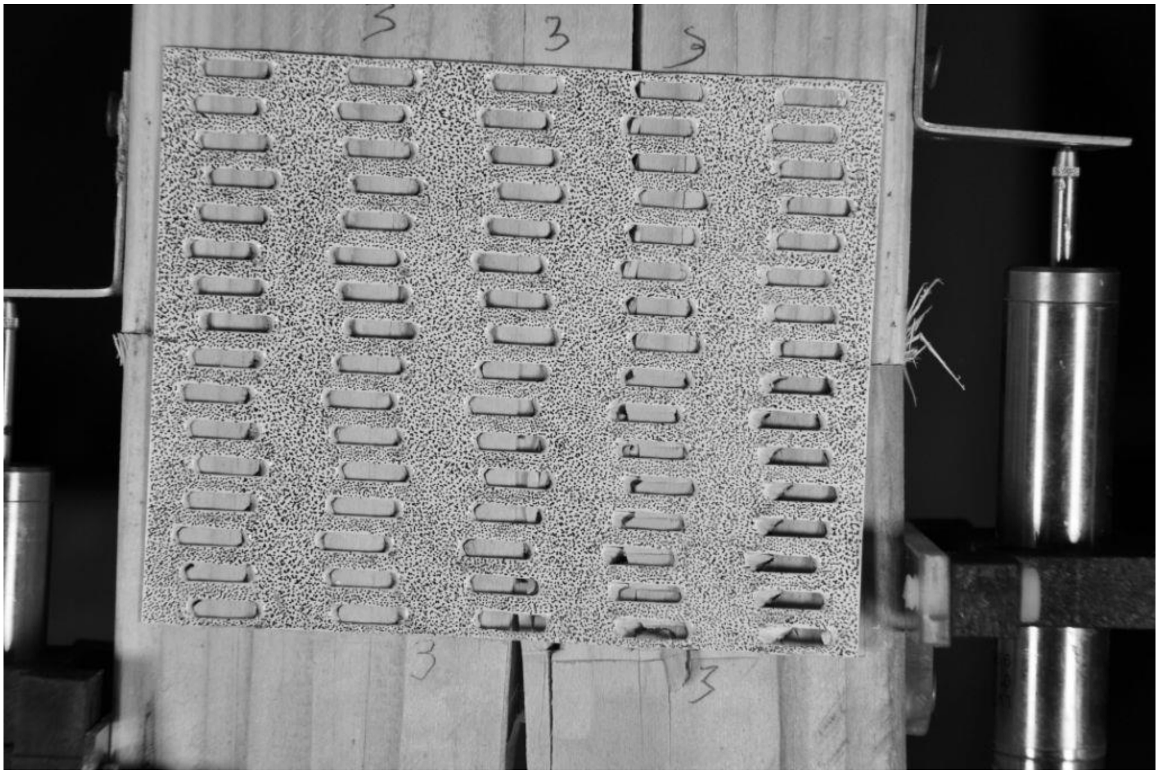

Figure 4-136: The last image at the failure

Twenty two (22) images were taken in addition to the reference image. The metal plate failed due to wood cracks and rotation of the specimen at the failure loading. As shown in the previous figures the wood members already had cracks before any loading. The specimen had rotated and the wood also had deeply cracked. Therefore, the main reason for failure was the wood cracks and the rotation of the specimen. The plate had failed at load equal to 4,500 pounds. The captured images were implemented in DIC-software to find the full-field strain measurements.

4.1.3.4.1 Analysis of the Full-Field Strain Results Obtained From DIC Software

All the test images, which were obtained from the lab tests, were implemented in the DIC software Vic-2D. Each image was analyzed in relation to a reference image. The full-field strain measurements were obtained from the DIC software. Figure 4-137 shows the strain (ε_{yy}) at 200 pounds.

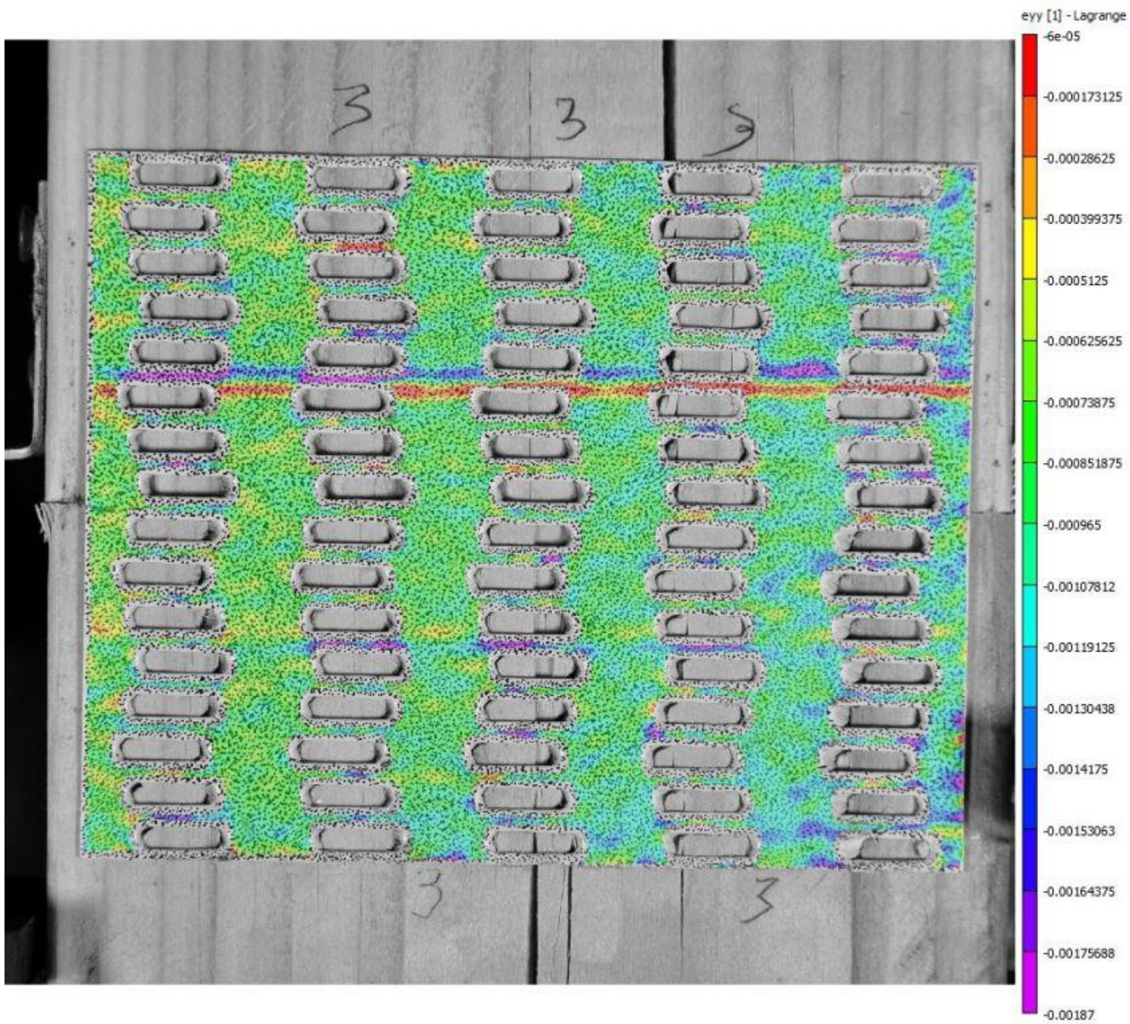

Figure 4-137: Full-field strain measurements (ε_{yy}) for the MPC at 200 pounds

The strain field's results at 200 pounds show very organized strain distribution over the entire plate. A strain strip with lower and higher strain values are seen on the top half of the plate. Increasing the load causes the strain as a compressive strain to decrease to load 1,000 pounds then it increases again as a compressive strain. The strain as a compressive strain increases again until 2,000 pounds. The strain (ε_{yy}) at 2,000 pounds is considered the maximum strain (ε_{yy}) image the specimen can reach in this test. Figure 4-138 show the strain (ε_{yy}) at 2,000 pounds.

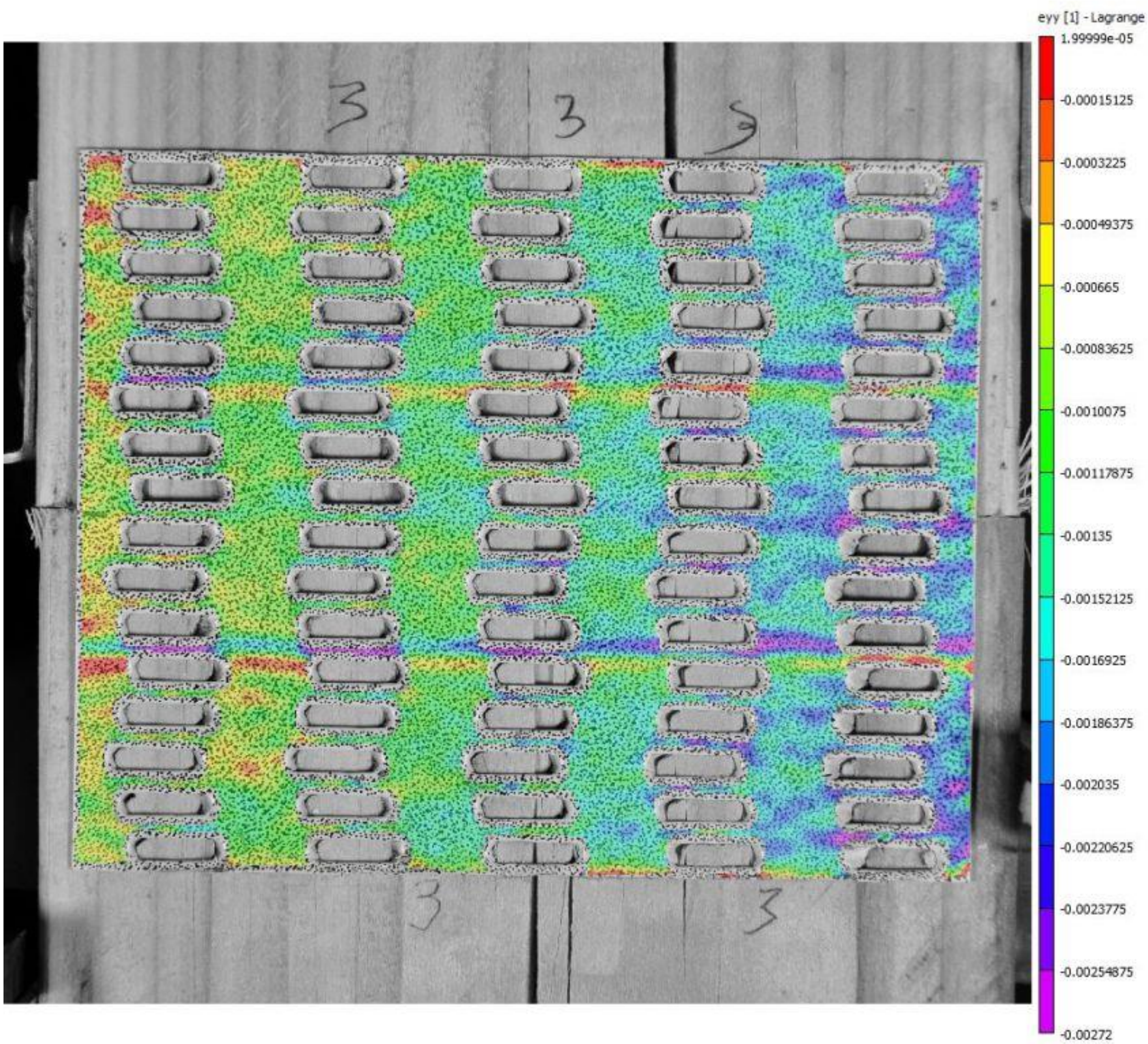

Figure 4-138: Full-field strain measurements (ε_{yy}) at 2,000 pounds

The full-field strain measurements show that the strain above and underneath the horizontal middle gap line is almost mirror to each other. A strain strip in the top half and the bottom half of the plate is shown on the last image and holds higher and lower strain values. After 2,000 pounds the strain (ε_{yy}) fields show unstable changes in the strain values and behavior until the failure at 4,500 pounds. The full-field strain (ε_{yy}) measurements show the strain decreases as a compressive strain until load 3,600 pounds then vary until failure. The last image at the failure is shown in Figure 4-139.

In this test the wood members have two deep vertical cracks from the beginning of the test in both the top and bottom wood members. The specimen fails due to these deep cracks in the wood, and more cracks also occur. The specimen is also influenced by a rotation to the left side from the horizontal middle gap line. The last captured image at load 4,500 pounds could not be processed by DIC code due to the rotation in the specimen. A strain strip is distributed horizontally on the top and the bottom half of the plate's full-field strain measurements and it is shown in each image. This strip has different strain values than the close strain field. This strip has high changes on the right vertical side of the plate due to the rotation in that area. The last image at failure shows tooth withdrawal to the bottom right quarter of the plate's area. And the wood cracks are shown deeper than that at earlier loading stages.

In general, the plate is in good condition with some exceptions. The bottom edges of the plate show some tooth withdrawal. The images show that the gap between the two wood members has been almost closed over the entire test.

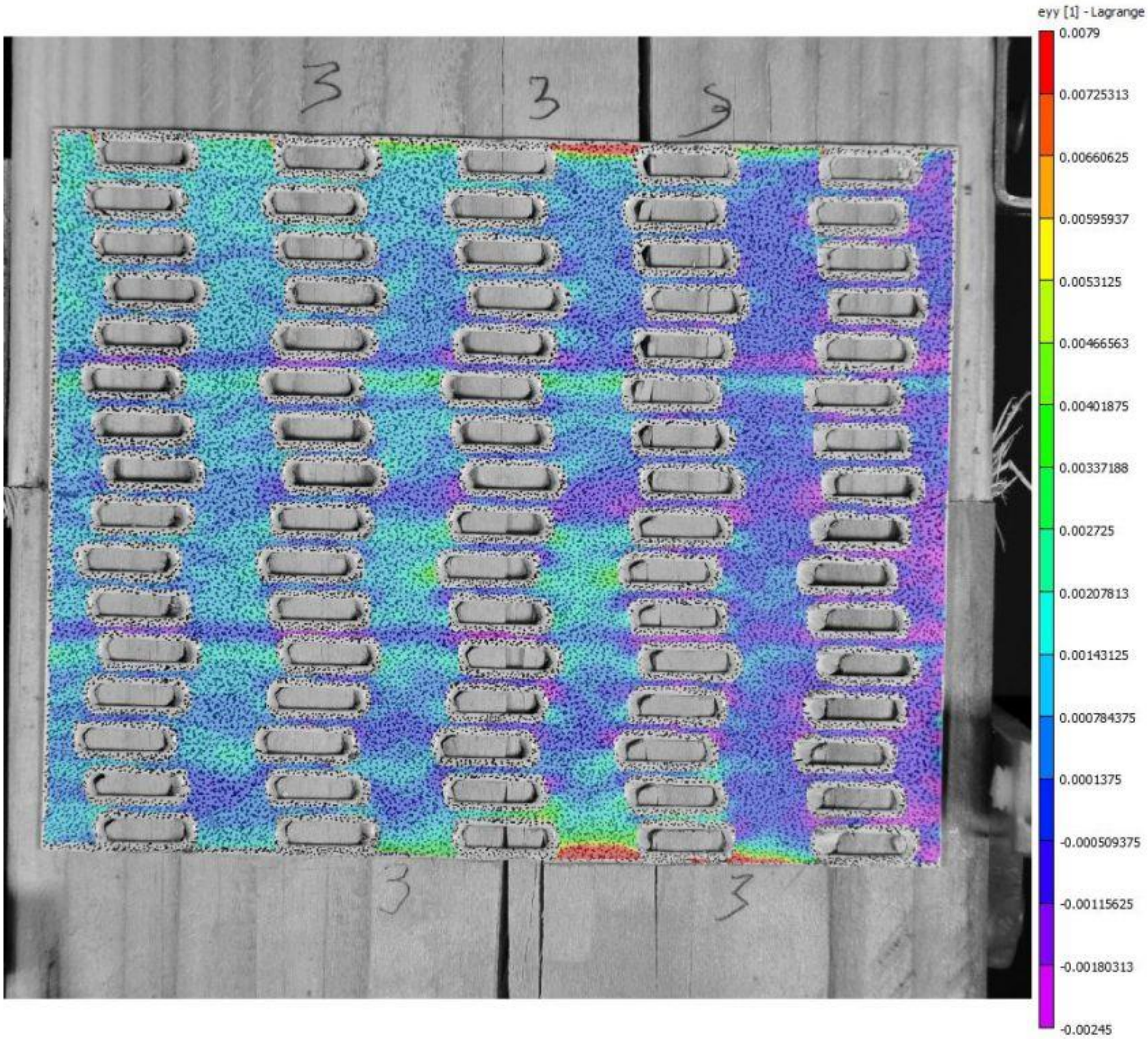

Figure 4-139: Full-field strain measurements (ε_{yy}) for the last image at failure at 4,400 pounds

The failure image shows tooth withdrawal in the bottom side of the plate. The full filed strain for the deformed images shows changes in strain by an increase in load. However, the general changes in the strain are very little due to loading because the specimen rotates and the wood fails. The plate is in good condition and can accept more loads but the failure in the wood and the rotation of the specimen has stopped the test. Thus, the plate needs more than 4,500 pounds to have self-failure.

The strain results in x-direction (ε_{xx}) can also be obtained from DIC code. The first full-field strain measurements (ε_{xx}) at 200 pounds are shown in Figure 4-140.

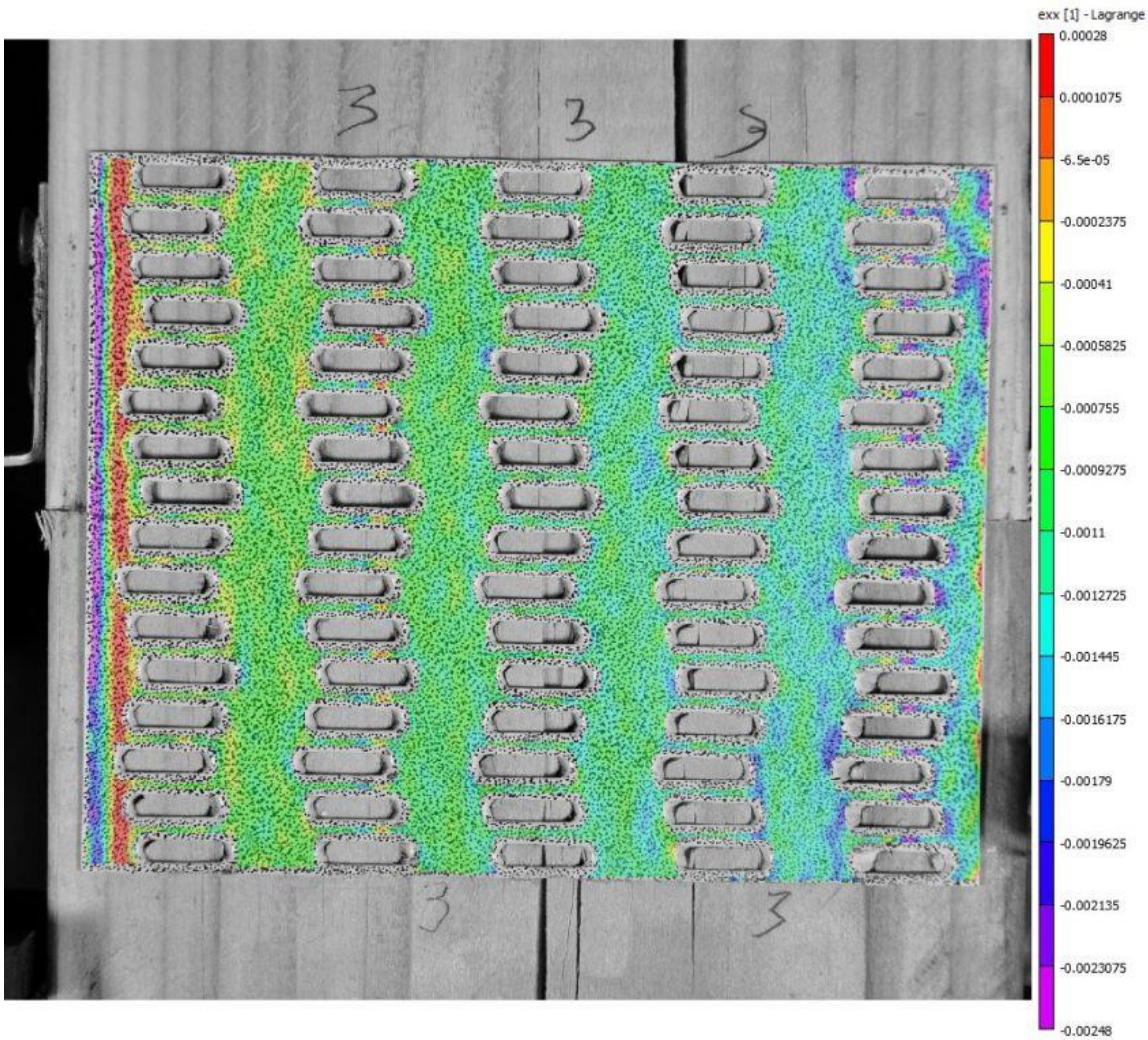

Figure 4-140: Full-field strain in x-direction (ε_{xx}) at load 200 pounds

The strain at 200 pounds is very low strain. The strain above and below the horizontal gap line is almost mirror to each other. High tensile strain (ε_{xx}) is shown along the left vertical side edge of the plate. By increasing the load to 1,000 pounds, the strain (ε_{xx}) decreases as a compressive strain, and the left side of the plate shows a turn to tensile strain instead of compressive strain. The right side of the plate is influenced by higher compressive strain (ε_{xx}) than the left side. The strain on the left side of the plate at higher load is a tensile strain not compressive stain (ε_{xx}). The full-field strain measurement images show that the right side behaves differently than the left side and the strain (ε_{xx}) above and underneath the horizontal middle gap line is almost mirror to each other. The next Figure 4-141 shows the full-field strain measurements (ε_{xx}) at load 2,000 pounds.

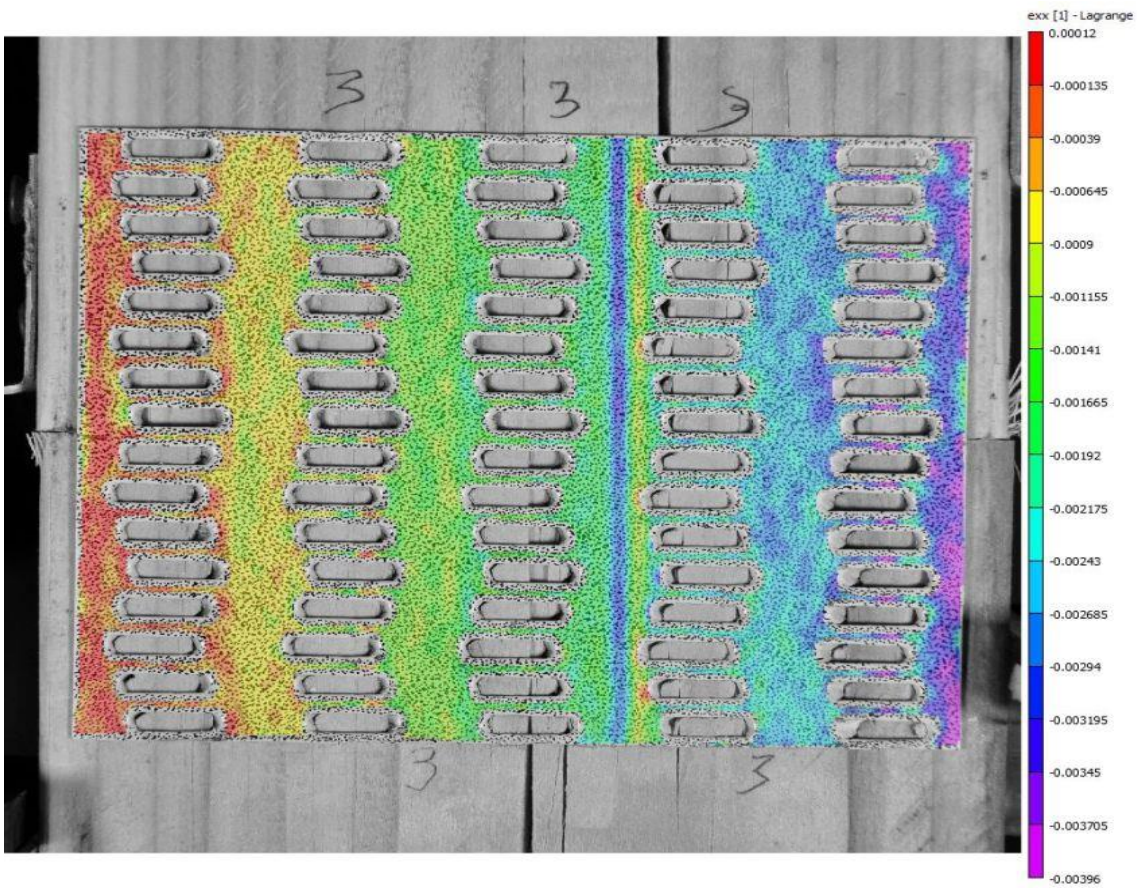

Figure 4-141: Full-field strain in x-direction (ε_{xx}) at load 2,000 pounds

The last image at 2,000 pounds shows how the top half of the strain (ε_{xx}) is almost mirror to the strain (ε_{xx}) on the bottom half. The strain (ε_{xx}) on the right side of the plate is compressive and it gradually decreases down to zero then it changes to tensile strain on the left side of the plate. A vertical strain strip, near the middle between the two upper and lower wood member's cracks, holds low compressive strain. This means that the area between the two wood cracks contracting as a result of these cracks as shown in the previous figure. Increasing the load causes the strain (ε_{xx}) to show an increase as compressive strain at load 3,000 pounds. The full field strain measurement at 3,000 pounds is very close to the image at 2,000 pounds regarding the distribution of the strain on the plate's surface. The full field strain (ε_{xx}) shows continuous spikes in the strain (ε_{xx}) with loading until failure. However, the general strain (ε_{xx}) has high compressive strain on the right side of the plate and very low compressive strain (ε_{xx}) or even tensile strain on the left side of the plate. The strain (ε_{xx}) for the image before failure at load 4,400 pounds is shown in Figure 4-142. This image shows how the strain grows gradually with a slope from the left to the right side.

In this test, the specimen failed due to wood cracks, rotation of the specimen toward the left side, and tooth withdrawal along the bottom quarter of the right side of the plate. Thus, the wood cracks influenced the strain (ε_{xx}) behavior of the entire test's images. The rotation of the specimen also affected the strain (ε_{yy}) and also it is shown here in the strain (ε_{xx}) behavior. The plate is divided into two sides the left side and the right side beside the middle side. However, the strain (ε_{xx}) is well organized in that the top

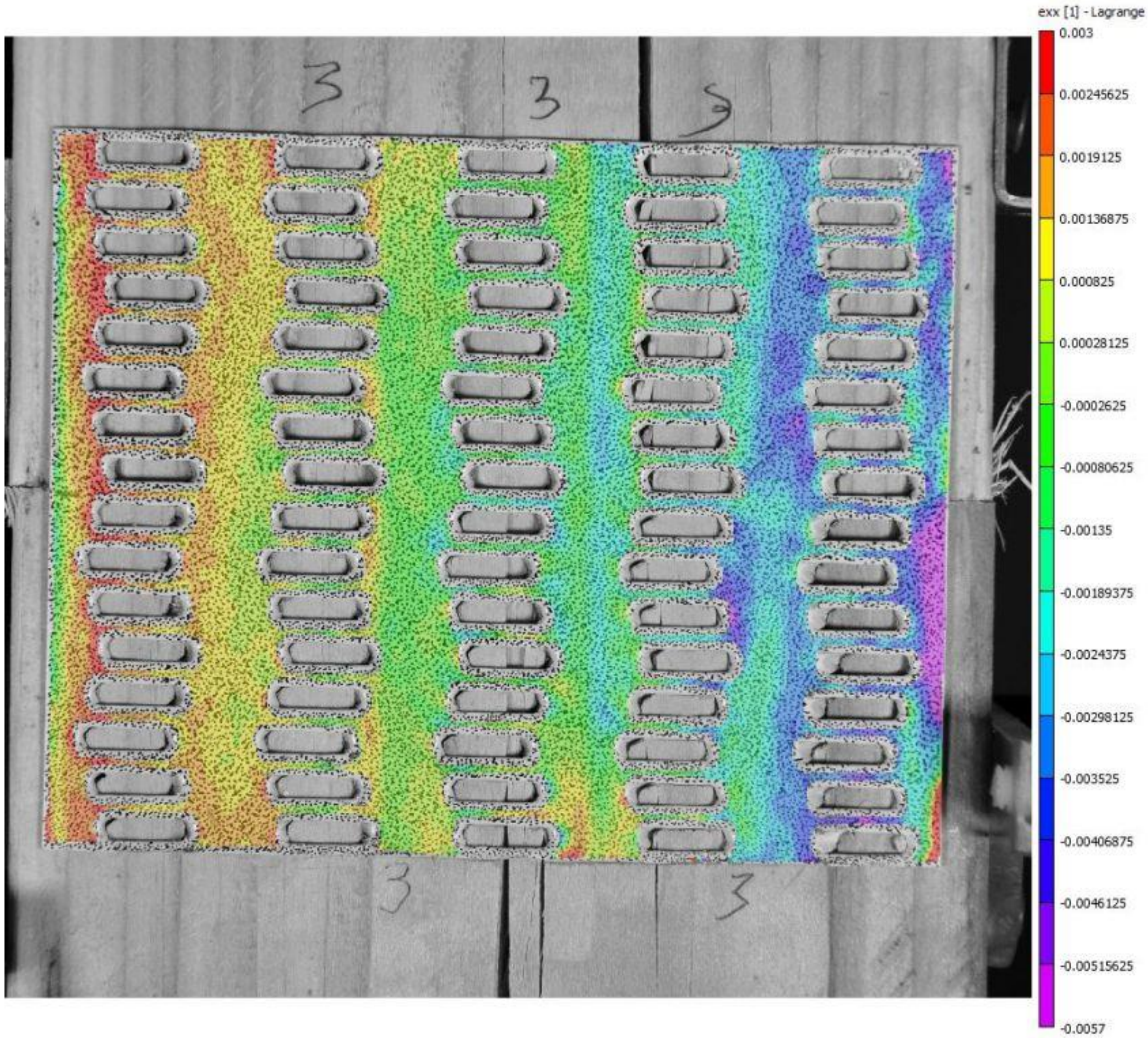

Figure 4-142: Full-field strain in x-direction ε_{xx} under load 4,400 pounds (the last image before failure)

half of the plate is almost mirror to the bottom half of the plate as shown in the (ε_{xx}) strain images. The last image before the failure shows that the strain (ε_{xx}) on the right bottom quarter of the plate, where the tooth withdrawal occurs there after 100 pounds, holds very low compressive strain on the edges and between the slots. The area of the wood through these slots shows the beginning of tooth withdrawal at that area.

4.1.3.5 Comparison between the Displacement from LVDT and DIC-Code gap:

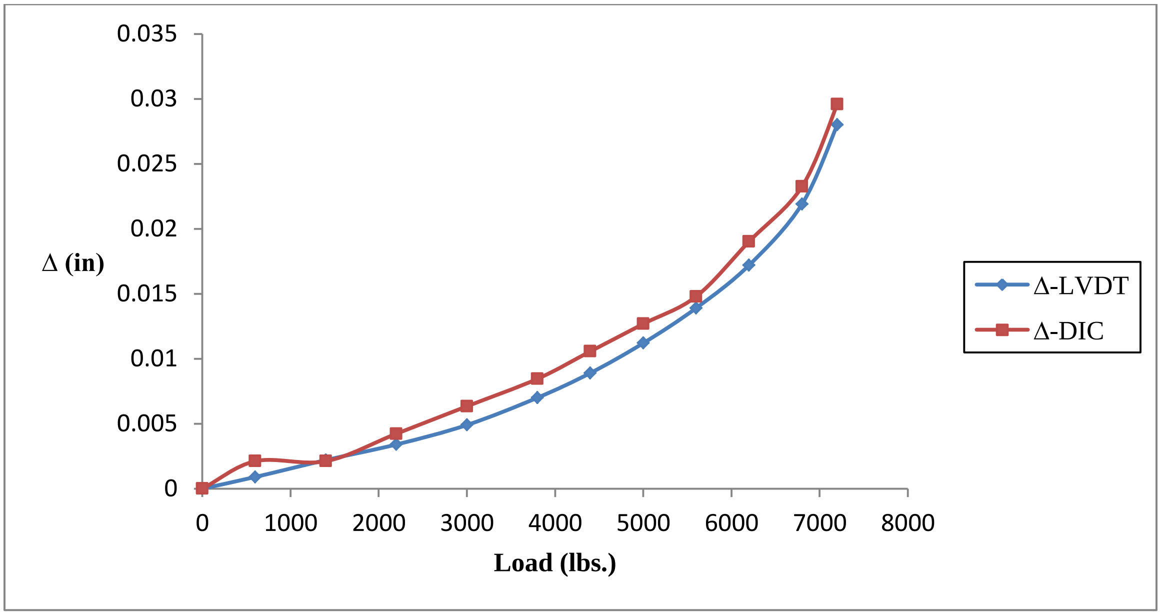

Figure 4-143: The displacement from LVDT vs. the displacement from DIC-code for the 1st EA test –the right side gap

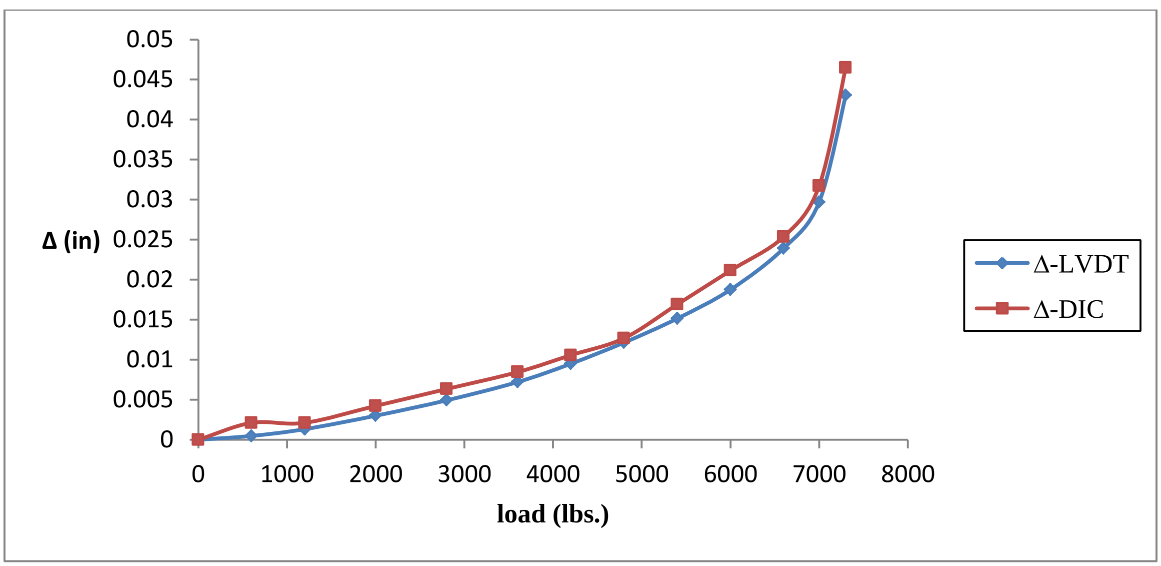

Figure 4-144: The displacement from LVDT vs. the displacement from DIC-code for the 1st EA test –the left side gap

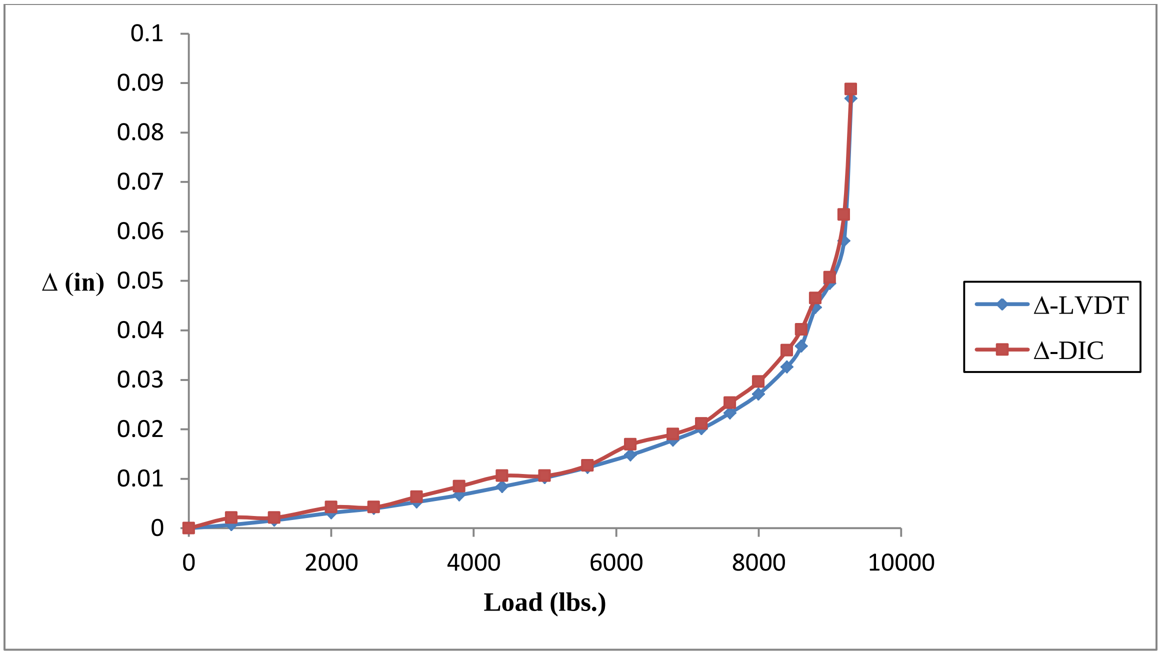

Figure 4-145: The displacement from LVDT vs. the displacement from DIC-code for the 2nd EA test –the right side gap

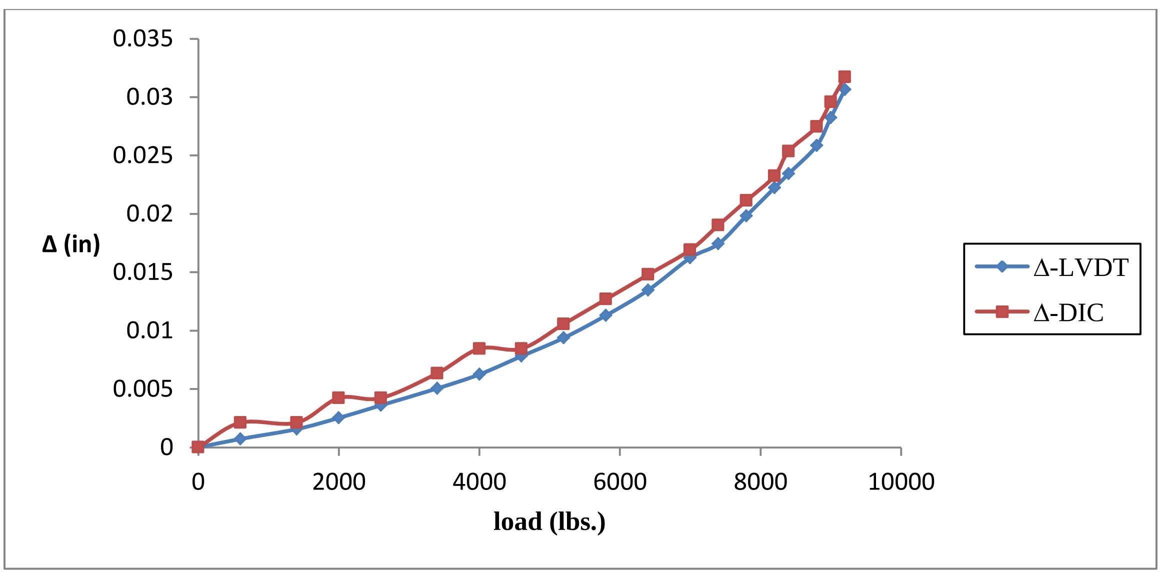

Figure 4-146: The displacement from LVDT vs. the displacement from DIC-code for the 2nd EA test –the left side gap

4.1.3.6 The EA-Tests Summary and Discussion

Three tests (EA) were conducted in the lab. The specimens were loaded until failure. A digital camera was used to capture images every 200 pounds. All the captured images were implemented in digital image correlation software Vic-2D to find the full-field strain measurements for each image with respect the non-deformed reference one. The first two tests failed due to tooth withdrawal and the third test failed due to wood cracks, rotation of the plate, and tooth withdrawal. Tables 4-8, 4-9 and 4-10 show a brief description for each test.

Table 4-8 : Brief description for each test-EA

EA-Test #	Failure load (lbs.)	Total Deformed Processed Images by DIC Code	Failure Behavior Descriptions
1	7,300	37	tooth withdrawal to the top half of the plate
2	8,300	43	tooth withdrawal to the bottom half of the plate
3	4,500	22	wood cracks, tooth withdrawal, and rotation of the specimen

Table 4-9: Brief comments on each EA-test

EA Test #	Comments on the Test and the Failure
1	The available captured images are 37 images plus the reference one. The last image at failure was processed by DIC-code. A significant strain changes on the plate due to tooth withdrawal
2	The available captured images are 47 images plus the reference one. The last image at failure was processed by DIC-code. A significant strain changes in the bottom due to tooth withdrawal.
3	The available captured images are 23 images plus the reference one. The last image at failure was not processed by DIC-code due to the rotation of the specimen. The plate has failed due to wood crack at 4,500 pounds and specimen rotation.

Table 4-10: Brief strain changes description for each EA-test

EA-Test #	The Strain (ε) Changes
1	The strain (ε_{yy}) started as a tensile strain. At load 6,000 pounds it turned to higher tensile strain. Due to tooth withdrawal in the top half of the plate, the strain behavior changed and it represented very high tensile strain (ε_{yy}) at the top of the plate.
2	The strain (ε_{yy}) started as a tensile strain. Then at load 6,000 pounds it significantly increased as tensile strain. The strain (ε_{yy}), from 6,000 pounds until 8,300 pounds, increased especially on the bottom half of the plate. The strain (ε_{xx}) was negative strain on most of the plate's regions. Due to tooth withdrawal in the bottom half of the plate, the strain behavior changed
3	The strain (ε_{yy}) started as a tensile strain. The strain (ε_{yy}) varied with loading until 4,000 pounds. It showed an increase to the tensile face. The plate failed due to tooth withdrawal, wood cracks and the rotation of the specimen. Strain (ε_{xx}) was negative on right side of the plate and positive on the left side.

The previous tables briefly describe the behavior of the plate under tensile load until failure. In this test the external load was parallel to the wood grains and perpendicular to the plate's major axis or to the slots. All the captured images were implemented in the digital image correlation software to obtain the full-field strain measurements. The third test had a rotation in the specimen so the DIC-code could not give the strain behavior for the last image at failure. The first and the second test failed due to tooth withdrawal of the plate while the third one failed due to tooth withdrawal, wood cracks, and rotation of the specimen.

In the first test, the plate starts with positive strain (ε_{yy}). Then the strain increases with loading. At 6,000 pounds, the strain shows a significant increase as tensile strain on the top and the bottom half of the plate. However, the strain (ε_{yy}) in the middle is compressive strain due to tooth withdrawal of the top half of the plate and due to the circular shape displacement for the plate around the gap line. The top left quarter of the plate's area is totally affected by tooth withdrawal at the failure. In general, the cross section line curves are very close to each other at low load but not at high loads. The top half of the plate failed due to tooth withdrawal and the wood cracks also helped to withdrawal the teeth. The plate has not yielded to show yielding strain and the other factors affect the strain behavior more than the external load. Thus, the strain is not fully-well organized or distributed. The images show that the top part has obvious tooth withdrawal while the bottom part had some minor changes. Thus, the load affected the top part of the plate more than the bottom part.

The left side of the specimen showed larger gap between the two wood members than on the right side. Increasing the load caused the left side gap to increase until tooth withdrawal occurred. The tooth withdrawal on the left side is very clear and is considered a major factor in the failure. The right side of the plate in the middle has not been affected by tooth withdrawal. The strain curves show that the strain underneath the horizontal middle gap line has very stable strain distribution and is well organized while the top is not due to tooth withdrawal and circular plate deformation.

The last image at failure shows that both strain (ε_{yy}) and (ε_{xx}) are tensile strain. That means the plate is not at yielding point. However, the strain behavior for the images before the tooth withdrawal influence shows that the strain (ε_{yy}) is tensile and the strain (ε_{xx}) is compressive which tends to yield. But after the tooth withdrawal, both strains have changed and the strain in both directions is tensile strain.

In the second test, the full-field strain measurements show that the strain increased as a tensile strain until load 2,000 pounds. Above 2,000 pounds the strain (ε_{yy}) fluctuates in its behavior and varies. At 6,000 pounds, the strain shows a change in the strain (ε_{yy}) behavior. The change in the strain behavior continues with loading and it is clear at load 8,000 pounds. At 6,000 pounds, the indication of tooth withdrawal has started to occur as shown earlier in the strain curves. The bottom wood member, which holds the grain that is parallel to the tension force, has a vertical crack before the test, which increased as a result of an increase of the load but, it is not the main reason for failure in this test. The gap size in the right side gradually increased from load 200 pounds until load 8,000 pounds. However, after 8,000 pounds the images show rapid increase in the gap size every 200 pounds. On the other hand, the images also show a plate withdrawal in the right bottom side first. The increase in the gap and the tooth withdrawal, especially in the right bottom side of the plate, occur together as the load is increased. The failure image shows tooth withdrawal in the bottom side of the plate, and it is very high in the right side where the gap also is large. However, the bottom of the plate has failed due to the tooth withdrawal. The last image shows tooth withdrawal for the whole bottom side of the plate.

In the third test, the strain also started as a tensile strain at 200 pounds. Then the strain increased as compressive strain until load 2,000 pounds because of a rotation occurrence. Once 2,000 pounds was applied, the strain (ε_{yy}) showed continuous spikes in the strain (ε_{yy}) curves. The strain before failure fluctuated. In general, the strain (ε_{yy}) on the top half of the plate was almost mirror to the strain curve on the bottom half of the plate with some exceptions. In this test, the wood members on the top and the bottom had deep cracks before the test. These cracks developed and became deeper during the test. Tooth withdrawal showed very clearly on the right middle side of the plate where the wood members had the cracks. The images also showed cracks in the wood through the slots. The right middle side of the plate was influenced by tooth withdrawal more than the left side. The last image at failure at load 4,500 pounds shows a complete tooth withdrawal to the right bottom-quarter side of the plate. The image at failure showed a deep wood crack in the bottom wood member. Besides all that was mentioned above, the specimen suffered a rotation which showed very well in the last image at failure. The specimen moved to the left side and the wood cracks in the bottom and the top wood members showed deeper cracks and this led to failure. The rotation of the specimen remained hidden during most of the test but, it was very clear in the last image at failure. This rotation can make a mess in the strain behavior in the entire test. Beside the rotation, the wood cracks that occurred in the test and developed with loading can also influence the strain behavior.

In these EA-tests, especially the first two tests, The images before the effect of tooth withdrawal shows that the strain (ε_{yy}) increased as a tensile strain while the strain (ε_{xx}) is a compressive strain which make sense. However, once the failure from external factors has occurred, the strain behavior also has changed. These external factors: 1) the tooth withdrawal affect and the pulling out of the plate. 2) Wood cracks which lead to failure and support tooth withdrawal. 3) Rotation of the specimen as shown in the third test. Due to these factors, the strain behavior changed and showed tensile strain again for both (ε_{yy}) and (ε_{xx}). This means that the plate was moving toward the yielding point and the strain toward a well-organized distribution. But once tooth withdrawal occurred, the strain behavior totally changed. The distribution of the strain (ε_{yy}) above and below the horizontal middle gap line no longer mirrored each other in the two tests due to the changes and failure indications of one half of the plate while the other half did not. The other half that did not fail showed more stable and well organized strain distribution as shown earlier in the strain curves. The tooth grip there seems to be very high.

The displacement of the gap between the two pieces of wood was found using the DIC Vic-2D software based on the number of pixels in the vertical direction in each image under loading. Then the calibration from the software was used to change the pixels to inches. The calibration factor was 0.002113. The results from the LVDT were used to compare the displacement of the gap from LVDT to the displacement that is found using the digital image correlation software Vic-2D. The results are not identical between the two methods but they are very close.

4.1.4 EE–Test

In EE-tension test the tension load is perpendicular to the plate's slots or the plates' major axis and to the wood grain. Three specimens of two members of wood connected by a metal plate connector were prepared for testing. After preparing the specimens they sat for 7 days before the test. They were tested under tension force in the civil engineering lab using the universal testing machine. The load increment was 200 pounds and an image was taken at each load increment until failure.

The LVDT machine was used to verify the results from the digital image correlation software. The LVDT was used for both sides of the specimen of wood members.

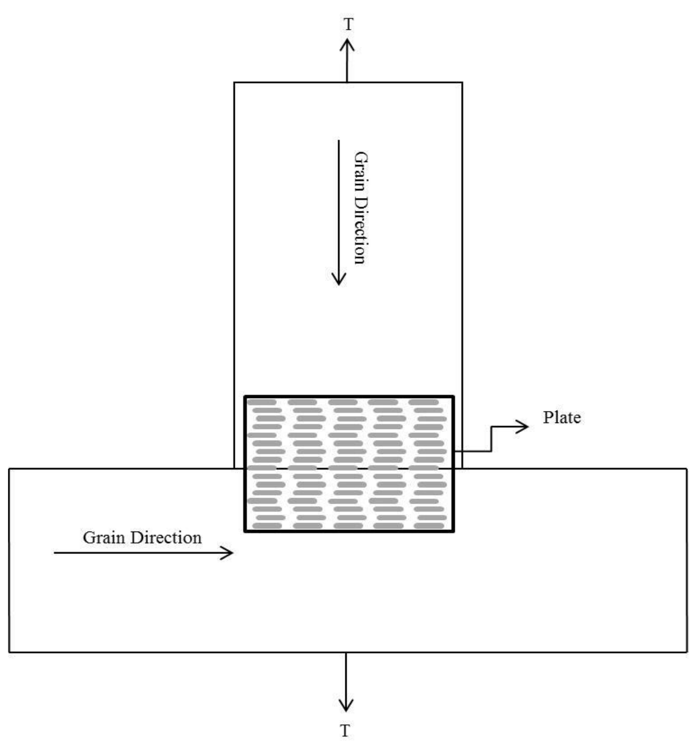

Figure 4-147: EE- sample test shape

4.1.4.1 Plate's Axes Direction Based on DIC Software

The direction of the x and y axis was obtained from the digital image correlation software as shown in the next two Figures 4-148, 4-149.

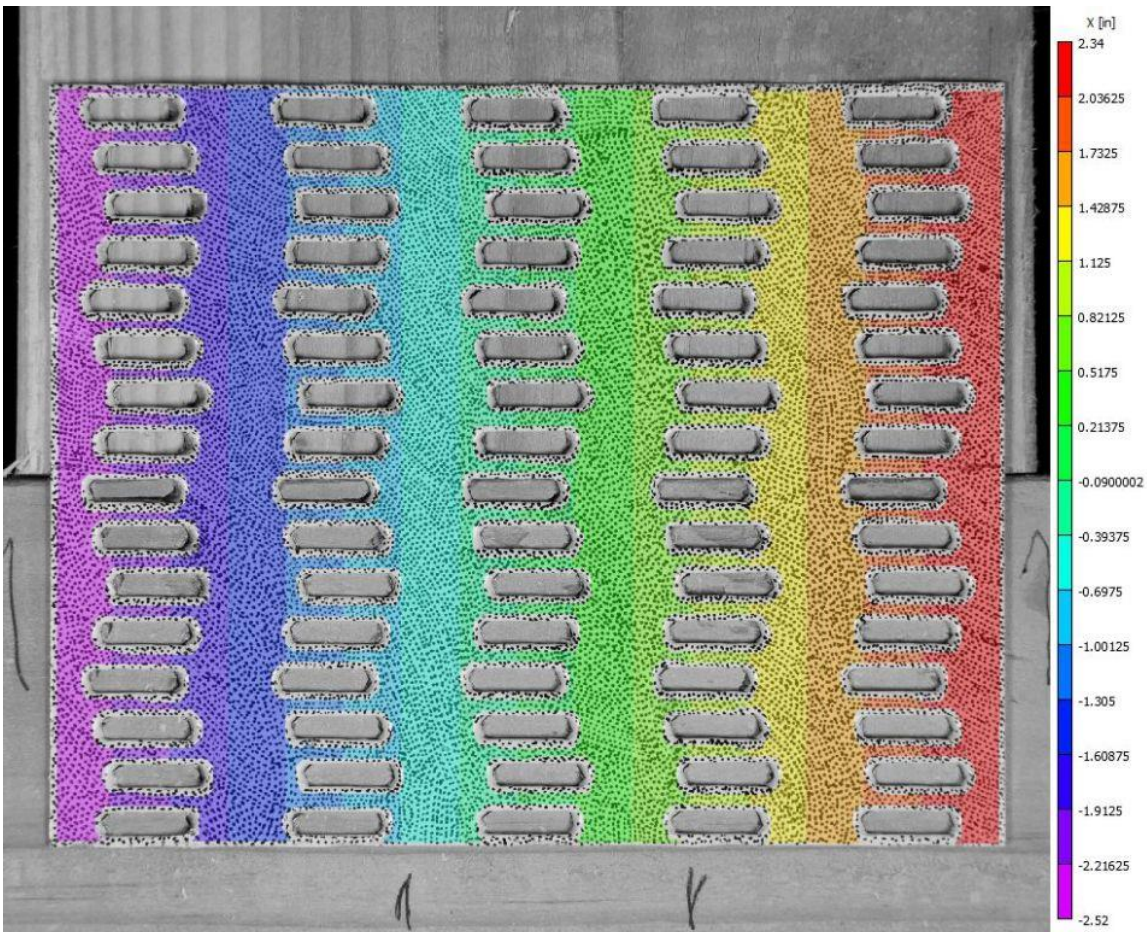

Figure 4-148: x-axis coordination system obtained from DIC software

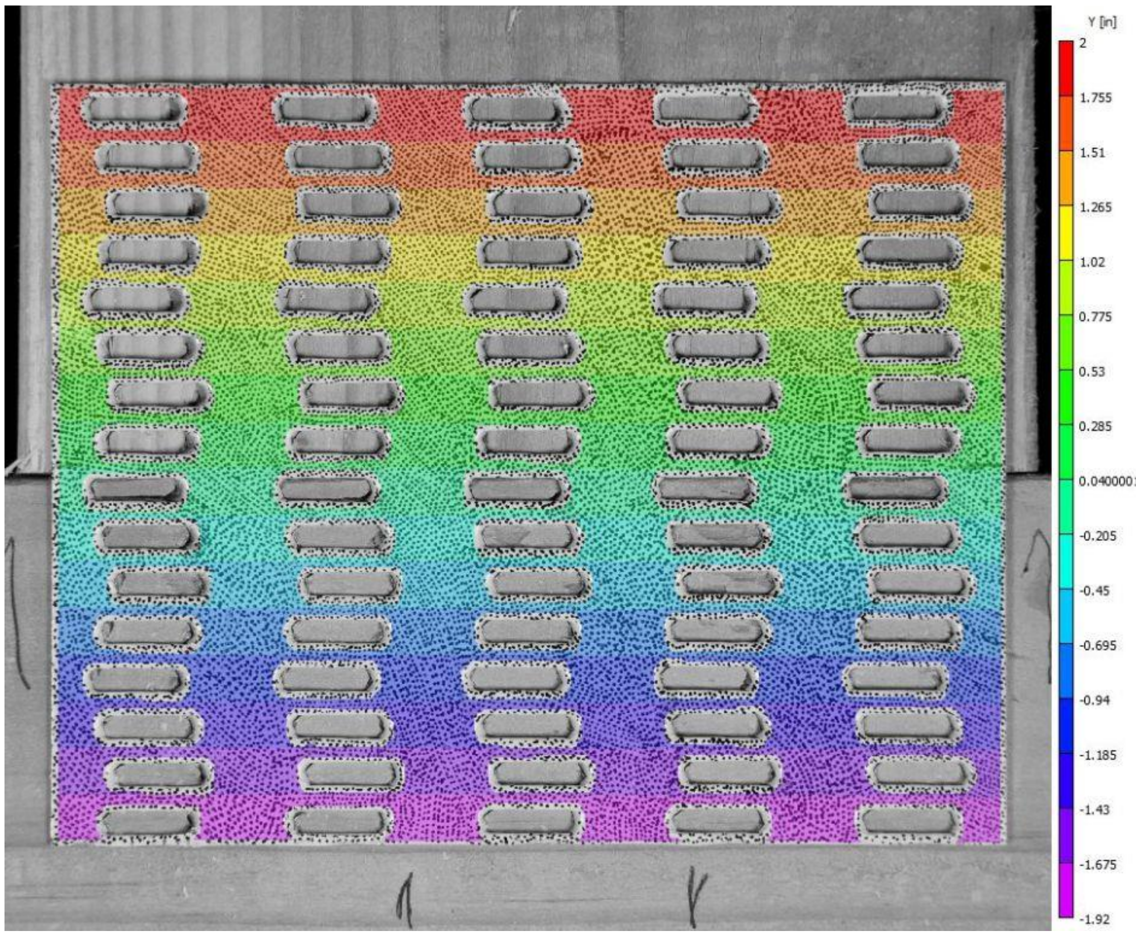

Figure 4-149: y-axis coordination system obtained from DIC software

4.1.4.2 The First Tension Test (EE-1st)

In this test, the two members of wood were connected by the MPC. The specimen was set on the universal testing machine. The first reference image was taken before applying any load. Figure 4-150 shows the first image which was considered as the reference image in digital image correlation technique.

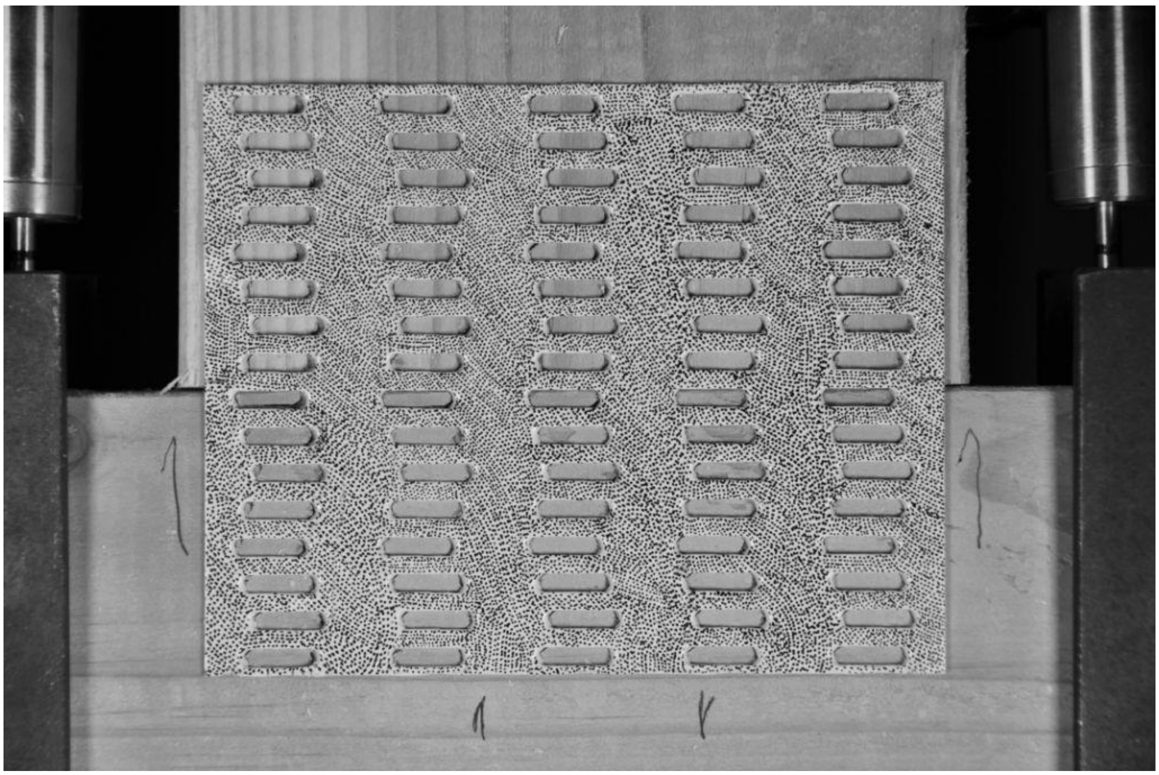

Figure 4-150: First image / reference image

After the first reference image was taken at load zero, the load was increased on the specimen until failure. The camera was placed on a fixed stand and the MPC was perpendicular to the camera's lenses. Images were taken for the MPC specimen at each

load increment of 200 pounds until failure. The failure was due to wood cracks. Figure 4-151 shows the last image at failure.

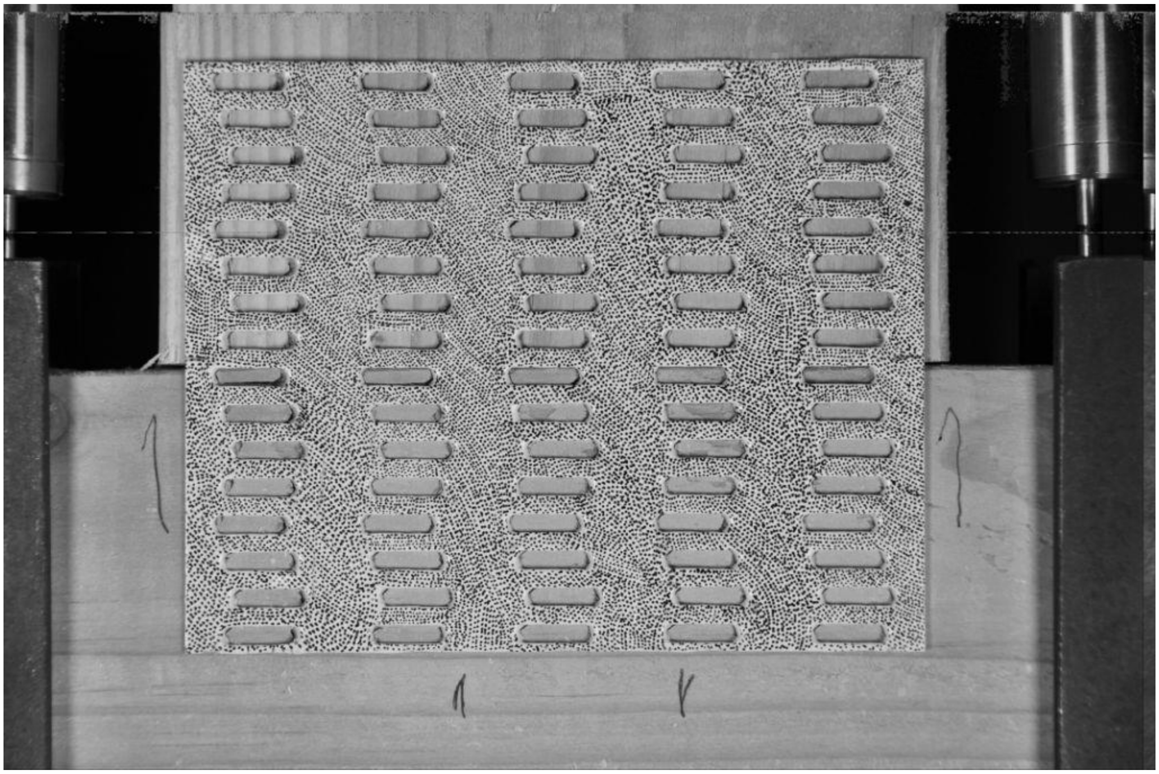

Figure 4-151: The last image at failure

Twenty (20) images were taken in addition to the reference image. The metal plate failed due to wood cracks. The cracks in the wood occurred under the supports so the plate and the wood under the plate at failure appears to be in good conditions but after this last image the crack expanded horizontally even under the plate. The plate did not fail and it was in good condition. The bottom wood member cracked. The specimen failed at load equal to 4000 pounds. The captured images were implemented in DIC-software to find the full-field strain measurements.

4.1.4.2.1 Analysis of the Full-Field Strain Results That Obtained From DIC Software

All the test images, which are obtained from the lab tests, are implemented in the digital image correlation software Vic-2D. Each image was analyzed in relation to a reference image. Thus, each deformed image is compared to the non-deformed reference image. The full-field strain measurements were obtained from the digital image correlation software. Figure 4-152 shows the strain in y-direction (ε_{yy}) for the image at 200 pounds.

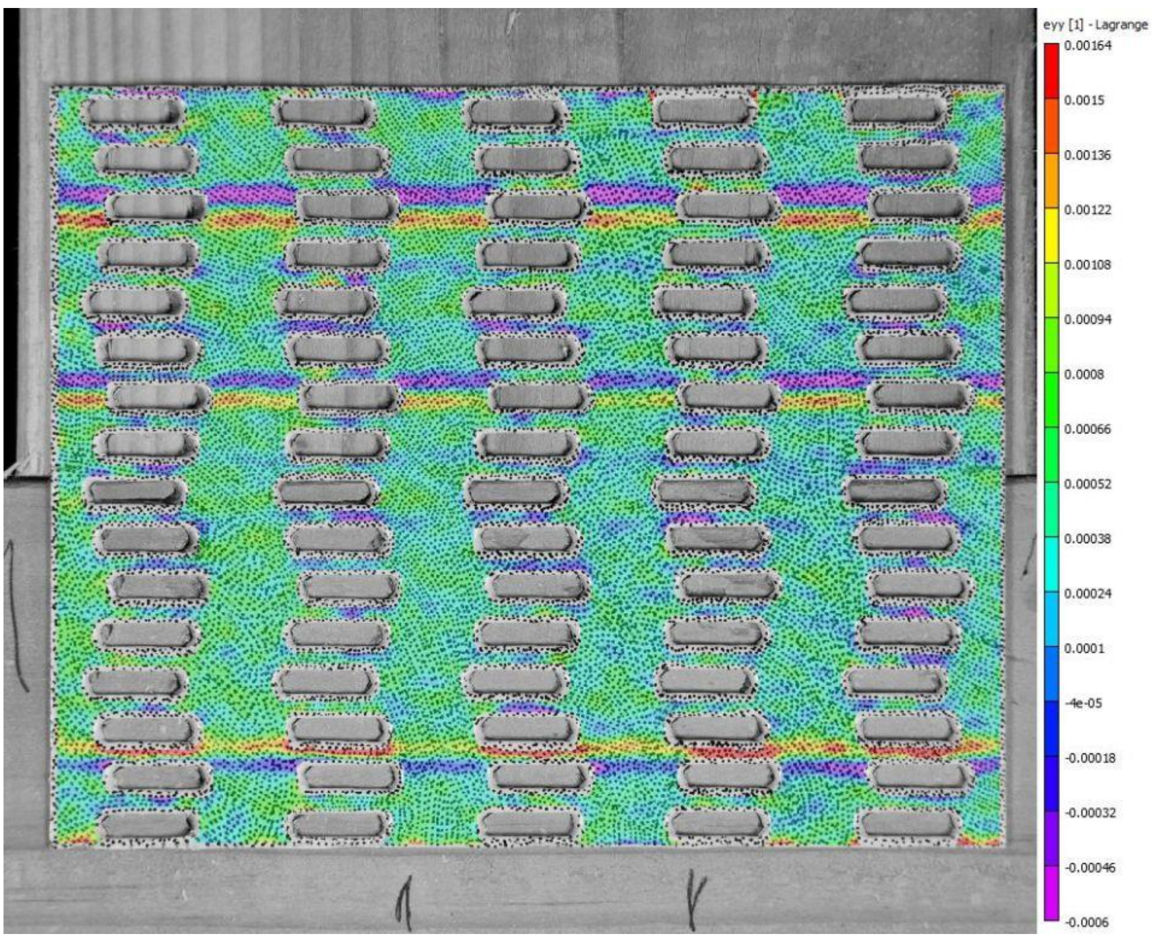

Figure 4-152: Full-field strain measurements (εyy) for the MPC at 200 pounds

The image at 200 pounds shows that the strain (ε_{yy}) is very low with some exceptions at some regions over the plate's surface. Strain (ε_{yy}) is tensile. The strain (ε_{yy}) values fluctuate with very low differences over the plate's strain field. As the load increases, the strain (ε_{yy}) also increases. Figure 4-153 shows the strain at 1,000 pounds.

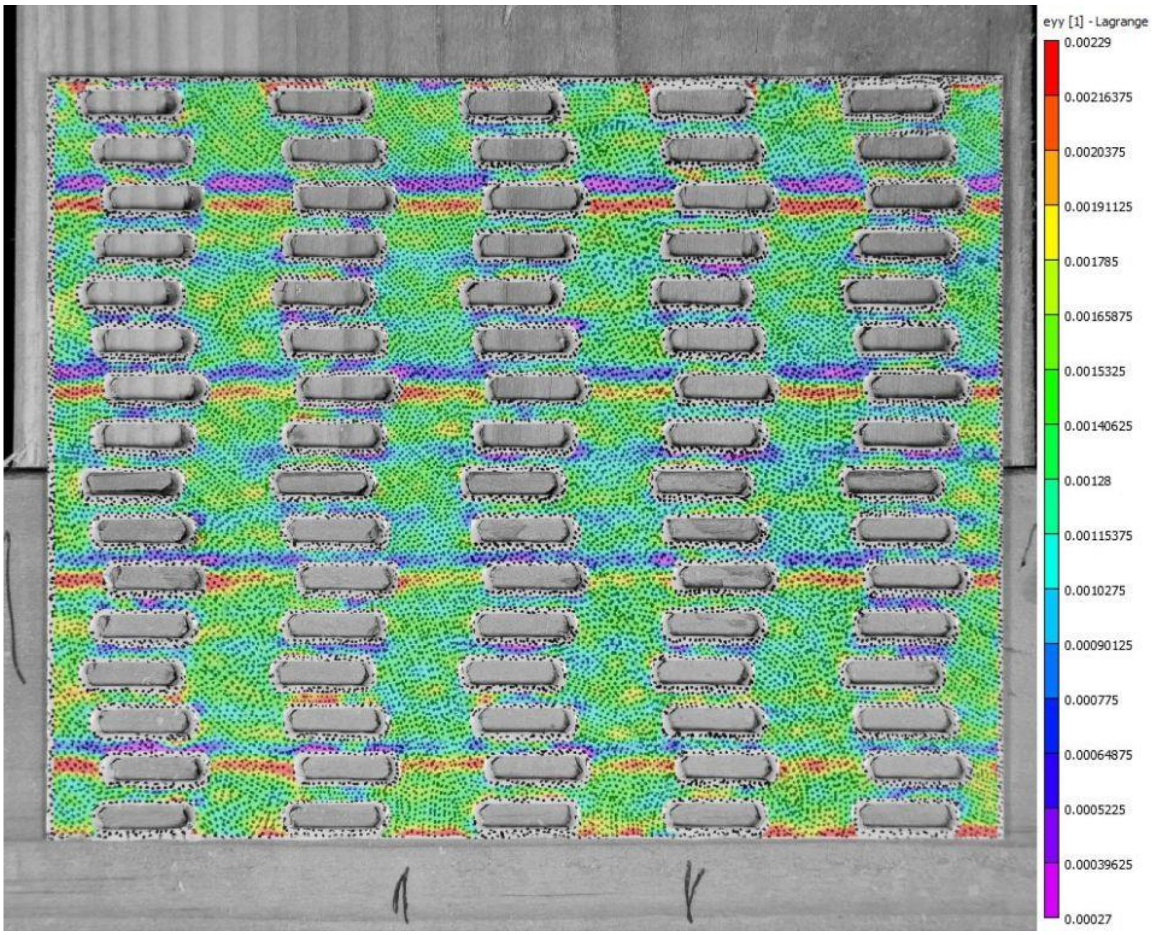

Figure 4-153: Full-field strain measurements (ε_{yy}) at 1,000 pounds

The strain field's results at 1,000 pounds shows higher strain values than the strain at 200 pounds and also it fluctuates over the plate. Some limited regions show lower strain values than the dominant strain. The strain field after 1,000 pounds experiences a decrease in its strain values (ε_{yy}). The strain (ε_{yy}) experience gradually decreases in its values until the failure at 4,000 pounds. The strain field is positive most of the time above the horizontal middle gap line. The right side of the plate shows some pulling out of the plate near the bottom edge so the strain is high as a tensile strain. The full-field strain measurements (ε_{yy}) at 3,200, 3,400, 3,600, 3800 and 4,000 are very close to each other. The images show how the area of the strain field beneath the horizontal middle gap line turns to different color due to the compressive strain (ε_{yy}) there. Figure 4-154 shows strain (ε_{yy}) for the last image at failure at 4,000 pounds.

The failure in this test was in the wood due to wood cracks in the bottom member under the two supports on the left and the right side. DIC software can be used to show the changes in strain under early different loading increments. From the full-field strain measurements, this test does not show any significant changes in the strain behavior to indicate any failure. The failure was in the wood under the support and even the last image at failure shows that the plate and the wood were in good condition. However, the loading machine stopped due to failure under the supports. The DIC strain images can give the strain field at early stages of loading before any indication of plate's failure.

In general, the plate in this test is in a good shape with some limited pulling out of the plate's edge that occurred at the bottom edge of the plate mainly from the right side. next images show the full field-strain measurements for different images.

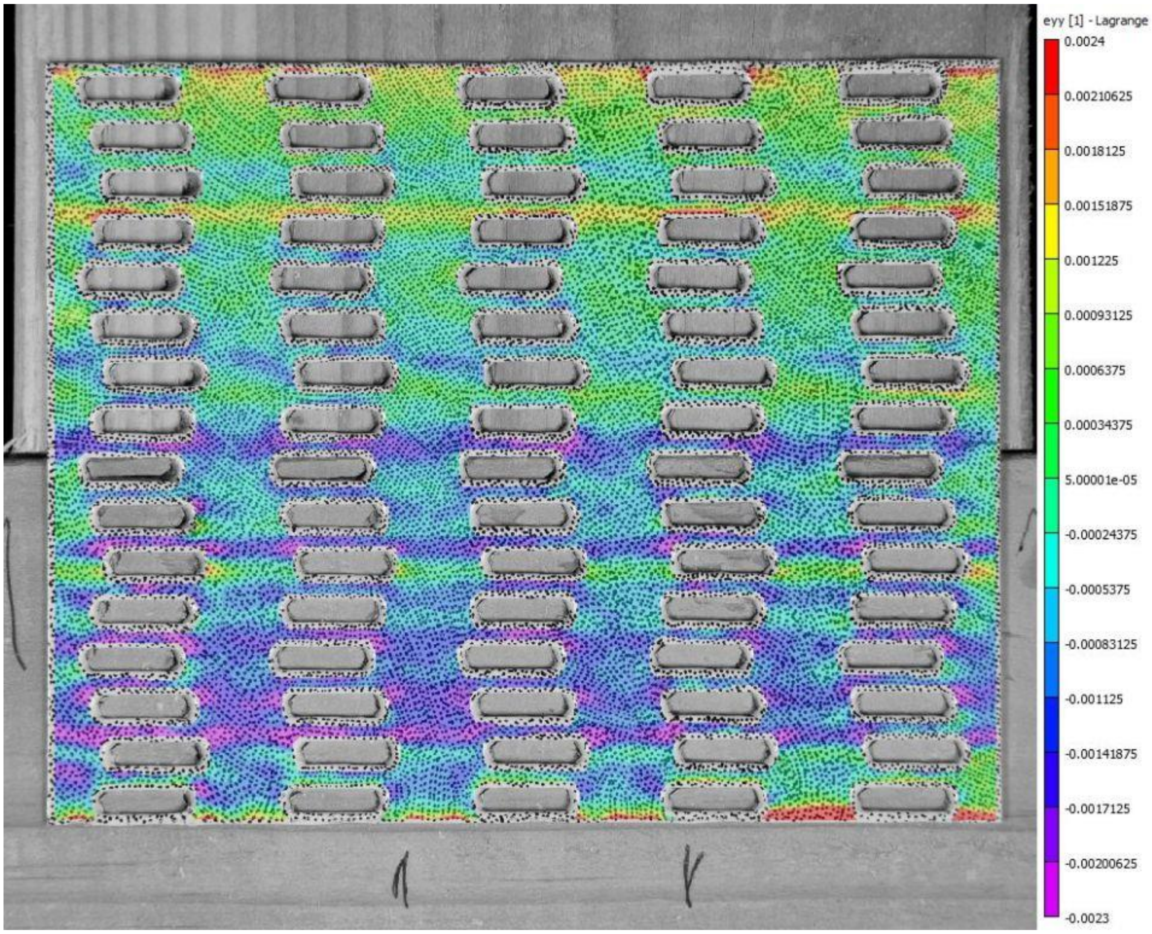

Figure 4-154: Full-field strain measurements (ε_{yy}) for the last image at the failure at 4,000 pounds

The strain field shows some spikes in the strain colors that means some sudden changes in the strain. These changes are close to the slots. Thus, the effect of the slots on the strain field is obvious and also some pulling out of the plate can make some sudden changes for the strain values. The maximum strain is found on the bottom right side of the plate. Some tooth withdrawal is shown at that corner. At 4,000 pounds the specimen cracked due to wood failure under the supports. The gap between the two wood members shows very small changes due to wood failure and the plate is in good condition. This test can show the changes in strain before the yielding point of the plate.

The strain results in x-direction (ε_{xx}) also can be obtained from digital image correlation code. The full-field strain (ε_{xx}) measurement is shown in Figure 4-155. The strain (ε_{xx}) is a tensile strain. The contour colors fluctuate across the plate, but in general the strain (ε_{xx}) is around 0.0004.

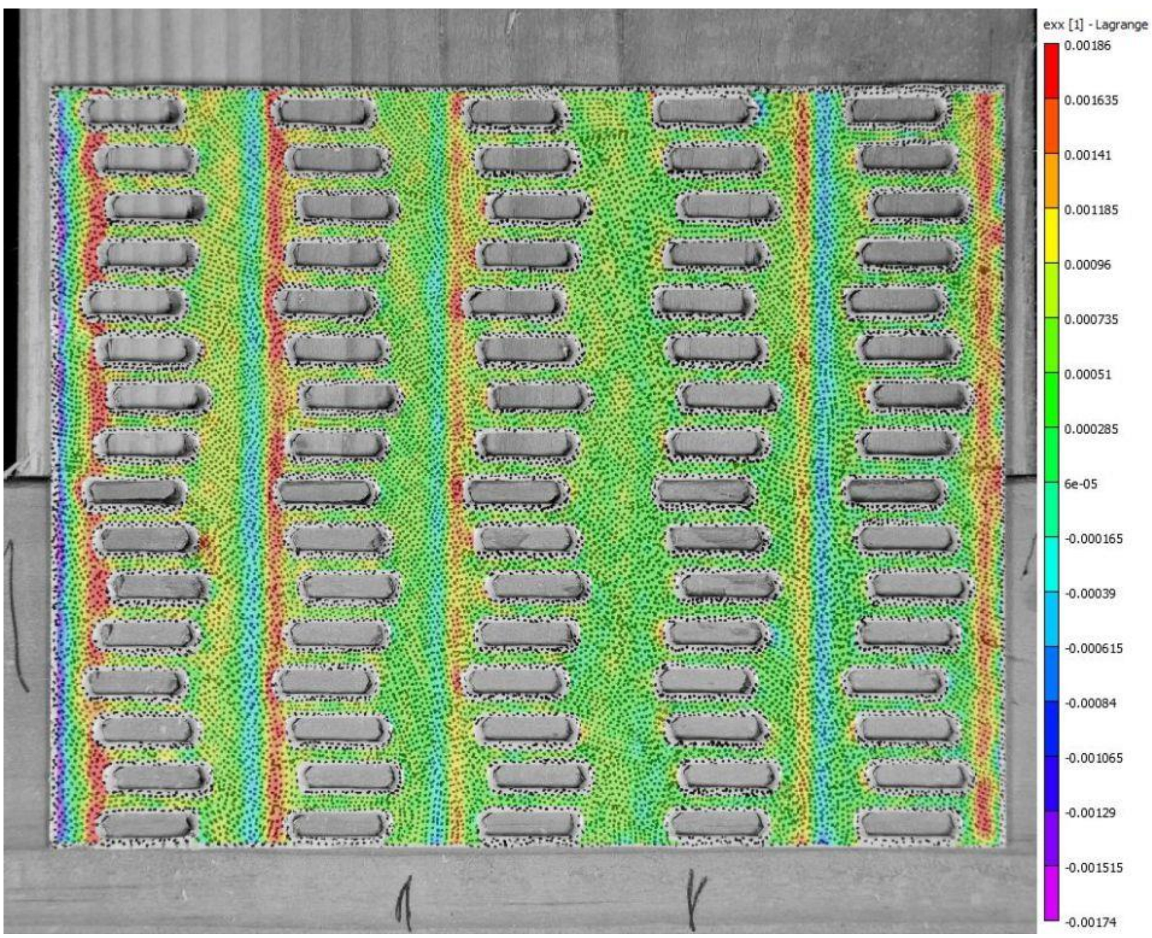

Figure 4-155: Full-field strain in x-direction (ε_{xx}) at load 200 pounds

Due to loading, the strain (ε_{xx}) also increases as a tensile strain until load 1,000 pounds as shown in Figure 4-156.

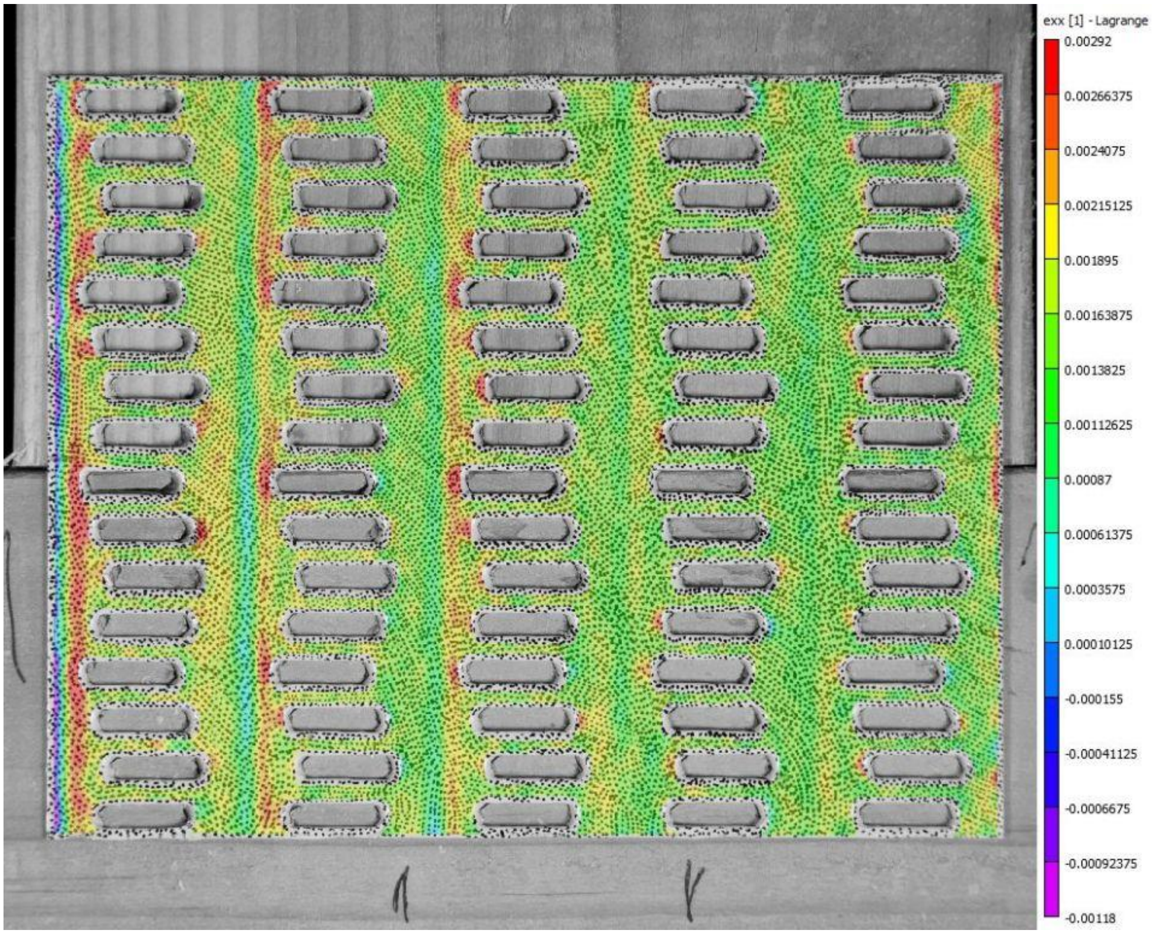

Figure 4-156: Full-field strain in x-direction (ε_{xx}) at load 1,000 pounds

After 1,000 pounds, the strain (ε_{xx}) fields decreases. At load 3,200 pounds; the strain (ε_{xx}) in the middle of the plate turns to compressive strain with some exceptions. But the strain (ε_{xx}) on the right-top of the plate holds tensile strain beside compressive strain. The bottom half of the plate mainly holds compressive strain with more strain values than the middle or the top part of the plate. The strain (ε_{xx}) behavior from load

3,200 pounds until the failure at 4,000 pounds is very close to each other. Figure 4-157 shows the last image at failure.

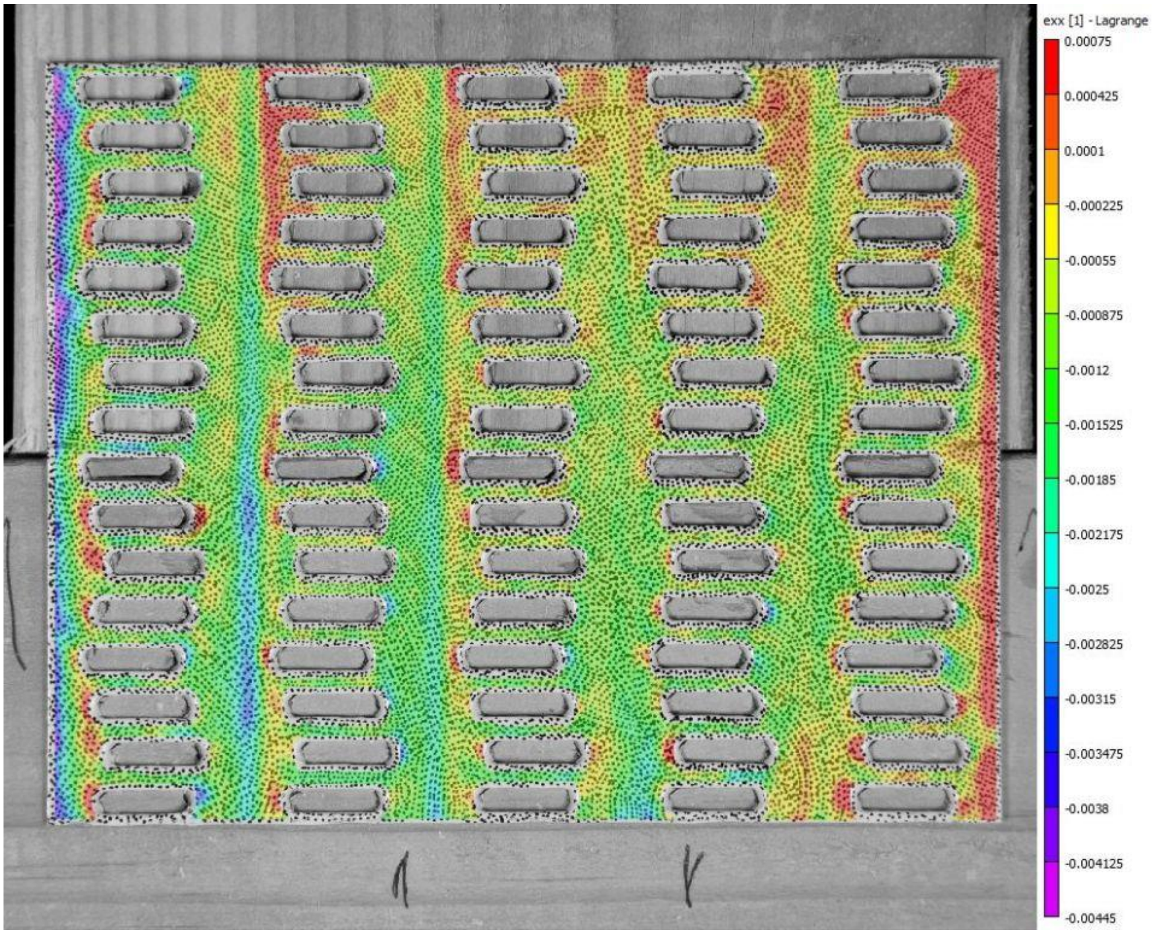

Figure 4-157: Full-field strain in x-direction (ε_{xx}) at load 4,000 pounds (the last image at failure)

The last image at the failure shows fluctuation in the strain values and shows rise in the strain in some areas on the plate. These spikes are due to the stress that is caused by the angle of the teeth, the stretch in the wood, and pulling out of the plate's edge with loading.

4.1.4.3 The Second Tension Test (EE-2nd)

In this test, the two members of wood were connected by the MPC. The specimen was set on the universal testing machine. The first reference image was taken before applying any load. Figure 4.202 shows the first image which was considered as the reference image in digital image correlation technique.

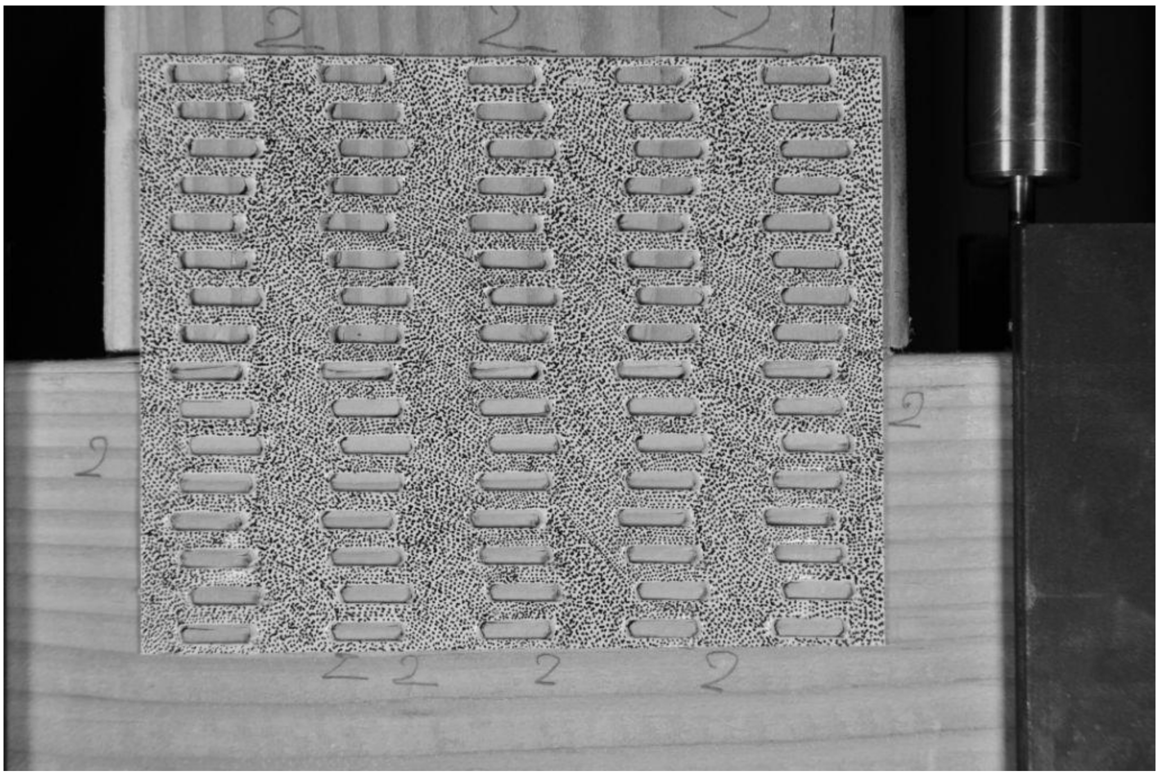

Figure 4-158: First image / reference image

After the first reference image was taken at load zero, the load was increased on the specimen until failure. The camera was placed on a fixed stand and the MPC was perpendicular to the camera's lenses. Images were taken for the MPC specimen at each

load increment of 200 pounds until failure. The failure was due to wood cracks and tooth withdrawal. Figure 4.203 shows the last image at the failure.

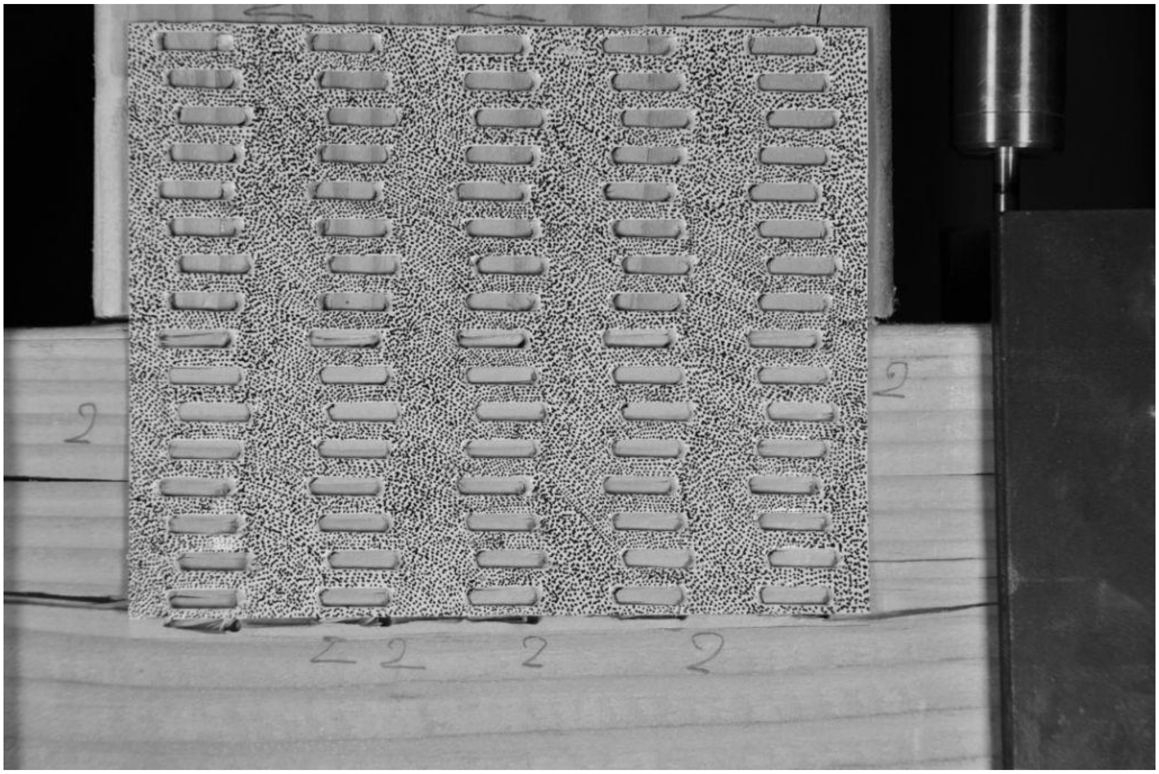

Figure 4-159: The last image at the failure

Thirteen (13) images were taken in addition to the reference image. The metal plate failed due to wood cracks and tooth withdrawal. As shown in Figure 4-159, the bottom wood member failed accompanied by some tooth withdrawal. The wood member in the top also had some cracks, but the main reason for failure was in the bottom wood member where the load was perpendicular to the wood grain. The specimen failed at load equal to 2,500 pounds. The captured images were implemented in DIC-software to find the full-field strain measurements.

4.1.4.3.1 Analysis of the Full-Field Strain Results Obtained From DIC Software

All the test images, which are obtained from the lab tests, are implemented in the digital image correlation software Vic-2D. Each image was analyzed in relation to a reference image. Thus, each deformed image is compared to the non-deformed reference image. The full-field strain measurements were obtained from the digital image correlation software. Figure 4-160 shows the strain in y-direction (ε_{yy}) for the image at 2,500 pounds.

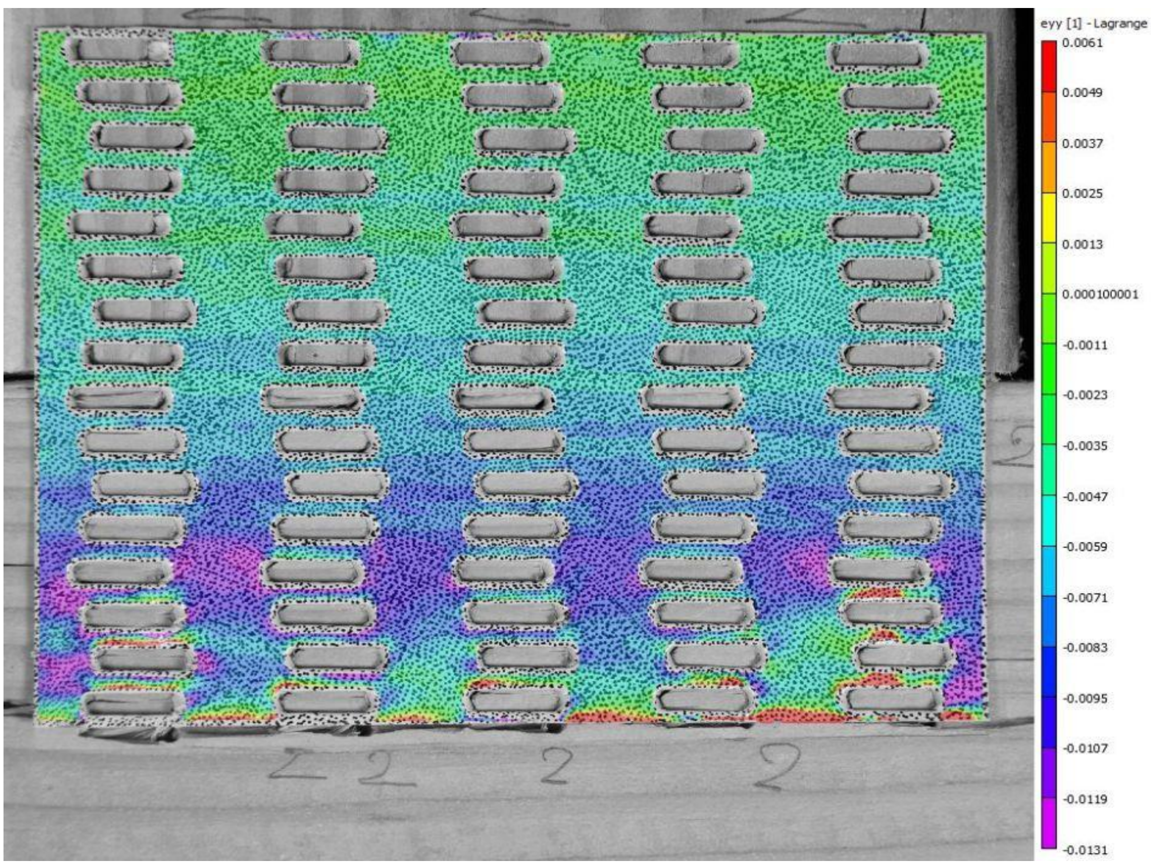

Figure 4-160: Full-field strain measurements (ε_{yy}) for the last image at failure at 2500 pounds

In general, from the full-field strain images, the strain values show fluctuations; however they are very close. The top half of the plate is behaves differently than the bottom plate which is imbedded in the wood that has the grain parallel to the load. The failure occurs due to the deep crack in the wood and tooth withdrawal in the bottom half of the plate. The last two images before the failure show different full-field strain than the earlier images. The gap between the two wood members shows very small changes due to wood failure and tooth withdrawal.

The strain results in x-direction (ε_{xx}) can be obtained from digital image correlation software. Figure 4-161 shows the strain (ε_{xx}) for the first image at 200 pounds.

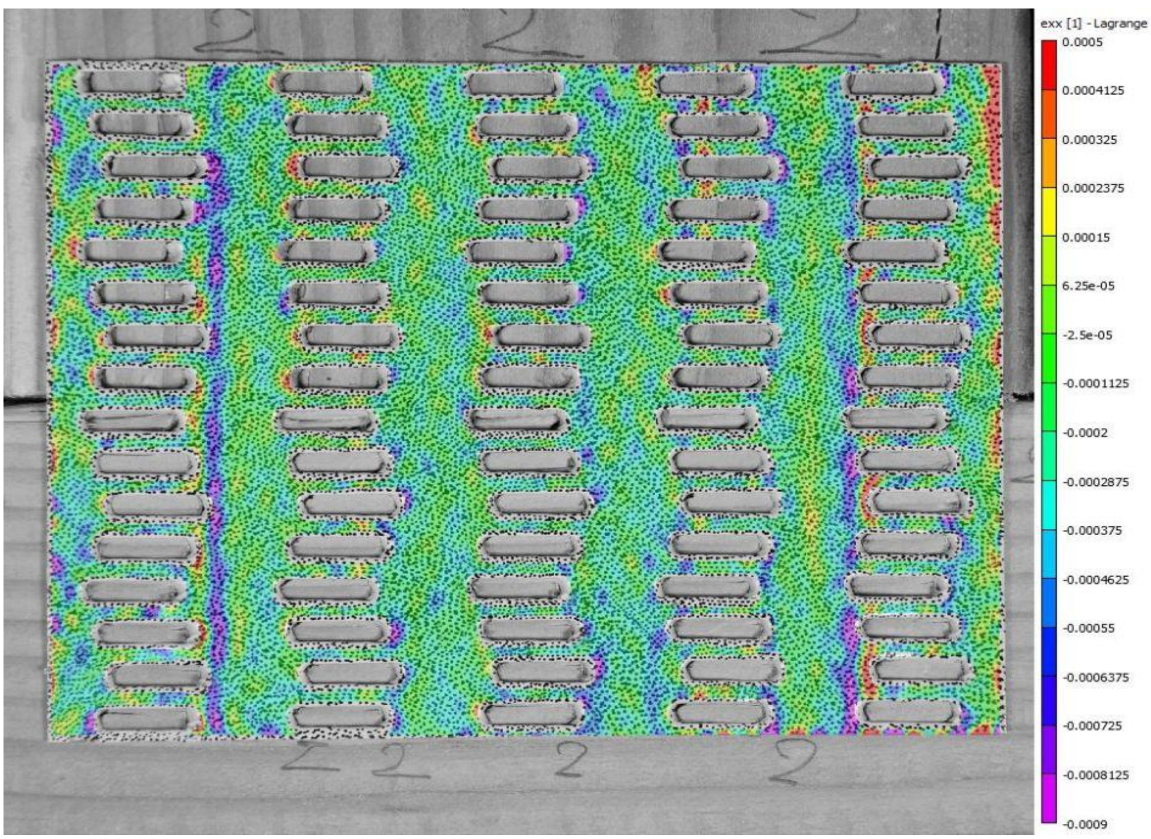

Figure 4-161: Full-field strain in x-direction (ε_{xx}) at load 200 pounds

At 2,400 pounds, the horizontal wood cracks in the bottom member occur. The cracks cross the wood under the plate. Thus, the plate's strain behavior is influenced by this crack. The strain behavior for the last two images at failure is different from the strain at 2,200 pounds. This shows the effect of the wood crack on the plate's strain behavior. Before this crack, all the strain behavior was based on the plate's response to the load. Figure 4-162 shows the strain field for the last image at failure.

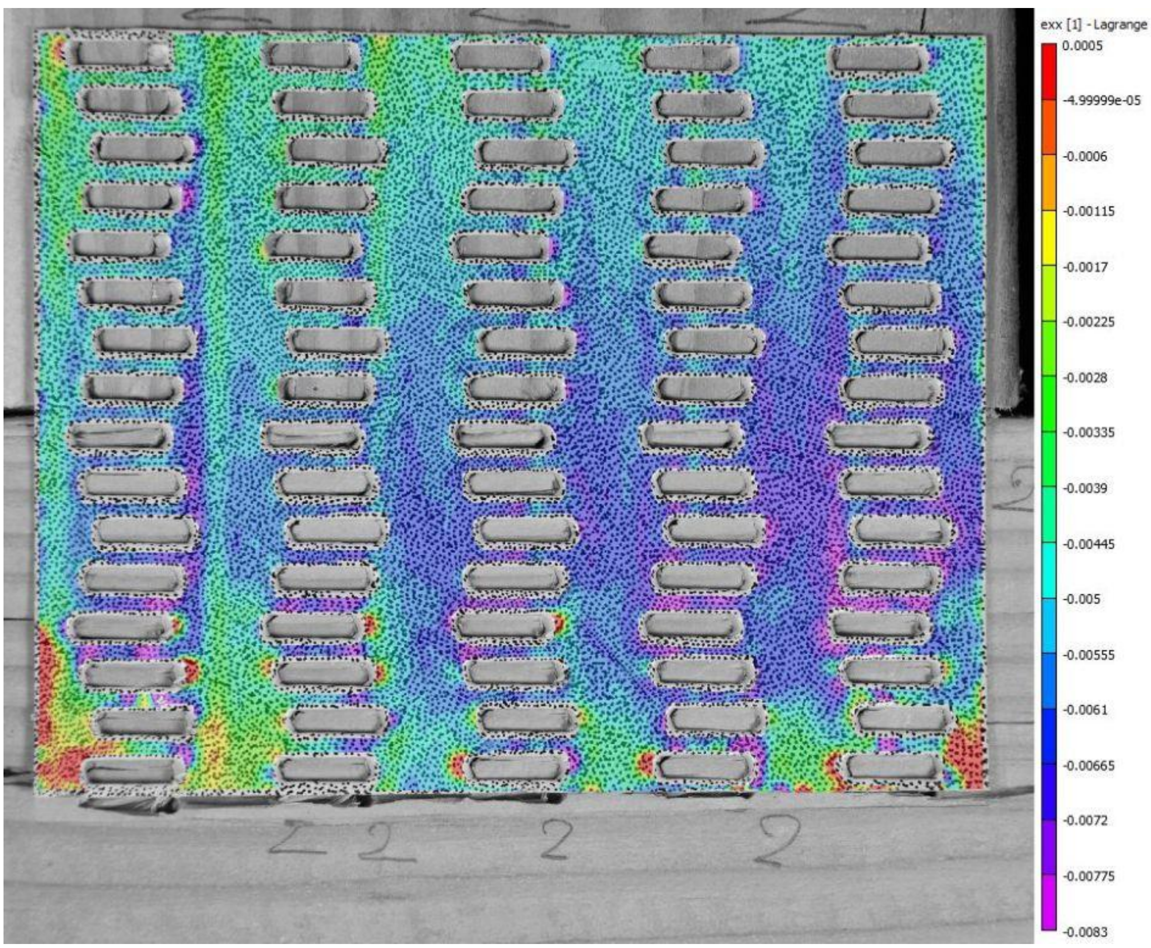

Figure 4-162: Full-field strain in x-direction ε_{xx} under load 2,500 pounds (the last image at failure)

4.1.4.4 The Third Tension Test (EE-3rd)

In this test, the two members of wood were connected by the MPC. The specimen was set on the universal testing machine. The first reference image was taken before applying any load. Figure 4-163 shows the first image which was considered as the reference image in digital image correlation technique.

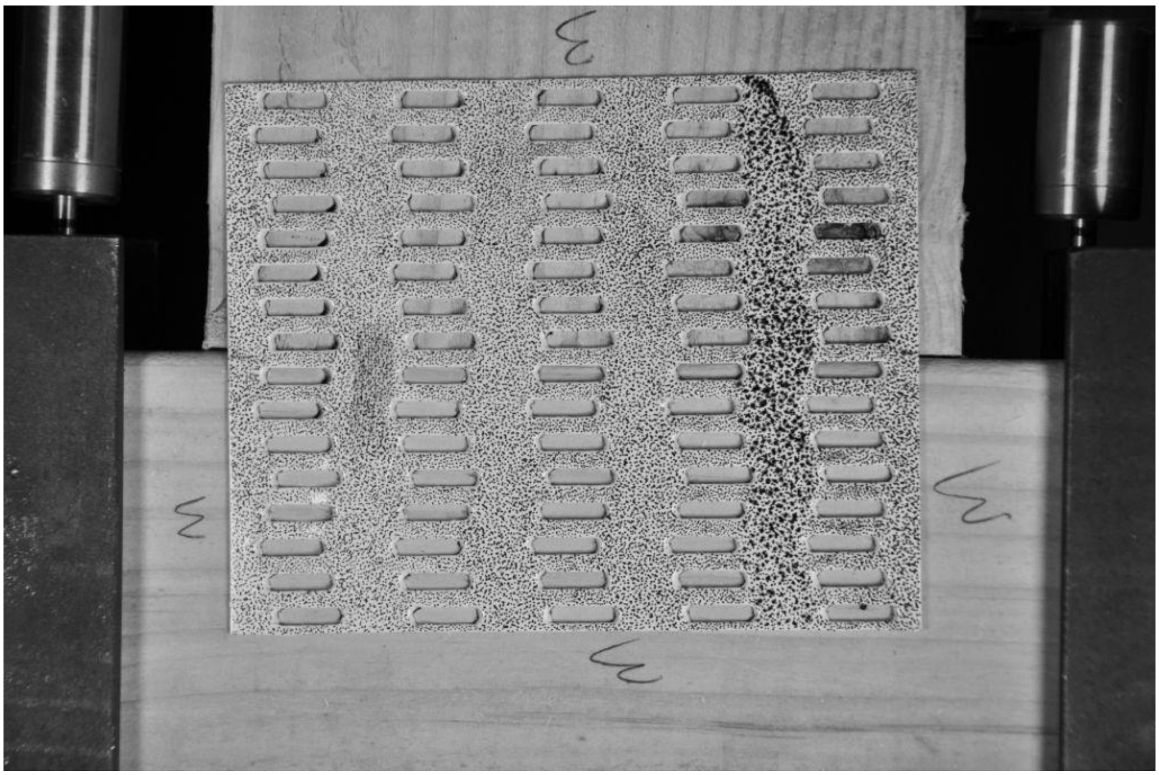

Figure 4-163: First image / reference image

After the first reference image was taken at load zero, the load was increased on the specimen until failure. The camera was placed on a fixed stand and the MPC was perpendicular to the camera's lenses. Images were taken for the MPC specimen at each

load increment of 200 pounds until failure. The failure was due to wood cracks and tooth withdrawal. Figure 4-164 shows the last image at the failure.

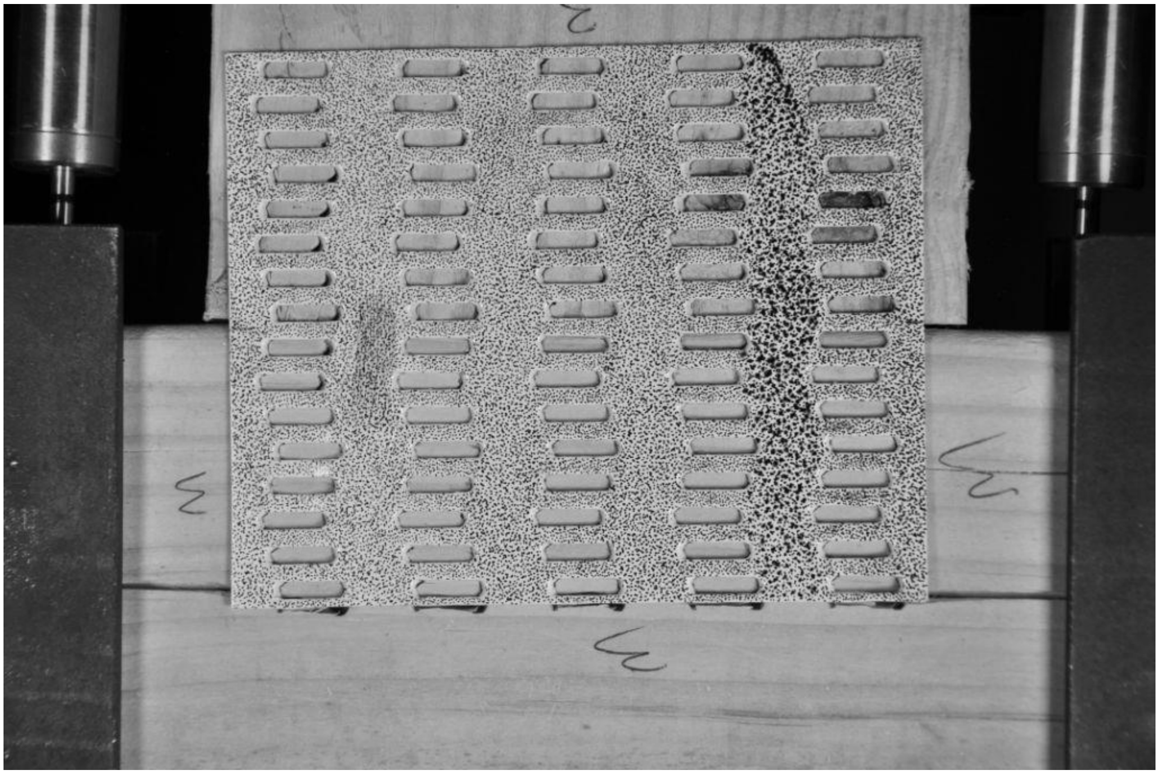

Figure 4-164: The last image after the failure

Twenty five (25) images were taken in addition to the reference image. The metal plate failed due to wood cracks and tooth withdrawal. As shown in Figure 4-164 the bottom wood failed with a horizontal crack across the wood that was beneath the metal plate and some tooth withdrawal accompanied by the wood failure. The wood member on the top also had some cracks, but the main reason for failure was in the bottom wood member where the load was perpendicular to the wood grain. The specimen failed at load equal to 5,000 pounds. The captured images were implemented in DIC-software to find the full-field strain measurements.

4.1.4.4.1 Analysis of the Full-Field Strain Results Obtained From DIC Software

All the test images, which are obtained from the lab tests, were implemented in the digital image correlation software Vic-2D. Each image was analyzed in relation to a reference image. So each deformed image is compared to the non-deformed reference image. The full-field strain measurements were obtained from the digital image correlation software. Figure 4-165 shows the strain (ε_{yy}) for the image at 200 pounds.

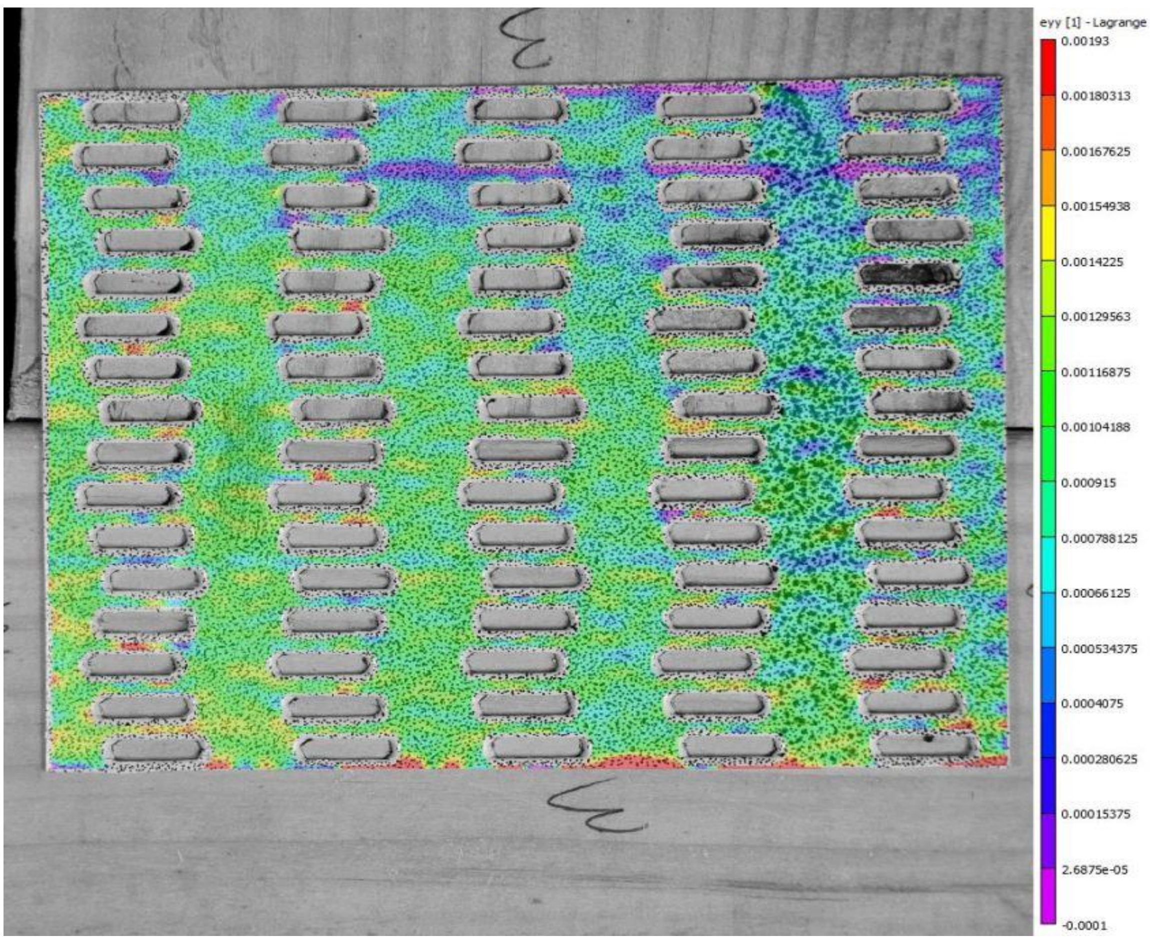

Figure 4-165: Full-field strain measurements (ε_{yy}) for the MPC at 200 pounds

The strain field's results show different levels of color and show that each level of color represents a specific number. The image at 200 pounds shows that the strain (ε_{yy}) is very low tensile strain over the entire plate's surface. Through loading, the strain field shows an increase in (ε_{yy}) values. In general, the strain on the top half of the plate is very close to the strain on the bottom half of the plate. At 4,000 pounds, the strain full-field is high as shown in Figure 4-166.

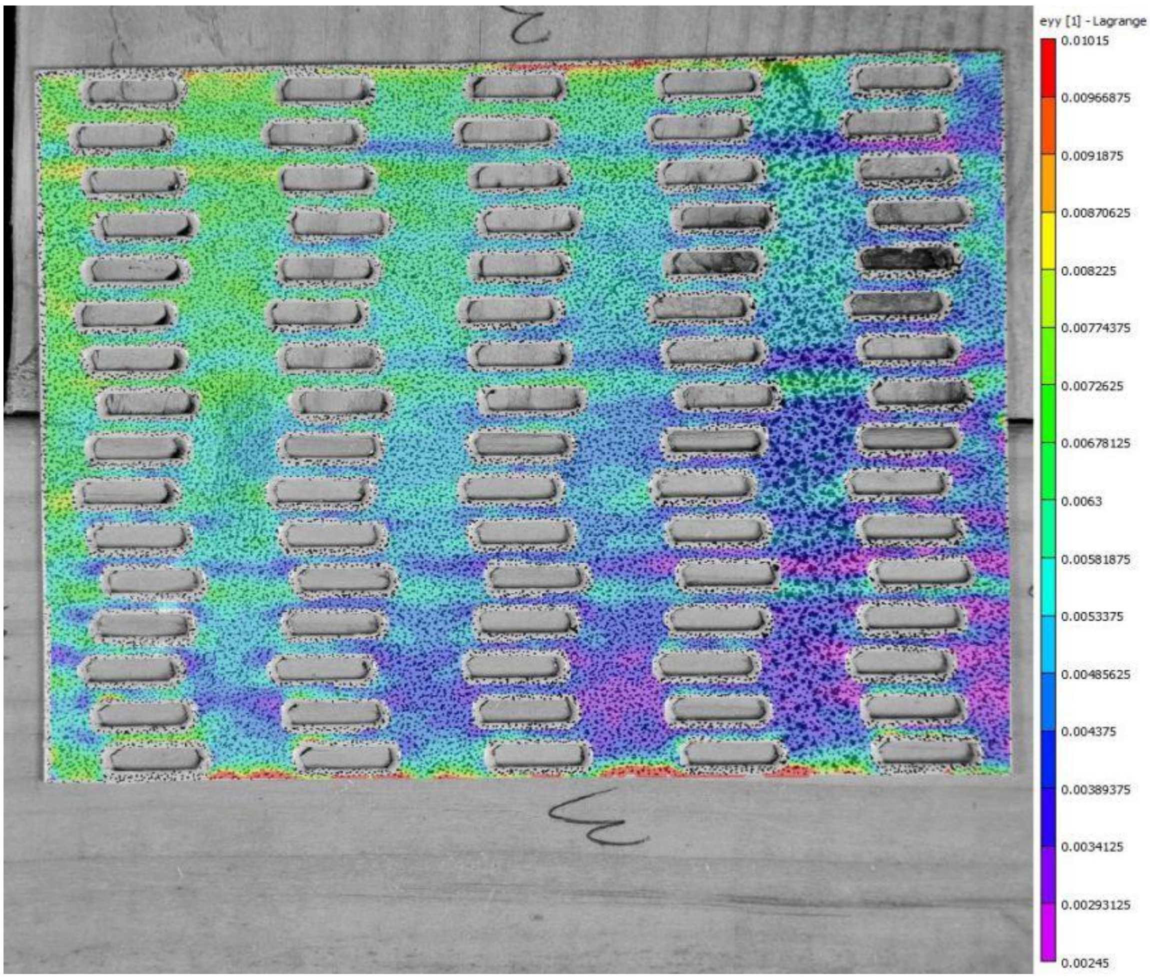

Figure 4-166: Full-field strain measurements (εyy) at 4,000 pounds

The full-field strain measurements at 4,000 pounds show a gradual increase in the strain (ε_{yy}) over the entire plate. The strain (ε_{yy}) is tensile strain with higher values than earlier strain field images. After 4,000 pounds, the strain fields show slight decrease but the strain is a tensile strain. At 4,800 pounds, the strain (ε_{yy}) increases again until the failure at 5,000 pounds. The full-field strain measurements (ε_{yy}) at 5,000 pounds are shown in Figure 4-167.

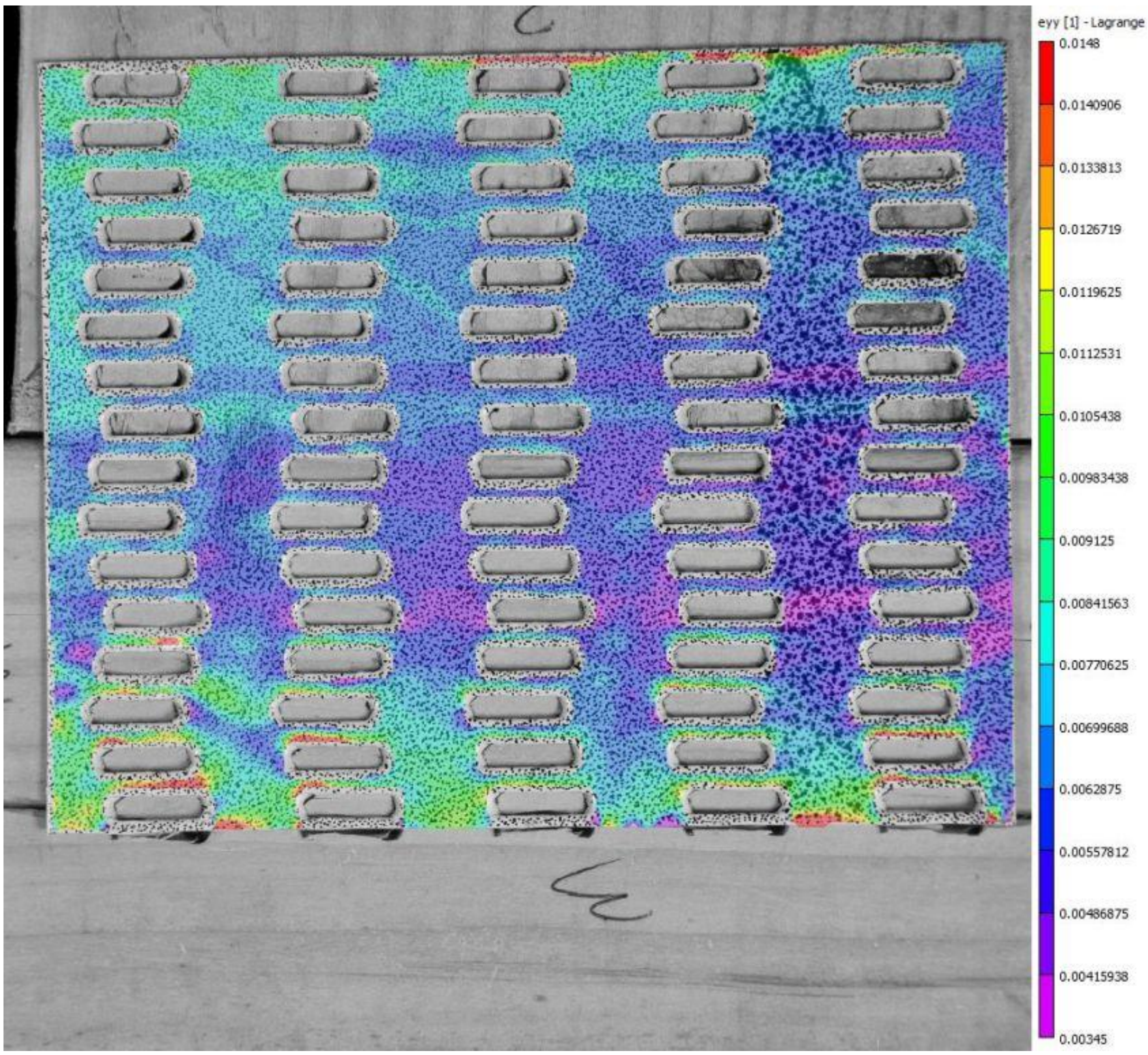

Figure 4-167: Full-field strain measurements (εyy) for the last image at failure at 5,000 pounds

The failure in this test is in wood due to wood cracks accompanied by tooth withdrawal in the bottom wood member. DIC software can be used to show the changes in strain under different loading increments. The last image at the failure in Figure 4-167 shows that the strain increased in the plate with some higher strains values around the left and the right edges of the plate. The full-field strain measurement shows a fluctuation in the strain colors and so the strain values. In general, there are some sudden changes in the strain colors all around the plate. The full-field strain measurement images that are obtained from DIC software show that the strain (ε_{yy}) increases with loading. The strain is positive from load 200 pounds until the failure. The strain is a tensile strain (ε_{yy}) in this test. The strain fields retreats down after applying 4000 pounds with very small strain values then the last two full-field strain images before the failure shows an increase in the strain then the failure.

A pulling out of the plate in circular shape has occurred in the bottom edge of the plate and has made the changes in the strain fields. The full-field strain images show high strain (ε_{yy}) at the very bottom edge of the plate. The highest tensile strain is 0.02.

The gap between the two wood members shows very small changes due to wood failure and tooth withdrawal. But the increase in the left side gap can be seen more easily than the right side. This test can show the changes in strain before the yielding point of the plate.

The strain results in x-direction (ε_{xx}) can also be obtained from digital image correlation software. The full-field strain measurements (ε_{xx}) for the first image at 200 pounds are shown in Figure 4-168. The strain (ε_{xx}) is a tensile strain with very low values. In general the strain is uniformly distributed over the plate's surface. The contour colors show very close results.

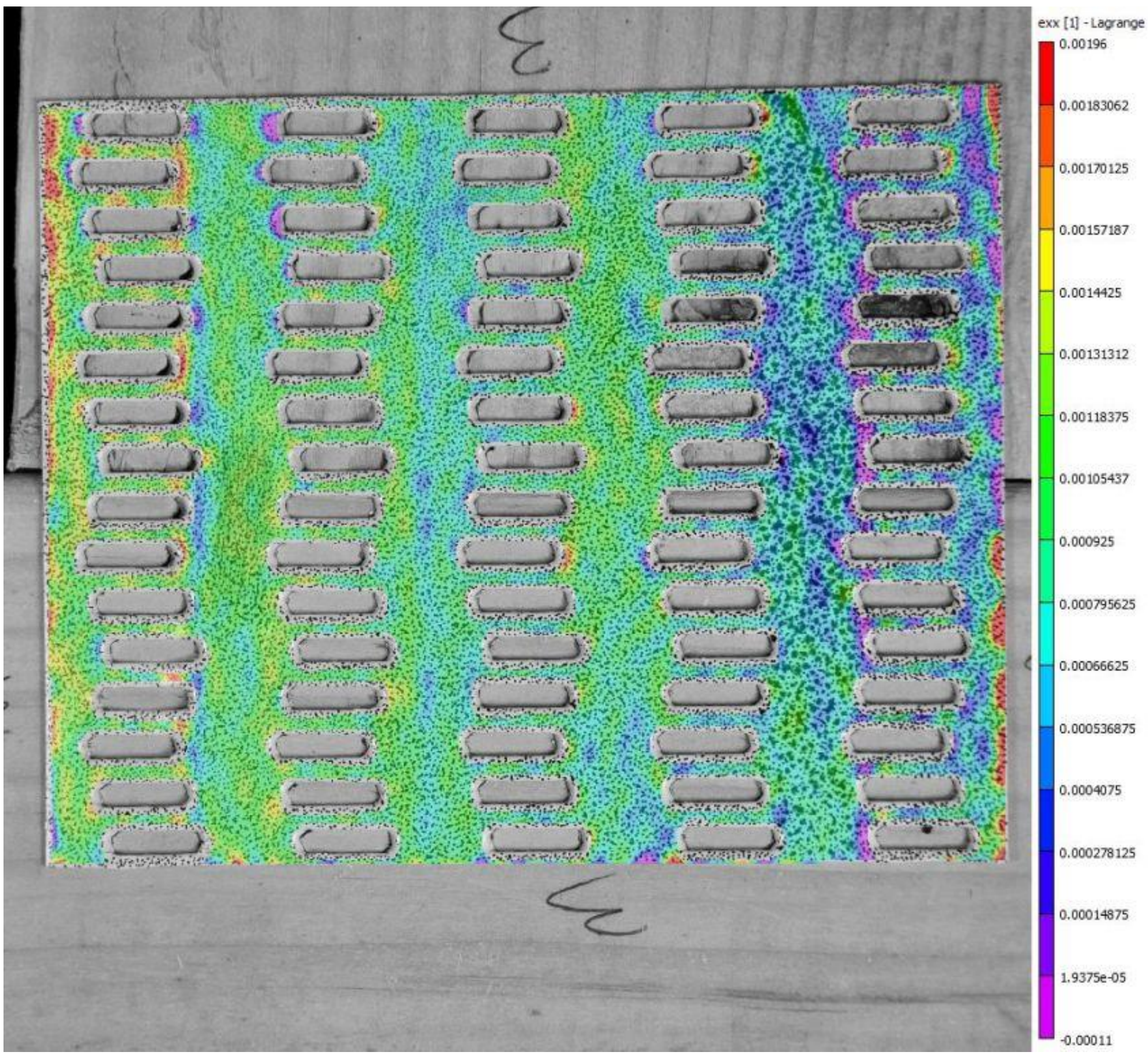

Figure 4-168: Full-field strain in x-direction (ε_{xx}) at load 200 pounds

As the load increases, the full-field strain measurement (ε_{xx}) shows an increase in the strain values until the 4,000 pounds. The full-field strain measurement at 4,000 pounds is shown in Figure 4-169. After applying 4,000 pounds, the full-field strain shows slight retreating in the strain values until applying 4,800 pounds. Thus, the strain (ε_{xx}) follows the strain (ε_{yy}) in its behavior. Both strains increase and decrease together. The full-field strain (ε_{xx}) shows that the right side strain (ε_{xx}) is lower in value than the left side strain (ε_{xx}).

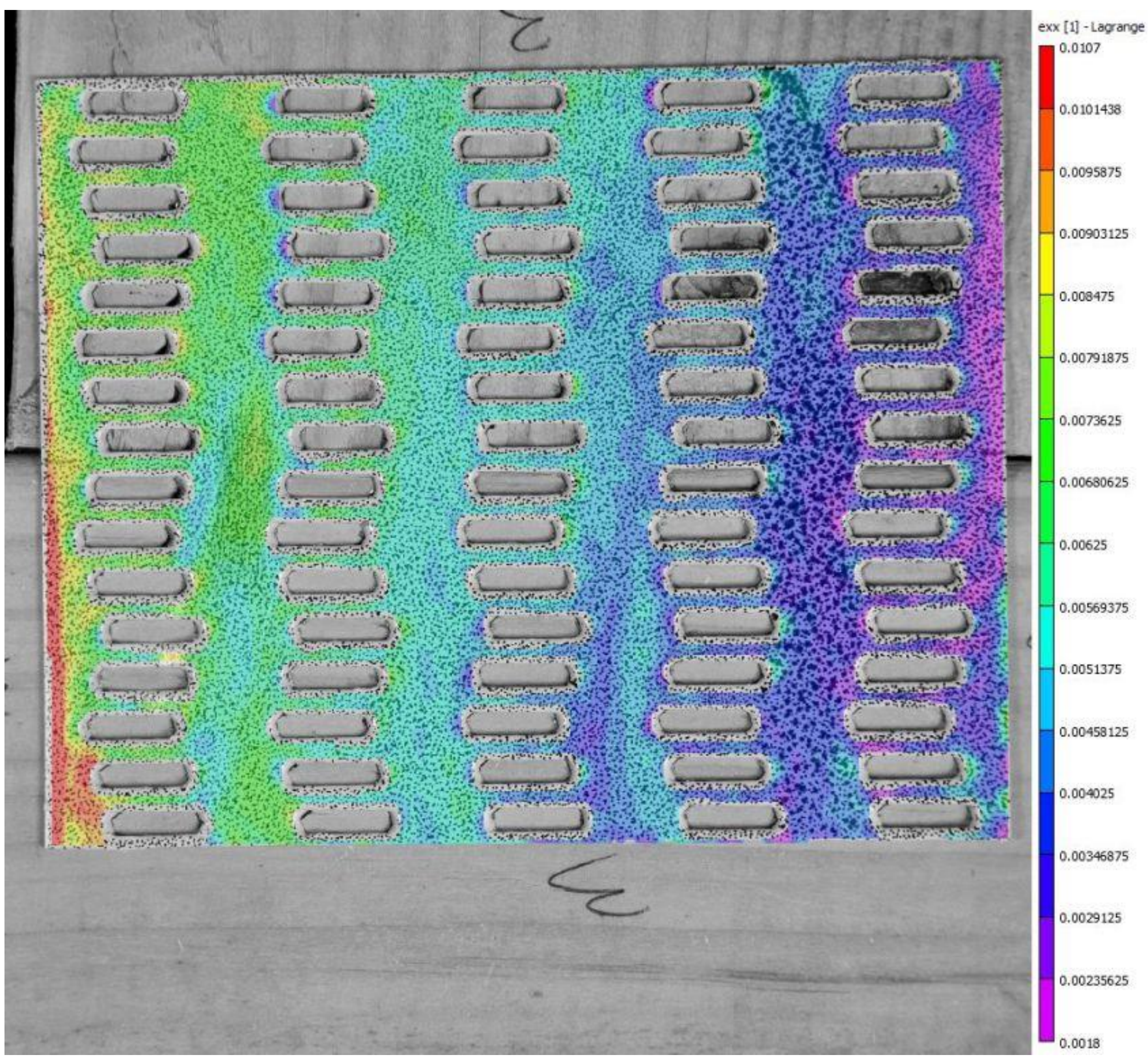

Figure 4-169: Full-field strain in x-direction (ε_{xx}) at load 4,000 pounds

At 4,800 pounds the strain (ε_{xx}) increases as a tensile strain. At failure at 5,000 pounds, the strain holds the highest strain (ε_{xx}) fields' values as shown in Figure 4-170. The last image at failure shows lower strain (ε_{xx}) on the right side than the left side of the plate. The very bottom of the plate shows more fluctuation in the strain (ε_{xx}) due to the wood crack across the bottom of the plate.

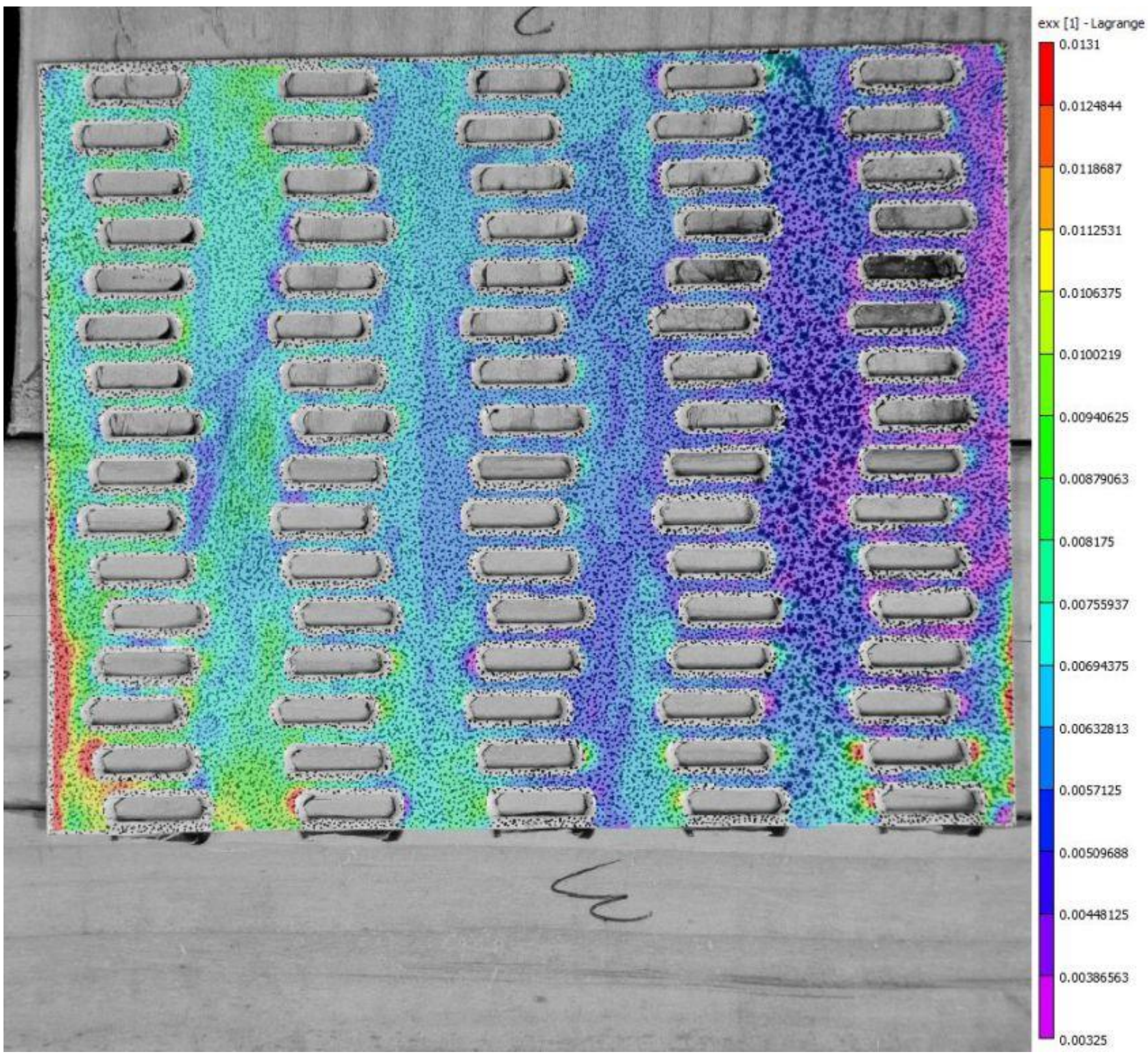

Figure 4-170: Full-field strain in x-direction (ε_{xx}) at load 5,000 pounds (the last image at failure)

4.1.4.4.2 Numerical Analysis for the Results

Two types of numerical analysis for the results are performed. The strain (ε_{yy}) is along the vertical direction and (ε_{xx}) is along the horizontal direction.

4.1.4.4.2.1 Strain in y-direction (ε_{yy}) along y-axis

To analyze the DIC results numerically, vertical cross section lines from the top of the plate to the bottom are taken for some images starting with the first image at 200 pounds and ending with the last image at failure. The cross section is taken in four different locations as shown in Figure 4-171.

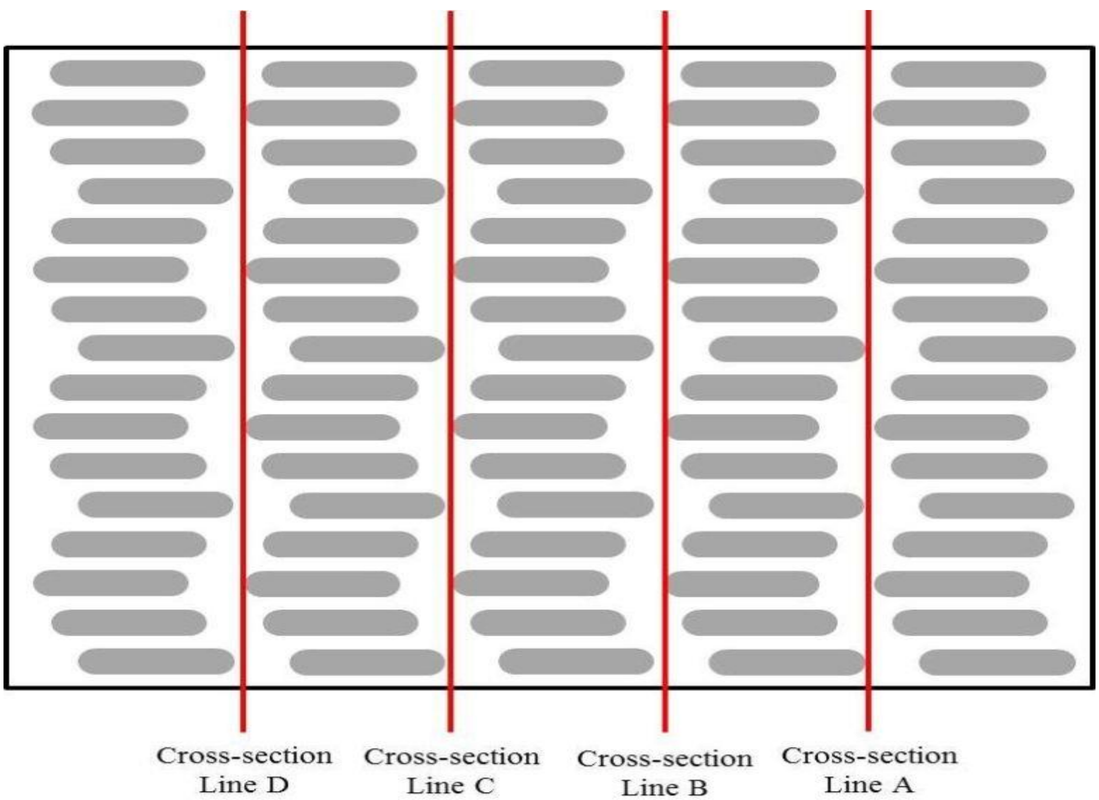

Figure 4-171: Metal plate with the cross-section lines along the vertical direction

The four locations of the cross section lines are as the following:

- The first cross section line (A-A) is from the right side of MPC @ x = 1.435 in.
- The second cross section line (B-B) is @ x = 0.456 in.
- The third cross section line (C-C) is @ x= -0.561 in.
- The fourth cross section line (D-D) is from the left side of MPC @ x= -1.551 in.

Four cross-section lines are taken for the strain field (ε_{yy}). The next four Figures 4-172 to 4-175 show the distribution of strain (ε_{yy}) at four different locations for 10 images. Each image represents the value of the loading that is applied on the specimen of the two wood members connected by the metal plate connector.

The curves show that the first considered load is 200 pounds then different increment of loading is taken until the failure at 5,000 pounds. The increments of load for the last 6 images are 200 pounds. The cross section lines show that the strain curve starts very stable after applying 200 pounds then it increases by loading until 4,000 pounds. The strain curve after 4,000 pounds retreats down until load 4,800 pounds. Then the strain curves increases up until the last strain curve at 5,000 pounds which has the highest strain (ε_{yy}).

In general, after applying 4,000 pounds, the strain curves show a slope along the vertical line. The strain at the top half of the plate holds higher strain than the bottom half of the plate. And the spikes in the strain curves are higher and noticeable. The strain curves show very high values in the last strain curve at the failure especially at cross section line (1-1) and (2-2). The cross section line (3-3) and (4-4) do not show that high strain changes near the edges. The plate on the bottom right side edge shows a circular deformation shape of pulling out for the plate but it does not occur on the left side edge. Thus, the tooth grip on the left side is higher than that for the right side. In this test the plate has failed due to wood cracks in the bottom half of the plate accompanying by tooth withdrawal and also pulling out for the plate's right vertical edge in a circular shape. Thus, the failure signs make the last strain curve different than the rest of the curves. The fluctuation in the strain (ε_{yy}) along the vertical cross section lines are due to many factors such as the effect of stretch in the wood especially when the load is perpendicular to the grain, pulling out of the plate in different places due to loading, and tooth withdrawal which is obvious around the edges of the plate. This test does not show a plate failure because the failure occurred in the wood not in the plate. The gap between the two wood members is very narrow as shown in the images, but this does not mean it has not increased.

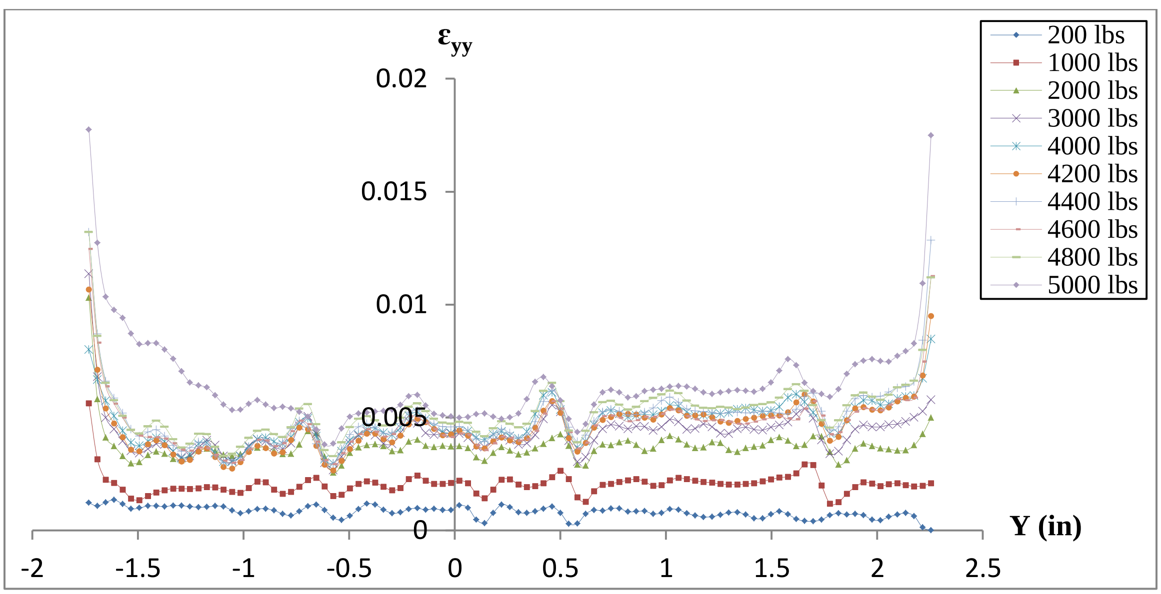

Figure 4-172: The strain distribution (ε_{yy}) along a cross section line (A-A) located on the right side of the plate

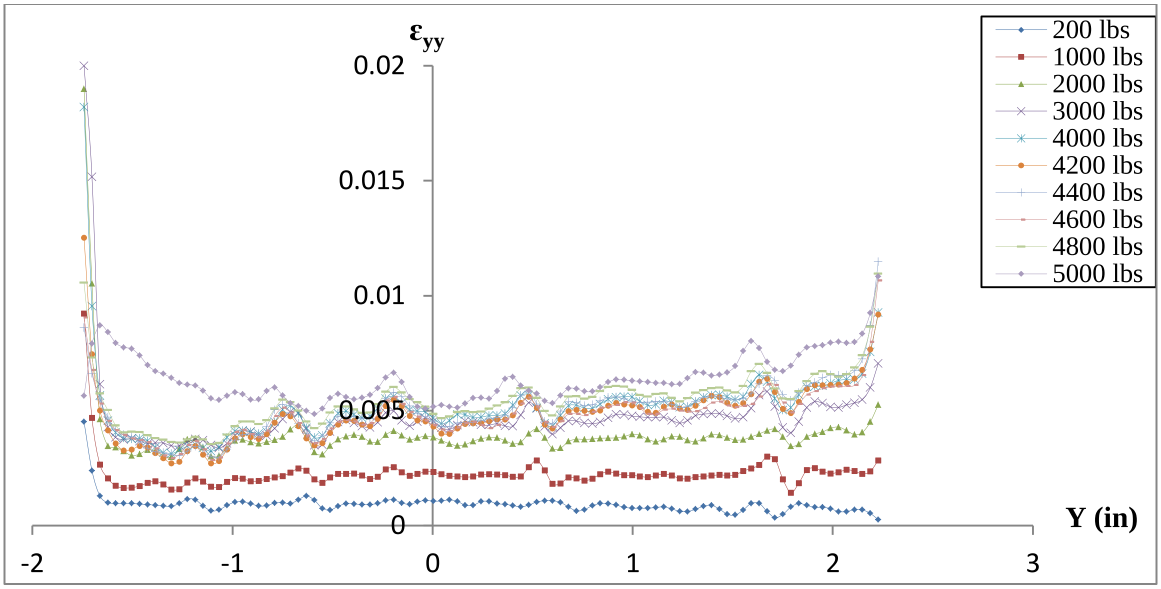

Figure 4-173: The strain distribution (ε_{yy}) along a cross section line (B-B)

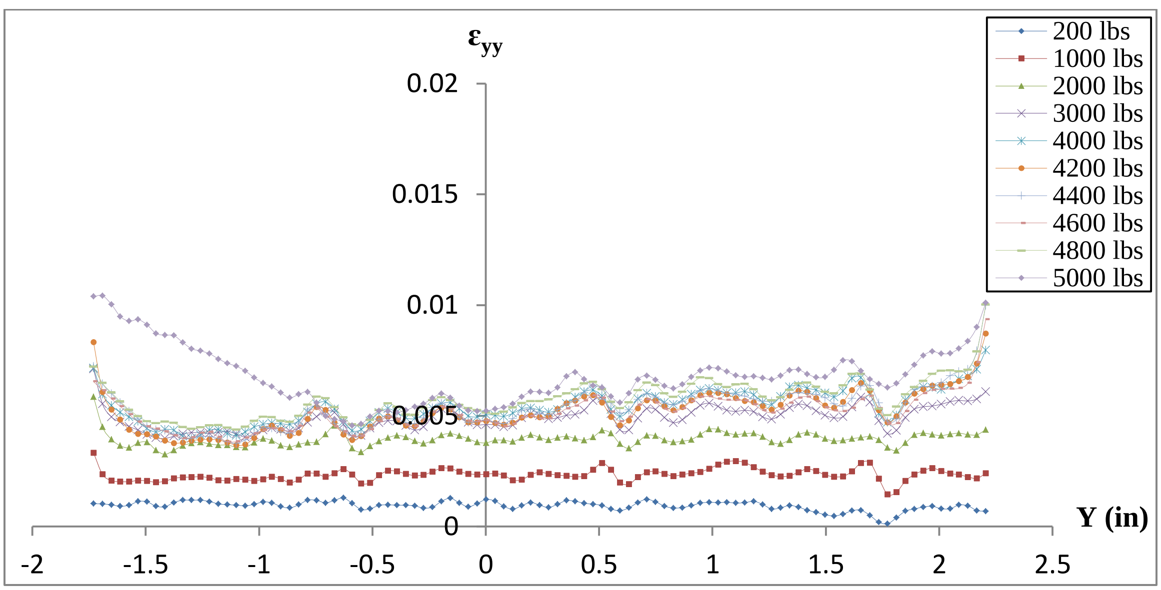

Figure 4-174: The strain distribution (ε_{yy}) along a cross section line (C-C)

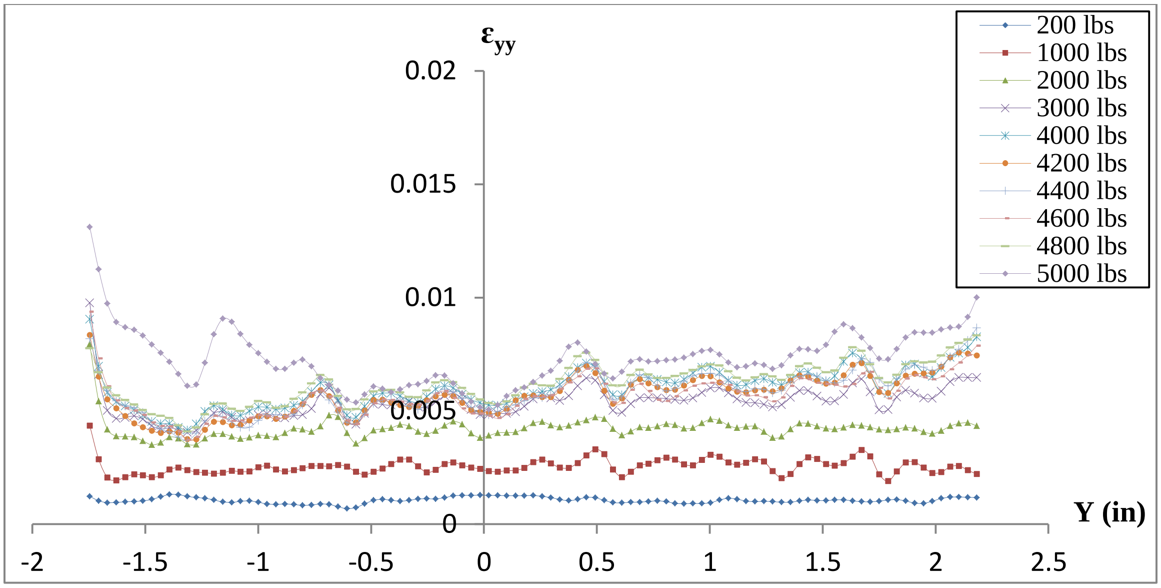

Figure 4-175: The strain distribution (εyy) along a cross section line (D-D) located on the left side of the plate

Figure 4-176 shows the strain (ε_{yy}) curves for the last image at 5,000 pounds.

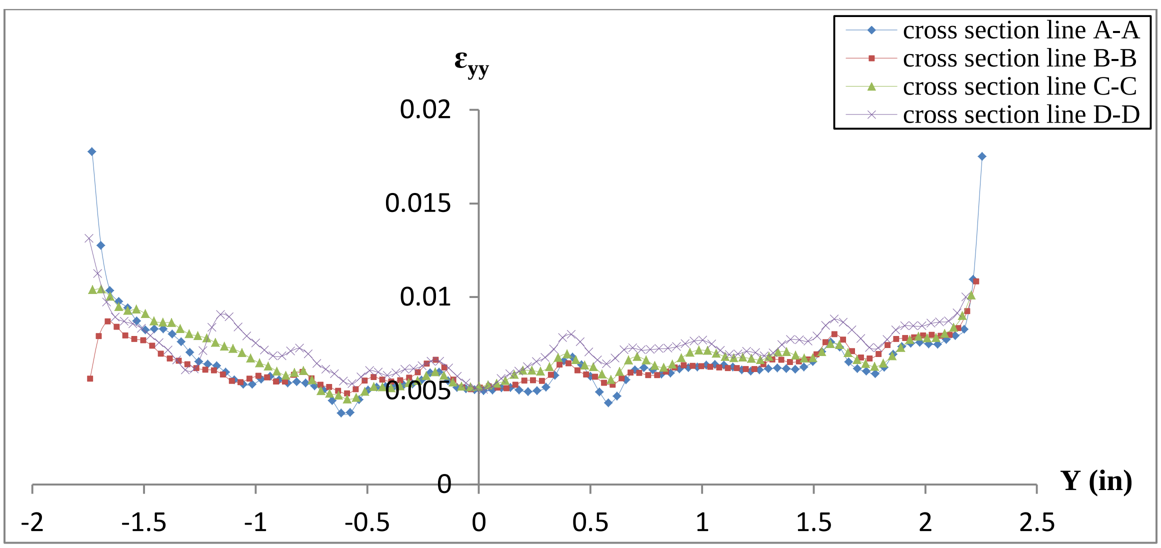

Figure 4-176: The strain distribution (εyy) along 4-cross section lines at the failure at load 5000 pounds

4.1.4.4.2.2 Strain in x-direction (ε_{xx}) along x-axis

To analyze the DIC results numerically, horizontal cross sectional lines from the right of the plate to the left are taken .The cross section lines are taken in three different locations as shown in Figure 4-177.

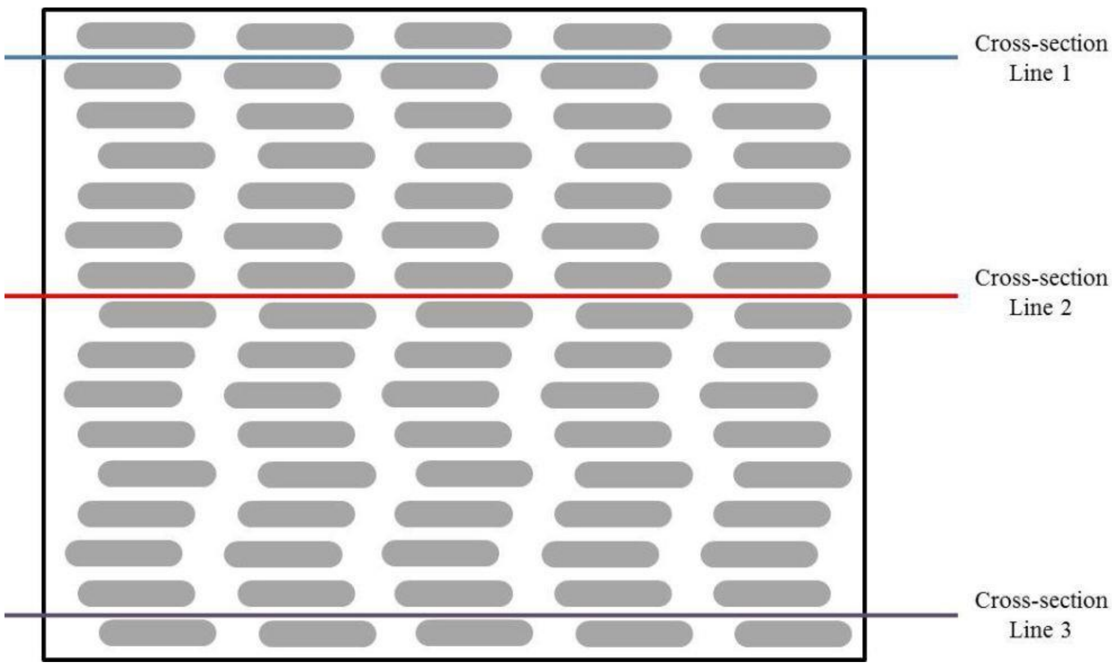

Figure 4-177: Metal plate with the cross-section lines along the horizontal direction

The three locations of the cross section lines are as the following:

- The first cross section line (1-1) is at the top of MPC @ y = 1.998 in.
- The second cross section line (2-2) is along the middle of the MPC @ y = 0.23 in.
- The third cross section line (3-3) is from the bottom of the MPC @ y = -1.51 in.

The strain (ε_{xx}) along x-direction can be obtained from digital image correlation software. Figures 4-178 to 4-180 show the strain (ε_{xx}) along the x-axis.

The curves in the three different places (top, middle, bottom of the plate) show very close results. The strain curves start with strain values at 200 pounds that are consistent across the plate from the right to the left side. Then the strain increases as tensile strain with loading until 4,000 pounds. At 4,000 pounds the strain (ε_{xx}) shows a slight retreat in their curves. At 4,800 and 5,000 pounds, a high strain is observed larger than the strain at lower load.

In general, the slope in the strain curves (ε_{xx}) over the plate's surface is very clear as shown in the next four figures. The right side of the plate holds less strain than the left side of the plate. The strain (ε_{xx}) along the cross section line (3-3) shows high sudden changes in the strain values at the strain curves at failure and close to failure. These sudden changes are due to wood cracks at load 4,800 pounds and 5,000 pounds. The very bottom side of the plate is highly influenced by wood failure more than the middle or the top half of the plate. The wood grain in the bottom wood member is perpendicular to the load which is weaker than perpendicular to the grain case.

In general, the variations in the strain values occur by loading due to many factors such as wood stretch and the angle of the teeth. The regularly spaced voids in the cross sectional area of the plate due to the slots also gives rise to variations in the strain curves. The pulling out of the plate due to loading is another factor that can affect the strain curves.

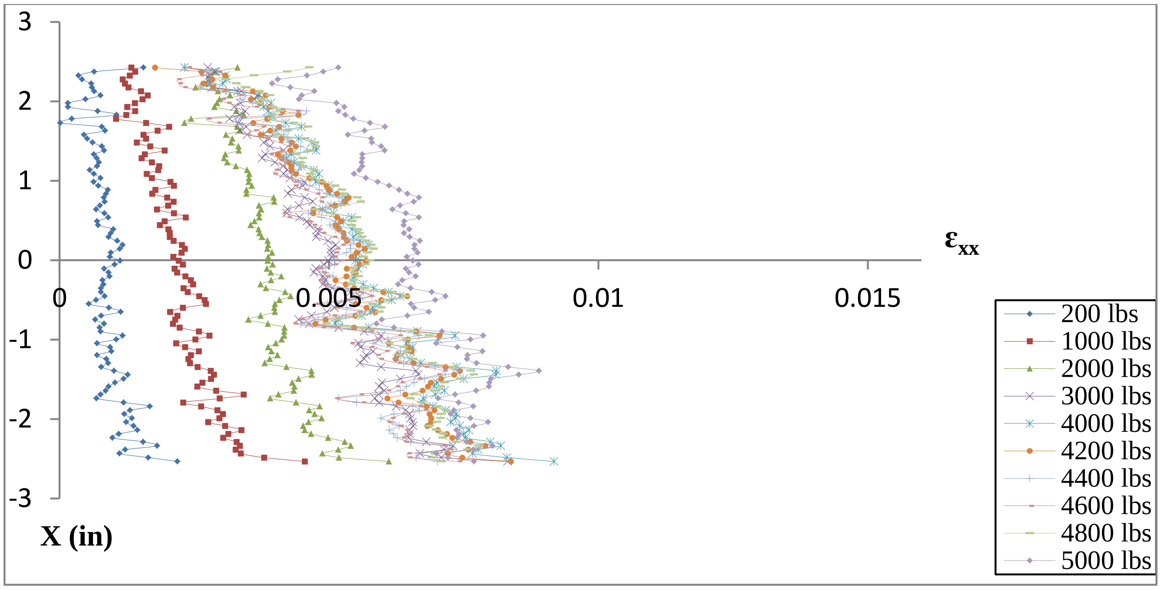

Figure 4-178: The strain distribution (ε_{xx}) along a cross section line (1-1) located on the top of the plate

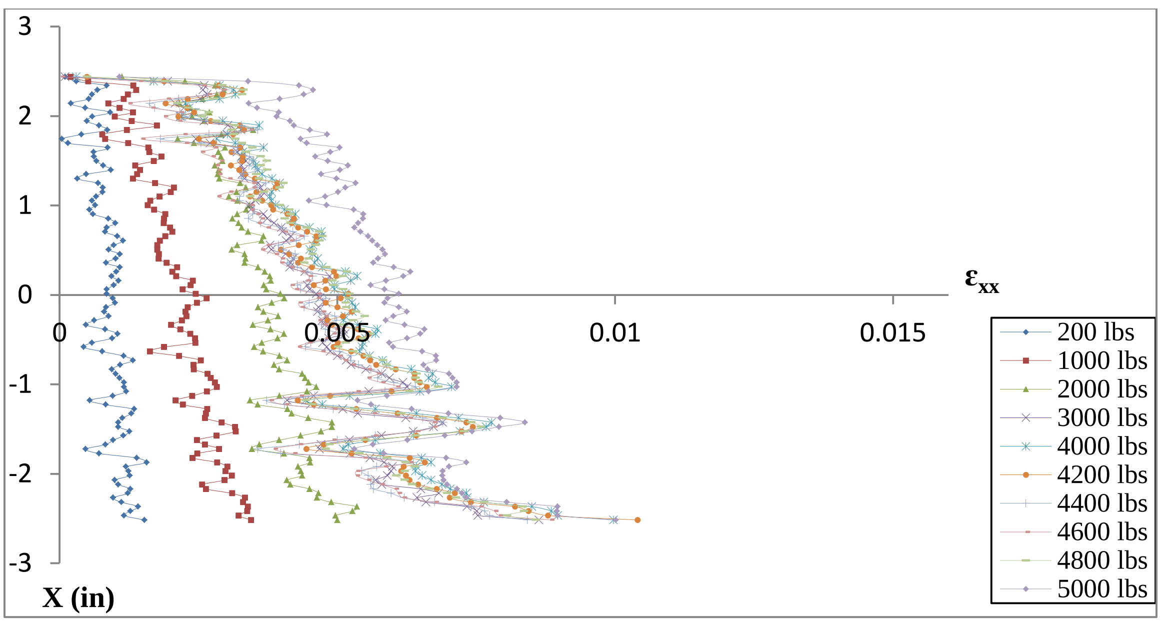

Figure 4-179: The strain distribution (ε_{xx}) along a cross section line (2-2) located on the middle of the plate

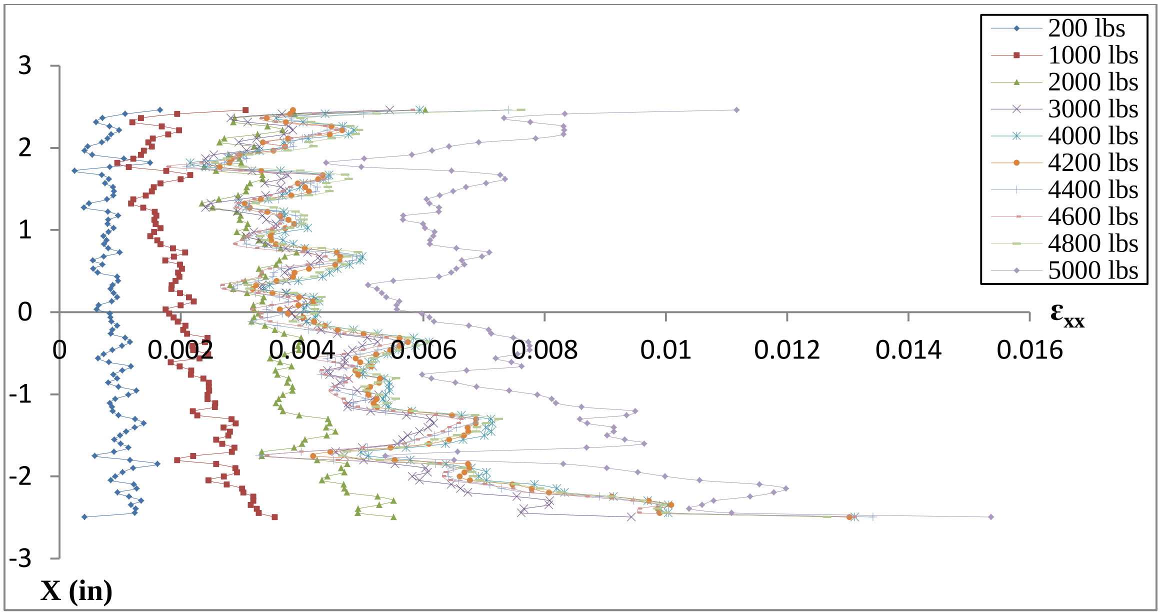

Figure 4-180: The strain distribution (ε_{xx}) along a cross section line (3-3) located on the bottom of the plate

Figure 4-181 shows the three lines strain (ε_{xx}) curves for the last image at 4,000 pounds.

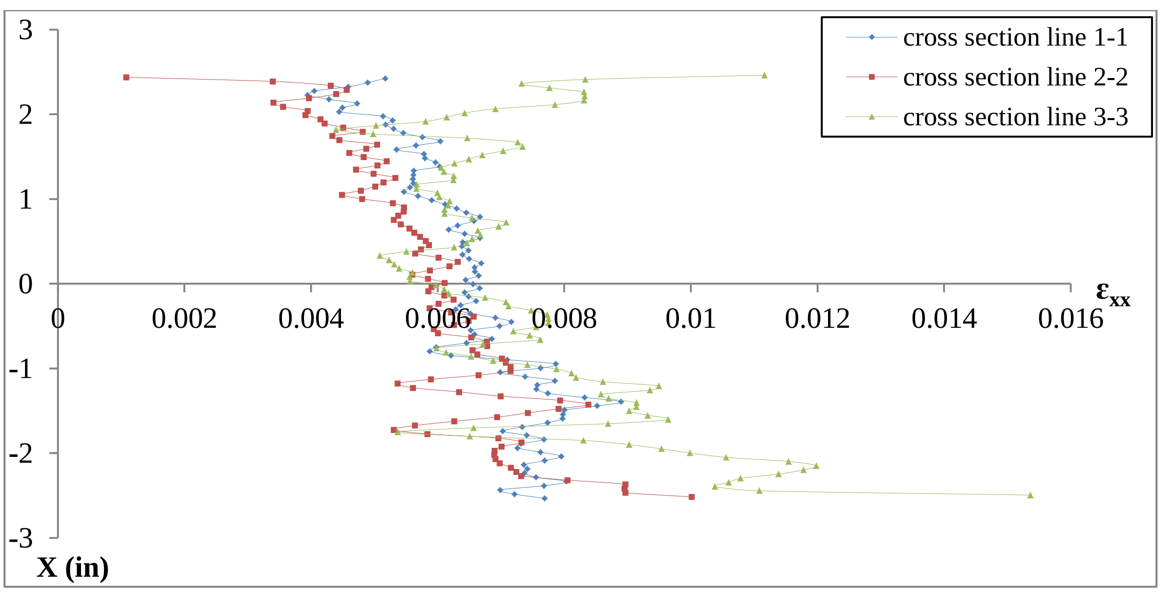

Figure 4-181: The strain (εxx) distribution along the three cross-section lines (1-1), (2-2), and (3-3) for the last image at the failure at load 5,000 pounds.

4.1.4.5 Comparison between the Displacement from LVDT and DIC-Code

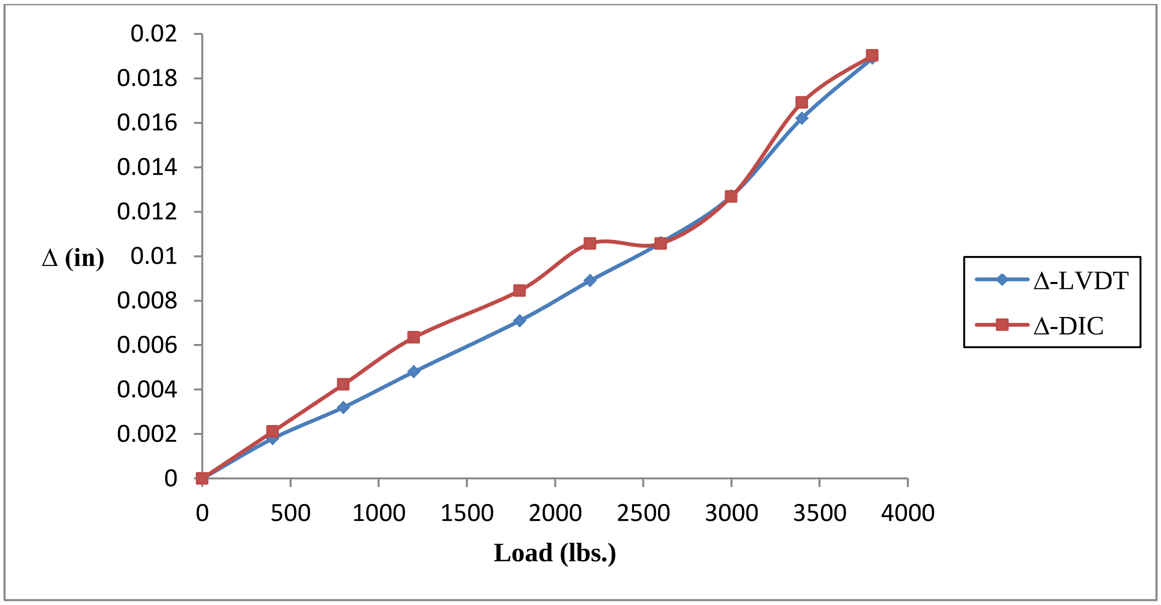

Figure 4-182: The displacement from LVDT vs. the displacement from DIC-code for the 1st EE test –the right side gap

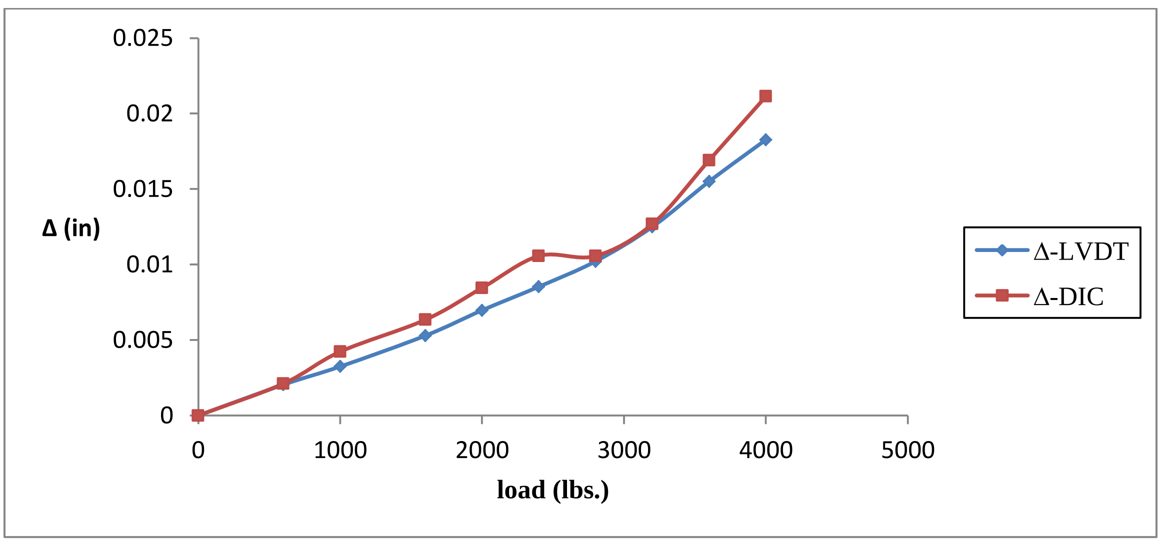

Figure 4-183: The displacement from LVDT vs. the displacement from DIC-code for the 1st EE test –the left side gap

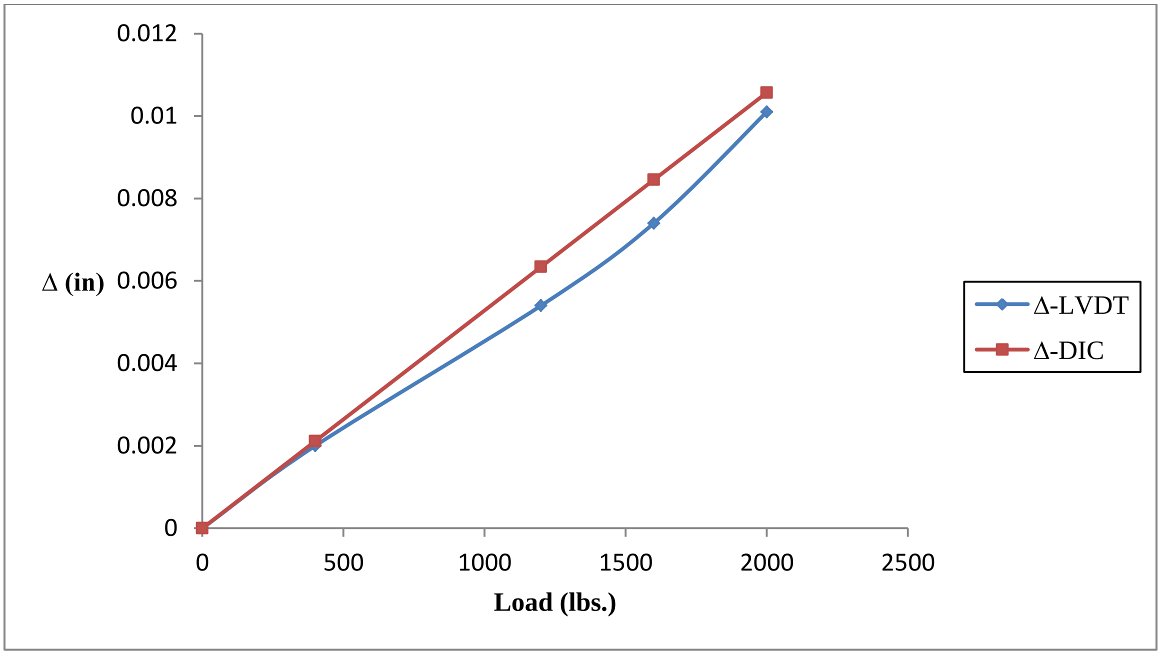

Figure 4-184: The displacement from LVDT vs. the displacement from DIC-code for the 2nd EE test –the right side gap

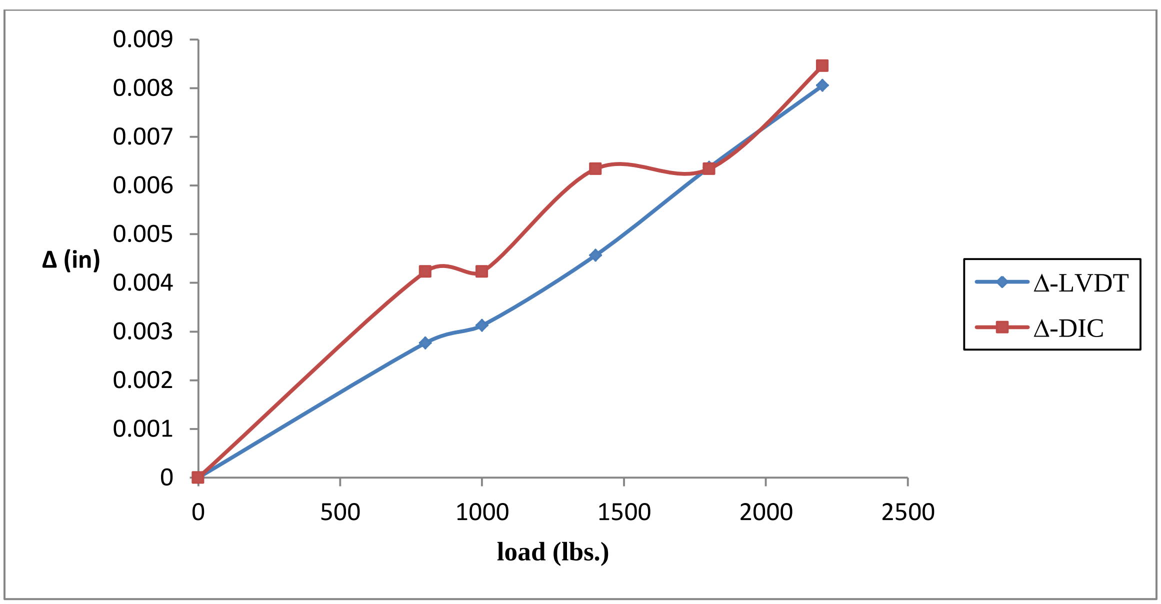

Figure 4-185: The displacement from LVDT vs. the displacement from DIC-code for the 2nd EE test –the left side gap

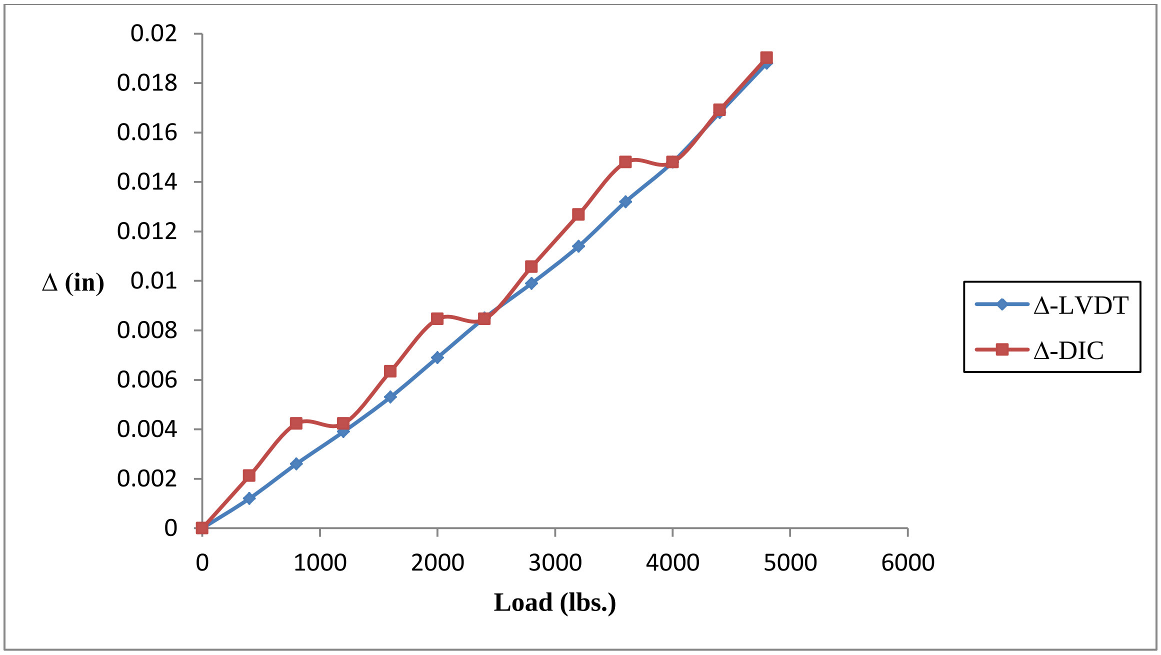

Figure 4-186: The displacement from LVDT vs. the displacement from DIC-code for the 3rd EE test –the right side gap

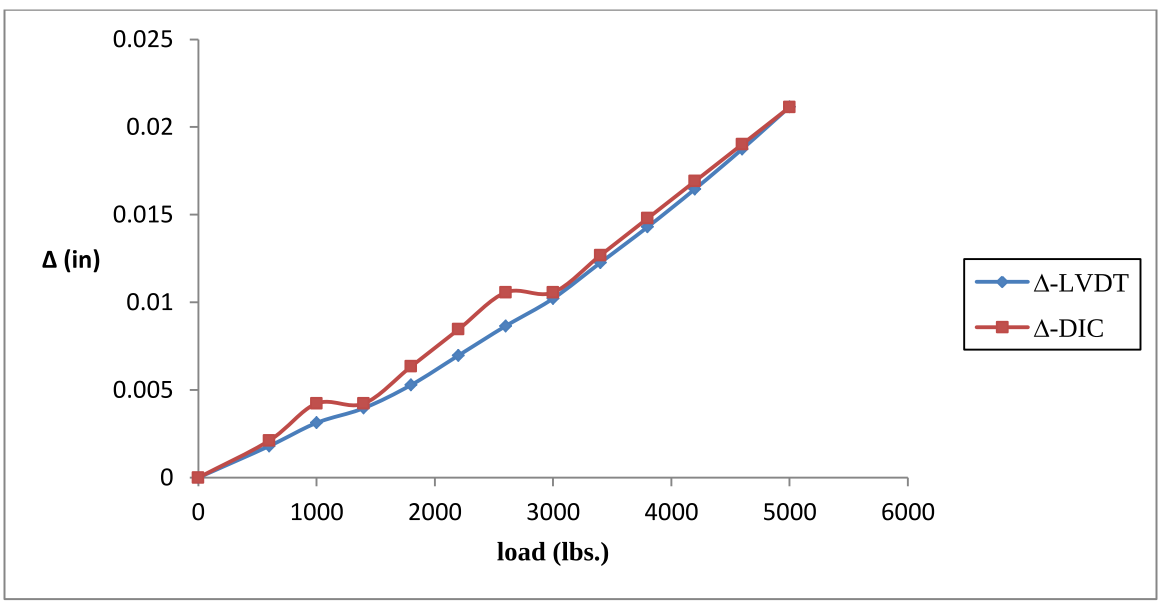

Figure 4-187: The displacement from LVDT vs. the displacement from DIC-code for the 3rd EE test –the left side gap

4.1.4.6 The EE-Tests Summary and Discussion

Three tests (EE) were conducted in the lab. The specimens were loaded until failure. A digital camera was used to capture images every 200 pounds. All the captured images were implemented in digital image correlation software Vic-2D. All three tests failed at the bottom wood member. Horizontal wood cracks occurred in the bottom wood member and under the steel support. The plate remained in good shape at the failure load. Tables 4-11, 4-12 and 4-13 show a brief description for each test.

Table 4-11: Brief description for each test-EE

EE-Test #	Failure load (lbs.)	Total Deformed Processed Images by DIC Code	Failure Behavior Descriptions
1	4,000	20	wood failure/ The bottom wood member cracked horizontally starting from the wood under the supports
2	2,500	13	wood failure/ The bottom wood member cracked horizontally besides the top wood member
3	5,000	25	wood failure/ The bottom wood member cracked horizontally and cross the wood under the plate

Table 4-12: Brief comments on each EE-test

EE Test #	Comments on the Test and the Failure
1	The available captured images are 20 images plus the reference one. The last image at failure was processed by DIC-code due to wood failure. No significant changes on the plate itself.
2	The available captured images are 13 images plus the reference one. The last image at failure was processed by DIC-code due to wood failure. No significant changes on the plate itself.
3	The available captured images are 25 images plus the reference one. The last image at failure was processed by DIC-code due to wood failure. The plate has failed due to wood crack at 4,800 pounds and 5,000 pounds along the bottom horizontal wood member.

Table 4-13: . Brief strain changes description for each EE-test

EE-Test #	The Strain (ε_{yy}) Changes
1	The tensile strain increases until load 1,000 pounds then it decreases. The strain at top half of the plate is tensile strain but the bottom half of the plate has low strain. Some pulling out for the bottom edge of plate is also shown.
2	The tensile strain increases until load 600 pounds then the strain varies. At 2,200 pounds the top half of the plate is positive and the bottom has very low strain. At failure, all the strain is compressive. The strain behavior at failure has changed due to wood cracks not plate failure.
3	The tensile strain increases until load from 200 pounds to 4,000 pounds then it shows slight decrease. At 4,800 and 5,000 pounds it shows high increase in tensile strain. The strain is high at area cross the wood crack line due to tooth withdrawal and pulling out of the plate especially on the right bottom side.

The three EE-tests are described briefly in the previous tables. In this test the external load is perpendicular to the wood grain direction and to the plate's major axis. The maximum recorded load in this test is 5,000 pounds and the least is 2,500 pounds. All the tests are influenced by wood failure in the bottom wood member where the grain direction is perpendicular to the external load direction. Due to wood failure, the strain behavior for the last images at failure changes and appears to be different than the dominant strain on the plate at earlier load stages.

The strain behavior for all images looks very close. The strain (ε_{yy}) increases with loading until a specific load value then it slightly decrease again. After the decrease in the strain, the strain increases again until the failure.

The entire three tests failed due to wood failure. The bottom wood member, which has a grain direction perpendicular to the external load, is influenced by horizontal cracks across the wood under the bottom half of the plate which leads to failure. The strain at the last images shows different behavior than the strain at earlier images before the wood crack effect. The wood cracks especially at the bottom cause tooth withdrawal and pulling out for the plate. Another failure style is on the bottom half –right edge (or –left edge) the plate shows circular pulling out as a result of failure. Thus, the strain is high at the edge of the plate where the tooth withdrawal and pulling out of the plate occur.

There are no significant changes in the strain behavior due to wood failure. This test does not show the exact procedures for the plate failure. However, the digital image correlation can provide the strain behavior for each image at low load. The maximum load before the failure is 5,000 pounds and the plate is in good condition and shape. From the strain behavior of the plate, the plate does not show any significant changes that would indicate yielding. The strain in both directions (ε_{yy}) and (ε_{xx}) have values so the strain (ε_{xx}) should be considered. The maximum changes in the strain are due to tooth withdrawal. This result shows that when it comes to the plate's failure the strain is high at higher load. Also this result shows that the external load doesn't control the plate and the plate has very high strength against the external force. The tooth grip is still very high. Thus, the strain curve is not fully well organized with respect to external loading. Some spikes of the strain curves are shown along the vertical curves due to slots distributed across the plate's surface where the teeth have been pressed out. The full-field strain measurement for the last image at failure load shows that the strain (ε_{xx}) is as high as the strain (ε_{yy}). Thus, at early stages of loading the strain (ε_{xx}) cannot be ignored and should be considered as the strain (ε_{yy}). Both strains (ε_{xx}) and (ε_{yy}) are tensile strain or compressive strain at the same time in the test with some limited exceptions. This indicates that many factors can play key roles in this test such as the wood stretch. The presence of teeth distributed in a wave pattern on the plate also plays a major role in changing the proposed behavior of the strain (ε_{xx}). Wood is anisotropic material, so the external load should be high enough to control the strain behavior and wood properties.

The strain values and the full-field strain measurements for the images show fluctuation in the strain values. This indicates that many factors still affect the strain behavior and the external load is low to take over the strain behavior of the plate. The wood grain is perpendicular to the load which makes it weaker. Pulling out of the teeth makes the strain field vary up and down and makes big changes in strain behavior. The teeth resistance in the bottom half of the plate is different than the shear resistance in the top half of the plate due to the difference in the wood grain direction. The angles of the teeth that are embedded in the wood also influence the teeth resistance and so the strain behavior. The tooth grip is very high and can resist higher external forces. The plate can withstand a higher load. Load values could be over 5,000 pounds. The strain's distribution over the plate's surface fluctuates and changes with loading. This indicates that the teeth resist the external load. The direction of the teeth angle and the cross sectional area controls the strain over the entire plate's surface. Thus, the external force needs to be higher to take over the influence of the teeth over the plate. Also the external force can take advantage of the lower cross sectional areas on some regions over the plate's surface.

The gap between the two wood members shows very small changes due to wood failure and tooth withdrawal.

The displacement of the gap between the two pieces of wood is found using the DIC Vic-2D software based on the number of pixels in the vertical direction in each image under loading. Then the calibration from the software is used to change the pixels to inches. The calibration factor is 0.002113. The results from the LVDT are used to compare the displacement of the gap from LVDT to the displacement that is found using the digital image correlation software Vic-2D. In DIC, the pixels are counted based on the image and the surface but the LVDT measures the displacement from the middle of the wood side. So the distance based on the pixels is controlled by the pixel size and the calibration number. While the LVDT gives the exact distance between gaps.

4.2 Heel Joint Tests

Four simple trusses were created. Figure 4-188 shows one of the simple trusses. The focus in this test will be on the left side heel joint. A (4X5) in of metal plate were used to connect the wood members together. The plate on the left side of heel joint was tested by placing the camera in front of it and all images were captured for that plate at a load increment of 200 pounds until failure.

All the trusses were set on the Universal Testing Machine as shown in Figure 4-188. Two pieces of wood were used as a support under the two heel joints. The top joint was supported by a C-shape hook to prevent it from swinging.

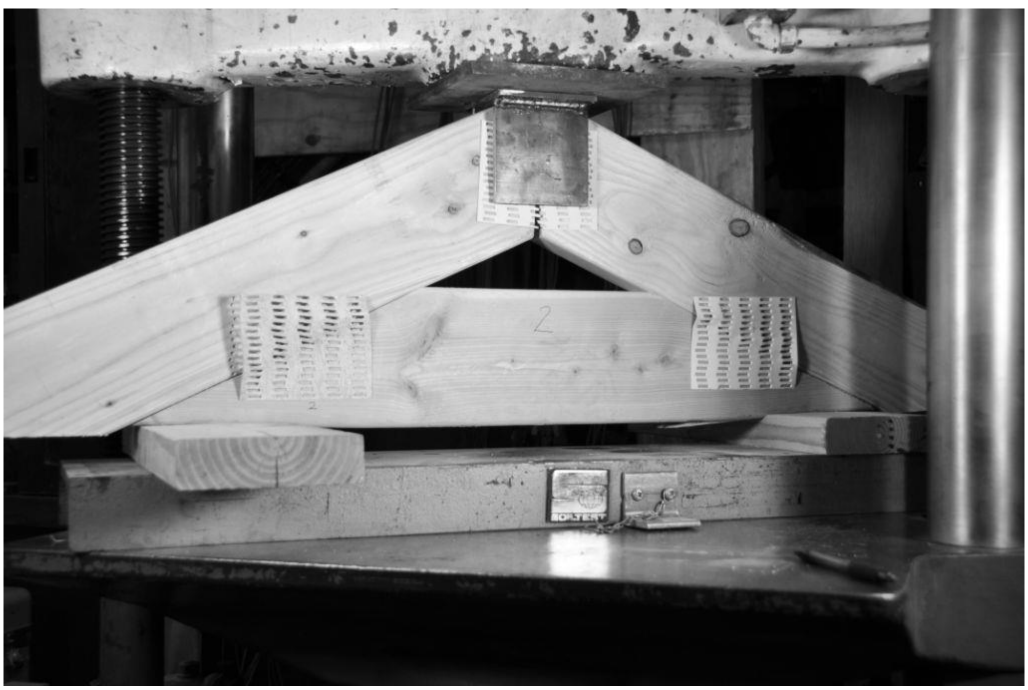

Figure 4-188: The typical truss in this research sitting on the Universal Testing Machine

The bottom table of the universal testing machine that holds the simple truss moved up until failure.

All images that were captured through the test until failure were implemented in the digital image correlation software to obtain the full-field strain measurements. The DIC software was used to analyze the strain field based on two main axes x and y. The x and y axes coordination system are shown in the next two Figures.

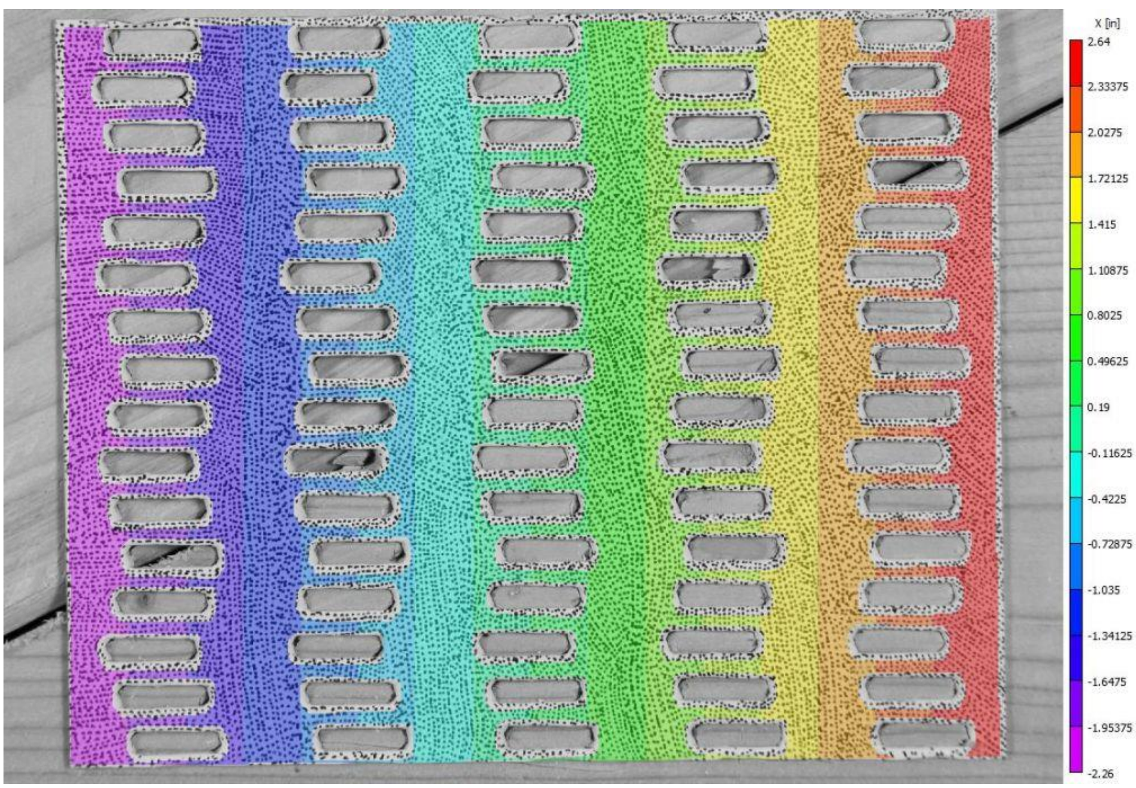

Figure 4-189: x-axis coordination system obtained from DIC software

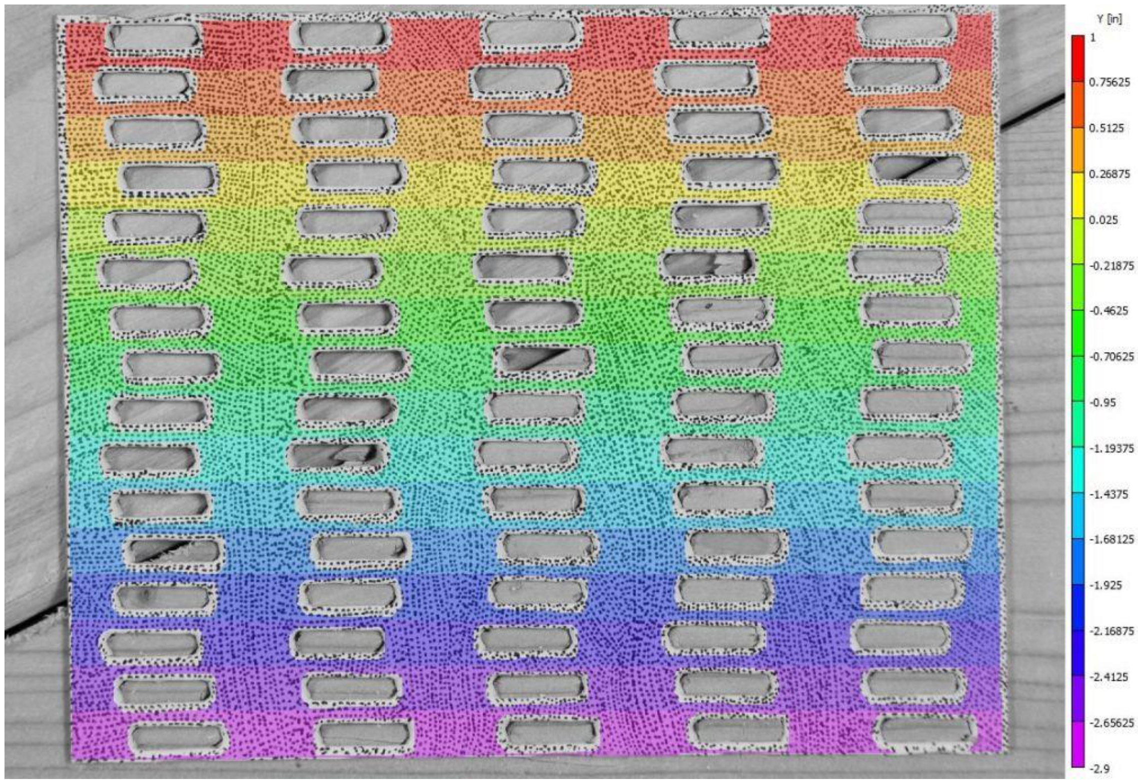

Figure 4-190: y-axis coordination system obtained from DIC software

The full-field strain results obtained from the DIC software were analyzed and presented numerically by considering a vertical and horizontal cross section lines from the top to the bottom and from the left to the right of the plate, respectively. The cross section is taken in four locations vertically and in three different locations horizontally as shown in Figure 4-191.

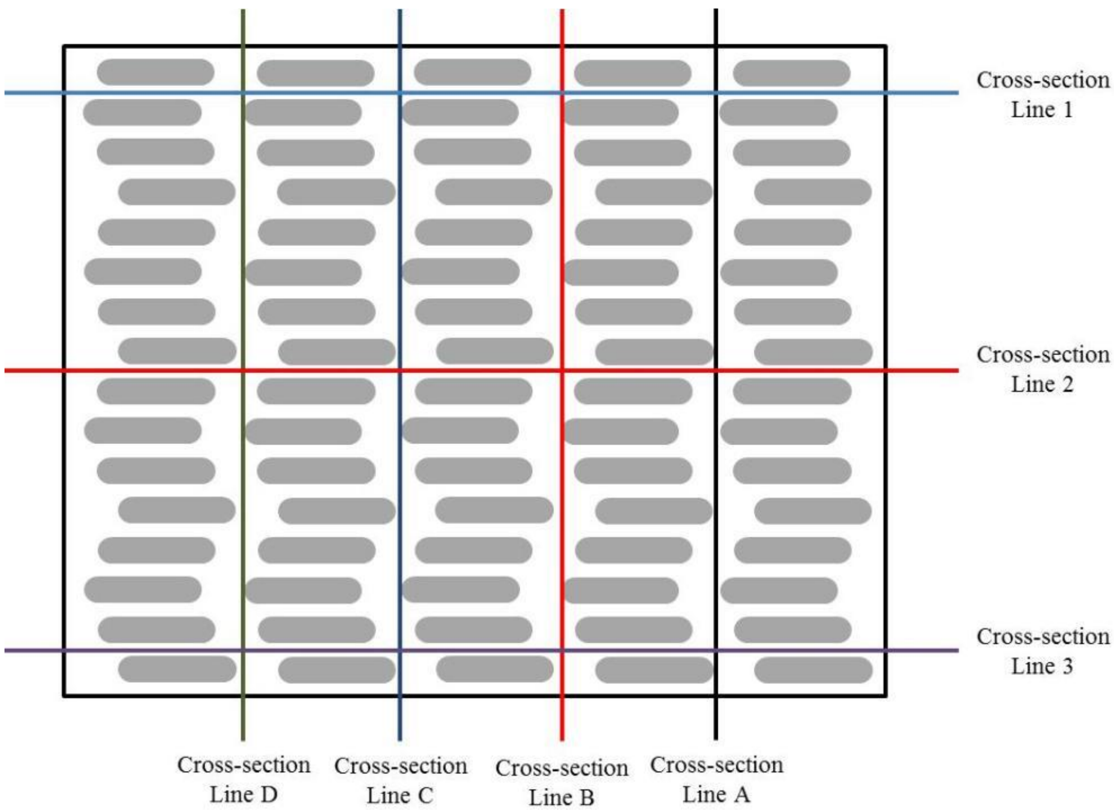

Figure 4-191: Metal plate with the cross-section lines along the vertical direction and the horizontal direction

4.2.1 1st Heel Joint Test:

In this test, the truss was set on the universal testing machine and the camera was placed at a fixed location in front of the speckled plate located on the left heel joint. The first image before loading was captured as a reference image, as shown in Figure 4-192.

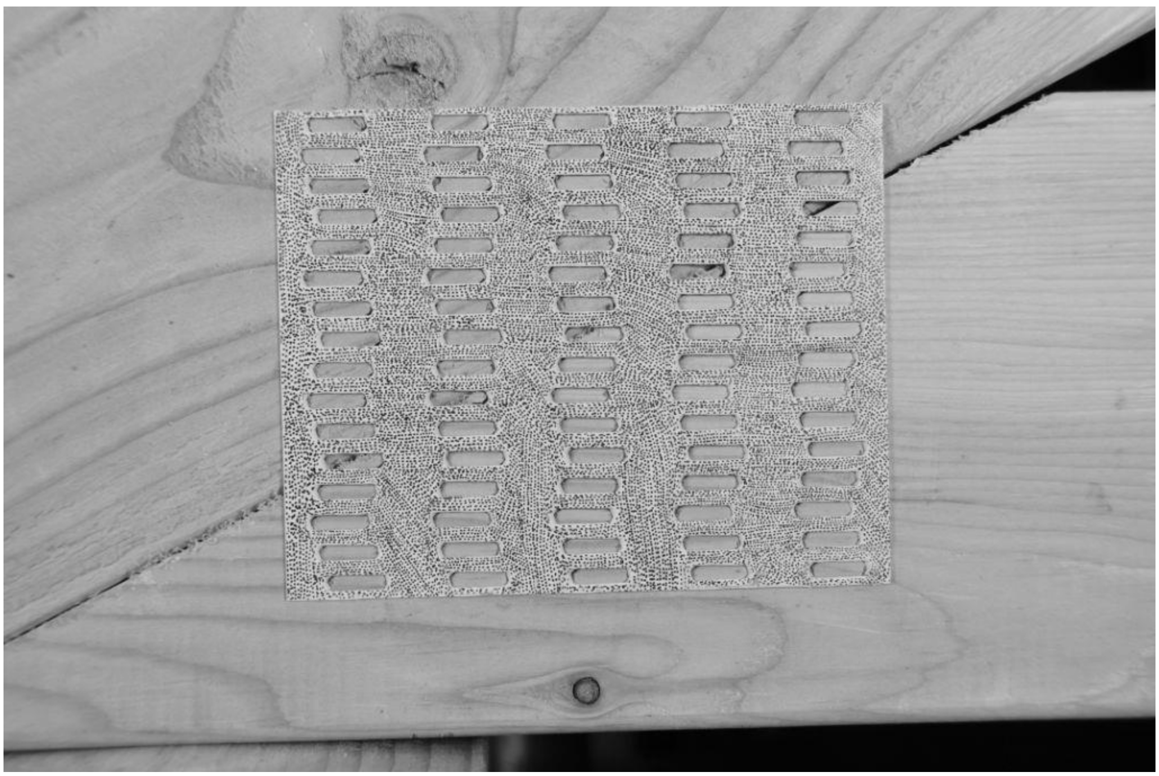

Figure 4-192: The reference image in the first heel joint

A total of 69 images were captured for this test before the failure besides the reference image. The truss failed at a load equal to 13,800 pounds. All the captured images were implemented in DIC software to find the full-field strain measurements.

4.2.1.1 Analysis of the Full-Field Strain Measurements Results Obtained From DIC Software

All the test images, which were obtained from the lab test, were implemented in the digital image correlation software Vic-2D. Each image was analyzed in relation to a reference image. Each deformed image was compared to the non-deformed reference image. The full-field strain measurements were obtained from the digital image correlation software. Figure 4-193 shows the strain in y-direction (ε_{yy}) for the first images at 200 pounds.

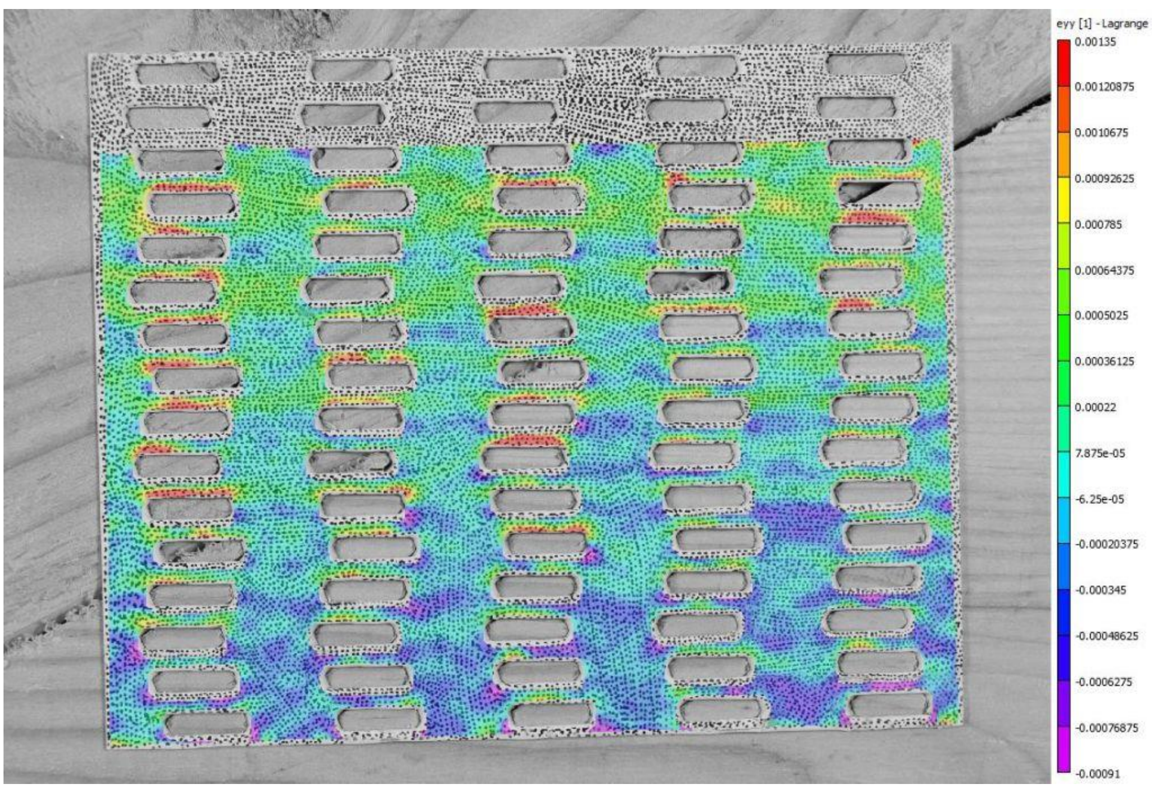

Figure 4-193: Full-field strain measurements (ε_{yy}) for the MPC after applying 200 pounds

The image shows that the strain (ε_{yy}) is distributed almost equally. The dominant strain (ε_{yy}) is positive with some little exceptions.

Increasing the load increases the strain (ε_{yy}) and changes throughout the plate. Figure 4-194 shows the strain at a load of 8,000 pounds.

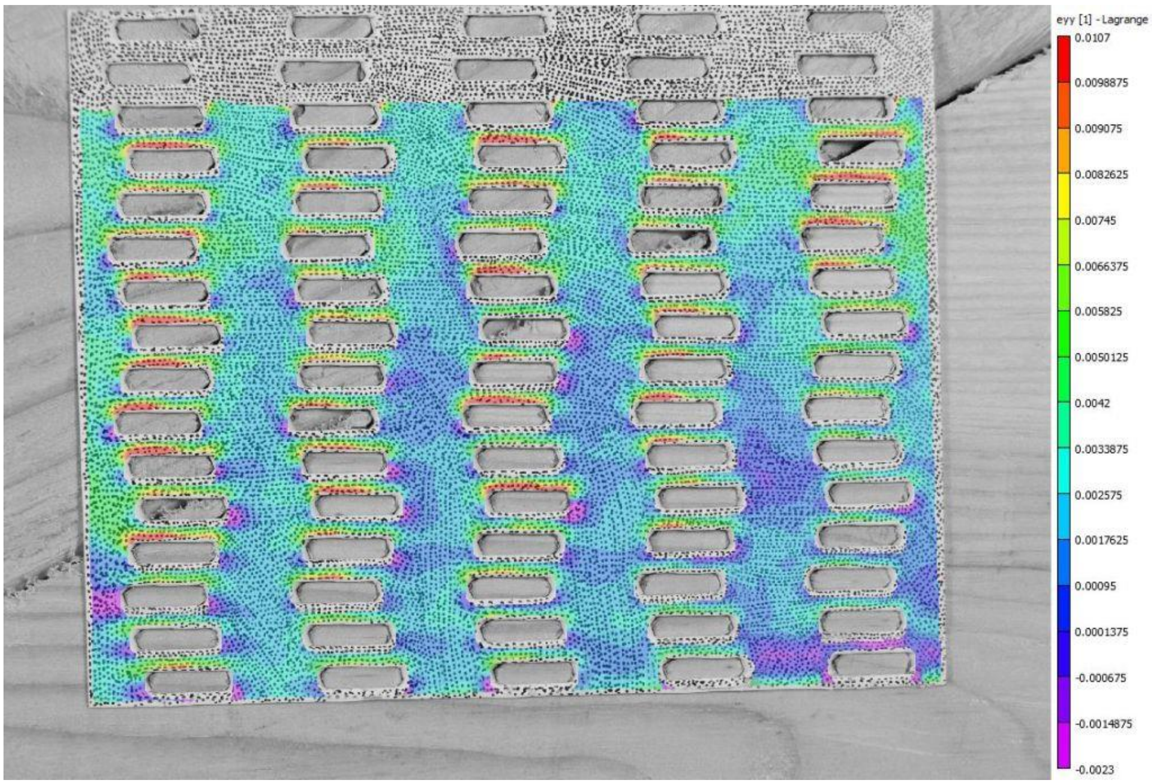

Figure 4-194: Full-field strain measurements (ε_{yy}) for the MPC after applying 8000 pounds

The previous figure shows that the strain (ε_{yy}) is equally distributed over the plate surface with some exceptions and the strain is low with a maximum value of 0.01. The strain over the entire plate is a tensile strain. The full-field strain measurements for the 69 images show that the strain field changes its behavior at image # 51, which is at a load of about 10,000 pounds as shown in Figure 4-195. The figure shows the changes which strain field (ε_{yy}) undergoes in the diagonal direction over the gap between the wood members. The strain around the diagonal line is compressive rather than tensile strain. However, the rest of the plate surface remains under tensile strain.

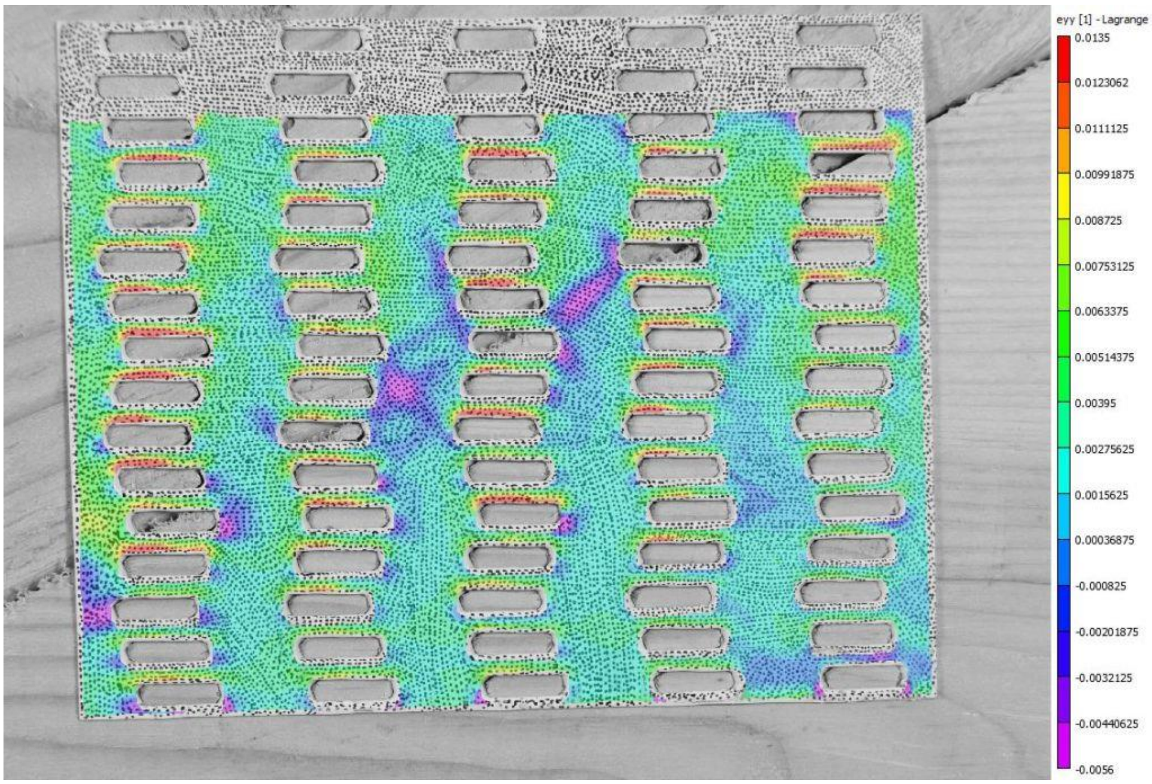

Figure 4-195: Full-field strain measurements (ε_{yy}) for the MPC after applying 10,000 pounds

After applying 10,000 pounds, the strain fields exhibit significant changes due to the forces from both horizontal and diagonal wood members. The next full-field strain images at increments of loading of 200 pounds show the diagonal compressive strain line created by loading until failure. Figure 4-196 shows the full-field strain measurements for the image # 61at 12,000 pounds. The strain (ε_{yy}) is compressive along the diagonal line over the gap between the wood members; however, it is a tensile strain over the rest of the plate. The tensile strain increases with loading to a value of 0.016 and the compressive strain also increases to a maximum value of about -0.038.

The strain field for the last image at the failure is shown in Figure 4-197, where the tooth withdrawal is evident especially in the left side of the plate.

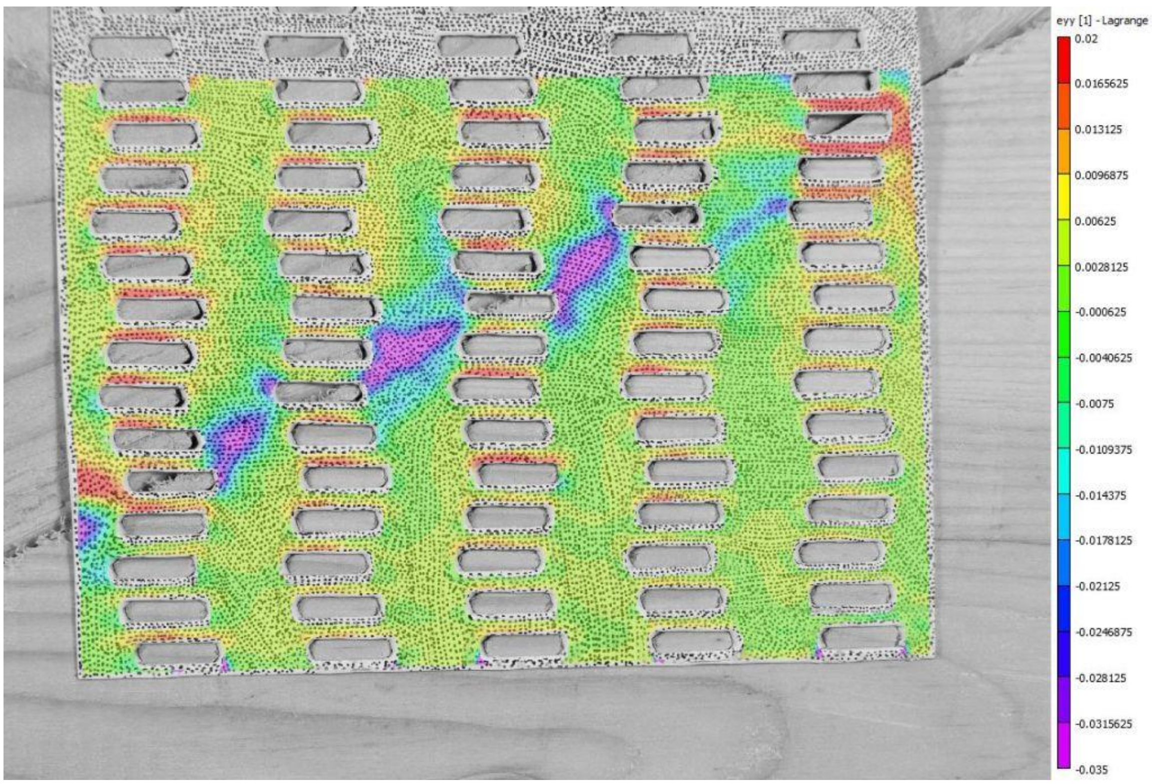

Figure 4-196: Full-field strain measurements (ε_{yy}) for the MPC after applying 12,000 pounds

The full-field strain measurements for the last image at failure shows high tensile strain in the upper right side; however, it shows compressive strain along the diagonal line over the gap between the two wood members. The strain is approximately tensile except at the regions close to the diagonal compressive strain. The tensile strain reaches a value of about 0.035 in certain regions over the plate surface and -0.1 as the maximum compressive strain. The plate also shows some circular withdrawal on the right side edge.

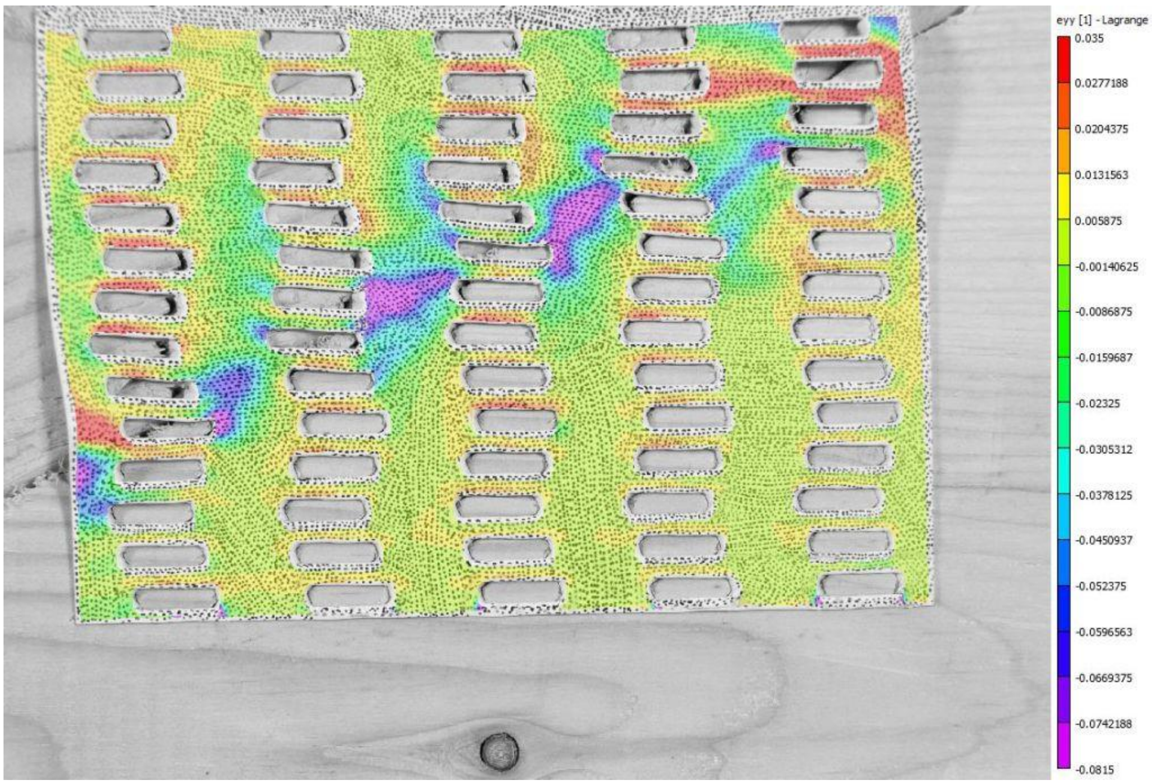

Figure 4-197: Full-field strain measurements (ε_{yy}) for the MPC at failure at 13,800 pounds

On the other hand, the full-field strain measurements in x-direction (ε_{xx}) can also be obtained from digital image correlation software. Figure 4-198 shows the strain (ε_{xx}) after applying 200 pounds. The image shows that the strain (ε_{xx}) is distributed over the plate with low values and reaches a maximum of 0.00045 and -0.00052. Some limited regions show compressive strain and the large region shows a tensile strain. By an increase the load, the strain (ε_{xx}) increases and changes throughout the surface of the plate. The increase in the strain (ε_{xx}) is also low and is not significant. The full-field strain measurements (ε_{xx}) from load 200 pounds until load 8,000 pounds show slight differences in the strain with loading. The compressive strain is in the bottom half of the plate and the tensile strain (ε_{xx}) is in the upper half of the plate.

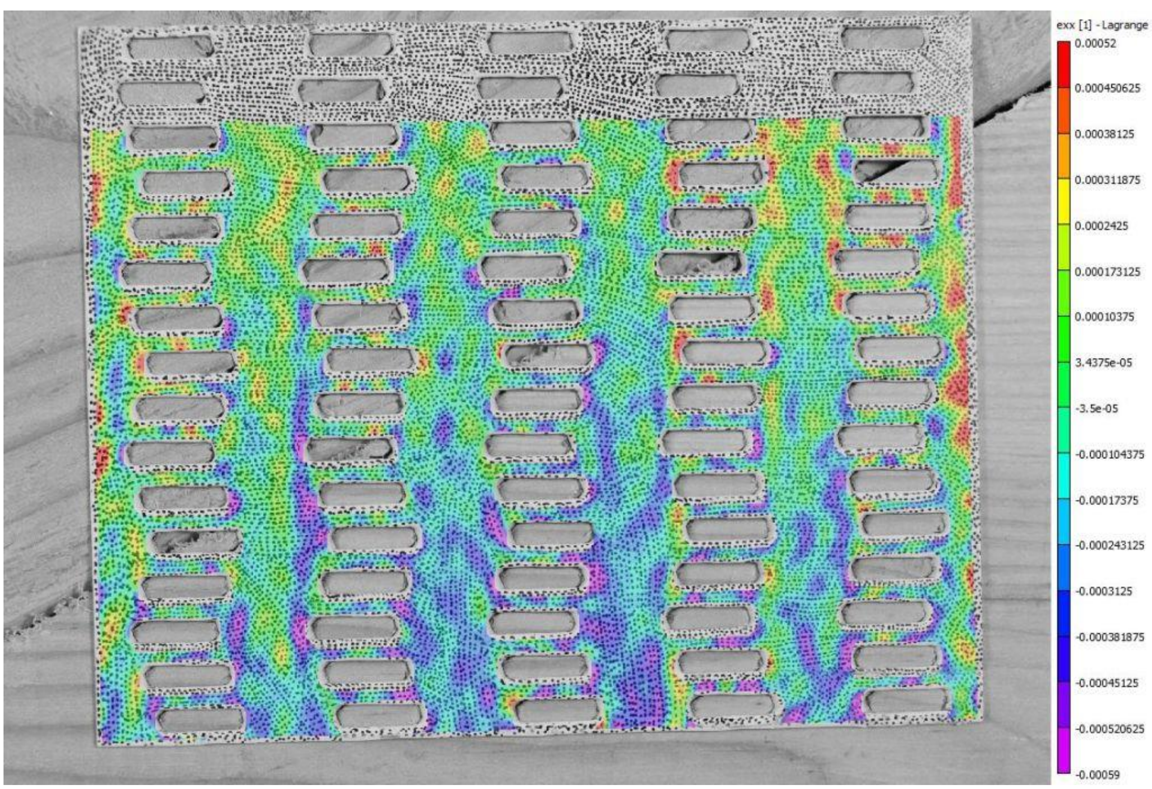

Figure 4-198: Full-field strain measurements (ε_{xx}) for the MPC after applying 200 pounds

At 8,000 pounds, the strain (ε_{xx}) behaves different than the earlier strain behavior. Figure 4.257 shows the strain (ε_{xx}) at 8,000 pounds. The bottom half of the plate is under low strain (ε_{xx}) especially from the right side of the plate. This result is evident from figure 4-199. The upper and middle half of the plate shows higher tensile strain (ε_{xx}) than the bottom half of the plate.

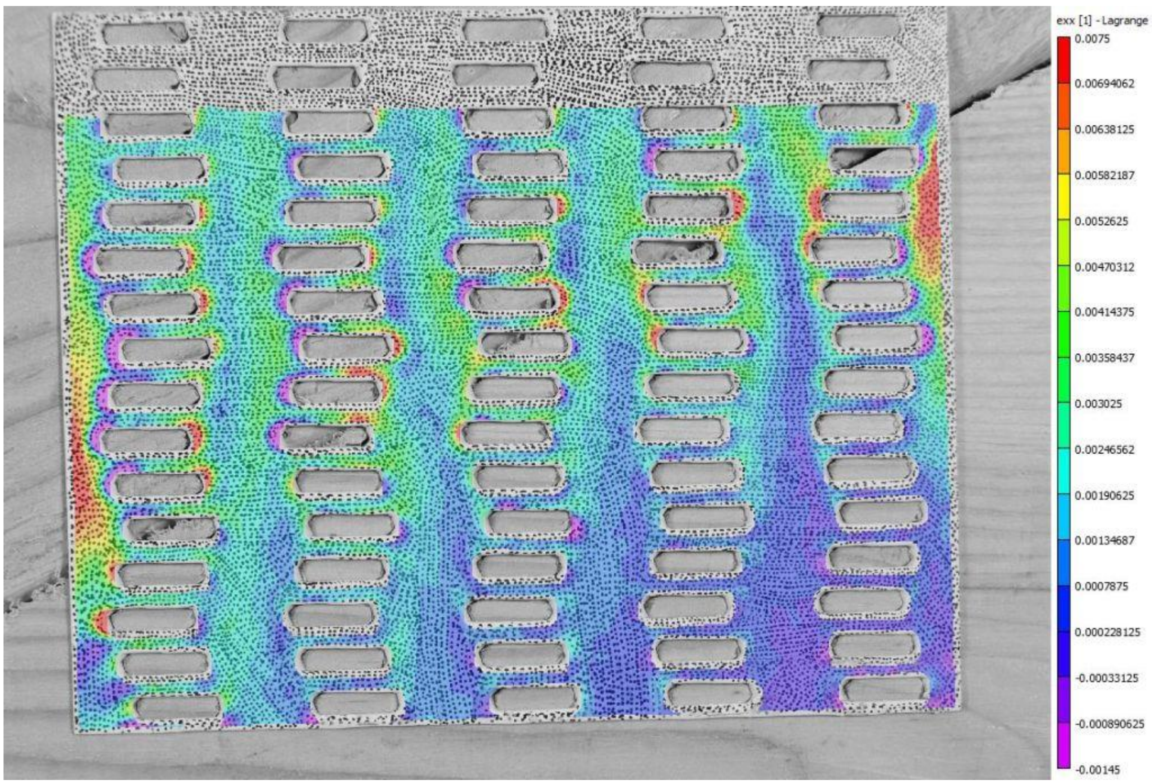

Figure 4-199: Full-field strain measurements (ε_{xx}) for the MPC after applying 8000 pounds

However, the full-field strain measurements for the 69 images show that the strain field changes its values and behavior at about image # 51, which is at load of 10,000 pounds as shown in Figure 4-200. This figure shows how the strain field (ε_{xx}) changes in the diagonal direction over the gap between the wood members. The strain around the diagonal line displays high tensile strain. However, the rest of the plate surface remains under tensile strain with some exceptions. The strain (ε_{xx}) at 10,000 pounds is shown in Figure 4-200. The strain (ε_{xx}) is higher over the diagonal line that is located over the gap between the two wood members.

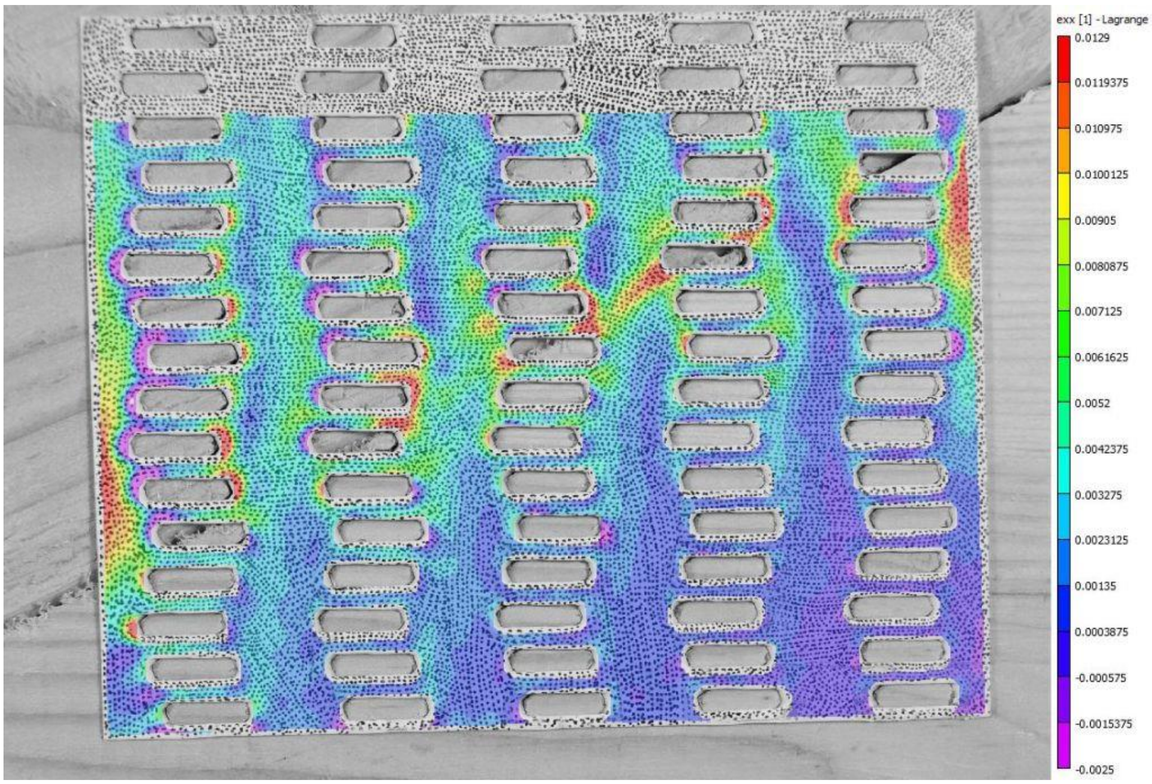

Figure 4-200: Full-field strain measurements (ε_{xx}) for the MPC after applying 10,000 pounds

The bottom area of the plate below the diagonal line has the lowest strain (ε_{xx}) on the plate surface. After applying 10,000 pounds, the strain fields show large changes due to the forces from both the horizontal and diagonal wood members. The next full-field strain measurement images at increments of loading of 200 pounds after the load of 10,000 pounds show that the diagonal tensile strain (ε_{xx}) line is created by loading until failure. Figure 4-201 shows the full-field strain measurements for the image #-61at 12,000 pounds. The strain (ε_{xx}) is tensile along the diagonal line over the gap between the two wood members, and it is tensile over the rest of the plate with some exceptions. The tensile strain has increased with loading, and other limited regions of the plate have tooth withdrawal and pulling out of the plate. The left side of the plate at these regions has a compressive strain (ε_{xx}).

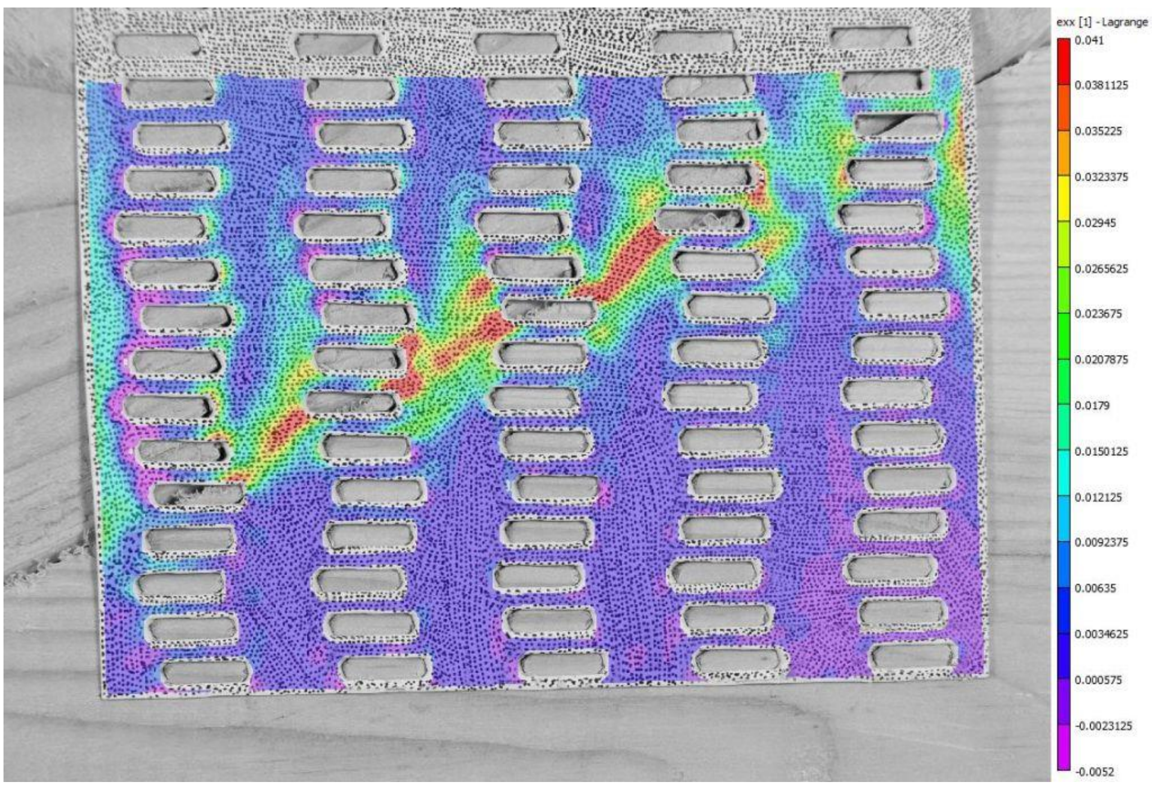

Figure 4-201: Full-field strain measurements (ε_{xx}) for the MPC after applying 12,000 pounds

The strain field for the last image at failure is shown in Figure 4-202. The figure shows tooth withdrawal especially on the left side of the plate. The full-field strain measurements for the last image at failure shows much higher tensile strain values on the diagonal line over the gap between the two connected wood members. The regions of the plate under the diagonal line exhibit lower strain values on the right side of the plate and higher strain values on the left side. The tensile strain reaches a value of 0.104. The plate also shows some circular withdrawal for the right side edge.

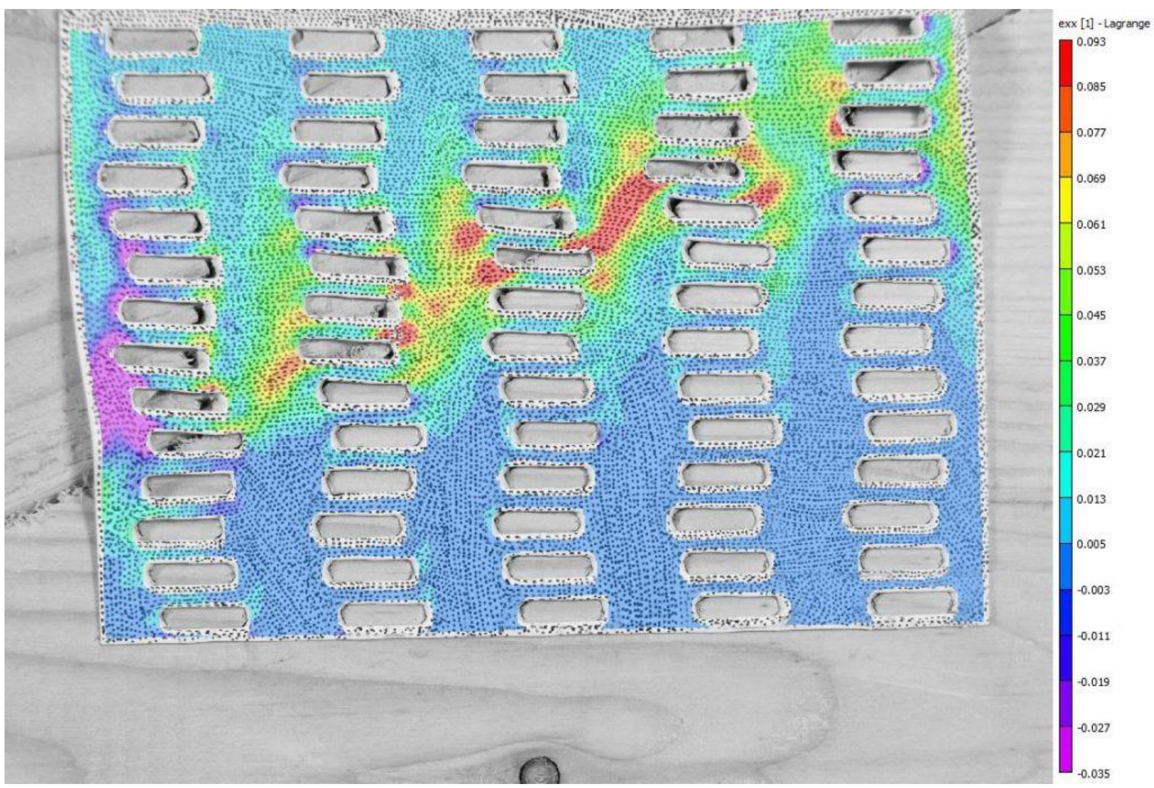

Figure 4-202: Full-field strain measurements (ε_{xx}) for the MPC at failure at 13,800 pounds

4.2.1.2 Numerical Analysis along the Vertical Strain Results

To analyze the DIC results numerically, a vertical cross section line from the top of the plate to the bottom is taken for some images starting with the first image at 200 pounds and ending with the last image at failure. The cross section is taken in four different locations as shown in Figure 4-203.

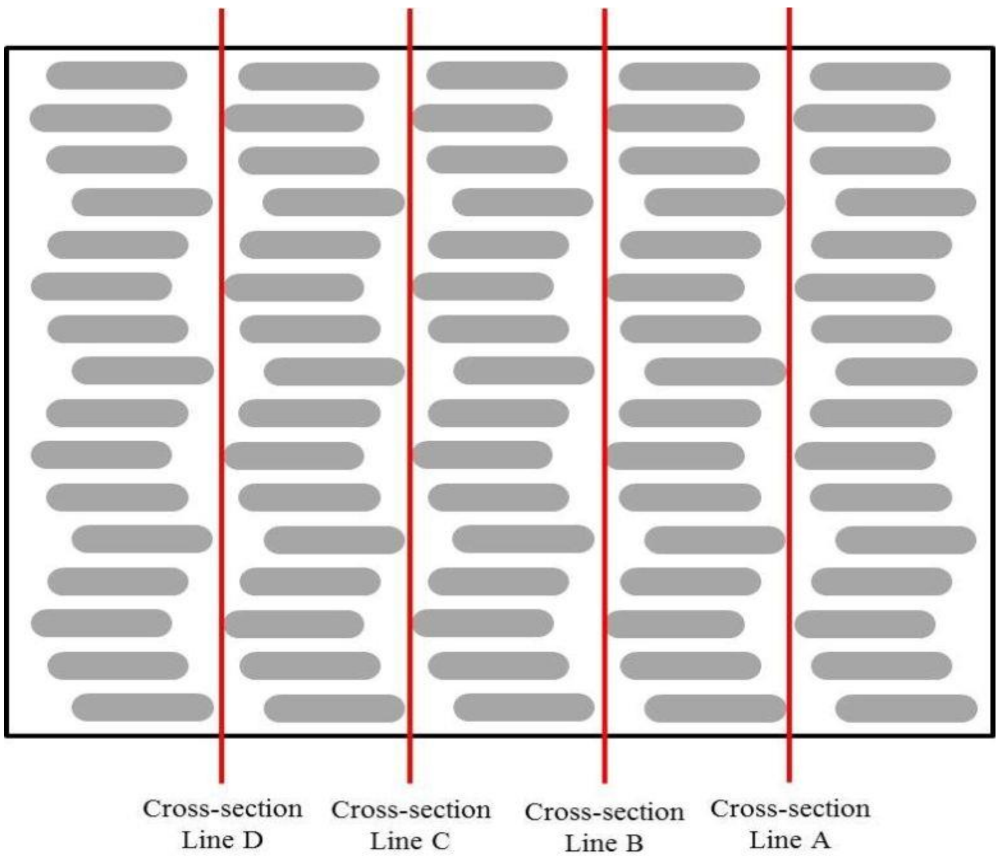

Figure 4-203: Metal plate with the cross-section lines along the vertical direction

The cross section is taken in four different locations:

- The first cross section is from the right side of MPC @ x = 1.52 in. cross-section A-A.
- The second cross section is @ x = 0.58 in. cross-section B-B.
- The third cross section is @ x = -0.44 in. cross-section C-C.
- The fourth cross section line is from the left side of MPC @ x= -1.44 in. cross-section D-D.

Four cross-section lines are taken for the strain field (ε_{yy}). The next Figures show the distribution of strain (ε_{yy}) accompanied by (ε_{xx}) at the same cross section line at four different locations for 12 images. Each image represents the value of the loading that is applied on the specimen of simple truss.

The curves show that the first considered load is 400 pounds and then different increment of loading is used to show the MPC behavior until failure. In general, the strain (ε_{yy}) exhibits similar strain results and almost equally distributed strain over the entire plate with some exceptions from the beginning of the test until 10,000 pounds of loading. After applying 10,000 pounds, the plate strain behavior shows some changes in the strain values over certain limited regions of the plate. The large change in the strain is limited in certain regions, which are over the diagonal gap between the two connected wood members. The dominant strain (ε_{yy}) is a tensile strain and it increases with loading through the test.

The strain (ε_{yy}) in Figure 4-204 shows the right side behavior of the MPC under loading at section (A-A). In this figure, the strain (ε_{yy}) is almost equally distributed from the top to the bottom of the plate along the cross section line (A-A).The strain (ε_{yy}) is also slightly increasing with loading from 200 pounds until 12,000 pounds. At 12,000, the strain (ε_{yy}) curve shows changes as some strain regions display negative strain and other regions display higher positive strain values. As a result of loading from 12,000 pounds to the failure at 13,800 pounds, the top region of the plate is in compressive strain (ε_{yy}) and a limited region has higher tensile strain (ε_{yy}) than that over the rest of the plate. The strain (ε_{xx}) in Figure 4-205 over the same cross section line (A-A) significantly increases after applying 12,000 pounds, it is tensile strain and it also increases with increasing load until failure at 13,000 pounds. The top of the plate after applying 12,000 pounds is under tensile strain (ε_{xx}) and compressive strain (ε_{yy}) while the remaining regions of the plate are under tensile strain (ε_{yy}) and (ε_{xx}).

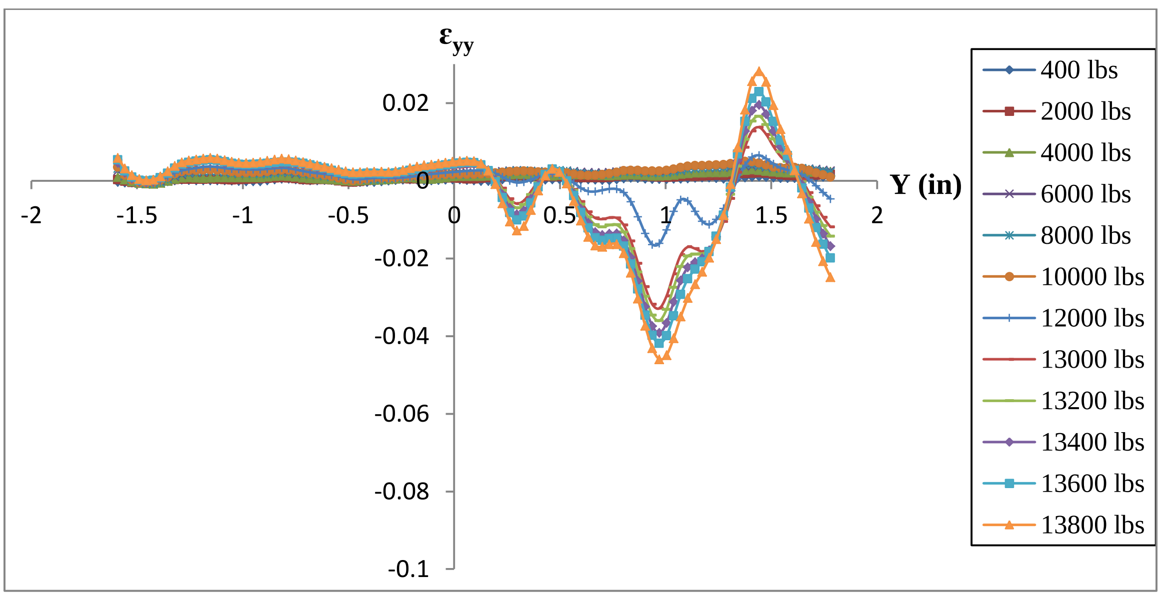

Figure 4-204: The strain distribution (ε_{yy}) along a cross section line (A-A) located on the right side of the plate

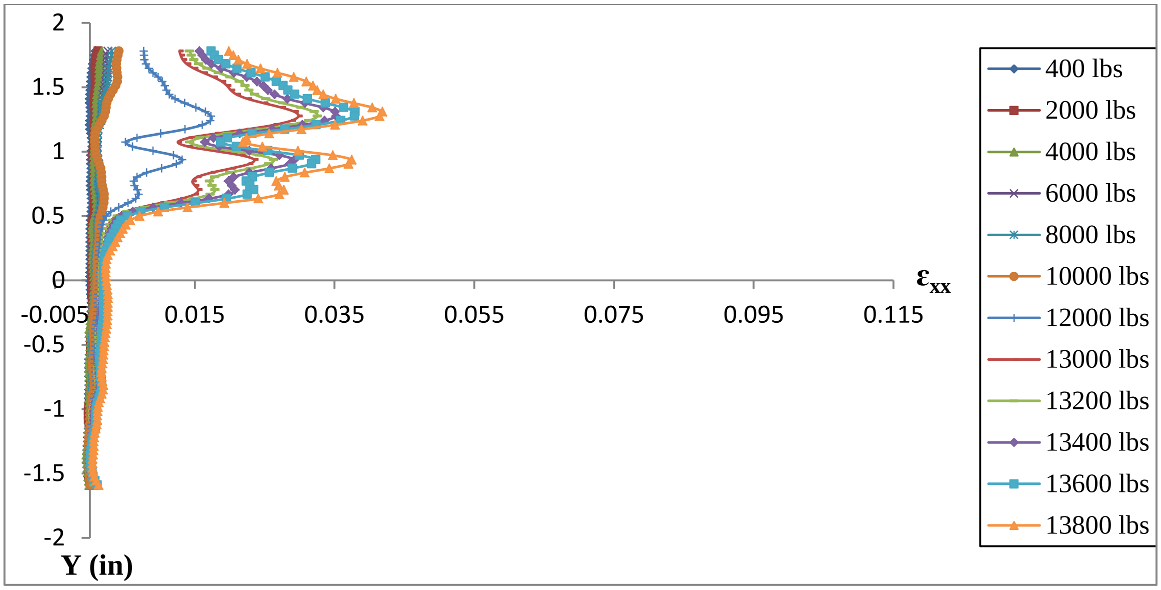

Figure 4-205: The strain distribution (ε_{xx}) along a cross section line (A-A) located on the right side of the plate

The next four Figures show the values of the strain (ε_{yy}) and (ε_{xx}) at the two middle cross section lines (B-B) and (C-C). The strain (ε_{yy}) shows almost equally distributed strain along the vertical cross section lines (B-B) and (C-C) starting from 400 pounds until 10,000 pounds. The strain curves (ε_{yy}) shows slightly increase with loading until 10,000 pounds. The strain (ε_{yy}) is tensile. After applying 10,000 pounds, the curves of strain (ε_{yy}) show an increase in the tensile strain and also a decrease in the tensile strain over a limited region of the plate. The strain over this limited region is also turning to compressive strain. This region is located over the diagonal line that is located over the gap between the two wood members. The curve at 12,000 pounds shows slight increase in the tensile strain; however, the increase is significant for the compressive strain over the same limited region and the limited region now is extending with loading. After

12,000 pounds until failure at 13,800 pounds, the strain (ε_{yy}) curves show high increase in compressive strain over the diagonal line and a constant increase in the tensile strain on the remaining regions of the plate.

On the other hand, the horizontal strain (ε_{xx}) is tensile strain from the beginning until the failure with certain limited exceptions. The strain (ε_{xx}) is low and equally distributed along the vertical line from the top to the bottom until the load 10,000 pounds where a significant increase in the tensile strain (ε_{xx}) over the same limited area that the strain (ε_{yy}) has a compressive strain. After applying 10,000 pounds until the failure at 13,800 pounds, the strain (ε_{xx}) over the limited area, which is located at the diagonal line over the two members of wood that are connected, increases significantly as a tensile strain (ε_{xx}) and the covered region is also extended with loading.

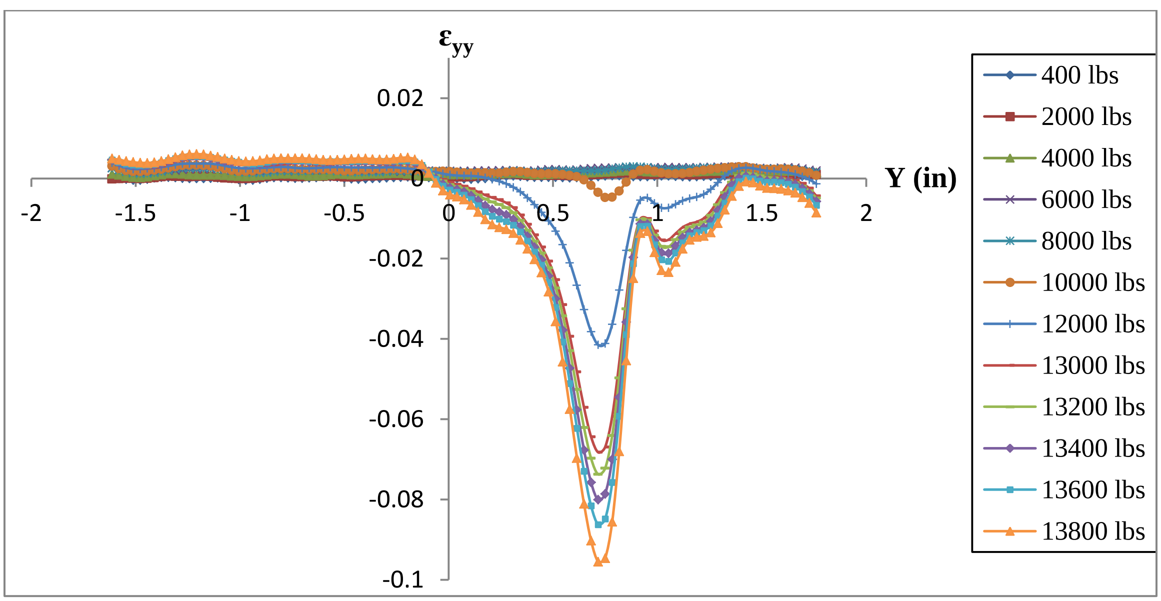

Figure 4-206: The strain distribution (ε_{yy}) along a cross section line (B-B)

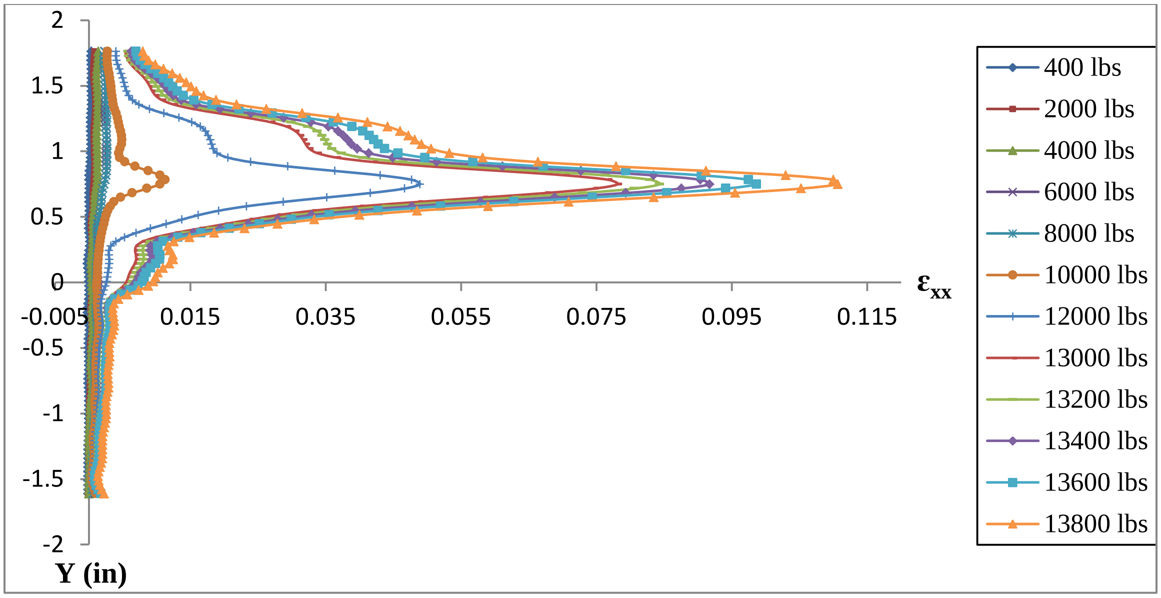

Figure 4-207: The strain distribution (ε_{xx}) along a cross section line (B-B)

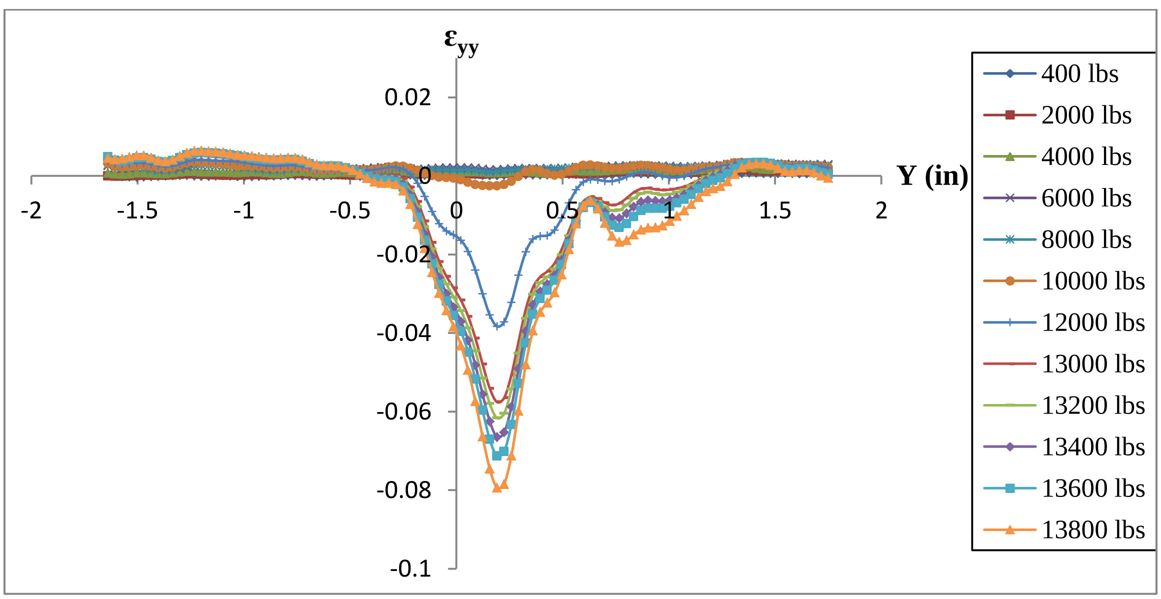

Figure 4-208: The strain distribution (ε_{yy}) along a cross section line (C-C)

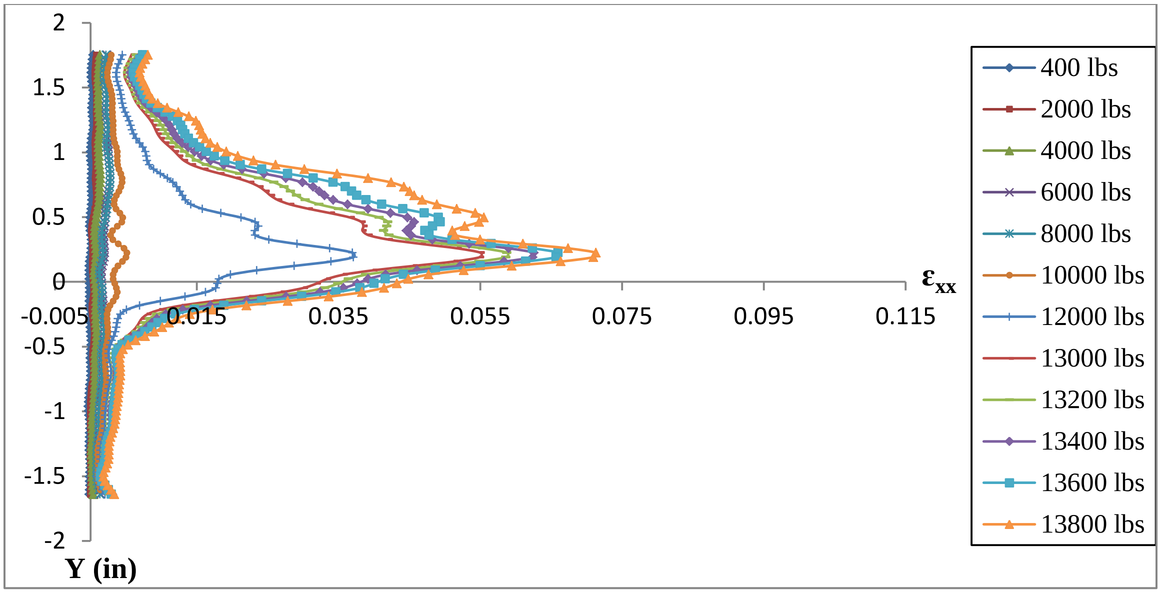

Figure 4-209: The strain distribution (ε_{xx}) along a cross section line (C-C)

Thus, at 10,000 pounds, the strain (ε_{xx}) is tensile while the strain (ε_{yy}) is a compressive strain. The maximum compressive strain (ε_{yy}) and (ε_{xx}) is -0.094 and 0.11 respectively. The cross section line (B-B) has been affected by loading more than the cross section line (C-C).

Figures 4-210 and 4-211 show the strain (ε_{xx}) and (ε_{yy}) along the vertical cross section line (D-D) located in the left side of the plate. In this cross section line, the strain slightly changes its behavior at 10,000 pounds of loading; however, at 12,000 pounds, the change in the strain curves (ε_{yy}) and (ε_{xx}) is significant until the failure at 13,800 pounds. The strain (ε_{yy}) changes to compressive strain over the limited area of the plate that is located over the diagonal line between the two members of wood that are connected while the strain (ε_{xx}) over the same limited area is tensile with higher values and increases with loading. As the load increases, the tensile strain (ε_{xx}) increases, and the vertical strain (ε_{yy}) increases also; however, it is a compressive strain. The curves show that the maximum vertical strain (ε_{yy}) is -0.0622 and the maximum horizontal (ε_{xx}) is 0.0732 at the failure at 13,800 pounds in the same point. The last cross section line (D-D) is less affected by the loading than the cross section line (C-C) which is located beside it.

Overall, the cross section line (B-B) shows the most section line that is affected by the loading and it possesses higher maximum strain values than other cross section lines. Then, the cross section line (C-C) follows the cross section line (B-B).

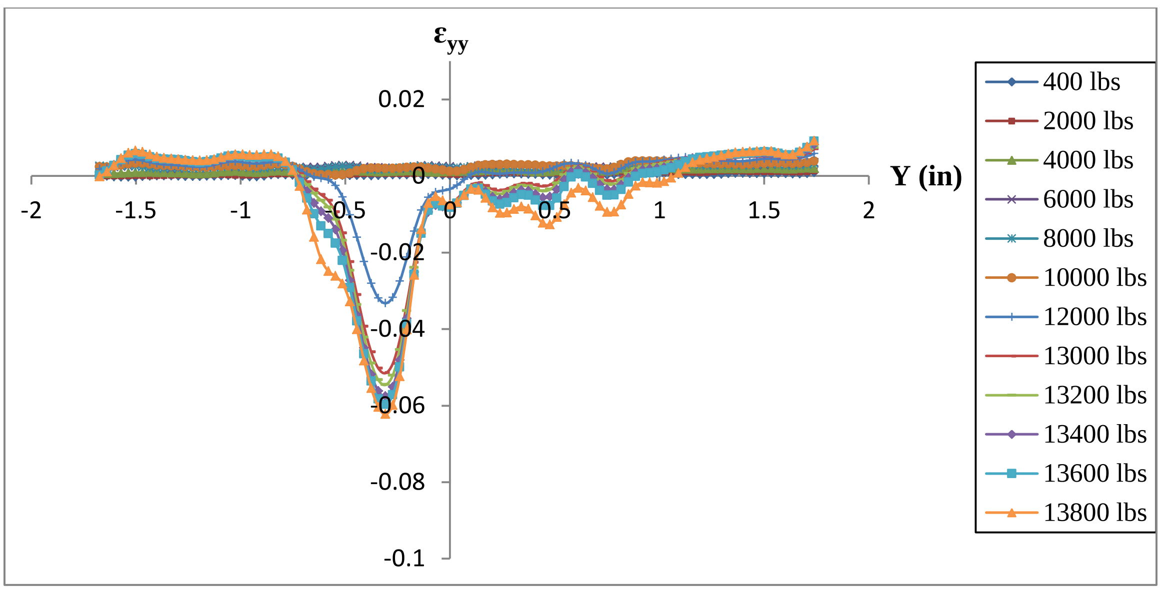

Figure 4-210: The strain distribution (ε_{yy}) along a cross section line (D-D) located on the left side of the plate

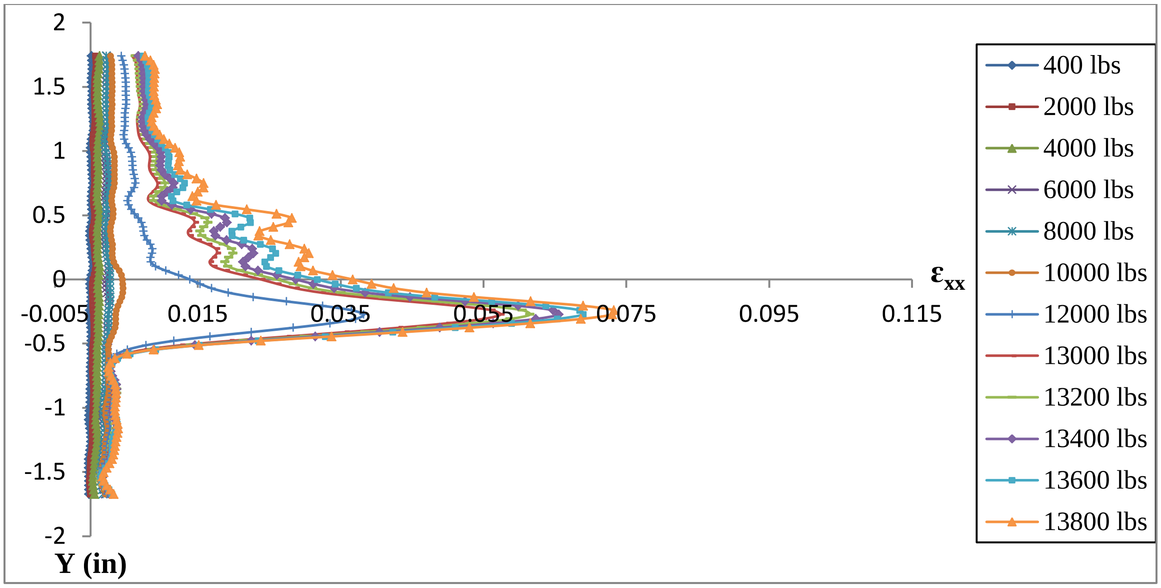

Figure 4-211: The strain distribution (ε_{xx}) along a cross section line (D-D) located on the left side of the plate

4.2.1.3 Numerical Analysis along the Horizontal Strain Results

To analyze the DIC results numerically, a horizontal cross section line from the right side to the left side the plate is taken for some images starting with the first image at 200 pounds and ending with the last image at failure. The cross section is taken in three different locations.

- The first cross section is on the top of MPC @ y = 1.59 in. cross-section 1-1.
- The second cross section is near the middle of the MPC @ y = 0.33 in. cross-section 2-2.
- The third cross section is bottom of MPC @ y = -1.39 in. cross-section 3-3.

Figure 4-212 shows the cross section lines on the metal plate

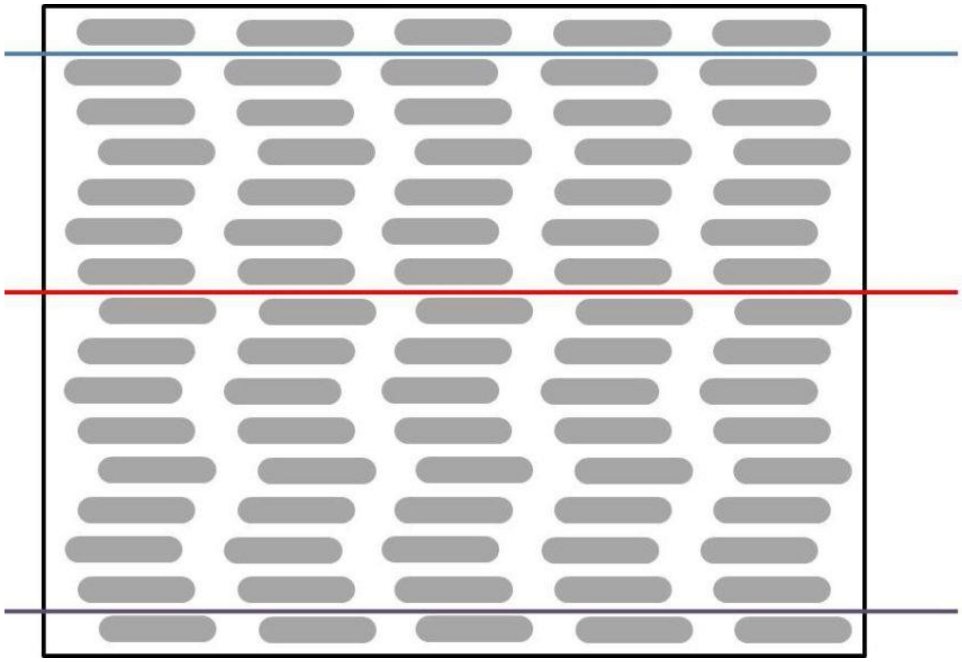

Figure 4-212: Metal plate with the cross-section lines along the horizontal direction

Three cross-section lines are taken for the strain field (ε_{xx}). The next Figures show the distribution of strain (ε_{xx}) accompanied with (ε_{yy}) at the same cross section line at three different locations for 12 images. Each image represents the value of the loading that is applied on the specimen of simple truss.

The curves show that the first considered load is 400 pounds then a different increment of loading is used to show the MPC behavior until the failure. In general, the strain (ε_{xx}) shows similar strain results and almost invariable horizontally distributed strain with some exceptions from the beginning of the test until 10,000 pounds of loading. After 10,000 pounds, the plate strain behavior shows some changes in strain values over a limited region of the plate. The high changes in the strain are limited with some regions which are over the diagonal gap between the two connected wood members. The dominant strain (ε_{xx}) is tensile strain, and it increases with loading throughout the test.

The strain (ε_{xx}) after applying 10,000 pounds shows a significant increase in the values in the middle of the plate at the cross section line (2-2). The lower part of the plate at cross section line (3-3) shows very low strain values comparing to cross section line (1-1) and (2-2).The strain (ε_{xx}) is high on the right side of the plate and gradually decreases to the left side of the plate as shown in Figure 4-213 at cross section line (1-1). At cross section line (2-2) as shown in Figure 4-215 the tensile strain is significantly high in the middle of the plate which crosses the diagonal line over the gap between the two wood members. The strain (ε_{xx}) is tensile strain except the left side of the plate which is influenced by tooth withdrawal and pulling out of the plate that makes the strain (ε_{xx}) turns to compressive strains at that region.

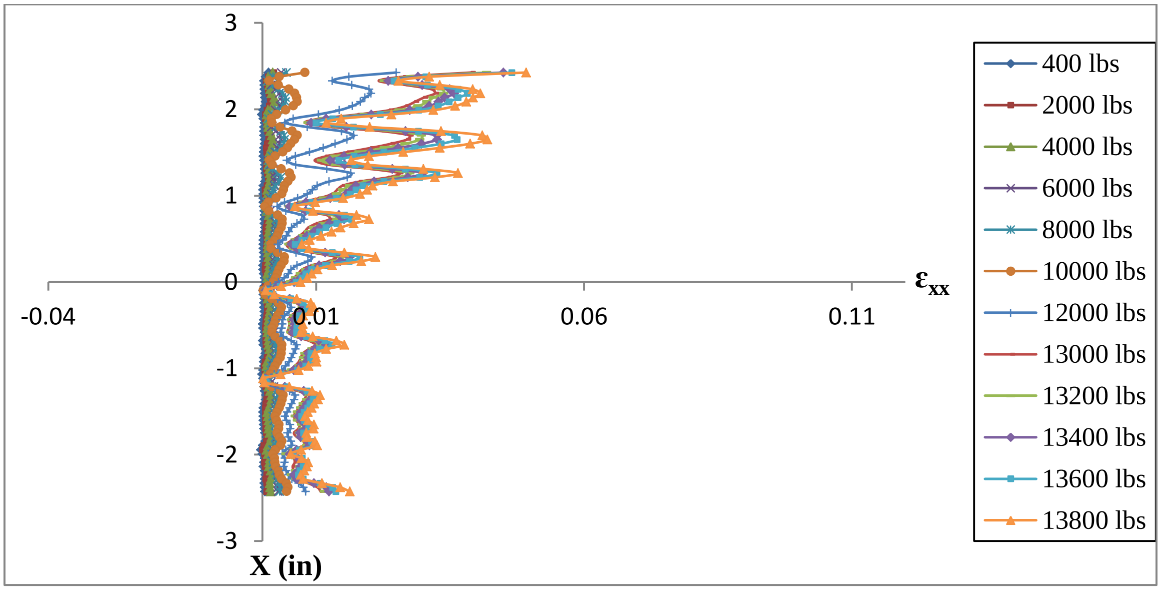

Figure 4-213: The strain distribution (ε_{xx}) along a cross section line (1-1)

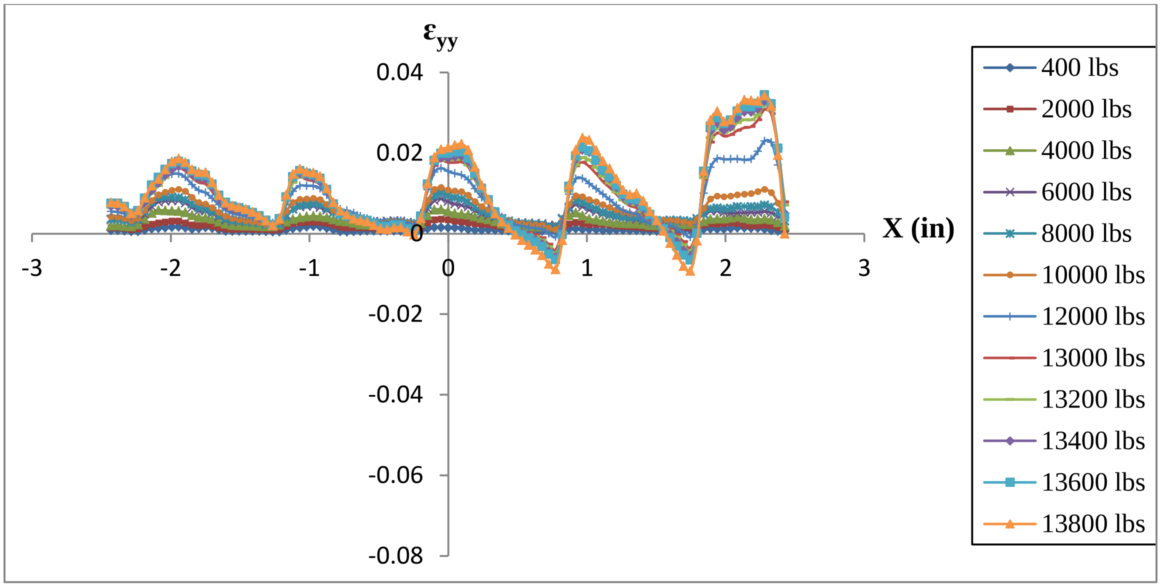

Figure 4-214: The strain distribution (ε_{yy}) along a cross section line (1-1)

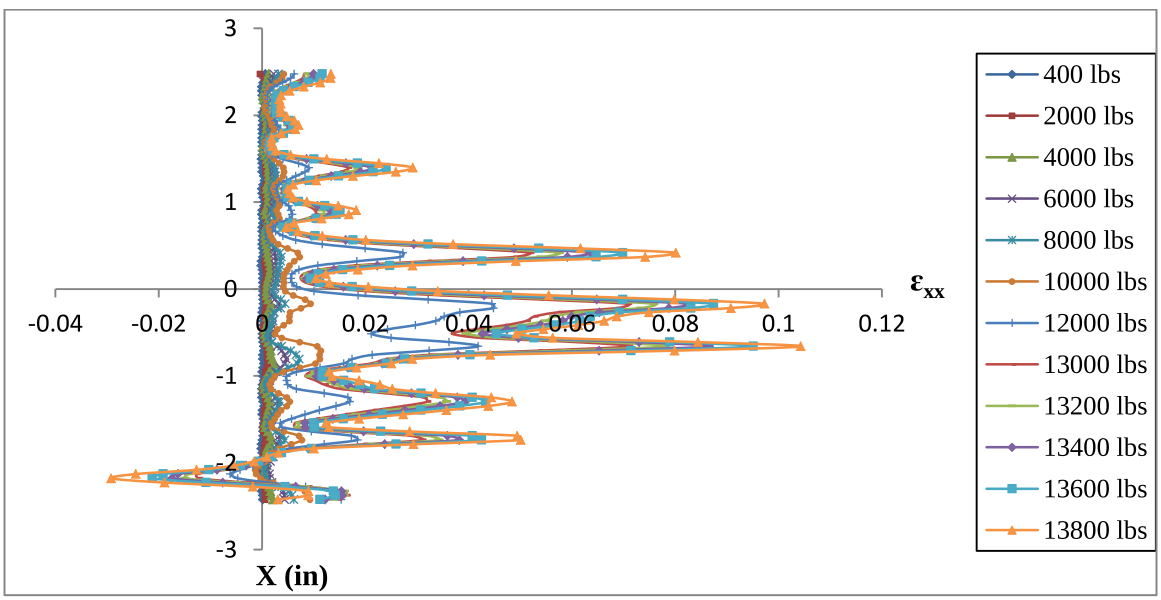

Figure 4-215: The strain distribution (ε_{xx}) along a cross section line (2-2)

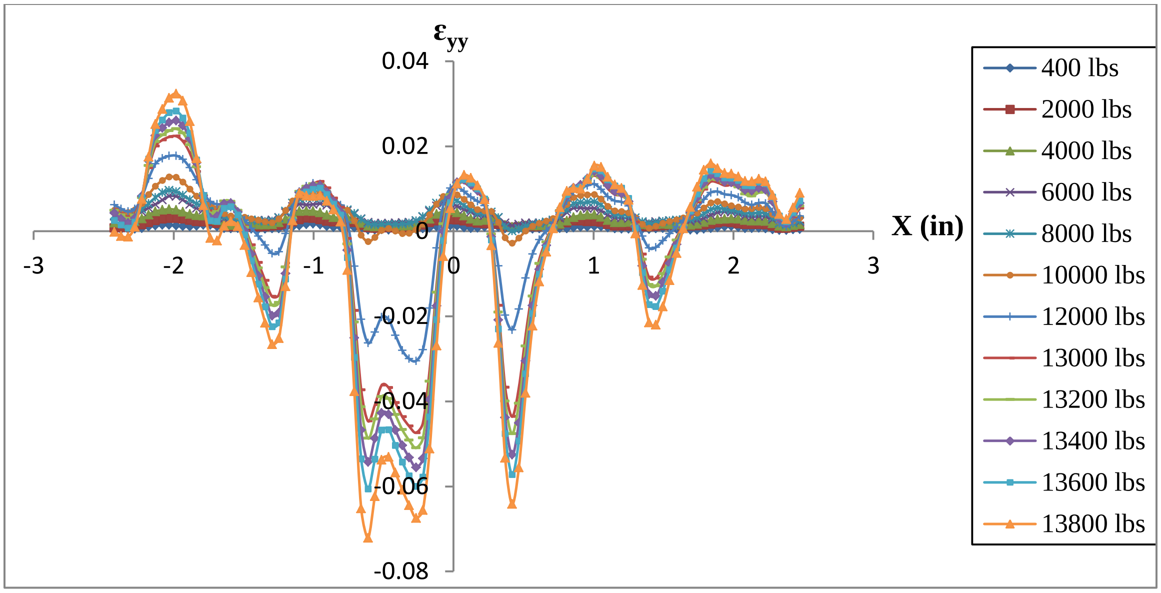

Figure 4-216: The strain distribution (ε_{yy}) along a cross section line (2-2)

The strain (ε_{xx}) at the cross section line (3-3) is very low; however, it increases from the right side of the plate to the left side as shown in Figure 4-217. The strain curve (ε_{xx}) shows repeated spikes which become significant at 10,000 pounds. The last strain curve at failure shows much larger spikes in strain values. These spikes in strain are due to the slot locations in the plate. The horizontal lines are taken from the right to the left through the little area between the adjacent slots; thus, the strain curve (ε_{xx}) changes significantly with loading.

Accompanied with each horizontal strain (ε_{xx}) curve, a vertical strain (ε_{yy}) is presented at the same horizontal line along the horizontal direction as shown in the previous figures. The strain (ε_{yy}) follows the strain (ε_{xx}) at these horizontal cross section lines. At cross section line (2-2) the strain (ε_{yy}) is also moving to higher compressive strain compared to the upper or the lower horizontal cross section line (1-1) and (3-3) respectively. The cross section line (3-3) does not show a significant change in the strain (ε_{xx}) or the strain (ε_{yy}).

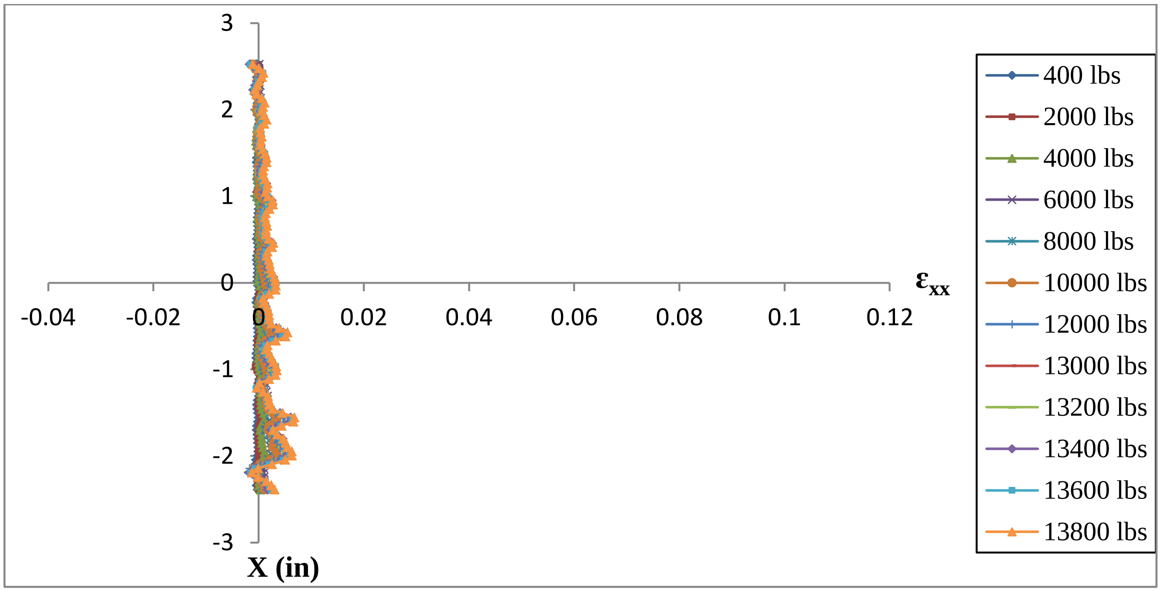

Figure 4-217: The strain distribution (ε_{xx}) along a cross section line (3-3)

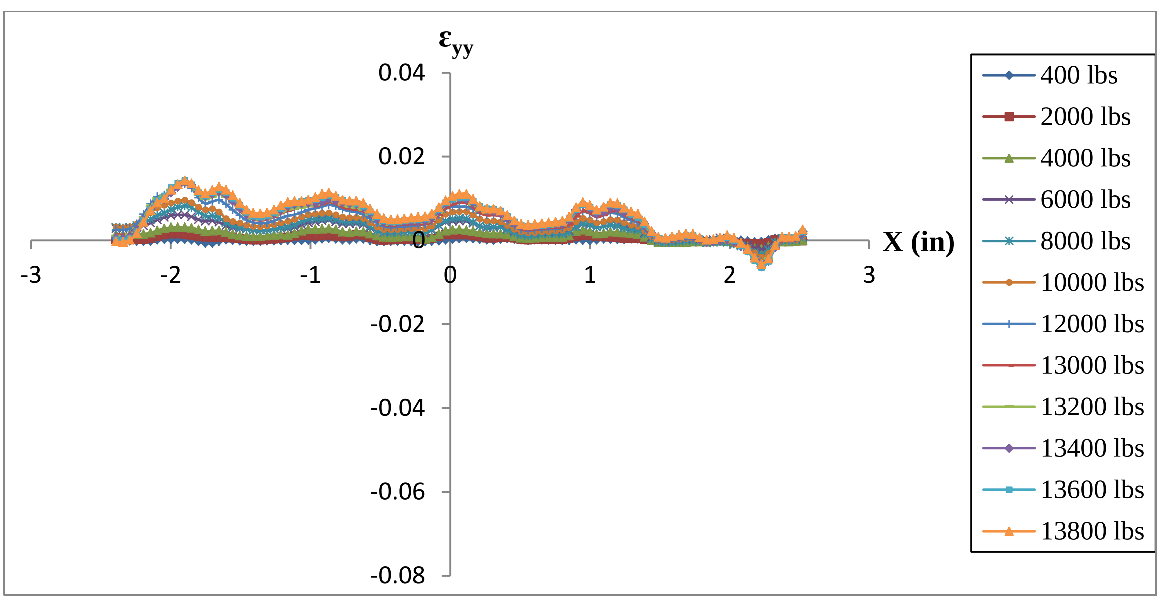

Figure 4-218: The strain distribution (ε_{yy}) along a cross section line (3-3)

4.2.1.4 The Truss Failure

The truss has failed at different places as shown in Figure 4-219.

Figure 4-219: The truss image after failure

Figure 4-219 shows that all the joints have failed. The left heel joint, where the speckled plate is located, is the worst failed joint. More detailed images for the three truss joints-plates are shown in Figures 4-220, 4-221 and 4-222.

The failure starts in the plate that is located on the top joint of the truss. A fracture (tear) starts from the bottom of the plate and increases with the load.

Figure 4-220: The left side heel joint-speckled plate just after failure

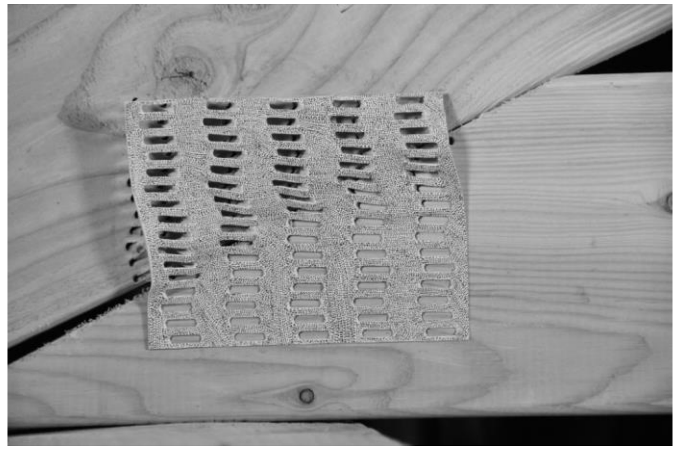

Figure 4-221: The plate on the top joint of the truss just after failure

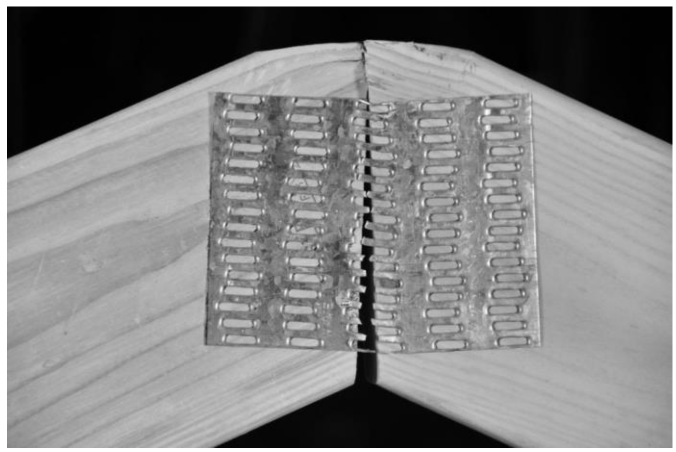

Figure 4-222: The right side heel joint- plate just after failure

When the top joint plate shows a fracture, the heel joints also show a failure. Some regions of the plates start to withdraw the teeth from the wood. The left heel joint-speckled plate shows a large area of the plate with tooth withdrawal. After that the truss fails and the earlier figures show the failure.

The top plate on the top joint starts to fracture as shown in Figure 4-221 from the bottom to the top of the plate. This shows that the place of the fracture is along the middle of the plate which has slots there. This area of the plate is half the surface area as places with no slots which makes it weaker and easier to crack than other places on the plate.

4.2.1.5 Summary of the 1st Heel Joint Test:

The strain curve at the vertical lines over the plate shows a tensile strain in both directions. The strain (ε_{xx}) and (ε_{yy}) is tensile strain from the beginning of loading until 10,000 pounds. That means the plate is stretching and expanding from both directions x and y. At 10,000 pounds the strain curves over the diagonal line, which is over the gap where the two members of wood are connected, shows a significant change in the strain values and the strain direction. At this load the strain (ε_{xx}) shows higher tensile strain in that region than the previous loading case; however, the strain (ε_{yy}) turns to compressive strain and its values increase with loading. The middle area of the plate is affected more by the loading than the right or the left area of the plate. The plate follows the principle: when a deformable body is subjected to a force, it will elongate in one direction and contract in the other. the strain (ε_{xx}) and (ε_{yy}) has the same case which is tensile. This result is due to the presence of the teeth which makes a shear stress over the entire plate.

The strain (ε_{xx}) in the horizontal direction shows very small strain values (ε_{xx}) in the lower areas of the plate than the middle or the top area. In general, the strain (ε_{xx}) below the diagonal line over the gap where the two wood members are connected is low comparing to the other strain values on the plate’s surface. The strain (ε_{xx}) at the diagonal line significantly increases after applying 10,000 pounds and it continues to increase until failure. The general (ε_{xx}) is tensile strain with some exceptions around the teeth and plate withdrawal regions.

4.2.2 Heel Joint- Second Test

In this test, the truss was set on the universal testing machine and the camera was placed on a fixed place in front of the speckled plate that was located on the left heel joint. The first image before loading was captured as a reference image Figure 4-223.

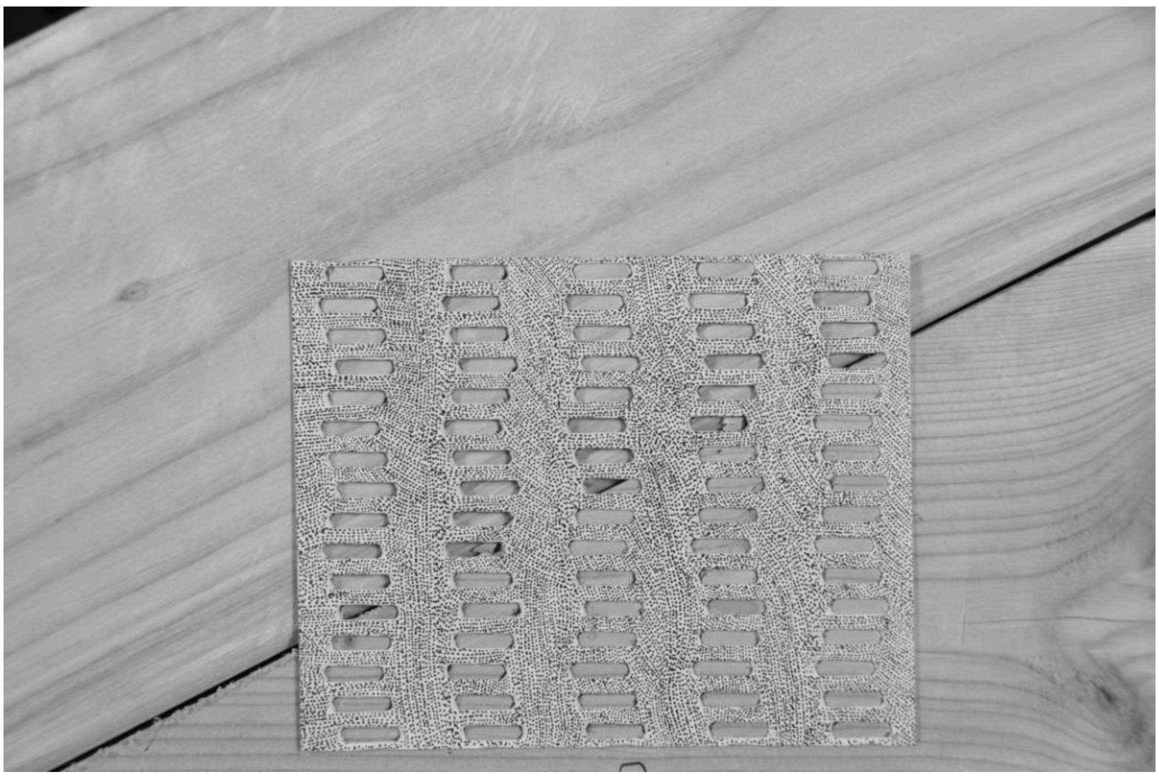

Figure 4-223: The reference image in the second heel joint test

A total of 54 images were captured for this test besides the reference image. The truss failed at load equal to 10,800 pounds. All the captured images were implemented in DIC software to find the full-field strain measurements.

4.2.2.1 Full-Field Strain Measurements Results Using DIC Software

The full-field strain measurements were obtained for the plate using the DIC software. A total of 54 images were implemented in the DIC software to find the full-field strain measurements in the horizontal and vertical direction. Figure 4.224 shows the strain in y-direction (ε_{yy}) for the first image at 200 pounds.

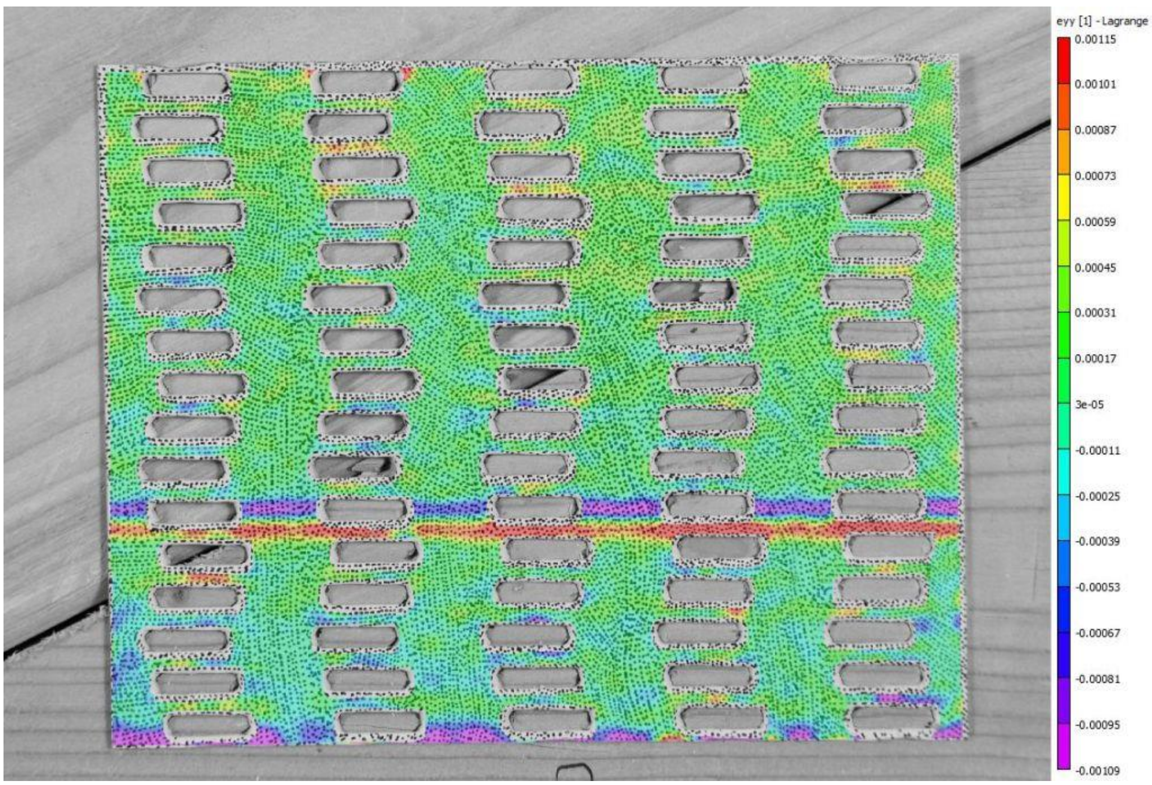

Figure 4-224: Full-field strain measurements (ε_{yy}) for the MPC after applying 200 pounds

The last image shows the strain (ε_{yy}) is almost equally distributed over the surface of the plate with certain exceptions. The dominant strain is positive which means a tensile strain. Increasing the load causes the strain (ε_{yy}) to increase and change throughout the plate. A significant change in strain (ε_{yy}) is shown after applying 9,000 pounds. Figure 4-225 shows the strain at 9,000 pounds.

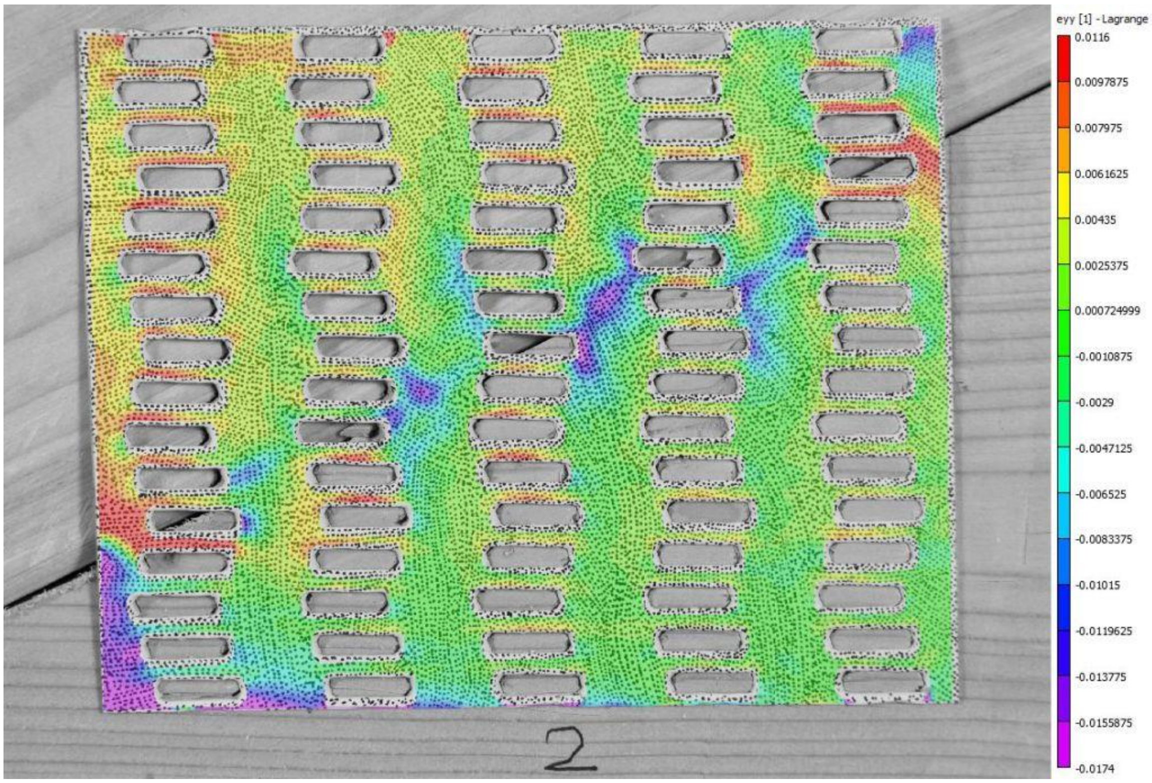

Figure 4-225: Full-field strain measurements (ε_{yy}) for the MPC after applying 9,000 pounds

The previous strain image shows low compressive strain (ε_{yy}) along the diagonal line that is located over the gap between the two connected wood members. The dominant strain (ε_{yy}) on the remaining plate's surface is tensile. The plate is influenced by tooth withdrawal on the left side of the plate and some limited area on the right side of the plate. The large changes in the strain (ε_{yy}) behavior are evident after applying 9,000 pounds until the failure at 10,800 pounds and comparing to the earlier strain-images. The strain (ε_{yy}) images show that the area of the plate under the diagonal line, over the gap between the two connected wood members, is moving to the right. The upper area of the plate above the diagonal line is moving to the left. The area around the diagonal line is twisting with loading until failure occurs. The strain (ε_{yy}) behavior before the failure at 10,600 pounds is shown in Figure 4-226.

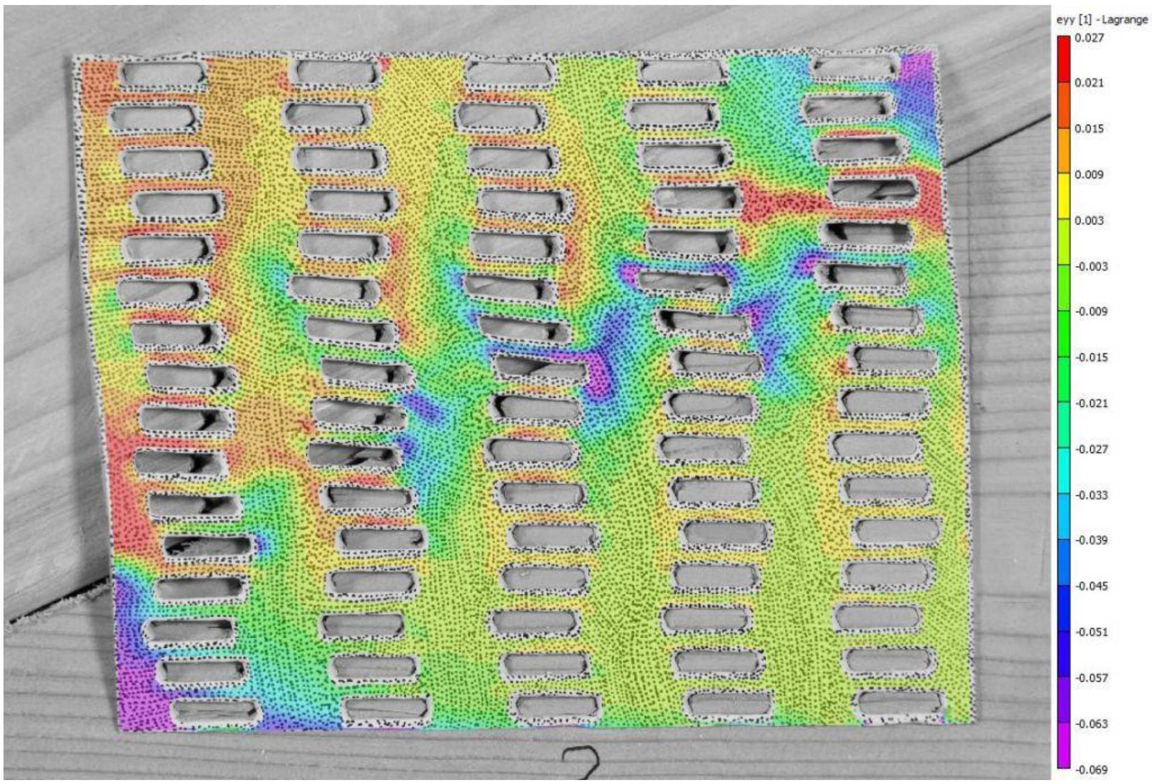

Figure 4-226: Full-field strain measurements (ε_{yy}) for the MPC after applying 10,600 pounds

The diagonal strain (ε_{yy}) is negative. The image clearly shows the twisting of the slots around the diagonal line. The left side of the plate also shows tooth withdrawal. The vertical strain (ε_{yy}) is tensile unless there is tooth withdrawal or pulling out of the plate especially from the edges. The full-field strain (ε_{yy}) behavior for the image at failure is shown in Figure 4-227. When the load is increased from 10,600 pounds to 10,800 pounds, the failure is observed on the plate. The plate fails due to tooth withdrawal for the area of the plate that is above the diagonal line. The twisting in the slots around the diagonal line is evident. The area of the plate that is underneath the diagonal line is not influenced by tooth withdrawal except the bottom left side of the plate.

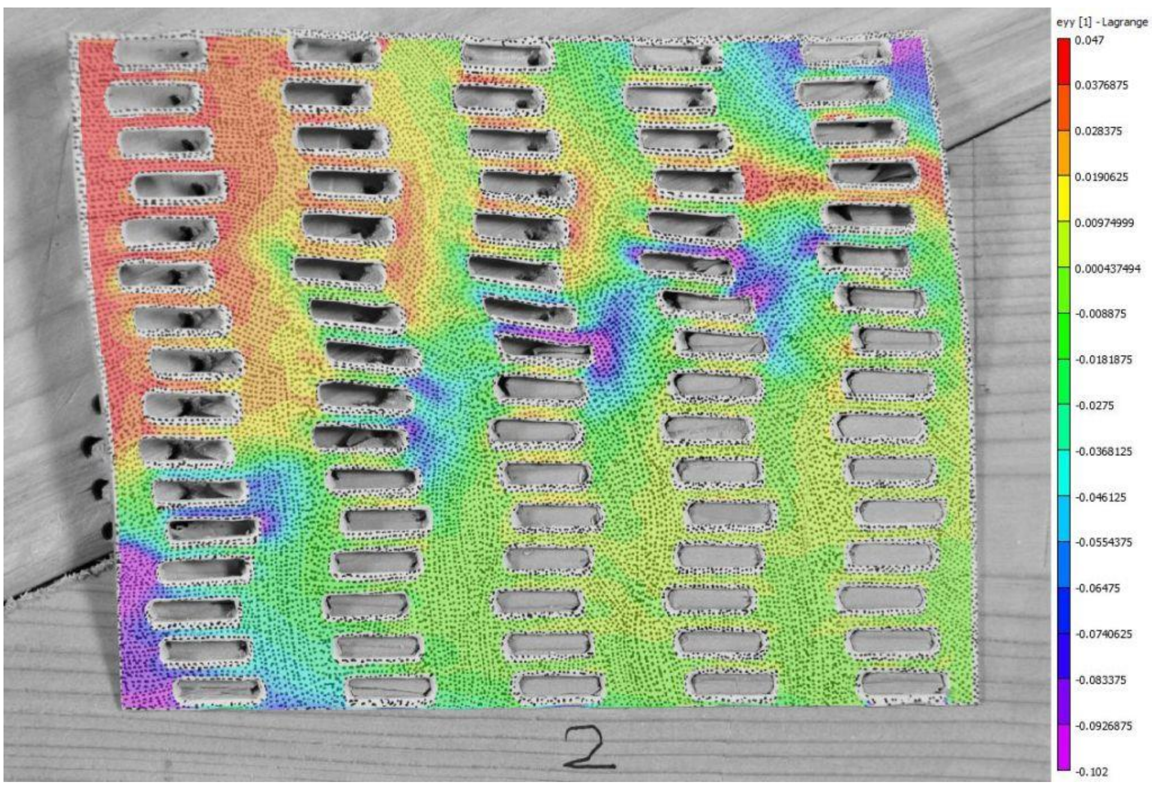

Figure 4-227: Full-field strain measurements (ε_{yy}) for the MPC at failure at 10,800 pounds

On the other hand, the full-field strain measurements in x-direction (ε_{xx}) can also be obtained from digital image correlation software. The next Figure 4-228 shows the strain (ε_{xx}) after applying 200 pounds. The strain (ε_{xx}) at 200 pounds is very low and holds negative and positive values.

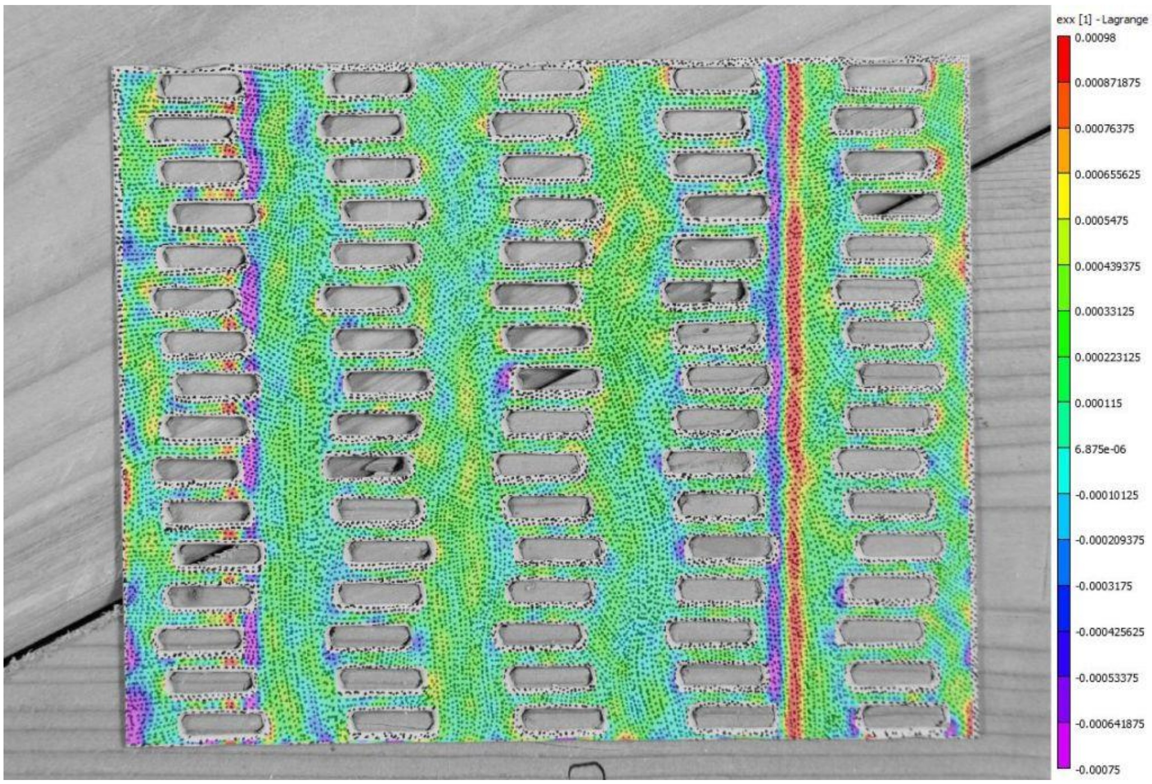

Figure 4-228: Full-field strain measurements (ε_{xx}) for the MPC after applying 200 pounds

After increasing the load, the strain (ε_{xx}) increases and changes its behavior. A significant change in the strain (ε_{xx}) is shown after applying 9,000 pounds as shown in Figure 4-229. The strain (ε_{xx}) along the diagonal line over the diagonal gap is high tensile strain while the strain (ε_{xx}) above and below the diagonal gap is very low compared to the tensile strain along the diagonal gap strain. Some high tensile strain also shows on the left end edge of the plate due to moving of the area of the plate above the diagonal gap to the left with twisting, which leads to tooth withdrawal at the edge. The strain (ε_{xx}) over the plate after applying 9,000 pounds is tensile with certain limited exceptions due to the moving of the plate's areas in different directions.

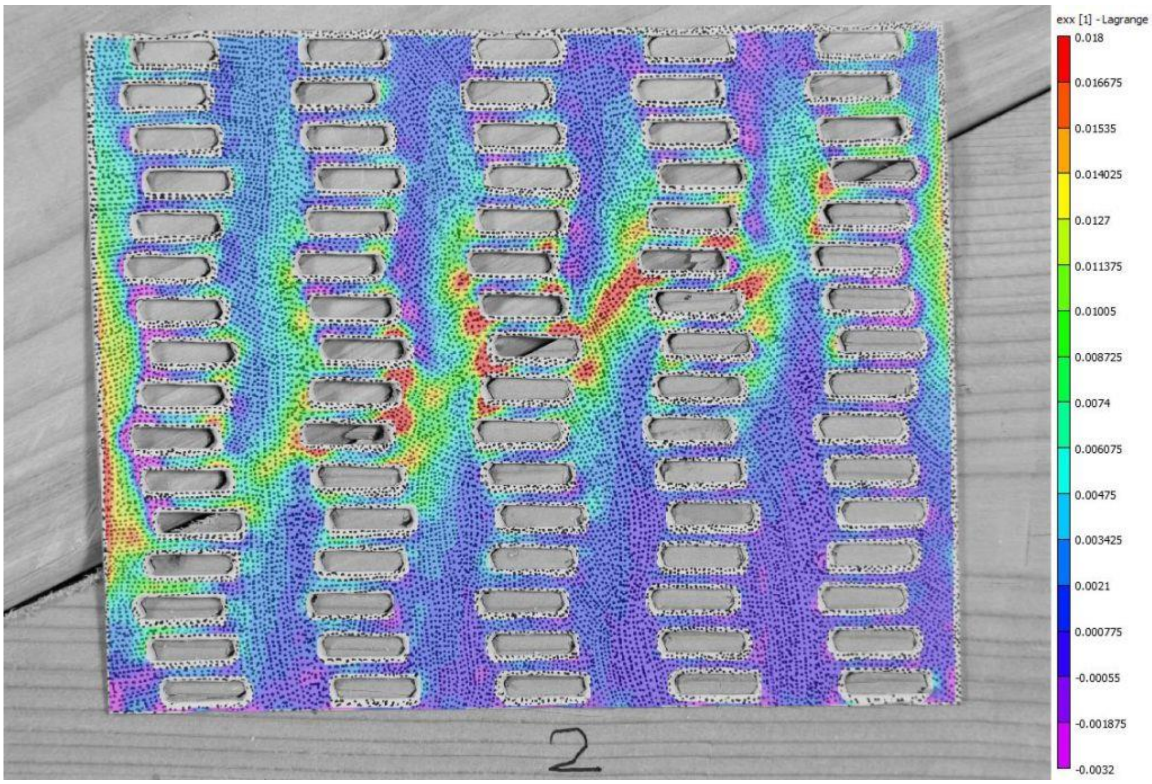

Figure 4-229: Full-field strain measurements (ε_{xx}) for the MPC after applying 9,000 pounds

The strain (ε_{xx}) after 9,000 pounds exhibits a significant influence by loading. The strain (ε_{xx}) increases with loading until failure at a load 10,800 pounds. Figure 4-230 and 4-231 shows the strain (ε_{xx}) behavior before and at failure respectively. The strain (ε_{xx}) before failure at a load 10,600 pounds is clearly influenced by a twisting in the plate's area along the diagonal gap line. The strain (ε_{xx}) there is higher than any other strain on the plate's surface. The area of the plate that is underneath the diagonal gap is influenced by lower strain (ε_{xx}) values than the area above the diagonal gap. By loading, the left end edge of the plate tends to have low compressive strain due to tooth withdrawal at the left side of the plate.

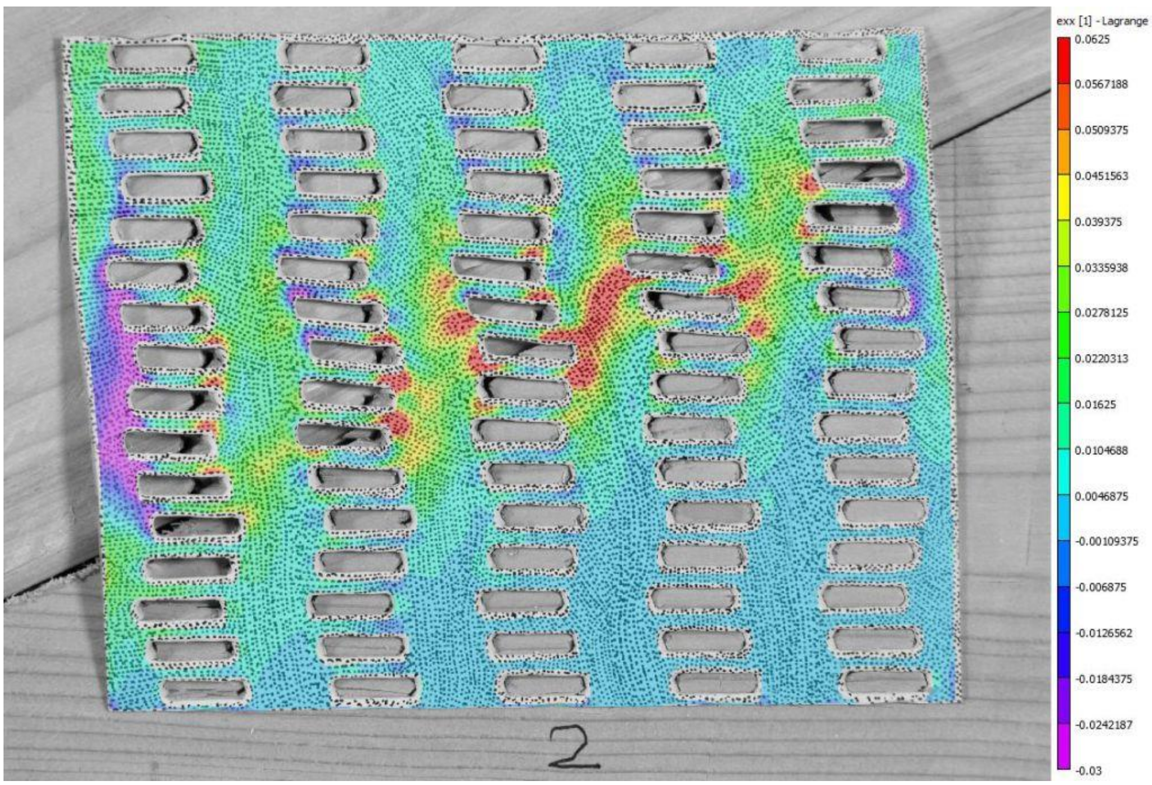

Figure 4-230: Full-field strain measurements (ε_{xx}) for the MPC after applying 10,600 pounds

The strain (ε_{xx}) behavior at failure is shown in Figure 4-231. The above part of the plate over the diagonal gap is completely influenced by tooth withdrawal. The strain (ε_{xx}) at that area is turning to compressive strain. The area of the plate underneath the diagonal gap remains tensile strain with values less than the tensile strain (ε_{xx}) values along the diagonal gap.

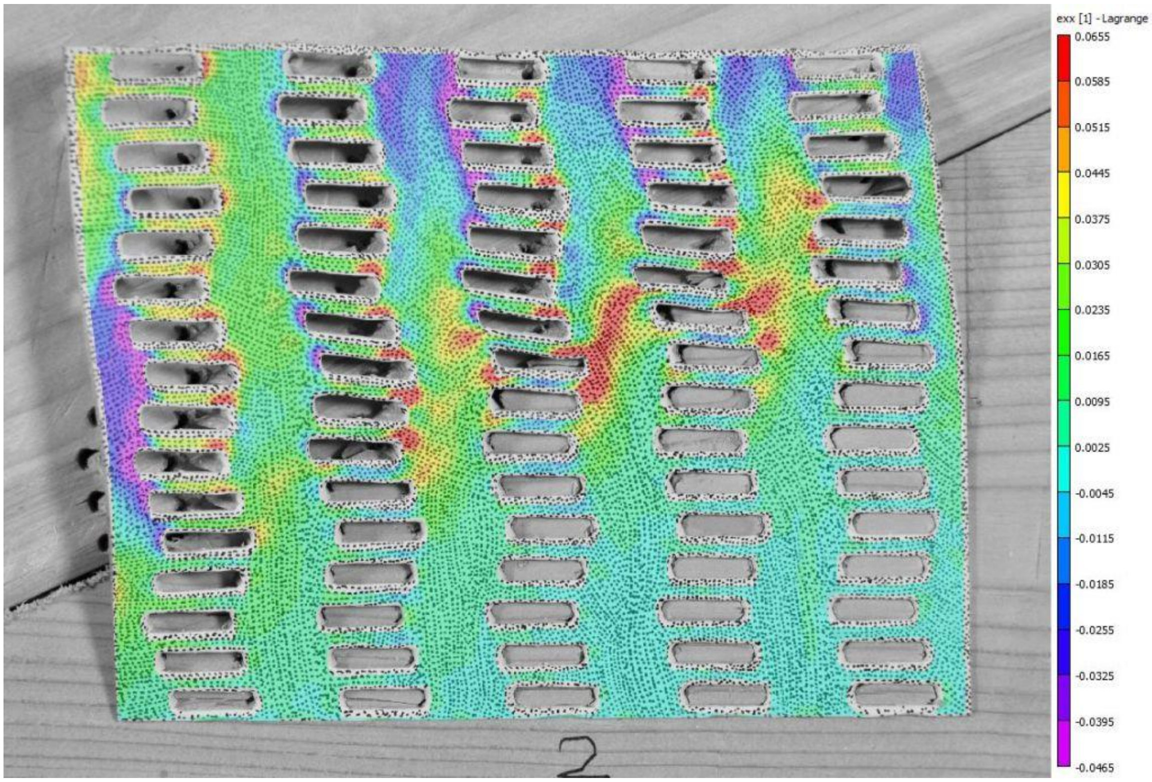

Figure 4-231: Full-field strain measurements (ε_{xx}) for the MPC at failure at 10,800 pounds

4.2.2.2 Numerical Analysis for the Vertical Strain Results

To analyze the DIC results numerically, a vertical cross section line from the top of the plate to the bottom is taken for some images starting with the first image at 200 pounds and ending with the last image at failure. The cross section is taken in four different locations as shown in Figure 4-232.

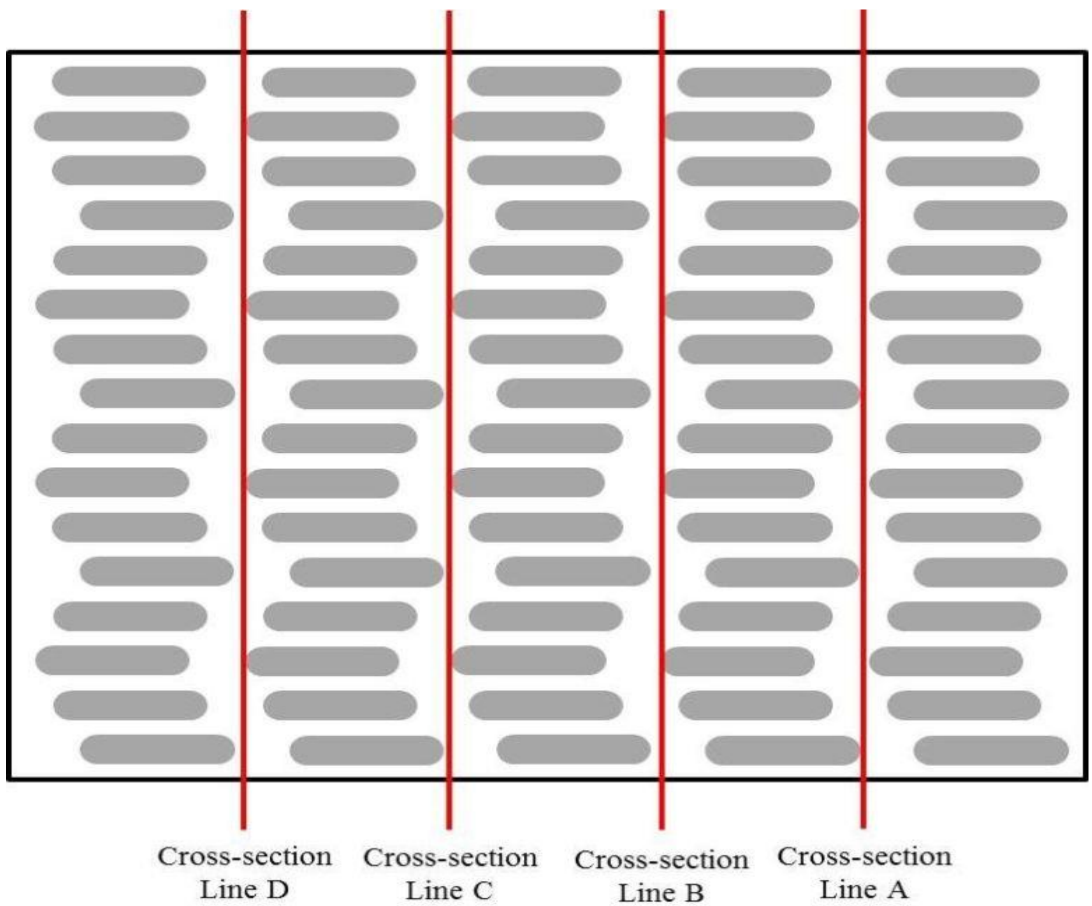

Figure 4-232: Metal plate with the cross-section lines along the vertical direction

The cross section is taken in four different locations:

- The first cross section is from the right side of MPC @ x = 1.71 in. cross-section A-A.
- The second cross section is @ x = 0.68 in. cross-section B-B.
- The third cross section is @ x = -0.254 in. cross-section C-C.
- The fourth cross section line is from the left side of MPC @ x= -1.31 in. cross-section D-D.

Four cross-section lines are taken for the strain field (ε_{yy}). The next figures show the distribution of strain (ε_{yy}) accompanied with (ε_{xx}) at the same cross section line at four different locations for 12 images. Each image represents the value of the loading that is applied on the specimen of simple truss.

The curves show that the first considered load is 400 pounds then a different increment of loading is used to show the MPC behavior until failure. In general, the strain (ε_{yy}) shows very close strain results and almost equally distributed strain over the entire plate with certain exceptions from the beginning of the test until 9,000 pounds of loading. At 9,000 pounds the plate's strain behavior shows some changes in the strain values over some limited plate's region. The large changes in the strain are limited to that region which is over the diagonal gap between the two connected wood members. The dominant strain (ε_{yy}) is tensile and it increases with loading throughout the test.

The strain (ε_{yy}) in Figure 4-232 shows the right side behavior of the MPC under loading at section (A-A). In this figure, the strain (ε_{yy}) is almost equally distributed from the top to the bottom of the plate along the cross section line (A-A). The strain (ε_{yy})

slightly increases from a load of 200 pounds up to a load of 9,000 pounds. At that load the strain (ε_{yy}) curve shows significant changes as some strain regions turn to negative strain and other regions move up as a tensile strain. As the load increases from 9,000 pounds to the failure at 10,800 pounds, the top region of the plate above the diagonal gap is influenced by a compressive strain (ε_{yy}) then it rises up as a tensile strain. The region around the diagonal gap is influenced by a large compressive strain (ε_{yy}) as shown in Figure 4-232. The lower area of the plate underneath the diagonal gap is influenced by a tensile strain (ε_{yy}). The strain (ε_{xx}) in Figure 4-233 over the same cross section line (A-A), significantly increases at a load of 9,000 pounds. The strain (ε_{xx}) is tensile along the cross section line (A-A). The strain curves after a load 9,000 pounds until failure shows a significant increase in the tensile strain (ε_{xx}) especially in the area around the diagonal gap. The strain (ε_{xx}) underneath the diagonal gap is very low compared to the values of the strain around the diagonal gap. The strain (ε_{xx}) underneath the diagonal gap is almost equally distributed without big spikes and significant changes in the strain curves.

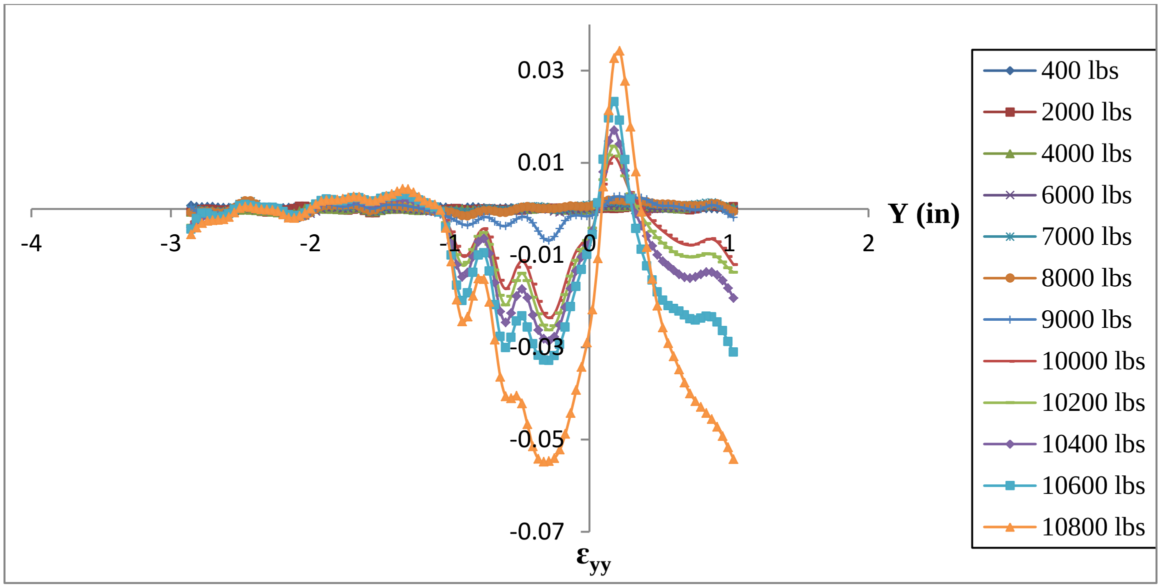

Figure 4-233: The strain distribution (ε_{yy}) along a cross section line (A-A) located on the right side of the plate

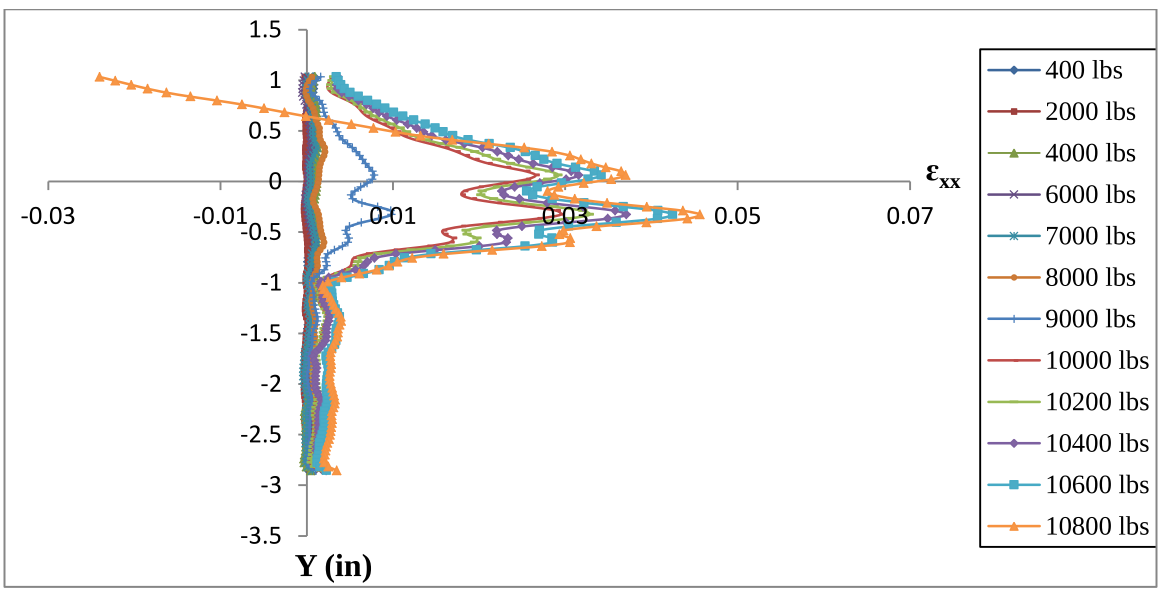

Figure 4-234: The strain distribution (ε_{xx}) along a cross section line (A-A) located on the right side of the plate

The next four strain curves show the strain (ε_{yy}) and (ε_{xx}) at the two middle cross section lines (B-B) and (C-C). The strain (ε_{yy}) shows almost equally distributed strain along the vertical cross section lines (B-B) and (C-C) starting from a load 400 pounds until a load 9,000 pounds. The strain curve (ε_{yy}) shows slight increase in the strain from the beginning of loading until a load 9,000 pounds. The strain (ε_{yy}) is tensile strain with certain limited exception area due to pulling out of the plate. At a load of 9,000 pounds the curves of strain (ε_{yy}) show a slight increase in the tensile strain and also higher decrease in the strain curve in some regions along the diagonal gap. The strain (ε_{yy}) around these regions is compressive. As the load increases from a load of 9,000 pounds until the failure at a load of 10,800 pounds, the compressive strain curves along the diagonal gap significantly increases as shown in the figures. The strain curve at failure shows some regions have higher tensile strain than the pre-strain curve at 10,600 pounds. This behavior is due to the complete failure that occurs for the plate in which the area of the plate above the diagonal gap is completely influenced by tooth withdrawal. The strain curves (ε_{yy}) along the cross section line (C-C) are less affected by loading than the strain curves along cross section line (B-B).

On the other hand, the horizontal strain (ε_{xx}) along the vertical direction is tensile from the beginning of the test until the failure with certain limited exceptions. The strain (ε_{xx}) is low and almost equally distributed along the vertical line from the top to the bottom until the load of 9,000 pounds at which point there is a significant increase in the tensile strain (ε_{xx}) over the same limited area in which strain (ε_{yy}) is a compressive strain. After applying 9,000 pounds until the failure at 10,800 pounds the strain (ε_{xx}) over the limited area, which is located at the diagonal gap, significantly increases as a tensile strain (ε_{xx}) as shown in the figures especially along the cross section line (B-B).

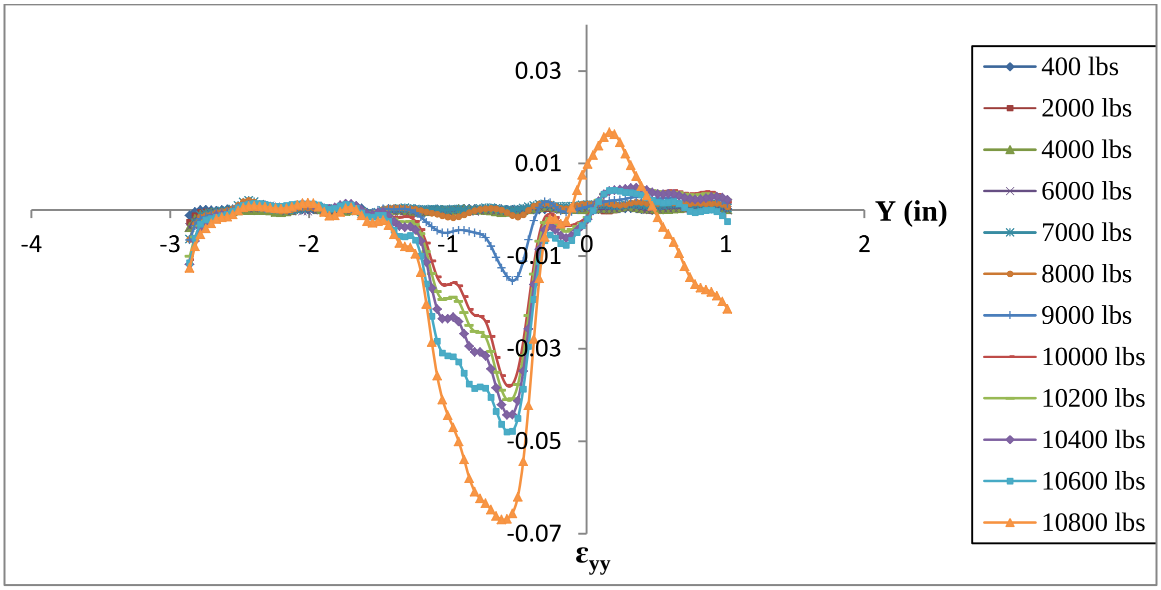

Figure 4-235: The strain distribution (ε_{yy}) along a cross section line (B-B)

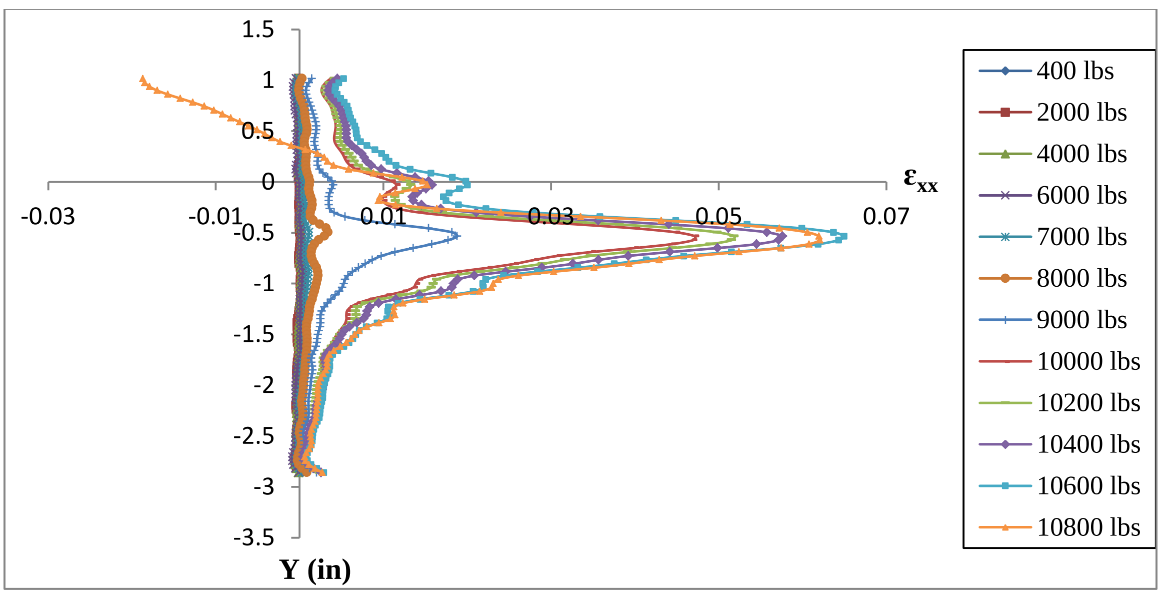

Figure 4-236: The strain distribution (ε_{xx}) along a cross section line (B-B)

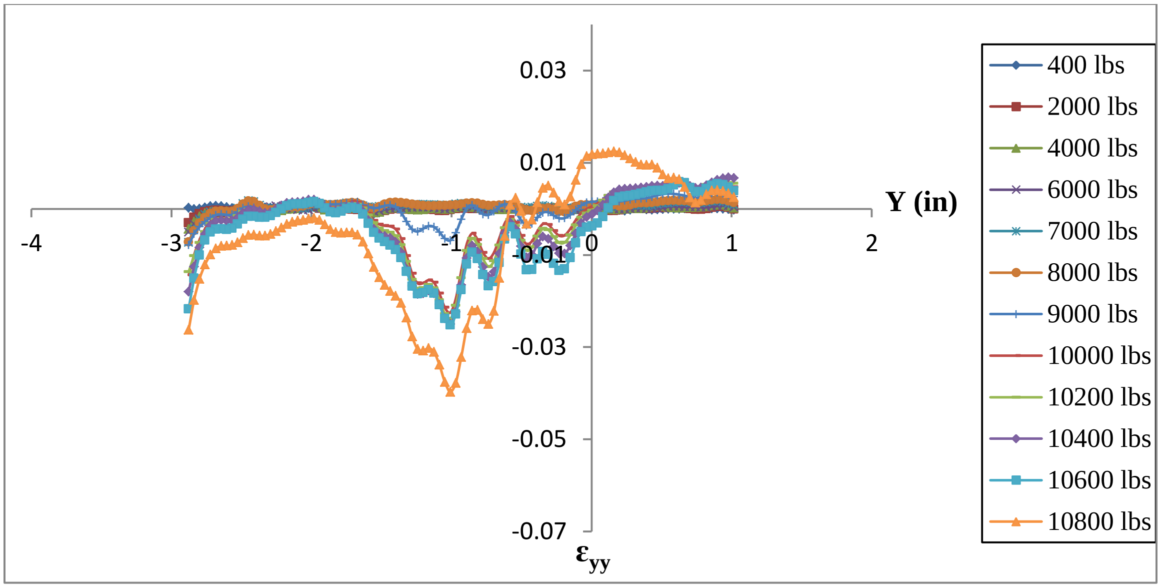

Figure 4-237: The strain distribution (ε_{yy}) along a cross section line (C-C)

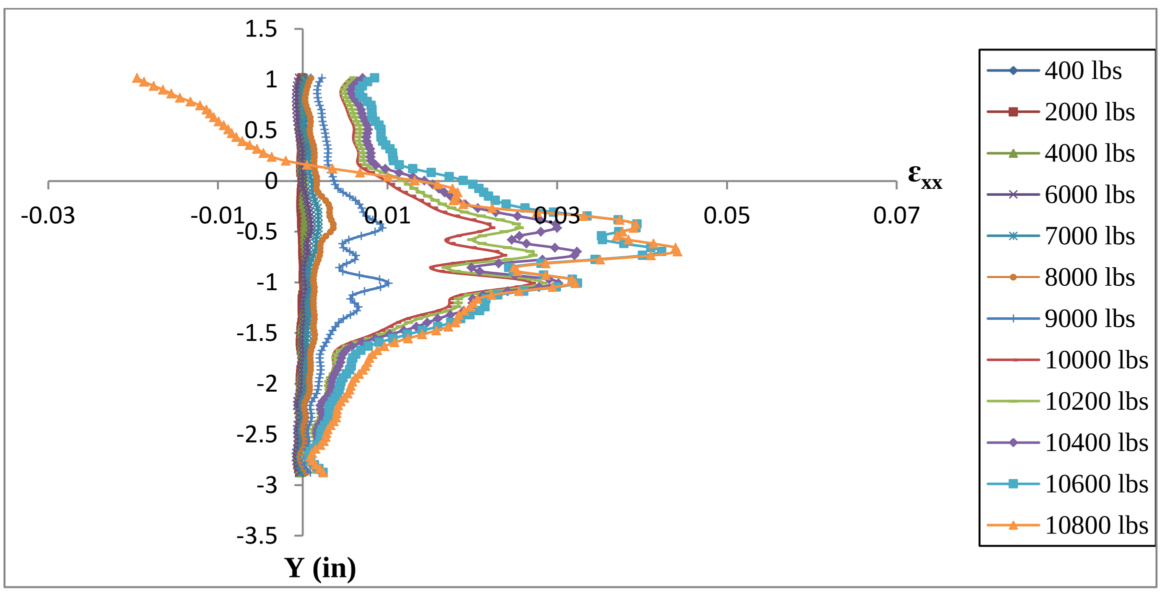

Figure 4-238: The strain distribution (ε_{xx}) along a cross section line (C-C)

The covered region is also extended with loading. Therefore, after applying a load of 9,000 pounds, the strain (ε_{xx}) is tensile and highest at the diagonal gap while the strain (ε_{yy}) is a compressive with and highest at the diagonal gap. The strains are very low compressive and tensile on the remaining regions of the plate. This strain distribution results since not all of the plate areas are influenced with the load and not all of the plate regions have yielded. Some regions on the plate are not near yield point. The cross section line (B-B) is affected by loading more than the cross section line (C-C).

Figures 4-239 and 4-240 show the strain (ε_{xx}) and (ε_{yy}) along the vertical cross section line (D-D) located on the left side of the plate. In this cross section line, the strain (ε_{yy}) slightly increases until a load of 9,000 pounds at which point the strain (ε_{yy}) curve changes from tensile strain (ε_{yy}) to compressive strain in the region of the diagonal gap. From a load of 9,000 pounds to a load of 10,800 pounds, the compressive strain (ε_{yy}) significantly increases and the bottom edge of the plate is also influenced by higher compressive strain. The strain (ε_{yy}) turns to compressive strain over the diagonal line between the two connected members of wood. The strain is compressive over the area that is influenced by tooth withdrawal at the edge of the plate.

The strain (ε_{xx}) along the cross section line (D-D) is tensile. The strain (ε_{xx}) is low starting from a load of 400 pounds and slightly increases with loading until a load of 9,000 pounds. From a load of 9,000 pounds until failure at a load of 10,800 pounds, the strain (ε_{xx}) significantly increases along the diagonal gap.

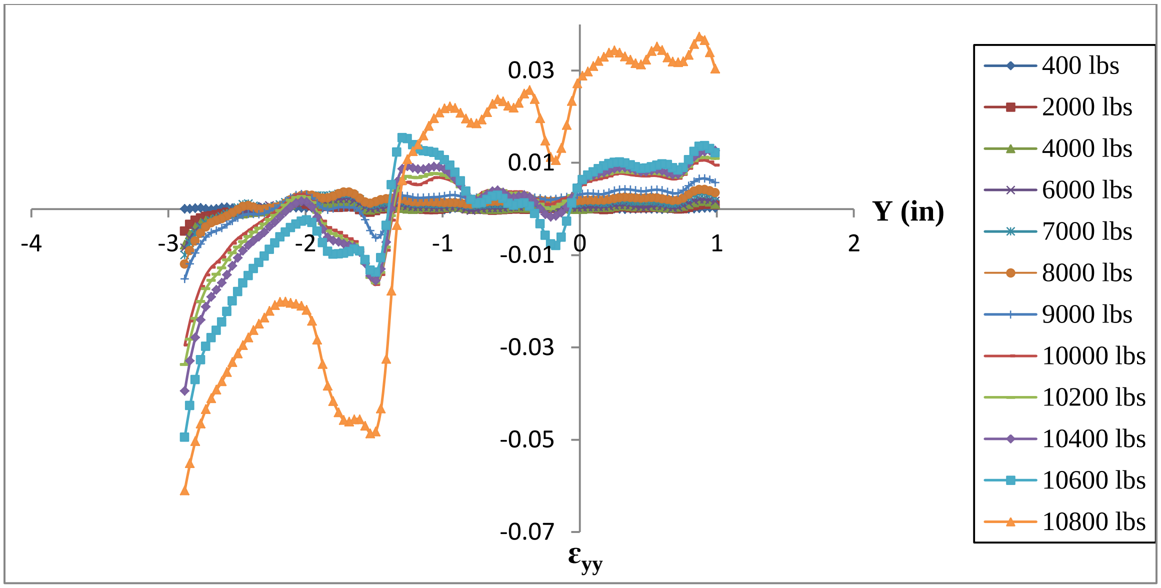

Figure 4-239: The strain distribution (ε_{yy}) along a cross section line (D-D) located on the left side of the plate

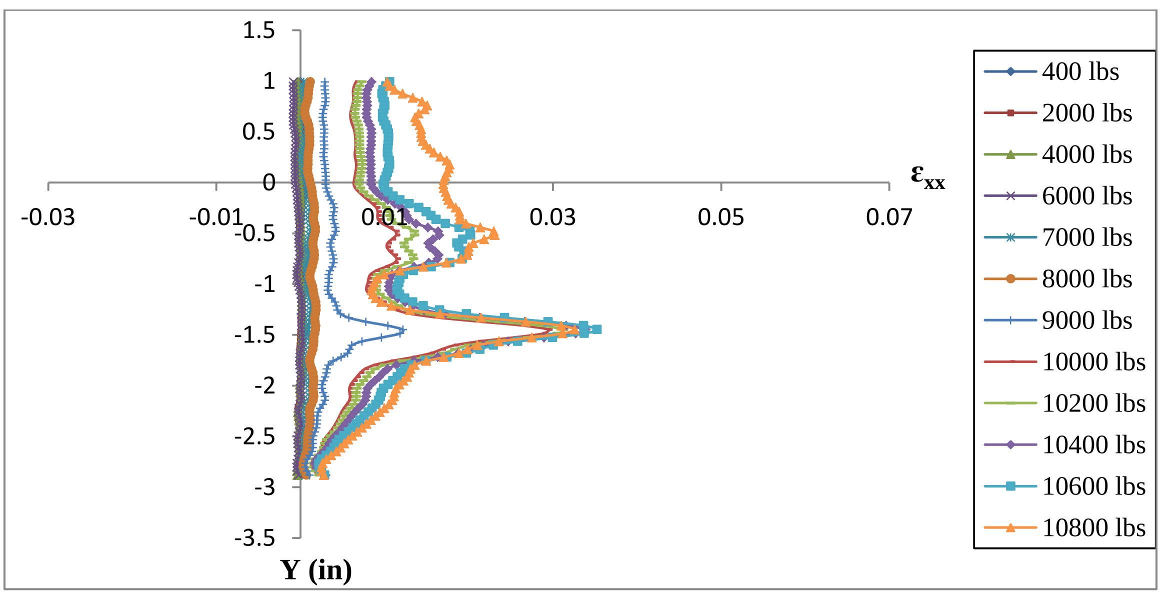

Figure 4-240: The strain distribution (ε_{xx}) along a cross section line (D-D) located on the left side of the plate

4.2.2.3 Numerical Analysis along the Horizontal Strain Results

To analyze the DIC results numerically, horizontal cross section lines from the right side to the left side the plate are taken for some images starting with the first image at a load of 200 pounds and ending with the last image at failure. The cross section is taken in three different locations.

- The first cross section is on the top of MPC @ y = 0.812 in. cross-section line 1-1.
- The second cross section is near the middle of the MPC @ y = -0.921 in. cross-section line 2-2.
- The third cross section is bottom of MPC @ y = -2.659 in. cross-section line 3-3.

Figure 4-241 shows the cross section lines on the metal plate

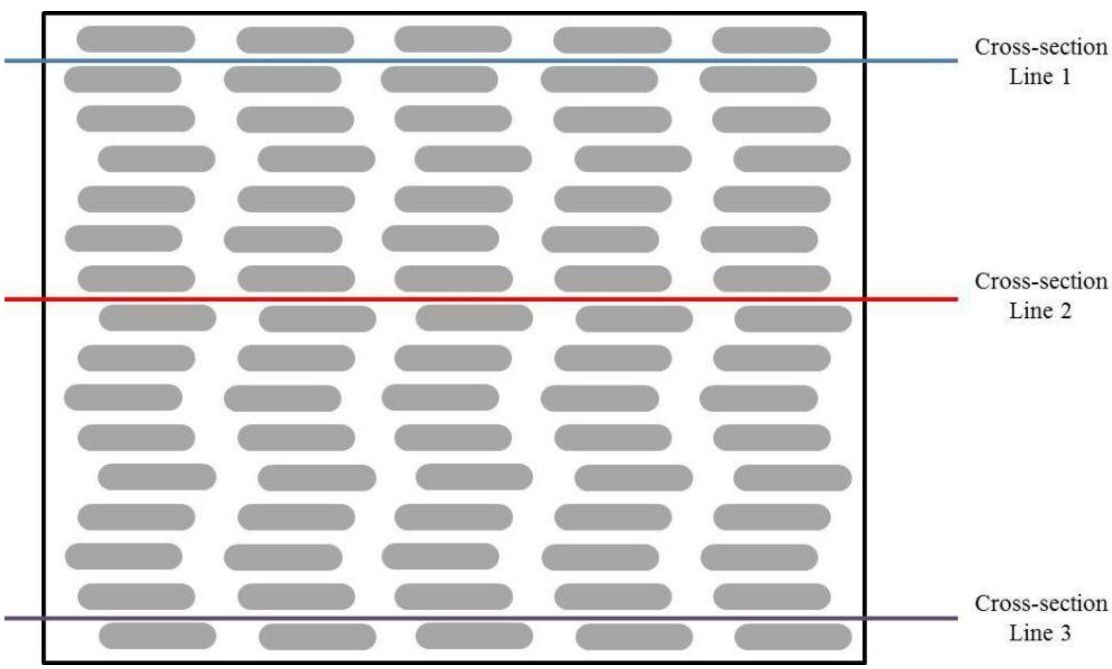

Figure 4-241: Metal plate with the cross-section lines along the horizontal direction

Three cross-section lines are taken for the strain field (ε_{xx}). The next figures show the distribution of strain (ε_{xx}) accompanied by (ε_{yy}) at the same cross section line at three different locations for 12 images. Each image represents the value of the loading that is applied on the specimen of simple truss.

The curves show that the first considered load is 400 pounds then a different increment of loading is used to show the MPC behavior until failure. In general, the strain (ε_{xx}) shows very close low strain values and almost equally horizontally distributed strain with some exceptions from the beginning of the test until a load of 9,000 pounds. From a load of 400 pounds until a load of 9,000 pounds, the strain (ε_{xx}) is low and spikes along the horizontal line. The strain sign is positive and negative; therefore, it is compressive and tensile at the same horizontal cross section line. The strain is close to zero. The strain (ε_{yy}) varies similar to the strain (ε_{xx}) along the horizontal line. This sudden change in the strain values and direction is due to many factors such as the presence of slots in the plate where teeth have been punched out. The presence of teeth which create a shear force depending on the angle of each tooth is also another factor that can make these sudden changes in the strain values and the plate's behavior.

At high loading after applying a load of 9,000 pounds, the plate strain behavior shows some changes in the strain values over some limited plate's region. The strain at the top of the plate at cross section (1-1) shows tensile strain all above the horizontal line except two regions which show compressive strain. Then from a load of 9,000 pounds until failure at a load of 10,800, the strain (ε_{xx}) increases as a tensile.

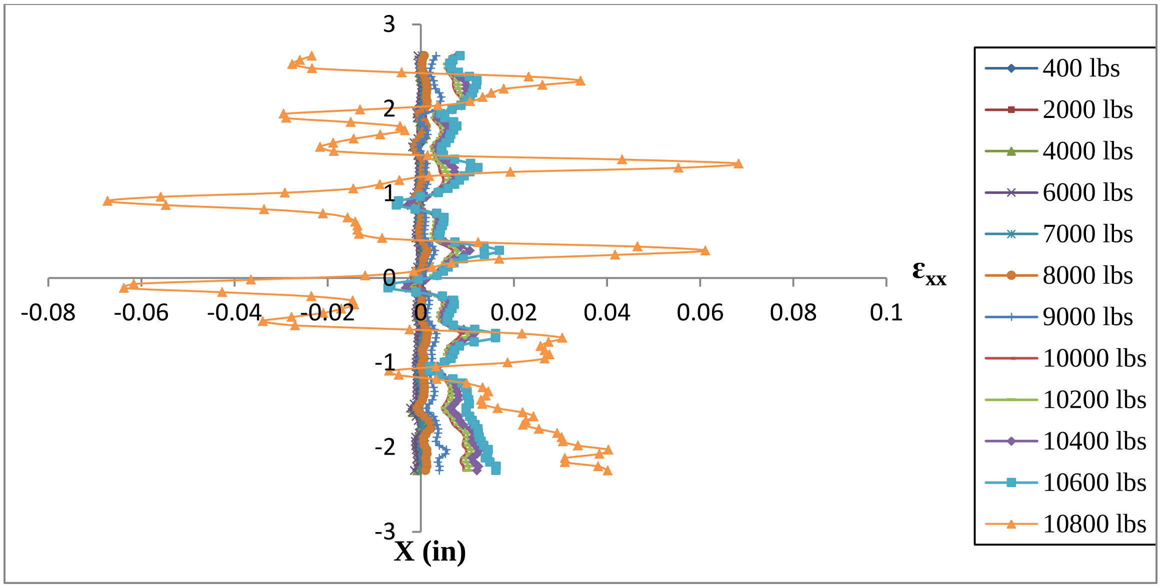

Figure 4-242: The strain distribution (ε_{xx}) along a cross section line (1-1)

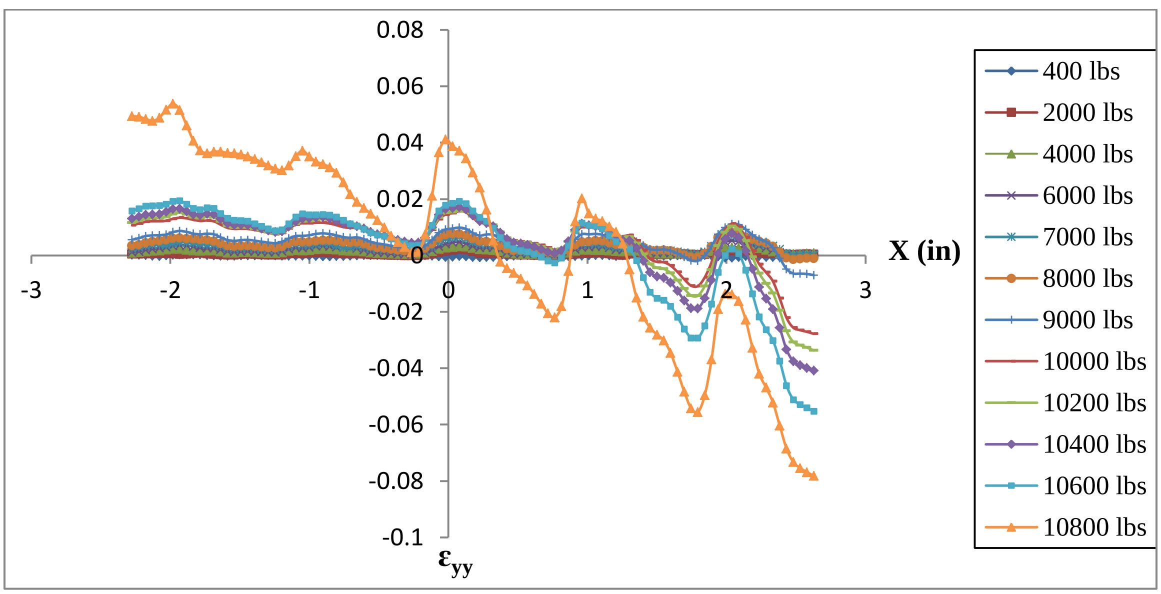

Figure 4-243: The strain distribution (ε_{yy}) along a cross section line (1-1)

The failure strain images show high compressive and tensile strain (ε_{xx}) and it is different from the prior strain behavior images at 10,600 pounds. This sudden change in strain behavior is due to the complete failure of the plate due to complete tooth withdrawal at that region. The strain (ε_{yy}) along the cross section line (1-1) also changes up and down. The strain (ε_{yy}) as a tensile starts from a load of 400 pounds and continues to a load of 9,000 pounds at which point strain (ε_{yy}) is a tensile strain; however, there is some compressive strain on some regions of the plate. Under load the strain (ε_{yy}) increases as a tensile and a compressive strain. The right side of the upper region of the plate is influenced by a compressive strain and the left side is influenced by a tensile strain (ε_{yy}). Thus, the right side of the cross section line at high loading is influenced by a tensile strain (ε_{xx}) and compressive strain (ε_{yy}); however, the left side is influenced by tensile (ε_{xx}) and (ε_{yy}). The effect of the shear stress from the teeth on the left side on the plate is more than the effect on the right side.

The strain (ε_{xx}) and (ε_{yy}) at the cross section line (2-2) along the horizontal middle of the plate is shown in figure 4-244 and 4-245, respectively. This cross section line-strain shows a tensile strain (ε_{yy}) at a load less than 9,000 pounds besides compressive and tensile strain (ε_{xx}). After applying a load of 9,000 pounds, the strain (ε_{yy}) shows changes in the strain curve from tensile to compressive strain at some limited regions of the plate. The compressive strain (ε_{yy}) significantly increases with loading until the failure at load of 10,800 pounds. On the other hand, the tensile strain also slightly increases with loading but the significant increase in the strain (ε_{yy}) is in the compressive strain (ε_{yy}). The strain (ε_{xx}) shows a sharp rise in the strain (ε_{xx}) curves with loading. At a load of 9,000 pounds, the strain (ε_{xx}) in the middle horizontal cross section line (2-2) displays a high tensile strain and reaches close to 0.1. This region is very close to the diagonal gap which makes large changes in strain. In general, the small plate's area between the two slots twists with loading and this phenomenon shows in the full-field strain measurement images. Therefore, this little area twists with loading, and the strain varies along the horizontal cross sectional line. The worst case strain scenario is the one that is closest to the diagonal gap.

The last horizontal cross section line (3-3) which is located along the bottom horizontal of the plate shows the least part of the plate that is influenced by the loading. The full-field strain measurement at failure shows that the area of the plate underneath the diagonal line is connected perfectly to the wood; however, the plate's area above the diagonal gap is highly influenced by the loading and fails by tooth withdrawal. Thus, the changes in the strain (ε_{xx}) and (ε_{yy}) is not significant compared to the horizontal cross sectional line at the middle or the top of the plate as shown in Figure 4-246 and 4-247 for strain (ε_{xx}) and (ε_{yy}). The stain (ε_{yy}) curve is influenced by a significant high compressive strain on the left side of the cross section horizontal line (3-3) at a load of 9,000 pounds. This change is due to a twisting of the plate along the diagonal gap. The left side of the line (3-3) is close to the end of the diagonal gap; thus, it affects the strain (ε_{yy}) curve. On the other hand, the strain (ε_{xx}) at the left side also shows a significant high strain in the same region that the strain (ε_{yy}) is influenced by a significant increase in the compressive strain. The rest of the plate's area shows slight changes in the strain (ε_{xx}) and (ε_{xx}) with loading compared to the left side of the line (2-2) and compared to the top or the middle cross section lines (1-1) and (2-2), respectively.

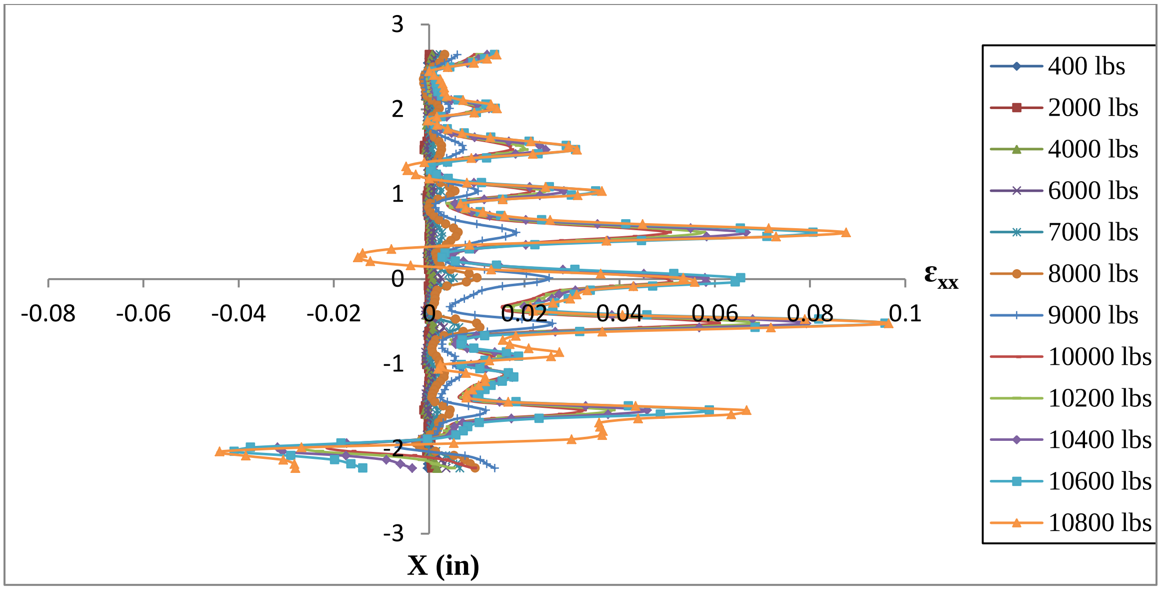

Figure 4-244: The strain distribution (ε_{xx}) along a cross section line (2-2)

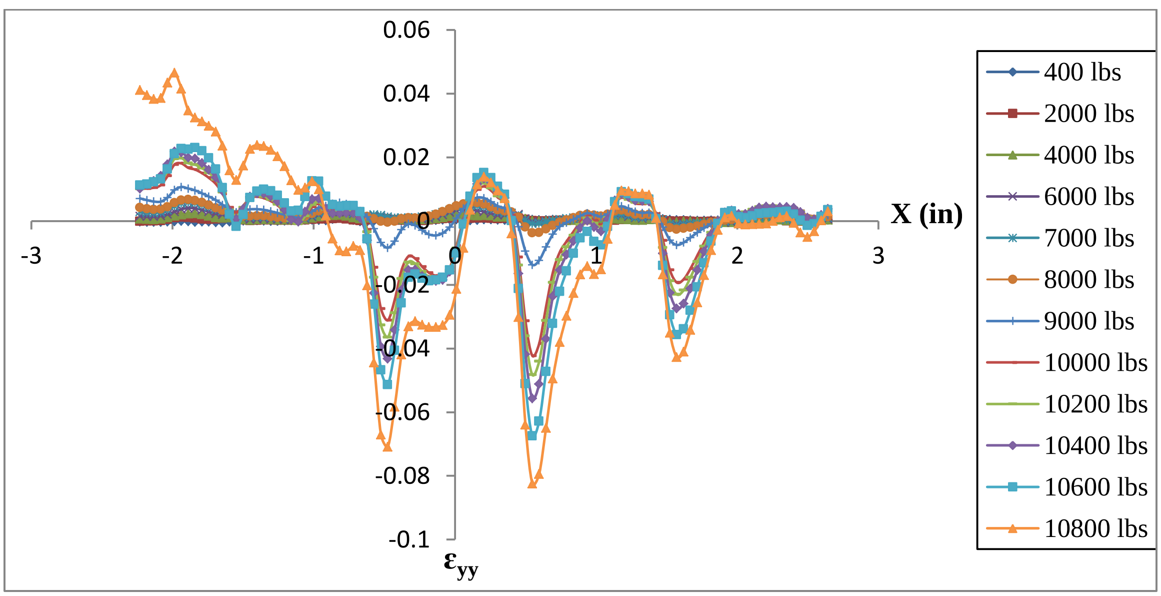

Figure 4-245: The strain distribution (ε_{yy}) along a cross section line (2-2)

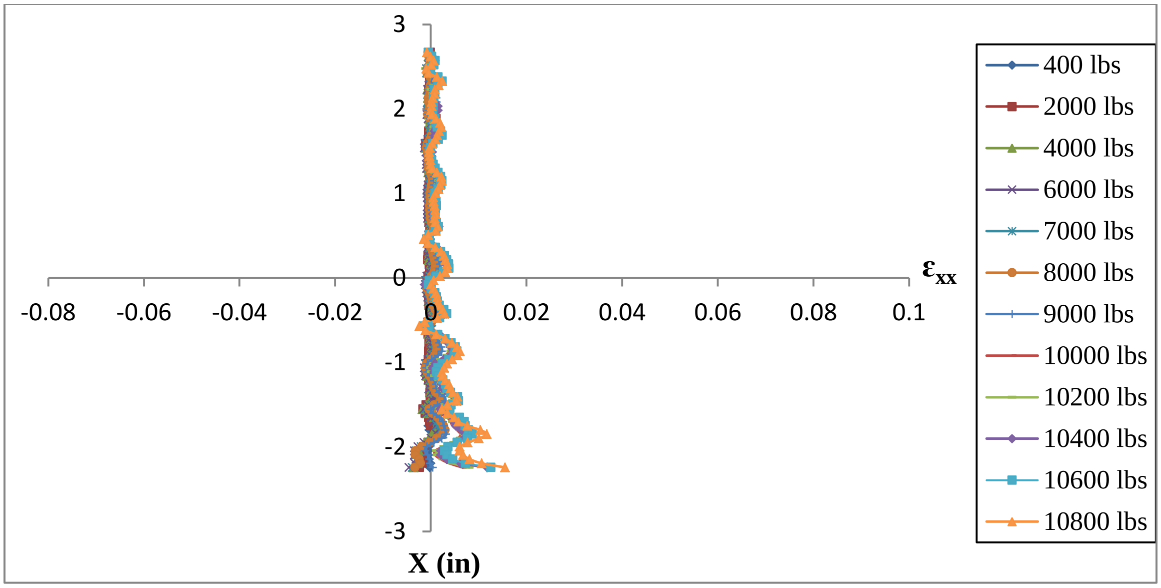

Figure 4-246: The strain distribution (ε_{xx}) along a cross section line (3-3)

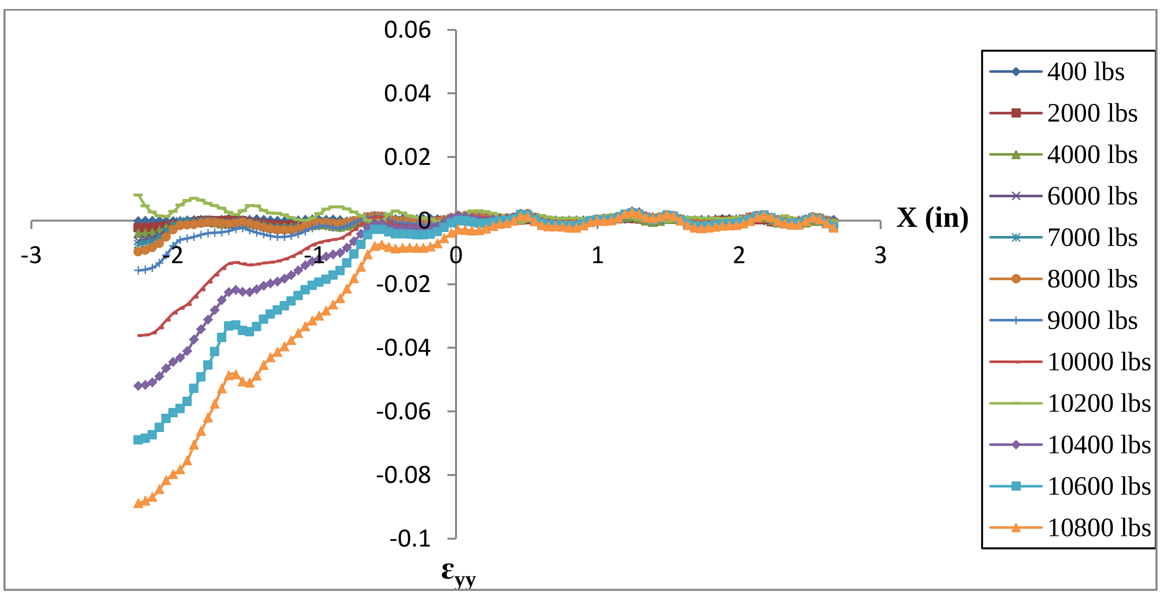

Figure 4-247: The strain distribution (ε_{yy}) along a cross section line (3-3)

4.2.2.4 The Truss Failure

The truss fails at different places as shown in Figure 4-248.

Figure 4-248: The truss image after failure

Figure 4-248 shows that all the joints starts to fail but the heel joint on the left, where the speckled plate is located, is the worst failed joint. More detailed images for the three truss joints-plates are shown in Figures 4-249 to 4-251.

The failure starts in the plate that located on the top joint of the truss. A fracture starts from the bottom of the plate and increases as the load increases. At the same time, the speckled plate on the left heel joint also starts to fail by tooth withdrawal.

Figure 4-249: The left side heel joint-speckled plate just after failure

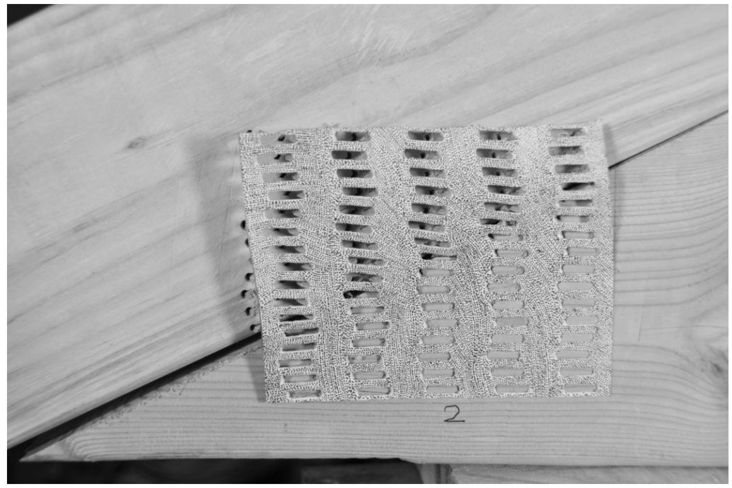

Figure 4-250: The plate on the top joint of the truss just after failure

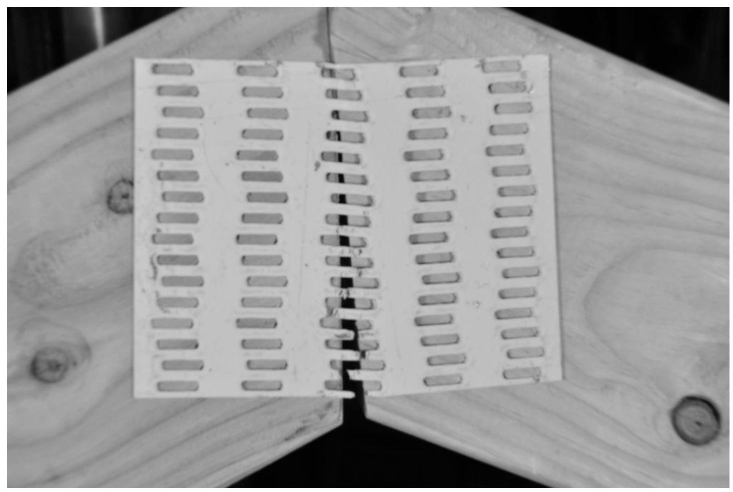

Figure 4-251: The right side heel joint-plate just after failure

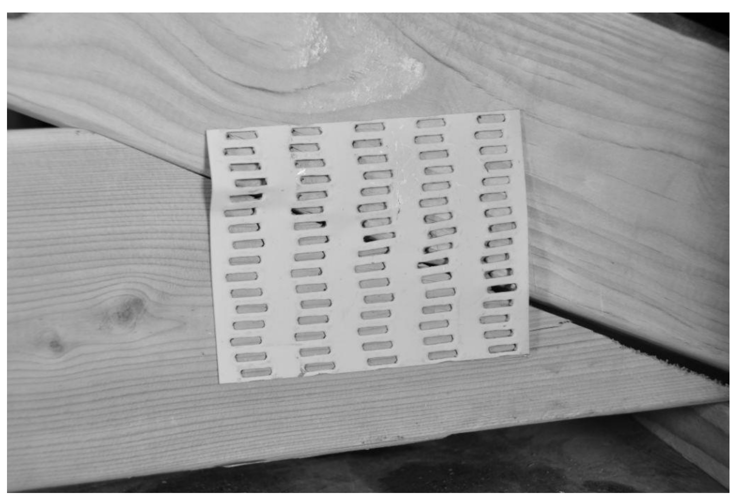

The plate on the right heel joint also is influenced by tooth withdrawal over some locations but this joint has less area of tooth withdrawal than the left heel joint-plate.

The truss fails due to tooth withdrawal of the left heel joint-speckled plate and the entire plate figures show the failure. The top plate on the top joint starts to fracture as shown in Figure 4-250 from the bottom to the top of the plate. This shows the place of the fracture along a row of slots in the middle of the plate. That part of the plate is half the area as other places which makes it weaker and easier to crack than other places on the plate. Examination of the two heel joints shows that failure starts in the axis of the plate located over the diagonal gap between the two wood members. This is clearly shown in the right heel joint-plate in Figure 4-251. This shows that the failure is initiated by tooth withdrawal starting at the axis of the plate over the diagonal gap between the two connected wood members. However, the main failure reason for the whole truss is due to the tooth withdrawal of the left heel joint-speckled plate.

4.2.2.5 Summary of the 2nd Heel Joint Test:

The strain curves at the vertical lines over the plate show tensile strain in both directions. ((ε_{xx}) and (ε_{yy})) are tensile strain from the beginning of loading until a load of 9,000 pounds. That means the plate is stretching and expanding from both directions x and y. At a load of 9,000 pounds the strain curves over the diagonal gap line where the two members of wood are connected shows significant changes in the strain values and the strain direction. At this load the strain (ε_{xx}) shows higher tensile strain values in that region than the previous loading. The strain (ε_{yy}) turns to compressive strain and its values increase with loading. The middle area at section (B-B) and the left side of the plate at section (D-D) are influenced and affected by loading more than the other areas of the plate. When a deformable body is subjected to a force, it will elongate in one direction and contract in the other. This occurs from a load of 9,000 pounds until failure. Before that, the strain (ε_{xx}) and (ε_{yy}) are both tensile strain. This result is due to the presence of the teeth which creates a shear stress over the entire plate and influences the plate's behavior. The plate has deformed by tooth withdrawal for all the plate's area above the diagonal gap but the area underneath the diagonal gap is under low tensile strain. This shows that some regions of the plate are below yield point; however, other regions are close or could be yielded. The 54 strain images show that the area of the plate above the diagonal gap is moving toward the left and the area of the plate underneath the diagonal gap is moving to the right. This phenomenon can be seen clearly after at a load of 9,000 pounds until the failure at a load of 10,800 pounds. The area of the plate along the diagonal gap is influenced by a shear twist which is evident in the last image at failure. The last image, which records the failure, shows clearly how the area of the plate above the diagonal gap is twisting and moving to the left.

The strain (ε_{xx}) in the horizontal direction shows smaller strain values (ε_{xx}) in the lower area of the plate than the middle or the top areas. In general, the strain (ε_{xx}) below the diagonal gap line over the gap of two connected wood members together is low compared to the other strain values on the plate's surface. The strain (ε_{xx}) at the diagonal line significantly increases from a load of 9,000 pounds until failure. In general, the strain (ε_{xx}) is tensile strain with some exceptions around the teeth and plate withdrawal regions. After applying a load of 9,000 pounds, the strain (ε_{xx}) in the area of the horizontal middle of the plate has the highest tensile strain (ε_{xx}) then the area above the diagonal gap is the next. The area of the plate located below the diagonal gap shows slow changes in the strain field results. This is a logical conclusion, as analysis of the images shows a clear twist of the plate along the diagonal gap which makes significant changes in the strain values, and the area above the diagonal gap is influenced by tooth withdrawal while the area below the diagonal gap is holding the wood perfectly; thus, no significant changes in strain are recorded there.

4.2.3 Heel Joint 3rd Test

In this test, the truss was set on the universal testing machine and the camera was placed on a fixed place in front of the speckled plate that was located on the left heel joint. The first image before loading was captured as a reference image Figure 4-252.

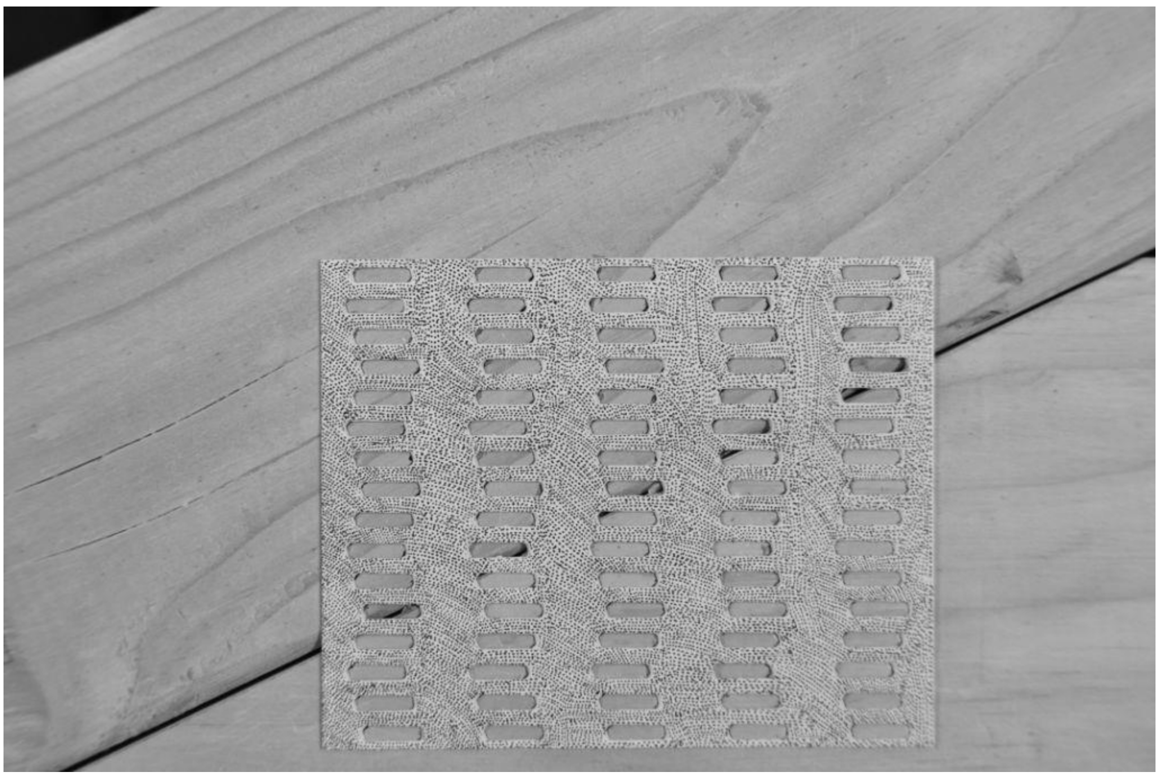

Figure 4-252: The reference image in the fourth heel joint test

A total of 63 images were captured for this test before the failure besides the reference image. The truss failed at load equal to 12,600 pounds. All the captured images were implemented in DIC software to find the full-field strain measurements.

4.2.3.1 Full-Field Strain Measurements Results Using DIC Software

Full-field strain measurements can be obtained for the metal plate using the DIC software. All the test images, which were obtained from the lab test, were implemented in the digital image correlation software Vic-2D. Each image was analyzed in relation to a reference image. Thus, each deformed image was compared to the non-deformed reference image. The full-field strain measurements were obtained from the digital image correlation software. Figure 4-253 shows the strain in y-direction (ε_{yy}) for the first images at 200 pounds.

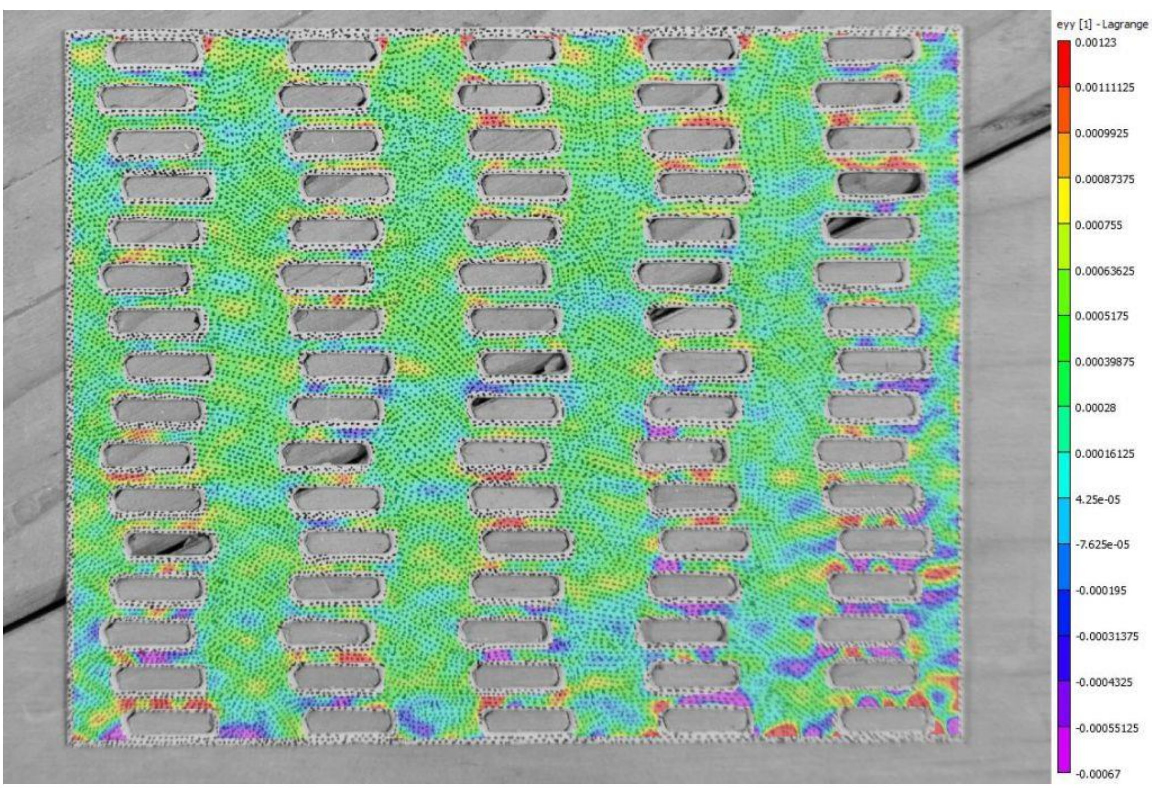

Figure 4-253: Full-field strain measurements (ε_{yy}) for the MPC after applying 200 pounds

The image shows that the strain (ε_{yy}) is almost equally distributed over the entire plate. In general, the strain (ε_{yy}) is a tensile strain with low values due to very low load which is 200 pounds. As the load increases, the strain (ε_{yy}) increases and shows slight changes in the strain until a load of 9,000 pounds at which point the plate shows some significant changes on some regions over the plate's area. Figure 4-254 shows the strain (ε_{yy}) field at 9,000 pounds.

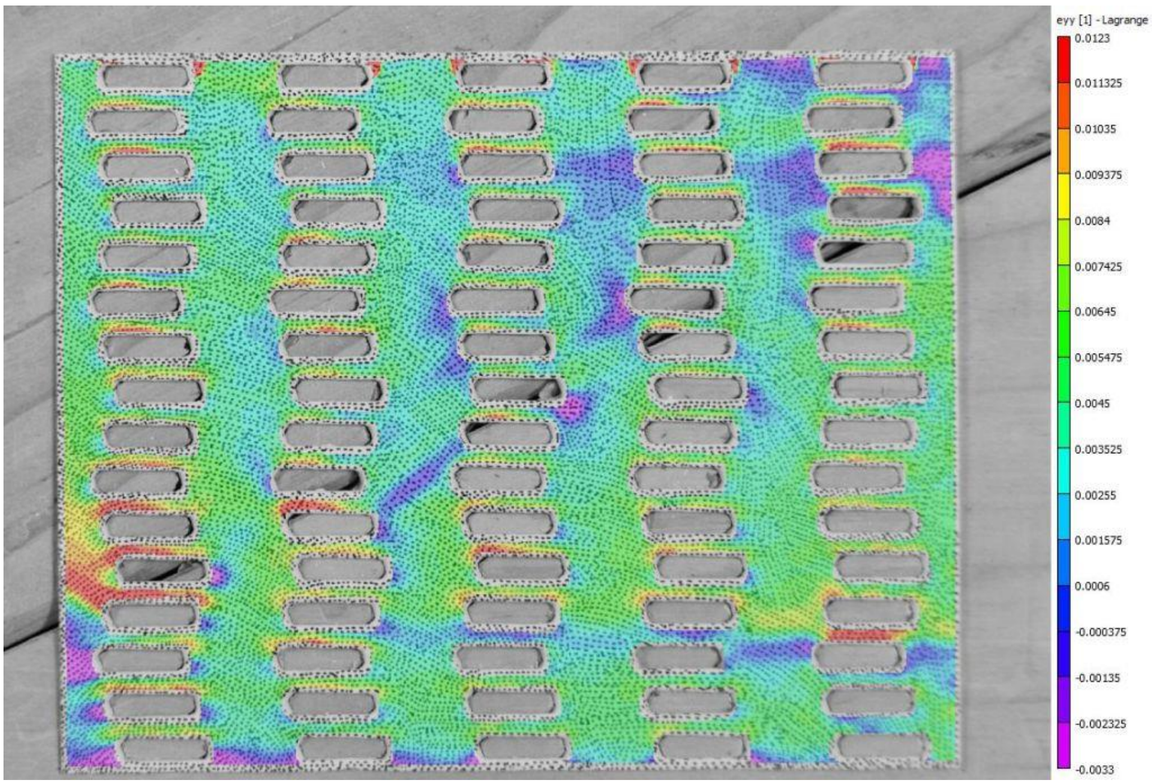

Figure 4-254: Full-field strain measurements (ε_{yy}) for the MPC after applying 9,000 pounds

The last figure shows that the strain (ε_{yy}) is a tensile strain over the general area of the plate. Some limited regions show compressive strain especially those close to the diagonal gap between the two connected wood members. Other areas on the top also turn to compressive strain. The strain at a load of 10,000 pounds shows more significant changes as shown in Figure 4-255.

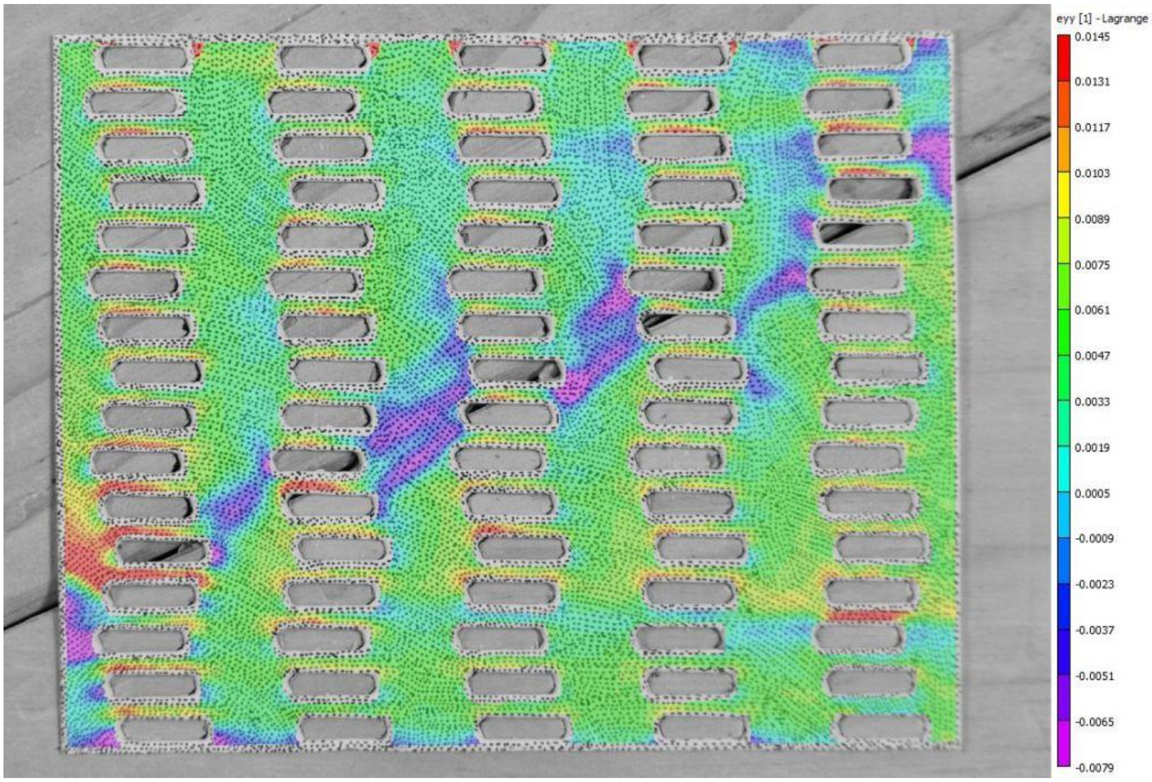

Figure 4-255: Full-field strain measurements (ε_{yy}) for the MPC after applying 10,000 pounds

The previous figure shows how the full-field strain measurements are significantly changed with loading. The strain line over the diagonal gap completely holds a different color than the dominant color over the plate. The strain there is compressive; however, it is tensile over the entire plate. The left-bottom side of the plate shows high tensile strain. Thus, this little area should show reaction to the load later on.

At a load of 10,000 pounds, the strain (ε_{yy}) increases and the areas between the two slots that are located over the diagonal gap between the two connected wood members shows a twist with loading. The significant change in the strain in that region is due to an increase in the gap between the two connected wood members. The tensile strain (ε_{yy}) underneath the diagonal gap line significantly increases and is higher than the tensile strain over the diagonal gap line. Figure 4-256 shows the full-field strain measurement (ε_{yy}) at 12,000 pounds.

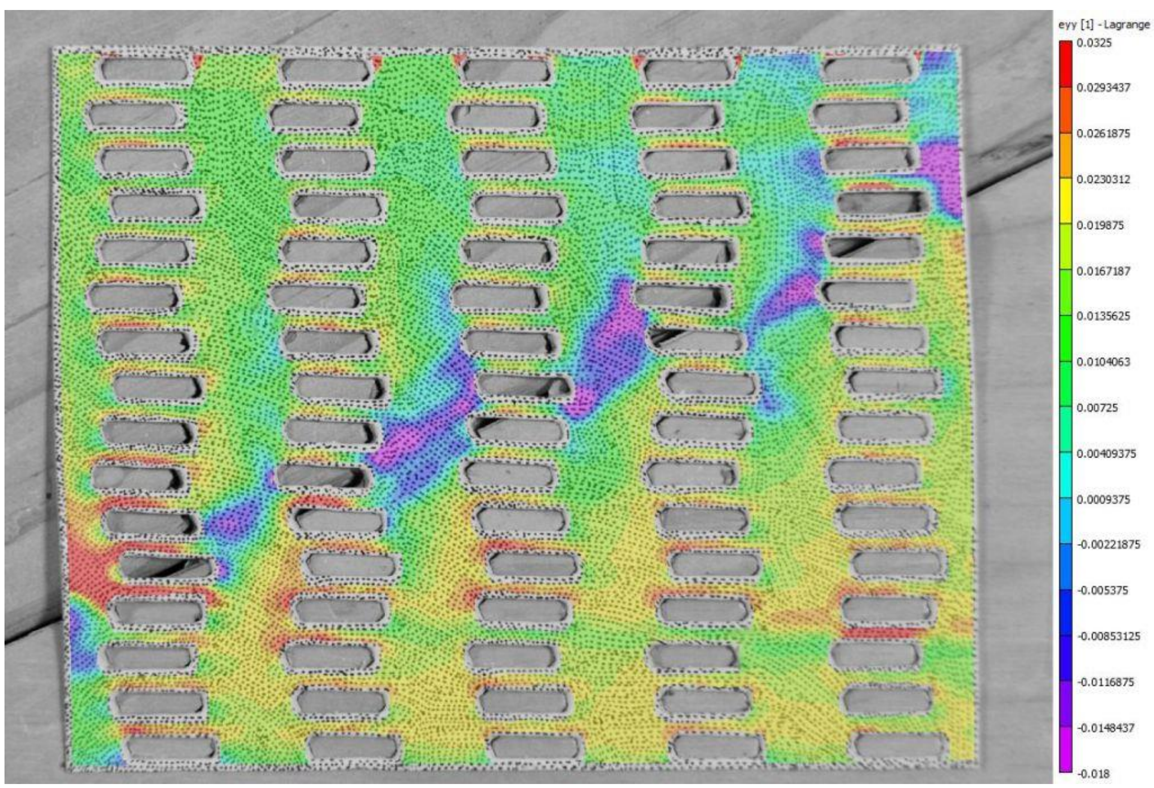

Figure 4-256: Full-field strain measurements (ε_{yy}) for the MPC after applying 12,000 pounds

The previous image shows the significant change in the tensile strain below the diagonal gap line. The strain (ε_{yy}) over the diagonal line is compressive; however, it has higher values than the earlier strain full-field images. The tensile strain on the bottom-left side is high. Some pulling out of the plate appears there as shown in Figure 4-256.

The last image at failure is shown in Figure 4-257 at 12,600 pounds. The truss fails at a load of 12,600 pounds; however, the speckled plate did not fail. The diagonal gap line shows very high compressive strain (ε_{yy}). The area of the plate underneath the diagonal gap line is influenced by high tensile strain (ε_{yy}). The area of the plate above the diagonal gap line is also influenced by tensile strain but it is less than the bottom tensile strain (ε_{yy}). Tooth withdrawal for the left- bottom side of the plate appears clearly in Figure 4-257 with high tensile strain (ε_{yy}). This speckled plate does not continue to explain more about the strain behavior of the plate failure, however, due to the failure that occurred in the other heel joint plate.

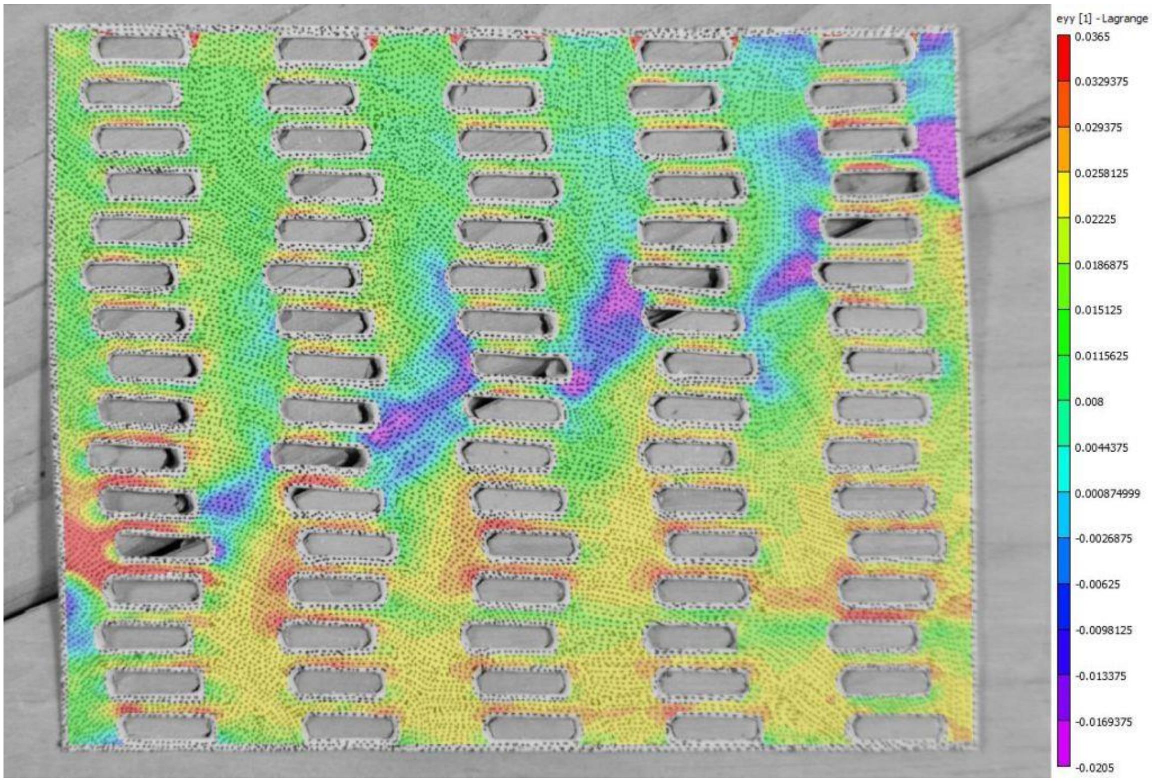

Figure 4-257: Full-field strain measurements (ε_{yy}) for the MPC after applying 12,600 pounds

On the other hand, the full-field strain measurements in x-direction (ε_{xx}) are also obtained from digital image correlation software. Figure 4-258 shows the strain (ε_{xx}) after applying a load of 200 pounds. The image shows that the strain (ε_{xx}) is a low tensile strain distributed over the plate and could reach up to 0.00072. Some regions show low compressive strain along the right side edge of the plate reaches up to -0.0009. Increasing the load causes the strain (ε_{xx}) to increase and change throughout the surface of the plate. The increase in the strain (ε_{xx}) is also low and not significant. The full-field strain measurements (ε_{xx}) from a load of 200 pounds until a load of 8,000 pounds show a slight difference in the strain values with loading. At a load of 9,000 pounds some changes in the strain (ε_{xx}) in the middle of the plate are observed.

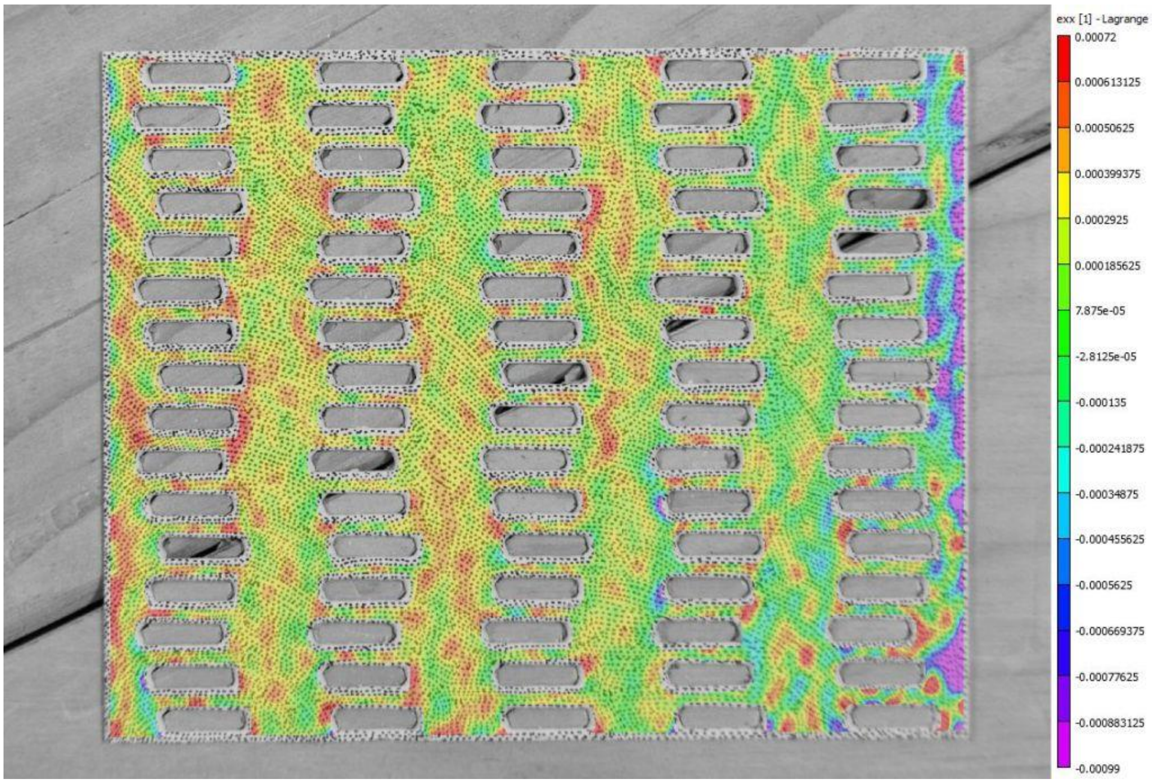

Figure 4-258: Full-field strain measurements (ε_{xx}) for the MPC after applying 200 pounds

The significant change in the strain is clearly shown at a load of 10,000 and 11,000 pounds especially along the diagonal gap line. Figure 4-259 shows the full-field strain (ε_{xx}) behavior at a load of 11,000 pounds.

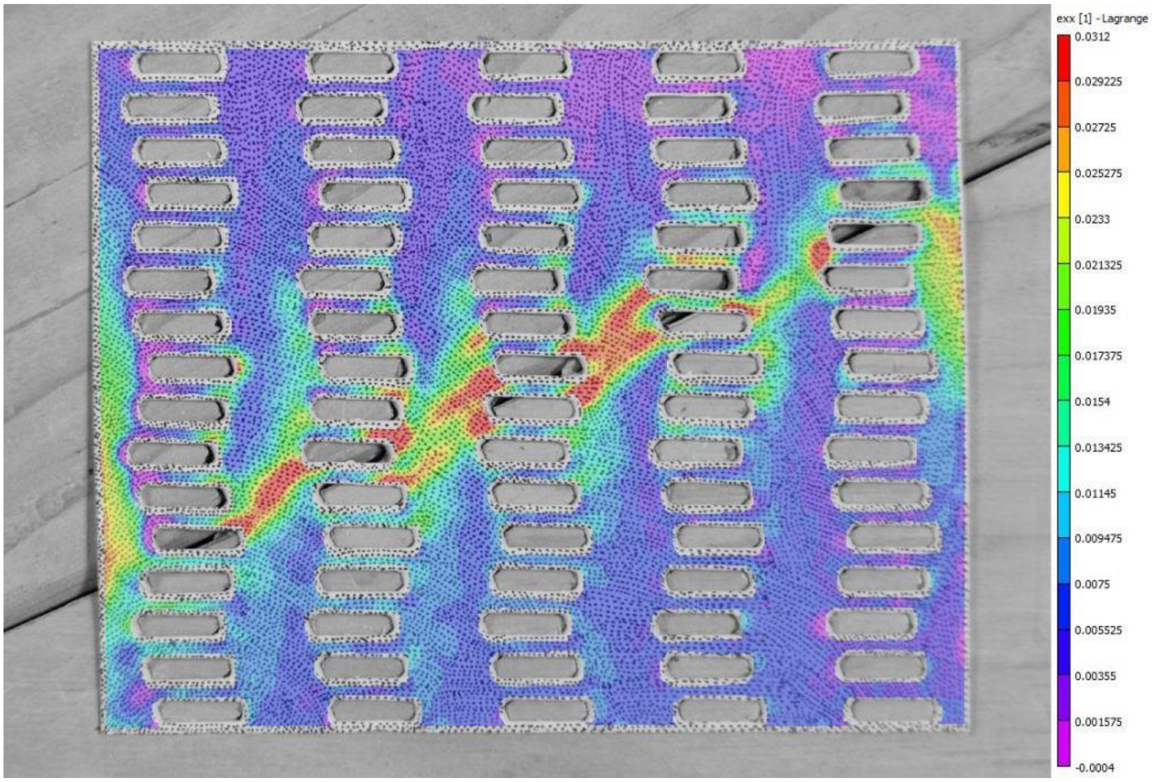

Figure 4-259: Full-field strain measurements (ε_{xx}) for the MPC at 11,000 pounds

The strain behavior at 11,000 pounds exhibits high tensile strain over the diagonal gap line and lower tensile strain above and below the diagonal gap line. Then as the load increases, the strain along the diagonal gap increases. The tensile strain above and below the diagonal gap line also increases. The last strain image at the failure is shown in Figure 4-260 where the pate is influenced by a load of 12,600 pounds.

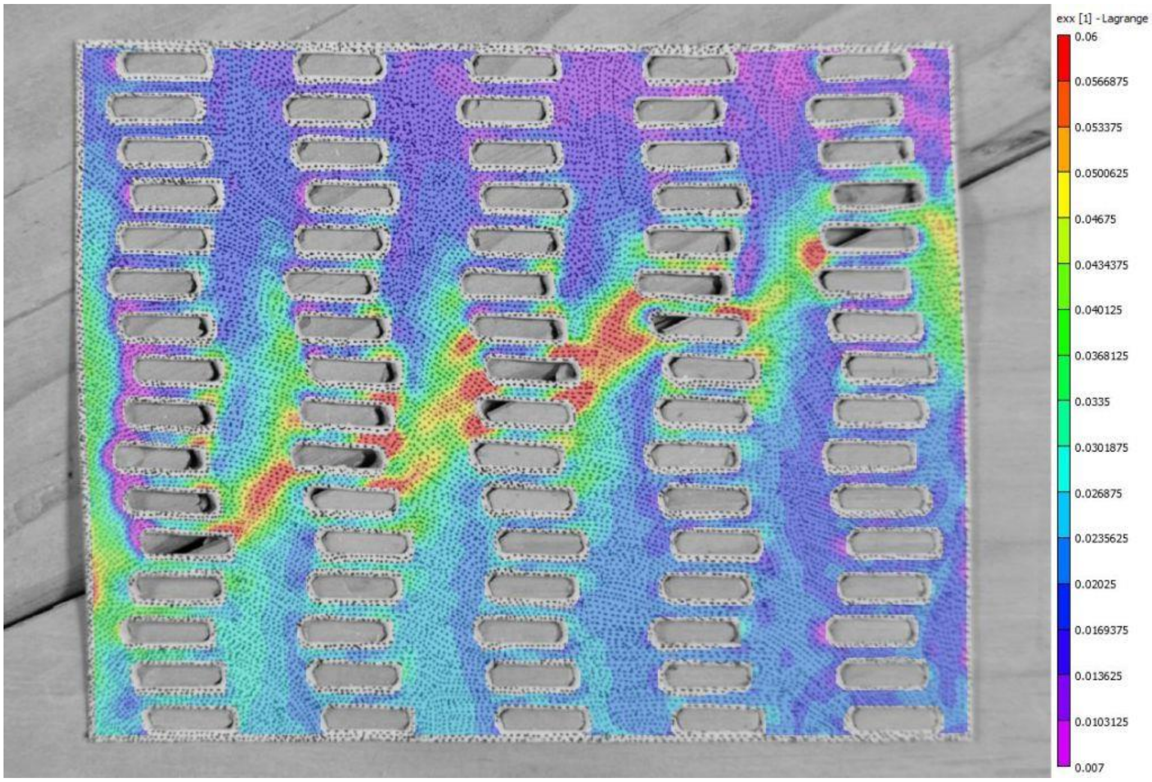

Figure 4-260: Full-field strain measurements (ε_{xx}) for the MPC at 12,600 pounds

The failure in this test is due to failure of the right heel joint plate, not the speckled one. Thus, the speckled plate is not in failure at a load of 12,600 pounds. However, the strain (ε_{xx}) shows significant changes along the diagonal gap line. The overall strain (ε_{xx}) is tensile strain with high values along the diagonal gap. The strain (ε_{xx}) fields show that the strain (ε_{xx}) is higher on the left side of the plate than the right side especially on the bottom parts of the plate.

4.2.3.2 Numerical Analysis along the Vertical Strain Results

To analyze the DIC results numerically, a vertical cross section line from the top of the plate to the bottom is taken for some images starting with the first image at a load of 200 pounds and ending with the last image at failure. The cross section is taken in four different locations as shown in Figure 4-261.

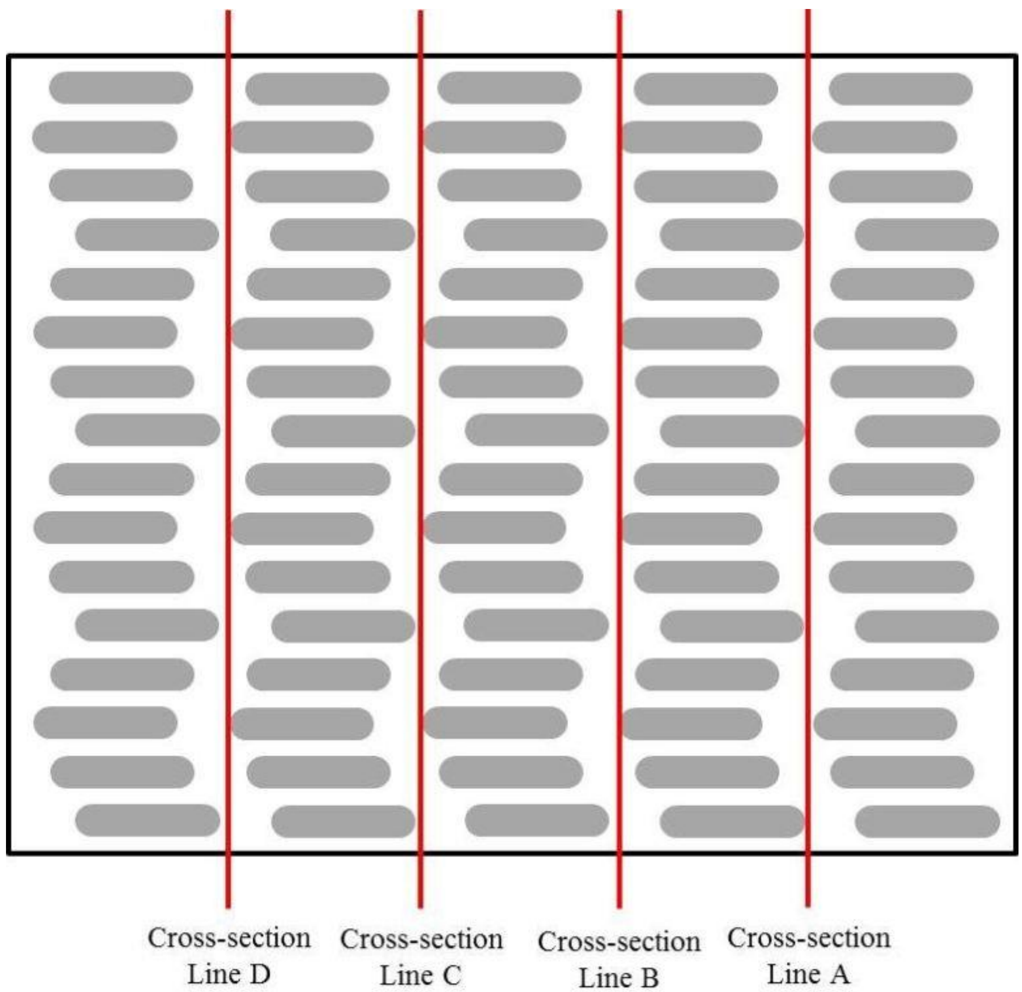

Figure 4-261: Metal plate with the cross-section lines along the vertical direction

The cross section is taken in four different locations:

- The first cross section is from the right side of MPC @ x = 1.87 in. cross-section A-A.
- The second cross section is @ x = 0.88 in. cross-section B-B.
- The third cross section is @ x = -0.10 in. cross-section C-C.
- The fourth cross section line is from the left side of MPC @ x= -1.11 in. cross-section D-D.

Four cross-section lines are taken for the strain field (ε_{yy}). The next figures show the distribution of strain (ε_{yy}) accompanied with strain (ε_{xx}) at the same cross section line at four different locations for 12 images. Each image represents the value of the loading that is applied on the specimen of simple truss.

The curves show that the first considered load is 400 pounds then a different increment of loading is used to show the MPC behavior until failure occurs. In general, the strain (ε_{yy}) shows similar strain values and almost equally distributed strain over the entire plate with some exceptions from the beginning of the test until a load 9,000 pounds. At a load of 10,000 pounds, changes in strain curves behavior are evident. The high changes in the strain are limited to that region along the diagonal gap between the two connected wood members. The dominant strain (ε_{yy}) is tensile strain, and it increases with loading throughout the test.

The strain (ε_{yy}) in Figure 4-262 shows the right side behavior of the MPC under loading at section (A-A). In this figure the strain (ε_{yy}) is almost equally distributed from the top to the bottom of the plate along the cross section line (A-A) with some exceptions. The strain (ε_{yy}) slightly increases with loading from a load of 400 pounds to a load of 10,000 pounds. At 10,000 pounds the strain (ε_{yy}) curve shows significant changes as some strain regions becomes negative strain and other regions show higher negative and positive strains than the earlier strain curves. As the loading is increased from a load of 10,000 pounds to the failure at a load 12,600 pounds, the top region of the plate is under tensile strain (ε_{yy}). A limited region has higher tensile strain (ε_{yy}) than the rest of the tensile strain over the plate. However, the strain (ε_{yy}) is compressive strain over the diagonal gap between the two connected wood members. The highest compressive strain is around the diagonal gap line. The strain below the diagonal gap is higher than the strain above the diagonal gap line.

The strain (ε_{xx}) in Figure 4-263 along the same cross section line (A-A) significantly increases at a load of 10,000 pounds. The strain (ε_{xx}) is tensile strain from the beginning of the test until the failure. The strain (ε_{xx}) increases with loading until failure at a load of 12,600 pounds. The area of the plate over the diagonal gap has the highest tensile strain (ε_{xx}) .The area of the plate below the diagonal gap line shows higher tensile strain than the area above the diagonal gap line. The strain (ε_{xx}) can reach up to 0.044 and the maximum tensile strain (ε_{yy}) is 0.028.

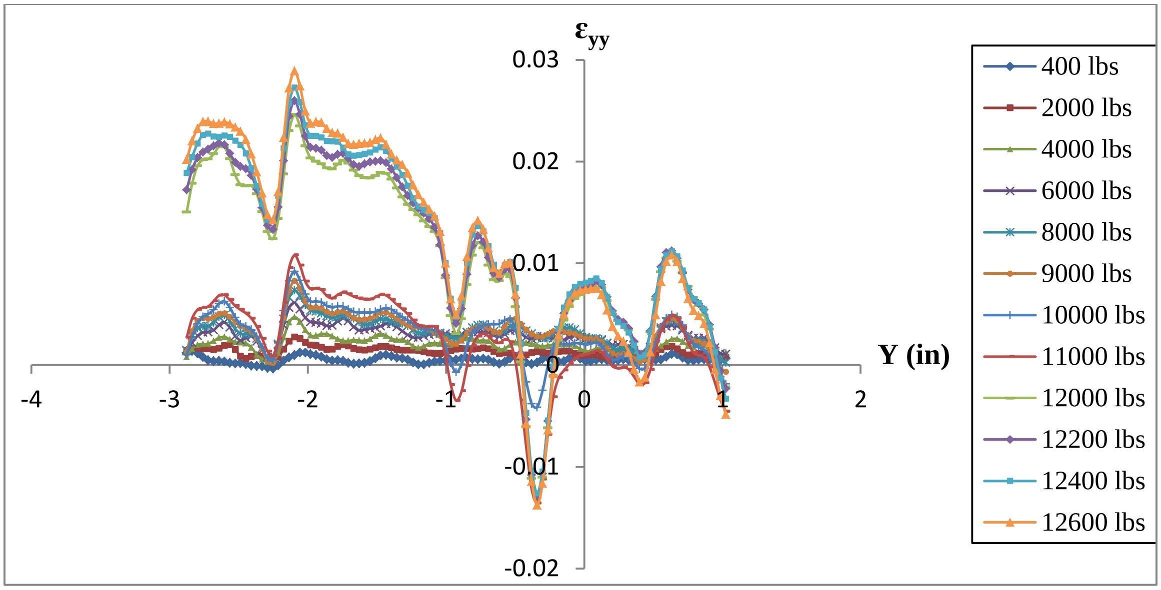

Figure 4-262: The strain distribution (ε_{yy}) along a cross section line (A-A) located on the right side of the plate

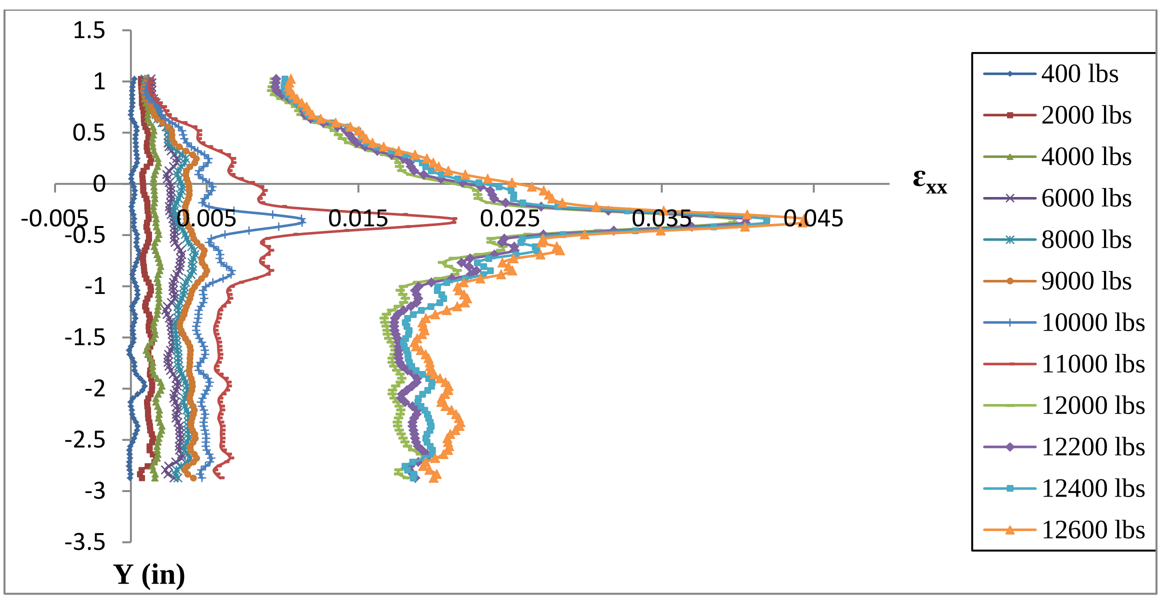

Figure 4-263: The strain distribution (ε_{xx}) along a cross section line (A-A) located on the right side of the plate

The strain curves behavior in the middle area of the plate along cross section line (B-B) and (C-C) is shown in Figures 4-264 to 4-267.The strain (ε_{yy}) shows almost equally distributed strain along the vertical cross section lines (B-B) and (C-C) starting from a load of 400 pounds until a load of 9,000 pounds. The strain curves (ε_{yy}) shows slight increase with loading up to this point. The strain (ε_{yy}) is tensile strain with some exceptions. At a load of 9,000 pounds, some changes are observed in the strain curve (ε_{yy}). However, a significant strain-curve change is clearly shown after applying a load of 10,000 pounds. The area of the plate over the diagonal gap line is moving to be negative strain (ε_{yy}) which means compressive strain. The rest of the pate's area is influenced by tensile strain. At a load of 11, 000 pounds, the strain curve (ε_{yy}) also follows the strain curve at load of 10,000 pounds but with a slight increase in the strain values. At a load of 12,000 pounds until the failure at a load of 12,600 pounds, the strain (ε_{yy}) possesses high compressive strain values on the area of the plate over the diagonal gap line. The area of the plate beneath the diagonal gap is influenced by higher tensile strain than the area above the diagonal gap line.

The strain (ε_{xx}) over the plate's area is tensile strain. The strain (ε_{xx}) increases with loading. The strain curves (ε_{xx}) in the middle along (B-B) and (C-C) shows that the strain (ε_{xx}) is almost equally distributed from the top to the bottom of the plate until a load of 9,000 pounds at which point a significant increase of the strain (ε_{xx}) on the area over the diagonal gap line is observed. The strain (ε_{xx}) shows a significant increase at a load of 10,000 pounds until failure. The last four strain curves show similar strain behavior. The tensile strain is high on the plate's area where the diagonal gap line is.

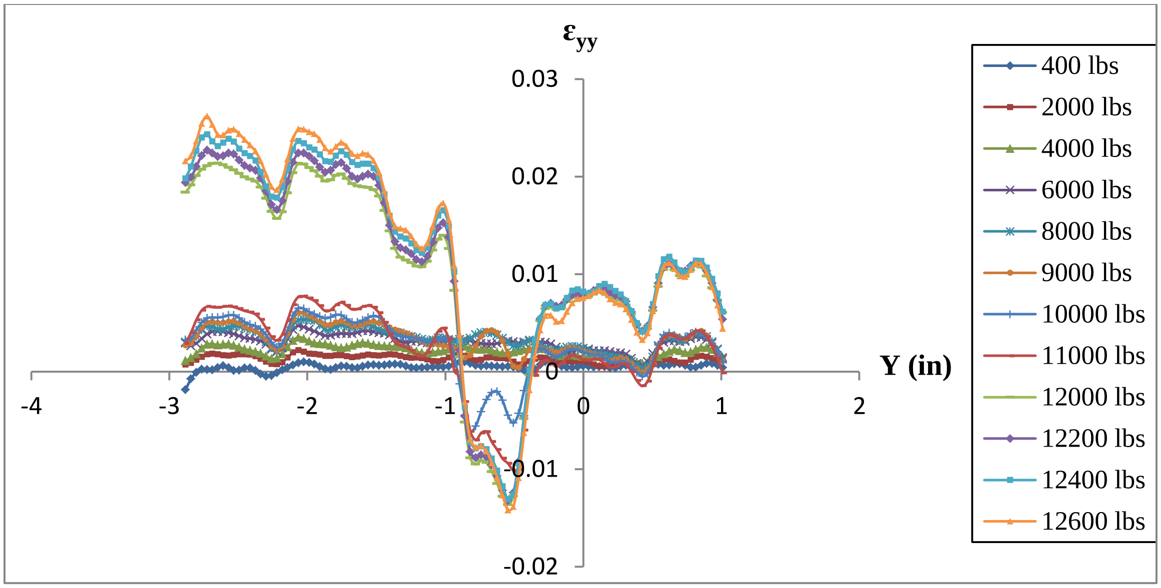

Figure 4-264: The strain distribution (ε_{yy}) along a cross section line (B-B)

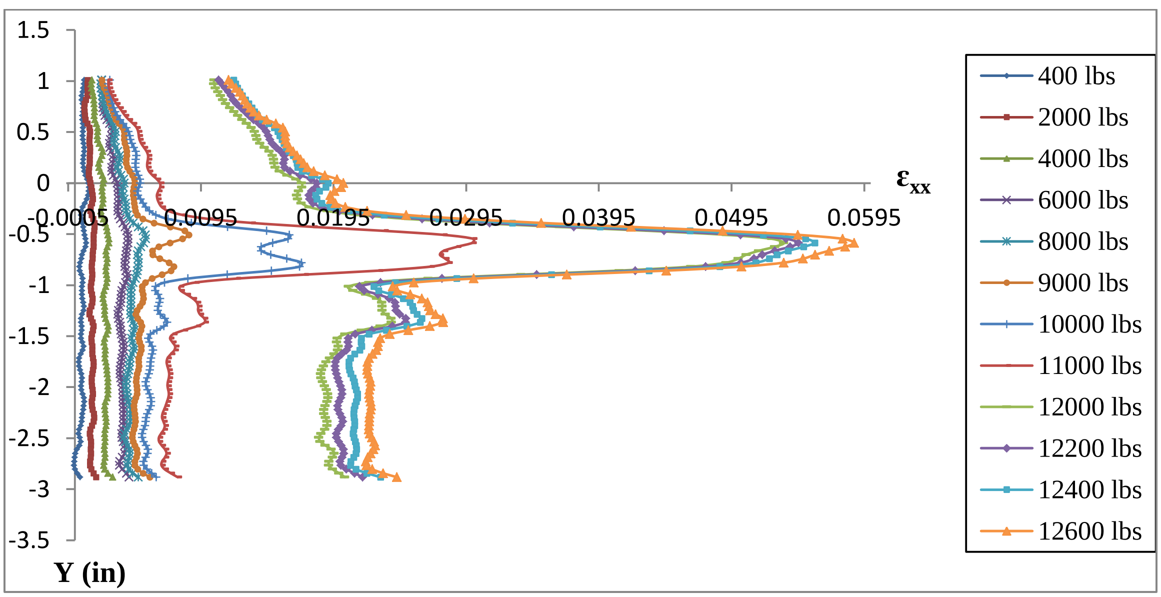

Figure 4-265: The strain distribution (ε_{xx}) along a cross section line (B-B)

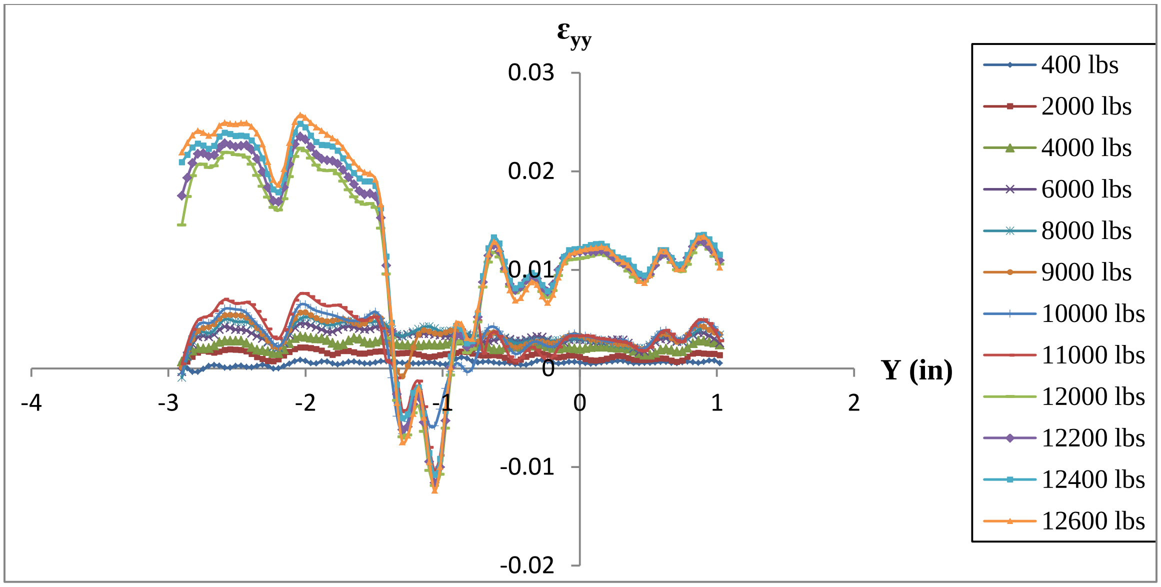

Figure 4-266: The strain distribution (ε_{yy}) along a cross section line (C-C)

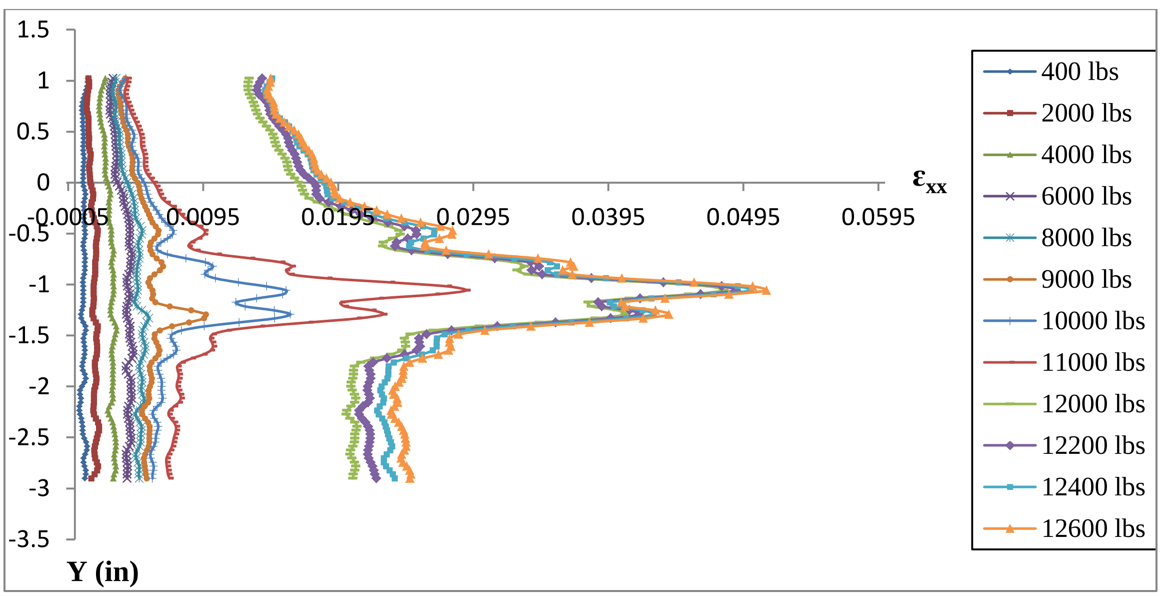

Figure 4-267: The strain distribution (ε_{xx}) along a cross section line (C-C)

The area of the plate beneath the diagonal line has higher tensile strain (ε_{xx}) than the area of the plate above the diagonal gap line.

Figures 4-268 and 4-269 show the strains (ε_{xx}) and (ε_{yy}) along the vertical cross sectional line (D-D) located in the left side of the plate. From a load of 400 pounds until a load of 8,000 pounds, the strain curves (ε_{yy}) are tensile strain. The tensile strain slightly increases with loading. At a load of 9,000 pounds, some changes start to influence the strain curves. At a load of 10,000 pounds, the strain (ε_{yy}) over the diagonal gap turns to compressive strain instead of tensile strain. Then the strain curve (ε_{yy}) at a load of 12,000 pounds until failure at a load of 12,600 shows high compressive strain on the area of the plate over the diagonal gap line. The strain (ε_{yy}) above the diagonal gap possesses higher tensile strain (ε_{yy}) than the area beneath the diagonal gap. The strain (ε_{yy}) reaches up to 0.025 as a maximum tensile strain and -0.0106 as the maximum compressive strain.

The strain (ε_{xx}) along the cross section line (D-D) is shown in Figure 4-269 . The strain (ε_{xx}) is tensile strain over the entire plate. Starting from a load of 400 pounds until a load of 8,000 pounds, the strain curves (ε_{xx}) show slightly increases by loading. The strain (ε_{xx}) shows almost equally distributed strain along the vertical cross section line (D-D). At a load of 9,000 pounds, the strain shows spikes in the curve especially in the area over the diagonal gap line. The strain curves (ε_{xx}) show that the strain over the diagonal gap is significantly increasing by loading as shown in the figure until the failure at a load of 12,600 pounds. At a load of 12,000 pounds, the strain (ε_{xx}) is higher on the plate's area beneath the diagonal gap line than the plate's area above the diagonal gap line. The strain curves behavior (ε_{xx}) almost follows the strain curve behavior (ε_{yy}) in the significant strain changes.

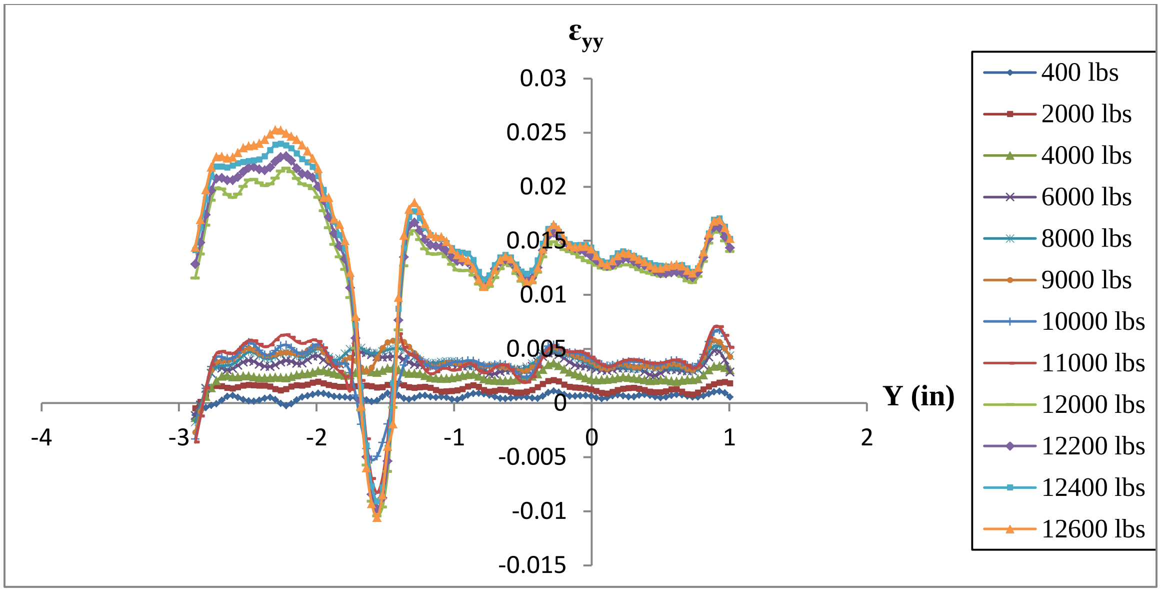

Figure 4-268: The strain distribution (ε_{yy}) along a cross section line (D-D) located on the left side of the plate

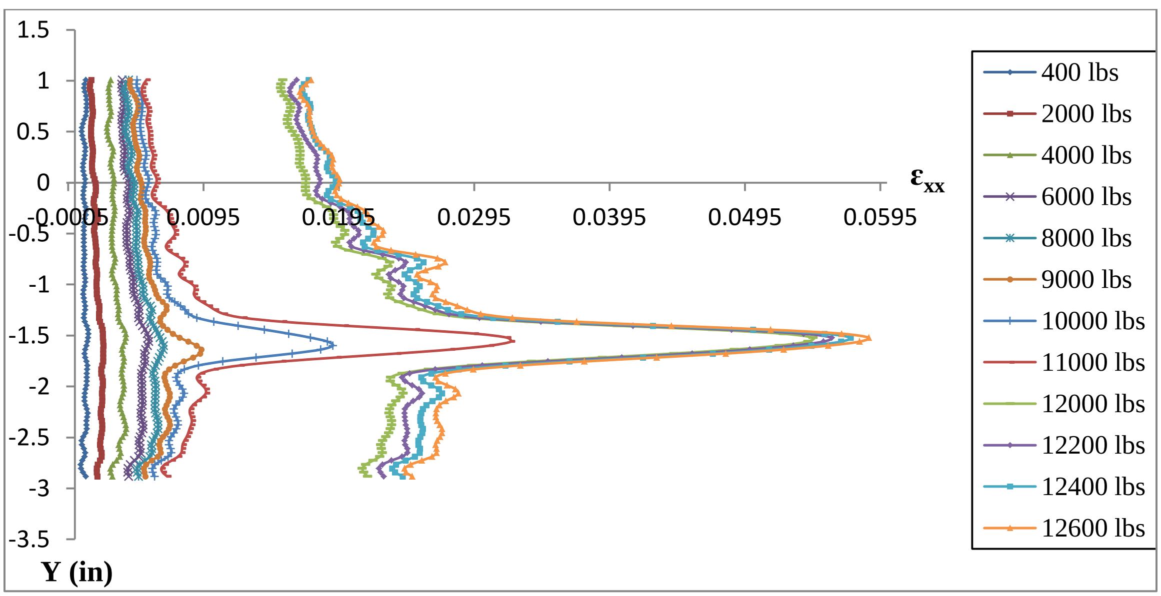

Figure 4-269: The strain distribution (ε_{xx}) along a cross section line (D-D) located on the left side of the plate

4.2.3.3 Numerical Analysis along the Horizontal Strain Results

To analyze the DIC results numerically, a horizontal cross section line from the right side to the left side of the plate is taken for some images starting with the first image at a load of 200 pounds and ending with the last image at failure. The cross section is taken in three different locations.

- The first cross section is on the top of MPC @ y = 0.81 in. cross-section 1-1.
- The second cross section is near the middle of the MPC @ y = -0.95 in. cross-section 2-2.
- The third cross section is bottom of MPC @ y = -2.69 in. cross-section 3-3.

Figure 4-270 shows the cross section lines on the metal plate

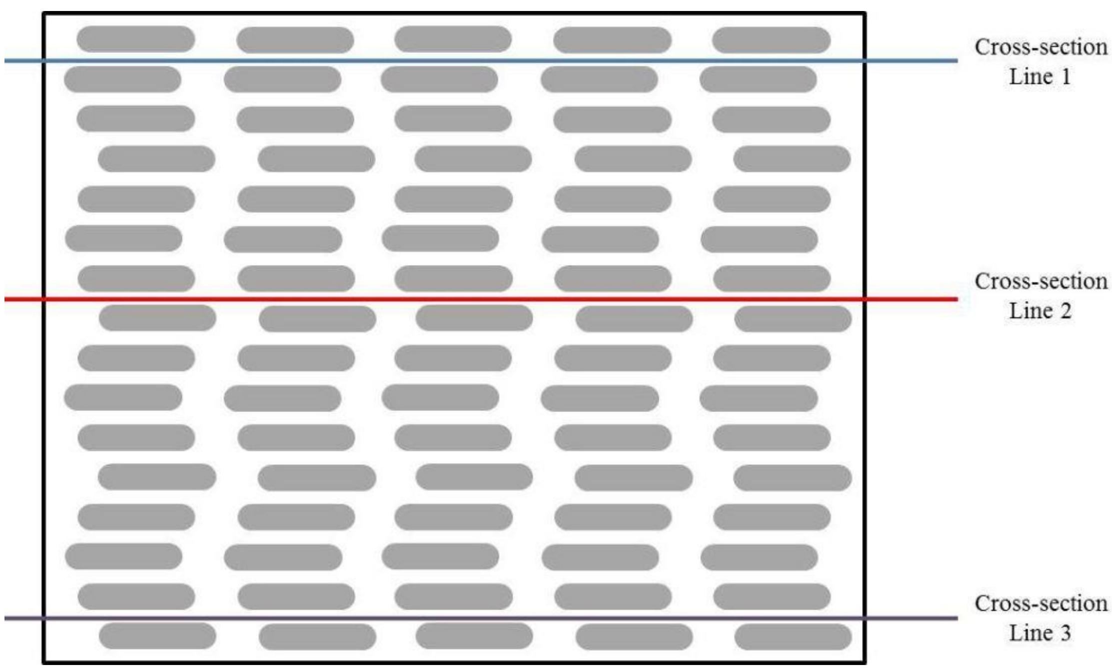

Figure 4-270: Metal plate with the cross-section lines along the horizontal direction

Three cross-section lines are taken for the strain field (ε_{xx}). The figures below show the distribution of strain (ε_{xx}) accompanied with (ε_{yy}) at the same cross section line at three different locations for 12 images. Each image represents the value of the loading that is applied on the specimen of simple truss.

The curves along the horizontal cross section line (1-1) and (3-3) show similar results while the cross section line (2-2) in the middle of the plate shows more changes in the strain results. The top cross section line (1-1) shows less change in the strain (ε_{xx}) with loading starting at 400 pounds until a load of 11,000 pounds. The cross section line (3-3) at Figure 4.275 shows a slight increase in the strain (ε_{xx}) with loading until a load of 11,000 pounds. At a load of 12,000 pounds, a big gap in the strain curves is shown in both cross section lines (1-1) and (3-3). The cross section line (3-3) holds higher tensile strain (ε_{xx}) than the top cross section line (1-1). The left side of the cross section line curves shows higher tensile strain than the right side. Thus, if this speckled plate will fail then the failure should start from the left side.

Accompanied with the strain (ε_{xx}) curves figures, the strain (ε_{yy}) displays along the same horizontal cross section line (1-1) and (3-3), respectively. The strain (ε_{yy}) along the bottom cross section line (3-3) is almost entirely tensile strain which increases with loading. A big gap in strain values occurs between the strain curve at a load of 11,000 pounds and 12,000 pounds. The strain curves at cross section line (1-1) shows spikes in the strain curve with loading. The top part of the plate shows less stability in strain changes than the bottom part of the plate. The bottom cross section line (3-3) holds higher tensile strain values than the top strain (ε_{yy}).

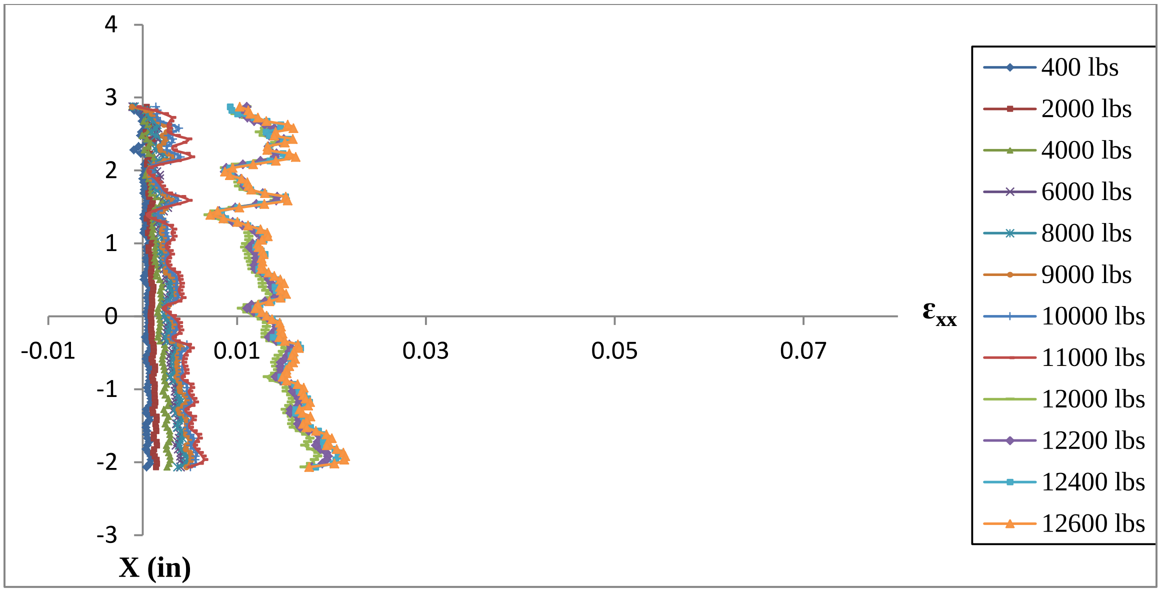

Figure 4-271: The strain distribution (ε_{xx}) along a cross section line (1-1)

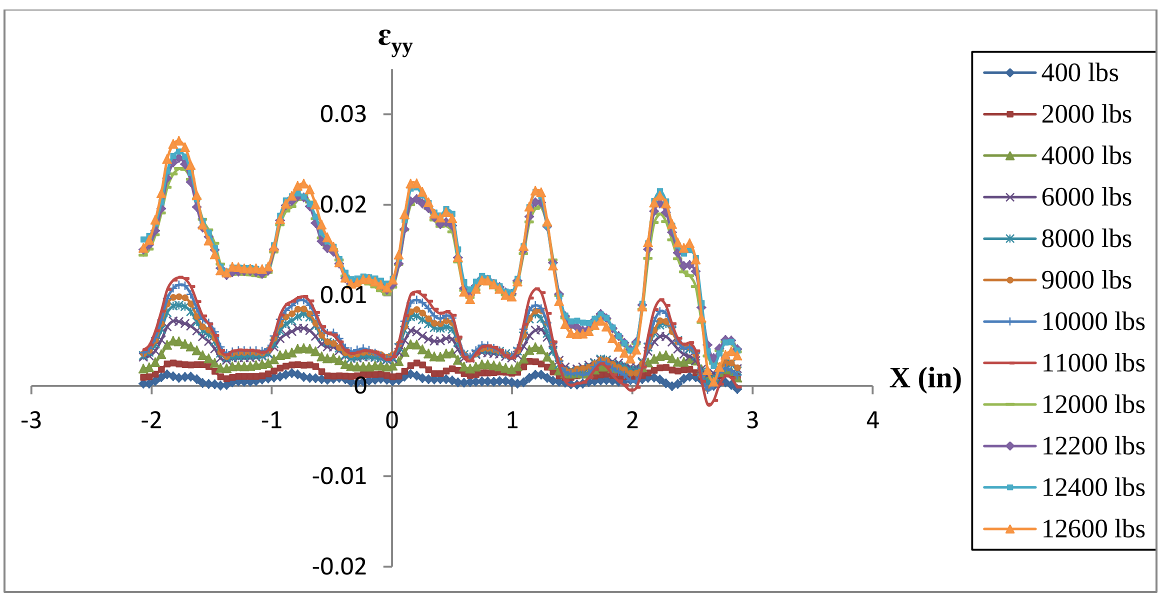

Figure 4-272: The strain distribution (ε_{yy}) along a cross section line (1-1)

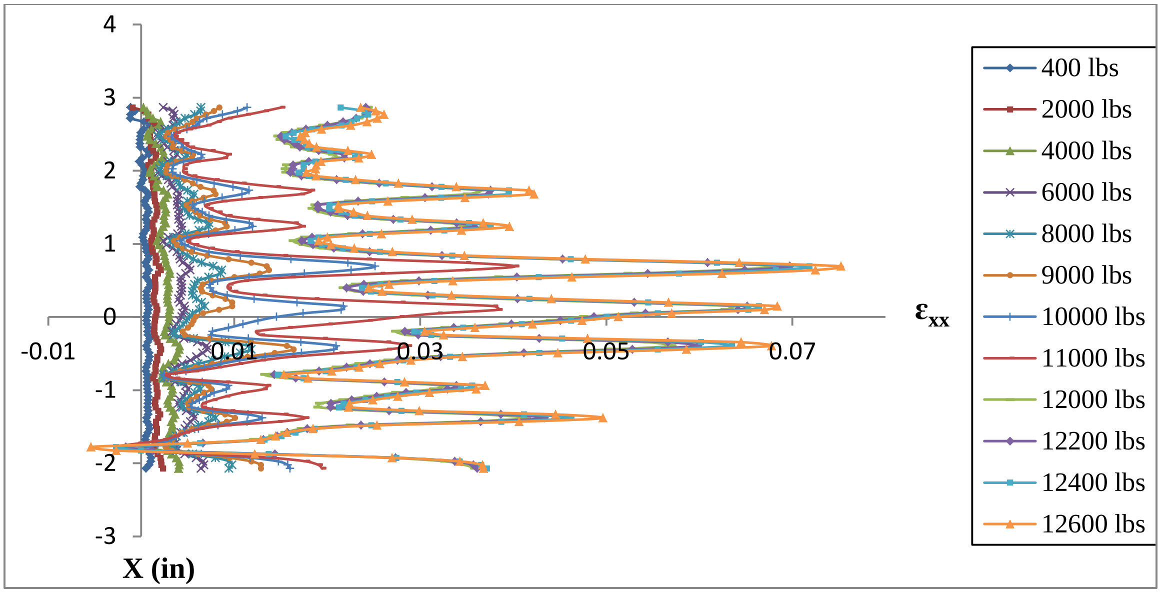

Figure 4-273: The strain distribution (ε_{xx}) along a cross section line (2-2)

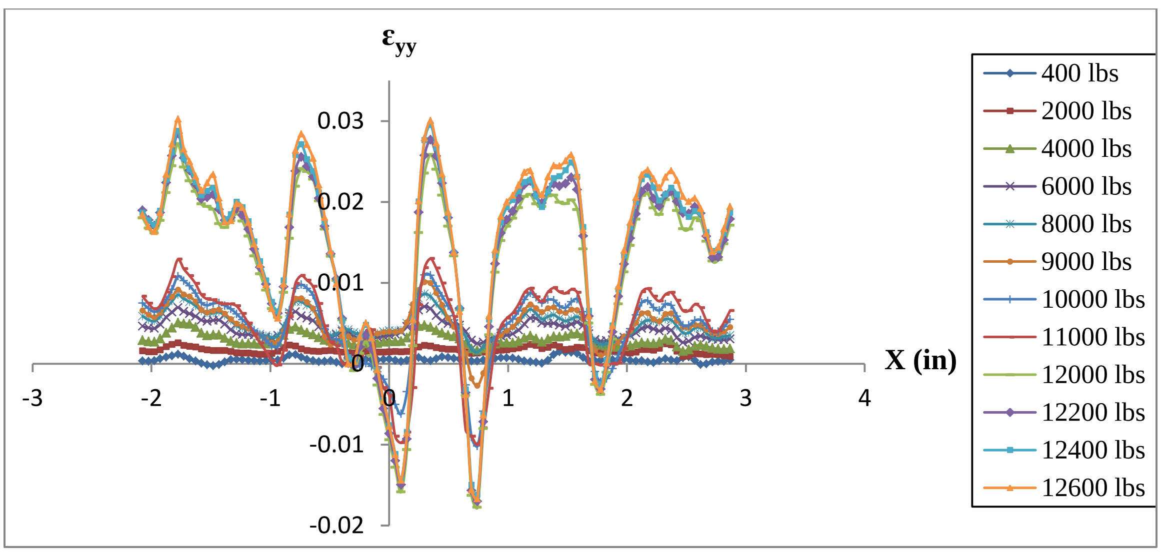

Figure 4-274: The strain distribution (ε_{yy}) along a cross section line (2-2)

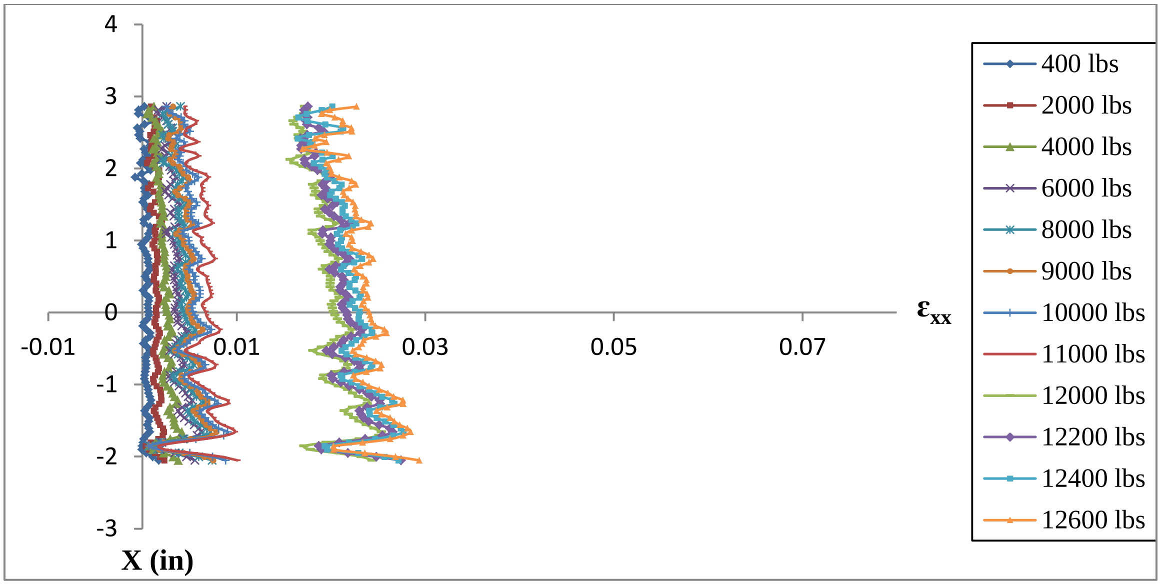

Figure 4-275: The strain distribution (ε_{xx}) along a cross section line (3-3)

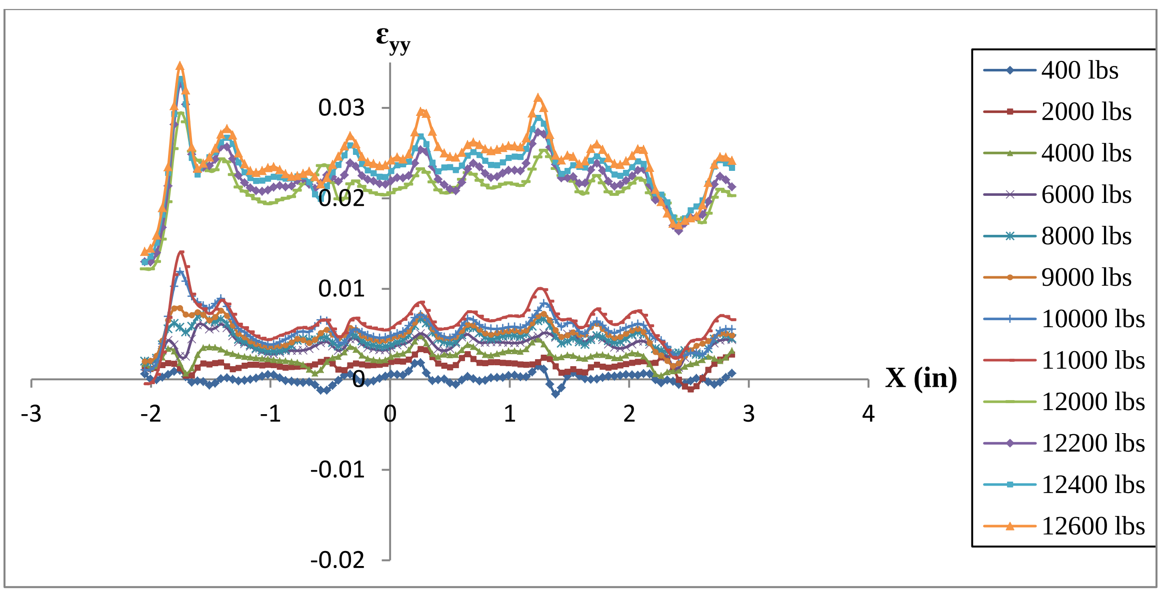

Figure 4-276: The strain distribution (ε_{yy}) along a cross section line (3-3)

The strain (ε_{xx}) and (ε_{yy}) along the middle horizontal cross section line (2-2) is shown in Figure 4.273 and 4-274 respectively. Over this cross section line, the strain (ε_{xx}) is tensile strain and shows spikes in the strain (ε_{xx}) starting from a load of 9,000 pounds. The spikes in the strain (ε_{xx}) curve increase with loading. The last four strain curves at a load of 12,000 pounds until failure at a load of 12,600 shows a similar strain (ε_{xx}) curve. This high sudden change in the strain curve is due to high influencing of the load on the middle of the plate. The cross section line (2-2) runs through the little area between two slots, and these little areas repeat along the cross section line (2-2). These areas are weak, so the large changes in the strain are in the middle of the plate. The strain along the diagonal line is the highest ones comparing to the other strain values. The strain (ε_{yy}) in the previous figures also shows high changes at a load of 12,000 pounds until the last image at a load of 12,600 pounds. The tensile strain turns to compressive strain over the diagonal gap line. However, the rest of the plate is influenced by tensile strain. A large gap is between the strain curve (ε_{yy}) at a load of 11,000 and 12,000 pounds. That means the plate after a load of 12,000 pounds becomes weaker. The vertical middle of the plate possesses the highest change in the strain.

4.2.3.4 The Third Truss Failure

The truss fails at different places as shown in Figure 4-277.

Figure 4-277: The truss image after failure

Figure 4-277 shows that all the joints start to fail by an increase of the load. The plate on the top joints starts first to fracture from the bottom to the top, then the right heel joint-plate shows more tooth withdrawal than the left heel joint-speckled plate. The tooth withdrawal is shown in many places on the plate especially on the axis of the plate over the diagonal gap between the two connected members of wood. More detailed images for the three truss joints-plates are shown in Figures 4-278 to 4-80.

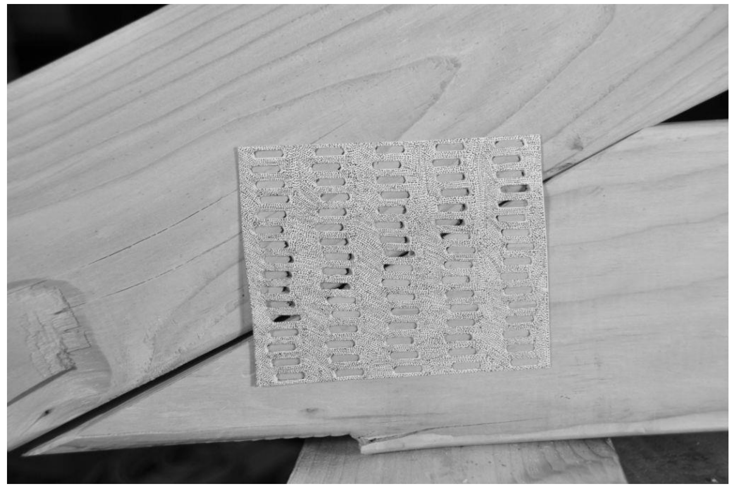

Figure 4-278: The left side heel joint-speckled plate just after failure

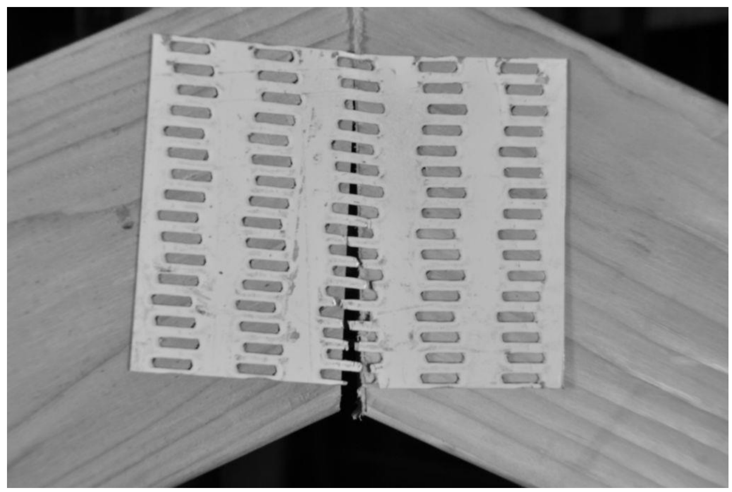

Figure 4-279: The plate on the top joint of the truss just after failure

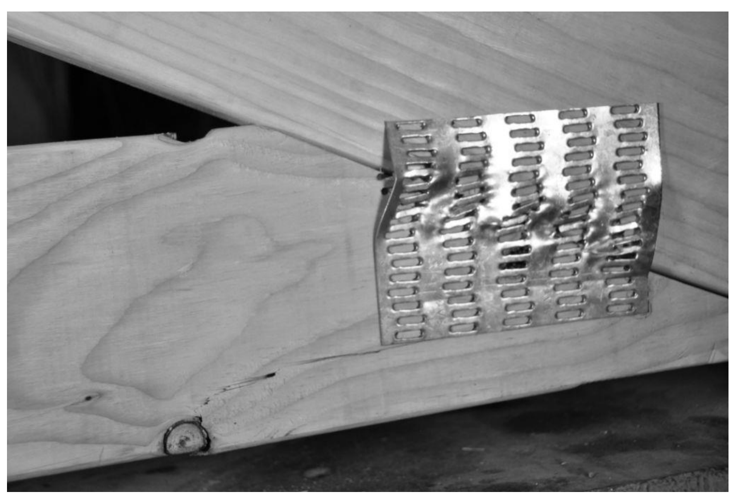

Figure 4-280: The right side heel joint-plate just after failure

The failure starts in the plate that is located on the top joint of the truss. A fracture starts from the bottom of the plate and increases as the load increases. At the same time, the plates on the heel joints also show tooth withdrawal. The right side heel joint-plate, which is the main point of failure, shows larger tooth withdrawal than the left side heel joint-speckled plate. The speckled plate on the left side heel joint also starts to fail by tooth withdrawal; however, it does not show large tooth withdrawal. The main reason for failure was not in this plate in this test. The tooth withdrawal is observed in the axis that is over the diagonal gap between the two connected wood members. The failure in the right side heel joint-plate along the axis that is located over the gap between the two connected wood members is evident as shown in the previous figures and shows a twist on the plate around that axis.

Besides the failure in the plates in this test, the bottom wood member also has cracked in the right side and it is shown in Figure 4-280. The crack is also under the right side heel joint-plate. There was a crack in the wood under the left side heel joint-speckled plate also.

4.2.3.5 Summary of the 3rd Heel Joint Test

The strain curve at the vertical lines over the plate shows tensile strain in both directions from a load of 200 pounds until a load of 9,000 pounds. That means the plate is stretching and expanding from both directions. At a load of 9,000 pounds the strain curves over the diagonal gap line, which is over the gap where the two members of wood are connected, shows a significant change in the strain values and the strain direction. The strain (ε_{yy}) at a load of 10,000 pounds shows compressive strain on the diagonal gap line. This strain increases with loading until the failure at a load of 12,600 pounds. The strain (ε_{yy}) is a tensile strain underneath and above the diagonal gap line; however, it is compressive along the diagonal gap line. The strain (ε_{xx}) along the vertical direction is tensile strain from the beginning of the test until the failure. The significant increase in the strain (ε_{xx}) is evident along the diagonal gap line. The strain (ε_{xx}) beneath the diagonal gap line is larger than that above the diagonal gap line.

The strain (ε_{xx}) in the horizontal direction shows slight changes in the strain curve starting from a load of 200 pounds until a load of 11,000 pounds on the top and the bottom of the plate. Then there is a large gap in the strain values between the strain curve (ε_{xx}) at a load of 11,000 pounds and a load of 12,000 pounds which indicates that the plate starts to be weaker. The middle horizontal line strain curves show more changes in the strain. Several spikes in the strain curves are observed to increase with loading. The full-field strain measurement (ε_{xx}) show the strain (ε_{xx}) is a high tensile strain along the diagonal gap line. The changes in strain (ε_{xx}) are higher on the left side of the plate than the right side.

In this test, when a deformable body is subjected to a force it will elongate in one direction and contract in the other, can be shown along the diagonal gap line. The remaining parts of the plate , the strain (ε_{yy}) is tensile strain not compressive strain.

The failure in this test is not in the left heel joint where the speckled plate is. Thus, the speckled plate is not in failure. The strain behavior for the speckled plate shows the behavior of the plate before failure and how the plate behaves under loading. The shear forces in the teeth still can hold more load.

4.2.4 Fourth 4^{th} Heel Joint Test

A fourth heel joint test was performed in the lab and the results were very similar to the third test results. A total of 61 images were captured and implemented in digital image correlation software. The truss failed at a load of 12,200 pounds. In this test, the truss was set on the universal testing machine and the camera was placed in a fixed location in front of the speckled plate that was located on the left heel joint. The first image before loading was captured as a reference image Figure 4-281. A total of 61 images were captured for this test before failure besides the reference image. The truss failed at load equal to 12,200 pounds. All the captured images were implemented in DIC software to find the full-field strain measurements.

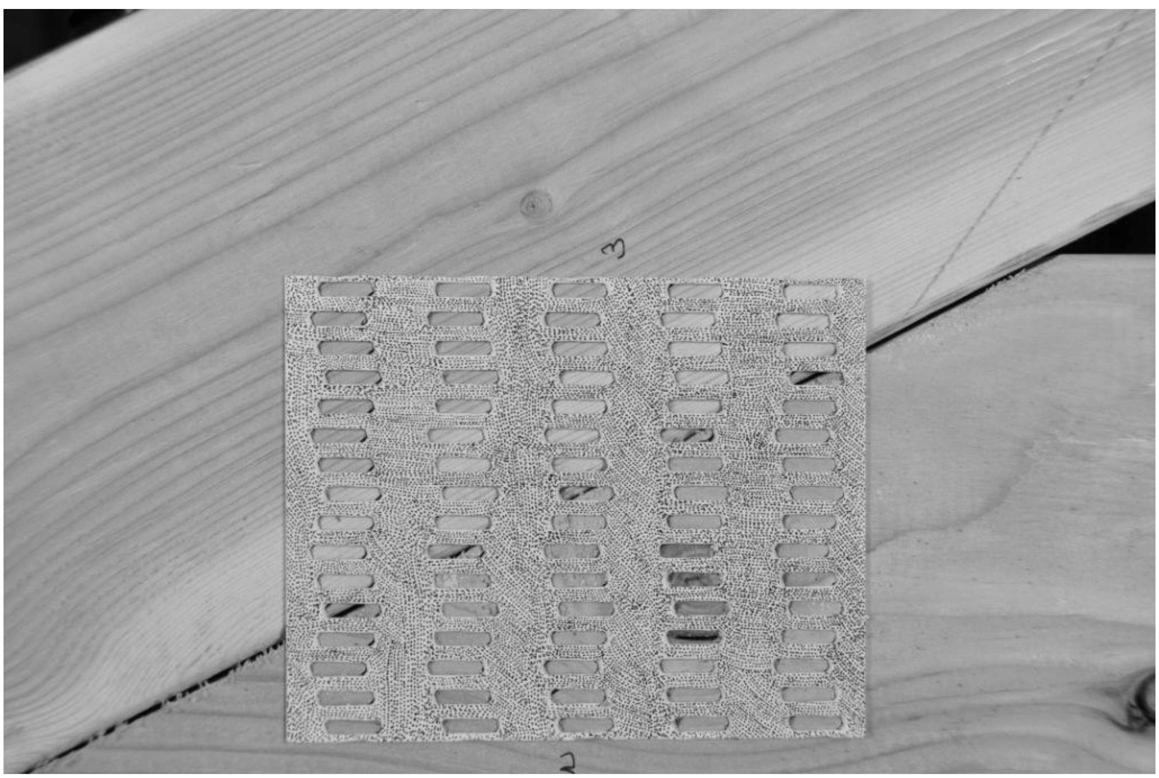

Figure 4-281: The reference image in the third heel joint test

4.2.4.1 The Truss Failure

The truss fails at different places as shown in Figure 4-282.

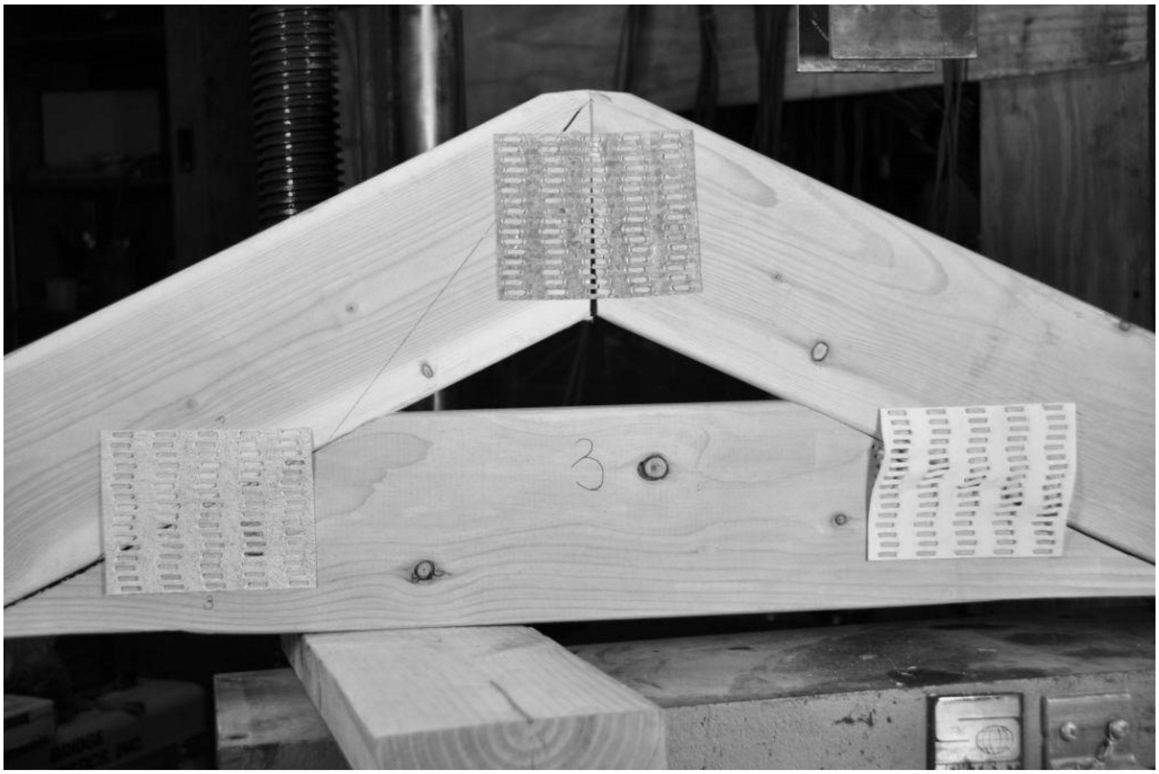

Figure 4-282: The truss image after failure

Figure 4-282 shows that all the joints start to fail by an increase of the load. The plate on the top joint starts first to fracture from the bottom to the top then the right heel joint-plate shows more failure tooth withdrawal than the left heel joint-speckled plate. The right heel joint-plate represents the failure for the whole truss. The tooth withdrawal is shown in many places on the plate especially the axis of the plate that is over the gap between the two connected members of wood. More detailed images for the three truss joints-plates are shown in Figure 4-283 to 4-285.

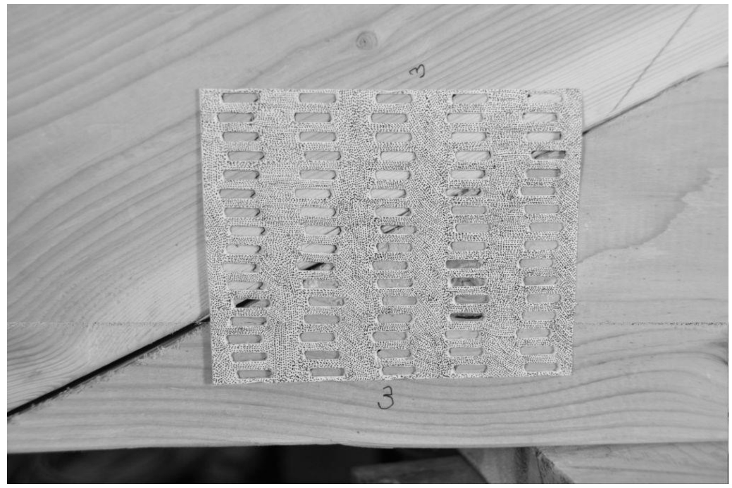

Figure 4-283: The left side heel joint-speckled plate just after failure

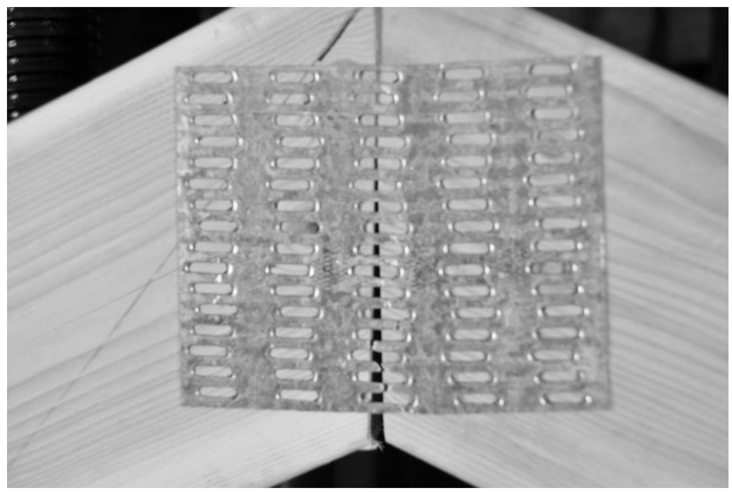

Figure 4-284: The plate on the top joint of the truss just after failure

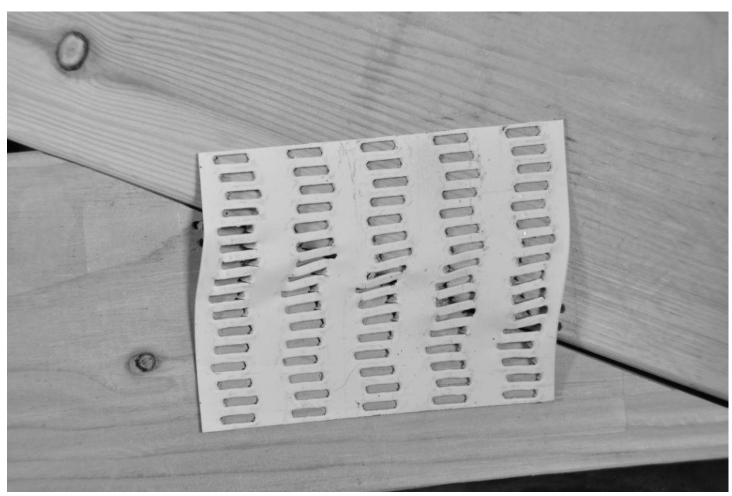

Figure 4-285: The right side heel joint - plate just after failure

The failure starts in the plate that located on the top joint of the truss. A fracture starts from the bottom of the plate and increases as the load increases. At the same time, the plates on the heel joints also show tooth withdrawal. The right side heel joint-plate shows larger tooth withdrawal leading to failure than the left side heel joint-speckled plate. The speckled plate on the left side heel joint also starts to fail by tooth withdrawal but, it does not show a large withdrawal. The main failure was not in the speckled plate. The tooth withdrawal is in the axis that is over the gap between the two connected wood members. The failure in the right side heel joint-plate along the axis over the gap between the two connected wood members is evident as shown in Figure 4-283 and shows a twist on the plate around that axis.

In general, in this test the truss fails due to tooth withdrawal of the right side heel joint-plate and the entire plate figures show the failure. The top plate on the top joint starts to fracture as shown in Figure 4-284 from the bottom to the top of the plate. This shows that the location of the fracture is along the middle of the plate which has slots there. Thus, the area of the plate is half of the area in other places which makes it weaker and easier to crack than other places on the plate.

4.2.5 Heel joints Summary and Discussion

The heel joint for the four previous tests shows similar results. All of the tests show that the strain (ε_{yy}) along the diagonal gap line holds very high compressive strain at loads of more than 9,000 pounds. The general strain (ε_{yy}) on the plate from the beginning of the test until a load of 9,000 pounds is tensile strain and the general horizontal strain (ε_{xx}) is tensile strain also. Therefore, the full-field strain measurements show tensile strain in both horizontal and vertical direction. This strain is tensile strain from beginning of the test until a load of 9,000 pounds. At a load of 9,000 pounds, the strain (ε_{xx}) significantly increases especially along the diagonal gap line that is located between the two connected wood members. However, the strain (ε_{yy}) on some regions of the plate, where it shows no indication of weakness or failure, is a tensile strain. Other regions may turn to compressive strain. Some regions also show lower tensile strain values with high load than the other strain regions at lower load. Therefore, the strain on the plate until a load of 9,000 pounds is tensile then the plate extends in both directions.

The truss is influenced by external force affecting the top of the truss. Two reactions are created on the two heel joints. The top external force is compressive and the reactions on the heel joints are also compressive force. The force that is created in the horizontal wood member (lower chord member) is a tensile force. The force in the diagonal wood member (top chord) is a compressive force. The logical strain results on the speckled heel joint plate are to have a tensile strain (ε_{xx}) in the horizontal direction and compressive strain (ε_{yy}) in the vertical direction. However, looking through the digital image correlation full-field strain measurements from the beginning of the test to a load of 9,000 pounds reveals that the strain (ε_{yy}) and (ε_{xx}) is tensile strain. What makes the strain (ε_{yy}) tensile instead of compressive strain is the presence of the teeth. The teeth are distributed over the plate regularly and in a wavy pattern. These teeth create shear stress and this shear stress is everywhere the teeth are. Thus, the external load will be transferred to the wood then from the wood to the plate throughout the teeth. The teeth will react against this external force as a shear force. The angles of the teeth significantly influence the direction and the value of the force that affects the metal plate.

The full-field strain results show that the vertical strain (ε_{yy}) is tensile strain instead of compressive strain until a load of 9,000 pounds and these results are due to the resist of the teeth. The teeth expand the plate vertically. After a load of 9,000 pounds, the strain (ε_{yy}) along the diagonal gap between the two connected wood members turns to compressive strain. On the other hand, the strain (ε_{xx}) holds a significant increase in the tensile stain along this diagonal gap. Thus, the teeth lose their effect on the plate after applying a load of 9,000 pounds along the diagonal gap region. The remaining areas of the plate show sometimes lower tensile strain (ε_{yy}) than the strain at lower load. Or sometimes some regions on the plate show compressive strain (ε_{yy}) along the vertical direction. Although the strain (ε_{yy}) is tensile strain after applying a load of 9,000 pounds, it is in general less than the earlier strain (ε_{yy}) which indicate that the shear forces from the teeth becomes weak and cannot hold higher load. In general, the strain (ε_{xx}) is tensile strain at most of the loading stages and shows a significant increase after applying a load of 9,000 pounds. The plate has failed in different ways in the four tests due to different reasons as shown in table 4.1. The maximum load that has been applied on the plate is 13,800 pounds. Tooth withdrawal in test #2 made the plate fail earlier than expected, as the truss failed due to tooth withdrawal at a load of only 10,800 pounds. The strain (ε_{yy})

holds high tensile and compressive strain values as high as the strain (ε_{xx}). The strain (ε_{yy}) and (ε_{xx}) can reach up to -0.1 and 0.11 respectively.

Table 4-14: 13 the failure descriptions of the four heel joint tests

Test #	Failure load (lbs.)	Total Deformed Images	Failure Behavior Descriptions
1	13,800	69	left speckled heel joint plate failed due to tooth withdrawal and fracture of the top plate
2	10,800	54	left speckled heel joint plate failed due to tooth withdrawal
3	12,600	63	plate failure on the right side of the heel joint and wood cracks
4	12,200	61	plate failure on the right side of the heel joint

Thus, the strain (ε_{xx}) cannot be ignored and should be considered as the strain (ε_{yy}). During the loading, the area of the plate that is located underneath the diagonal gap line moves to the right while the area above the diagonal gap line moves to the left. A twist of the plate's area that is located along the diagonal gap line can be observed after applying a load of 9,000 pounds. Figure 4-286 shows a failure due to the twisted area.

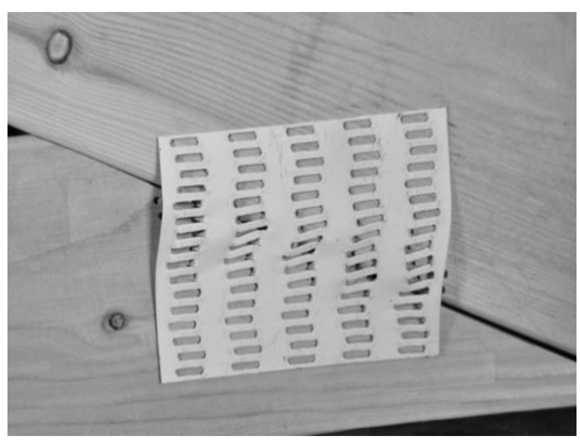

Figure 4-286: Twisted plate of some regions of the plate

CHAPTER V

CONCLUSION

The overall goal of this research is to find the full-field strain measurements for the metal plate connections using the digital image correlation DIC technique. Also, to provide deeper understanding for the failure mode based on strain analysis.

Four basic tension joints tests (AA, AE, EA and EE) were performed in the laboratory. Each test was repeated three times. A Nikon CCD camera was used to capture the deformed images at a load increment of 200 pounds until the failure occurs. All the captured images were implemented in the digital image correlation software Vic-2D to obtain the full-field strain measurements for each deformed image.

A simple truss was made in the laboratory to obtain a heel joint. Four simple trusses were tested until failure. One camera was used to capture the deformed images of one heel joint-speckled plate. The captured images were implemented in digital image correlation software to obtain the full-field strain measurements.

.

Chapter 3 in this research describes the tests' apparatus, material, and the methodology of testing and related conditions. It also clarifies the DIC technique as methodology and its basics and related conditions.

Chapter 4 shows the testing laboratory results and the digital image correlation-strain results. Each test has its own strain behavior. A total of 16 tests were performed in the lab and each test had several deformed images. The deformed images from each test were analyzed by the DIC software to obtain the full-field strain measurements. Chapter 4 showed and discussed the resulting strain field images. A summary and a discussion of each test are provided at the end of the test section.

5.1 Why this research is useful?

- Digital image correlation method is an optical, nondestructive and non-contact method in which the surface of the specimen can be analyzed directly regardless of the properties of material such as wood or concrete or ceramics. These advantages make DIC a desirable approach to find the strain or to track any cracks in addition to using it in medical research.

- Metal plate connections (MPC) are an important member in the wood truss industry. Thus, deeper understanding for its strain behavior under different stages of loading can be useful in future modeling and explaining failure modes. Strain behavior of MPC can give indication of the strength of MPC.

5.2 Heel Joint

A simple truss is made to obtain a heel joint as shown in Figure 5-1. Four simple trusses are made to test the heel joint. The interested heel joint is the left one where the speckled plate is set there to connect the two wood members together. The full-field strain measurements in both directions are obtained from digital image correlation Vic-2D code.

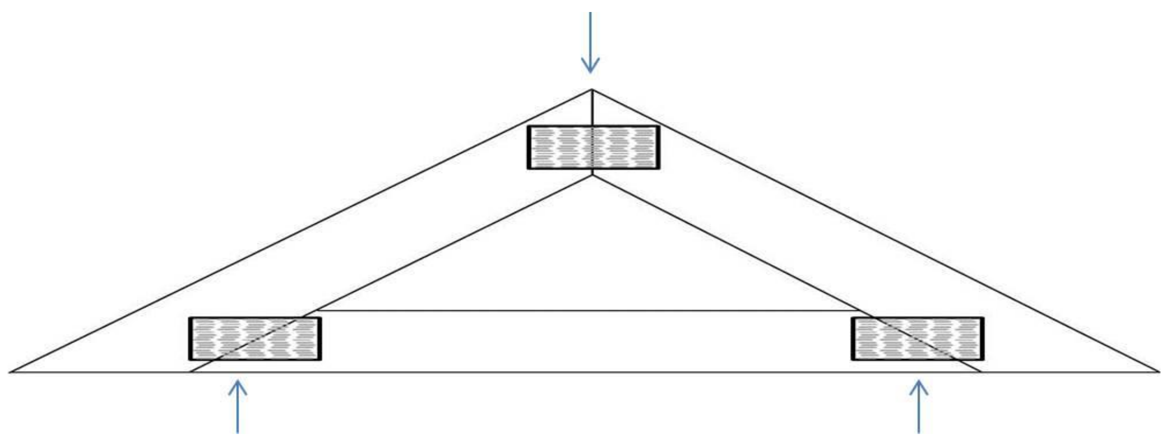

Figure 5-1: the simple truss with three metal plates connects the wood member at the front joints

The truss is influenced by external compressive force affecting the top of the truss. A compressive reaction is created on the two heel joints. The force that is created in the horizontal wood member (bottom chord) is a tensile force. The force created in the diagonal wood member (top chord) is a compressive force. Based on these reactions, the logical strain results on the speckled heel joint plate are to have a tensile strain (ε_{xx}) in the horizontal direction and compressive strain (ε_{yy}) in the vertical direction. The full-field strain measurements can be obtained from DIC software. All four heel joint tests show that the strain (ε_{yy}) along the diagonal gap line holds high compressive strain. And the strain (ε_{xx}) shows a significant increase in its values especially along the diagonal gap line that is located between the two connected wood members. However, there are some exceptions for this general information. The strain (ε_{yy}) in some regions of the plate does not show any indication of weakness or failure and it is influenced by tensile strain but other regions may turn to compressive strain. In general, the strain on the plate until a load of 9,000 pounds is tensile strain and the plate is extending in both directions. After applying a load of 9,000 pounds, the influence of the external force increases and this result is shown along the diagonal gap line. The strain (ε_{xx}) is tensile strain; however, after applying a load of 9,000 pounds, a significant increase occurs in the tensile strain (ε_{xx}) along the diagonal gap line. The strain (ε_{yy}) shows a decrease in the tensile strain and some regions turns to compressive strain especially along the diagonal gap line.

In general, the load is applied on the top metal plate as a compressive force on the top and the two bottom heel joints. The top (wood member) chord is supposed to hold compressive force and the bottom chord holds tensile force. Due to loading the top plate tears from the bottom toward the top as shown in figure 5-2.

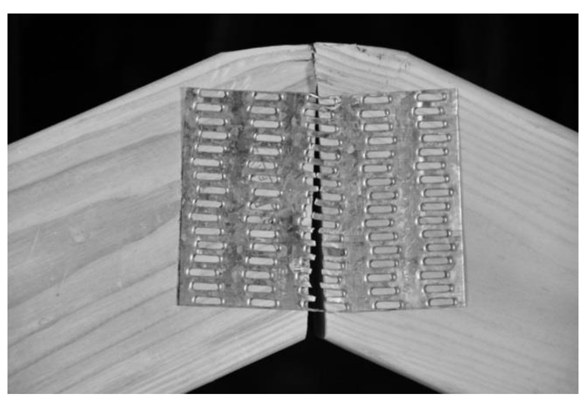

Figure 5-2: the top plate on the simple truss after failure

At the same time, the plates at the heel joints show also significant changes. The area of the plates along the diagonal gap line shows a disorder. This disorder is a result of many forces affecting the plate at the same time. Figure 5-3 shows the plate before failure and the disorder of the plate's area along the diagonal gap line.

Figure 5-3: The plate on the heel joint shows the disorder of the plate's area along the diagonal line

Under load the area of the plate under the diagonal gap line is affected by tensile strain thus, the strain in x-direction (ε_{xx}) moves away from the top chord member toward the direction of the tensile strain in the bottom chord member. The tensile strain (ε_{xx}) is highest on the diagonal gap line. The area of the plate above the diagonal gap line moves away from the bottom chord. The strain in x-direction is tensile strain and high along the diagonal gap line. The strain in y-direction is very low tensile strain and very high compressive strain along the diagonal gap line. Thus, along the diagonal gap line the strain in x-direction (ε_{xx}) is high tensile strain and in y-direction it is high compressive strain (ε_{yy}). This kind of movement is due to a combination of forces acting on the heel joint. One of these combinations is the rotation that is created in the top chord member of the truss due to the tear of the top plate. The gap at the end (to the left of speckled plate) increases with loading due to the effect of tensile force while the gap on the right side of the speckled plate closes with loading due to the effect of compressive force. Figure 5-4 show the truss after failure.

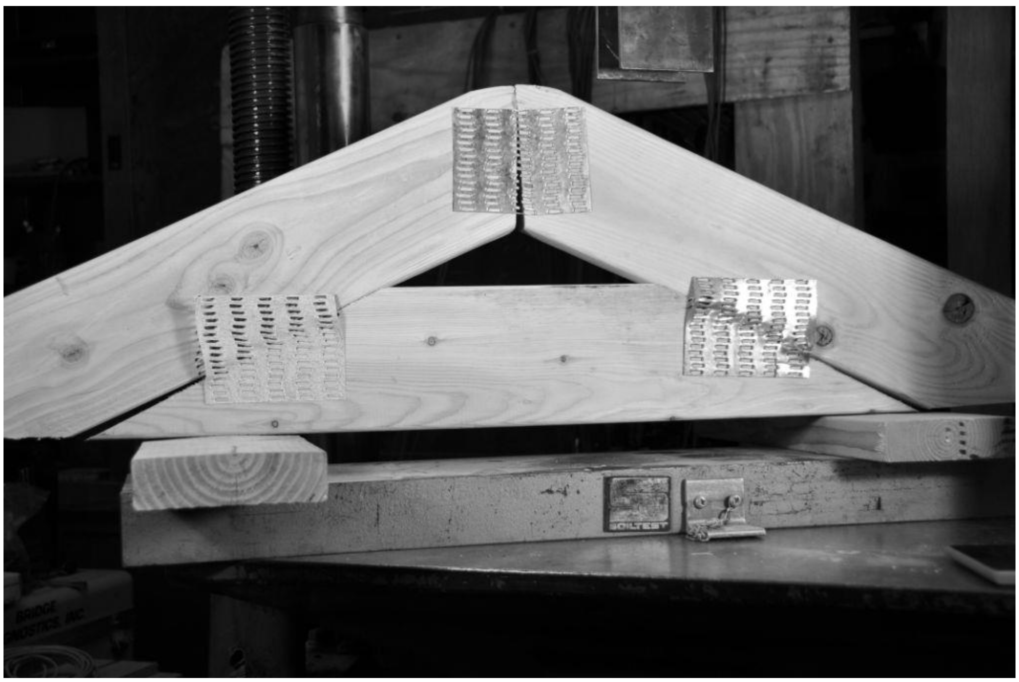

Figure 5-4: The truss after failure show the failure at the three front joints

The last figure shows the tear of the top plate and the movement of the plate under loading as shown in the right heel joint. The left speckled joint has failed due to tooth withdrawal. The tear in the top plate leads to a rotation in the top chord member. This rotation of the top chord member makes changes in the plate’s strain behavior. Buckling of the plate occurs on the top right edge and the bottom left edge of the plate where it crosses the diagonal gap line. This buckling is due to the influence of the rotation. Due to the rotation, the area of the plate above the diagonal gap line is under low tensile strain (ε_{yy}). The area of the plate beneath the diagonal gap line is also under low tensile strain in y-direction due to the effect of the tensile stress in the bottom chord member. Along the diagonal gap line the strain (ε_{yy}) is high compressive strain and the strain (ε_{xx}) is high tensile strain. The influence of the rotation causes the plate to fail due to tooth withdrawal. The plate along the diagonal gap line does not tear because of the rotation of the top chord member which leads the top area of the plate on the heel joint to fail due to tooth withdrawal as shown in figure 5-5.

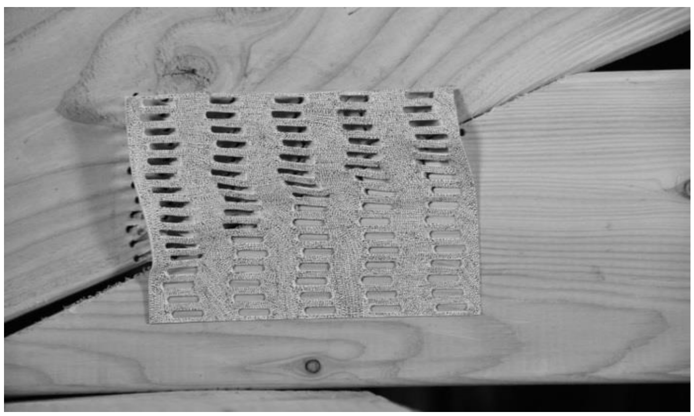

Figure 5-5: The heel joint-speckled plate fails due to tooth withdrawal for the area above the diagonal gap line

The heel joint plates in all tests show buckling in both sides the top right and the bottom left in all tests as shown in figure 5-6. This buckling is an introduction to tooth withdrawal. The buckling is especially shown on these two sides as a result of compressive force from the top chord member and the rotation of this member due to the tear of the top plate from the bottom to the top. Due to the rotation of the top chord member, the plates tend to fail by tooth withdrawal. The diagonal gap line is influenced by compressive strain (ε_{yy}) which increases with loading; the strain (ε_{xx}) in the horizontal direction is tensile strain and increases with loading.

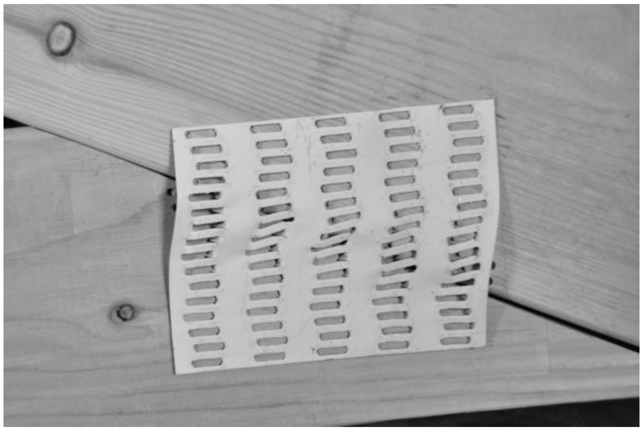

Figure 5-6: The heel joint-plate shows buckling of the plate on both sides

There are different load combinations and circumstances in the heel joint plate. The truss is made of wood which is anisotropic material. The heel joint of interest is the one on the left side. The images just show the left speckled heel joint plate and at the failure all the three front plates can be seen. However, the truss also has another three plates on the back and they are under the same situation of the front three plates. Their behavior also influences the behavior of the front plates. The camera just catches the front plates that connect the joints.

5.3 Four Basic Tensile-Joint Tests

Four basic tension-joint tests are conducted in the lab to obtain the full-field strain measurements. The four tests are different based on the direction of the load with respect to the plate's major axis and the wood grain. The tests are AA, AE, EA and EE. A letter indicates the load direction which is parallel to the plate's major axis or the wood grain. E indicates to the load direction when it is perpendicular to the plate's major axis or to the wood grain. The previous four lab tests show different strain behavior and failure mode for each test. In the first test AA, the plate is ruptured at the failure. The strain along the horizontal line above the gap shows a significant increase then it yields. The plate fails due to plate tear. The strain above the horizontal middle gap line is almost mirror to the strain underneath the gap line. In the test EA, the plate fails due to tooth withdrawal. The strain field results show an increase in the strain with loading until failure. The strain above the middle horizontal gap line is higher than the strain underneath the gap line. Along the horizontal gap line, the strain tends to be high. The plate in this test does not yield. The tooth withdrawal is the main reason for failure. The part of the plate where tooth withdrawal occurs shows higher tensile strain than the other part as shown in images in chapter 4. The region of the plate that does not influence by tooth withdrawal remains in stable well-organized strain distribution. This strain behavior explains the failure mode and direction. The strain distribution over the plate changes on the plate's side that shows tooth withdrawal later; however, there is no significant changes in the strain field to show yielding point. The next two tests AE and EE fail due to cracks in the bottom wood members. However, digital image correlation code is able to analyze the strain behavior at low loads. The full filed strain behavior and analysis for the two tests are shown in chapter 4. The strain field shows that when the load is low then the strain over the plate fluctuates and varies; however, the strain increases with increasing load. The strain will show an organized distribution when the external load takes over the teeth shear forces (teeth resistance).

Finally, the strain field shows similar strain values over the plate's surface at low load. The strain above the horizontal middle line over the gap is almost mirror to the strain underneath the horizontal gap line unless tooth withdrawal or wood cracks occur. If the joint shows high gripping teeth, the plate will yield and a significant rise in the strain (ε_{yy}) and (ε_{xx}) is observed. The regions of the plate that do not show any indication for failure tends to have high teeth gripping; thus, the teeth resistance controls the plate. The results show that when the load is parallel to the wood grain, the plate show high strength and high teeth griping than the load when it is perpendicular to the wood grain.

5.4 Stress-Strain Diagram

The stress strain diagram is constructed between the external tensile load and the resulting strain from DIC code. The first tensile test AA is contributes the stress-strain diagram because it is the only test showing yielding and then tearing of the plate. Thus, the plate yields and then fails due to the rupture along the middle horizontal gap line under loading affect. The area along the middle horizontal gap line is considered to define the stress-strain diagram and the modulus of elasticity (E) from the slope of the curve. Figure 5-7 shows the metal plate at AA-test before loading and at failure.

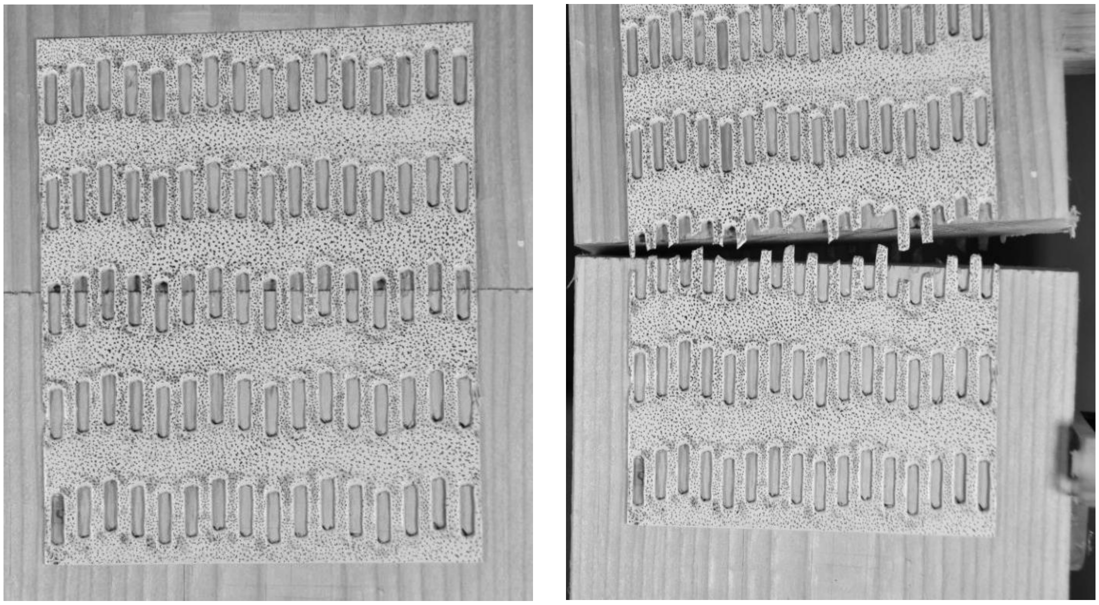

Figure 5-7: The plate before loading and at failure for AA test

The stress-strain diagram is found at three different locations as shown in Figure 5-8 where the vertical lines cross the horizontal line along the gap. The first location is where the first cross section line (1-1) crosses the horizontal line which is located to the right side of the plate. The second location is near the middle along the cross section line (2-2) and the third location is to the left side of the plate along the cross section line (3-3).

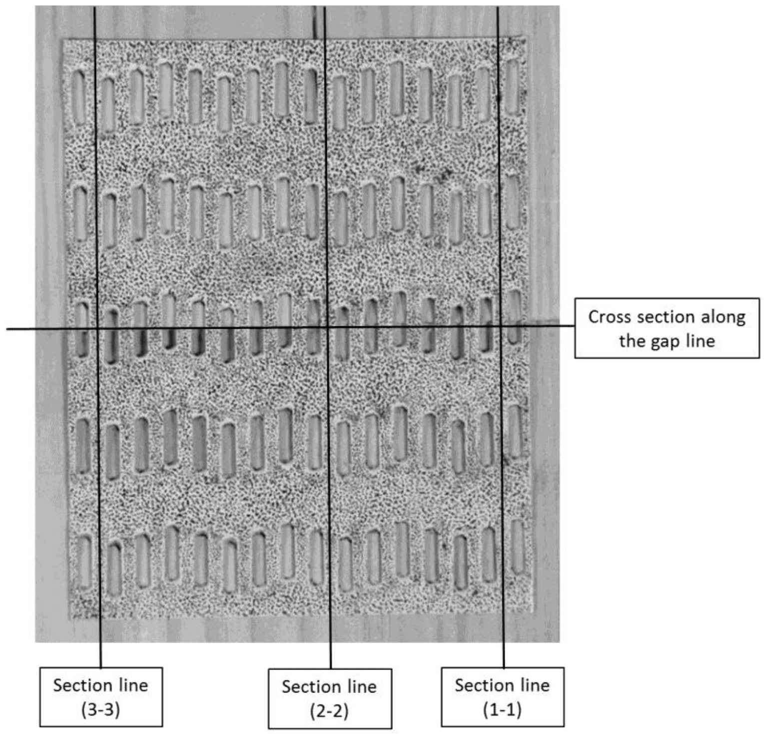

Figure 5-8: The locations of the three cross sectional lines on the plate surface

The load is assumed to be uniformly distributed over the area. The teeth are supposed to transfer the entire external tensile load to the plate. The friction between the plate and the wood is ignored. The load is applied on the top wood member. There are two metal plates to connect the joint. One is on the front and the other is on the back of the joint. Thus, the load is equally divided between them. The width along the middle horizontal gap line is half of the width (4 in) due to the holes (slots). The thickness of the plate is 0.0359 in. the stress is calculated based on the load divided by the area. The area is the thickness of the plate multiplied by the width which is equal to 0.0718 in^2. The strain is found from the DIC strain field with results derived from the three locations mentioned above at different loads ranging from 200 pounds to 8,600 pounds before failure. After constructing the stress strain diagram, the modulus of elasticity can be found by finding the slope of the curve at elastic region. A linear regression is used to find the best slope. The stress strain diagram does not show an exact yielding point thus, an offset of 0.002 on the strain axis is used to construct a new slope parallel to the modulus of elasticity slope and intersect with the curve which then shows the yielding point as shown in Figure 5-9. The avg. modulus of elasticity (E) is found in table 4.1.

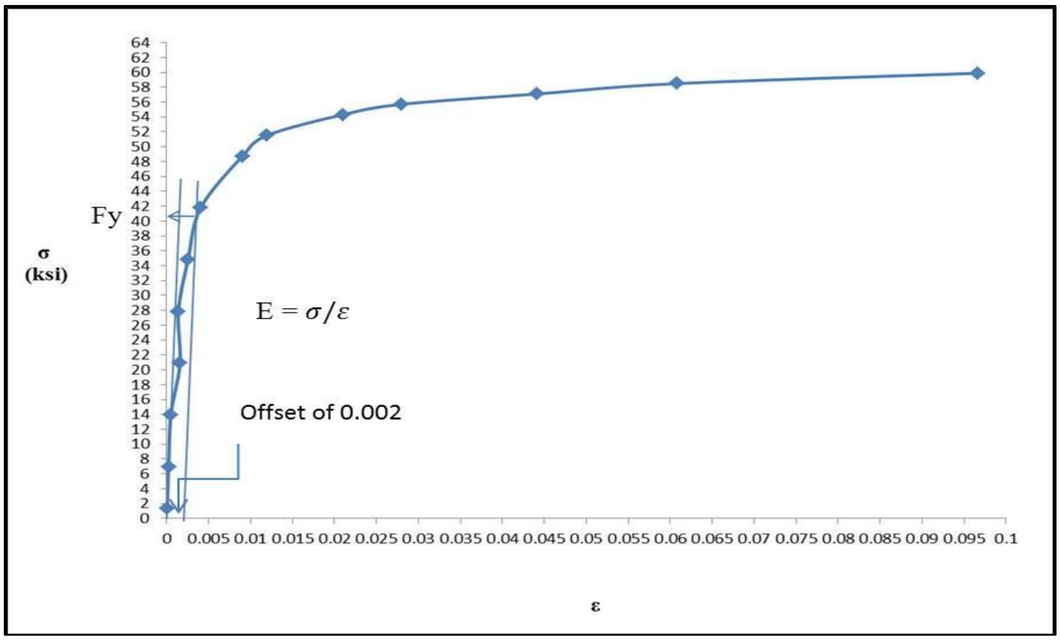

Figure 5-9: the offset in stress-strain diagram for test AA

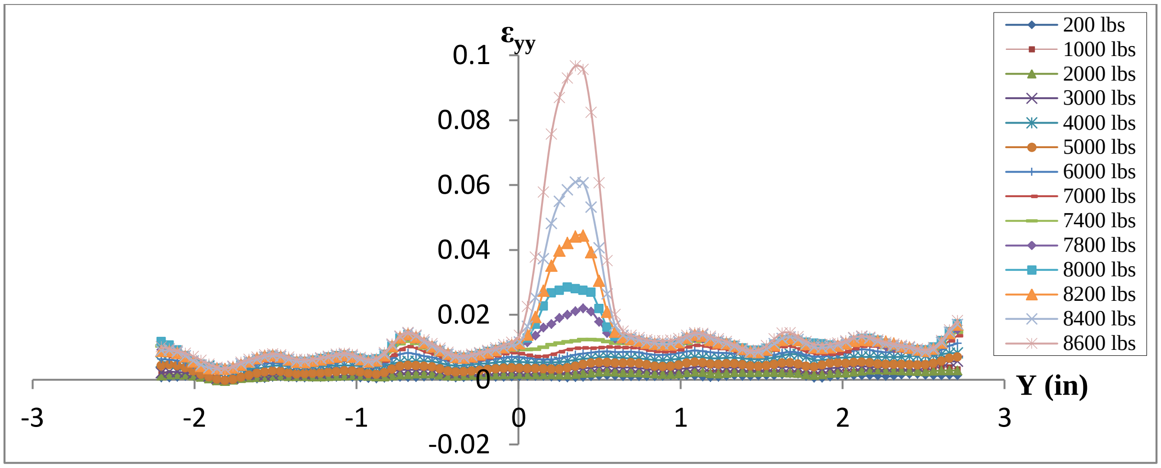

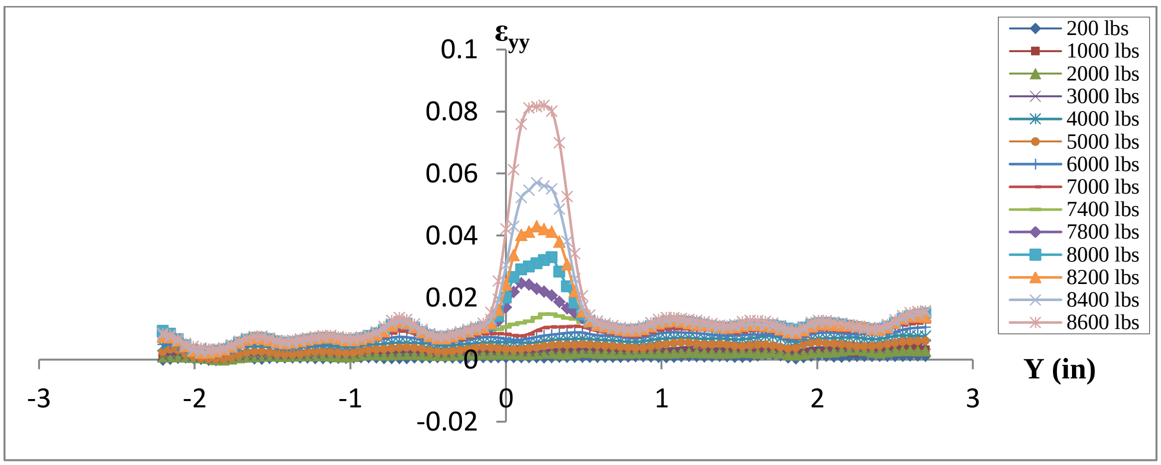

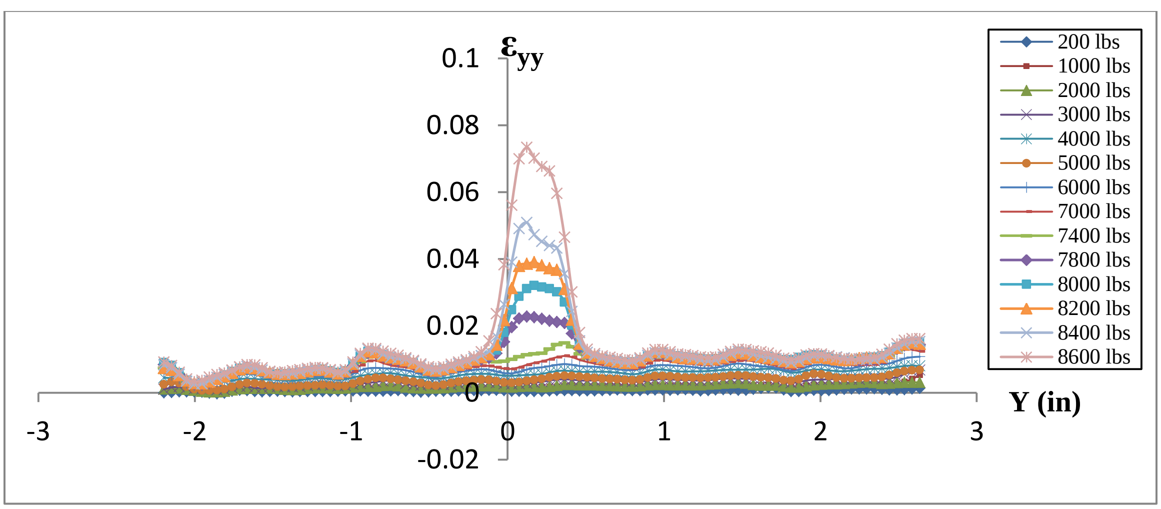

Figure 5-10: the strain along the cross section (1-1), (2-2) and (3-3) respectively for the second test AA

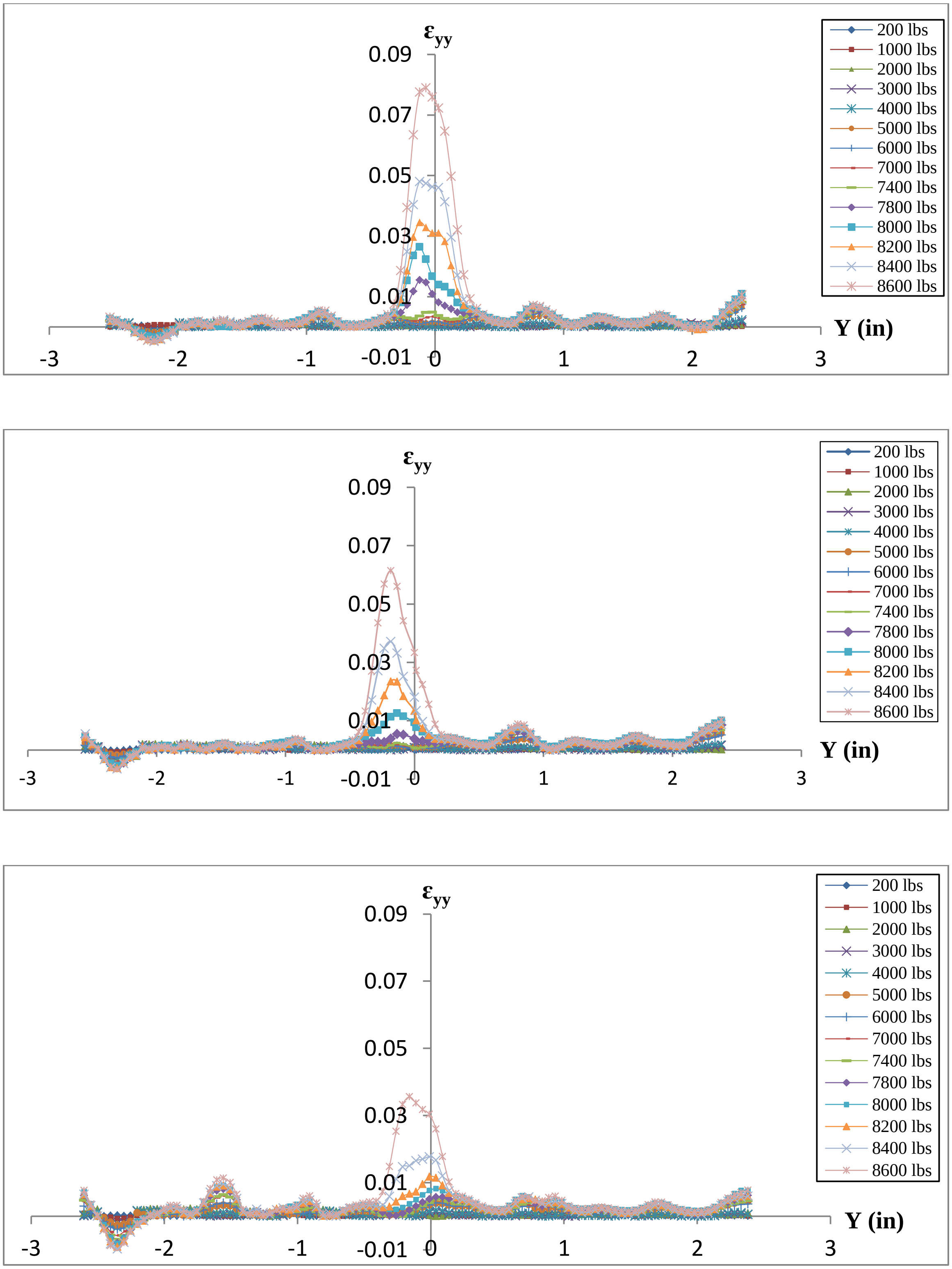

Figure 5-11: the strain along the cross section (1-1), (2-2) and (3-3) respectively for the third test AA

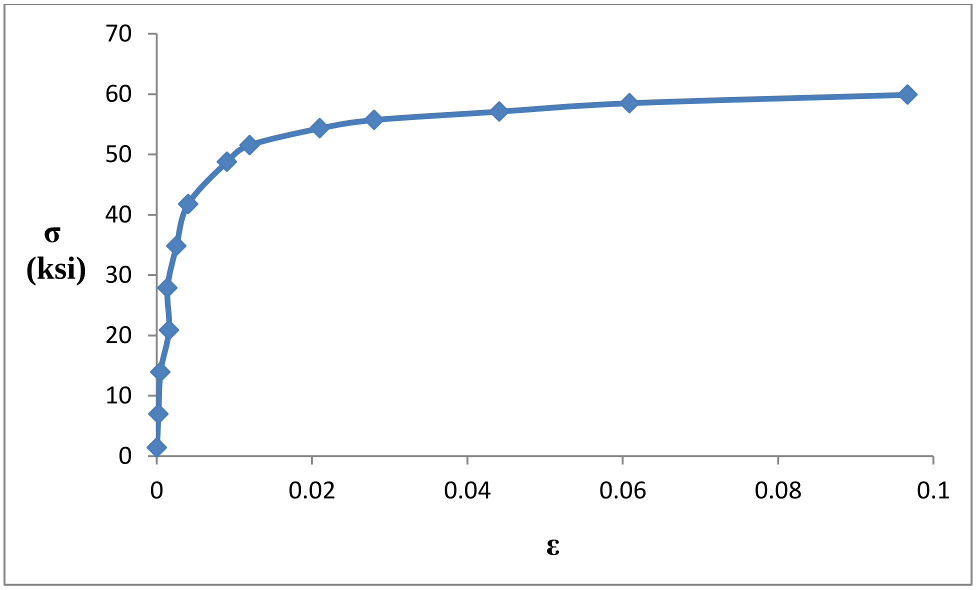

Figure 5-12: Stress-strain diagram for AA-2nd test at cross section line (1-1)

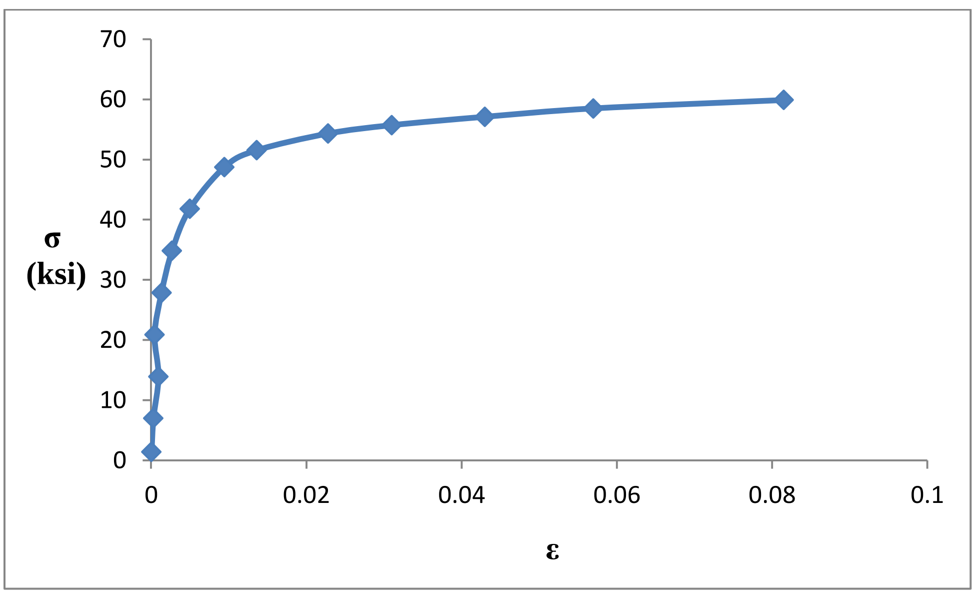

Figure 5-13: Stress-strain diagram for AA-2nd test at cross section line (2-2)

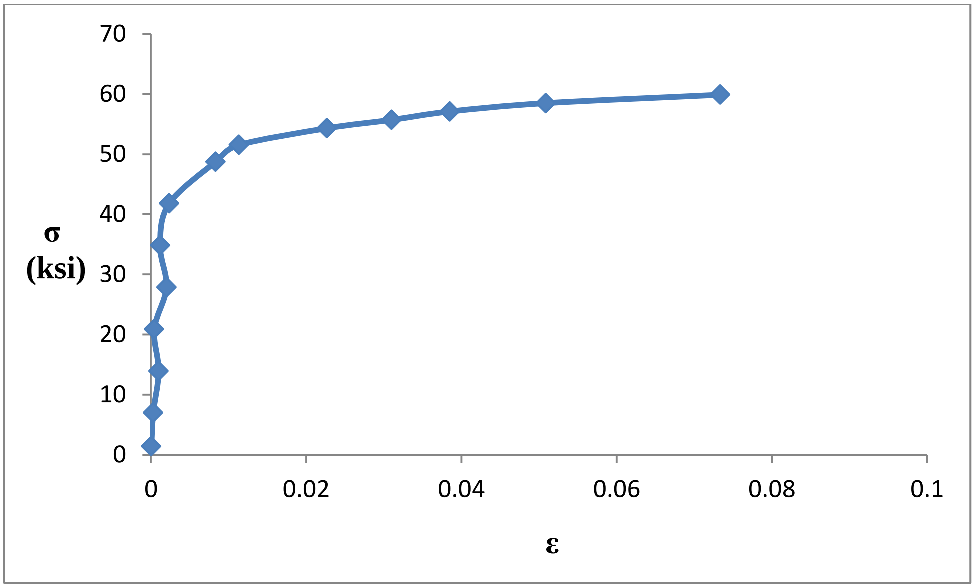

Figure 5-14: Stress-strain diagram for AA-2nd test at cross section line (3-3)

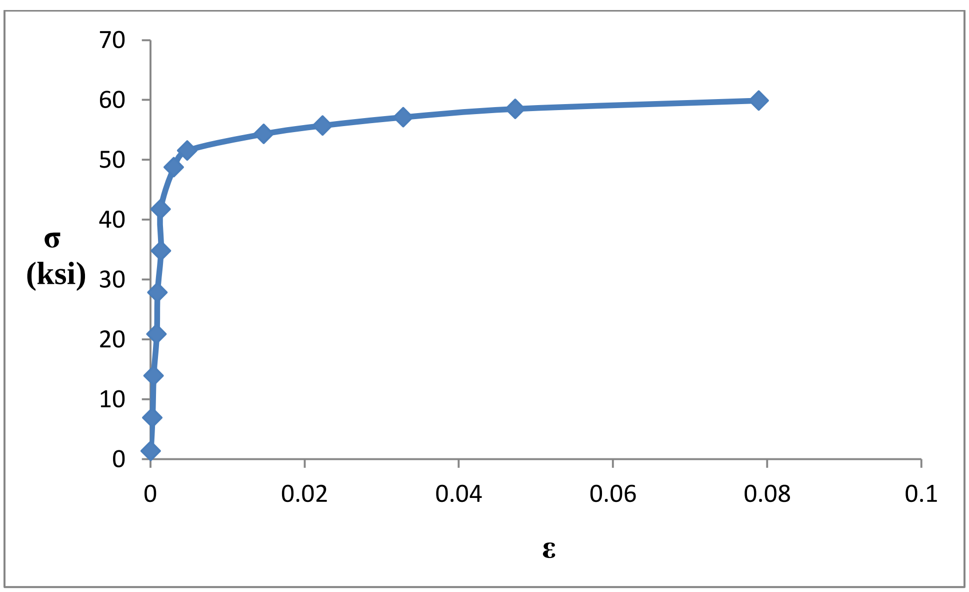

Figure 5-15: Stress-strain diagram for AA-3rd test at cross section line (1-1)

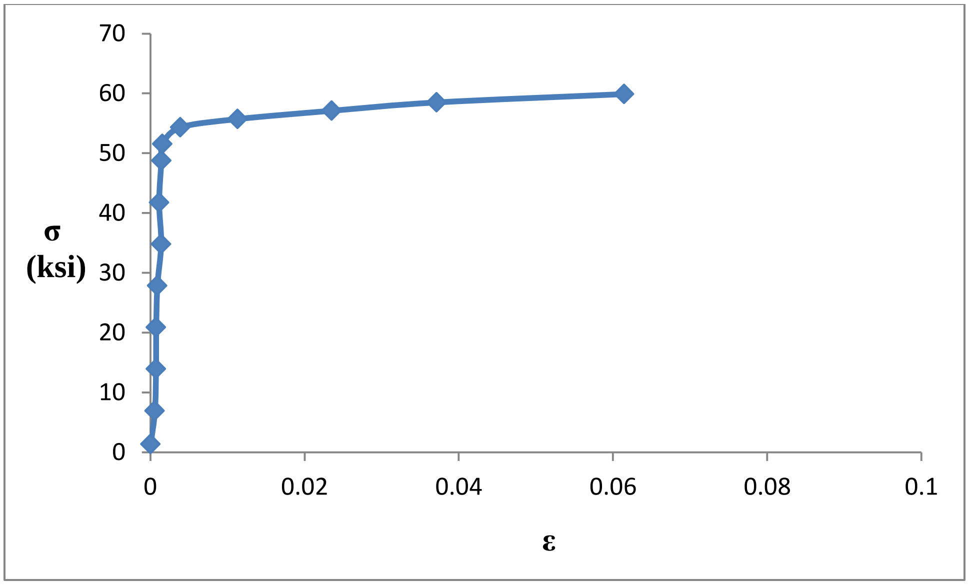

Figure 5-16: Stress-strain diagram for AA-3rd test at cross section line (2-2)

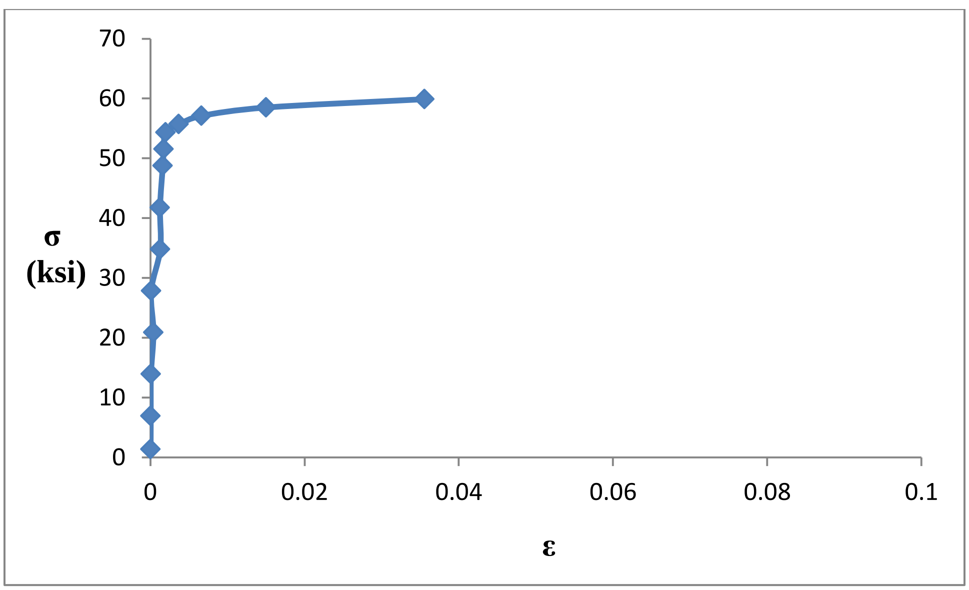

Figure 5-17: Stress-strain diagram for AA-3rd test at cross section line (3-3)

Table 5-1: The modulus of elasticity and the yielding stress for the metal plate at test AA obtained from the stress strain diagrams

Test	position	E (ksi)	Fy (ksi)	F @ fracture(K)	Ft (ksi)
test AA-2nd	Line 1-1	27.7	40.5	8.65	60
test AA-2nd	Line 2-2	27.1	38.5	8.65	60
test AA-2nd	Line 3-3	28.7	44	8.65	60
test AA-3rd	line 1-1	27.2	49	8.64	59.88
test AA-3rd	Line 2-2	30.8	53	8.64	59.88
test AA-3rd	Line 3-3	29.9	55	8.64	59.8
	AVG. =	28.57	46.67	8.65	59.93

The plate is G40 steel gauge 20. The specifications of this plate based on ASTM A653ss G40, Fy (minimum) is 40 ksi and Ft (minimum) is 55 ksi. The ASTM specifications agree with the full field strain results found using the DIC technique.

The stress-strain diagram from the digital image correlation can be changed to a load-displacement diagram in order to compare it to the load-displacement diagram from LVDT. The LVDT machines are placed on the right side of the first AA test and on the left and the right side on the second AA test. Figure 5-18 shows the location where the strain values are averaged then they are changed to displacement Δl. The original length of the segment is 0.5 in. The average strain is multiplied by 0.5 inches to find the displacement Δl. The strain is found by averaging the strain values at the interested segment at different loading conditions.

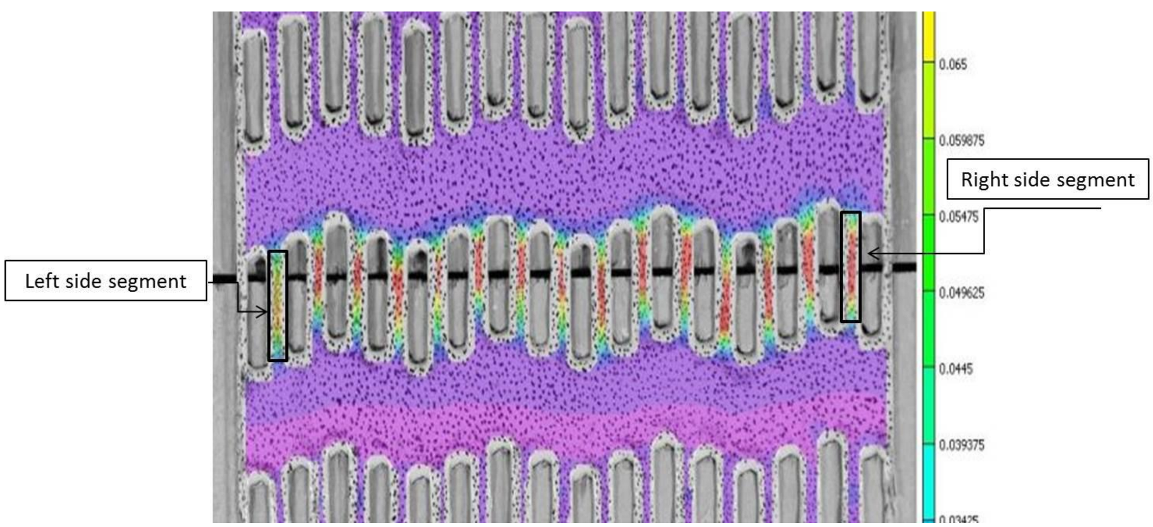

Figure 5-18: The locations of the plate's segments used to draw the load-displacement curve

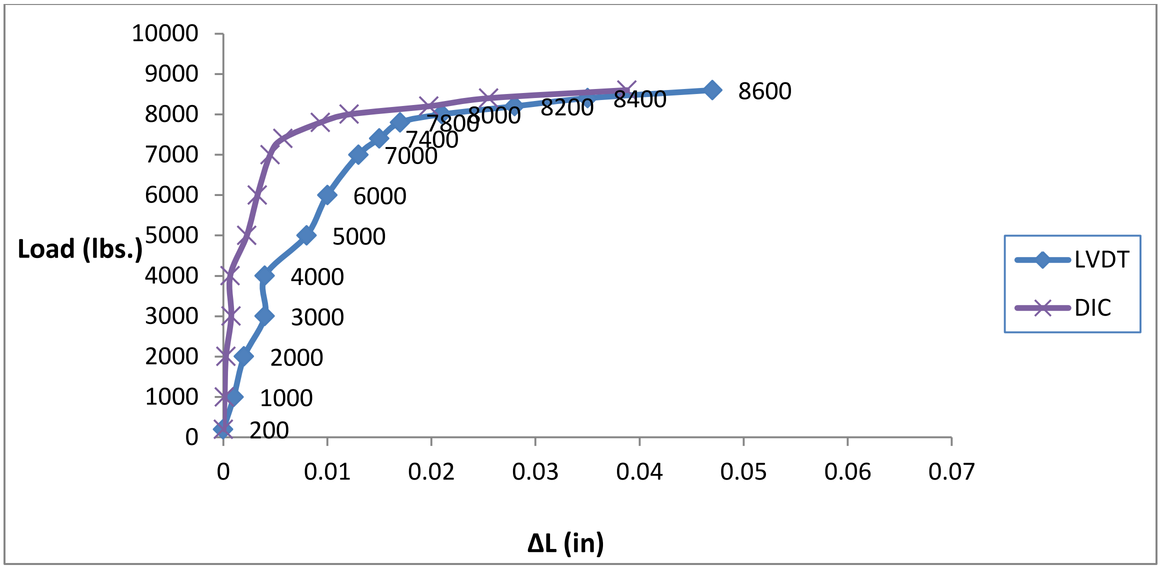

Figure 5-19: The load–displacement diagram for the left side segment of AA-1st

The curves show close results with divergence between the LVDT machine and the DIC technique through the middle of the test. However, they are not identical. The next figures show the curves for the second test AA. The results show more divergence between the LVDT and DIC than the divergence in test AA-1st. The right side segment shows higher displacement than the left side segment in both DIC and LVDT. Both curves from LVDT and DIC show the same direction of the increase in displacement with loading but they are not identical. Several factors cause this divergence between these two methods. The load is assumed to be uniformly distributed over the plate's area. However, the teeth may lose some of the load due to partial tooth withdrawal thus the displacement on the plate is ignored in all the calculations and the plate is considered as a free plate.

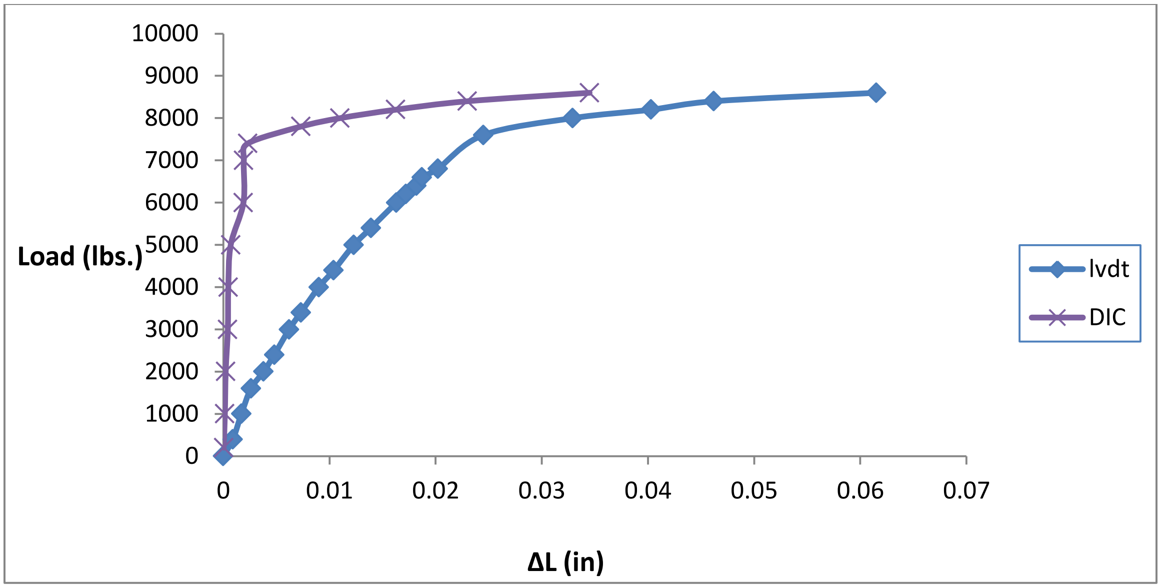

Figure 5-20: The load –displacement diagram for the right side segment of AA-2nd

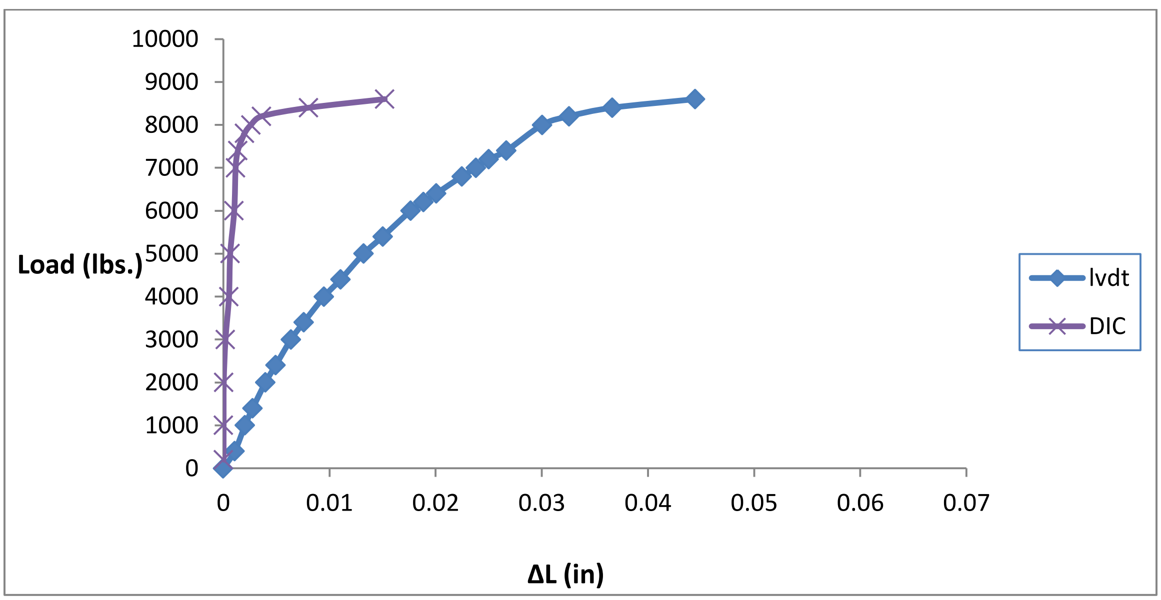

Figure 5-21: The load –displacement diagram for the left side segment of AA-2nd

The teeth of the plate are embedded inside the wood which is considered as an anisotropic material which has different properties in different direction thus the change between the LVDT and the DIC strain is under 0.02 inches, so all these factors can truly influence the strain results.

It is shown that the strain has a maximum value less than 0.1 and the displacements are less than 0.07inches. Thus due to the low numbers that are used in the strain and the displacement calculations, several factors could affect the results. The nature of the connected joint is complicated. It is a combination of the plate, the wood, and the teeth. The angle of the teeth embedded in the wood is supposed to be perpendicular to the wood plane. The teeth may have an angle inside the wood plane that can introduce some changes in the force transformation from the wood to the plate and could affect the displacement of the plate. The plate also has out-of-plane displacement that affects the DIC displacement and strain results. The DIC technique is used in 2D not 3D in this research. The gap on the right side is larger than the gap on the left side; it slightly increases linearly from the right to the left as shown in Figure 5-22 to 5-24 for AA test. Thus, the gap on the right side is higher than the left side in AA. The segment of the plate of interest on the right side, which was used to find the displacement, is located approximately 2 inches away from the LVDT location thus; the gap under that segment is less than the gap on the LVDT side. Thus, the load-displacement curve shows some divergence between the LVDT and DIC results. The bottom wood member surface in test AA-2nd shows a slope on the left side as shown in Figure 5-25 and some wood cracks are shown in Figure 5-24.

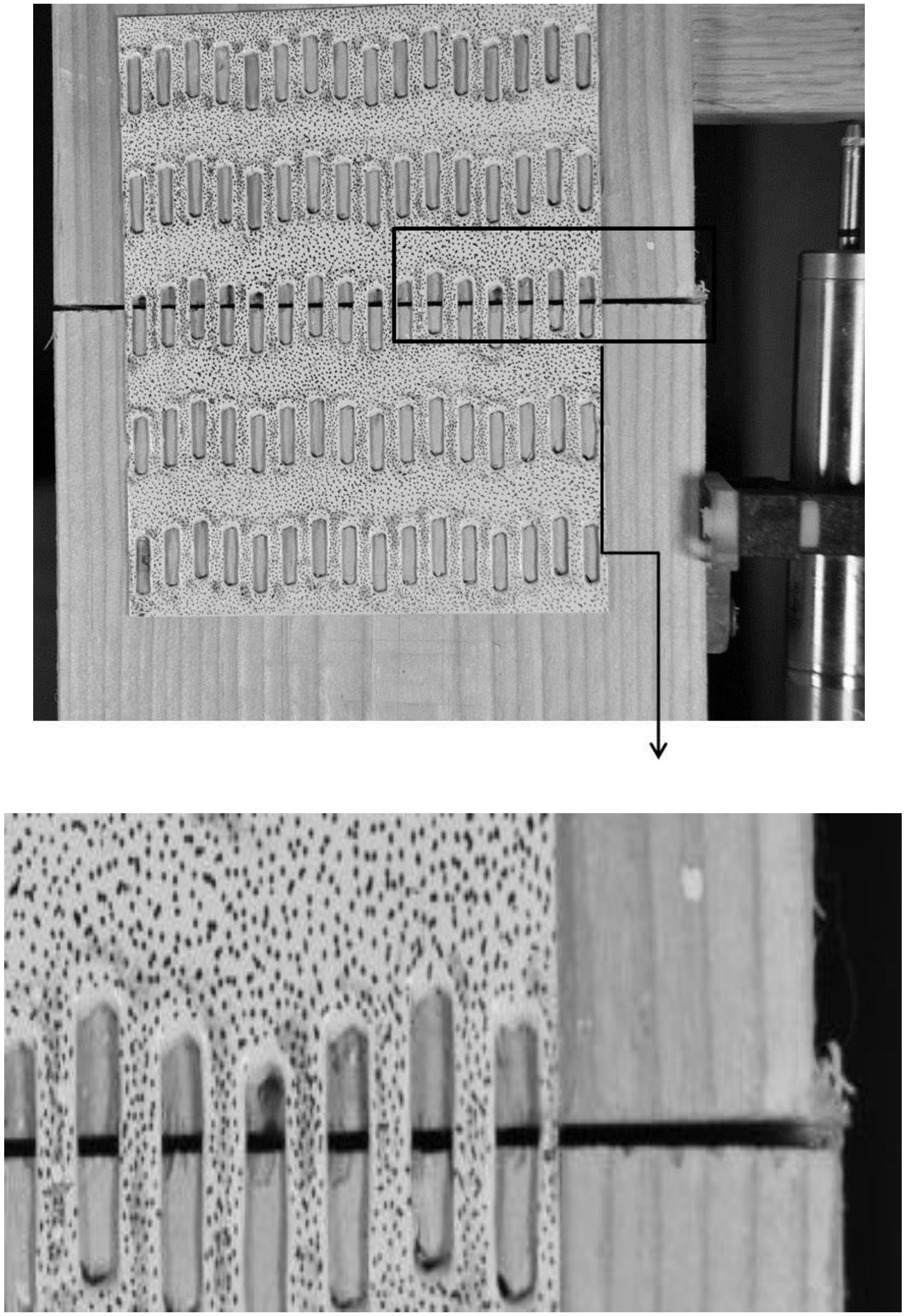

Figure 5-22: the gap at test AA-1st on the right side where the LVDT is higher than the gap under the segment of interest of the plate

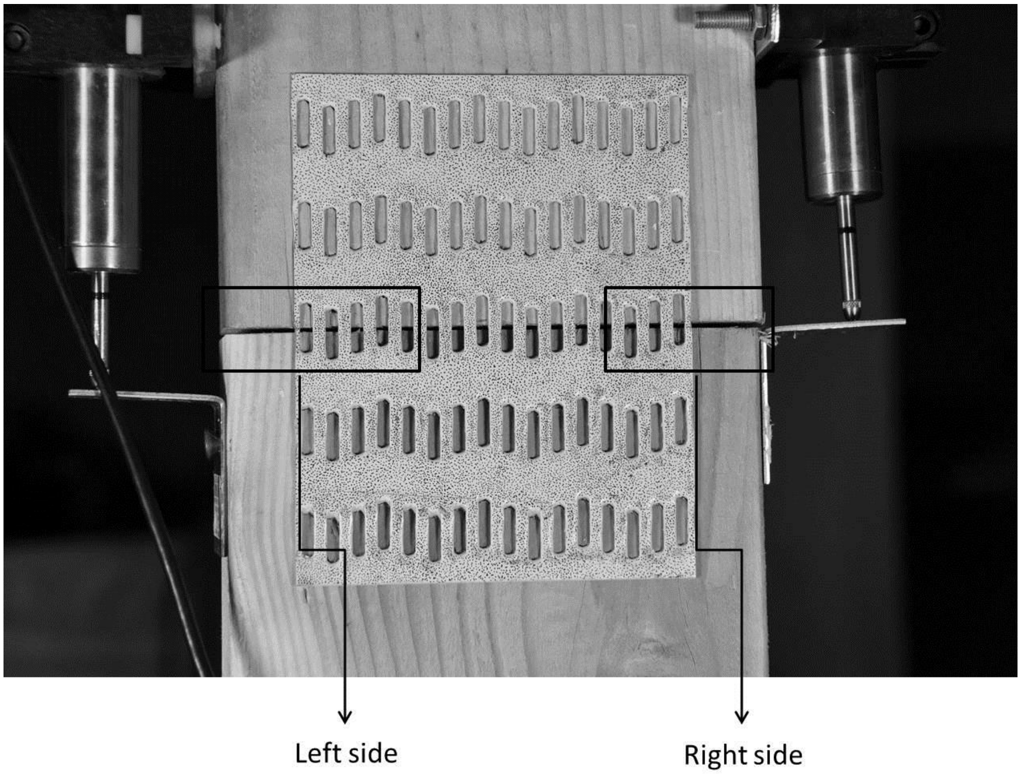

Figure 5-23: The gap at test AA-2nd on the right side and the left side where the LVDT is located

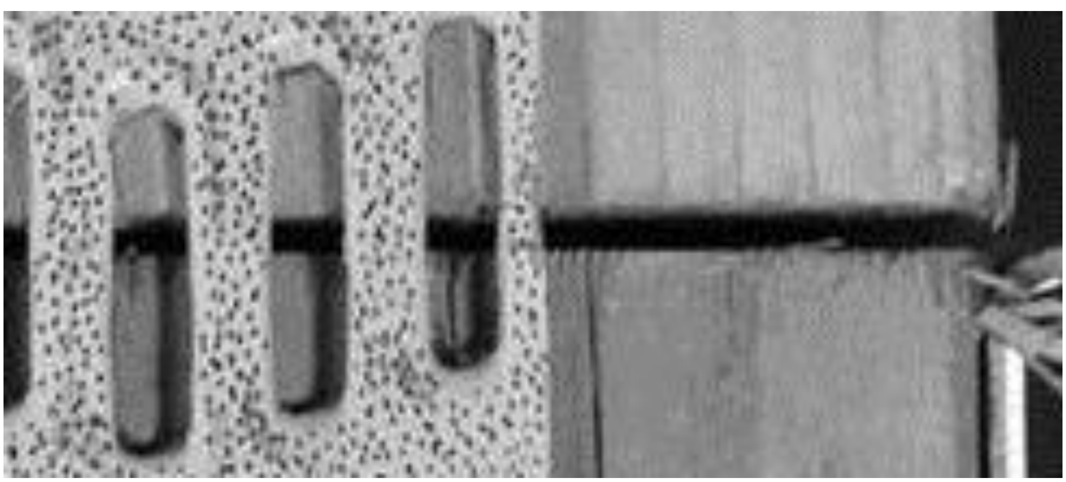

Figure 5-24: The gap at test AA-2nd on the right side segment

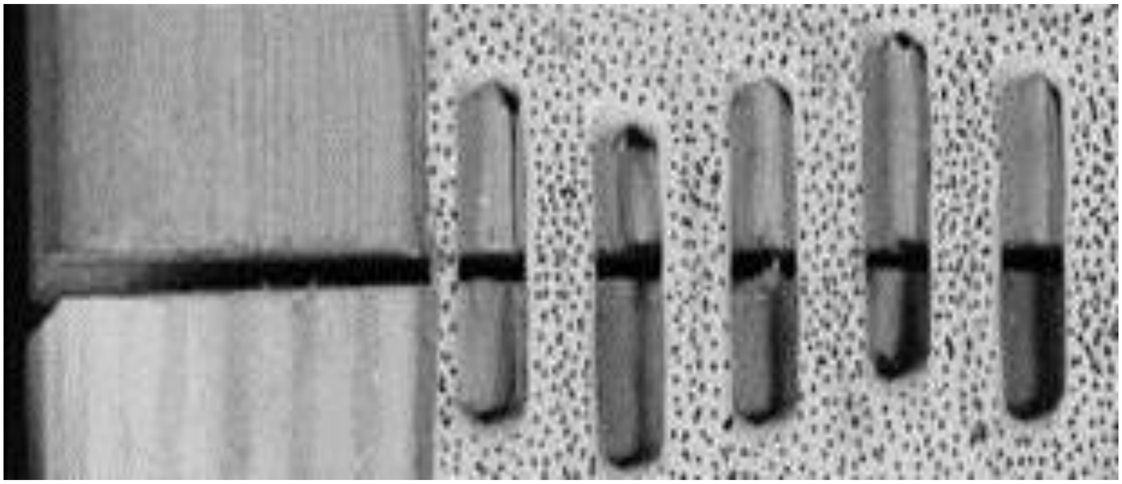

Figure 5-25: The gap at the test AA-2nd on the left side segment

The LVDTs are set on the side of the joint not on the front, so it measures the gap between the two wood members under loading. This gap is the sides gap not the front gap and it measures the gap between the wood not the plate itself. The LVDT is not exactly placed on the gap. Also, as shown in the figures the LVDT machine is not exactly placed perpendicular to the front surface, a slight slope can be seen.

The images show that there is gauge length of the LVDT which gives the displacement for the gap and the wood member length so that the LVDT displacement is higher than the DIC displacement. In the future the wood members should be speckled and the DIC used to find the displacement between them, and the LVDT should be placed on the interested speckled wood members to provide more accurate results.

One of the most important factors that affect the divergence between the LVDT and DIC test results is the local deformation of the wood around the tooth. When the load is applied on the wood member, it will be transferred to the teeth. Each tooth will react against this force, and it will move due to this force. Thus the movement of the tooth will cause a local wood deformation. This local deformation will affect the load that is transferred to the plate surface. Finally the amount of the load that the plate will receive from the tooth is less than the real amount. Therefore, if the relative displacement of the wood and the plate are different, then the gap between the two wood members will be higher than the displacement of the plate surface.

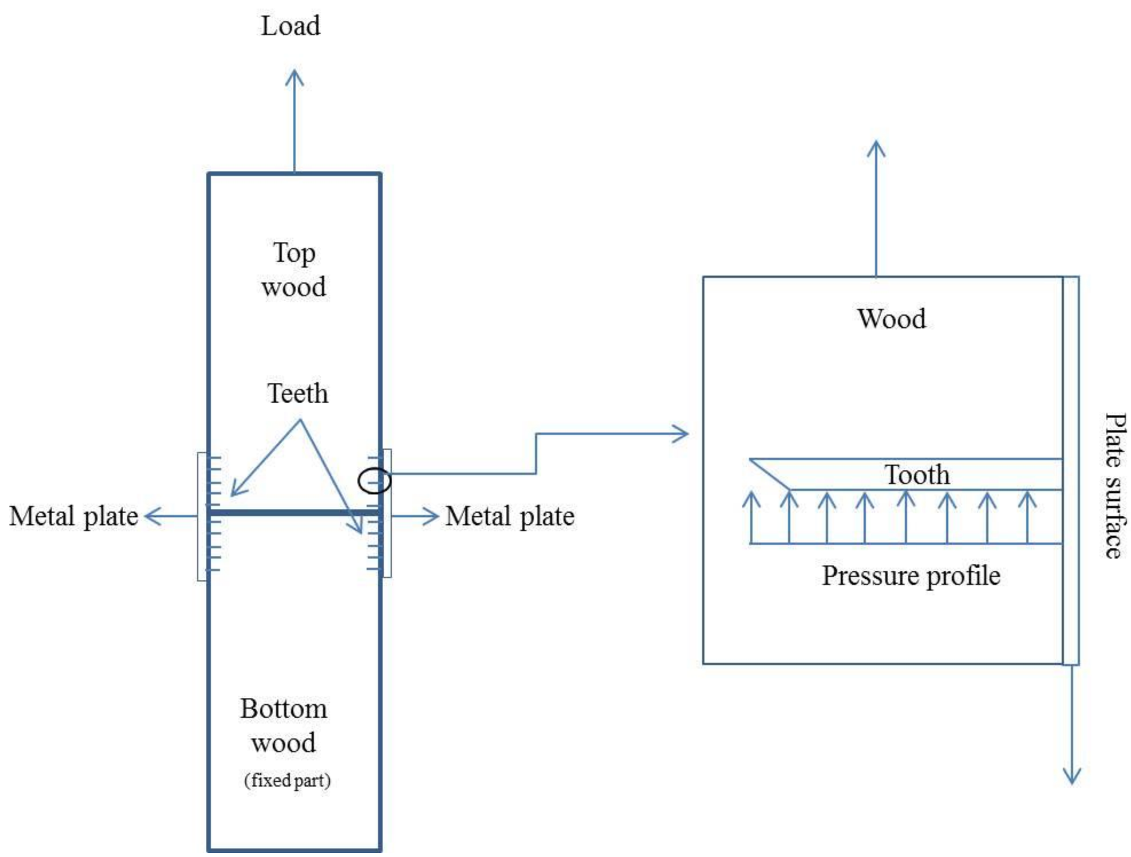

Figure 5-26: Analog of a tooth of metal plate inside the wood

Thus, overall there is a difference between the LVDT load-displacement curve and the DIC load-displacement curve. However, both curves move toward the same direction and the difference between them starts higher in the middle of the test then it becomes narrower by increasing the load as shown in the previous figures. The LVDT load-displacement curve gives an indication of the direction of load and displacement and can be compared to the DIC load-displacement curve. In the future the LVDT should be placed close to the interested plate segment to compare the displacement between the LVDT and DIC method.

(Montemayor, 2003) used the DIC technique to find the deformation in in cyclic triaxial testing. The results from DIC technique were compared to the LVDT measurements. There were a divergence between both techniques but they had the same trend. (De Keyser, 2011) also compared the deformation results that were obtained from DIC technique to the deformation results that measured using LVDT. The results showed divergence between the two techniques.

5.5 What Factors Can Affect the Strain Behavior and Strain Changes Over the MPC?

The metal plate connector (MPC) cannot be treated as simple steel plate because of the teeth which are distributed over its surface in a special pattern. A stamping machine is used to punch out the teeth to the required dimensions and different forms. Holes or slots are left in the plate as a result of this process. These holes decrease the cross sectional areas of the plate at some places to half its original area. In this research the slots are distributed in a wavy pattern so that the teeth are distributed based on the slots pattern. The metal plate connectors (MPC) are designed in this way to connect wood members together and then to transfer the load between the wood members. Thus, the teeth function is to join the MPC with the wood members and to transfer the shear forces which should not exceed the allowable load per tooth or per unit area.

In the plate design, there are three strength sources of the plate:

- Lateral resistance (tooth withdrawal): the plate area should be designed to provide the required number of teeth that will develop the required design strength in the plate.
- Tension strength of plate net section (width)
- Shear strength of plate net section (width)

Digital image correlation (DIC) can present the strain as a local strain not global strain. Usually the average of local strains on a homogenous surface is a good estimate of the average global strain in the materials which can be compared to the typical stress-strain curve for that material. However, in the case of MPC the procedure for finding global strain and the stress-strain curve using the local strain are complicated by the holes in the MPC. These holes complicate the stress concentration and so the displacements and the strain values. A small local area can suffer from high stress and strain, as shown earlier, which is more likely to yield than other regions. Having areas of different concentrations of stress or strain in the specimen makes accurately averaging local strain values extremely difficult. Based on that, the strain will not be uniform as in the classic stress-strain diagram. So expecting matching between the average strain using DIC technique and the classical strain for MPC (steel plate) is actually not valid. In the case of MPC, besides having the holes and slots all around the surface, it is also clamped or pressed in the wood by its teeth. That means it is not a free plate.

From the four tension joint tests and the heel joint tests, several factors can affect the strain behavior:

- The slots that are distributed in a wavy pattern over the plate's surface make the cross sectional areas on some locations less than other locations. Thus, the stress will be higher across the slot regions and these regions will be weaker than other regions.
- The angle of the teeth that are embedded in the wood. The teeth play an important role in the MPC. The teeth transfer the force from the wood to the plate. The angle of the teeth affects the strain behavior and direction on the surface of the plate.
- The wood type, wood cracks, grain direction, and the stretch in the wood also affect the strain behavior. When the wood grain is parallel to the external force, the tensile strength is high.
- The gripping of the teeth. In order to show a yielding point for the plate, the external force should be high and tooth gripping should also be high; thus, the plate will yield. However, when the teeth lose their resistance and the external load takes over and controls the plate, tooth withdrawal will occur. As long as the external load and tooth gripping are high, the strain behavior and strain field of the plate will be well organized. However, at the beginning of the tests

at low external load values, the teeth resistance controls the plate then strain behavior varies.

- The load is not transferred uniformly from the teeth to the plate
- The out of plan movement

LVDT machine is used to confirm the results of the DIC code. The results were very close and similar to each other. Another manual check is also done over the plate's surface and also confirms the DIC strain results. Thus the DIC technique is successfully analyzed the strain behavior of the plate.

5.6 Future work

In this research the full-field strain measurements are found for the metal plate connector using DIC technique. VIC-2D is used as a DIC code in 2 dimensions in which one camera is used on one plane surface. Strain fields can be obtained also by using DIC technique in 3 dimensions (3D) in which two cameras will be used from 2 different locations. 3D DIC can provide 3-dimensional measurements of shape and strain.

More comprehensive investigation needs to be undertaken into the influence of the teeth angle that is embedded in the wood on the strain behavior. Also the influence of the area of wood that is covered by plate on the strain behavior needs to be addressed.

Groom (1991) showed that the tensile behavior of MPC can be modified by the addition of an adhesive layer to the tip of each tooth of MPC immediately prior to joint assembly. During the pressing process, the adhesive layer extended along most of the tooth length. After applying tension load for tensile test, the results showed that the initial stiffness values of adhesive teeth increased by around 90% compared with the non-adhesive teeth. Further, the load-slip diagram (Fig. 2-4) showed that the non-adhesive teeth begin to yield at around 25% of ultimate load compared to %50 for adhesive treated teeth. Thus the adhesive layer around the teeth increased the connection between the MPC and the wood member by reorganizing the stresses along the length of the teeth to support the applied lateral force which in turn increased the resistance of the teeth to withdrawal forces. Based on Groom's research, DIC should be applied to show the strain behavior of adhesive teeth and how the adhesive teeth can influence the strain behavior and the failure mode based on DIC full-field strain measurements.

The camera was not perfectly perpendicular to the plates' samples, thus, a future research can show the influence of the camera's position and direction on the strain results.

Begin typing or pasting the rest of your chapter 5 text here.

This template is best used for directly typing in your content. However, you can paste text into the document, but use caution as pasting can produce varying results.

REFERENCES

Amanuel, S., et al. (2000). "Modeling the interface of metal-plate-connected tension-splice joint by finite element method." transactions of the American Society of Agricultural Engineers, ASAE **43**(5): 1269-1277.

Amodio, D., et al. (2003). "Digital speckle correlation for strain measurement by image analysis." Experimental Mechanics **43**(4): 396-402.

Amstutz, B. E., et al. (1995). "An experimental study of CTOD for mode I/mode II stable crack growth in thin 2024-T3 aluminum specimens." ASTM special technical publication **1256**: 256-271.

ANSI/TPI (1995). "National design standard for metal plate connected wood truss connections. ANSI/TPI 1 - 1995. Corp Author(s): Truss Plate Institute. Madison, WI.".

Avril, S., et al. (2008). "Overview of identification methods of mechanical parameters based on full-field measurements." Experimental Mechanics **48**(4): 381-402.

Avril, S., Vautrin, A.,Surrel, Y. (2004). "Grid method: Application to the characterization of cracks." Experimental Mechanics **44**(1): 37-43.

Bart-Smith, H., et al. (1998). "Compressive deformation and yielding mechanisms in cellular Al alloys determined using X-ray tomography and surface strain mapping." Acta materialia **46**(10): 3583-3592.

Bastawros, A., et al. (2000). "Experimental analysis of deformation mechanisms in a closed-cell aluminum alloy foam." Journal of the Mechanics and Physics of Solids **48**(2): 301-322.

Bay, B. K. (1995). "Texture correlation-a method for the measurement of detailed strain distributions within trabecular bone." J. Orthop. Res **13**: 258-267.

Beineke, L. and S. Suddarth (1979). "Modeling joints made with light-gage metal connector plates." Forest Products Journal **29**(8): 39-45.

Bing Pan, K. Q., Huimin Xie and Anand Asundi (2009). "Two-dimensional digital image correlation for in-plane displacement and strain measurement: a review." Meas. Sci. Technol **20**.

Bornert, M., Brémand, F.,Doumalin, P.,Dupré, J. C.,Fazzini, M.,Grédiac, M.,Hild, F.,Mistou, S.,Molimard, J.,Orteu, J. J.,Robert, L.,Surrel, Y.,Vacher, P.,Wattrisse, B. (2009). "Assessment of Digital Image Correlation Measurement Errors: Methodology and Results." Experimental Mechanics **49**(3): 353-370.

Brillaud, J., Lagattu, Fabienne (2002). "Limits and Possibilities of Laser Speckle and White-Light Image-Correlation Methods: Theory and Experiments." Appl. Opt. **41**(31): 6603-6613.

Bruck, H. M., S.,Sutton, M.,Peters, W. (1989). "Digital image correlation using Newton-Raphson method of partial differential correction." Experimental Mechanics **29**(3): 261-267.

Caárdenas-García, J. F., et al. (1998). "Digital image correlation procedure to characterize soil surface layer cracking." Agronomy journal **90**(3): 438-441.

Cabrero, J. M. and K. G. Gebremedhin (2009). "Finite Element Model for Predicting Stiffness of Metal-Plate-Connected Tension-Splice and Heel Joints of Wood Trusses." ASAE **52**(2): 565-573.

Canadian Standard Association, C. (1980). " Methods of testing for evaluation of truss plates used in lumber joints. CSA Standard S-347-M1980.Rexdale, Ontario, Canada.".

Carlson, D. O. (1991). "Automated Builder -Dictionary/Encyclopedia of Industrialized Housing.".

Carroll, J. (2011). Relating Antique Crack Growth to Microstructure Via Multiscale Digital Image Correlation. Civil Engineering Department. Illinois, University Of Illinois. **Doctor Of Philosophy**.

Carroll, J. (2011). Relating fatigue crack growth to microstructure via multiscale digital image correlation. United States -- Illinois, University of Illinois at Urbana-Champaign. **3478621:** 177.

Chen, D. J., Chiang, F.P., Tan, Y.S., Don, H.S. (1993). "Digital speckle-displacement measurement using a complex spectrum method." Appl. Opt **32**: 1839-1849.

Cheng, P., et al. (2002). "Full-field speckle pattern image correlation with B-spline deformation function." Experimental Mechanics **42**(3): 344-352.

Cho, S., Chasiotis, I.,Friedmann, T.A.,Sullivan, J.P. (2005). "Young's modulus, Poisson's ratio and failure properties of tetrahedral amorphous diamond-like carbon for MEMS devices." Journal of Micromechanics and Microengineering **15**(4): 728.

Choi, D., Thorpe, J.L.,Cote, WA.,Hanna, R.B. (1996). "Quantification of compression failure propagation in wood using digital image pattern recognition." Forest Products Journal **46**(10): 87-93.

Choi, D., Thorpe, JL.,Hanna, RB (1991). "Image analysis to measure strain in wood and paper." Wood Science and Technology **25**(4): 251-262.

Choi, S., Shah, SP (1997). "Measurement of deformations on concrete subjected to compression using image correlation." Experimental Mechanics **37**(3): 307-313.

Chu, T., et al. (1985). "Applications of digital-image-correlation techniques to experimental mechanics." Experimental Mechanics **25**(3): 232-244.

Claire, D., Hild, F.,Roux, S. (2002). "Identification of damage fields using kinematic measurements." Comptes Rendus Mecanique **330**(11): 729-734.

Corr, D., Accardi, M.,Graham-Brady, L.,Shah, S. (2007). "Digital image correlation analysis of interfacial debonding properties and fracture behavior in concrete." Engineering Fracture Mechanics **74**(1): 109-121.

Cramer, C. O. (1968). "Load distribution in multiple bolt tension joints. ." J. of Structural Div., ASCE **94**: No. ST5.

Cramer, S., et al. (1993). "Computation of member forces in metal plate connected wood trusses." Structural Engineering Review **5**(3): 209-218.

Cramer, S. M., et al. (1990). "Theoretical Consideration of Metal-Plate-Connected Wood-Splice Joints." Journal of Structural Engineering **116**(12): 3458-3474.

Crovella, P. L. and K. G. Gebremedhin (1990). "Analysis of light frame wood truss tension joint stiffness." Forest Products Journal **40**(4): 41-47.

Dally, J. W., W.F.Riley (2005). "Experimental Stress Analysis." (4th ed. Knoxville, TN : College House Enterprises, LLC).

Dawicke, D. and M. Sutton (1994). "CTOA and crack-tunneling measurements in thin sheet 2024-T3 aluminum alloy." Experimental Mechanics **34**(4): 357-368.

Dawicke, D., et al. (1995). "Measurement and analysis of critical CTOA for an aluminum alloy sheet." ASTM special technical publication **1220**: 358-358.

Demarkles, L. R. (1955). "Investigation of the use of a rubber analog in the study of stress distribution in riveted and cemented joints. National Advisory Committee for Aeronautics Tech. Note No. 3413."

Durig, B., et al. (1988). "Digital Image Correlation Measurements of Strain in Bovine Retina." Optical Testing and Metrology.

Ellegaard, P. (2006). "Finite- element modeling of timber joints with punched metal plate fasteners " Journal of structural Engineering ASCE **132**(3): 409-417.

Gaudette, G. R., Todaro, J., Krukenkamp, I.B., Chiang, F.P. (2001). "Computer aided speckle interferometry: a technique for measuring deformation of the surface of the heart." Ann. Biomed. Eng. **29**(775-80).

Gebremedhin, K. G. and P. L. Crovella (1991). "Load Distribution In Metal Plate Connectors of Tension Joints In Wood Trusses." ASAE **34**(1): 281-0287.

Giachetti, A. (2000). "Matching techniques to compute image motion." Image and Vision Computing **18**(3): 247-260.

Groom, L. and A. Polensek (1992). "Nonlinear Modeling of Truss-Plate Joints." Journal of Structural Engineering **118**(9): 2514-2531.

Groom, L. H. (1991). "Effect of Adhesive Applied to the Tooth-Wood interface on Metal-Plate-Connections Loaded in Tension." Forest Products Journal **41**(4): 33-35.

Gupta, R. and K. G. Gebremedhin (1990). "Destructive Testing of Metal-Plate-Connected Wood Truss Joints " Journal of Structural Engineering **116**(7): 1971-1982.

Gupta, R., et al. (1996). "Metal-plate-connected wood joints: a literature review." Forest Research Laboratory

Oregon State University.

Gupta, R. and B. Wagner (2002). "Effect of Metal Connector plate on the Bending Strength of Solid Sawn Lumber and LVL: A Pilot Study." Forest Products Journal **52**(10): 71-74.

Haddadi, H., Belhabib, S. (2008). "Use of rigid-body motion for the investigation and estimation of the measurement errors related to digital image correlation technique." Optics and Lasers in Engineering **46**(2): 185-196.

Han, G., et al. (1994). "A study of stationary crack-tip deformation fields in thin sheets by computer vision." Experimental Mechanics **34**(2): 125-140.

Han, G., et al. (1995). "A study of stable crack growth in thin SEC specimens of 304 stainless steel by computer vision." Engineering Fracture Mechanics **52**(3): 525-555.

He, R. S., Horn, C.T.,Wang, H.J.,Hwang, S.F. (2006). "Deformation measurement by a digital image correlation method combined with a hybrid genetic algorithm." Key Engineering Materials **326**: 139-142.

He, Z., et al. (1984). "Two-dimensional fluid-velocity measurements by use of digital-speckle correlation techniques." Experimental Mechanics **24**(2): 117-121.

He, Z. H., Sutton, M.A.,Ranson, W.F.,Peters, W.H. (1984). "Two-dimensional fluid-velocity measurements by use of digital-speckle correlation techniques." Experimental Mechanics **24**(2): 117-121.

Helm, J. D. (2008). "Digital image correlation for specimens with multiple growing cracks." Experimental Mechanics **48**(6): 753-762.

Hild, F. and S. Roux (2006). "Digital image correlation: from displacement measurement to identification of elastic properties–a review." Strain **42**(2): 69-80.

Hung, P.-C., Voloshin, AS (2003). "In-plane strain measurement by digital image correlation." Journal of the Brazilian Society of Mechanical Sciences and Engineering **25**(3): 215-221.

Hung, P. C. and A. Voloshin (2003). "In-plane strain measurement by digital image correlation." Journal of the Brazilian Society of Mechanical Sciences and Engineering **25**(3): 215-221.

Huntley, J. M. (1996). "Interview on Computer-Aided Analysis of Photographic Specklegrams,Optical Testing Digest,August, SPIE online publication.http://www.spie.org/otd."

Hwang, S.-F., Wu, Wei-Jie (2012). "Deformation measurement around a high strain-gradient region using a digital image correlation method." Journal of Mechanical Science and Technology **26**(10): 3169-3175.

Isyumov, N. (1967). "Load distribution in multiple shear-plate joints in timber. Canadian Department of Forestry Publication No. 1203."

Jin, H. and H. A. Bruck (2005). "POINTWISE DIGITAL IMAGE CORRELATION USING GENETIC ALGORITHMS." Experimental Techniques **29**(1): 36-39.

Kifetew, G. (1996). "Application of the deformation field measurement method to wood during drying." Wood Science and Technology **30**(6): 455-462.

Kifetew, G., Lindberg, H.,Wiklund, M. (1997). "Tangential and radial deformation field measurements on wood during drying." Wood Science and Technology **31**(1): 35-44.

Knauss, W. G., Chasiotis, Ioannis,Huang, Ying (2003). "Mechanical measurements at the micron and nanometer scales." Mechanics of Materials **35**(3): 217-231.

Lantos, G. (1969). "Load distribution in a row of fasteners subjected to lateral load. ." Wood Sci. **1**(3): 129-136.

Laurence Mott, S. M., Shaler, and Leslire H. Groom (1994). "Application of Imaging Technologies to Experimental Mechanics." Techniques in Experimental Mechanics Applicable to Forest Products Research. Proceeding of the Experimental Mechanics Plenary Session at the Forest Products Research Society Annual Meeting. Prtland, ME: 17-22.

Lecompte, D., Smits, A.,Bossuyt, S.,Sol, H.,Vantomme, J.,Van Hemelrijck, D.,Habraken, AM (2006). "Quality assessment of speckle patterns for digital image correlation." Optics and Lasers in Engineering **44**(11): 1132-1145.

Lecompte, D., Smits, Arwen,Sol, Hugo,Vantomme, John,Van Hemelrijck, Danny (2007). "Mixed numerical–experimental technique for orthotropic parameter identification using biaxial tensile tests on cruciform specimens." International Journal of Solids and Structures **44**(5): 1643-1656.

Liu, J., et al. (1998). "Experimental characterization of crack tip deformation fields in alloy 718 at high temperatures." Journal of engineering materials and technology **120**(1): 71-78.

Lu, H. and P. Cary (2000). "Deformation measurements by digital image correlation: implementation of a second-order displacement gradient." Experimental Mechanics **40**(4): 393-400.

Lyons, J., et al. (1996). "High-temperature deformation measurements using digital-image correlation." Experimental Mechanics **36**(1): 64-70.

Lyons, J., Liu, J.,Sutton, MA (1996). "High-temperature deformation measurements using digital-image correlation." Experimental Mechanics **36**(1): 64-70.

Mahmoud, S. and K. Lease (2003). "The effect of specimen thickness on the experimental characterization of critical crack-tip-opening angle in 2024-T351 aluminum alloy." Engineering Fracture Mechanics **70**(3): 443-456.

McNeill, S., et al. (1997). "Measurement of surface profile using digital image correlation." Experimental Mechanics **37**(1): 13-20.

Misra, R. D. (1964). "An analytical and experimental investigation of stress distribution in the punched metal plate of a timber joint. Ph.D. thesis. Michigan State Univ., East Lansing, Mich.".

Mizuno, Y., et al. (1995). "In situ measurement of sintering shrinkage in powder compacts by digital image correlation method." Powder metallurgy **38**(3): 191-195.

Montemayor, E. (2003). Determination of Strains in Cyclic Triaxial Using Digital Image Correlation. Civil and Environmental Engineering. South Carolina, University of South Carolina. **Doctor of Philosophy**.

Mott, L., Shaler, S.M.,Groom, L.H. (1996). "A technique to measure strain distributions in single wood pulp fibers." Wood and Fiber Science **28**(4): 429-437.

Orteu, J.-J., Garcia, Dorian,Robert, Laurent,Bugarin, Florian (2006). "A speckle texture image generator." 63410H-63410H.

Pan, B. (2011). "Recent Progress in Digital Image Correlation." Experimental Mechanics **51**(7): 1223-1235.

Pan, B., Wang, Z.,Xie, H. (2009). "Generalized spatial-gradient-based digital image correlation for displacement and shape measurement with subpixel accuracy." The Journal of Strain Analysis for Engineering Design **44**(8): 659-669.

Pan, B., Xie, H.,Wang, Z.,Qian, K. (2008). "Study on subset size selection in digital image correlation for speckle patterns." Optics Express **16**(10): 7037-7048.

Pan Bing, X. H.-m., Xu Bo-qin and Dai Fu-long (2006). "Performance of sub-pixel registration algorithms in digital image correlation." Meas. Sci. Technol **17**: 1615-1621.

Peters, W., Ranson, WF.,Sutton, MA.,Chu, TC.,Anderson, J. (1983). "Application of digital correlation methods to rigid body mechanics." Optical Engineering **22**(6): 226738-226738-.

Poissant, J. and F. Barthelat (2010). "A Novel “Subset Splitting” Procedure for Digital Image Correlation on Discontinuous Displacement Fields." Experimental Mechanics **50**(3): 353-364.

Quaile, A. T. and F. J. Keenan (1979). Truss plate testing in Canada: Test procedures and factors affecting strength properties. Proceedings - Metal Plate Wood Truss Conference., St Louis, MO, USA, For Prod Res Soc (FPRS Proc P-79-28).

Rassam, H. Y. and J. R. Goodman (1970). "Buckling behavior of layered wood colums." Wood Science **2**(4): 238-246.

Rastogi, P. K. (2000). "Digital speckle pattern interferometry and related techniques." Digital Speckle Pattern Interferometry and Related Techniques, by PK Rastogi (Editor), pp. 384. ISBN 0-471-49052-0. Wiley-VCH, December 2000. **1**.

Redlinger, M. J. (1998). Behavior of Metal-Plate-Connected Wood Truss Joints Under Wind and Impact Loads. Civil Engineering. Oregon, Oregon State University

Réthoré, J., Hild, F.,Roux, S. (2007). "Shear-band capturing using a multiscale extended digital image correlation technique." Computer Methods in Applied Mechanics and Engineering **196**(49): 5016-5030.

Réthoré, J., Hild, F.,Roux, S. (2008). "Extended digital image correlation with crack shape optimization." International journal for numerical methods in engineering **73**(2): 248-272.

Riley, G. J. (May 1998). "Analytical model of metal-plate-connected wood truss joint stiffness."

Riley, G. J. and K. G. Gebremedhin (1999). "Axial and rotational stiffness model of metal-plate-connected wood truss joints." Transactions of the American Society of Agricultural Engineers **42**(Compendex): 761-770.

S.F. Hwang, Y. J. H., W.J. Wu (2008). "Deformation Measurement by a Digital Image Correlation With a Hybrid Genetic Algorithm " Conference: 2008 SEM XI International Congress & Exposition on Experimental & Applied Mechanics.

Sabaté, N., Vogel, D.,Gollhardt, A.,Keller, J.,Michel, B.,Cané, C.,Gràcia, I.,Morante, JR (2006). "Measurement of residual stresses in micromachined structures in a microregion." Applied physics letters **88**(7): 071910-071910-071913.

Sasaki, Y. and T. Takemura (1990). "Non-linear analysis of metal-plate wood trusses." 1990 International Timber Engineering Conference, Tokyo, Japan.: 701-708.

Schreier, H., Sutton, Michael (2002). "Systematic errors in digital image correlation due to undermatched subset shape functions." Experimental Mechanics **42**(3): 303-310.

Schreier, H. W., Braasch, Joachim R.,Sutton, Michael A. (2000). "Systematic errors in digital image correlation caused by intensity interpolation." Optical Engineering **39**(11): 2915-2921.

Schreier, H. W., Sutton, M.A. (2002). "Systematic errors in digital image correlation due to undermatched subset shape functions." Experimental Mechanics **42**(3): 303-310.

Schriver, A. B. and B. Wood (1990). Strength of truss plate timber connections under transverse loading. Proceedings of the Annual Conference and the First Biennial Environmental Speciality Conference, May 16 - 18 1990, Hamilton, Ont, Can, Publ by Canadian Soc for Civil Engineering.

Sjodahl, M. (1997). "Accuracy in electronic speckle photography " Appl. Opt. **36**: 2875-2885.

Sjödahl, M. (1994). "Electronic speckle photography: increased accuracy by nonintegral pixel shifting." Applied Optics **33**(28): 6667-6673.

Sjodahl, M., Benckert, L.R. (1993). "Electronic speckle photography: analysis of an algorithm giving the displacement with subpixel accuracy " Appl. Opt. **32**: 2278-2284.

Sjodahl, M., Benckert, L.R. (1994). "Electronic speckle photography-increased accuracy by nonintegral pixel shifting " Appl. Opt. **33**: 6667-6673.

Sjodahl, M., Benckert, L.R. (1994). "Systematic and random errors in electronics speckle photography " Appl. Opt. **33**: 7461-7471.

Slabinski, M. S. (2005). Finite Element Analysis of Unsupported Metal Plate Connector Area of Timber Joints Under Buckling Loads. Syrecuse, New York, State University of New York. **Master of science**.

Smith, B. W., Li, M.,Tong, W. (1998). "ERROR ASSESSMENT FOR STRAIN MAPPING BY DIGITAL IMAGE CORRELATION." Experimental Techniques **22**(4): 19-21.

Stelmokas, J. W., Zink, A.G.,Loferski, J.R. (1997). "Image correlation analysis of multiple-bolt wood connections." Wood and Fiber Science **29**(3): 210-227.

Su, C. and L. Anand (2003). "A new digital image correlation algorithm for whole-field displacement measurement."

Suddarth, S. and D. H. Percival (1972). Increasing the Application Efficiency of Performance of Metal Plate Connectors. Metal Plate Wood Truss Conf. Forest Prod. SOC.**:** PP : 98-104.Madison, WI.

Suddarth, S., et al. (1979). "Variability in tension performance of metal plate connections. Metal Plate Wood Truss Conference." Forest Products Research Society.

Suddarth, S. and R. W. Wolfe (1984). "Purdue plane structures analyzer II (PPSAII) : a computerized wood engineering system. General Technical Report FPL-40, United States Department of Agriculture, Forest Service, ." Forest Products Laboratory, Madison, WI.

Sun, Z., Lyons, Jed S.,McNeill, Stephen R. (1997). "Measuring Microscopic Deformations with Digital Image Correlation." Optics and Lasers in Engineering **27**(4): 409-428.

Sutton, M., McNeill, S.,Helm, J.,Chao, Y. (2000). "Advances in two-dimensional and three-dimensional computer vision for shape and deformation measurement." Photomechanics: 323-372.

Sutton, M., et al. (1992). "Experimental investigations of three-dimensional effects near a crack tip using computer vision." International journal of fracture **53**(3): 201-228.

Sutton, M. A., Boone, M.L.,Ma, F.,Helm, J.D. (2000). "A combined modeling–experimental study of the crack opening displacement fracture criterion for characterization of stable crack growth under mixed mode I/II loading in thin sheet materials." Engineering Fracture Mechanics **66**(2): 171-185.

Sutton, M. A., et al. (2000). Computer vision applied to shape and deformation measurement. Proc. Int. Conf. on Trends in Optical Non-Destructive Testing and Inspection.

Sutton, M. A., Mingqi, Cheng,Peters, W. H.,Chao, Y. J.,McNeill, S. R. (1986). "Application of an optimized digital correlation method to planar deformation analysis." Image and Vision Computing **4**(3): 143-150.

Sutton, M. A., Orteu, J.J.,Schreier, H. (2009). Image correlation for shape, motion and deformation measurements: Basic Concepts, Theory and Applications, Springer.

Sutton, M. A., Wolters, W. J.,Peters, W. H.,Ranson, W. F.,McNeill, S. R. (1983). "Determination of displacements using an improved digital correlation method." Image and Vision Computing **1**(3): 133-139.

Tong, W. (1997). "Detection of plastic deformation patterns in a binary aluminum alloy." Experimental Mechanics **37**(4): 452-459.

Tong, W. (2005). "An Evaluation of Digital Image Correlation Criteria for Strain Mapping Applications." Strain **41**(4): 167-175.

Triche, M. and S. Suddarth (1988). "Advanced design of metal plate connector joints." Forest Products Journal **38**(9): 7-12.

Truss Plate Institute TPI (2007). "National design standard for metal plate connected wood truss construction. ANCI/TPI 1 - 2007. Corp Author(s): Truss Plate Institute.".

Vatovec, M. (1995). Analytical and experimental investigation of the behavior of metal-plate-connected wood truss joints.

Vatovec, M., et al. (1996). "Modeling of Metal-plate-connected Wood Truss Joints." transactions of the American Society of Agricultural Engineers ASAE **39**(3): 1101-1111.

Vendroux, G. and W. Knauss (1998). "Submicron deformation field measurements: Part 2. Improved digital image correlation." Experimental Mechanics **38**(2): 86-92.

Wang, Y. and A. M. Cuitiño (2002). "Full-field measurements of heterogeneous deformation patterns on polymeric foams using digital image correlation." International Journal of Solids and Structures **39**(13–14): 3777-3796.

Wang, Y. Q., Sutton, M. A.,Bruck, H. A.,Schreier, H. W. (2009). "Quantitative Error Assessment in Pattern Matching: Effects of Intensity Pattern Noise, Interpolation, Strain and Image Contrast on Motion Measurements." Strain **45**(2): 160-178.

Wattrisse, B., et al. (2001). "Analysis of strain localization during tensile tests by digital image correlation." Experimental Mechanics **41**(1): 29-39.

Wu W., P. W. H., Hammer M. (1987). "basic mechanical properties of retina in simple tension, trans." ASME, J Biomech. Eng. **109**: 1.

Yaofeng, S. and J. H. L. Pang (2007). "Study of optimal subset size in digital image correlation of speckle pattern images." Optics and Lasers in Engineering **45**(9): 967-974.

Yaofeng, S., Pang, J.H.L. (2007). "Study of optimal subset size in digital image correlation of speckle pattern images." Optics and Lasers in Engineering **45**(9): 967-974.

Yoneyama, S., Kikuta, H.,Kitagawa, A.,Kitamura, K. (2006). "Lens distortion correction for digital image correlation by measuring rigid body displacement." Optical Engineering **45**(2): 023602-023602-023609.

Yoneyama, S., Kikuta, Hisao,Kitagawa, Akikazu,Kitamura, Koji (2006). "Lens distortion correction for digital image correlation by measuring rigid body displacement." Optical Engineering **45**(2): 023602-023602.

Yuanhao, H. (2004). "Development of Digital Image Correlation mthod for Displacement and Shape Measurement." Thesis,National University of Singapore.

Zhang, D., Luo, M.,Arola, D.D. (2006). "Displacement/strain measurements using an optical microscope and digital image correlation." Optical Engineering **45**(3): 033605-033605-033609.

Zhang D, Z. X. a. C. G. (1999). "Compression strain measurement by digital speckle correction." Exp. Mech. **39**: 62-65.

Zhang, Z. F., Kang, Y.L.,Wang, H.W.,Qin, Q.H.,Qiu, Y.,Li, X.Q. (2006). "A novel coarse-fine search scheme for digital image correlation method." Measurement **39**(8): 710-718.

Zhou, P. a. G., K. E. (2001). "Subpixel displacement and deformation gradient measurement using digital image/ speckle correlation." Optical Engineering **40**: 1613-1620.

Zink, A. G., Davidson, R.W.,Hanna, R.B. (1996). "Experimental measurement of the strain distribution in double overlap wood adhesive joints." J. Adhes. **56**: 27.

APPENDICES

Appendix A

The displacement results from LVDT vs. the displacement from DIC Vic-2D for the four tension tests

A.1

The displacement results from LVDT vs. DIC Vic-code are presented in the next tables for the test AA.

Table A-1. the displacement of LVDT vs. DIC.Code for test AA 2^{nd}

AA-Test 2^{nd}

Δ @ **R** - deformation of the right side gap of the specimen (LVDT set on the right side) **LVDT # 5**			
Load (lbs.)	**Δ - LVDT (in)**	**Δ - DIC.Code (pixels)**	**Δ - DIC.Code (in)**
0	0	0	0
200	0	0	0
400	0	0	0
600	0	0	0
800	0.001	1	0.0021133
1000	0.001	1	0.0021133
1200	0.001	1	0.0021133
1400	0.001	1	0.0021133
1600	0.002	2	0.0042266
1800	0.002	2	0.0042266
2000	0.002	2	0.0042266
2200	0.003	2	0.0042266
2400	0.003	2	0.0042266
2600	0.003	2	0.0042266
2800	0.003	2	0.0042266
3000	0.004	2	0.0042266
4000	0.004	3	0.0063399
4200	0.005	3	0.0063399
4600	0.006	4	0.0084532
4800	0.007	4	0.0084532
5000	0.008	4	0.0084532
5200	0.008	4	0.0084532
5400	0.009	4	0.0084532
5600	0.009	5	0.0105665
5800	0.009	5	0.0105665
6000	0.01	5	0.0105665
6200	0.01	6	0.0126798

6400	0.012	6	0.0126798
6600	0.012	6	0.0126798
6800	0.012	6	0.0126798
7000	0.013	7	0.0147931
7200	0.013	7	0.0147931
7400	0.015	8	0.0169064
7600	0.016	8	0.0169064
7800	0.017	9	0.0190197
8000	0.021	10	0.021133
8200	0.028	12	0.0253596
8400	0.035	18	0.0380394
8600	0.047	23	0.0486059

Table A-2. the displacement of LVDT vs. DIC.Code for test AA- 3rd from the right side gap

AA-Test 3rd

Δ @ **R** - deformation of the right side gap of the specimen (LVDT set on the right side) **LVDT # 5**			
Load (lbs.)	**Δ - LVDT (in)**	**Δ - DIC.Code (pixels)**	**Δ - DIC.Code (in)**
0	0	0	0
400	0.0009	0	0
1000	0.0017	1	0.0021133
1600	0.0026	2	0.0042266
2000	0.0038	3	0.0063399
2400	0.0048	3	0.0063399
3000	0.0062	4	0.0084532
3400	0.0073	4	0.0084532
4000	0.009	5	0.0105665
4400	0.0104	5	0.0105665
5000	0.0123	6	0.0126798
5400	0.0139	7	0.0147931
6000	0.0163	8	0.0169064
6200	0.0172	9	0.0190197
6400	0.0182	9	0.0190197
6600	0.0187	10	0.021133
6800	0.0202	10	0.021133
7600	0.0245	12	0.0253596
8000	0.0329	16	0.0338128
8200	0.0403	20	0.042266
8400	0.0462	22	0.0464926
8600	0.0615	30	0.063399

Table A-3. The displacement of LVDT vs. DIC.Code for test AA- 3rd from the left side gap

AA-Test 3rd

Δ @ L - deformation of the left side gap of the specimen (LVDT set on the left side) **LVDT # 4**			
Load (lbs.)	**Δ - LVDT (in)**	**Δ - DIC.Code (pixels)**	**Δ - DIC.Code (in)**
0	0	0	0
400	0.001081575	1	0.0021133
1000	0.002042975	2	0.0042266
1400	0.002764024	2	0.0042266
2000	0.003965774	3	0.0063399
2400	0.004927174	3	0.0063399
3000	0.006369274	4	0.0084532
3400	0.007571023	4	0.0084532
4000	0.009493823	5	0.0105665
4400	0.011056098	6	0.0126798
5000	0.013219247	7	0.0147931
5400	0.015021872	8	0.0169064
6000	0.017665721	9	0.0190197
6200	0.018867471	9	0.0190197
6400	0.020069221	10	0.021133
6800	0.02247272	11	0.0232463
7000	0.023794645	11	0.0232463
7200	0.024996395	12	0.0253596
7400	0.026678844	13	0.0274729
8000	0.030043744	14	0.0295862
8200	0.032567418	15	0.0316995
8400	0.036653367	18	0.0380394
8600	0.044464741	22	0.0464926

A.2

The displacement results from LVDT vs. DIC Vic-code are presented in the next tables for the test AE.

Table A-4. The displacement of LVDT vs. DIC.Code for test AE-1st from the right side gap

Δ @ **R** - deformation of the right side gap of the specimen (LVDT set on the right side) **LVDT # 5**			
Load (lbs.)	**Δ - LVDT (in)**	**Δ - DIC.Code (pixels)**	**Δ - DIC.Code (in)**
0	0	0	0
600	0.0037	2	0.0042266
1200	0.0084	4	0.0084532
1800	0.0175	9	0.0190197

Table A-5. The displacement of LVDT vs. DIC.Code for test AE- 3rd from the left side gap

Δ @ **L** - deformation of the left side gap of the specimen (LVDT set on the left side) **LVDT # 4**			
Load (lbs.)	**Δ - LVDT (in)**	**Δ - DIC.Code (pixels)**	**Δ - DIC.Code (in)**
0	0	0	0
800	0.004206074	2	0.0042266
1400	0.009734056	5	0.0105665

Table A-6. The displacement of LVDT vs. DIC.Code for test AE-2nd from the right side gap

Δ @ **R** - deformation of the right side gap of the specimen (LVDT set on the right side) **LVDT # 5**			
Load (lbs.)	**Δ - LVDT (in)**	**Δ - DIC.Code (pixels)**	**Δ - DIC.Code (in)**
0	0	0	0
400	0.0022	1	0.0021133
1000	0.0047	3	0.0063399
1400	0.0064	3	0.0063399
1800	0.0083	4	0.0084532
2200	0.0104	5	0.0105665
2600	0.0129	6	0.0126798
3000	0.0141	7	0.0147931
3400	0.017	8	0.0169064

Table A-7. The displacement of LVDT vs. DIC.Code for test AE-2nd from the left side gap

Δ @ **L** - deformation of the left side gap of the specimen (LVDT set on the left side) **LVDT # 4**			
Load (lbs.)	**Δ - LVDT (in)**	**Δ - DIC.Code (pixels)**	**Δ - DIC.Code (in)**
0	0	0	0
600	0.002523644	2	0.0042266
800	0.003605206	2	0.0042266
1600	0.006369197	3	0.0063399
2000	0.0081718	4	0.0084532
2400	0.010094577	5	0.0105665
2800	0.012137527	6	0.0126798
3200	0.014060303	7	0.0147931

Table A-8. The displacement of LVDT vs. DIC.Code for test AE-3rd from the right side gap

Δ @ **R** - deformation of the right side gap of the specimen (LVDT set on the right side) **LVDT # 5**			
Load (lbs.)	**Δ - LVDT (in)**	**Δ - DIC.Code (pixels)**	**Δ - DIC.Code (in)**
0	0	0	0
400	0.0015	1	0.0021133
800	0.0027	2	0.0042266
1200	0.0043	2	0.0042266
1600	0.0059	3	0.0063399
2200	0.0091	5	0.0105665
2600	0.0108	5	0.0105665
3000	0.0223	12	0.0253596

Table A-9. The displacement of LVDT vs. DIC.Code for test AE-3rd from the left side gap

Δ @ **L** - deformation of the left side gap of the specimen (LVDT set on the left side) **LVDT # 4**			
Load (lbs.)	**Δ - LVDT (in)**	**Δ - DIC.Code (pixels)**	**Δ - DIC.Code (in)**
0	0	0	0
600	0.002283297	2	0.0042266
1000	0.003485032	2	0.0042266
1400	0.005167462	3	0.0063399
1800	0.006729718	4	0.0084532
2400	0.009613882	5	0.0105665
2800	0.01189718	6	0.0126798
3200	0.016824294	8	0.0169064

A.3

The displacement results from LVDT vs. DIC Vic-code are presented in the next tables for the test EA.

Table A-10. The displacement of LVDT vs. DIC.Code for test EA-1st from the right side gap

Δ @ **R** - deformation of the right side gap of the specimen (LVDT set on the right side) **LVDT # 5**			
Load (lbs.)	**Δ - LVDT (in)**	**Δ - DIC.Code (pixels)**	**Δ - DIC.Code (in)**
0	0	0	0
600	0.0009	1	0.0021133
1400	0.0022	1	0.0021133
2200	0.0034	2	0.0042266
3000	0.0049	3	0.0063399
3800	0.007	4	0.0084532
4400	0.0089	5	0.0105665
5000	0.0112	6	0.0126798
5600	0.0139	7	0.0147931
6200	0.0172	9	0.0190197
6800	0.0219	11	0.0232463
7200	0.028	14	0.0295862

Table A-11. The displacement of LVDT vs. DIC.Code for test EA-1st from the left side gap

Δ @ L - deformation of the left side gap of the specimen (LVDT set on the left side) **LVDT # 4**			
Load (lbs.)	**Δ - LVDT (in)**	**Δ - DIC.Code (pixels)**	**Δ - DIC.Code (in)**
0	0	0	0
600	0.0004807	1	0.0021133
1200	0.001321925	1	0.0021133
2000	0.003004374	2	0.0042266
2800	0.004927174	3	0.0063399
3600	0.007210498	4	0.0084532
4200	0.009493823	5	0.0105665
4800	0.012137672	6	0.0126798
5400	0.015142047	8	0.0169064
6000	0.018747296	10	0.021133
6600	0.02391482	12	0.0253596
7000	0.029683219	15	0.0316995
7300	0.043022641	22	0.0464926

Table A-12. The displacement of LVDT vs. DIC.Code for test EA-2nd from the right side gap

Δ @ **R** - deformation of the right side gap of the specimen (LVDT set on the right side) **LVDT # 5**			
Load (lbs.)	**Δ - LVDT (in)**	**Δ - DIC.Code (pixels)**	**Δ - DIC.Code (in)**
0	0	0	0
600	0.0007	1	0.0021133
1200	0.0016	1	0.0021133
2000	0.0031	2	0.0042266
2600	0.004	2	0.0042266
3200	0.0053	3	0.0063399
3800	0.0067	4	0.0084532
4400	0.0084	5	0.0105665
5000	0.0102	5	0.0105665
5600	0.0123	6	0.0126798
6200	0.0148	8	0.0169064
6800	0.0178	9	0.0190197
7200	0.0201	10	0.021133
7600	0.0233	12	0.0253596
8000	0.0271	14	0.0295862
8400	0.0326	17	0.0359261
8600	0.0368	19	0.0401527
8800	0.0446	22	0.0464926
9000	0.0495	24	0.0507192
9200	0.0581	30	0.063399
9300	0.0869	42	0.0887586

Table A-13. The displacement of LVDT vs. DIC.Code for test EA-2nd from the left side gap

Δ @ L - deformation of the left side gap of the specimen (LVDT set on the left side) **LVDT # 4**			
Load (lbs.)	**Δ - LVDT (in)**	**Δ - DIC.Code (pixels)**	**Δ - DIC.Code (in)**
0	0	0	0
600	0.000721041	1	0.0021133
1400	0.001562256	1	0.0021133
2000	0.002523644	2	0.0042266
2600	0.003605206	2	0.0042266
3400	0.005047288	3	0.0063399
4000	0.006249024	4	0.0084532
4600	0.007811279	4	0.0084532
5200	0.009373535	5	0.0105665
5800	0.011296312	6	0.0126798
6400	0.013459435	7	0.0147931
7000	0.016223427	8	0.0169064
7400	0.017425162	9	0.0190197
7800	0.019828633	10	0.021133
8200	0.022232103	11	0.0232463
8400	0.023433838	12	0.0253596
8800	0.025837309	13	0.0274729
9000	0.02824078	14	0.0295862
9200	0.03064425	15	0.0316995

A.4

The displacement results from LVDT vs. DIC Vic-code are presented in the next tables for the test EE.

Table A-14. The displacement of LVDT vs. DIC.Code for test EE-1st from the right side gap

Δ @ **R** - deformation of the right side gap of the specimen (LVDT set on the right side) **LVDT # 5**			
Load (lbs.)	**Δ - LVDT (in)**	**Δ - DIC. Code (pixels)**	**Δ - DIC. Code (in)**
0	0	0	0
400	0.0018	1	0.0021133
800	0.0032	2	0.0042266
1200	0.0048	3	0.0063399
1800	0.0071	4	0.0084532
2200	0.0089	5	0.0105665
2600	0.0106	5	0.0105665
3000	0.0127	6	0.0126798
3400	0.0162	8	0.0169064
3800	0.0189	9	0.0190197

Table A-15. The displacement of LVDT vs. DIC.Code for test EE-1st from the left side gap

Δ @ L - deformation of the left side gap of the specimen (LVDT set on the left side) **LVDT # 4**			
Load (lbs.)	**Δ - LVDT (in)**	**Δ - DIC. Code (pixels)**	**Δ - DIC. Code (in)**
0	0	0	0
600	0.00204295	1	0.0021133
1000	0.003244685	2	0.0042266
1600	0.005287635	3	0.0063399
2000	0.006970065	4	0.0084532
2400	0.008532321	5	0.0105665
2800	0.01021475	5	0.0105665
3200	0.012498047	6	0.0126798
3600	0.015502385	8	0.0169064
4000	0.018266377	10	0.021133

Table A-16. The displacement of LVDT vs. DIC.Code for test EE-2nd from the right side gap

Δ @ L - deformation of the left side gap of the specimen (LVDT set on the left side) **LVDT # 4**			
Load (lbs.)	**Δ - LVDT (in)**	**Δ - DIC. Code (pixels)**	**Δ - DIC. Code (in)**
0	0	0	0
800	0.002763991	2	0.0042266
1000	0.003124512	2	0.0042266
1400	0.004566594	3	0.0063399
1800	0.006369197	3	0.0063399
2200	0.008051627	4	0.0084532

Table A-17. The displacement of LVDT vs. DIC.Code for test EE-2nd from the left side gap

Δ @ **L** - deformation of the left side gap of the specimen (LVDT set on the left side) **LVDT # 4**			
Load (lbs.)	**Δ - LVDT (in)**	**Δ - DIC. Code (pixels)**	**Δ - DIC. Code (in)**
0	0	0	0
800	0.002763991	2	0.0042266
1000	0.003124512	2	0.0042266
1400	0.004566594	3	0.0063399
1800	0.006369197	3	0.0063399
2200	0.008051627	4	0.0084532

Table A-18. The displacement of LVDT vs. DIC.Code for test EE-3rd from the right side gap

Δ @ **R** - deformation of the right side gap of the specimen (LVDT set on the right side) **LVDT # 5**			
Load (lbs.)	**Δ - LVDT (in)**	**Δ - DIC. Code (pixels)**	**Δ - DIC. Code (in)**
0	0	0	0
400	0.0012	1	0.0021133
800	0.0026	2	0.0042266
1200	0.0039	2	0.0042266
1600	0.0053	3	0.0063399
2000	0.0069	4	0.0084532
2400	0.0085	4	0.0084532
2800	0.0099	5	0.0105665
3200	0.0114	6	0.0126798
3600	0.0132	7	0.0147931
4000	0.0148	7	0.0147931
4400	0.0168	8	0.0169064
4800	0.0188	9	0.0190197

Table A-19. The displacement of LVDT vs. DIC.Code for test EE-3rd from the left side gap

Δ @ L - deformation of the left side gap of the specimen (LVDT set on the left side) **LVDT # 4**			
Load (lbs.)	**Δ - LVDT (in)**	**Δ - DIC. Code (pixels)**	**Δ - DIC. Code (in)**
0	0	0	0
600	0.001802603	1	0.0021133
1000	0.003124512	2	0.0042266
1400	0.003965727	2	0.0042266
1800	0.005287635	3	0.0063399
2200	0.006970065	4	0.0084532
2600	0.008652494	5	0.0105665
3000	0.01021475	5	0.0105665
3400	0.0122577	6	0.0126798
3800	0.01430065	7	0.0147931
4200	0.016463774	8	0.0169064
4600	0.018747071	9	0.0190197
5000	0.021150541	10	0.021133

Appendix-B

Weight loss (lbs.) for 6 wood members since January 22/2013-April 10/2013.

Table B-1. the weight of six wood members Vs. the day

Test #	1	2	3	4	5	6
21-Jan	1173.5	1545.9	1605.2	1235.6	1480.8	1350.2
22-Jan	1140.5	1515.3	1573.6	1199.9	1442.9	1320.9
23-Jan	1110.5	1489.5	1542.6	1170.5	1412.9	1295.2
24-Jan	1083.5	1446.4	1490.8	1144.8	1375.6	1255.3
25-Jan	1069.3	1419.1	1460.3	1120.2	1363.5	1231.2
28-Jan	1045.9	1394.4	1404.5	1099.5	1340.4	1216.7
29-Jan	1038.2	1385.6	1399.2	1093.3	1331	1208.8
30-Jan	1032	1376.7	1385.6	1087.1	1320.3	1200.2
31-Jan	1022.9	1367.4	1371.5	1080.5	1308.7	1191.3
1-Feb	1018.8	1357.8	1363.5	1072.3	1302	1184.8
4-Feb	1008.6	1340.8	1340.3	1058.7	1288.2	1171.3
5-Feb	1006.4	1337.8	1334.6	1055.7	1282.3	1166.8
6-Feb	1003.7	1335.9	1331.7	1054.2	1279.5	1163.3
7-Feb	1002.2	1333.9	1329.5	1054.2	1277	1161.2
8-Feb	1001.9	1332.6	1327.4	1054.2	1275.7	1159.9
11-Feb	994.8	1321.5	1313.6	1045.9	1267.7	1151.9
12-Feb	992.1	1318.7	1310.1	1044.7	1265.3	1148.7
13-Feb	990.6	1316.5	1308.6	1044.4	1263	1147.4
14-Feb	989	1313.5	1304.3	1042	1258.7	1143.5
15-Feb	988	1309	1300	1040.5	1254.3	1141.3
18-Feb	987	1300	1290.5	1035.3	1249.5	1137.5
19-Feb	986.5	1298	1288.6	1033.5	1247.3	1135.2
20-Feb	986	1296.3	1287.3	1032.2	1246	1133.5
21-Feb	985.8	1295.4	1286.1	1031.7	1244.9	1131.7
22-Feb	985.2	1294.1	1285.6	1031.2	1244	1129.9
25-Feb	985	1289.5	1282.5	1029	1243.1	1127.8
26-Feb	984.5	1288.5	1281.6	1028	1242.5	1126
27-Feb	984.1	1287	1280.3	1026.7	1241.1	1124.8
28-Feb	984.1	1286.1	1279.5	1025.8	1240.2	1123.5

1-Mar	984	1285	1279	1024.3	1239.6	1122
4-Mar	983	1282.1	1277.3	1023.8	1238.8	1120.6
5-Mar	982.6	1281.1	1276	1023.1	1237.9	1119.7
6-Mar	982.3	1280.3	1275.3	1022.4	1237.1	1117.8
7-Mar	982.1	1279.5	1274.4	1021.6	1236.2	1116.5
8-Mar	982	1278.3	1273.7	1021	1235.7	1115
12-Mar	981.8	1277.3	1273.1	1020.3	1235	1114.2
13-Mar	981.6	1276.7	1272.7	1019.7	1234.5	1113.3
14-Mar	981.5	1275.8	1272.3	1019.2	1234.1	1112.6
15-Mar	981.4	1275	1272	1018.7	1233.6	1112
18-Mar	981.2	1273.5	1271.5	1018.2	1233.2	1111.5
19-Mar	981	1273	1271.1	1017.8	1232.9	1111.1
20-Mar	980.8	1272.5	1270.8	1017.4	1232.6	1110.7
21-Mar	980.6	1272	1270.6	1017.1	1232.3	1110.4
22-Mar	980.5	1271.6	1270.4	1016.8	1232.2	1110.2
25-Mar	980.3	1271.1	1270.2	1016.6	1232	1110.1
26-Mar	980.2	1270.8	1270	1016.4	1231.9	1110.1
27-Mar	980.1	1270.5	1269.5	1016.4	1231.8	1110
28-Mar	980	1270.3	1269.3	1016.4	1231.7	1109.9
29-Mar	979.9	1270.2	1269.3	1016.3	1231.6	1109.9
1-Apr	979.9	1270.1	1269.2	1016.3	1231.6	1109.9
2-Apr	979.8	1270.1	1269.2	1016.3	1231.5	1109.8
3-Apr	979.7	1270.1	1269.2	1016.3	1231.5	1109.8
4-Apr	979.7	1270	1269.1	1016.2	1231.4	1109.7
5-Apr	979.6	1270	1269.1	1016.2	1231.4	1109.7
8-Apr	979.6	1270	1269.1	1016.2	1231.4	1109.6
9-Apr	979.5	1269.9	1269.1	1016.2	1231.3	1109.6
10-Apr	979.5	1269.9	1269.1	1016.2	1231.3	1109.5

Table B-2. The weight loss between the two days weight measurements of six wood members

test #	1	2	3	4	5	6
22-Jan	33	30.6	31.6	35.7	37.9	29.3
23-Jan	30	25.8	31	29.4	30	25.7
24-Jan	27	43.1	51.8	25.7	37.3	39.9
25-Jan	14.2	27.3	30.5	24.6	12.1	24.1
28-Jan	23.4	24.7	55.8	20.7	23.1	14.5
29-Jan	7.7	8.8	5.3	6.2	9.4	7.9
30-Jan	6.2	8.9	13.6	6.2	10.7	8.6
31-Jan	9.1	9.3	14.1	6.6	11.6	8.9
1-Feb	4.1	9.6	8	8.2	6.7	6.5
4-Feb	10.2	17	23.2	13.6	13.8	13.5
5-Feb	2.2	3	5.7	3	5.9	4.5
6-Feb	2.7	1.9	2.9	1.5	2.8	3.5
7-Feb	1.5	2	2.2	0	2.5	2.1
8-Feb	0.3	1.3	2.1	0	1.3	1.3
11-Feb	7.1	11.1	13.8	8.3	8	8
12-Feb	2.7	2.8	3.5	1.2	2.4	3.2
13-Feb	1.5	2.2	1.5	0.3	2.3	1.3
14-Feb	1.6	3	4.3	2.4	4.3	3.9
15-Feb	1	4.5	4.3	1.5	4.4	2.2
18-Feb	1	9	9.5	5.2	4.8	3.8
19-Feb	0.5	2	1.9	1.8	2.2	2.3
20-Feb	0.5	1.7	1.3	1.3	1.3	1.7
21-Feb	0.2	0.9	1.2	0.5	1.1	1.8
22-Feb	0.6	1.3	0.5	0.5	0.9	1.8
25-Feb	0.2	4.6	3.1	2.2	0.9	2.1
26-Feb	0.5	1	0.9	1	0.6	1.8
27-Feb	0.4	1.5	1.3	1.3	1.4	1.2
28-Feb	0	0.9	0.8	0.9	0.9	1.3
1-Mar	0.1	1.1	0.5	1.5	0.6	1.5
4-Mar	1	2.9	1.7	0.5	0.8	1.4
5-Mar	0.4	1	1.3	0.7	0.9	0.9
6-Mar	0.3	0.8	0.7	0.7	0.8	1.9
7-Mar	0.2	0.8	0.9	0.8	0.9	1.3
8-Mar	0.1	1.2	0.7	0.6	0.5	1.5
12-Mar	0.2	1	0.6	0.7	0.7	0.8

13-Mar	0.2	0.6	0.4	0.6	0.5	0.9
14-Mar	0.1	0.9	0.4	0.5	0.4	0.7
15-Mar	0.1	0.8	0.3	0.5	0.5	0.6
18-Mar	0.2	1.5	0.5	0.5	0.4	0.5
19-Mar	0.2	0.5	0.4	0.4	0.3	0.4
20-Mar	0.2	0.5	0.3	0.4	0.3	0.4
21-Mar	0.2	0.5	0.2	0.3	0.3	0.3
22-Mar	0.1	0.4	0.2	0.3	0.1	0.2
25-Mar	0.2	0.5	0.2	0.2	0.2	0.1
26-Mar	0.1	0.3	0.2	0.2	0.1	0
27-Mar	0.1	0.3	0.5	0	0.1	0.1
28-Mar	0.1	0.2	0.2	0	0.1	0.1
29-Mar	0.1	0.1	0	0.1	0.1	0
1-Apr	0	0.1	0.1	0	0	0
2-Apr	0.1	0	0	0	0.1	0.1
3-Apr	0.1	0	0	0	0	0
4-Apr	0	0.1	0.1	0.1	0.1	0.1
5-Apr	0.1	0	0	0	0	0
8-Apr	0	0	0	0	0	0.1
9-Apr	0.1	0.1	0	0	0.1	0
10-Apr	0	0	0	0	0	0.1

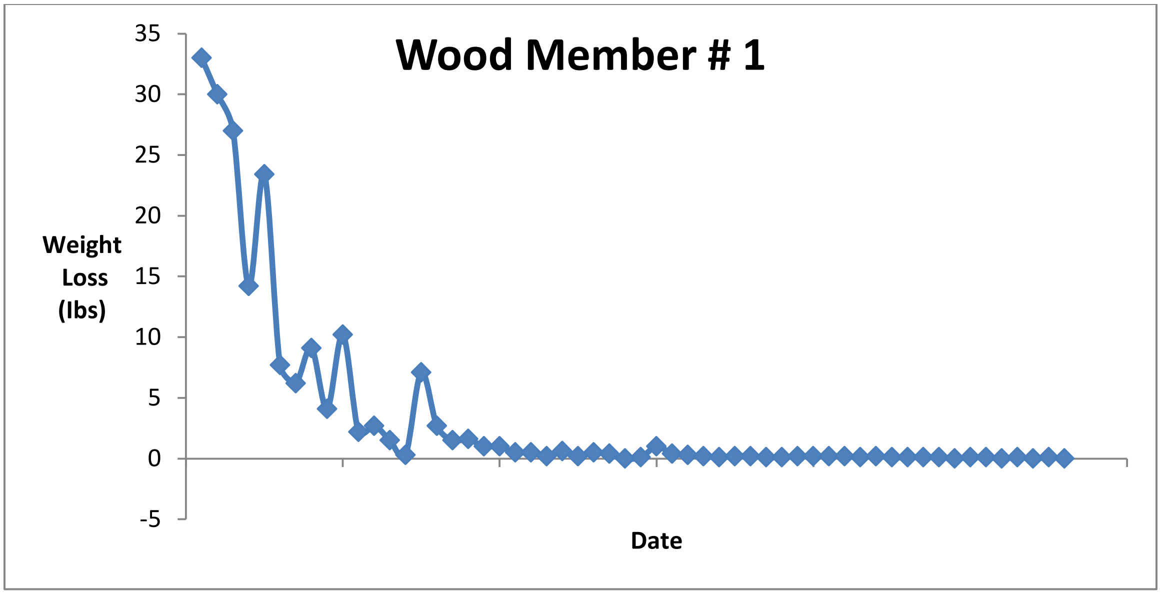

Figure B-1. The weight loss curve with time for wood member #1

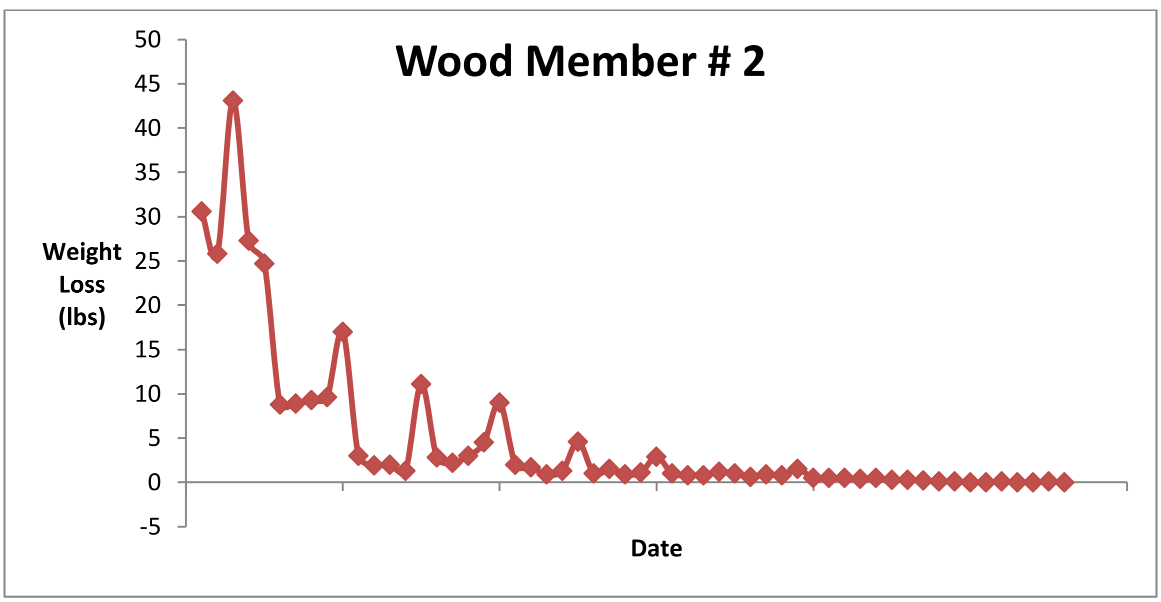

Figure B-2. the weight loss curve with time for wood member #2

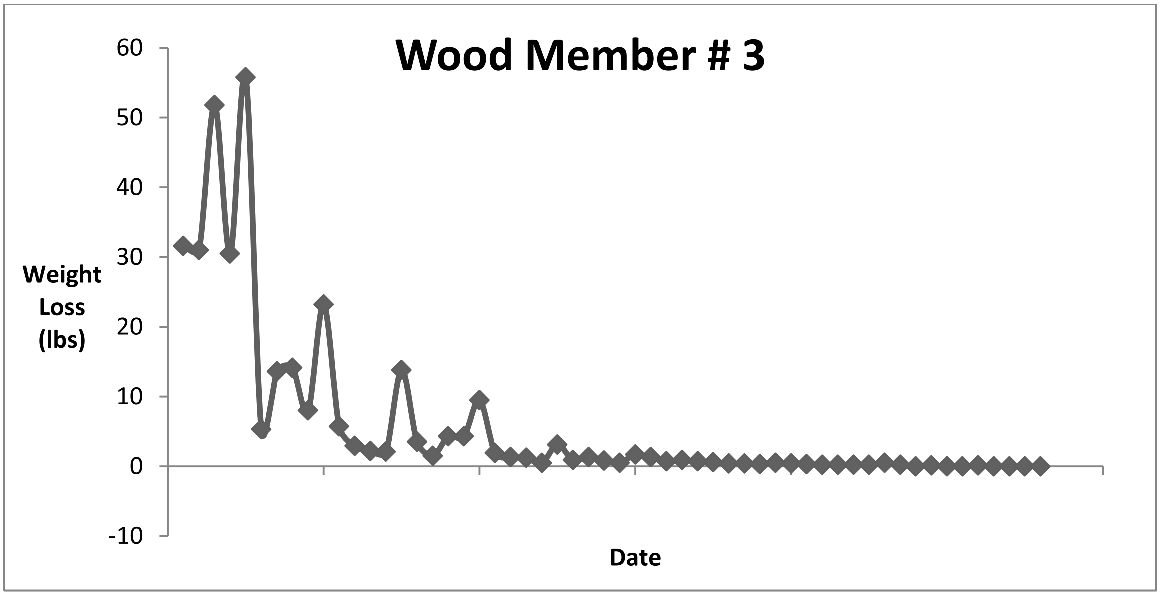

Figure B-3. The weight loss curve with time for wood member #3

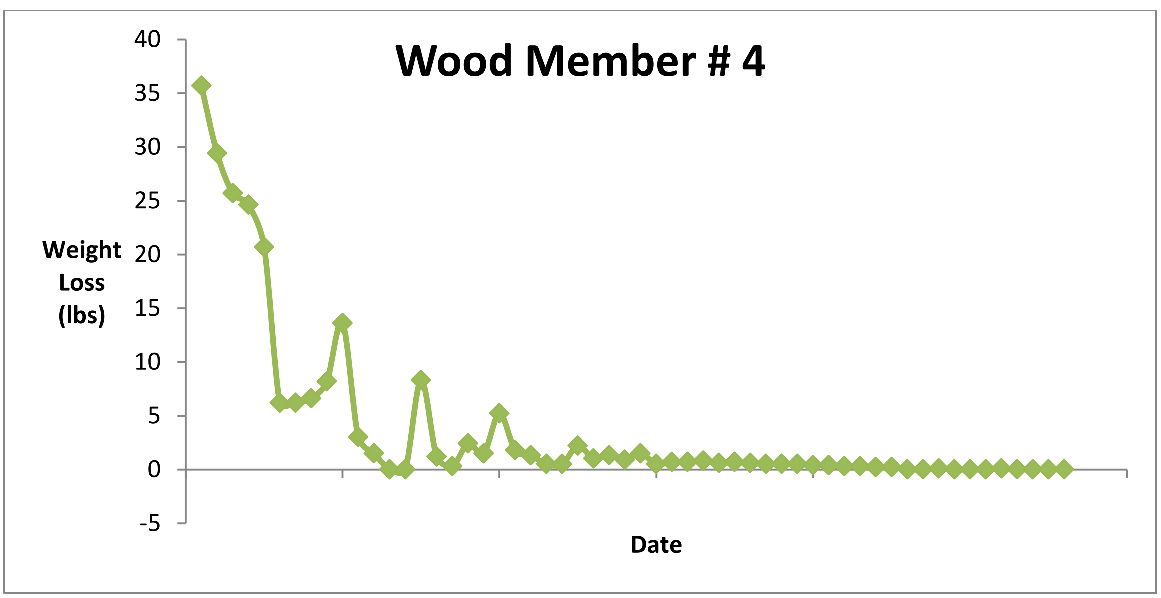

Figure B-4. The weight loss curve with time for wood member #4

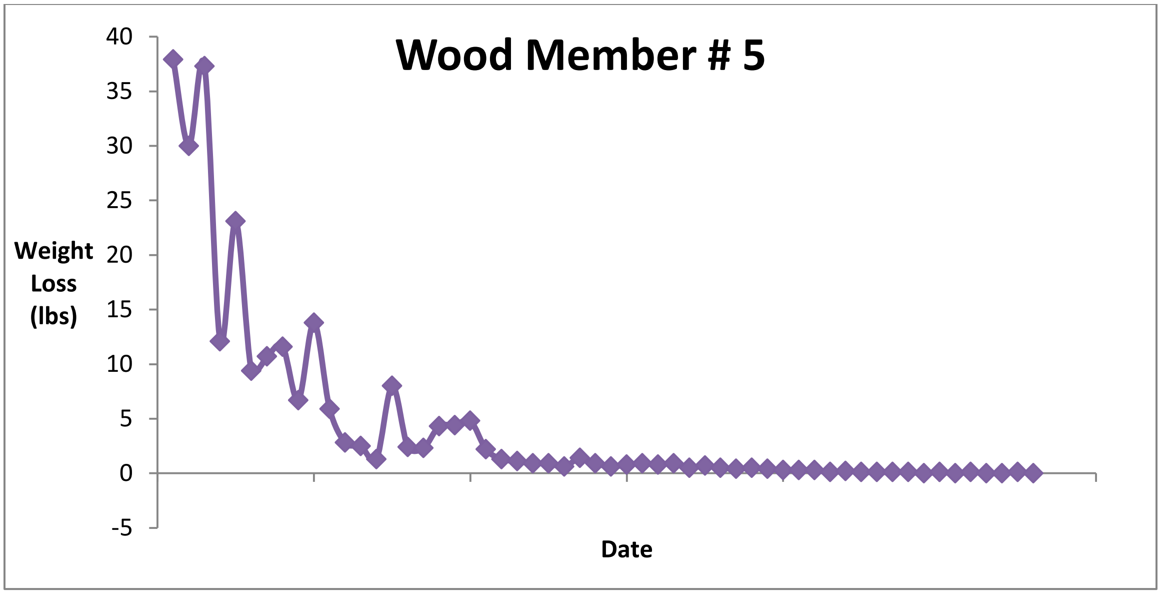

Figure B-5. The weight loss curve with time for wood member #5

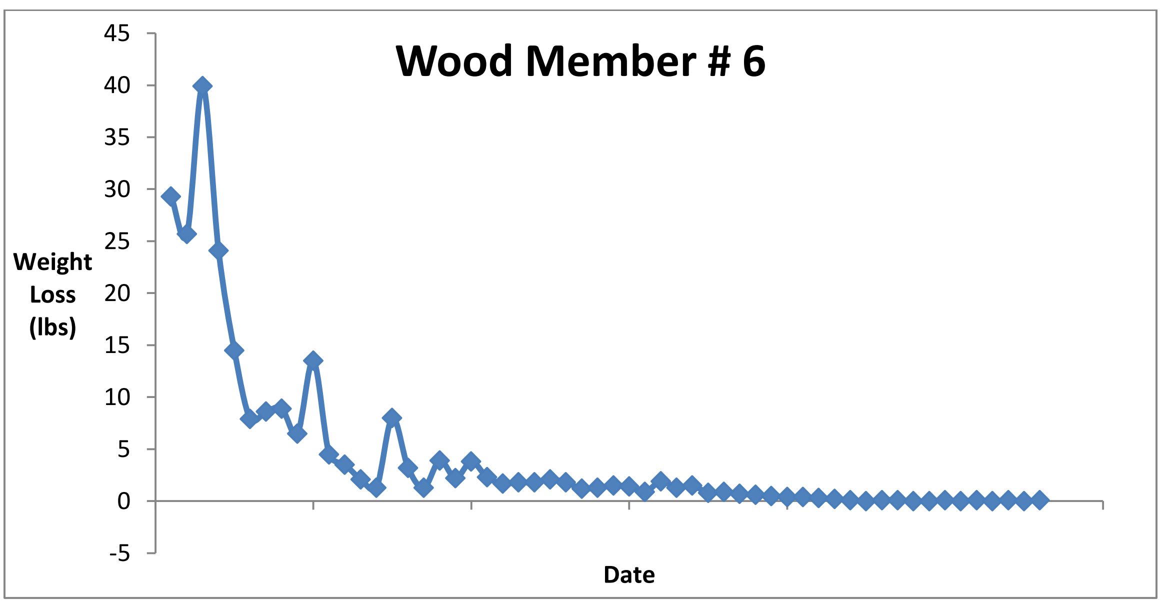

Figure B-6. The weight loss curve with time for wood member #6

Appendix C

Obstacles and Challenges in this Research (Trials and Errors):

In this research, there were several obstacles that have been encountered until finding the right results, and theses obstacle are:

- DIC is an electrical engineering subject. Thus, understanding first DIC technique was the most important part. Many data and research papers had been collected from different journals to understand what DIC is, what the history of this technique is and how this works.
- Choosing the right software: choosing the right software was not easy. There is a lot of academic software in the research papers. A lot of them had been contacted but just few replied. These contact procedures took a long time. However, having the software is not a last solution. You need to understand how this software works and all the conditions and limitations of this software. Usually who wrote the software tried not to show its weakness or where this software cannot be applied. Thus, as a student you should try and see if this works or not. In the first time, software was chosen and a good time was spent on it to be understood and why the researcher wrote it in this way and why it is different. After the software was understood, it was used in this research. However, after a while the results from this first software did not mean anything. Then the creature of this software was contacted to ask several questions about the software. Then, after around 30 days he declared that this software does not work in this research case because the

plates that were examined have slots everywhere. The software will read these slots as a fracture on the plate. Then the software will struggle reading these fracture especially if it is not capable of analyzing it. After that, the need for new software was repeated again but this time the needed software should be able to cut out some parts from the area of interest and analyze it without having these slots. Finally, after many attempts, software was found and it can be used on the plates with slots on. The software was used for several times to make sure it works and it can be used to cut the slots off and run it after that without any problems. The Vic-2D code successfully analyzed the metal plate connections with the slots on.

- Speckle pattern: as mentioned in chapter 3 that the speckle is very important in the DIC technique and influences the results. The speckle pattern was also one of the obstacles that had been a problem in this research. The first speckle pattern was created by using the brush to randomly make the black dots. However, with no experience in making the speckle pattern on the plate using the brush, the dots were not regular and dense. Some specimens were examined and used the DIC code to analyze them but the analysis did not work. Another search was made to find the right speckle way. There were several ways to do it other than using the brush. However, all of them need other equipment. Since this research is funded research the speckled plates were done by hand dot by dot. These procedures by hand were time consuming but it worked well. Around 5 hours was consumed to make speckles on each plate by using the hand. Dr. Sutton mentioned several methods to do speckle pattern and the last one was the manual one by the hand.

- In heel joint test, big plates were chosen (8X8 in) first to do the test. All the big plates were speckled then tested in the lab. However, the failure took so long time and finally it was in the wood or due to teeth withdrawal. Then, the heel joint tests were repeated with smaller plate (4X5 in). The test took less than 20 minutes and the failure occurred in the plate itself and the changes in the plate due to load was clear.
- Universal testing machine is just 29X29 in which makes the size of the truss limited to its size.

VITA

Deema Rashad Alsheiab

Candidate for the Degree of

Doctor of Philosophy/Civil Engineering / structural Engineering

Thesis: FULL-FIELD STRAIN MEASUREMENTS OF METAL PLATE CONNECTIONS USING DIGITAL IMAGE CORRELATION TECHNIQUE

Major Field: Structural Engineering

Biographical:

Education:

Completed the requirements for the Doctor of Philosophy in civil engineering at Oklahoma State University, Stillwater, Oklahoma in December, 2013.

Completed the requirements for the Master of Science in civil engineering at Oklahoma State University, Stillwater, Oklahoma in 2006.

Completed the requirements for the Bachelor of Science in civil engineering at Jordan University of Science and Technology, Irbid, Jordan in 2002

Experience:

Professional Memberships:

A member in ACI since 2007